Title
SKS03: Centrifuge Test of Liquefaction-Induced Downdrag in Interbedded Soil Deposits

Authors
Sinha, Sumeet Kumar
Ziotopoulou, Katerina
Kutter, Bruce L

Publication Date
2021

DOI
10.17603/DS2-WJGX-TB78

Data Availability
The data associated with this publication are available at: https://www.designsafe-ci.org/data/browser/public/designsafe.storage.published/PRJ-2828

REPORT NO.
UCD/CGMDR-21/02

CENTER FOR GEOTECHNICAL MODELING

DATA REPORT FOR SKS03:

CENTRIFUGE TESTING OF LIQUEFACTION-INDUCED DOWNDRAG ON AXIALLY LOADED PILES

BY

S. K. SINHA

K. ZIOTOPOULOU

B. L. KUTTER

UCDAVIS

DEPARTMENT OF CIVIL & ENVIRONMENTAL ENGINEERING
COLLEGE OF ENGINEERING
UNIVERSITY OF CALIFORNIA AT DAVIS

November 2020

CENTRIFUGE TESTING OF LIQUEFACTION-INDUCED DOWNDRAG ON AXIALLY LOADED PILES
Centrifuge Data Report for SKS03

S.K. Sinha, K. Ziotopoulou, B.L. Kutter

Center for Geotechnical Modeling Data Report UCD/CGMDR – 21/02

Date:	November, 2020
Date of testing:	27-28th August, 2020
Project:	Validation of Design for Liquefaction-Induced Downdrag on Piles
Sponsor:	California Department of Transportation (CALTRANS)

ACKNOWLEDGEMENTS

This work was supported primarily by the California Department of Transportation (CALTRANS) under the project titled ‘Validation of Design for Liquefaction-Induced Downdrag on Piles’. The contents of this report are solely the authors’ and do not necessarily reflect the views or opinions of the sponsors. The authors would like to acknowledge the suggestions and assistance of Dan Wilson, Tom Kohnke, Chad Justice and Anatoily Ganchenko of the UC Davis CGM and the UC Davis undergraduate researcher Jared May and masters’ researcher student James Heins for their help during model preparation and testing. The author would also acknowledge the help towards the development of the large centrifuge at UC Davis, which was supported primarily by the National Science Foundation (NSF) via the Natural Hazards Engineering Research Infrastructure (NHERI) and Network of Earthquake Engineering Simulation (NEES).

CONDITIONS AND LIMITATIONS

CONTENTS

LIST OF FIGURES

LIST OF TABLES

1 ABSTRACT

Earthquake shaking can cause significant soil settlements, especially if the shaking causes liquefaction. Soil settlements will induce drag loads that can significantly increase the axial loads in a pile foundation and/or cause significant pile settlement (Figure 1). The liquefaction-induced downdrag on piles is affected by the complex interplay and timing of a variety of processes including the development and dissipation of pore water pressures, soil settlement, sand boils and gaps that provide vents for high excess pore pressures. Since it has not been possible to accurately model all these complex processes, simplifying assumptions are used to account for downdrag in the current design procedures. A series of centrifuge tests were designed to investigate the complex processes and the validity of the simplifying assumptions. This report describes the details of the second (SKS03) of the two model tests performed under this project. Sinha et al. (2021b) describes the previous centrifuge test series (SKS02). In SKS03, the soil profile consisted of (from top to bottom in prototype dimensions) 1 m of coarse sand, a 2 m clay crust, about 4.7 m of loose sand, 1.3 m of silt, 4 m of medium dense sand and 8 m of dense sand. Three 635 mm diameter piles were embedded about 15 m into the deposit, with their tips embedded about 1.9 m into the deeper dense sand. The three piles were loaded by lumped masses clamped just above the pile head; the static loads were different on each pile (500 kN, 1500 kN, and 2400 kN). The piles were instrumented with several strain gauge bridges designed to measure the axial load distribution in the piles. The base of the model was shaken with multiple earthquake ground motions with peak horizontal accelerations ranging from 0.08 g to 0.61 g. In addition to earthquake shaking, a pile load test was performed on one of the piles.

As in SKS02, drag loads were observed to increase from earthquake shaking. Most of the pile settlement occurred during shaking, and very minimal settlement happened post shaking. Among all piles, the heavily loaded piles suffered the most settlement. Higher drag loads were observed on lightly loaded piles as compared to the heavily loaded piles. As expected, the neutral plan was found to be relatively deep for the lightly loaded pile and shallow for the heavily loaded pile.

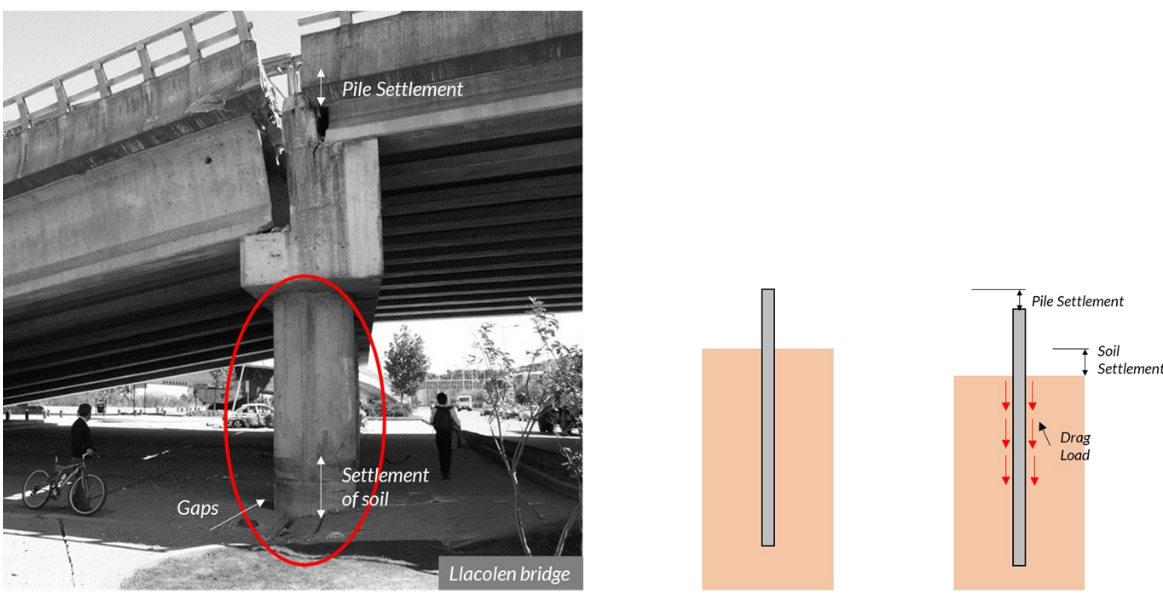

Source: https://www.flickr.com/photos/ewm/4417936107/

Figure 1. Liquefaction-induced settlement results in drag load and settlement in piles.

2 PROBLEM STATEMENT

Pile foundations are designed to transfer loads to deeper depths through skin friction and tip resistance while undergoing acceptable settlements. For sites where earthquake-induced (liquefaction) ground settlement is expected to occur, estimating the drag load and pile settlement becomes an important design objective. The prediction is often based on simplifying assumptions that arise from the incomplete understanding of the phenomenon, resulting in over- or underestimating of drag loads and settlements. It mainly results from an incomplete understanding of the complex interplay and timing of the different mechanisms during/post liquefaction. Sinha et al. (2021b) described several factors affecting liquefaction induced downdrag and mechanism occurring at the interface (Figure 2). To investigate these mechanisms and expand our current understanding and propose revisions to existing procedures on pile design, a series of centrifuge model tests were performed.

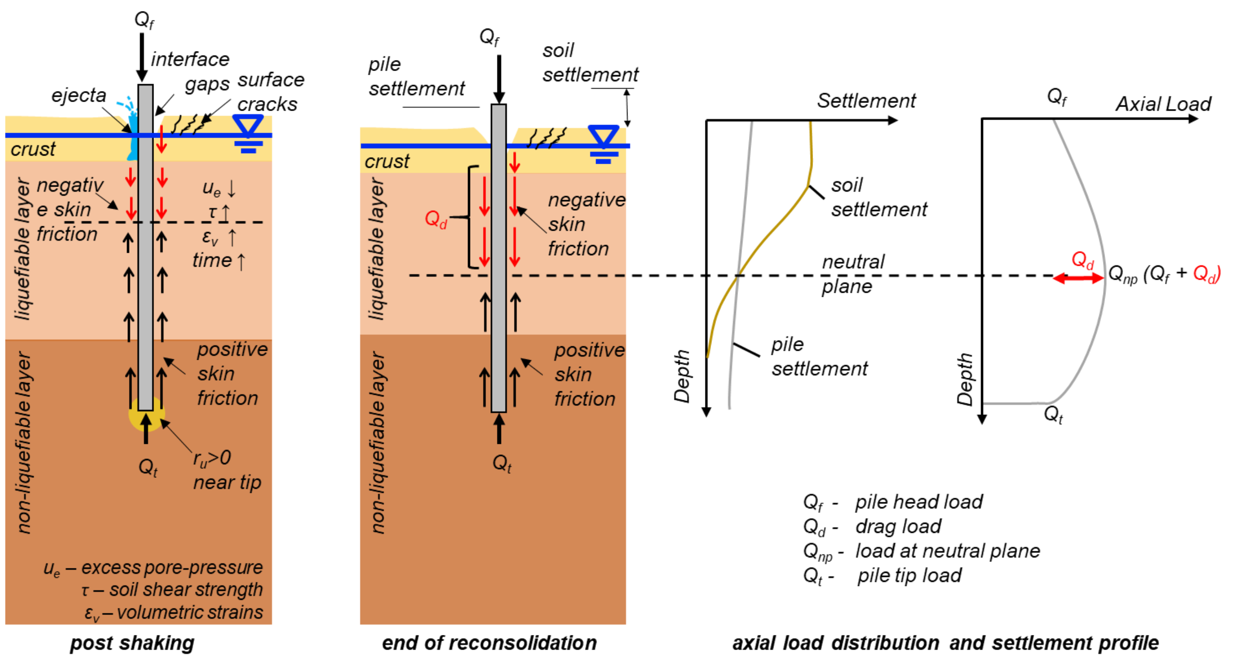

Figure 2. Illustration of liquefaction-induced downdrag in piles.

Figure 3 shows the development of the drag load in a uniform layered liquefiable deposit as recorded in centrifuge test SKS02 (Sinha et al. 2021b). With multiple shakings, the drag load on piles increased and attained saturation. About 15-20 mm (prototype scale) of soil settlement was found enough to mobilize the full negative skin friction. As far as piles' performance is concerned, the experimental results clearly showed that the presence of high excess pore pressures near the tip could significantly reduce the tip resistance and result in excessive settlement in pile. Overall, most of the pile settlement occurred during shaking, and < 10 mm occurred post-shaking.

In SKS03, the effect of pile head load, intermediate soil layers, and presence of clay crust on liquefaction-induced downdrag are studied. Cracks in the clay crust layer can expedite dissipation and create gaps at the interface, significantly lowering the development of negative skin friction near the surface. The presence of deep low permeable soil layers can slow the dissipation process in the layers beneath it, inducing slow settlement and thus high negative skin friction in the layers above. With a large pile head load, the neutral plan would be shallower, and correspondingly, the drag loads would be smaller. However, a larger pile load could result in higher settlement in pile. This report describes the second large centrifuge test (SKS03) performed on 27-28th August 2020 as an effort to understand the mechanisms involved with iquefaction-induced downdrag phenomenon.

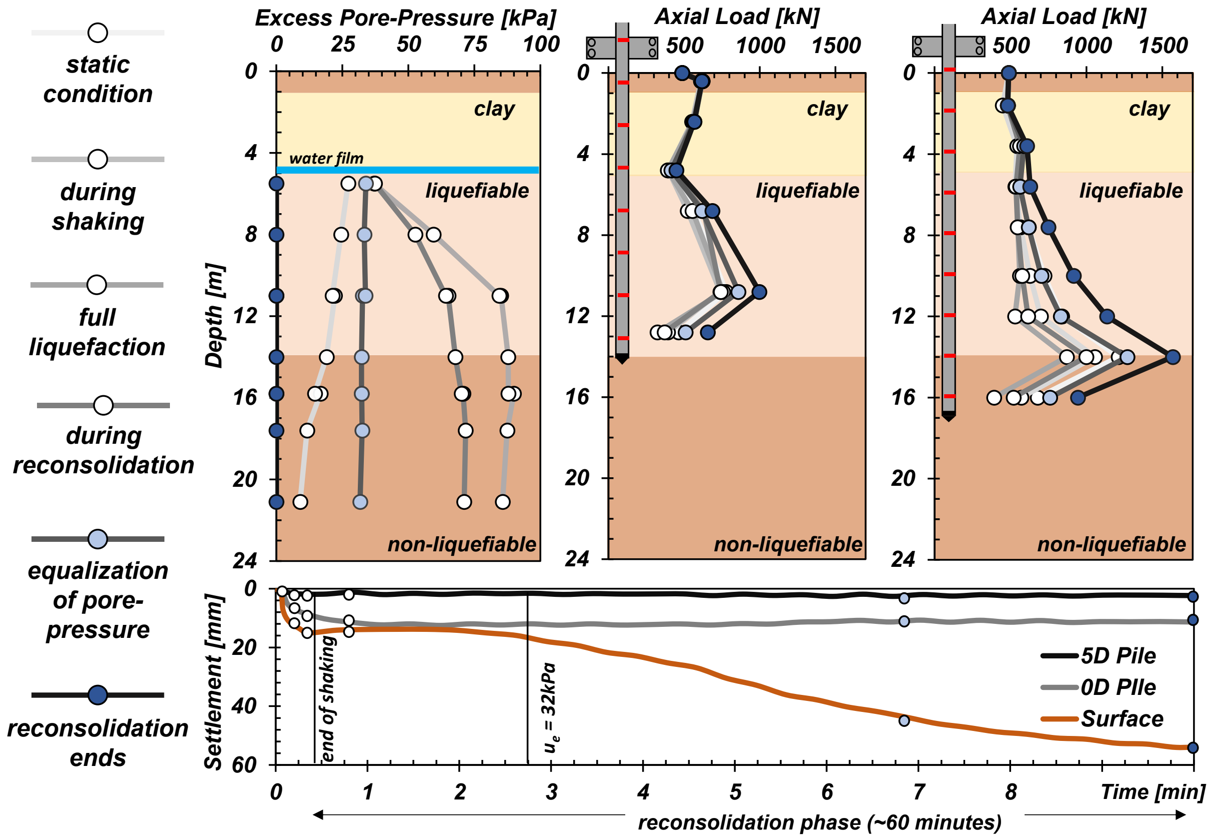

Figure 3. Excess pore pressure, axial load profile and settlement in soil and pile recorded during the earthquake event EQM₃ in centrifuge test SKS02.

3 CENTRIFUGE MODEL DESCRIPTION

The results from the centrifuge test SKS02 and the factors affecting downdrag, as discussed in Sinha et al. (2021b), guided the design of this centrifuge test. SKS03 included three aluminum pipe piles in a more interbedded layered soil deposit. The three piles were loaded by different lumped masses at the pile head, producing static factors of safety of about 8, 2.5, and 1.5, respectively, and all their tips were embedded about 15 m into the soil deposit, including 1.9 m (3 diameters) into the dense sand layer. Several sensors were placed in the model to track the pore pressure generation/dissipation, induced soil/pile settlements, accelerations, and axial loads generated in the piles. Four high speed (up to 10000 fps) Photron cameras were used to obtain the images and TEMA tracking software was used to process the image data to determine three-dimensional movements of many markers on the model. Sinha et al. (2021a) describes the techniques and tools used to obtain and process the image data. The model was tested on the large 9 m centrifuge at the Center of Geotechnical Modeling at the University of California Davis.

3.1 Scaling Laws

All numerical quantities in this report, unless explicitly specified, have been converted into prototype units according to the scaling laws described by Kutter (1992). For example, the model length is multiplied by the scale factor N to obtain the equivalent length in the prototype scale, where N is the centrifugal acceleration applied to the model. For this test, the centrifugal acceleration on the model was 40 g ($N = 40$) at the center of model 8.635 m from the axis of rotation. The angular speed of the centrifuge was 64.4 rpm.

Table 1. Scaling factors in centrifuge testing.

	Parameters		***Model/Prototype***
General	Length [m]	L	$1/N$
	Density [kg/m^3]	ρ	1
	Stress, Strain	σ,τ,ε	1
	Force [N]	F	$1/N^2$
	Mass [Kg]	M	$1/N^3$
	Time [s]	T	$1/N$
Dynamic	Time [s]	T	$1/N$
	Frequency [Hz]	f	N
	Velocity [m/s]	v	1
	Acceleration [g]	a	N
	Diffusion Time [s]	T_{dif}	$1/N^2$

3.2 Cross-section and Instrumentation Layout

Figure 4 shows the plan view of the model in model scale dimensions (in cm). To convert into prototype scale, all dimensions should be multiplied by the scale factor of N=40. The model consisted of 3 medium pipe piles: Pile 1, Pile 2, and Pile 3 of model diameter (D) 15.88 mm. The piles were installed at the middle cross-section of the model container (Section F-F) with their tip embedded 3D into the dense sand layer. The minimum lateral separation between the piles and the container was about 20D. A vertical array of accelerometers (Section F-F) and pore pressure transducers (Section E-E) were installed at the center of the model in between Pile 2 and Pile 3. Four Photron Cameras on the east side and line lasers (Laser 1, Laser

2) were installed to track the movement of the model surface and the piles. Additionally, Cone Penetration Test ($CPT_{\#}$), Pile Load Test ($PLT_{\#}$), Hand Vane Shear Test ($VST_{\#}$) were performed to obtain the strength of soil at different stages of the test. The location of the line lasers (shown in green color), cone penetration test, pile load test and vane shear test are shown in Figure 4.

Figure 5 shows the model cross-section view in model scale dimensions (in cm). Table 2 shows soil layer properties (thickness and saturated densities). For convenience, on the right side of the model, the prototype depth (in m) measured from the soil surface is shown. The soil profile consists of 1 m of Monterey sand, 2 m of cemented Yolo loam (s_u≈28-35kPa), 4.7 m of loose sand (D_r≈40%), ~1.3 m of silty clay (20% clay and 80% silt) and 4 m of medium dense sand (D_r≈60%). The water table was located on the surface. The pile head mass of the installed piles (Pile 1 and Pile 2) was 1 m above the ground surface. Pile 3 mass was about 1.3 m above the soil surface. ICP and MEMS accelerometers were installed on the pile head mass to monitor accelerations and rotations during earthquake loading events. The piles were instrumented with 9 full-bridge axial strain gages at spacing of 2 m (prototype scale) to fully capture the axial load distribution. Just below the clay layer, pore pressures transducers were installed to track the movement of the hydraulic head during/after the shaking event. Accelerometers on the containers were installed to measure the input earthquake motion and any vertical accelerations generated. Additionally, horizontal, and vertical accelerometers were also installed on the beams holding the cameras.

Similar to SKS02 test, MS54XXX SMD PPTs (see Section 4.2.2) shown in yellow color in Figure 5, were again used. Although these sensors had a very low success rate of about 1/3 in SKS02 test, the data provided some useful information. These sensors were installed at non-critical locations. To improve their success rate in the current test, the sensors were prepared with three or more layers of adhesive coating.

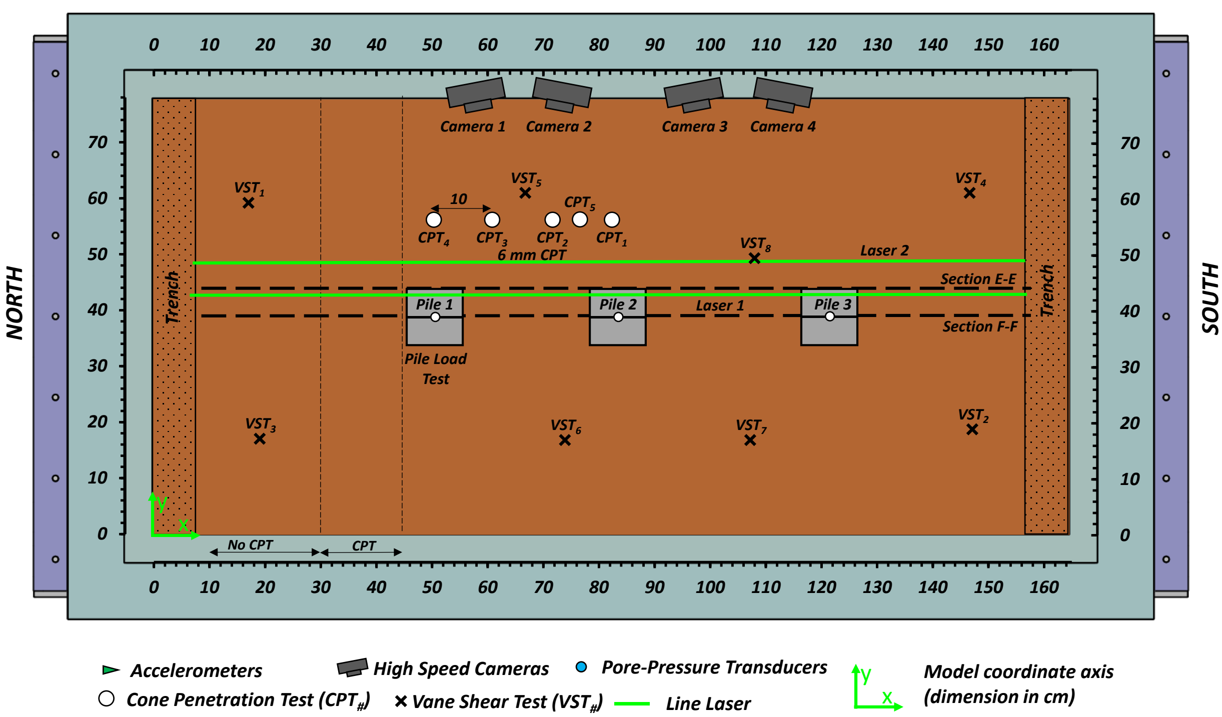

Figure 4. Plan view of the model (dimensions shown in model scale in cm).

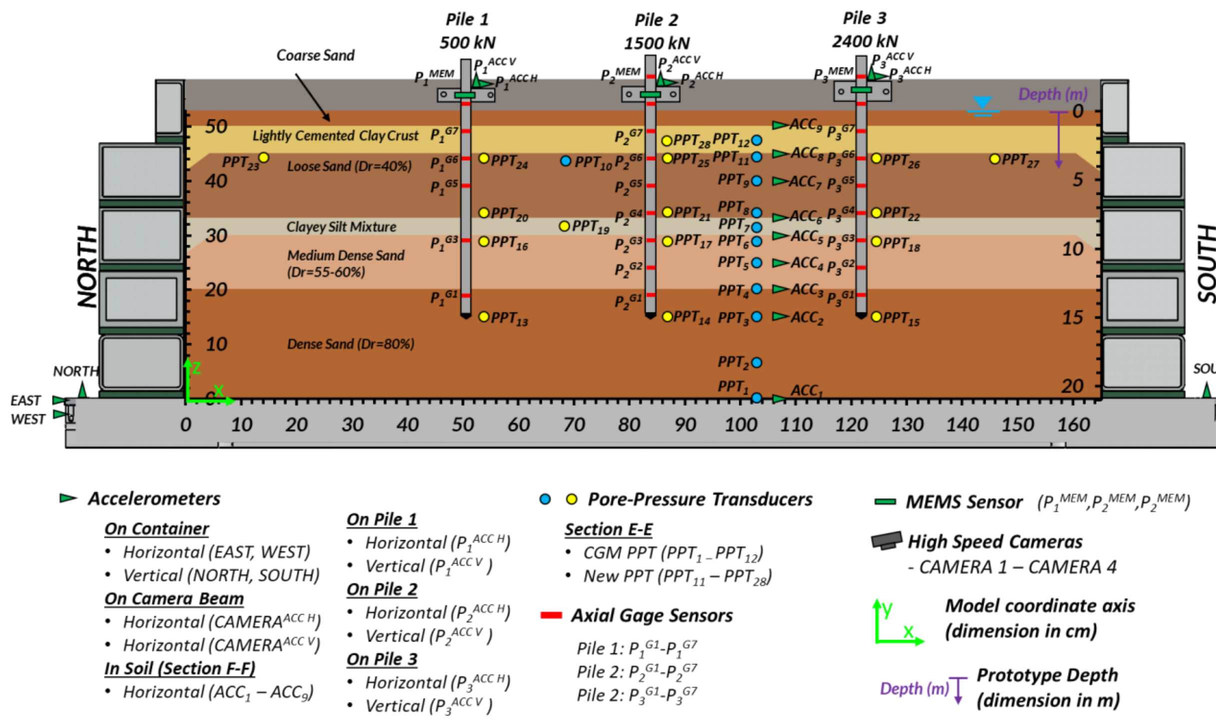

Figure 5. Cross-section view of the model. Model dimensions are shown in centimeters (z-scale on the left and x-scale at the bottom). Prototype depth is shown in meters using the scale on the right.

Table 2. Soil layer thickness and saturated density.

Soil Type	***Thickness [cm]***	***Saturated Density [Kg/m³]***
Monterey Sand	*2.5*	*2054*
Clay Crust	*5.0*	*1700*
Loose Sand	*11.7*	*1971*
Clayey Silt	*3.3*	*2000*
Medium Dense Sand	*10*	*2019*
Dense Sand	*20*	*2051*

3.3 Soil Properties

3.3.1 Sand

The loose, medium dense and dense soil layer below the clay layer consisted of Ottawa F-65 sand purchased from US Silica Engineered Performance Materials. The top layer consisted of Monterey sand. The properties of the soils are summarized in Table 3 below.

Table 3. Properties of sand used in the test.

Soil Type	G_s	e_{min}	e_{max}	D_{50} ***[mm]***	***USCS***	***Description***
Ottawa F-65	2.65	0.52	0.83	0.2	SP	US Silica: F-65 whole grain Quartz sand
Monterey Sand	2.64	0.536	0.843	0.95	SP	Cemex: Clean graded kiln dried Monterey sands #0/30

3.3.2 Clay Crust

Lightly cemented Yolo loam soil was used to model the clay crust layer. Yolo loam was excavated from the yard of Center for Geotechnical Modeling at UC Davis and then later sieved with #15 sieve to retain particles less than ~1.69 mm. Figure 6(a) shows the gradation curve of the sieved Yolo loam. The Atterberg limits of the sieved Yolo Loam had a liquid limit (LL) of w=29% and plasticity index of PI = 10.

Park (2011) found that mixtures of Yolo Loam and Portland cement can produced highly sensitive clays. In SKS03 test, to create weakly cemented clay layer, Basalite type II-V (Portland Cement) was mixed with Yolo loam. Different proportion of soil, cement and water was tested to design the clay crust with peak undrained shear strength around 80-100 kPa. A kitchen mixer was used to create 3 kg samples which were later tested for undrained shear strength. First a mixture of cement and dry soil was prepared, upon which appropriate amount of water was slowly added and then mixed over 5 minutes. Hand vane shear (Figure 6) with a blade width of 19 mm and height of 30 mm was used to test the undrained shear strength of the specimen as the cement in the mixture cured with time. Additionally, fall cone (apex angle of 30^{o}) tests (Figure 6) were also performed to measure the undrained shear strength of the cement clay mixture. However, as the shear strength of the sample increased with time, the large decrease in penetration depth of falling cone made it useless for further strength measurements.

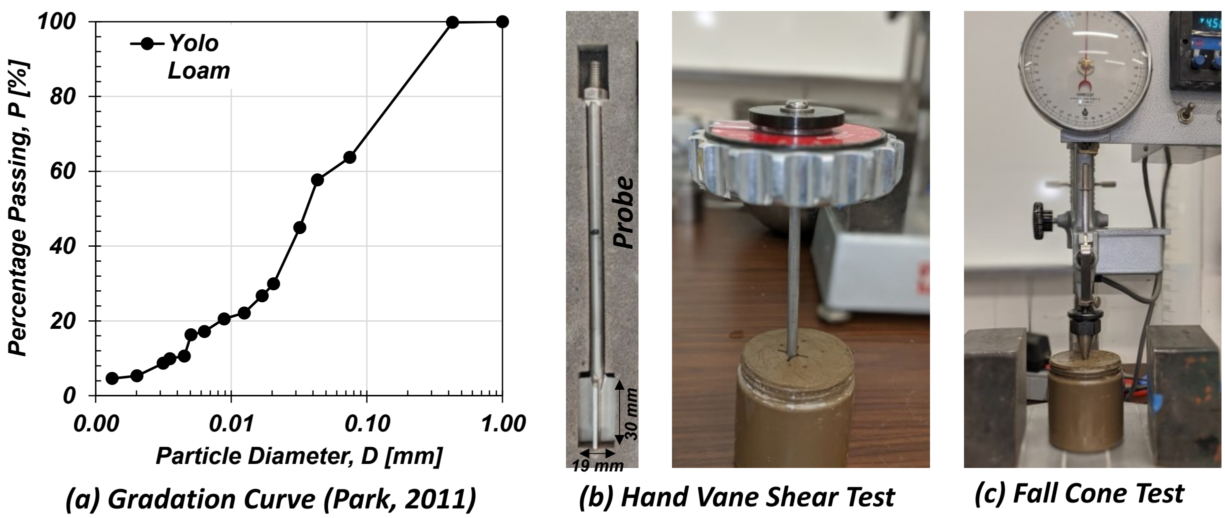

Figure 6. (a) Gradation Curve of Yolo Loam soil. (b) Hand Vane Shear and (c) Fall Cone test used for estimating the undrained shear strength of cemented clay mixture.

In the first series of tests, samples were prepared and stored in multiple sealed containers as shown in Figure 7. This was made to ensure constant water content in the samples. The water content (w) in the samples was kept as 50%. The strength of the samples was monitored over three weeks. Figure 7, shows the results for two samples prepared with cement-soil ratio of 3% and 2%, respectively.

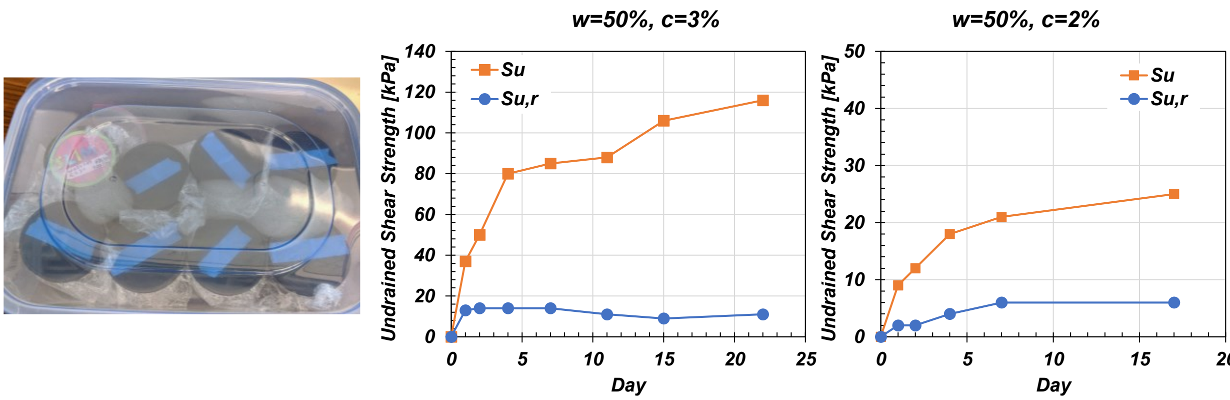

Figure 7. Peak and residual undrained shear strength of weekly cemented Yolo loam samples prepared with water content (w) of 50% and cement-soil (c) percentage of 3% and 2%, respectively placed in an airtight sealed container. The undrained shear strength was measured with 19 mm wide and 30 mm long hand vane shear.

In the second series of tests, the sample was prepared and submerged under water. This was done to simulate similar conditions as it would happen while building the model. The samples were prepared and poured in containers under ~1 inch of water as shown in Figure 8. The water content (w) in the samples was kept as 50%. The strength of the samples was again monitored over three weeks. Figure 8 shows the results for two samples prepared with cement-soil ratio of 3% and 4%, respectively. From the results received, water content of w=50% and soil-cement ratio of 3% was used for the design of clay crust. The build-in strengths obtained during the centrifuge tests are discussed in section 6.2.

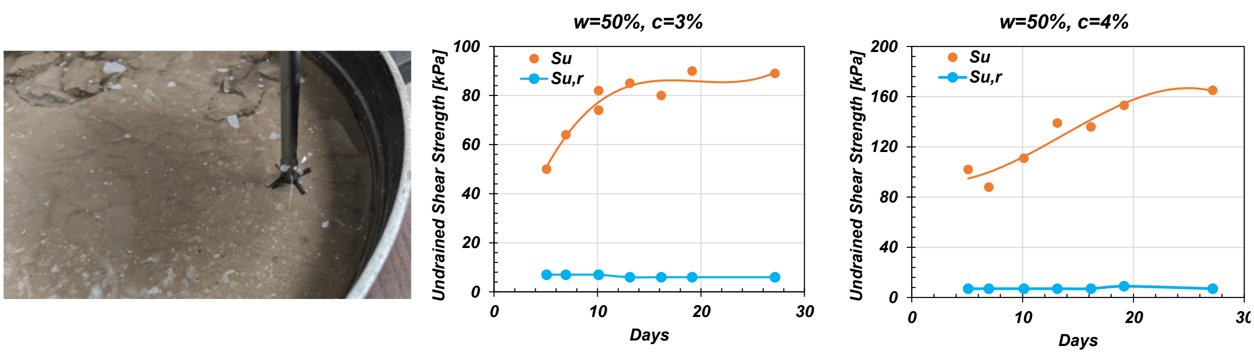

Figure 8. Peak and residual undrained shear strength of weekly cemented Yolo Loam samples prepared with water content (w) of 50% and cement-soil (c) percentage of 3% and 4% cured under 1 inch of water bath. The undrained shear strength was measured with 19 mm wide and 30 mm long hand vane shear.

3.3.3 Clayey Silt

The clayey silt layer was prepared with 20% of Kaolin clay mixed with 80% of silt (SIL-CO-SIL-250). The properties of Kaolin clay and silt used are summarized in Table 4. The permeability of the mixture was found to be 9×10^{-8} m/s. The mixture was prepared at a water content (w) of 44.6%. Price (2018) reported a PI of 6 for the mixture containing 80% silt and 20% clay. The clayey silt layer was designed for an OCR of 1 i.e., a consolidation stress (σ'_p) of 80kPa. From one-dimensional consolidation tests, the coefficient of consolidation (c_v) was measured to be increasing from 5 mm^2/s at low stress ($\sigma'_p \leq 5$ kPa) to 45 mm^2/s for high consolidation stresses ($\sigma'_p \geq 80$ kPa). At $\sigma'_p \geq 80$ kPa, the volumetric compression was estimated to be about 24 %. The cyclic properties of the mixture are reported in Price (2018).

Table 4. Properties of kaolin clay and silt used in the test.

Soil Type	G_s	*LL [%]*	*PL [%]*	*PI*	*USCS*	*Description*
Kaolin Clay	2.58	46.8	28.3	18.5	ML	Hydrite Flat DS IMREYS Company
Silt	2.64	-	NP	NP	ML	SIL-CO-SIL-250, US SILICA

3.4 Pile Properties

Table 5 summarizes the dimensions and properties of the selected pile at prototype and model scale. The selected pile corresponded to an industrial medium steel pipe pile of diameter 0.635 m and thickness of 11 mm.

Table 5. Properties of the instrumented piles.

Parameters	*Prototype*	*Model*
Material	Aluminum 6061	
Young's Modulus [GPa]	69	
Yield Stress [MPa]	290	
Outer Diameter [mm]	635	15.9
Thickness [mm]	36	0.90
Length [m]	27.6	0.69
Area [mm^2]	21563.9	41.9
Bending Stiffness (I) [mm^4]	3.02E+09	1179
Elastic Section Modulus S_y [mm^3]	9.50E+06	148.5
Plastic Section Modulus $S_{y,plastic}$[mm^3]	1.28E+07	199.9
Axial Load [kN]	19408	12.13
$M_{elastic}$ [kN-m]	2752	0.043
$M_{plastic}$ [kN-m]	3648	0.057
Instrumentation Spacing [m]	2	0.05
Length with embedment in soil (3D) [m]	14.92	0.373

Three piles: Pile 1, Pile 2, and Pile 3 were placed in the model with an embedment of 3D into the dense sand layer as shown in Figure 5. The bottom of the pile mass was about 0.5 m (model scale 12.5 mm) above the soil surface. The center of the pile mass above the soil surface was about 1 m for Pile 1 and Pile 2 and 1.27 m for Pile 3. The piles had a slenderness (L/D) ratio of about 25.

Detains on the design of pile mass, assembly, interface roughness and instrumentation details can be found in the SKS02 data report (Sinha et al. 2021b). The residual interface friction angle (δ) of the pile was $\delta = 30^o$. Pile 1 in SKS03 test was restored from a pile that was damaged prior to SKS02 test. Pile head loads of 500 kN, 1500 kN and 2400 kN on Piles 1, 2, and 3 respectively, were modeled by model masses of 800 gm, 2495 gm, and 3992 gm (including nuts and bolts). The model dimensions of the designed steel mass blocks for Piles 2 and 3 are shown in Figure 9 and Figure 10. For Pile 1 aluminum steel block mass with a width of 4 inches and thickness of 1 inch was used. The drawing of the Pile 1 head mass can be seen in Sinha et al. (2021b).

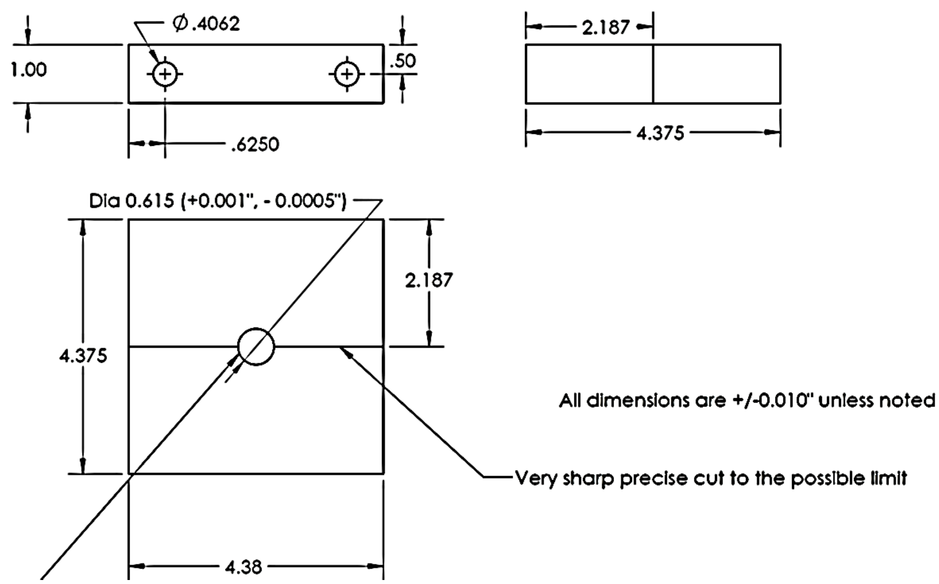

Figure 9. Model dimension (in inches) of Pile 2 head mass.

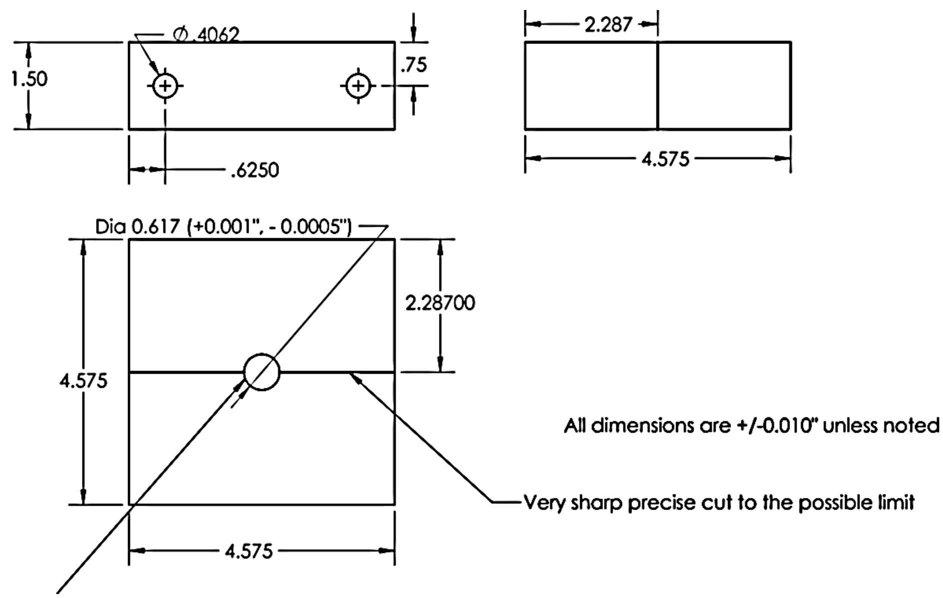

Figure 10. Model dimension (in inches) of Pile 3 head mass.

3.4.1 Pile Design

All the piles were loaded with different pile head loads (i.e., designed with different static factor of safety). Figure 10 shows the static pile capacity calculated using different methods based on an estimated cone tip resistance of 13 MPa at pile's tip and a skin friction of 1700 kN. The median pile load capacity was found to be about 4000 kN. The piles (Pile 1, Pile 2, and Pile 3) were designed for an embedment of 3D in dense sand with a pile head load of 500 kN, 1500 kN, and 2400 kN which resulted in a static factor of safety of 8, 2.6, and 1.6, respectively. Section 6.4 discusses the achieved pile capacity obtained from static pile load test conducted during the centrifuge test.

Soil Drained Critical Friction Angle [Degrees]		30
Scale Factor		40
Pile Properties		***At 40 g***
Outer Dia [mm]	15.88	635
Inner Dia [mm]	14.10	564
Length [mm]	660.40	26416
Crossectional Area [mm^2]	41.85	66966
Base Area [mm^2]	197.93	316692
Pile Self Weight [kN]	0.00146	2
I [mm^4]	1179.08	3018453162
Young's Modulus, E [Pa]	70000000000.00	70000000000
Bending Stiffness EI [Pam^4]	82.54	211291721.35
Skin Friction Capacity [kN]		1700
Drag Load [kN]		1200
$N_{1,60}$ @ 3D in Dense Sand (Dr=80%))		40
Cone Tip Resistance @ 3D in Dense Sand (Dr=80%) [MPa]		13
Effective Stress [kPa]		139.55

Design Method	***Pile Base Stress [MPa]***	***Pile Base Resistance [kN]***	***Total Pile Resistance [kN]***	***Base Resistance Factor***	***Nominal Pile Resistance [kN]***
Based on Cone Tip Resistance	13.0	4117.0	5817.0	0.50	2823
Norddlund/Thurman Method	9.4	2983.1	4683.1	0.45	2107
Meyerhof	4.6	1455.7	3155.7	0.30	1202
Nottingham and Schmertmann method	9.6	3040.2	4740.2	0.50	2285
Dutch Method (qc average over 8D above and 4D below tip)	12.1	3827.2	5527.2	0.50	2679
Aoki and Velloso's method	7.4	2352.6	4052.6	0.50	1941
LCPC Method	5.2	1646.8	3346.8	0.50	1588
FHWA/IN/JTRP-99/8 (Rodrigo Salgado,Junhwan Lee) s/d=10%	5.2	1646.8	3346.8	0.50	1588
ICP-05	5.2	1646.8	3346.8	0.50	1588
Lehane, Scheider and Xu (2005)	7.3	2296.3	3996.3	0.50	1913
Kenneth Gavina, Meho Sasa Kovacevic, David Igoec	7.8	2470.2	4170.2	0.50	2000
Mean	7.9	2498.4	4198.4	0.50	2014
Median	7.4	2352.6	4052.6	0.50	1941
Max	13.0	4117.0	5817.0	0.50	2823

Figure 11. Determination of static pile capacity using different design methods.

4 INSTRUMENTATION PLAN AND LAYOUT

Figure 4 and Figure 5 show the instrumentations placed in the model. For defining sensor locations (X,Y,Z), the origin was taken at the bottom most north-west corner of the model as shown in Figure 5. For convenience, the figure also has a scale on right to show the prototype depth (Z) in m measured form the surface of the model. In Figure 4, Section F-F represents the center of the model in transverse direction, whereas Section E-E is 5 cm (model scale) east of section F-F. The different types of sensors used in the model are shown in Figure 12. For an easier reference in the rest of the report, all the sensors are named as described in the sub-sections below.

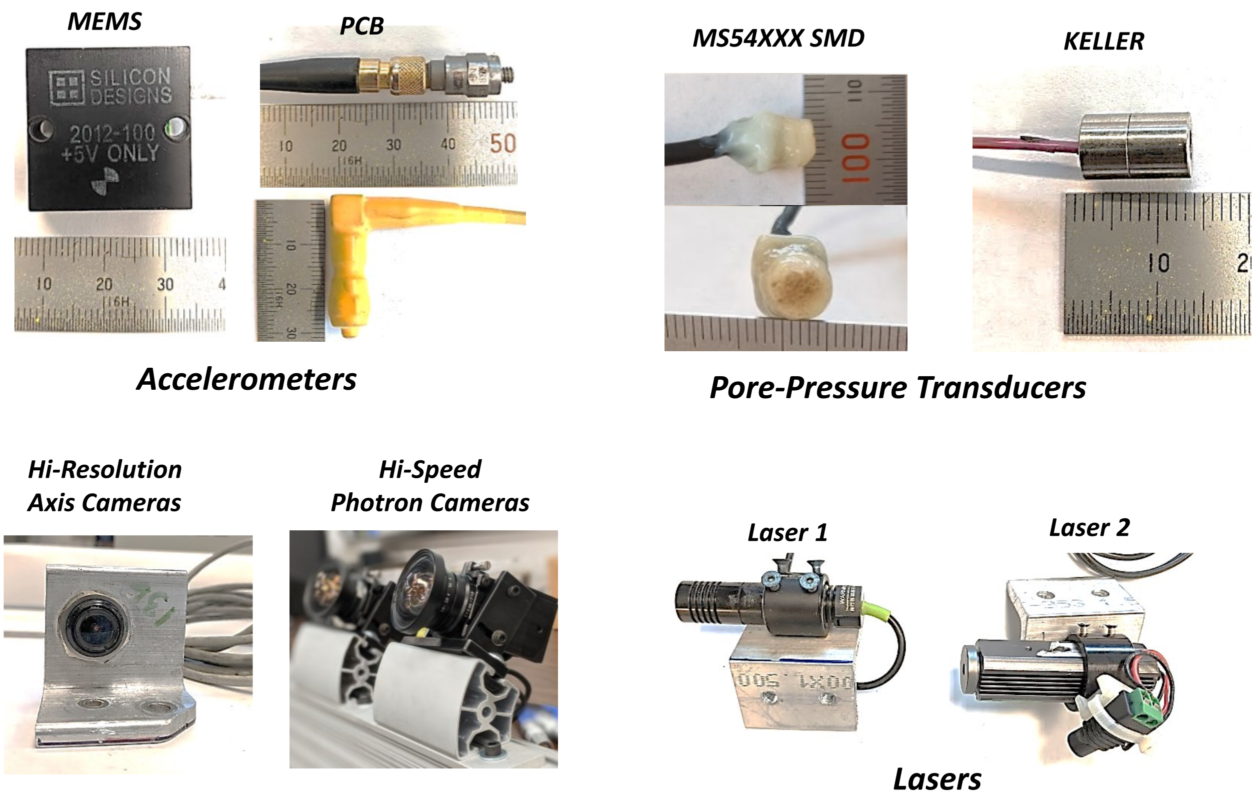

Figure 12. Sensors used in the centrifuge test.

4.1 Accelerometers

An array of horizontal piezoelectric accelerometers (PCBs) was placed in soil on Section F-F at the longitudinal center of the model as shown in Figure 5. The accelerometers in the soil were named as ACC_1 – ACC_9, beginning from the bottom of the model to the top. Four accelerometers: EAST, WEST, NORTH, and SOUTH were installed on the model container. The descriptions of all the accelerometers in the model are shown below. Table 6 and Table 7 summarizes the location and RESDAQ configuration of the accelerometers used. Accelerometers installed on piles and camera beam are discussed in Section 4.3 and Section 4.4, respectively.

<u>*Accelerometers in Soil*</u>

- ACC_1 - ACC_9: measures acceleration in soil occurring at different depths.

Accelerometers on Container

- EAST, WEST: placed on east and west of the base plate to measure applied input acceleration.
- NORTH, SOUTH: placed on north and south on the base plate to measure vertical acceleration.

Table 6. Accelerometers placed in the model and their location.

	Name	***Serial Number***	***X [cm]***	***Y [cm]***	***Z [cm]***		***Comments***
					Construction Phase	***Post Excavation***	
Accelerometers on Container	EAST	East 6025	-	-	-	-	facing south (+X)
	WEST	West 6021	-	-	-	-	facing south (+X)
	NORTH	21063	-	39.25	-	-	facing down (-Z)
	SOUTH	99516	-	39.25	-	-	facing down (-Z)
Accelerometers in Soil	ACC$_1$	73959	103	44.25	0.35	0.35	facing south (+X)
	ACC$_2$	127922	103	44.25	15.09	14.85	facing south (+X)
	ACC$_3$	108847	103	44.25	20.01	19.66	facing south (+X)
	ACC$_4$	107644	103	44.25	24.99	24.7	facing south (+X)
	ACC$_5$	99517	103	44.25	29.99	28.8	facing south (+X)
	ACC$_6$	107039	103	44.25	33.25	32.49	facing south (+X)
	ACC$_7$	21061	103	44.25	39.14	37.47	facing south (+X)
	ACC$_8$	127926	103	44.25	44.99	43.35	facing south (+X)
	ACC$_9$	99518	103	44.25	49.98	48.71	facing north (-X)

Table 7. RESDAQ configuration for all the accelerometers placed in the soil and on container.

	Name	***Sensitivity***		***Sensitivity Units***	***Xdcr Range***	***Xdcr units***	***Bridge Type***	***Terminal Configuration***	***DAQ Range***	***DAQ Range Units***	***Excitation Source***	***Excitation Value***	***Excitation Units***
		Construction Phase	***Post Excavation***										
Accelerometers on Container	EAST	52.400	52.400	mV/g	100.0	g	N/A	Pseudo	5	Volts	Internal	2	mA
	WEST	53.600	53.600	mV/g	100.0	g	N/A	Pseudo	5	Volts	Internal	2	mA
	NORTH	50.600	50.600	mV/g	100.0	g	N/A	Pseudo	5	Volts	Internal	2	mA
	SOUTH	50.100	50.100	mV/g	100.0	g	N/A	Pseudo	5	Volts	Internal	2	mA
Accelerometers in Soil	ACC$_1$	52.300	52.300	mV/g	100.0	g	N/A	Pseudo	5	Volts	Internal	2	mA
	ACC$_2$	50.600	50.600	mV/g	100.0	g	N/A	Pseudo	5	Volts	Internal	2	mA
	ACC$_3$	49.700	49.700	mV/g	100.0	g	N/A	Pseudo	5	Volts	Internal	2	mA
	ACC$_4$	48.600	48.600	mV/g	100.0	g	N/A	Pseudo	5	Volts	Internal	2	mA
	ACC$_5$	52.000	52.000	mV/g	100.0	g	N/A	Pseudo	5	Volts	Internal	2	mA
	ACC$_6$	49.500	49.500	mV/g	100.0	g	N/A	Pseudo	5	Volts	Internal	2	mA
	ACC$_7$	49.500	49.500	mV/g	100.0	g	N/A	Pseudo	5	Volts	Internal	2	mA
	ACC$_8$	51.700	51.700	mV/g	100.0	g	N/A	Pseudo	5	Volts	Internal	2	mA
	ACC$_9$	49.600	49.600	mV/g	100.0	g	N/A	Pseudo	5	Volts	Internal	2	mA

4.2 Pore pressure Transducers

Two different types of pore pressure transducers: Keller and MS54XXX SMD were placed in the model which are summarized in the sub-sections below. The Keller transducers were regularly used, expensive (~$1000/piece) relatively durable pore pressure transduces used in centrifuge modeling applications at CGM, UC Davis. The MS54XXX SMD transducer were new cheap sensors (~$10/piece) used in SKS02 centrifuge test (Sinha et al. 2021b). Although, MS54XXX SMD transducers had very low success rate (about 30% in SKS02 test), they produced some sensible data. They were again tried in SKS03, but with low expectations regarding their performance. For all the critical locations Keller transducers were used.

4.2.1 Keller Transducers

Table 7 and Table 8 shows the location and the RESDAQ configuration of these sensors. It also shows the sensor location when the model was constructed and when the model was excavated after the test.

The change in position (Z coordinate) of the sensor is an indication of soil settlement. One may estimate the settlement by taking the difference of the initial and final Z coordinate. Section 6.6 shows the settlement in the soil layers evaluated from the measurement of the colored sand elevation before and after the test. It was found that the settlement obtained from the change in position of pore pressure transducers were larger than obtained from the surface measurements and the ones recorded from the colored sand elevation measurements.

<u>*Keller Pore pressure transducers*</u>

- $PPT_1 - PPT_9$, $PPT_{11} - PPT_{12}$: array placed at the center of the model on section E-E.
- PPT_{10}**:** placed at the interface of clay and loose sand layer to measure lateral hydraulic gradient.

Table 8. Keller transducers placed in the model and their location.

	Name	***Serial Number***	***X [cm]***	***Y [cm]***	***Z [cm]***	
					Construction Phase	***Post Excavation***
Keller PPTs	PPT_1	PPT_6661	103	39.25	0.21	0.2
	PPT_2	PPT_6157	103	39.25	7	6.98
	PPT_3	PPT_5757	103	39.25	15.09	14.85
	PPT_4	PPT_5882	103	39.25	20	19.77
	PPT_5	PPT_5885	103	39.25	24.99	24.51
	PPT_6	PPT_6664	103	39.25	29.49	28.82
	PPT_7	PPT_5861	103	39.25	31.34	30.36
	PPT_8	PPT_5884	103	39.25	33.76	31.64
	PPT_9	PPT_6158	103	39.25	39.14	36.98
	PPT_{10}	PPT_6666	67.25	39.25	44.49	42.24
	PPT_{11}	PPT_5758	103	39.25	44.49	42.61
	PPT_{12}	PPT_6668	103	39.25	46.97	45.26

Table 9. RESDAQ configuration for all Keller transducers.

	Name	Sensitivity		Sensitivity Units	Xdcr Range	Xdcr units	Bridge Type	Terminal Configuration	DAQ Range	DAQ Range Units	Excitation Source	Excitation Value	Excitation Units
		Construction Phase	Post Excavation										
Keller PPTs	PPT_1	37.822	-	mV/Volt	689.5	kPa	Full	DIFF	25	mV	Internal	3.3	Volts
	PPT_2	40.094	40.094	mV/Volt	689.5	kPa	Full	DIFF	25	mV	Internal	3.3	Volts
	PPT_3	36.491	36.491	mV/Volt	689.5	kPa	Full	DIFF	25	mV	Internal	3.3	Volts
	PPT_4	36.471	36.835	mV/Volt	689.5	kPa	Full	DIFF	25	mV	Internal	3.3	Volts
	PPT_5	33.118	33.638	mV/Volt	689.5	kPa	Full	DIFF	25	mV	Internal	3.3	Volts
	PPT_6	36.647	35.991	mV/Volt	689.5	kPa	Full	DIFF	25	mV	Internal	3.3	Volts
	PPT_7	43.520	43.520	mV/Volt	689.5	kPa	Full	DIFF	25	mV	Internal	3.3	Volts
	PPT_8	40.792	41.833	mV/Volt	689.5	kPa	Full	DIFF	25	mV	Internal	3.3	Volts
	PPT_9	33.310	33.310	mV/Volt	689.5	kPa	Full	DIFF	25	mV	Internal	3.3	Volts
	PPT_{10}	32.840	32.840	mV/Volt	689.5	kPa	Full	DIFF	25	mV	Internal	3.3	Volts
	PPT_{11}	43.389	43.389	mV/Volt	689.5	kPa	Full	DIFF	25	mV	Internal	3.3	Volts
	PPT_{12}	35.540	35.540	mV/Volt	689.5	kPa	Full	DIFF	25	mV	Internal	3.3	Volts

4.2.2 MS54XXX SMD Transducers

The MS54XXX series of sensors were prepared following the procedure specified in Sinha et al. (2021b). To improve their performance and usability in SKS03 centrifuge test, multiple (at least three) coatings of adhesive were used. This increased their success rate from 30% to about 50%. It was found that the increased exposure of these sensors to water decreased the bond between the sensor and the porous stone. The description of these sensors used in the model are shown below.

MS54XXX SMD Pore pressure Transducers

- PPT_{13} - PPT_{15}: placed close to the pile tip.
- PPT_{16} - PPT_{18}: placed close to the pile at the interface of silty sand and medium dense sand layer.
- PPT_{20} - PPT_{22}: placed close to the pile at the interface of silty sand and loose sand layer.
- PPT_{23} - PPT_{27}: placed below the clay layer to track hydraulic gradient developed during drainage.
- PPT_{19} , PPT_{28}: measure pore-water pressure in silt and clay layer, respectively.

During the test, the MS54XXX sensors placed in the clayey silt layer (PPT_{19}), clay layer (PPT_{28}) and ones near the interface of clay and loose sand (PPT_{25}-PPT_{27}) failed to record any data.

Table 10. MS54XXX transducers placed in the model and their location.

	Name	Serial Number	X [cm]	Y [cm]	Z [cm] Construction Phase	Z [cm] Post Excavation	Comments
MS54XXX SMD PPTs	PPT_{13}	MS5407_116	52.5	39.25	15.09	14.66	
	PPT_{14}	MS5407_117	86	39.25	15.09	14.65	
	PPT_{15}	MS5407_118	124	39.25	15.09	14.67	
	PPT_{16}	MS5407_119	52.5	39.25	29.49	-	
	PPT_{17}	MS5407_120	86	39.25	29.49	-	
	PPT_{18}	MS5407_121	124	39.25	29.49	28.93	
	PPT_{19}	MS5407_130	67.25	39.25	31.64	31.27	*failed during test*
	PPT_{20}	MS5407_122	52.5	39.25	33.74	33.34	
	PPT_{21}	MS5407_123	86	39.25	33.74	33.59	
	PPT_{22}	MS5407_124	124	39.25	33.74	32.78	
	PPT_{23}	MS5407_125	14	39.25	44.49	43.78	
	PPT_{24}	MS5407_126	52.5	39.25	44.49	43.89	
	PPT_{25}	MS5407_127	86	39.25	44.49	43.32	*failed during test*
	PPT_{26}	MS5407_128	124	39.25	44.49	40.05	*pushed during pile installation, failed during test*
	PPT_{27}	MS5407_129	150	39.25	44.49	43.07	*failed during test*
	PPT_{28}	MS5407_131	86	39.25	46.97	46.97	*failed during test*

Table 11. RESDAQ configuration for all MS54XXX transducers.

	Name	Sensitivity Construction Phase	Sensitivity Post Excavation	Sensitivity Units	Xdcr Range	Xdcr units	Bridge Type	Terminal Configuration	DAQ Range	DAQ Range Units	Excitation Source	Excitation Value	Excitation Units
MS54XXX PPTs	PPT_{13}	74.843	74.843	mV/Volt	689.5	kPa	N/A	DIFF	5	Volts	External	5	Volts
	PPT_{14}	74.843	74.843	mV/Volt	689.5	kPa	N/A	DIFF	5	Volts	External	5	Volts
	PPT_{15}	74.843	74.843	mV/Volt	689.5	kPa	N/A	DIFF	5	Volts	External	5	Volts
	PPT_{16}	74.843	-	mV/Volt	689.5	kPa	N/A	DIFF	5	Volts	External	5	Volts
	PPT_{17}	76.402	76.402	mV/Volt	689.5	kPa	N/A	DIFF	5	Volts	External	5	Volts
	PPT_{18}	76.264	76.264	mV/Volt	689.5	kPa	N/A	DIFF	5	Volts	External	5	Volts
	PPT_{19}	76.161	-	mV/Volt	689.5	kPa	N/A	DIFF	5	Volts	External	5	Volts
	PPT_{20}	76.406	76.406	mV/Volt	689.5	kPa	N/A	DIFF	5	Volts	External	5	Volts
	PPT_{21}	76.263	76.263	mV/Volt	689.5	kPa	N/A	DIFF	5	Volts	External	5	Volts
	PPT_{22}	76.329	76.329	mV/Volt	689.5	kPa	N/A	DIFF	5	Volts	External	5	Volts
	PPT_{23}	75.456	75.456	mV/Volt	689.5	kPa	N/A	DIFF	5	Volts	External	5	Volts
	PPT_{24}	76.161	76.161	mV/Volt	689.5	kPa	N/A	DIFF	5	Volts	External	5	Volts
	PPT_{25}	76.681	-	mV/Volt	689.5	kPa	N/A	DIFF	5	Volts	External	5	Volts
	PPT_{26}	77.488	-	mV/Volt	689.5	kPa	N/A	DIFF	5	Volts	External	5	Volts
	PPT_{27}	76.268	-	mV/Volt	689.5	kPa	N/A	DIFF	5	Volts	External	5	Volts
	PPT_{28}	75.738	-	mV/Volt	689.5	kPa	N/A	DIFF	5	Volts	External	5	Volts

4.3 Instrumentation on Pile

The piles: Pile 1, Pile 2 and Pile 3 were instrumented with 9 full bridge axial strain gages to measure the axial load distribution. Additionally, ICP accelerometers and MEMS accelerometers, (Figure 13) were placed to measure the horizontal and vertical accelerations and rotation of pile mass.

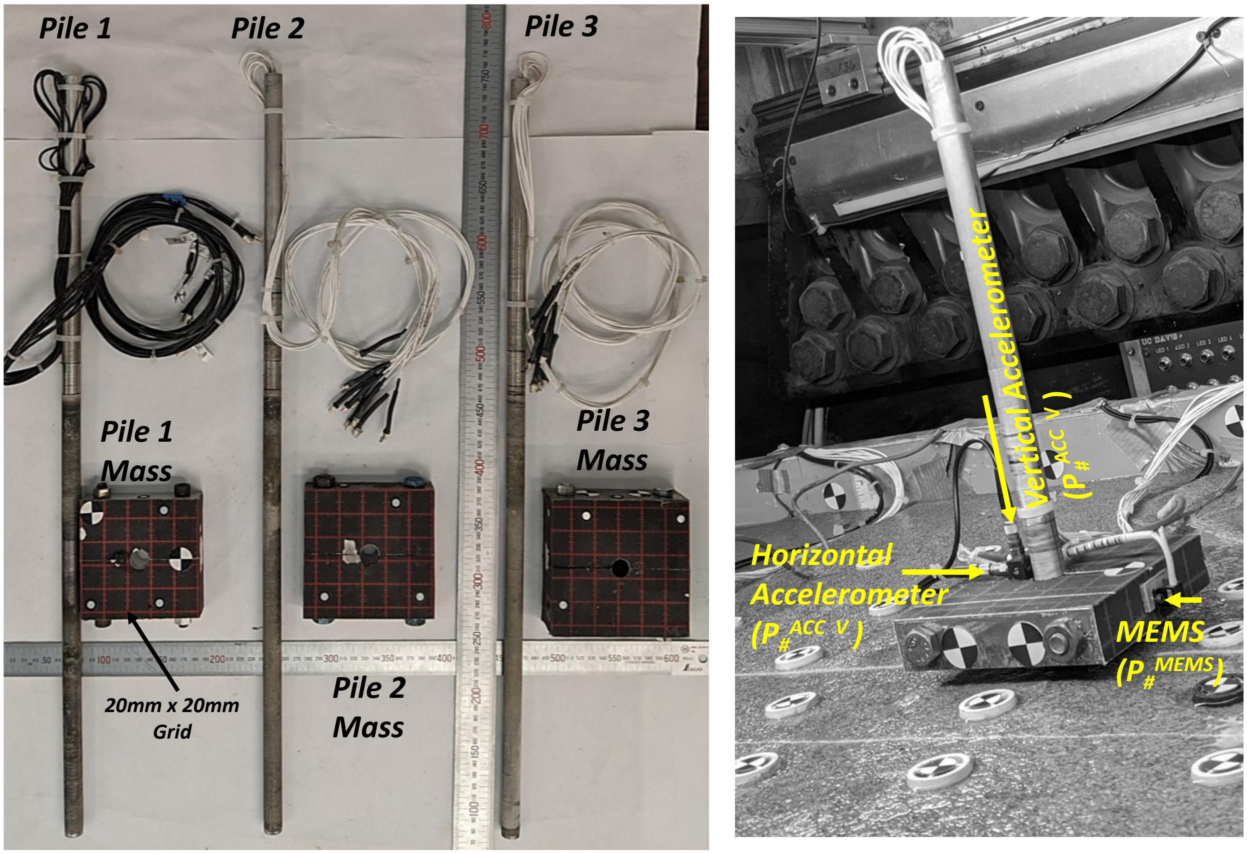

Figure 13. Instrumented piles: Pile 1, Pile 2, and Pile 3 (on left) and sensors installed on pile head mass (on right).

4.3.1 Pile 1

The descriptions of instrumentation on pile 1 is shown below. Table 12 and Table 13 shows the location and RESDAQ configuration of sensors attached to pile 1. Since, Pile 1 was a salvaged pile, few of the gages (P_1^{G2} and P_1^{G4}) did not work.

<u>*Axial Strain Gages*</u>

- P_1^{G1}, P_1^{G3}, P_1^{G5} – P_1^{G8}: full bridge axial strain gage array to measure the axial load response.

<u>*Sensors Installed on Pile Head Mass*</u>

- *ICP Accelerometers*
  - $P_1^{ACC\ H}$, $P_1^{ACC\ V}$: records horizontal and vertical response.
- *MEMS Accelerometers*
  - P_1^{MEM}: measures the acceleration normal to the plane of the sensor.

Table 12. Location of sensors installed on Pile 1.

	Name	Serial Number	X [cm]	Y [cm]	Z [cm] Construction Phase	Z [cm] Post Excavation	Comments
Pile 1 Strain Gages	P_1^{G1}	Pile_1_Gage_1	50.5	39.25	18.73	17.96	
	P_1^{G3}	Pile_1_Gage_3	50.5	39.25	28.89	28.12	
	P_1^{G5}	Pile_1_Gage_5	50.5	39.25	39.05	38.28	
	P_1^{G6}	Pile_1_Gage_6	50.5	39.25	44.13	43.36	
	P_1^{G7}	Pile_1_Gage_7	50.5	39.25	49.21	48.44	
	P_1^{G8}	Pile_1_Gage_8	50.5	39.25	54.29	53.52	
Pile 1 Sensors	$P_1^{ACC\ H}$	128307	52	39.25	56.31	55.54	facing north (-X)
	$P_1^{ACC\ V}$	21067	52	39.25	56.31	55.54	facing down (-Z)
	P_1^{MEM}	A109714	45	39.25	55.04	54.2	facing south (+X)

Table 13. RESDAQ configuration of sensors on Pile 1.

	Name	Sensitivity Construction Phase	Sensitivity Post Excavation	Sensitivity Units	Xdcr Range	Xdcr units	Bridge Type	Terminal Configuration	DAQ Range	DAQ Range Units	Excitation Source	Excitation Value	Excitation Units
Pile 1 Strain Gages	P_1^{G1}	1.259	0.964	mV/Volt	449.6	lbf	Full	DIFF	25	mV	Internal	2.5	Volts
	P_1^{G3}	0.943	0.961	mV/Volt	449.6	lbf	Full	DIFF	25	mV	Internal	2.5	Volts
	P_1^{G5}	0.910	0.927	mV/Volt	449.6	lbf	Full	DIFF	25	mV	Internal	2.5	Volts
	P_1^{G6}	0.940	0.972	mV/Volt	449.6	lbf	Full	DIFF	25	mV	Internal	2.5	Volts
	P_1^{G7}	0.918	0.949	mV/Volt	449.6	lbf	Full	DIFF	25	mV	Internal	2.5	Volts
	P_1^{G8}	0.945	0.963	mV/Volt	449.6	lbf	Full	DIFF	25	mV	Internal	2.5	Volts
Pile 1 Sensors	$P_1^{ACC\ H}$	49.200	49.200	mV/g	100.0	g	N/A	Pseudo	5	Volts	Internal	2	mA
	$P_1^{ACC\ V}$	54.100	54.100	mV/g	100.0	g	N/A	Pseudo	5	Volts	Internal	2	mA
	P_1^{MEM}	9.570	9.570	mV/Volt	50.0	g	Full	DIFF	25	mV	Internal	2.5	Volts

4.3.2 Pile 2

The descriptions of instrumentation on pile 2 is shown below. Table 14 and Table 15 shows the location and RESDAQ configuration of the sensors attached to pile 2.

Axial Strain Gages

- $P_2^{G1} – P_2^{G9}$: full bridge axial strain gage array to measure the axial load response.

Sensors Installed on Pile Head Mass

- *ICP Accelerometers*
  - $P_2^{ACC\ H}$, $P_2^{ACC\ V}$: records horizontal and vertical response.
- *MEMS Accelerometers*
  - P_2^{MEM}: measures the acceleration normal to the plane of the sensor.

Table 14. Location of sensors installed on Pile 2.

	Name	Serial Number	X [cm]	Y [cm]	Z [cm] Construction Phase	Z [cm] Post Excavation	Comments
Pile 2 Strain Gages	P_2^{G1}	J7623-02-01	84	39.25	18.73	17.83	
	P_2^{G2}	J7623-02-02	84	39.25	23.81	22.91	
	P_2^{G3}	J7623-02-03	84	39.25	28.89	27.99	
	P_2^{G4}	J7623-02-04	84	39.25	33.97	33.07	
	P_2^{G5}	J7623-02-05	84	39.25	39.05	38.15	
	P_2^{G6}	J7623-02-06	84	39.25	44.13	43.23	
	P_2^{G7}	J7623-02-07	84	39.25	49.21	48.31	
	P_2^{G8}	J7623-02-08	84	39.25	54.29	53.39	
Pile 2 Sensors	$P_2^{ACC\ H}$	107067	85.5	39.25	56.31	55.47	facing north (-X)
	$P_2^{ACC\ V}$	99509	85.5	39.25	56.31	55.47	facing down (-Z)
	P_2^{MEM}	A109770	78	39.25	55.04	54.2	facing south (+X)

4.3.3 Pile 3

The descriptions of instrumentation on pile 3 is shown below. Table 16 and Table 17 shows the location and RESDAQ configuration of the sensors attached to pile 3.

Axial Strain Gages

- $P_3^{G1} – P_3^{G9}$: full bridge axial strain gage array to measure the axial load response.

Sensors Installed on Pile Head Mass

- *ICP Accelerometers*
  - $P_3^{ACC\ H}$, $P_3^{ACC\ V}$: records horizontal and vertical response.

- *MEMS Accelerometers*
  - P_3^{MEM}: measures the acceleration normal to the plane of the sensor.

Table 15. RESDAQ configuration of sensors on Pile 2.

	Name	Sensitivity: Construction Phase	Sensitivity: Post Excavation	Sensitivity Units	Xdcr Range	Xdcr units	Bridge Type	Terminal Configuration	DAQ Range	DAQ Range Units	Excitation Source	Excitation Value	Excitation Units
Pile 2 Strain Gages	P_2^{G1}	1.096	1.054	mV/Volt	449.6	lbf	Full	DIFF	25	mV	Internal	2.5	Volts
	P_2^{G2}	0.856	0.834	mV/Volt	449.6	lbf	Full	DIFF	25	mV	Internal	2.5	Volts
	P_2^{G3}	0.744	0.634	mV/Volt	449.6	lbf	Full	DIFF	25	mV	Internal	2.5	Volts
	P_2^{G4}	0.800	0.775	mV/Volt	449.6	lbf	Full	DIFF	25	mV	Internal	2.5	Volts
	P_2^{G5}	0.897	0.885	mV/Volt	449.6	lbf	Full	DIFF	25	mV	Internal	2.5	Volts
	P_2^{G6}	0.869	0.918	mV/Volt	449.6	lbf	Full	DIFF	25	mV	Internal	2.5	Volts
	P_2^{G7}	0.899	0.870	mV/Volt	449.6	lbf	Full	DIFF	25	mV	Internal	2.5	Volts
	P_2^{G8}	0.740	0.991	mV/Volt	449.6	lbf	Full	DIFF	25	mV	Internal	2.5	Volts
Pile 2 Sensors	$P_2^{ACC\ H}$	49.100	49.100	mV/g	100.0	g	N/A	Pseudo	5	Volts	Internal	2	mA
	$P_2^{ACC\ V}$	49.300	49.300	mV/g	100.0	g	N/A	Pseudo	5	Volts	Internal	2	mA
	P_2^{MEM}	6.985	6.985	mV/Volt	50.0	g	Full	DIFF	25	mV	Internal	2.5	Volts

Table 16. Location of sensors installed on Pile 3.

	Name	Serial Number	X [cm]	Y [cm]	Z [cm]: Construction Phase	Z [cm]: Post Excavation	Comments
Pile 3 Strain Gages	P_3^{G1}	J7623-01-01	122	39.25	18.73	16.04	
	P_3^{G2}	J7623-01-02	122	39.25	23.81	21.12	
	P_3^{G3}	J7623-01-03	122	39.25	28.89	26.2	
	P_3^{G4}	J7623-01-04	122	39.25	33.97	31.28	
	P_3^{G5}	J7623-01-05	122	39.25	39.05	36.36	
	P_3^{G6}	J7623-01-06	122	39.25	44.13	41.44	
	P_3^{G7}	J7623-01-07	122	39.25	49.21	46.52	
	P_3^{G8}	J7623-01-08	122	39.25	54.29	51.6	
Pile 3 Sensors	$P_3^{ACC\ H}$	108953	123	39.25	57.58	54.89	facing north (-X)
	$P_3^{ACC\ V}$	21051	123	39.25	57.58	54.89	facing down (-Z)
	P_3^{MEM}	A109732	115.5	39.25	55.67	52.985	facing south (+X)

Table 17. RESDAQ configuration of sensors on Pile 3.

	Name	Sensitivity		Sensitivity Units	Xdcr Range	Xdcr units	Bridge Type	Terminal Configuration	DAQ Range	DAQ Range Units	Excitation Source	Excitation Value	Excitation Units
		Construction Phase	Post Excavation										
Pile 3 Strain Gages	P_3^{G1}	0.443	0.460	mV/Volt	224.8	lbf	Full	DIFF	25	mV	Internal	2.5	Volts
	P_3^{G2}	0.244	0.238	mV/Volt	224.8	lbf	Full	DIFF	25	mV	Internal	2.5	Volts
	P_3^{G3}	0.413	0.317	mV/Volt	224.8	lbf	Full	DIFF	25	mV	Internal	2.5	Volts
	P_3^{G4}	0.360	0.155	mV/Volt	224.8	lbf	Full	DIFF	25	mV	Internal	2.5	Volts
	P_3^{G5}	0.418	0.186	mV/Volt	224.8	lbf	Full	DIFF	25	mV	Internal	2.5	Volts
	P_3^{G6}	0.416	0.273	mV/Volt	224.8	lbf	Full	DIFF	25	mV	Internal	2.5	Volts
	P_3^{G7}	0.431	0.226	mV/Volt	224.8	lbf	Full	DIFF	25	mV	Internal	2.5	Volts
	P_3^{G8}	0.449	0.373	mV/Volt	224.8	lbf	Full	DIFF	25	mV	Internal	2.5	Volts
Pile 3 Sensors	$P_3^{ACC\ H}$	50.500	50.500	mV/g	100.0	g	N/A	Pseudo	5	Volts	Internal	2	mA
	$P_3^{ACC\ V}$	52.100	52.100	mV/g	100.0	g	N/A	Pseudo	5	Volts	Internal	2	mA
	P_3^{MEM}	6.025	6.025	mV/Volt	50.0	g	Full	DIFF	25	mV	Internal	2.5	Volts

4.4 High Speed Photron Cameras

Four high speed cameras (Photron MH6) were used to obtain 3-dimesnional positions of target makers placed in the model. Sinha et al. (2021a) describes the details on camera setup. Cameras were attached on a T-20/80 2040 2″ x 4″ Camera Beam running from north to south of the model as shown in Figure 14. The camera beam rested on two East-West T-20/80 2040 (2″ x 4″) Beams 1 and Beam 2 as shown in Figure 14. A 3D SolidWorks drawing of the model placed on the centrifuge bucket is shown in Figure 15. The figure shows how the camera was attached to the Camera Beam. It also shows the location and configuration of different beams in the model. Three LED strips were installed for illumination, one on each of the Camera Beam and the two East-West Beams. The location and orientation of the cameras and the sensors associated with camera beam are summarized in Table 18.

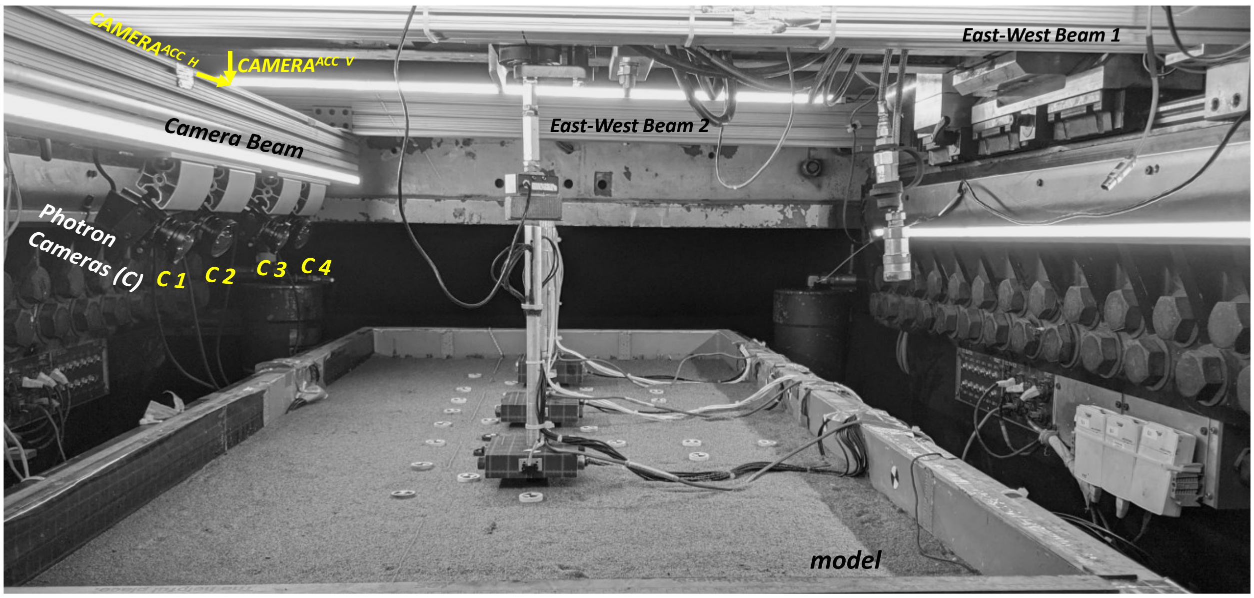

Figure 14. Front view of the finished model showing the four Photron cameras mounted on the camera beam.

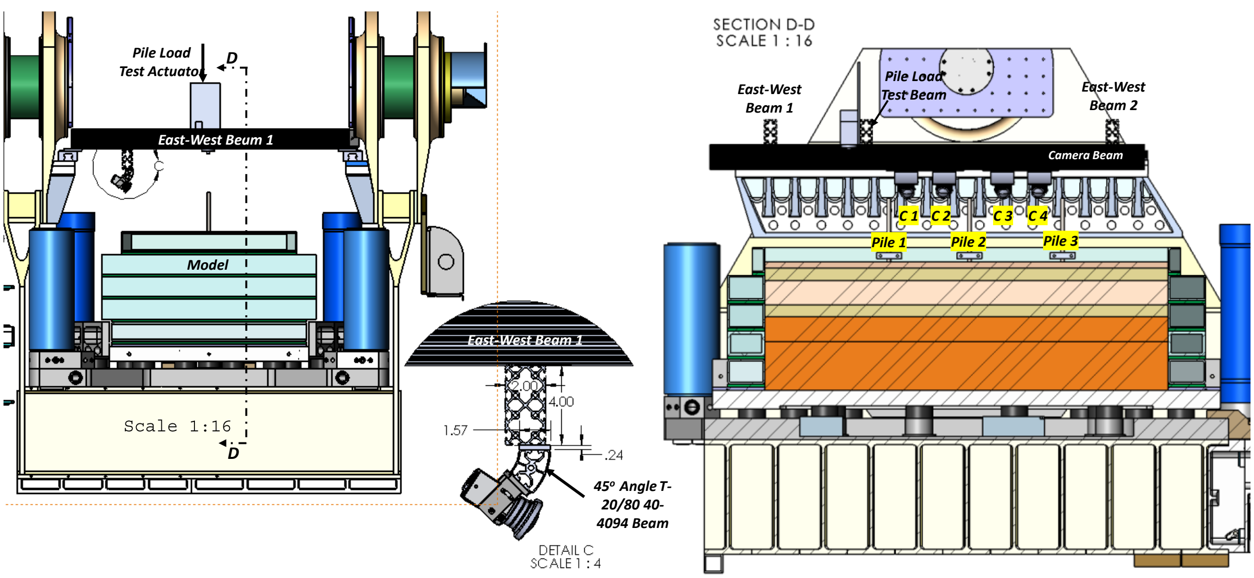

Figure 15. 3D SolidWorks model showing the configuration of the beams and camera mounting system.

Table 18. Location of camera and camera sensors.

	Name	Serial Number	X [cm]	Y [cm]	Z [cm]		Comments
					Construction Phase	Post Excavation	
Photron Cameras	CAMERA 1	-	58	78.5	78.94	78.94	~33° clockwise in Z-X plane, Twist (~5°)
	CAMERA 2	-	73	78.5	79.44	79.44	~33° clockwise in Z-X plane, Twist (-~5°)
	CAMERA 3	-	97.5	78.5	79.2	79.2	~33° clockwise in Z-X plane, Twist (~5°)
	CAMERA 4	-	114.6	78.5	79.24	79.24	~33° clockwise in Z-X plane, Twist (-~5°)
Camera Sensors	CAMERA$^{ACC\ H}$	107649	85.5	80.46	99.3	99.3	installed on camera beam
	CAMERA$^{ACC\ V}$	108848	85.5	80.46	99.3	99.3	installed on camera beam
	CAMERA^{Trigger}	Camera_Trigger_1	-	-	-	-	trigger to start recording
	SNAPSHOT^{Trigger}	Camera_Trigger_1	-	-	-	-	trigger to take snapshots

Table 19. RESDAQ configuration of camera sensors.

	Name	Sensitivity		Sensitivity Units	Xdcr Range	Xdcr units	Bridge Type	Terminal Configuration	DAQ Range	DAQ Range Units	Excitation Source	Excitation Value	Excitation Units
		Construction Phase	Post Excavation										
Camera Sensors	CAMERA$^{ACC\ H}$	48.2	48.2	mV/g	100	g	N/A	Pseudo	5	Volts	Internal	2	mA
	CAMERA$^{ACC\ V}$	50	50	mV/g	100	g	N/A	Pseudo	5	Volts	Internal	2	mA
	CAMERA^{Trigger}	1000	1000	mV/Volt	3	inch	N/A	DIFF	10	Volts	External	5	Volts
	SNAPSHOT^{Trigger}	1000	1000	mV/Volt	3	inch	N/A	DIFF	10	Volts	External	5	Volts

4.4.1 Camera Properties

Two triggers: CAMERA^{Trigger} to start recording and SNAPSHOT^{Trigger} to take snapshots were set up. The cameras ware only triggered when a snapshot was required to be taken. Sinha et al. (2021a) describes the triggering sequence of the cameras during the test. The shutter speed of the camera was set to 4000Hz. The resolution used for recording was 1280 px x 800 px. The physical pixel size of the camera sensor was 6.6 microns. Two sets of camera frame rates (frames per second (FPS)) were used. A higher frame rate was used to record movements during shaking and a lower frame rate for movements during reconsolidation (i.e., post shaking). Table 20 lists the frame rate and duration of each shaking event. Figure 16 shows the model view from the four cameras.

Table 20. Photron camera recording details for each shaking event.

Day	***Event***	***Time***	***During Shaking***		***Post Shaking***		***Total Recording Duration [sec]***
			Frame Rate	***Total Frames***	***Frame Rate***	***Total Frames***	
8/27/2020	*SWM_1*	*10:41*	1600	1920	4	240	61.2
	EQM_1	*11:33*	1600	1920	4	3600	901.2
8/28/2020	*SWM_2*	*10:03*	1600	1920	4	600	151.2
	EQM_2	*10:25*	1600	2560	4	3600	901.6
	EQM_3	*11:03*	1600	2560	4	3600	901.6
	EQM_4	*11:43*	1600	3250	2	2412	1208.03125
	EQM_5	*12:09*	1600	3250	2	2412	1208.03125

Note: To get the list of the description of the events refer to Table 24. PLT_2_Axis_Camera_North_of_CPT_Rig.asf contains the recording of pile load test PLT_2.

Figure 16. A view of recording from four cameras in Photron viewer software.

4.4.2 Camera Target Markers

To track 3-D movements of model features, target markers were placed on soil, pile masses, the model container, and the centrifuge bucket as shown in Figure 17. Quadrant markers of size 15 mm and 20 mm were placed on the soil and pile, (Figure 17). Suggestions regarding marker design are described in Sinha et al. (2021a).

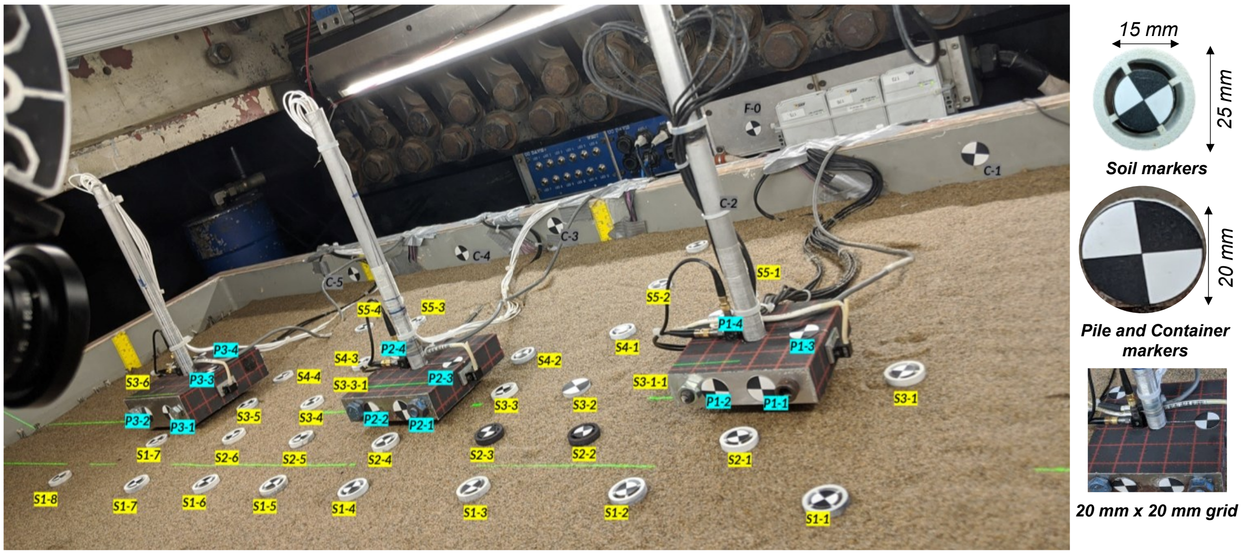

Figure 17. Camera target markers placed on soil, pile, model container and centrifuge bucket.

4.4.3 Methodology to Obtain 3-D Movements

Obtaining 3-D positions of targets require the use of two or more cameras viewing the target of interest at different view angles and a software to perform the image analysis. In this centrifuge test, the four cameras: Camera 1 (C1), Camera 2 (C2), Camera 3 (C3) , and Camera 4 (C4) were oriented accordingly to view different parts of the model. Camera 1 (C1) and Camera 2 (C2) was responsible for monitoring much of the North portion of the model container as well as Pile 1 and Pile 2. Camera 3 (C3) and Camera 4 (C4) monitored much of the south side of the container as well as Pile 2 and Pile 3. Figure 16 shows the view of the model as seen by the four cameras.

Image analysis overall involved two steps. The first step involved calibrating cameras to obtain its extrinsic and intrinsic properties. 3D measurements (at the center) of the camera target markers were recorded to calibrate the camera and obtain its extrinsic properties (i.e., the orientation and position) of the camera. Additionally, lens calibration was performed to obtain its intrinsic properties (i.e., focal length, distortion, skew, and image center). The second step involved the use of an image processing software (such as TEMA) to track the position of placed camera target markers. Sinha et al. (2021a) describes the process of obtaining 3D displacements in centrifuge tests using high-speed Photron cameras and TEMA.

All the positions determined by the TEMA software were processed to obtain displacements relative to the top ring of the model container. The relative displacement data is presented in the appendix. The plots show the cumulative displacement of target markers for different events during each spin. The reference time in cumulative plots is taken at the beginning of step wave motions SWM_1 and SWM_2 for Spin 1 and Spin 2, respectively. The archived data includes both the position data and the displacement data.

4.5 Centrifuge Cone Penetration Test

A 6 mm (model scale) centrifuge cone penetration test (CPT) was performed between each shaking events. The probe used was of Liquefaction Experiments and Analysis Projects' (LEAP-2017) design (Carey et al. 2018), where an external load cell attached to the head of the pile is internally connected to the pile's tip (Figure 18). A 500 lbf load cell was attached to the probe to measure the tip load during cone penetration testing. The locations of the CPT tests are shown in Figure 4. The probe was pushed with a 16 inch (model scale) hydraulic actuator which made investigation possible up to a depth of about 15 m (in prototype scale). Table 21 describes the details of RESDAQ configuration of the CPT probe. CPTs were performed at a penetration rate of 1 cm/s (model scale).

Figure 18. 6mm LEAP centrifuge cone penetration test (CPT) probe.

Table 21. RESDAQ configuration of load cells and displacement transducer attached to the CPT probe.

	Name	Sensitivity: Construction Phase	Sensitivity: Post Excavation	Sensitivity Units	Xdcr Range	Xdcr units	Bridge Type	Terminal Configuration	DAQ Range	DAQ Range Units	Excitation Source	Excitation Value	Excitation Units
CPT Sensors	CPT	1.959	1.959	mV/Volt	2224.1	N	Full	DIFF	25	mV	Internal	2.5	Volts
	CPT Disp	1000	1000	mV/Volt	3.2	inch	N/A	DIFF	10	mV	Internal	1	Volts

4.6 Centrifuge Pile Load Test

A pile load test (PLT) was conducted on Pile 1 to estimate the static load capacity of the piles. A 2-inch (model scale) actuator connected with a 1000 lbf load cell was used for the load test. A constant rate of penetration test (ASTM D1143) was used to push Pile 1 at a displacement rate of 1 mm/minute. Two pile load tests: PLT_1 and PLT_2 were conducted. PLT_1 was performed at the beginning of the centrifuge test, whereas PLT_2 was performed at the end of the centrifuge test. The details on these tests are shown below:

Pile Load Test Details

- *PLT_1:* Penetrated at the rate of 1 mm/minute with a maximum tip movement of 5.2 mm i.e., ~35%D.
- *PLT_2:* Penetrated at the rate of 1 mm/minute with a maximum tip movement of 13 mm i.e., ~82%D.

The RESDAQ configuration of the sensors attached to the PLT probe are shown in Table 22.

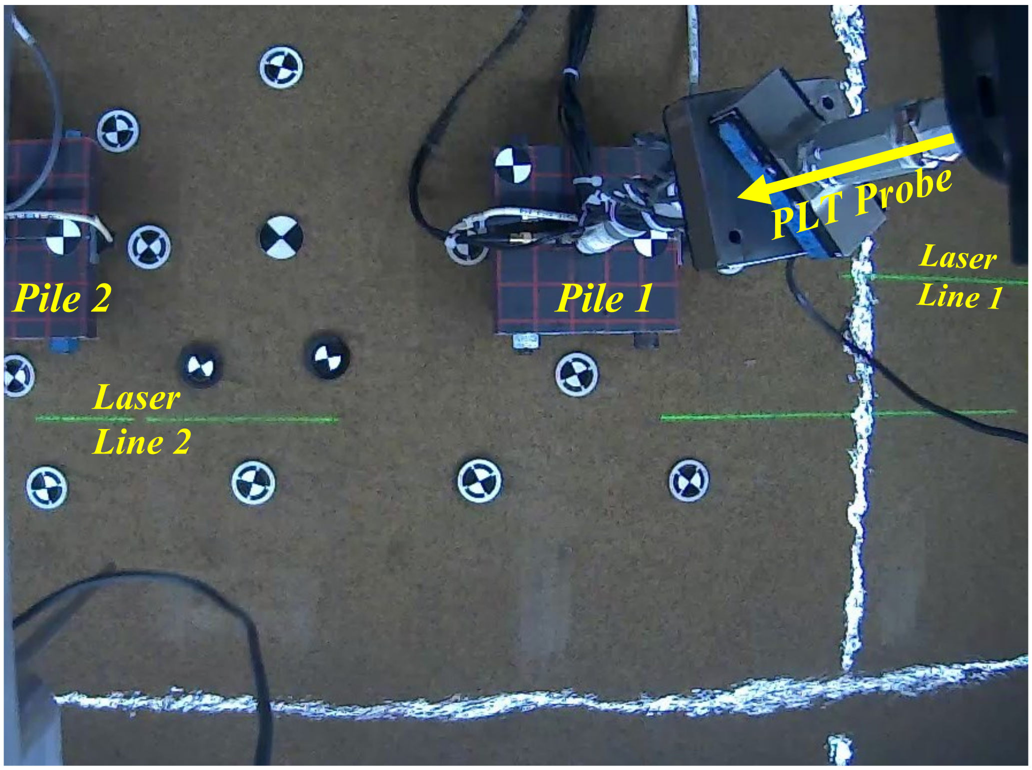

Figure 19. A snapshot during the second centrifuge pile load test (PLT_2).

Table 22. RESDAQ configuration of load cells and displacement transducer attached to the PLT probe.

	Name	Sensitivity		Sensitivity Units	Xdcr Range	Xdcr units	Bridge Type	Terminal Configuration	DAQ Range	DAQ Range Units	Excitation Source	Excitation Value	Excitation Units
		Construction Phase	Post Excavation										
PLT Sensors	PLT	1.99	1.99	mV/Volt	1000	lbf	Full	DIFF	25	mV	Internal	2.5	Volts
	PLT Disp	1000	1000	mV/Volt	5.4	mm	N/A	DIFF	10	mV	Internal	1	Volts

4.7 Lasers

Similar to SKS02, two line lasers were installed which created a laser line across the piles and the soil (see Figure 20). The lines lasers were mounted on the swinging axis of the bucket in Y-Z plane. On the model, the line lasers produced laser lines in X-Y plane as shown in Figure 20. The specifications of line lasers used in this test are described in SKS02 test (Sinha et al. 2021b).

Figure 20. A view of laser lines on the model.

Since no displacement transducers were used in SKS03 test, the movement of laser lines were analyzed to estimate real time settlements of soil and pile settlements during testing. The methodology on processing laser lines and obtaining settlements is discussed in Sinha et al. (2020). The details on the laser angles and the laser lines are summarized below.

Laser 1 (projected laser line 1)

- *Line laser source coordinates*: X = 84 cm, Y = 97.5 cm, Z = 157.89 cm
- *Line laser angle: 62^o (with respect to z plane)*
- *Laser line 1 coordinates on soil:* Y=40.3 cm, Z=52.5 cm
- *Laser line 1 coordinates on piles' head:* Y=43.0 cm and Z correspondingly

Laser 2 (projected laser line 2)

- *Line laser source coordinates*: X = 78 cm, Y = 98.5 cm, Z = 158.89 cm
- *Line laser angle: 65^o (with respect to z plane)*
- *Laser line 2 coordinates on soil:* Y=49.7 cm, Z=52.5 cm

4.7.1 Axis Camera Recordings

High-definition cameras from Axis Communications were installed on the cone penetration test (CPT) rig to take the snapshots and track laser lines during shakings and during pile load tests. The Axis Cameras were mounted on either side of the CPT rig as shown in Figure 21. The cameras mounted on the north and south side of the CPT rig was named correspondingly as North and South Axis Cameras. Figure 21 shows the view of the model from south and north axis cameras. From the center of the CPT rig (or the center of the CPT exploration), the cameras were located 13.4 cm in north and south direction, respectively. The cameras moved with the CPT rig in X-direction as more CPT explorations were conducted. The description, coordinates and orientation of the axis cameras are shown below. The log of snapshots and recordings taken by the cameras are summarized in Table 23.

Hi-Resolution Cameras (North and South of CPT rig)

- Model: AXIS P1214-E Network Cameras
- Frame Rate: 30 fps
- Resolution: 1280px x 720px
- Pixel Size:

North Axis Camera:

- *Coordinates:* Y=41.5 cm, Z = 113 cm, X = -13.4 cm from CPT location
- *Orientation:* looked vertically down in Z-direction i.e., 90° in Y-Z plane

South Axis Camera:

- *Coordinates:* Y=41.5 cm, Z = 113 cm, X = 13.4 cm from CPT location
- *Orientation:* looked vertically down in Z-direction i.e., 90° in Y-Z plane

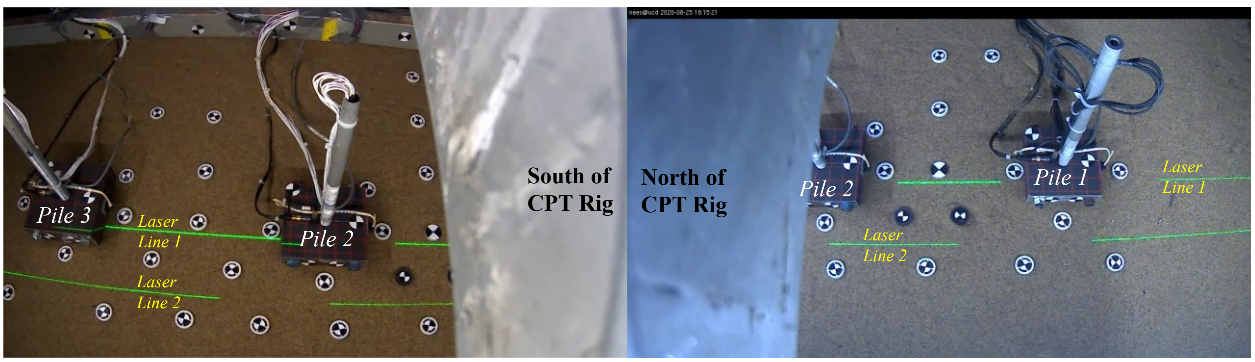

Figure 21. A view of the model from south and north axis cameras.

Table 23. Log of snapshots taken from axis cameras.

Day	Time	*Event*	*Snapshots File Name*
8/27/2020	9:20	At 1 g	At_1g_Day_1_Spin_1_Axis_Camera_North_of_CPT_Rig.jpg
			At_1g_Day_1_Spin_1_Axis_Camera_South_of_CPT_Rig.jpg
	9:55	During Spin-up 1	At_12g_Day_1_Spin_1_Axis_Camera_North_of_CPT_Rig.jpg
			At_12g_Day_1_Spin_1_Axis_Camera_South_of_CPT_Rig.jpg
	10:03		At_25g_Day_1_Spin_1_Axis_Camera_North_of_CPT_Rig.jpg
			At_25g_Day_1_Spin_1_Axis_Camera_South_of_CPT_Rig.jpg
	10:26	SWM_1	Before_SWM_1_Axis_Camera_North_of_CPT_Rig.jpg
			Before_SWM_1_Axis_Camera_South_of_CPT_Rig.jpg
	10:40		After_SWM_1_Axis_Camera_North_of_CPT_Rig.jpg
			After_SWM_1_Axis_Camera_South_of_CPT_Rig.jpg
	11:29	EQM_1	Before_EQM_1_Axis_Camera_North_of_CPT_Rig.jpg
			Before_EQM_1_Axis_Camera_South_of_CPT_Rig.jpg
	11:38		After_EQM_1_Axis_Camera_North_of_CPT_Rig.jpg

	11:49		After_EQM_1_Axis_Camera_South_of_CPT_Rig.jpg 10_Minutes_After_EQM_1_Axis_Camera_North_of_CPT_Rig.jpg 10_Minutes_After_EQM_1_Axis_Camera_South_of_CPT_Rig.jpg
	11:53	CPT_2	Before_CPT_2_Axis_Camera_North_of_CPT_Rig.jpg Before_CPT_2_Axis_Camera_South_of_CPT_Rig.jpg
	12:12	During Spin-down 2	At_1g_During_Spin_Down_Day_1_Spin_2_Axis_Camera_North_of_CPT_Rig.jpg At_1g_During_Spin_Down_Day_1_Spin_2_Axis_Camera_South_of_CPT_Rig.jpg
8/28/2020	9:23	During Spin-up 1	At_1g_Day_2_Spin_1_Axis_Camera_North_of_CPT_Rig.jpg At_1g_Day_2_Spin_1_Axis_Camera_South_of_CPT_Rig.jpg
	9:59	SWM_2	Before_SWM_2_Axis_Camera_North_of_CPT_Rig.jpg Before_SWM_2_Axis_Camera_South_of_CPT_Rig.jpg
	10:04		After_SWM_2_Axis_Camera_North_of_CPT_Rig.jpg After_SWM_2_Axis_Camera_South_of_CPT_Rig.jpg
	10:25	EQM_2	Before_EQM_2_Axis_Camera_North_of_CPT_Rig.jpg Before_EQM_2_Axis_Camera_South_of_CPT_Rig.jpg
	10:26		After_EQM_2_Axis_Camera_North_of_CPT_Rig.jpg After_EQM_2_Axis_Camera_South_of_CPT_Rig.jpg
	11:02	EQM_3	Before_EQM_3_Axis_Camera_North_of_CPT_Rig.jpg Before_EQM_3_Axis_Camera_South_of_CPT_Rig.jpg
	11:08		After_EQM_3_Axis_Camera_North_of_CPT_Rig.jpg After_EQM_3_Axis_Camera_South_of_CPT_Rig.jpg
	11:33	EQM_4	Before_EQM_4_Axis_Camera_North_of_CPT_Rig.jpg Before_EQM_4_Axis_Camera_South_of_CPT_Rig.jpg
	11:38		After_EQM_4_Axis_Camera_North_of_CPT_Rig.jpg After_EQM_4_Axis_Camera_South_of_CPT_Rig.jpg
	11:58	EQM_5	Before_EQM_5_Axis_Camera_North_of_CPT_Rig.jpg Before_EQM_5_Axis_Camera_South_of_CPT_Rig.jpg
	12:12		After_EQM_5_Axis_Camera_North_of_CPT_Rig.jpg After_EQM_5_Axis_Camera_South_of_CPT_Rig.jpg
	13:58	During Spin-up 2	At_40g_Day_2_Spin_2_Axis_Camera_North_of_CPT_Rig.jpg At_40g_Day_2_Spin_2_Axis_Camera_South_of_CPT_Rig.jpg
	13:58	SWM_3	After_SWM_3_Axis_Camera_North_of_CPT_Rig.jpg
	14:18	PLT_2	Before_PLT_2_Axis_Camera_North_of_CPT_Rig.jpg
	14:40		After_PLT_2_Axis_Camera_North_of_CPT_Rig.jpg

Note: To get the list of the description of the events refer to Table 24. PLT_2_Axis_Camera_North_of_CPT_Rig.asf contains the recording of pile load test PLT_2.

5 MODEL CONSTRUCTION

The model container used was (Flexible Shear Beam) FSB 2.1 of dimensions 165 cm x 78.5 cm x 58.3 cm. Shear rods were placed on both east and west ends of the container to provide complementary shear. Paper scale were stick on the container to monitor the soil placement during pluvitaion. Additionally, wooden yard stick was glued on the top ring of the container to measure X, Y, and Z coordinates. The prepared model container is shown in Figure 22. The sequence of steps involved in building the model are described in Section 5.1 to Section 5.8.

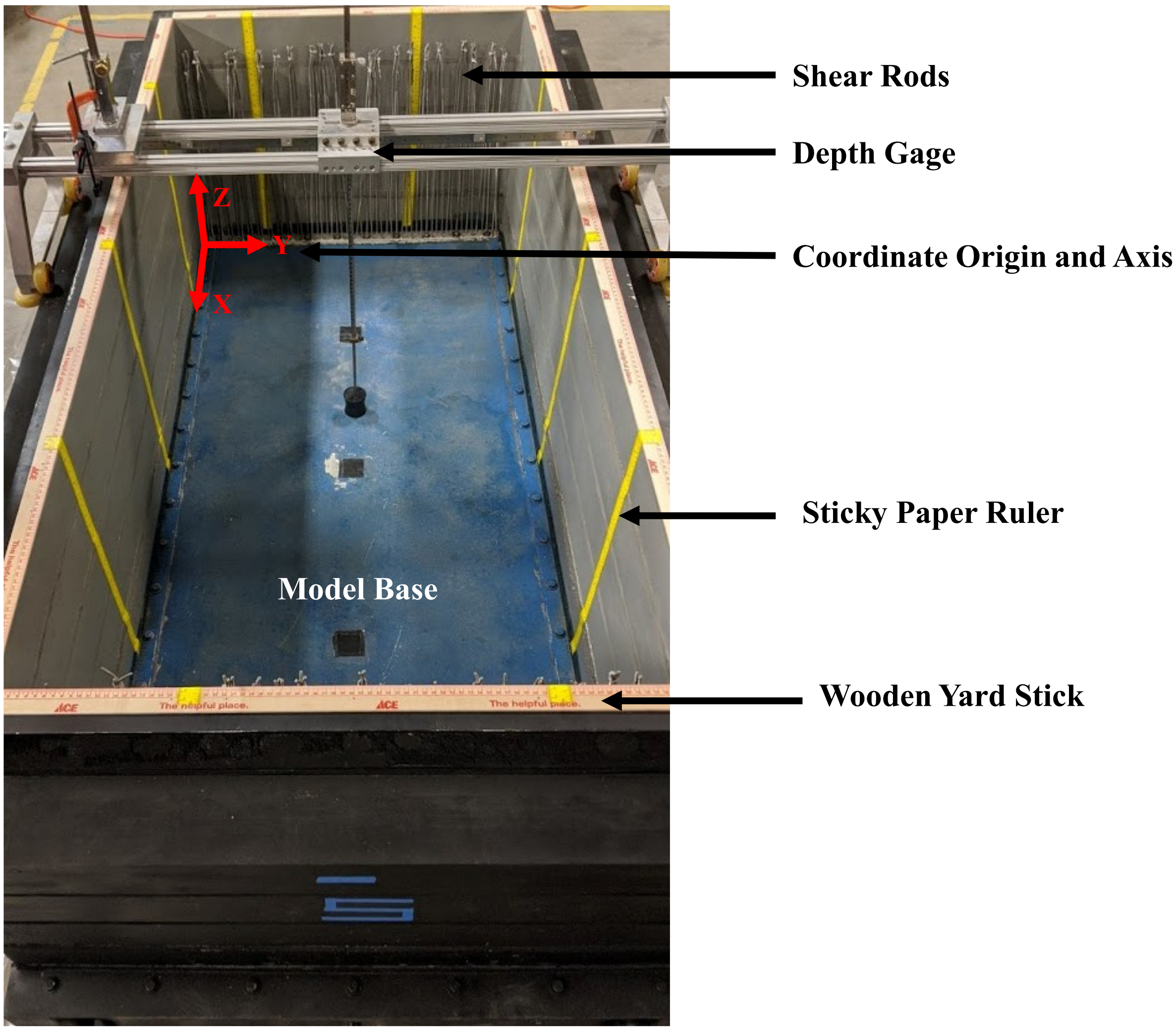

Figure 22. The model container ready for building the model.

5.1 Dense and Medium Dense Layers

Dry pluviation method was used to place the dense and medium dense sand layers. The CGM's drum pluviator was used to place the dense sand layer whereas the pluviator with a hose along with a diffusing screen was used to place the medium dense sand layer. The procedure used for placing the sand layers and placing the sensors are described Sinha et al. (2021b). Figure 23 shows the model view at the end of placement of the dense sand layer. Colored sand was sprinkled at selected depths to visually define the interface of medium sand layer and dense sand layer as shown in Figure 23.

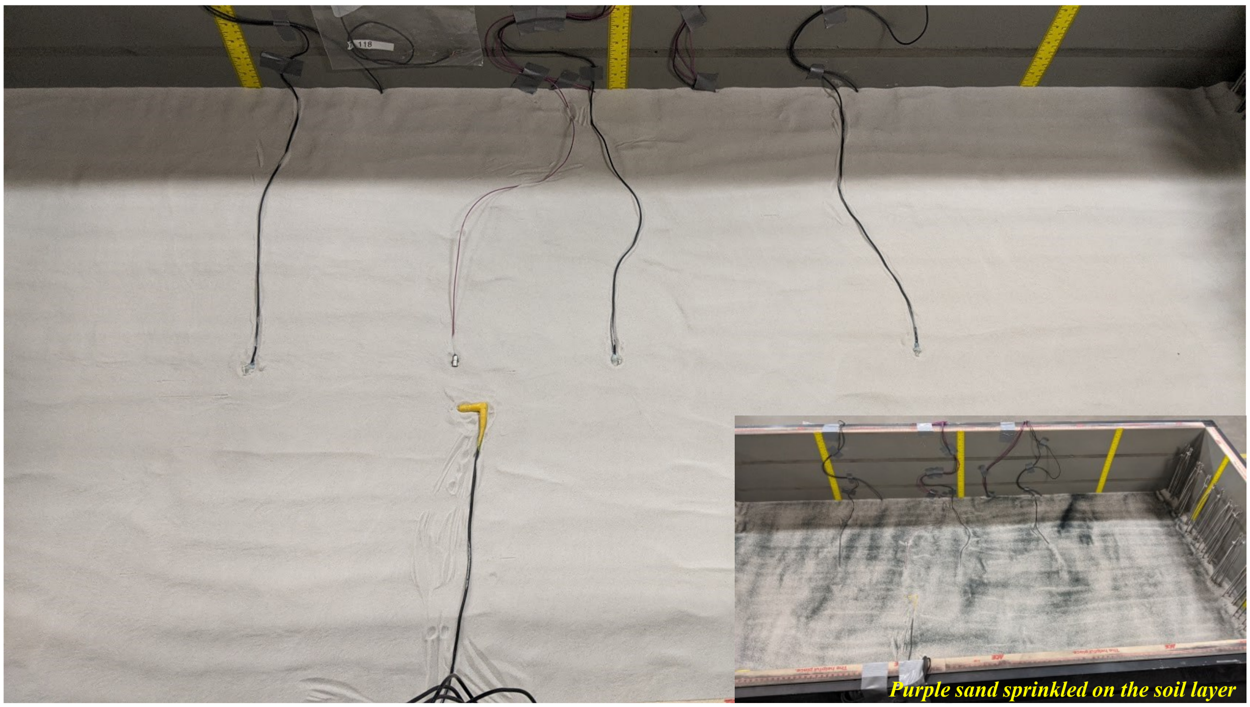

Figure 23. Plan view of the model after placement of the dense sand layer.

5.2 Saturation

The model was saturated on the centrifuge arm to eliminate the possibility of disturbance from transporting the model after saturation. A viscous fluid mixture of deionized water and 1.65% methyl cellulose was used for saturation, which had a viscosity of about 27 times than that of water. According to the scaling rules, the viscosity of the fluid should be scaled inversely with the length scale factor, which for this experiment was 1/40. This rule is only applicable if a specific prototype is envisioned, and the same soil is used in model and prototype. In the current test, the scaling of viscosity was necessary to ensure that the sedimentation of the sand is slow relative to the duration of the earthquake shaking and the pore pressures do not dissipate during shaking. For SKS03 test, a viscosity scale factor of 27 was chosen to represent a realistic prototype and ensure dissipation of pore pressures in the sand layer significantly greater than the duration of shaking and faster than the time required for consolidation of the clay layer. The preparation of methyl cellulose mixture followed the standards presented in Stewart et al. (2009).

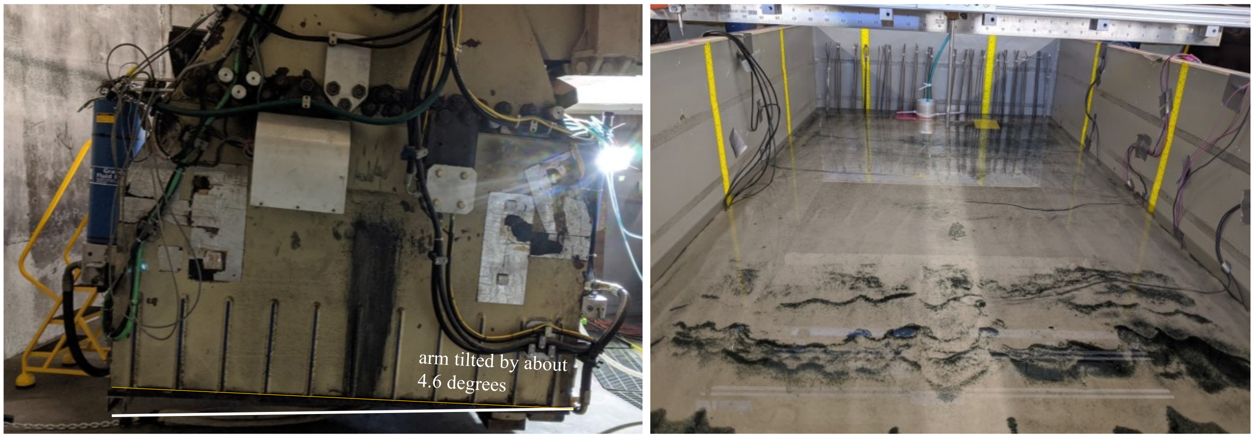

Figure 24. Top-down saturation on the arm with tilt in the model to about 4.6^o (on left). View of the model after saturation (on right) showing colored sand and pore water pressure sensors visible on the submerged sand surface.

A top-down saturation method with water introduced at one end of the tilted container (Figure 24) was used to saturate the model. The procedures on saturation of the model are described in Sinha et al. (2021b). A view of the model after saturation is also shown in Figure 24.

5.3 Clayey Silt Layer and Consolidation

The clayey silt layer was placed as a slurry directly on top of the medium dense sand layer. The mixture contained 20% clay and 80% silt with a water content of w=44%. The slurry was mixed under vacuum of 45 kPa. It was then placed in the model and consolidated on the centrifuge with an equivalent load of 80 kPa. The method and preparation required to place and consolidate a silt layer is described in Sinha et al. (2021b). The difference in consolidation between SKS02 and SKS03 test was the way consolidation was performed. In SKS02, consolidation was performed at 1 g using a consolidation press whereas in SKS03 test consolidation was performed on centrifuge at 40 g. To get a consolidation load of 80 kPa at 40 g on centrifuge, the silt layer was loaded with a dead weight of about 250 kg (model scale).

(a) (b) (c)

Figure 25. Silt layer placement and consolidation. View of the model (a) after placing the silt layer, (b) with applied dead load and (c) at the end of consolidation.

Figure 25 shows the view of the model at different times stages of the consolidation process. First, the silt layer was placed as a slurry. Then, 250 kg (~2 kPa) of dead load was placed slowly over several days to consolidate the model to develop sufficient strength to hold the dead load for consolidation on centrifuge. The model was then consolidated on centrifuge by very slowly increasing the g-level in steps (1g → 2g→ 4g→8g→12g→20g→30g→40g). Settlement and pore pressures transducers were connected to continuously monitor the soil settlement and excess pore pressures build up and dissipation during the consolidation process. Figure 25 (c) shows the view of the model at the end of consolidation.

5.4 Loose Sand Layer

The loose sand layer was placed as a slurry on top of the medium dense sand layer. To achieve this, the model was moved from the centrifuge arm and carefully placed on the ground floor. Several trials were performed to design the slurry composition and the placement procedure, to achieve a target relative density of D_r=40%. Figure 26 show the model setup during the preparing and placement of sand slurry. The procedure is described below.

- The sand was mixed at a moisture content of 41% by mass. Instead of water, the saturating fluid was of 1.7% HPMC-water solution. The sand-water-HPMC mixture was blended in the sealed concrete mixer under vacuum pressure of 98 kPa for about 30 minutes to remove air from the soil.
- While the sand was getting mixed, the vacuum pump was paused, and CO_2 was added until the pressure in the sealed concrete mixer decrease to zero. This process took about about 40 seconds. (Later it was realized that it may have been preferable to stop the mixing and then quickly release the vacuum by venting to atmosphere.)
- Following vacuum release, the lid was opened, and the mixer was tilted to pour the slurry in a bucket.
- The slurry was then quickly moved and placed in the model.

For each batch of slurry placement, the above process took about 33 minutes. During the slurry placement, the model was always submerged with at least 1 inch of deaired 1.7% HPMC solution. The steps involved in the procedure described above were tried several times to make it efficient and consistent across different batches. A small metal sheet was used to guide the slurry in the model to cause less disturbance in the placed sand layers beneath. This step also helped in producing less vigor during slurry placement reducing any chances of air entrapment. For a uniform placement of slurry, the model was separated into three sections using thin sheets of steel as shown in Figure 26. A total of about 18 batches of slurry were used. Figure 27 show the view of the model after placement of loose sand layer.

Figure 26. Setup for placing the loose sand layer as slurry.

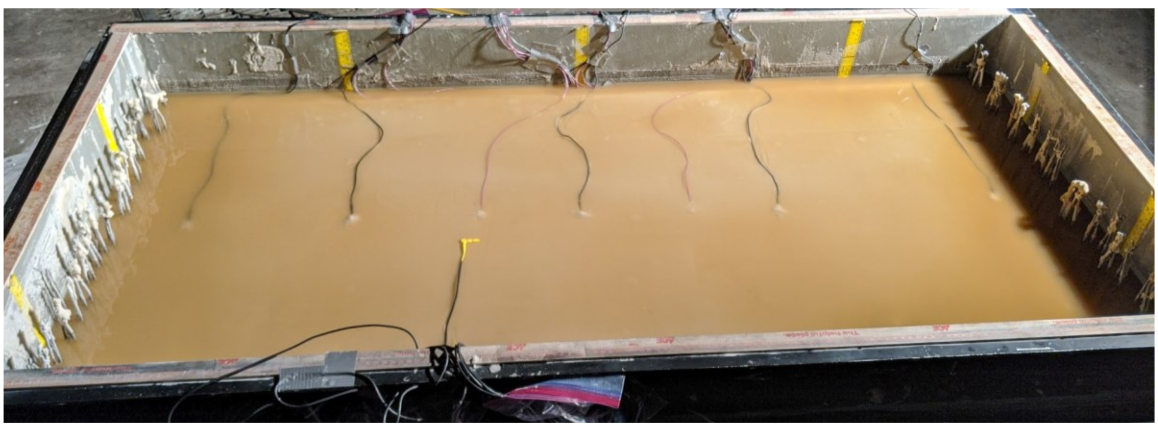

Figure 27. View of the model after the placement of loose sand layer.

5.5 Lightly Cemented Clay Layer

Clay layer was also placed as a slurry. The slurry was prepared in the clay mixer under vacuum pressure of 45 kPa. The composition consisted of 3% cement and 50% water. The procedure used for mixing and placing the clay slurry is outlined below.

- Appropriate quantities of Yolo Loam clay and water (for a water content of 50%) was mixed in a larger ribbon mixer for more than three 3 hours.
- The mixing was performed under vacuum pressure of 45 kPa.
- Cement equal to 3% of soil mass was added and then mixed for additional 20 minutes.
- The slurry was then transported though a hose from the mixer to the model using a pneumatic pump as shown in Figure 28.
- As the slurry was placed in the model, it was levelled with a levelling tool as shown in Figure 28. Samples were taken to monitor the development of shear strength in the slurry as the cement hydrated and bonded the clay particles.

Figure 28. Placement of clay slurry in the model.

The whole process from the start of adding cement to the mixer to pouring of the clay slurry in the model lasted for about 40 minutes. Immediately as the cement was mixed to the slurry, hydration of the cement began, and the mixture thickened. When slurry was pumped after 20 minutes of mixing, it flowed as a thick viscous mixture as shown in Figure 28. Section 6.2 describes the achieved undrained shear strength of the placed clay layer during the test.

5.6 Pile Installation

After the two days of placement of the clay slurry, piles were installed in the soil. Three holes were made in the cemented clay layer to help guide the insertion of piles. A 1000 lbs dead weight was used to push the piles in soil. Hand-held surveyor's level and spirit level was attached to the pile masses to maintain verticality of the pile during installation. The procedure of pile installation is described in detail in Sinha et al. (2021b).

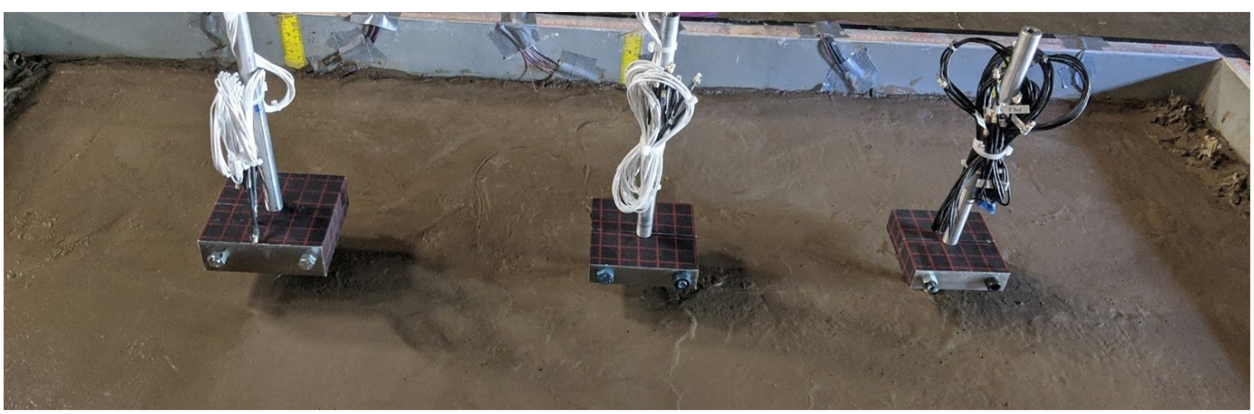

Figure 29. View of the model with three piles installed.

5.7 Monterey Sand Layer

Monterey sand was pluviated in the model using a drum pluviator. Canopies made with paper were used to cover the piles (see Figure 30 (a)) and help the sand particles slide down instead of bouncing from the pile masses. Soil beneath the piles was manually placed carefully using a funnel and then levelled using a trowel. The relative density (D_r) achieved was about 95%. The layer was then saturated with 1.7% deaired HPMC solution. Figure 30 shows the model view before and after the placement of Monterey sand.

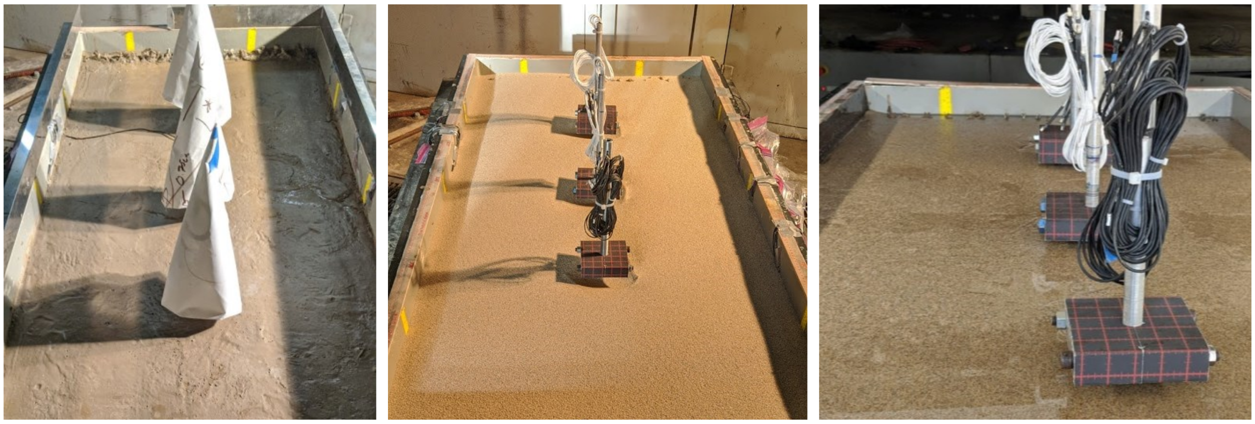

(a) (b) (c)

Figure 30. (a) Model setup for pluvitaion and view of the model (b) after placing and (c) saturation of the Monterey sand layer.

5.8 Work on the Arm

After placement of the Monterey sand, the model was lifted and carefully placed on the centrifuge arm using a chain fall as described in SKS02 data report (Sinha et al. 2021b). Work on the arm involved placing the camera beams and light beams, installing cameras and line lasers, placing sensors on the piles, and routing all the sensor cables to the data acquisition (DAQ) system. Soil markers and camera target markers were also placed on the model and can be seen in Figure 17. During this process, the model was occasionally sprinkled with water at regular intervals to prevent drying of the clay surface. Figure 31 shows the finished view of the model with three instrumented piles installed.

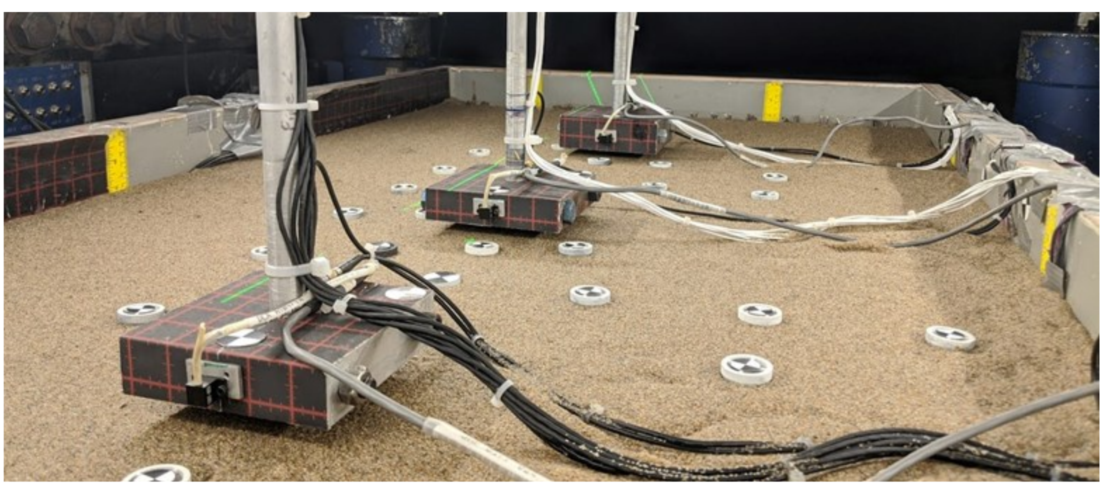

Figure 31. Finished view model showing three fully instrumented piles.

6 CENTRIFUGE TEST

6.1 Test Chronology and Log Details

The test was conducted on 27th and 28th of August 2020. Table 24 outlines the log of events on the days of testing and the datafiles associated with it. Table 20 and Table 23 summarizes the snapshots and videos taken during these events.

Table 24. Log of events and their description on Day 1 and Day 2 of test (27th and 28th of August).

Date	Spin	Time	Event	Location	Event Description	Fast Data file / other data	Slow Data
26th August	-	18:16	VST_1	X=16.4 cm, Y = 58.5 cm, Z = middle of clay layer	Hand Vane Shear Test, 19 mm blade	$s_{u,p}$ = 31 kPa, $s_{u,r}$ = 4 kPa	-
	-	18:34	VST_2	X=147 cm, Y = 19.5cm, Z = middle of clay layer	Hand Vane Shear Test, 19 mm blade	$s_{u,p}$ = 38 kPa, $s_{u,r}$ = 4 kPa	-
27th August	1	7:10	-	-	Slow data started	-	08272020@091814.bin
		9:25	-	-	Started spinning	-	
		10:40	SWM_1	-	Step wave (AF=0.6, IF=4000, P-P=2.5g)	08272020@091814@104029@64.5rpm.bin	
		10:52	CPT_1	X=82 cm, Y=56.5 cm	6 mm centrifuge cone penetration test	08272020@091814@105210@64.4rpm.bin	
		11:14	PLT_1	on Pile 1	Pile load test	08272020@091814@111447@64.5rpm.bin	
		11:33	EQM_1	-	Small Santa Cruz (AF =4.4, IF=2000, P-P=7.0g)	08272020@091814@113338@64.4rpm.bin	
		11:56	CPT_2	X=72 cm, Y=56.5 cm	6 mm centrifuge cone penetration test	08272020@091814@115643@64.2rpm.bin	
		11:59	-	-	Spin down initiated	-	
28th August	-	6:50	VST_3	X=19.32 cm, Y = 17 cm, Z = middle of clay layer	Hand Vane Shear Test, 19 mm blade	$s_{u,p}$ = 30 kPa, $s_{u,r}$ = 4 kPa	-
	-	7:05	VST_4	X=145.6 cm, Y =60.9 cm, Z = middle of clay layer	Hand Vane Shear Test, 19 mm blade	$s_{u,p}$ = 43 kPa, $s_{u,r}$ = 4 kPa	-
	1	8:28	-	-	Slow Data started	-	08282020@091729.bin
		9:27	-	-	Started Spinning	-	
		10:01	SWM_2	-	Step wave (AF=0.6, IF=4000, P-P=0.325g)	08282020@091729@100121@64.5rpm.bin	
		10:25	EQM_2	-	Medium Santa Cruz (AF =5.8, IF=2000, P-P=10g)	08282020@091729@102507@64.5rpm.bin	
		10:42	CPT_3	X=61 cm, Y=56.5 cm	6 mm centrifuge cone penetration test	08282020@091729@104225@64.5rpm.bin	
		11:07	EQM_3	-	Large Santa Cruz (AF =8.1, IF=2000, P-P=13g)	08282020@091729@110705@64.4rpm.bin	
		11:23	CPT_4	X=51 cm, Y=56.5 cm	6 mm centrifuge cone penetration test	08282020@091729@112326@64.4rpm.bin	
		11:43	EQM_4	-	Large EJM01 motion (IF=1428, AF=0.85, P-P=29g)	08282020@091729@114313@64.2rpm.bin	
		12:09	EQM_5	-	Large EJM01 motion (IF=1428, AF=1.275, P-P=42.5g)	08282020@091729@120938@64.5rpm.bin	
		12:26	-	-	Spin down initiated	-	
	2	13:46	-	-	Started Spinning	-	
		14:04	SWM_3		Step wave (AF=1.0, IF=4000, P-P=0.9g)	08282020@091729@140425@64.4rpm.bin	
		14:21	PLT_2	on Pile 1	Pile load test	08282020@091729@142116@64.6rpm.bin	
		14:44	CPT_5	X=76.5 cm, Y=56.5 cm	6 mm centrifuge cone penetration test	08282020@091729@144401@64.7rpm.bin	
		14:48	-		Spin down initiated	-	
	-	17:28	VST_5	X=66.5 cm, Y = 61.5 cm, Z = middle of clay layer	Hand Vane Shear Test, 19 mm blade	$s_{u,p}$ = 35 kPa, $s_{u,r}$ = 3 kPa	-
	-	17:33	VST_6	X=74 cm, Y =16.6 cm, Z = middle of clay layer	Hand Vane Shear Test, 19 mm blade	$s_{u,p}$ = 33 kPa, $s_{u,r}$ = 3 kPa	-
	-	17:39	VST_7	X=107 cm, Y = 17.7 cm, Z = middle of clay layer	Hand Vane Shear Test, 19 mm blade	$s_{u,p}$ = 37 kPa, $s_{u,r}$ = 3 kPa	-
	-	17:44	VST_8	X=108.3 cm, Y =49.5 cm, Z = middle of clay layer	Hand Vane Shear Test, 19 mm blade	$s_{u,p}$ = 38 kPa, $s_{u,r}$ = 3 kPa	-

Event Description: VST: Vane Shear Test, PLT: Pile Load Test, SWM: Step Wave Motion, CPT: Centrifuge Cone Penetration Test, EQM: Earthquake Motion
Earthquake Motion Terminologies: AF: Amplification Factor for input motion, IF: Input Frequency for input motion, P-P: Peak to Peak
Slow Data Filename Description: Date@Time.bin
Fast Data Filename Description: SlowDataDate@SlowDataTime@FastDataTime.bin
Undrained Shear Strength: $s_{u,p}$: peak, $s_{u,r}$: residual

6.2 Vane Shear Tests

Vane shear tests were performed at 1 g at the times listed in Table 25. During the placement of the clay layer, samples were taken aside (see Table 24) to monitor the development of shear strength of the clay as the cement reacted. Hand vane shear tests were performed in the middle of the clay layer i.e., at the depth of 5.0 cm (model scale). Figure 32 shows the development of peak undrained shear strength of clay during the initial 2 weeks of hydration process. It also shows the undrained shear strength of the clay crust before and after each day of testing.

From the plots shown in Figure 32, the undrained shear strength of the weekly cemented clay during the test ended up being ~35 kPa, significantly smaller than the targeted undrained shear strength of 80-100 kP) (see Section 3.3.2). This might be explained by the longer mixing time (~20 minutes) of clay-cement mixture in the large ribbon mixer compared to 5 minutes of mixing in the kitchen mixer while designing the targeted strength. The duration of mixing and/or the type of mixer and batch size might have also affected the strength gain.

Table 25. Vane shear test performed on the samples taken aside and on the model during centrifuge testing.

Date	***Time***	***Day #***	***Undrained Shear Strength [kPa]***		***Sensitivity S***	***Description***
			$s_{u,p}$	***$s_{u,r}$***		
8/11/2020	11:25	0	0	0		- Mixing done @ 11:25 am on August 11th, 2020
Tests Performed on the sample taken aside in small container						
8/12/2020	17:13	1.2	9.5	0.5	19	The procedure used was the following :  - The vane shear tip was pushed 40 mm from the surface to the center of the clay layer. - The penetrated vane was left for a minute to dissipate the excess pore pressures generated. - Torque was then slowly applied to the vane until the soil failed. The peak reading was recorded. - The vane was rotated 5 more times to measure the residual undrained shear strength of the cemented clay.
8/13/2020	16:42	2.2	17	1	17	
8/14/2020	17:53	3.3	21	3	7	
8/16/2020	19:36	5.3	24	3	8	
8/17/2020	17:56	6.3	24	3.5	7	
8/18/2020	17:54	7.3	28	3	9	
8/19/2020	21:10	8.4	26	3	9	
8/20/2020	17:21	9.2	26	3	9	
8/21/2020	18:43	10.3	24	3	8	
8/24/2020	19:50	13.4	26	3	9	
8/25/2020	17:58	14.3	26	3	9	
Tests Performed on the model** **(using the same procedure as specified above)						
8/26/2020	6:16	14.8	31	4	8	VST_1, X=16.4cm, Y=58.8cm, Z=middle of clay layer
8/26/2020	6:34	14.8	38	4	10	VST_2, X=147cm, Y=19.5cm, Z=middle of clay layer
8/28/2020	6:50	16.8	30	4	8	VST_3, X=19.32cm, Y=17cm, Z=middle of clay layer
8/28/2020	7:05	16.8	43	4	11	VST_4, X=145.66cm, Y=60.9cm, Z=middle of clay layer
8/28/2020	17:28	17.3	35	3	12	VST_5, X=66.5cm, Y=61.5cm, Z=middle of clay layer
8/28/2020	17:33	17.3	33	3	11	VST_6, X=74cm, Y=16.6cm, Z=middle of clay layer
8/28/2020	17:39	17.3	37	3	12	VST_7, X=107cm, Y=17.7cm, Z=middle of clay layer
8/28/2020	17:44	17.3	38	3	13	VST_8, X=108.3cm, Y=49.5cm, Z=middle of clay layer

$s_{u,p}$: peak undrained shear strength, $s_{u,r}$: residual undrained shear strength

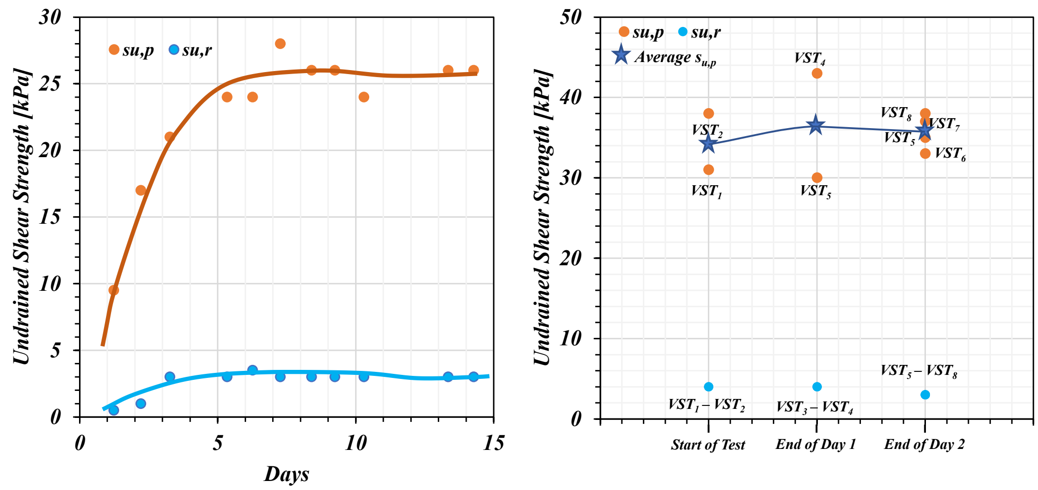

(a) *During first 2 weeks of placement* (b) *During the centrifuge test*

Figure 32. Peak and residual undrained shear strength (s_u) of the clay crust layer estimated from vane shear tests.

6.3 Centrifuge Cone Penetration Tests

Centrifuge cone penetration tests were performed with a 6 mm (model scale) diameter probe with tip angle of 60 degrees (see Figure 18) at different stages of the centrifuge test (see Table 24). The cone was pushed at the rate of 1 cm/s. Interpretations from CPTs are shown in Figure 33. Normalized cone tip resistance (qc1N) and relative density (D_r) was estimated based on Idriss and Boulanger (2008) CPT correlation with constants C_1=1.893 and C_2=0.7284 calibrated for Ottawa F-65 sand. In the plots, the qc1N and relative densities for clay and silt layers are not shown.

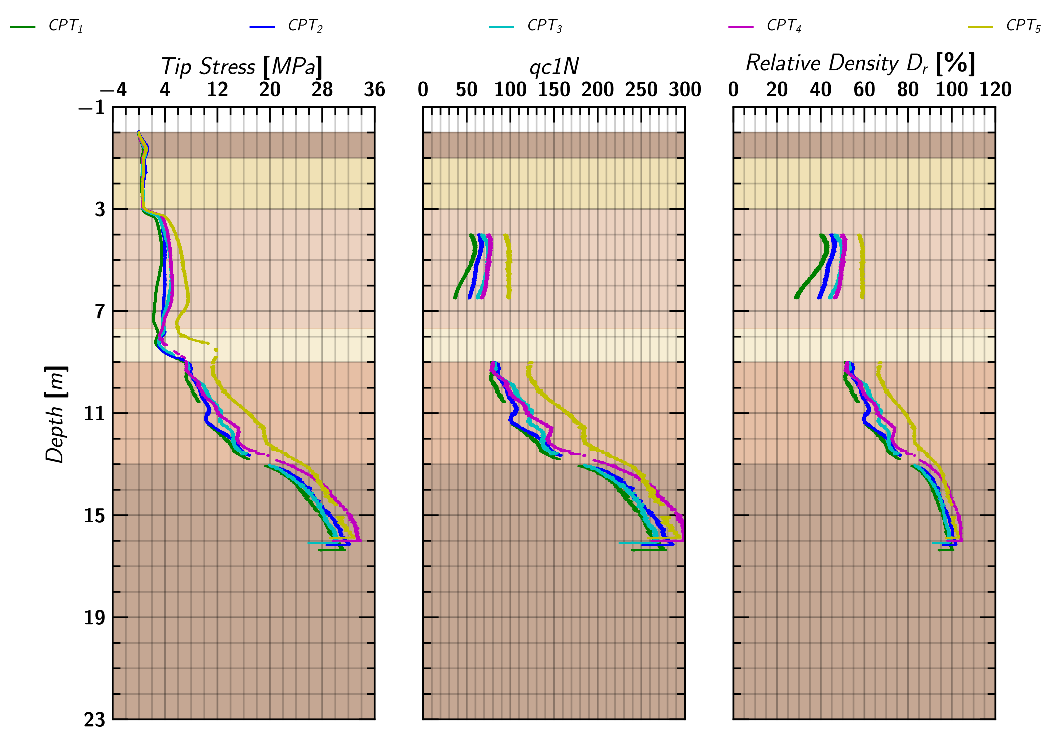

Figure 33. Centrifuge cone penetration test results (CPT_1, CPT_2, CPT_3, CPT_4, and CPT_5).

6.4 Centrifuge Pile Load Tests

A centrifuge pile load test (PLT) was conducted to estimate the static pile load capacity. The test was conducted on Pile 1 which had an initial applied head load of 500 kN. A 2-inch actuator attached to a cross beam pushed the Pile 1 at a penetration rate of 1 mm/minute and the applied actuator load, and its displacement were measured. Figure 35 (a) shows the recorded actuator load and recorded (uncorrected) actuator movement during the pile load tests. PLT_1 was conducted at the beginning of the centrifuge test whereas PLT_2 was conducted at the end of the centrifuge test (see Table 24). During the tests, the reaction from the actuator caused deflection in the cross beam in the opposite direction. As a result, the movement recorded by the actuator was consistently larger than the actual penetration of the pile. To correct this, an unloading stiffness for the soil-pile-beam was estimated from pile rebound once the load was removed. Figure 34 shows the table calculating elastic unloading stiffness for pile load tests PLT_1 and PLT_2 from elastic unloading in piles and elastic unloading of soil at its tip. An average elastic stiffness of 36.86 kN/mm (prototype scale) was applied to correct the actuator movement and obtain the actual penetration of the pile. Figure 34 (b) shows pile load test results with estimated pile penetration. Section 6.4.1 and Section 6.4.2 plot the results from the pile load tests PLT_1 and PLT_2. In the plots, the applied head load is the sum of the actuator load and the initial pile head load of 500 kN and the penetration is normalized to the percentage of pile diameter.

PLT $_1$	
Max Tip Load [kN]	3300
Max Pile Head Load [kN]	4200
Length of pile above soil [m]	11.5
Length of pile in soil [m]	14.9
Pile elongation due to unloading [mm]	22.22
Pile elongation due to unloading [%D]	3.50
Soil rebound during unloading [%D]	1.56
Total rebound at pile head [%D]	5.1
Elastic Unloading Stiffness [kN/%D]	244.35
PLT $_2$	
Max Tip Load [kN]	4800
Max Pile Head Load [kN]	6200
Length of pile above soil [m]	11.5
Length of pile in soil [m]	14.9
Pile elongation due to unloading [mm]	32.69
Pile elongation due to unloading [%D]	5.15
Soil rebound during unloading [%D]	2.37
Total rebound at pile head [%D]	7.52
Elastic Unloading Stiffness [kN/%D]	223.8

Soil rebound at Pile's Tip					
ν	0.3	- Poisson's ratio			
η	0.9	- influence value			
r	0.3175	- radius [m]			
G	125	- Shear Modulus [MPa]	- for Vs=250m/s		
Pb_{PLT1}	2500.000	-stress [KN]			
Pb_{PLT2}	3800.000	-stress [KN]			
Se_{PLT1}	9.921	- elastic reboud [mm]		1.56	-[%D]
Se_{PLT2}	15.080	- elastic rebound [mm]		2.37	-[%D]

$$S_e = \frac{P_b(1-\nu)\eta}{4rG}$$

Analysis of Deformation of Vertically Loaded Piles, Randolph, Mark F. Wroth, C. Peter (1979)

Figure 34. Table showing the calculations for estimating the total rebound in pile and elastic unloading stiffness during pile load tests PLT_1 *and* PLT_2.

Figure 36 shows the determination of static pile load capacity from pile load tests PLT_1 and PLT_2 using the DeBeer (1968) yield load method. The determined static pile load capacity from PLT_1 and PLT_2 was found to be 3800 kN and 4550 kN, respectively. The penetration of the piles at 3800 kN and 4550 kN for pile load test PLT_1 and PLT_2 were about 12% and 15% of pile diameter, respectively (see Figure 36). For PLT_1 test, the mobilized skin friction and tip resistance with the pile head load of 3800 kN were found to be 1200 kN and 2600 kN, respectively. For PLT_2 test, the mobilized skin friction and tip resistance at the total pile head load of 4550 kN were found to be 1950 kN and 2600 kN, respectively.

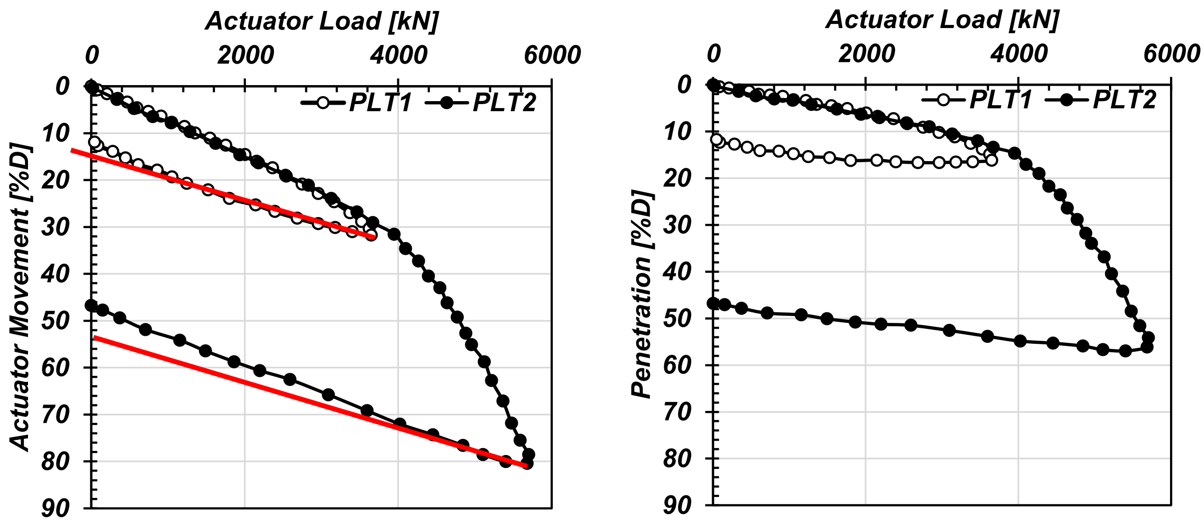

Figure 35. Results of pile load tests PLT_1 and PLT_2 showing the actuator load versus (a) actuator movement and (b) estimated pile penetration from the unloading curve. The red line indicates the elastic stiffness of the cross beam on which the load actuator was installed.

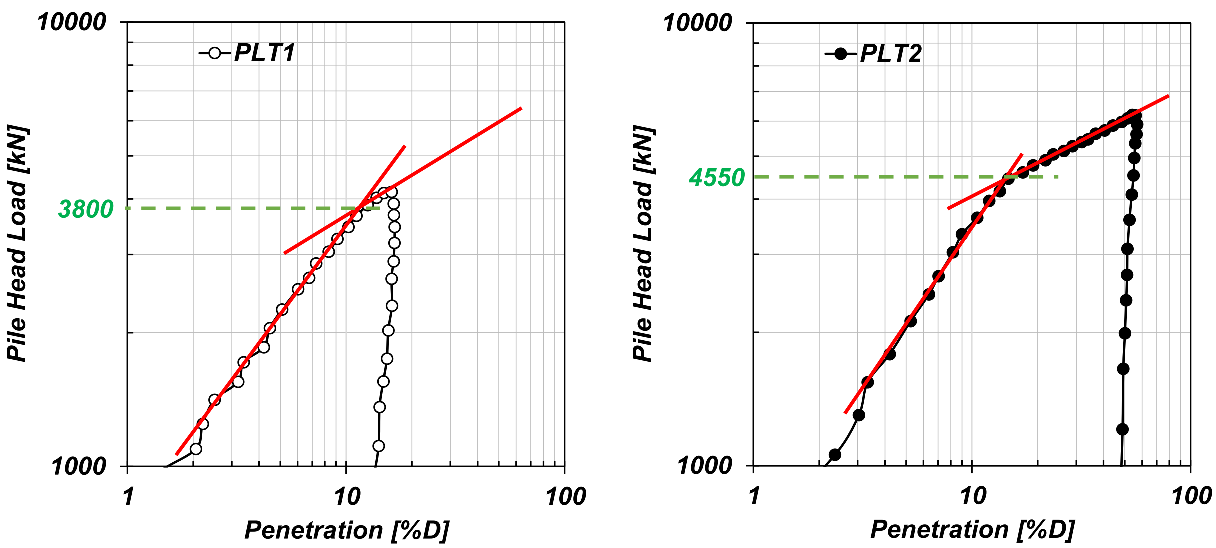

(a) PLT_1 (b) PLT_2

Figure 36. Determination of static pile load capacity from (a) PLT_1 and (b) PLT_2 from DeBeer's (1968) method.

6.4.1 Centrifuge Pile Load Test PLT_1

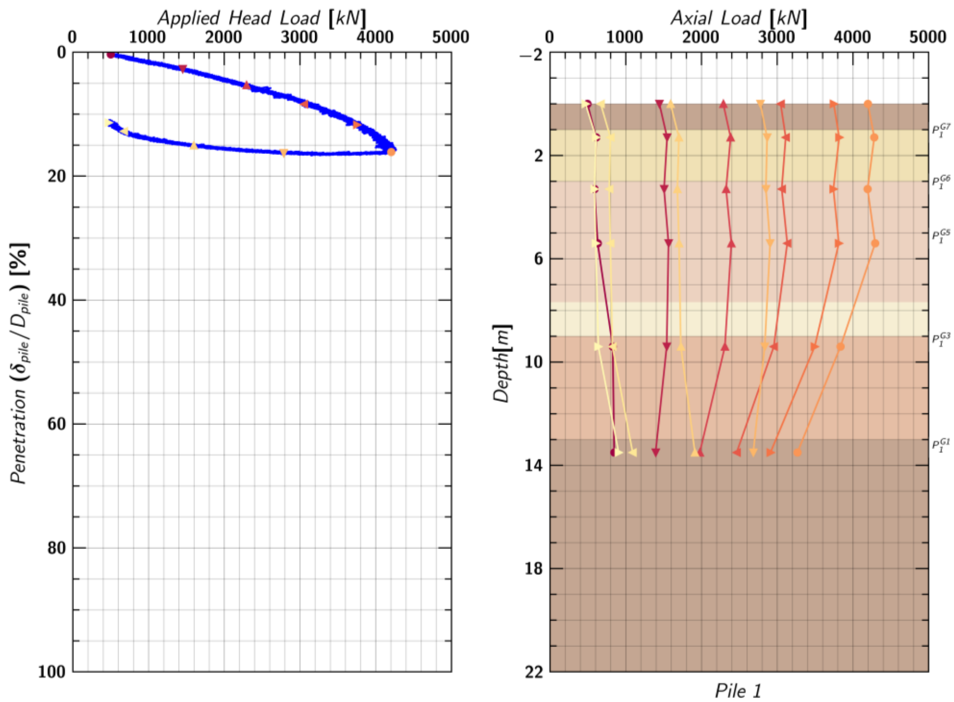

Figure 37. Applied head load, estimated penetration, and axial load profile during pile load test PLT_1.

6.4.2 Centrifuge Pile Load Test PLT_2

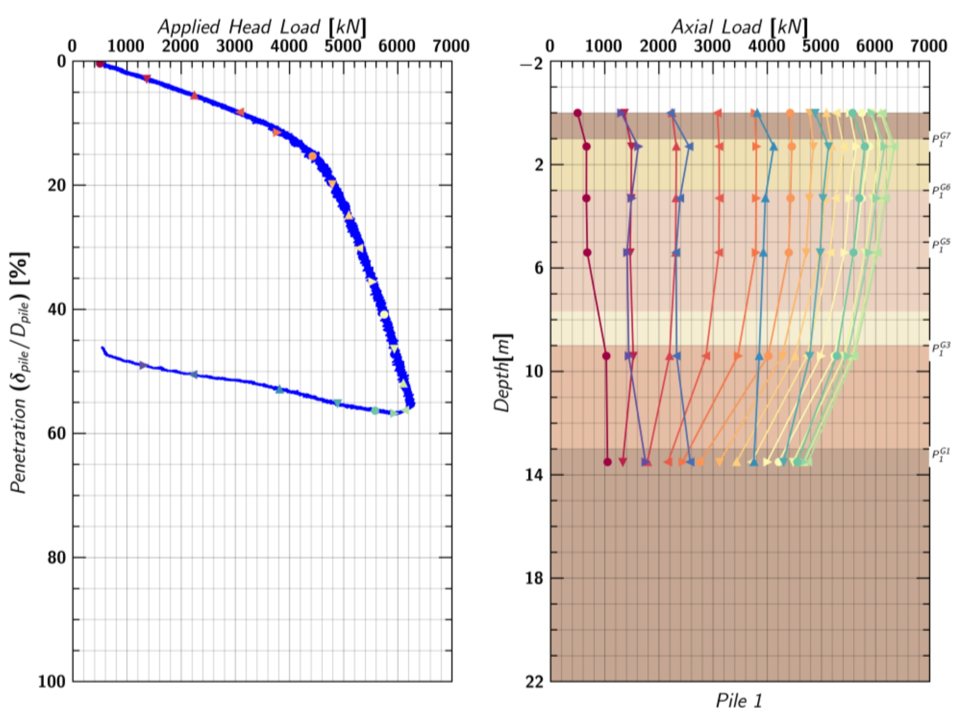

Figure 38. Applied head load, estimated penetration, and axial load profile during pile load test PLT_2.

6.4.3 Load Curve

A load curve was estimated from the axial load distribution in Pile 1 from the pile load tests. Figure 39 shows the load curve estimated from Pile load test (PLT_2). The load curve had a shaft and tip resistance of 1950 kN and 2600 kN, respectively.

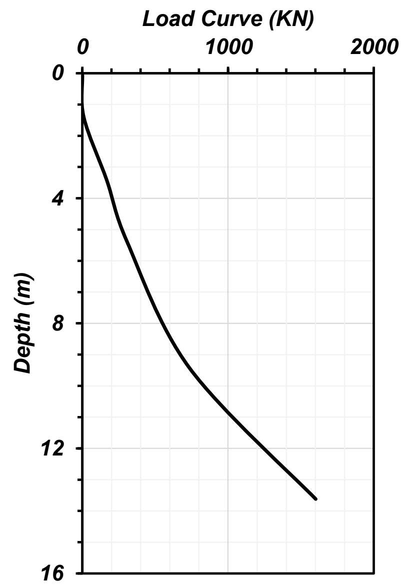

Figure 39. Load curve estimated from pile load test PLT_2.

During both the pile load tests (see Figure 37 and Figure 38), The initial developed drag load on Pile 1 diminished as more load were applied to it. The load and the corresponding settlement in the pile for which drag loads diminished were evaluated for both the tests. It was found that at about 1200 kN, the initial drag loads in the piles diminished. At this load, the magnitude of penetration in piles were measured to be about 3% of the pile diameter, which at model scale is about 0.5 mm. This illustrates that a small relative movement of 3% pile diameter (2.5 times D_{50} of soil) at pile's interface can result in full mobilization of skin friction.

6.5 Step Wave Motion Tests

Step wave motion tests SWM_1 and SWM_2 were performed on Day 1 and Day 2 respectively to characterize the natural frequencies of the piles and the camera beam on which Photron cameras were installed. Section 6.5.1 and Section 6.5.2 shows the response of piles during these tests. The natural periods of the piles and the camera beam obtained from these tests are summarized in Table 26.

Table 26. Natural period of piles evaluated from the step wave motion tests.

Test	Natural Period (s)				
	Pile 1	Pile 2	Pile 3	Camera Beam	
	Hor[1]	Hor[1]	Hor[1]	Hor[1]	Ver[2]
SWM_1	1.18	1.67	2	0.5	0.5
SWM_2	1	1.17	1.4	0.5	0.5

[1]Horizontal [2]Vertical

6.5.1 Step Wave Motion SWM_1

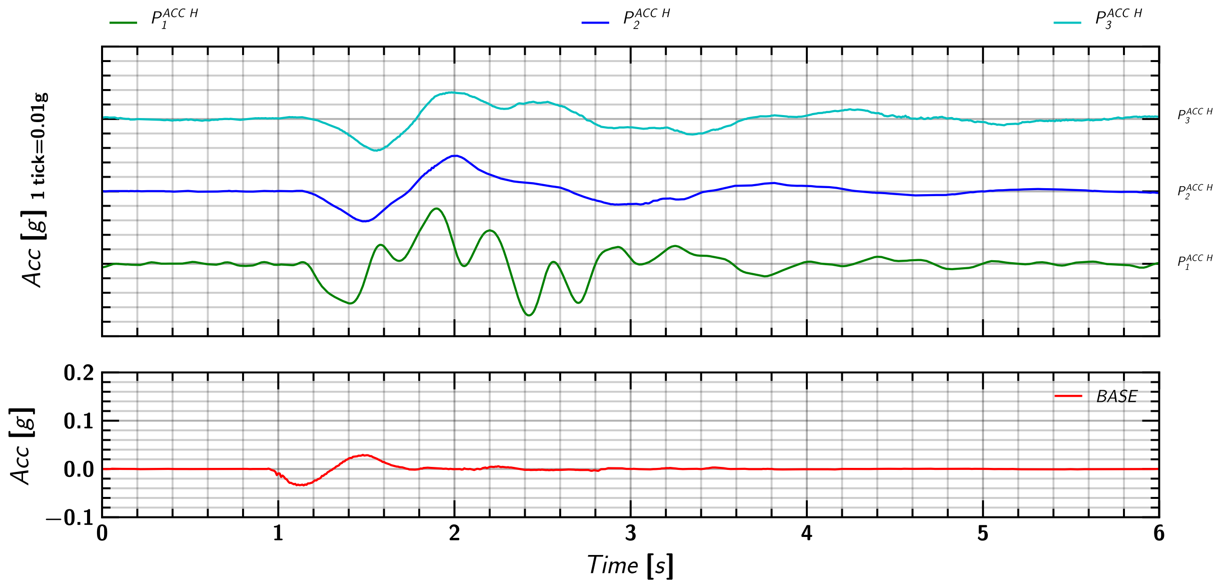

Note: BASE refers to the average of acceleration measured from EAST and WEST sensors.

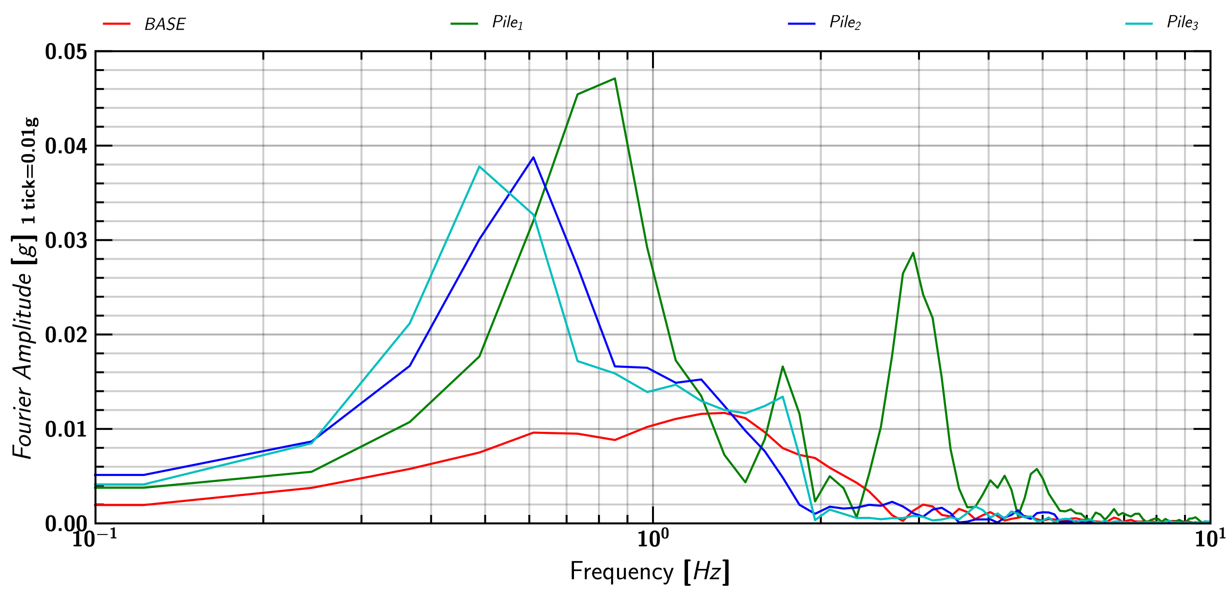

Figure 40. Dynamic response of piles during step wave motion SWM_1.

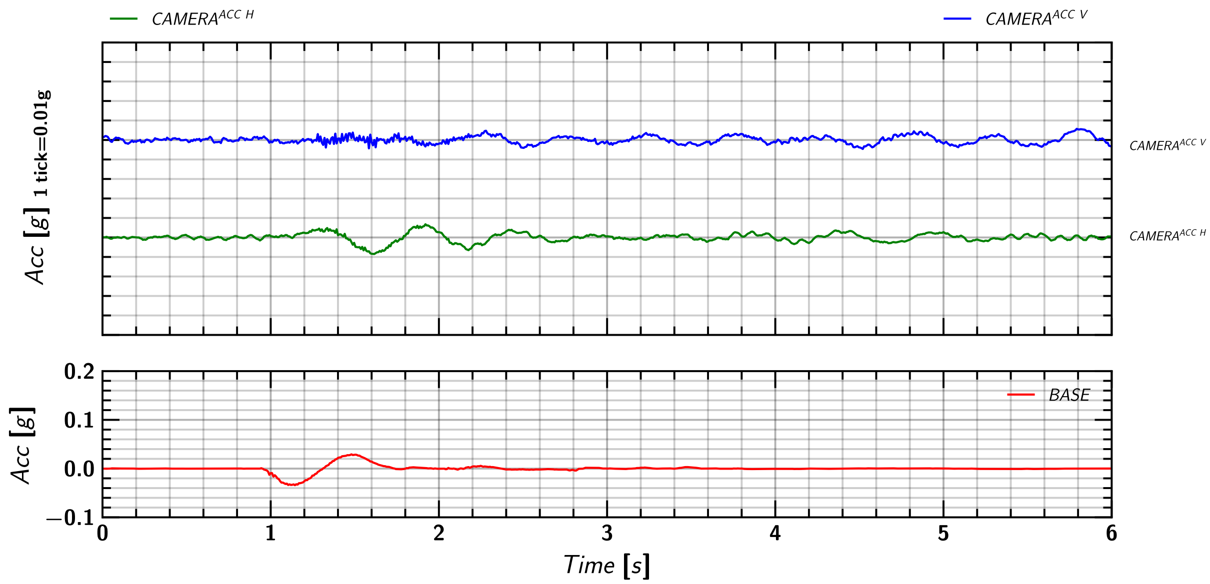

Note: BASE refers to the average of acceleration measured by EAST and WEST sensors.

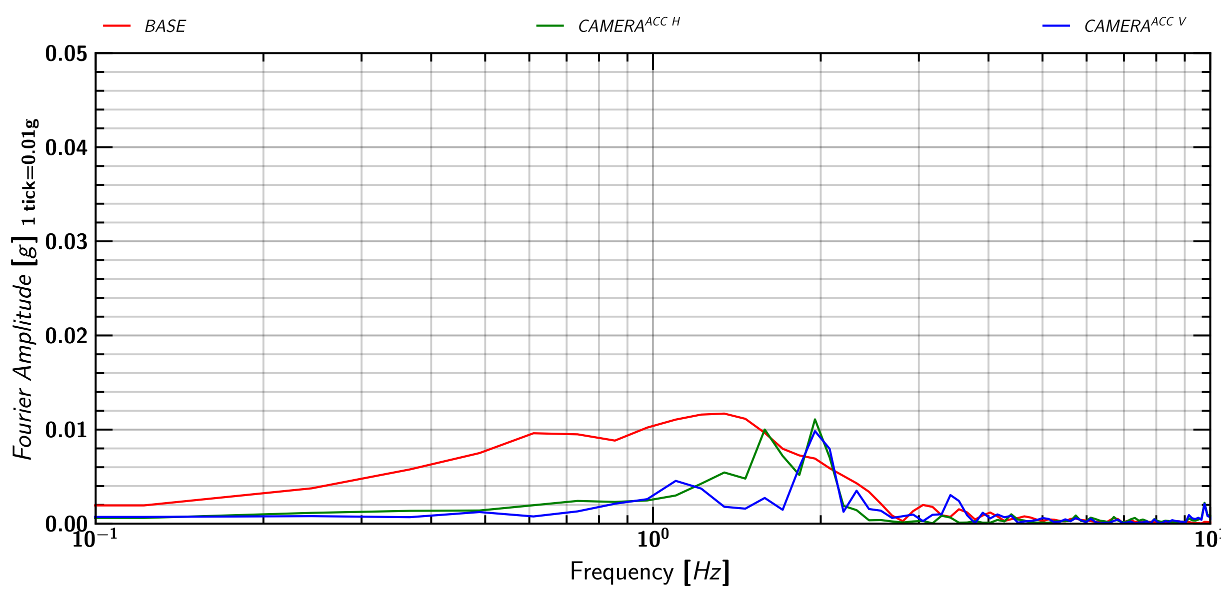

Figure 41. Dynamic response of camera beam during step wave motion SWM_1.

6.5.2 Step Wave Motion SWM_2

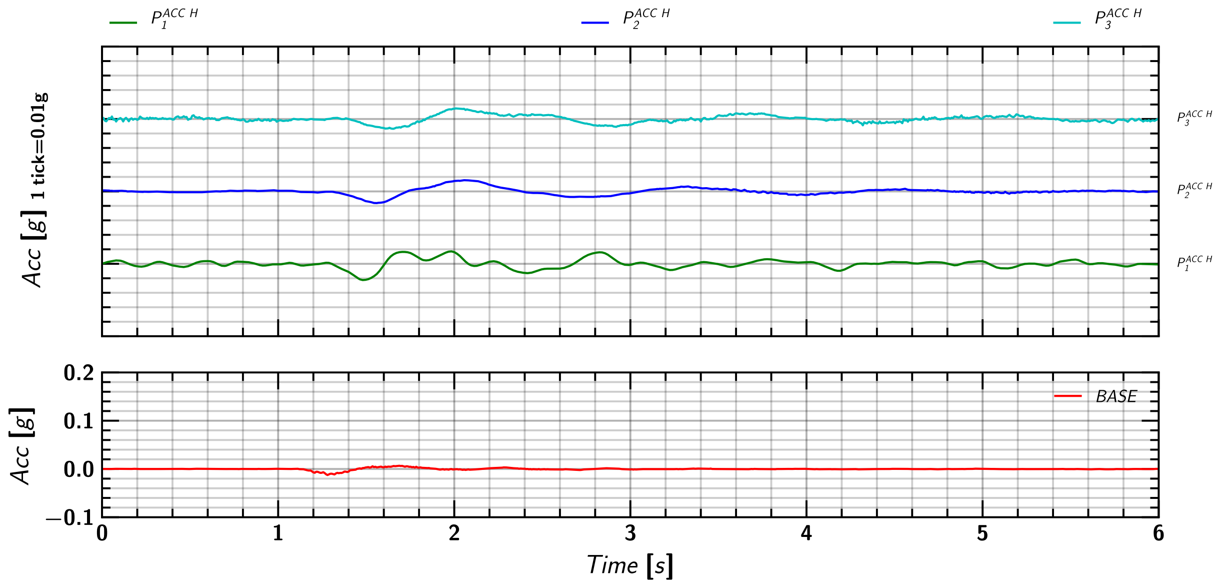

Note: BASE refers to the average of acceleration measured by EAST and WEST sensors.

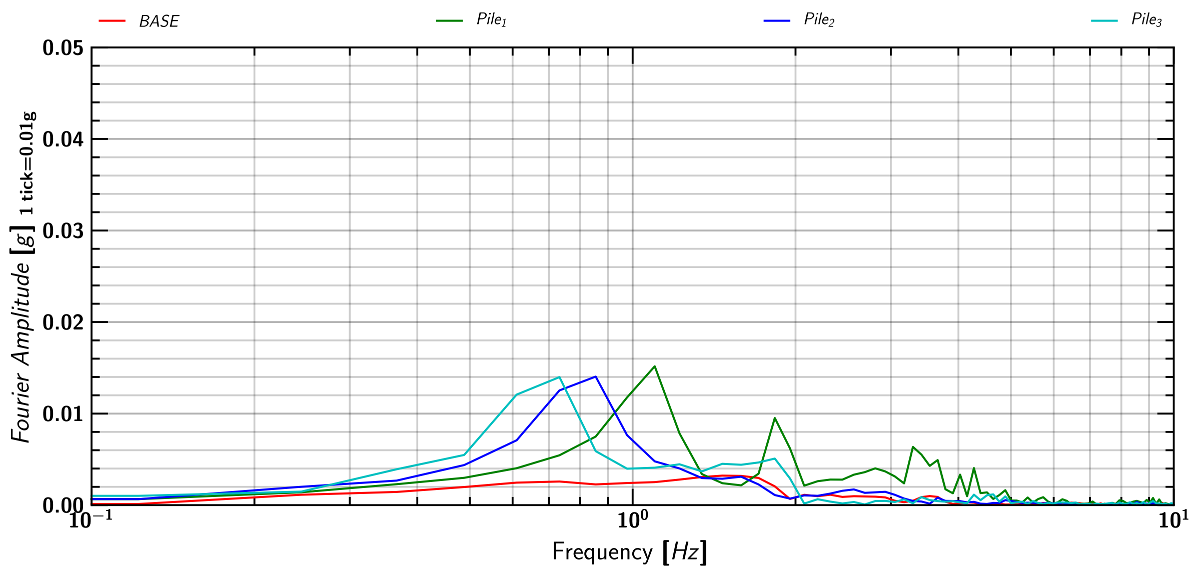

Figure 42. Dynamic response of piles during step wave motion SWM_2.

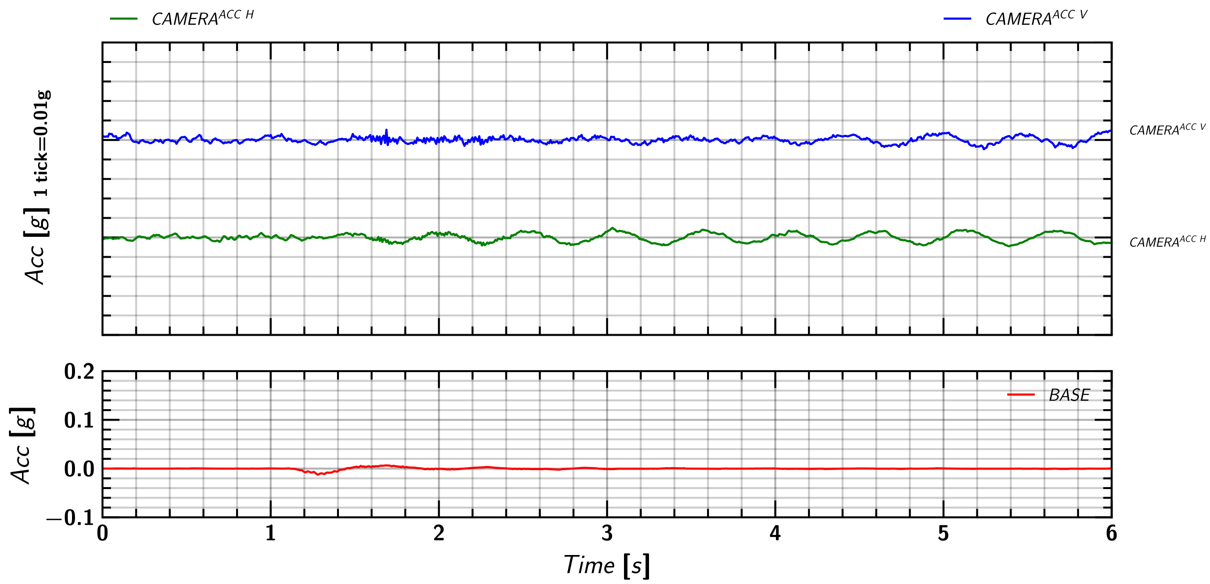

Note: BASE refers to the average of acceleration measured by EAST and WEST sensors.

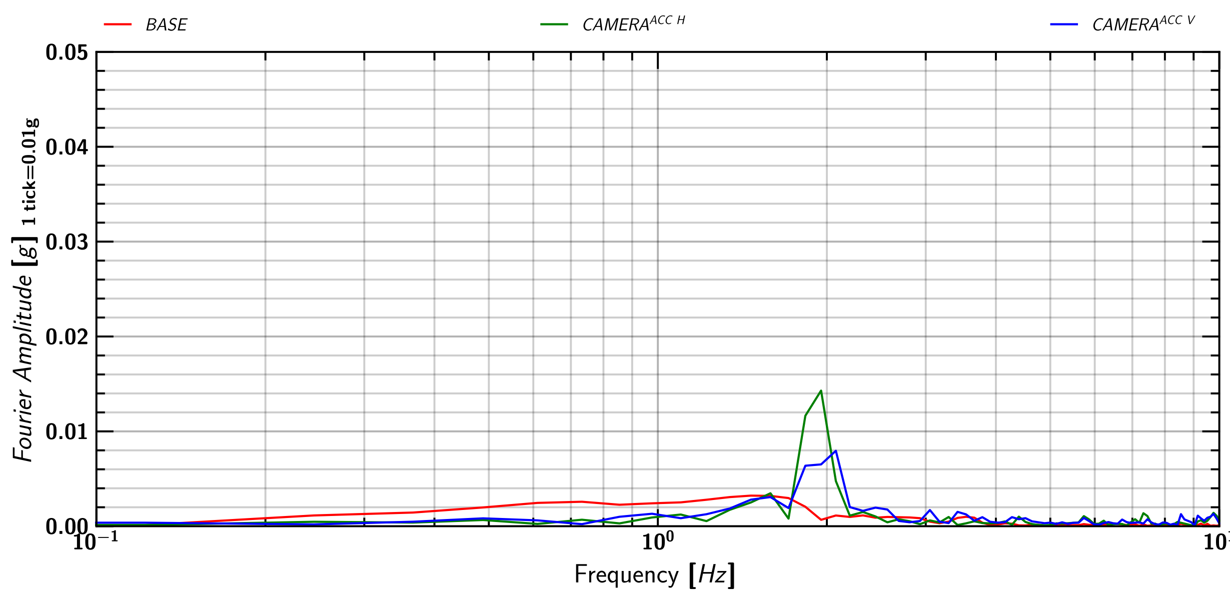

Figure 43. Dynamic response of camera beam during step wave motion SWM_2.

6.6 Soil and Pile Movement

The recordings from the Photron cameras were processed in TEMA (Image Systems Motion Analysis 2020). Sinha et al. (2021a) describes the process of obtaining 3D displacements using TEMA. 3D displacement fields were obtained for all the target markers (see Figure 44) placed on the model. The target markers placed on soil, pile, model container, and centrifuge bucket are summarized below.

Figure 44. Camera target markers placed on soil, pile, model container, and centrifuge bucket.

<u>Piles</u>

- *Pile 1*: P1-1, P1-2, P1-3, and P1-4
- *Pile 2*: P2-1, P2-2, P2-3, and P2-4
- *Pile 3*: P3-1, P3-2, P3-3, and P3-4

<u>Soil</u>

- *Row 1*: S1-1, S1-2, S1-3, S1-4, S1-5, S1-6, S1-7
- *Row 2*: S2-1, S2-2, S2-3, S2-4, S2-5, S2-6, S2-7
- *Row 3*: S3-1, S3-2, S3-3, S3-4, S3-5, S3-6, S3-7
- *Row 4*: S4-1, S4-2, S4-3, S4-4, S4-5, S4-6, S4-7
- *Row 5*: S5-1, S5-2, S5-3, S5-4, S5-5, S5-6, S5-7

<u>Container</u>

- *Top Ring*: C-1, C-2, C-3, C-4, C-5

<u>Bucket</u>

- *West Side:* F-0

APPENDIX E, G, I, K, and M, plots the lateral movement (i.e. X direction) and settlement (i.e. in Z-direction) of container, piles, and soil target markers in prototype scale. The plots show the movements relative to the top ring of the container (i.e., relative to the average movement of target markers C-1 to C-5). The Y-movement of the target markers are not shown in these plots. There magnitude was small and did not present any useful information in the analysis.

The plots also show the cumulative relative movement of target markers during each spin. The reference time for obtaining the cumulative movements was taken at the beginning of step wave motions SWM_1 and SWM_2 for Spin 1 and Spin 2, respectively. Since the video recordings were discontinuous and were taken only at specific times during each event, when they were processed to obtain cumulative readings, errors could have been introduced from the change in position of the target markers while processing the images for each event. As a result, the cumulative readings presented in this report should be taken carefully as only a qualitatively estimate of target markers movement. However, the computed movement presented within each individual event (once the target marker position was fixed) is accurate.

The sub-sections in the appendix are:

- *Container Movement in X and Z direction*
- *Soil (Row 1 i.e., S1-#) Movement in X and Z direction*
- *Soil (Row 2 i.e., S2-#) Movement in X and Z direction*
- *Soil (Row 3 i.e., S3-#) Movement in X and Z direction*
- *Soil (Row 4 i.e., S4-#) Movement in X and Z direction*
- *Soil (Row 5 i.e., S5-#) Movement in X and Z direction*
- *Pile 1 Mass (P1-#) Movement in X and Z direction*
- *Pile 2 Mass (P2-#) Movement in X and Z direction*
- *Pile 3 Mass (P3-#) Movement in X and Z direction*

Please note that the plots do not include the results of the target points that could not be tracked properly.

Note: The archived data includes both the position data and the displacement data and can be downloaded from DesignSafe.

6.7 Shaking Events

In total five earthquake shaking events were applied to the model with three Santa Cruz motions and two EJM01 motion. Table 27 lists these motions.

Table 27. Applied earthquake motions.

Motion	***Recording***	***Filename***
Santa Cruz	1989 Loma Prieta earthquake - UCSC/Lick Lab, Ch. 1 - 90 degrees	SC60696.txt
EJM01	Modified Northridge Motion (Malvick et al. 2002)	EJM01.txt

The chronological order in which the five motions EQM_1-EQM_5 are applied is shown in Table 24. The description of the motions and the achieved peak ground acceleration (PGA) is shown below. The results are plotted in the APPENDIX[1].

- EQM_1: Small Santa Cruz Earthquake (PGA=0.026g): see APPENDIX D
- EQM_2: Medium Santa Cruz Earthquake (PGA=0.14g): see APPENDIX F
- EQM_3: Large Santa Cruz Earthquake (PGA=0.24g): see APPENDIX H
- EQM_4: Large EJM01 Modified Northridge Motion (PGA=0.40g): see APPENDIX J
- EQM_5: Large EJM01 Modified Northridge Motion (PGA=0.40g): see APPENDIX L

Note: The recorded centrifuge data was corrected with post-excavation sensitivities as shown in RESQAQ Tables (Table 7 to Table 22). The processed data (as reported in this report and plots) are archived in DesignSafe.

For all the sensors (except instrumented piles) the post-excavation sensitivities were almost same to the sensitivities before testing (also referred as during construction phase in this report). For the piles, the post-excavation sensitivities were more representative and accurate as they were obtained by a more careful calibration. Since, the instrumented piles had some sensitivity to bending (see discussion in SKS02 data report (Sinha et al. 2021b)) and the calibration device was not perfectly aligned, the orientation of the pile effected the calibration results.

The correction from the change in sensitivity can be applied as follows.

$$\text{Corrected Data} = \text{Raw Data}\,\frac{\text{Approximate sensitivity (i. e. obtained during Construction Phase)}}{\text{More accurate sensitivity (i.. e. obtained Post Excavation)}}$$

All figures shown in the Appendix plots the corrected data as obtained from the above equation. For all the sensors, the sensitivities during construction phase and the post-excavation sensitivities are reported in tables in Section 4. As an example: the sensitivities for the instrumented piles are summarized in Table 11, Table 13, and Table 15 for Pile 1, Pile 2, and Pile 3, respectively under section 4.3.

6.7.1 EQM Event Plots

Appendix A, B, and C plot the slowly sampled data throughout the course of each spin. These long duration plots are useful for understanding the sequence of the test and for observing slow processes such as consolidation of the clay. The high-speed data is shown for each earthquake motion in the APPENDIX sections listed above.

For each EQM event the following plots are shown.

- *Input motion:* The applied motion measured by EAST and WEST sensor. An average of these motions is represented as BASE motion, where BASE=0.5(EAST+WEST).
- *Spectral Acceleration:* Spectral acceleration computed for the input motion (BASE), Pile 1, Pile 2, and Pile 3.
- *Container Acceleration:* Response of accelerometers attached to the container.
- *Soil Acceleration:* Response of accelerometers placed in soil.

[1] To plot the response of each sensors, an initial offset reading was applied for each centrifuge spin as described below.

- PPT_1- PPT_{28} – offset reading at 1g, corrections made for pore-pressure at 1 g.
- Accelerometers ($ACC_{\#}$)– offset reading was taken as just before the start of event.
- Axial strain gages – offset reading at 1 g.

- *Pile Mass Acceleration:* Response of accelerometers placed on pile mass.
- *Soil and Pile Mass Lateral Movement in X direction:* Movement of the piles and nearby soil in the shaking (X) direction. The movement of the pile mass in X direction was computed by taking the average movements of target markers (P1-1,P1-2) for Pile 1, (P2-1,P2-2) for pile 2, and (P3-1 , P3-2) for Pile 3. The soil target markers selected nearby the piles were S2-1, S2-4, and S2-7 respectively for Pile1, Pile 2, and Pile 3. It also shows the contour plot of the soil movement at the end of shaking and after full reconsolidation. From the contour plots lateral movement of soil in +X direction was observed i.e., the soil moved towards the south end of the container.
- *Soil and Pile Settlement (movement in Z direction):* Settlement of the piles and the nearby soil (i.e., movement in Z direction). The settlement of the pile masses was computed by taking the average settlement of target markers (P1-1,P1-2) for Pile 1, (P2-1,P2-2) for pile 2, and (P3-1 , P3-2) for Pile 3. The soil target markers selected nearby the piles were S2-1, S2-4, and S2-7 respectively for Pile1, Pile 2 and Pile 3. It also shows the contour plot of the soil settlement at the end of shaking and after full reconsolidation. The settlement contour shows that the surface settlement was non-uniform. Large settlements were observed in the center of the container and smaller towards the edges. Since during construction the soil at the surface was flat and not curved in accordance with the g-field, this would have resulted in larger settlement in the middle of the container and smaller towards the edges.
- *Pore pressure:* Measured pore pressure in soil by Keller and MS54XXX transducers.
- *Excess Pore pressure Ratio (r_u):* The excess pore pressure ratio (r_u) in soil was estimated using the formula $r_u(t) = (u(t) - u_o)/\sigma'_{vo}$, where u_o and σ'_{vo} is the hydrostatic and initial vertical effective stress respectively before the start of EQM event and u is the pore pressure at any given time (t) during the event. To compute the effective stress (σ'_{vo}), the total stress (σ_{vo}) was computed based on the initial densities and layer depth as summarized in Table 2.
- *Axial Load:* Axial load measured by the strain gages installed in the piles. The apparent oscillations of axial load were thought to be primarily associated with the cross-axis sensitivity of the axial strain gauges. Although the bridges were designed to optimize the sensitivity to axial load, small errors in the alignment of the piles and the installation of the gauges lead to moment sensitivity, and we do expect large moments to develop in the piles as a result of the lateral shaking. To remove/reduce the effect of moment on the axial load measurements during shaking, a moving mean with a window of 6 seconds is taken for the recorded axial load by the strain gages (shown as dashed line).
- *Pore pressure and Axial Load Profile:* Plot of axial load profiles for pile 1 and pile 2 and pore pressure profiles with depth. It must be noted that the axial load profiles use the moving mean data of the axial measurements (shown as dashed line in Axial Load plots) to remove/reduce the effect of moment on the measured axial responses during shaking.

Note: Unless specified, raw data measured from the sensors are shown in the plots. During the event, some of the sensors failed and might show erratic responses. Some of the MS54XXX transducers that failed have not been reported in these plots. The legend of color used to show different soil layers in these figures is shown in Figure 45. Additionally, for convenience the color legend is provided in the footer of each page.

Dense Sand	Medium Dense Sand	Clayey Silt	Loose Sand	Clay Crust

Figure 45. Legend of colors used for showing different soil layers in the plots shown in APPENDIX.

7 MODEL DISSECTION

On completion of the test, the model was moved to the model prep room and its surface was scanned with a 3D handheld scanner, to preserve the surface digitally for future measurements. Figure 46 show the 3D model of the scanned surface. Following that, dissection of the model was carried out. The model was cut carefully longitudinally from the west to east side of the container as shown in Figure 46 and Figure 47.

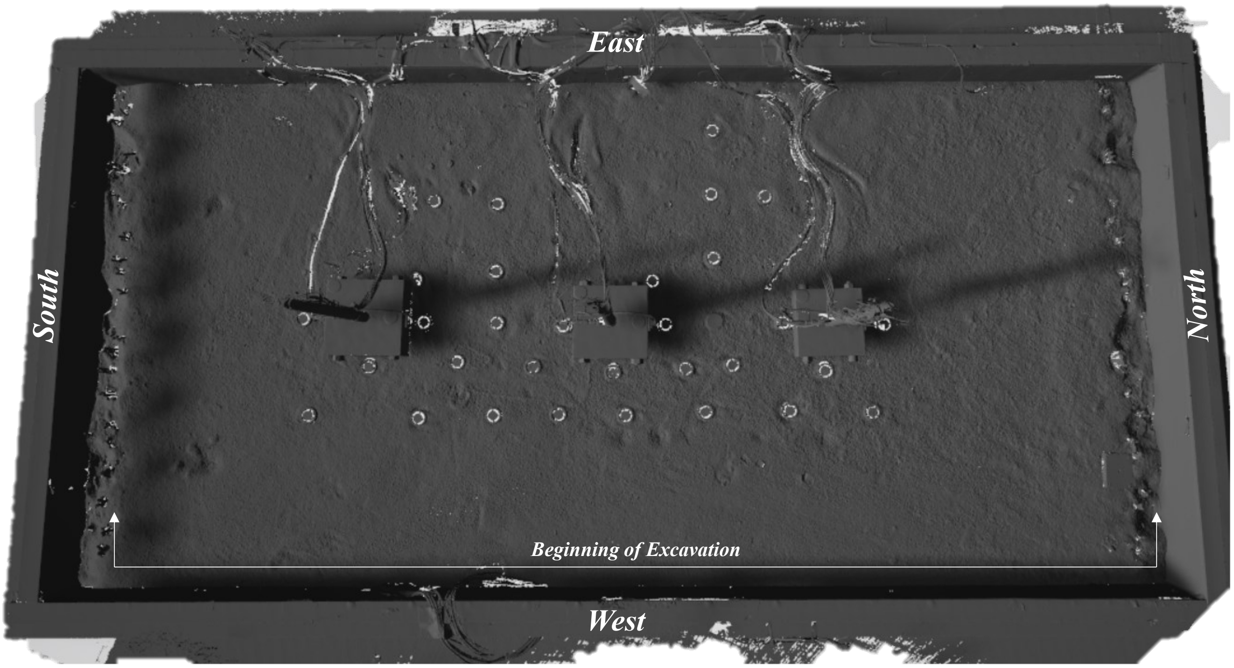

Figure 46. 3D surface mapping of the model using a hand-held surface scanner.

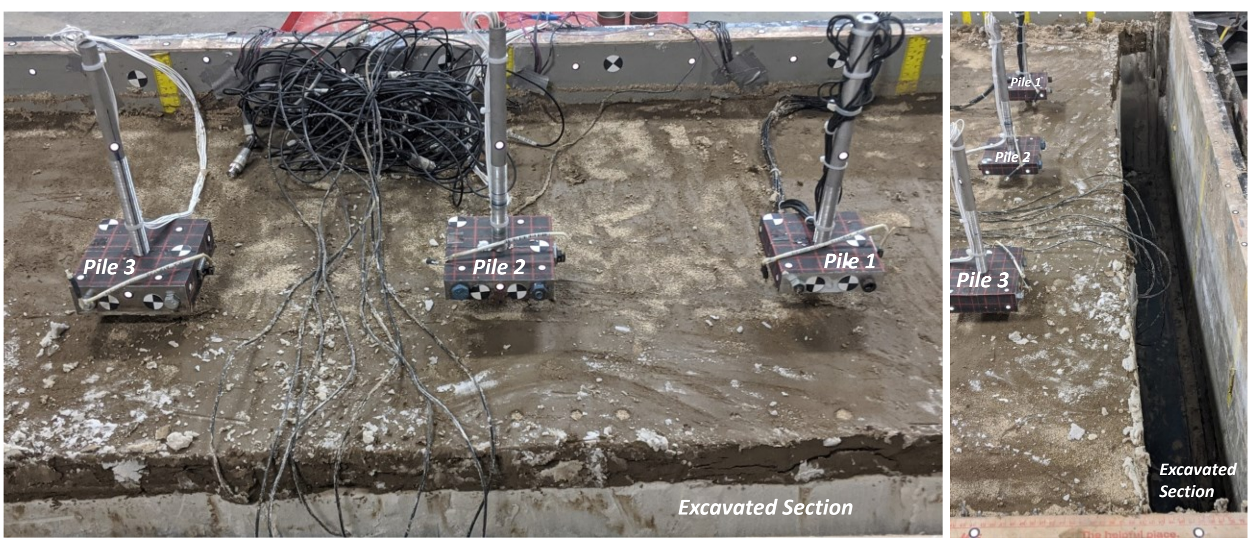

Figure 47. View of model during dissection.

7.1 Cracks in the Clay Crust

The clay layer in the model was expected to develop cracks during shaking. The top Monterey sand layer was carefully removed as shown in Figure 48. Initially, no surface cracks were found to be clearly visible.

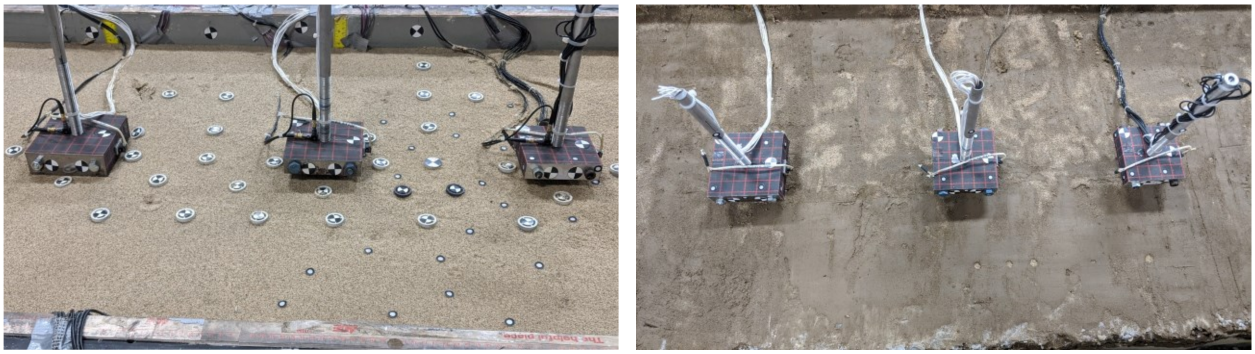

Figure 48. Removal of the Monterey sand layer to expose the clay crust.

As excavation continued (from the west side of the model), surface cracks started to be more clearly visible on the top of the clay layer. The force required to cut the layers and possibly desiccation from drying of clay could have stressed the soil especially in the weak hairline cracks zones, making them larger. Figure 49 maps few of the surface cracks observed in the clay layer during the dissection process.

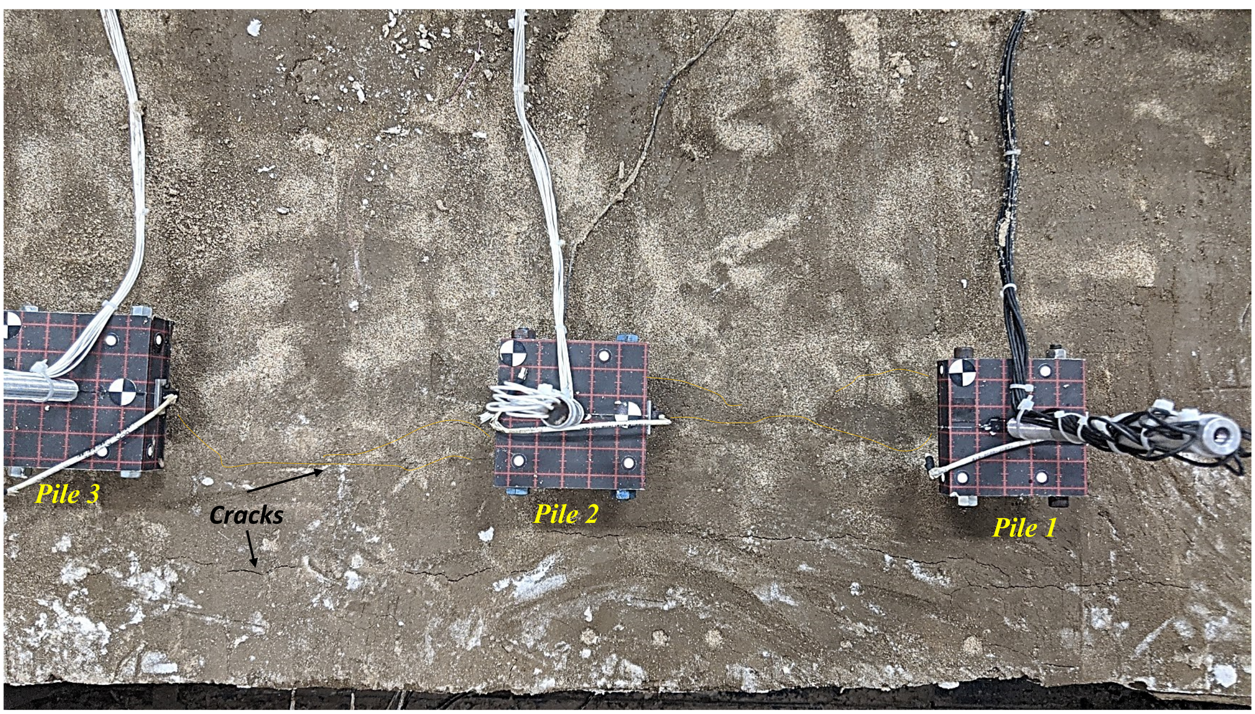

Figure 49. Cracks observed on the clay surface. Major cracks are clearly visible by the naked eye whereas few fine hair-like cracks are shown in brown color.

Continued excavation further, exposed more cracks on the surface and near the piles. Figure 50 shows the cracks growing near pile 1, pile 2, and pile 3. The way cracks propagated during model excavation indicate the presence of initial fine hairline cracks from the conducted centrifuge test.

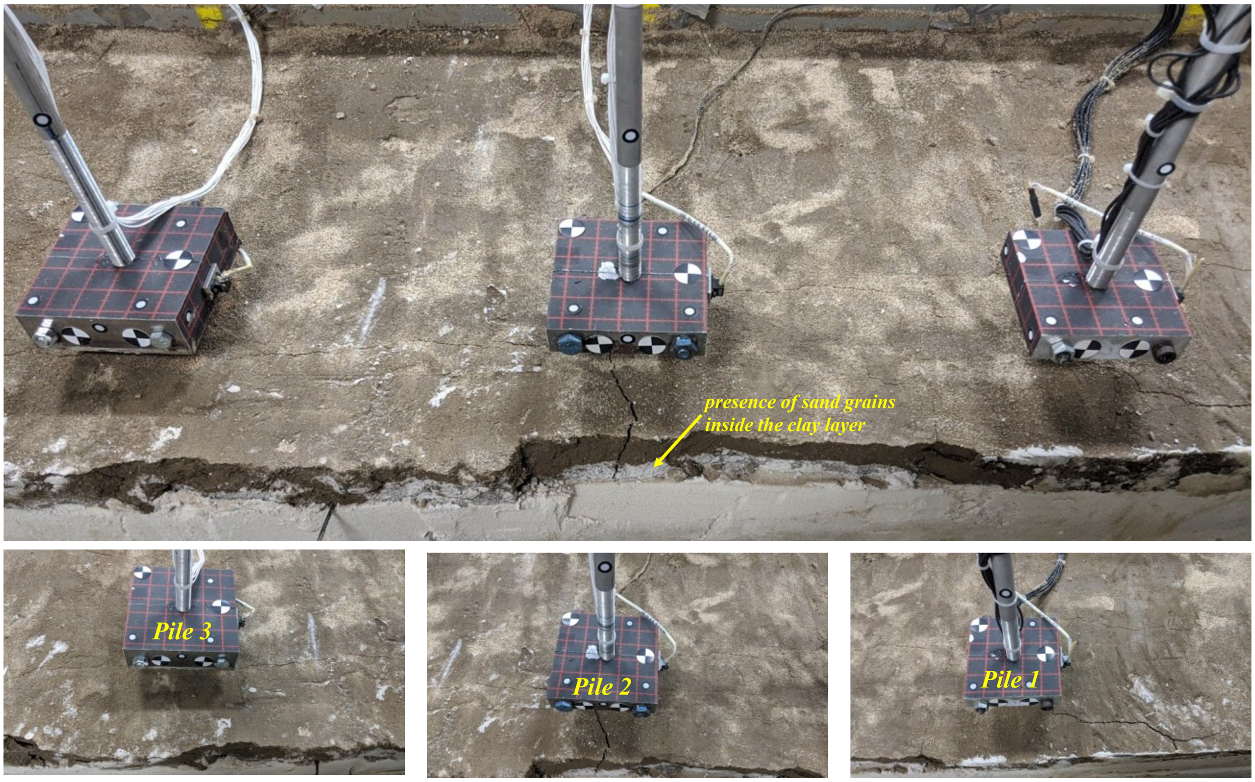

Figure 50. Surface ejecta observed in the model.

With careful inspection of model cross-section during excavation process, loose sand beneath the clay layer was seen to have risen inside the cracks from bottom of the clay layer (see Figure 51). This indicated the presence of boils in the loose soil beneath the clay layer. During shaking, the liquefied soil must have tried to escape from the cracks of the clay layer to the surface but could not achieve so because of the small size of the cracks and low permeability of the clay layer. Consequently, no surface manifestations of sand boils were observed during testing. Figure 51 and Figure 52 show a cross-section view of a crack in the clay layer and the migration of sand particles from the layer beneath.

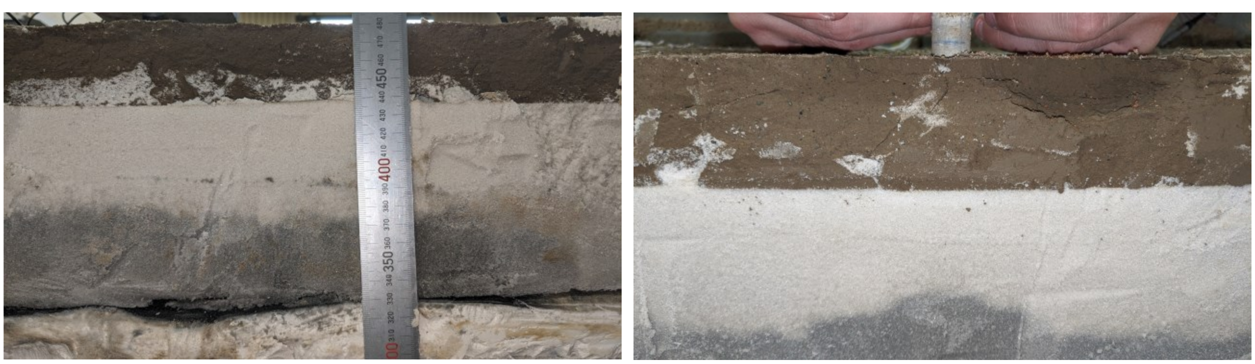

Figure 51. Cross-section view of cracks in the clay layer and migration of sand particles in them from the layer beneath.

Figure 52. Cross-section view of the model showing movement of sand grains inside the clay layer from the soil beneath.

Chunks of clay crust samples were carefully extracted to expose the cracks beneath the clay layer. Figure 53 and Figure 54 shows the bottom of the clay layer with exposed cracks. In Figure 53 (right), sand particles can be seen inside these cracks. While one would expect these cracks to have initiated from shaking events, Figure 54 reveal that some of these cracks might have already been present inside the clay layer from the way it was placed in the model. Figure 54 shows clumps at the bottom of the clay layer like the way it was placed in model.

Figure 53. A view of the bottom of the clay layer showing presence of cracks.

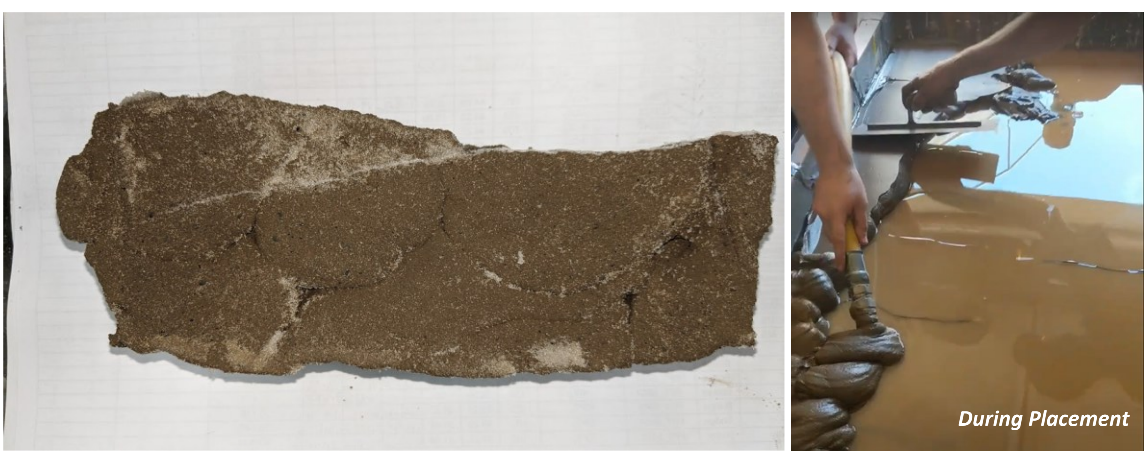

Figure 54. The bottom of the clay layer (on left) can be seen in clumps, like the way it was placed in the model (right).

7.2 Ejecta

Figure 55. Ejecta observed below the clay layer

The migration of sand particles from the layer beneath to inside the clay layer provided evidence of the initiation of sand boils during the test. Figure 55 shows one of the most prominent of the incipient sand boil found at the mid-south end of the model.

7.3 Soil Settlement

Several measurements were taken during model dissection to measure the change in position of the soil layers and colored sand layers placed during model construction. The measurements were taken at different longitudinal (North-South) and (East-West) sections and are summarized in Table 28. Figure 56 (left) shows the model cross-section with all the soil layers during excavation. An average final soil settlement profile is also shown in the Figure 56 (right). Please note that the black color appearing in the sand layer is a result of mold (fungus) that could have grown while the model was sitting in the model preparation room for about a week before the excavation began. When the excavated surface was exposed in air for a day, the mold disappeared, and the color changed back from black to white.

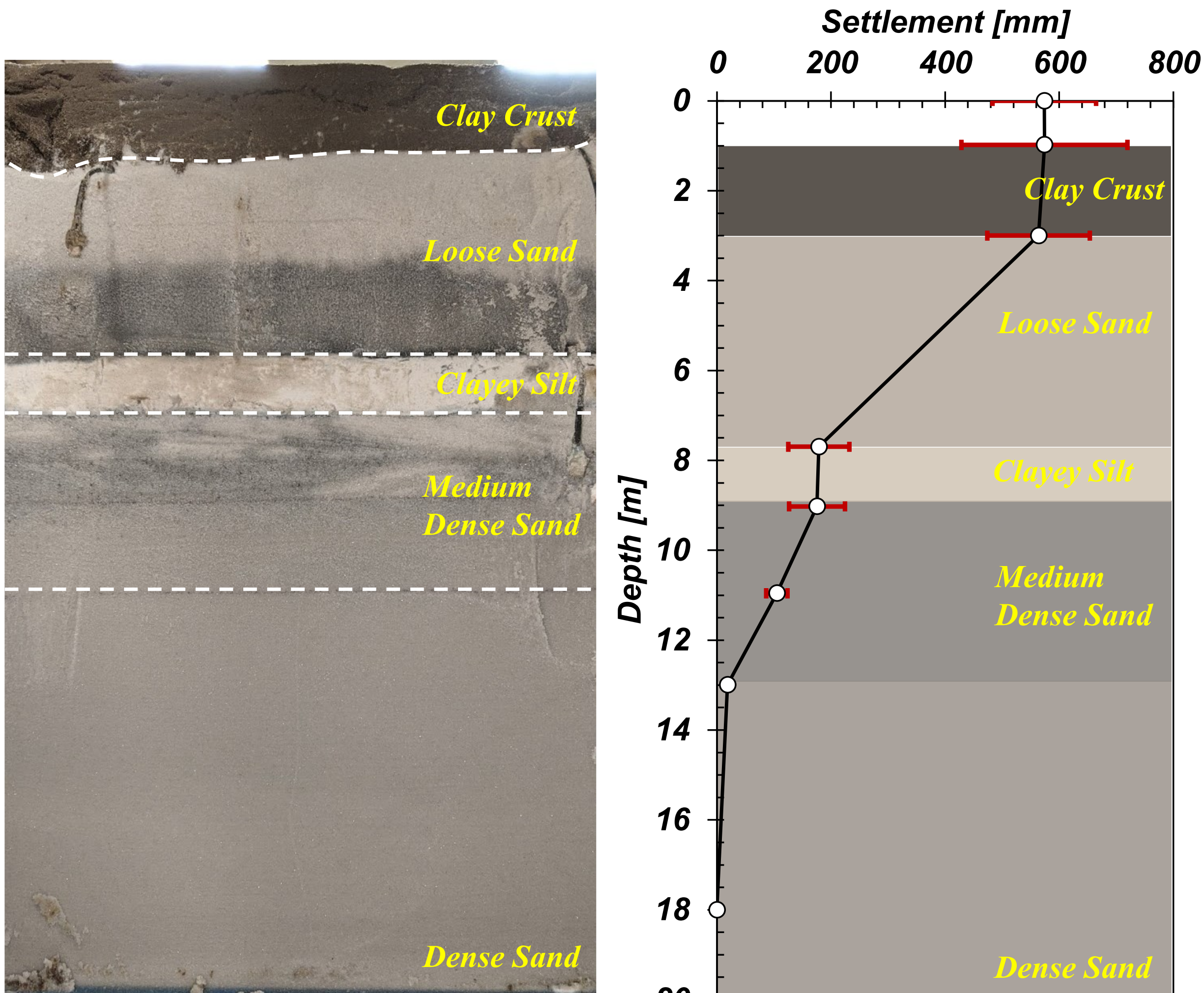

Figure 56. Model cross-section showing soil layers (left) and average soil settlement profile (with ± one standard deviation) at prototype scale.

Table 28. Coordinates of soil layers measured (in model scale) across multiple sections during model dissection.

		Z coordinate of layers during model excavation [mm]					
X [mm]	**Y [mm]**	**Top of Clay Crust Layer**	**Top of Loose Sand Layer**	**Top of Clayey Silt Layer**	**Top of Medium Dense Sand Layer**	**Middle of Medium Dense Sand Layer**	**Top of Dense Sand Layer**
1430	618	488	436.5	326	293.5	247.5	200
1200	618	488	438	327	294	246.5	199.5
840	618	489.5	438	326.5	294	247	200
640	618	487	438	327.5	296.5	247	199.5
480	618	485	435	327	294.5	247	200
300	618	484	434	326	293.5	246.5	199.5
1430	520	488.2	428.4	328.4	295.3	249.5	200.1
1200	520	487.4	437.5	326.5	295.1	248	199.2
1000	520	486.4	439.2	329.7	296.8	249.6	198.6
840	520	487.3	438.5	328.4	296.5	246.8	200.2
640	520	484.3	439.5	328.7	295.4	248.1	199.8
480	520	484.5	436.4	329.7	294.7	249.5	200.6
300	520	485.3	432.8	325.5	292.4	245.7	199
1430	390	486.7	430.6	326.1	295.3	250.8	199.5
1200	390	483.8	434.2	325.9	295.6	247.8	200
1000	390	485.3	436.6	323.7	294.7	247.8	200.5
840	390	484.6	434.3	327.8	292.6	248.6	200.7
640	390	482.2	436.4	330.6	295.2	249.9	199.6
480	390	481.9	435.6	331.4	296.4	247.8	199.2
300	390	484.4	436.4	330	293.5	250.2	199.3
1430	300	488.1	430.4	326.1	295.6	248	199.8
1200	300	485.2	423.3	325.6	294.7	248.4	199.3
1000	300	486.9	437.5	330.1	293.8	247.9	199.6
840	300	488	439.4	329.8	295.7	249.8	200.1
640	300	482.8	440.7	332.2	298.9	249.8	199.9
480	300	483.2	439	332.4	297.2	249.7	200.1
300	300	483.4	436.1	332.2	293.8	249	199.2
1430	150	491.9	431.4	324.6	295.8	249.3	200.1
1200	150	487.6	437.1	328	293.7	249	199.9
1000	150	489.4	438	325.8	294.9	249.9	199.7
840	150	487.5	439.2	329.1	296	249.2	199.8
640	150	487.6	439.1	328.9	294.2	248.9	199.8
480	150	488.4	439.7	329.9	296	248.9	199.9
300	150	486.5	435.6	329.4	294.8	248.7	199
Average Z coordinate [mm]		486.19	435.95	328.13	295.02	248.47	199.74
Standard Deviation		2.27	3.64	2.25	1.34	1.23	0.46
Z During Construction [mm]		500.54	450.05	332.6	299.4	251.1	200.2
Average settlement [mm]		14.35	14.10	4.47	4.38	2.63	0.46
Prototype Depth [m]		1.0	3.0	7.7	9.0	11.0	13.0
Prototype Settlement [mm]		574.2	563.9	178.7	175.3	105.1	18.6

-All dimensions are in model scale unless stated otherwise

7.4 Pile Settlement

Surface measurements were taken to evaluate the settlement of the pile. All the piles appeared very vertical during the excavation process. The pile tip positions before and after the test are summarized in Table 29. Figure 57 and Figure 58 shows the cross-section view of the piles and the soil around it as observed during the excavation process.

Table 29. Summary of pile tip positions and tilt measured (at model scale) during model dissection.

	*Z Coordinate of Pile Tip [cm]**		*Settlement [mm]**
	After Pile Installation	*Post-Excavation*	
Pile 1	15.24	14.37	8.7
Pile 2	15.24	14.56	6.8
Pile 3	15.24	12.75	24.9

*All dimensions are in model scale

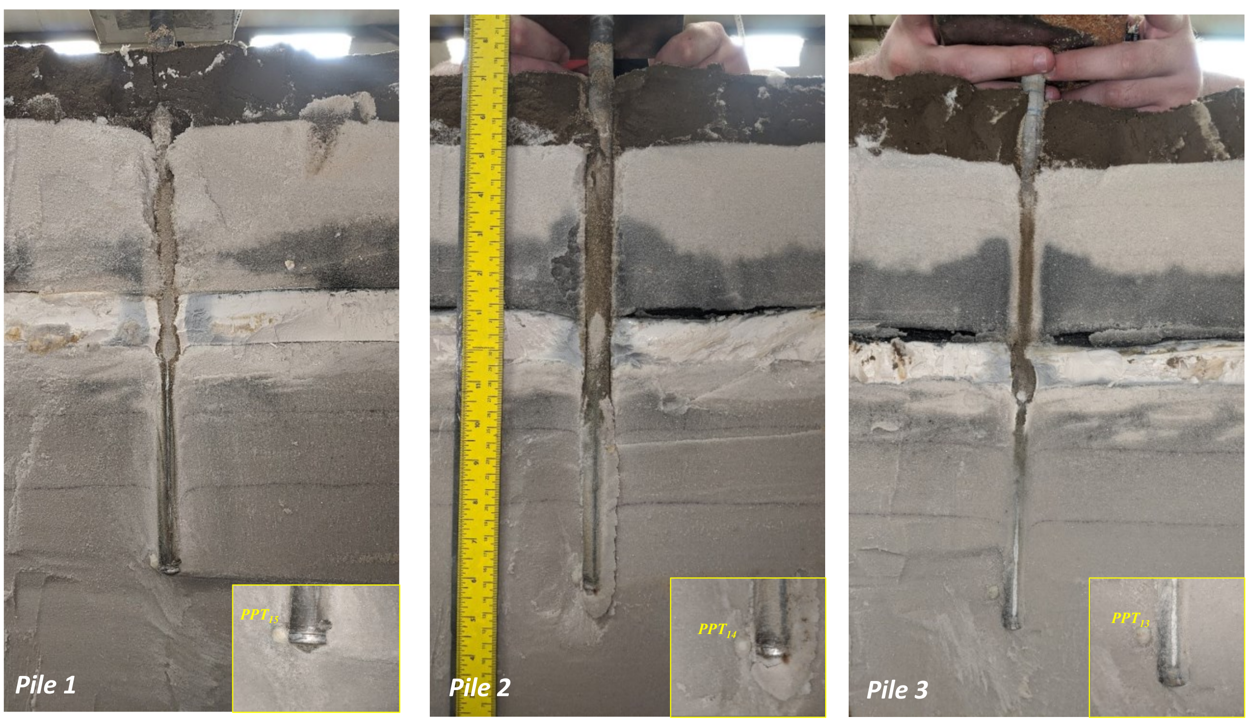

Figure 57. Cross-section view of Pile 1, Pile 2, and Pile 3 during the excavation process.

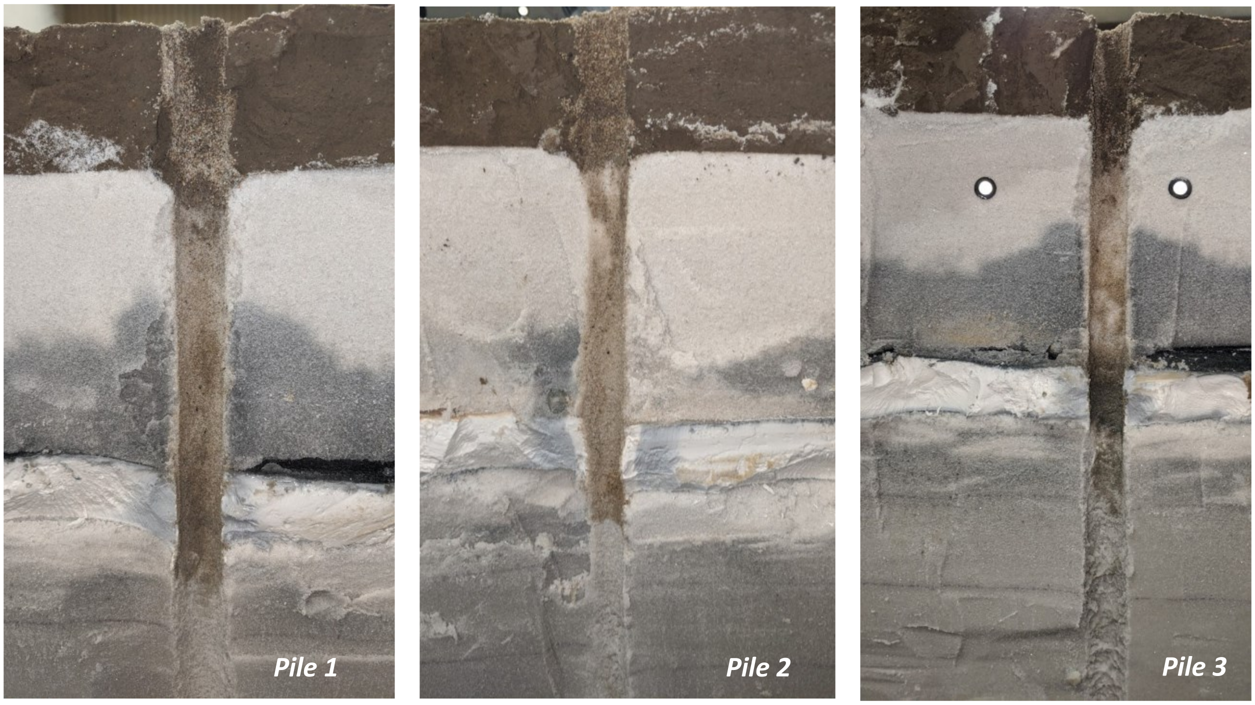

Figure 58. Cross-section view of soil around Pile 1, Pile 2, and Pile 3 during the excavation process.

7.5 Centrifuge Pile Load Test

Figure 59 shows the cross-section view of the Pile 1 after the end of pile load test PLT_2. Hand measurement before and after the test measured a tip penetration of 6.5 mm. The large penetration of the pile tip displaced and stressed the soil nearby creating a bulb like contours as shown in Figure 59. These contours could have been formed from the drying of the soil, and simultaneously the growing of the mold (fungus) in the dried regions. The shearing from the pile load test and the dilatancy of the soil near the pile, would have resulted in a local movement of water from the soil nearby towards the pile. This local variation in water content when dried could have resulted in the formation of contours around the pile. As a result, the contours indirectly represent the volume of stressed soil. Figure 59 (top-right corner) shows an inner bulb and an outer bulb. The color of the bulb indicates that the inner bulb (white color) was stressed more than the outer bulb (blackish color). The diameter of the inner and outer bulb was measured to be about 2 and 5 times the diameter (D) of the pile.

Figure 59. Cross-section view of Pile 1 after pile load test PLT_2.

7.6 Sensor Position and Recalibration

During model dissection, the new position of the sensors was recorded. The sensors were recalibrated to check the change in sensitivities. The depth and post-excavation sensitivities of the sensors are listed in Table 6 through Table 18. Figure 60 shows the view of the sensors during model dissection.

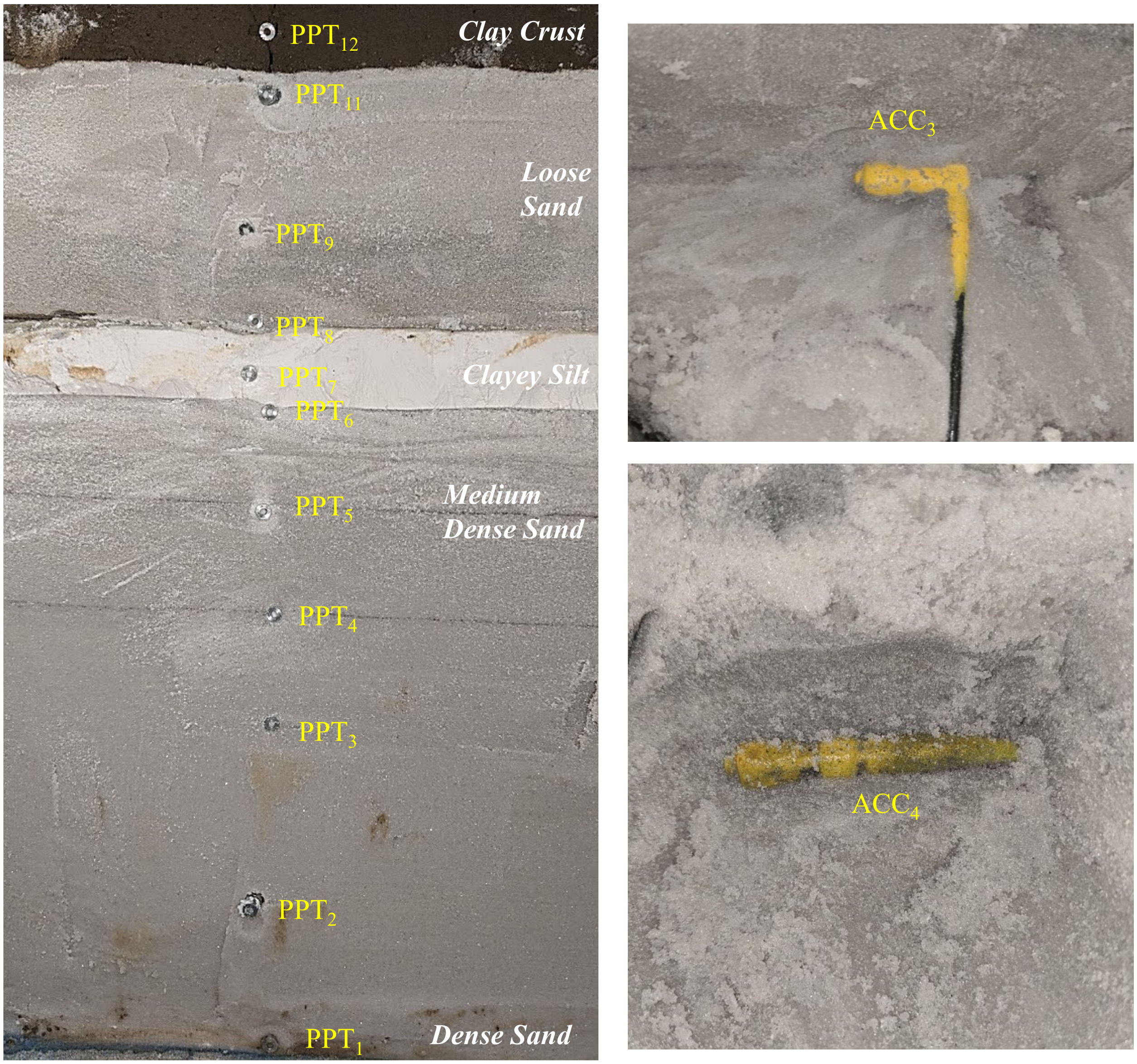

Figure 60. A view of the pore pressure transducers array and accelerometers during model dissection.

8 REFERENCES

Carey, T., Gavras, A., Kutter, B., Haigh, S. K., Madabhushi, S. P. G., Okamura, M., Kim, D. S., Ueda, K., Hung, W. Y., Zhou, Y. G., Liu, K., Chen, Y. M., Zeghal, M., Abdoun, T., Escoffier, S., and Manzari, M. (2018). "A new shared miniature cone penetrometer for centrifuge testing." *Physical Modelling in Geotechnics*, 1, 293–298.

Idriss, I. M., and Boulanger, R. W. (2008). *Soil liquefaction during earthquakes*. Earthquake Engineering Research Institute.

Image Systems Motion Analysis. (2020). *TEMA Classic 3D, Version 2020c*.

Kutter, B. L. (1992). "Dynamic centrifuge modeling of geotechnical structures." *Transportation Research Record*, (1336), 24–30.

Malvick, E. J., Kulasingam, R., Boulanger, R. W., and Kutter, B. L. (2002). *Effects of void redistribution on liquefaction flow of layered soil – centrifuge data report for EJM01*. Center for Geotechnical Modeling, University of California Davis.

Park, D. S. (2011). "Strength Loss and Softening of Sensitive Clay Slopes." University of California Davis.

Price, A. B. (2018). "Cyclic Strength and Cone Penetration Resistance for Mixtures of Silica Silt and Kaolin." University of California Davis.

Sinha, S. K., Kutter, B. L., Wilson, D., Carey, T., and Ziotopoulou, K. (2021a). *Use of Photron cameras and TEMA software to measure 3D displacements in centrifuge tests*. Center for Geotechnical Modeling, University of California Davis.

Sinha, S. K., Kutter, B. L., and Ziotopoulou, K. (2020). "New Method to Measure Vertical Displacement Using Laser lines and Cameras." *International Journal of Physical Modelling in Geotechnics*.

Sinha, S. K., Ziotopoulou, K., and Kutter, B. L. (2021b). *Centrifuge testing of liquefaction-induced downdrag on axially koaded piles : Data Report for SKS02*. Center for Geotechnical Modeling, University of California Davis.

Stewart, D., Chen, Y.-R., and Kutter, B. (2009). "Experience with the Use of Methylcellulose as a Viscous Pore Fluid in Centrifuge Models." *Geotechnical Testing Journal*, 21(4), 365.

APPENDIX

A. DAY 1 Spin 1

A.1 Pore Pressures in Soils

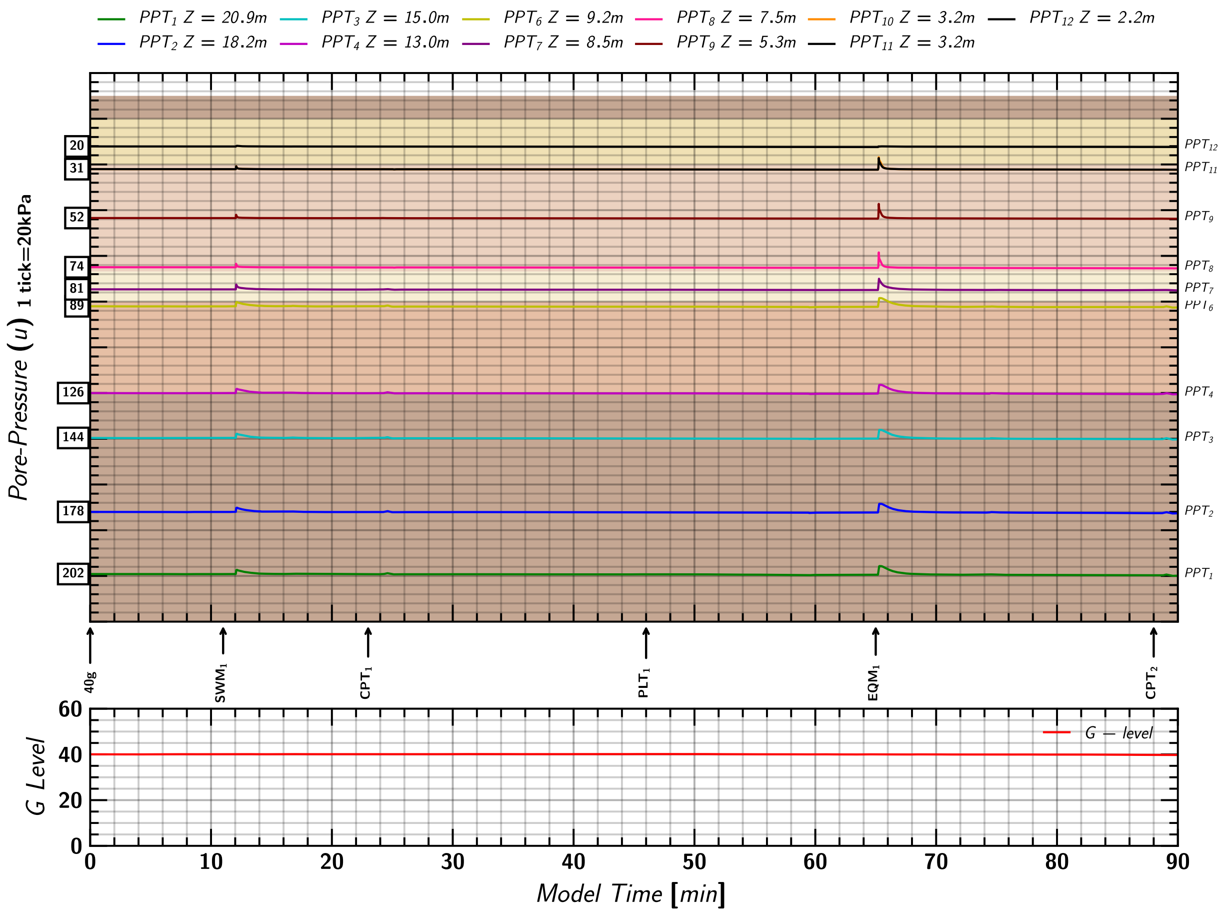

Figure 61. Day 1 Spin 1: Pore pressures measurements in soil from Keller transducers.

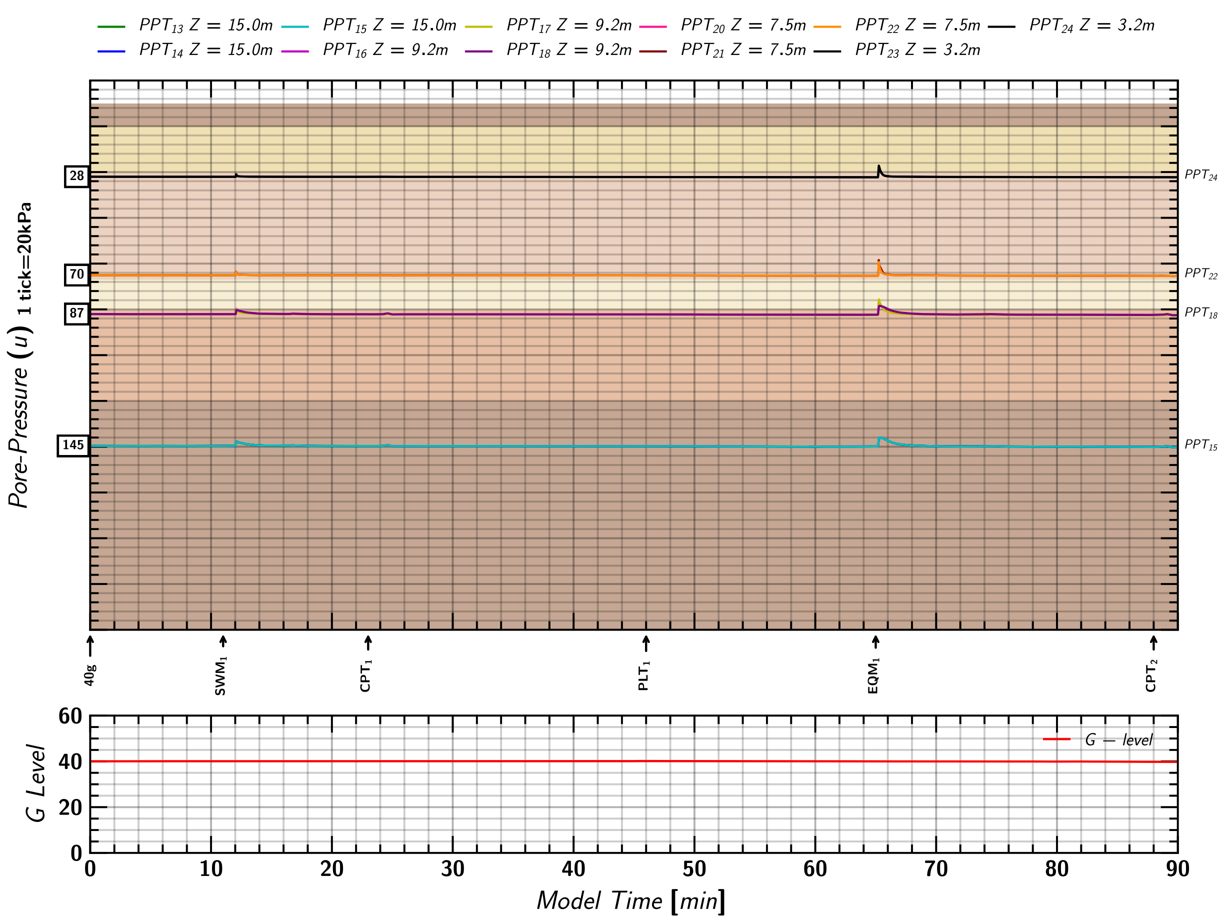

Figure 62. Day 1 Spin 1: Pore pressures measurements in soil from MS54XXX transducers.

A.2 Axial Load in Piles

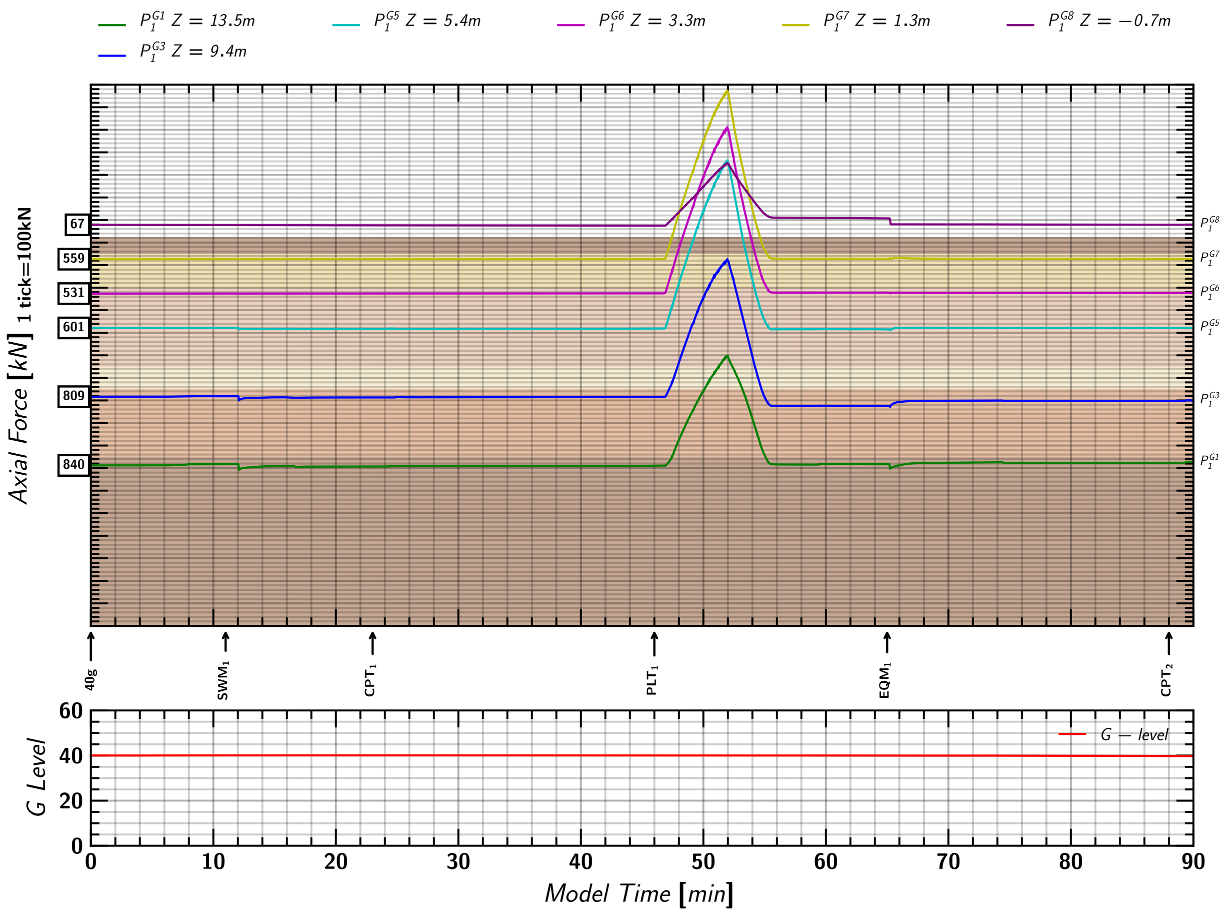

Figure 63. Day 1 Spin 1: Axial load measurements in Pile 1.

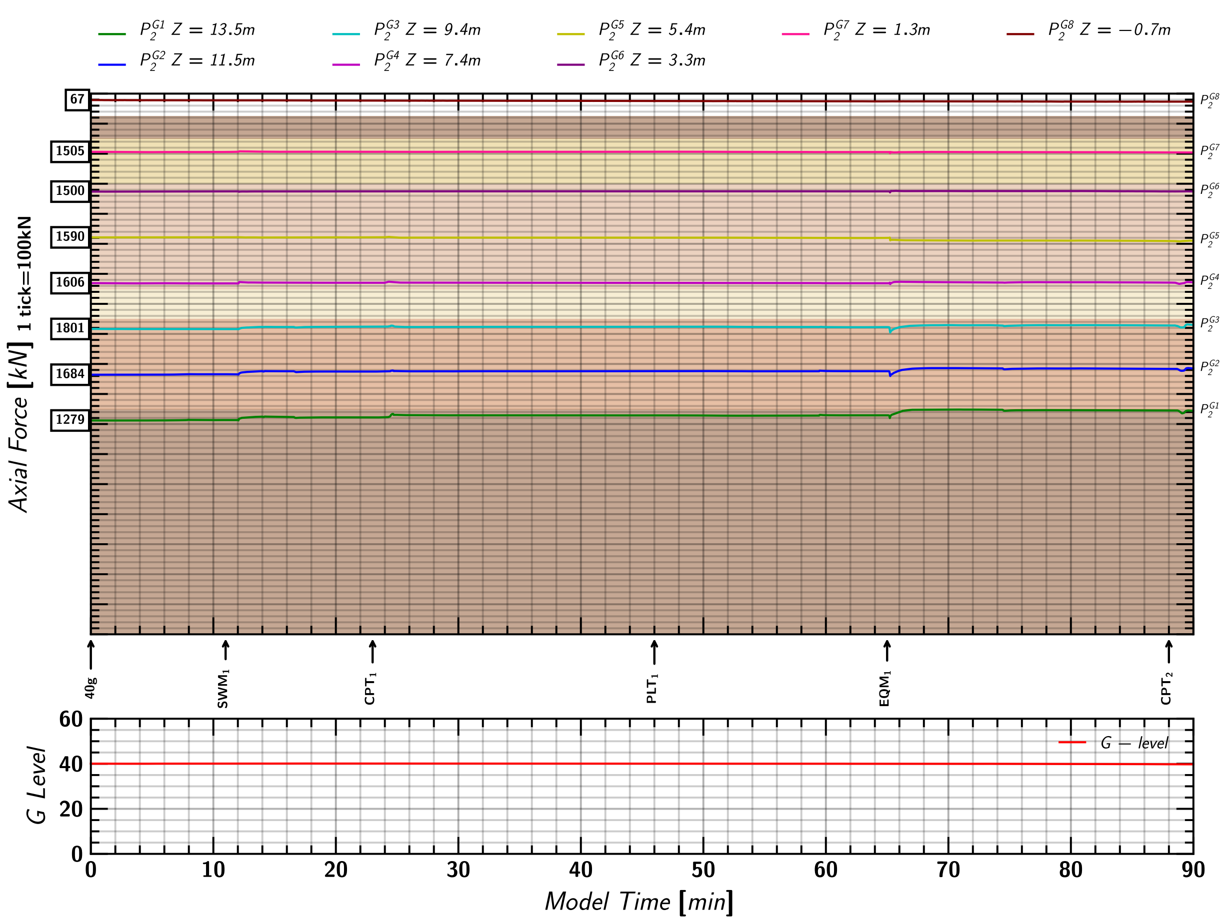

Figure 64. Day 1 Spin 1: Axial load measurements in Pile 2.

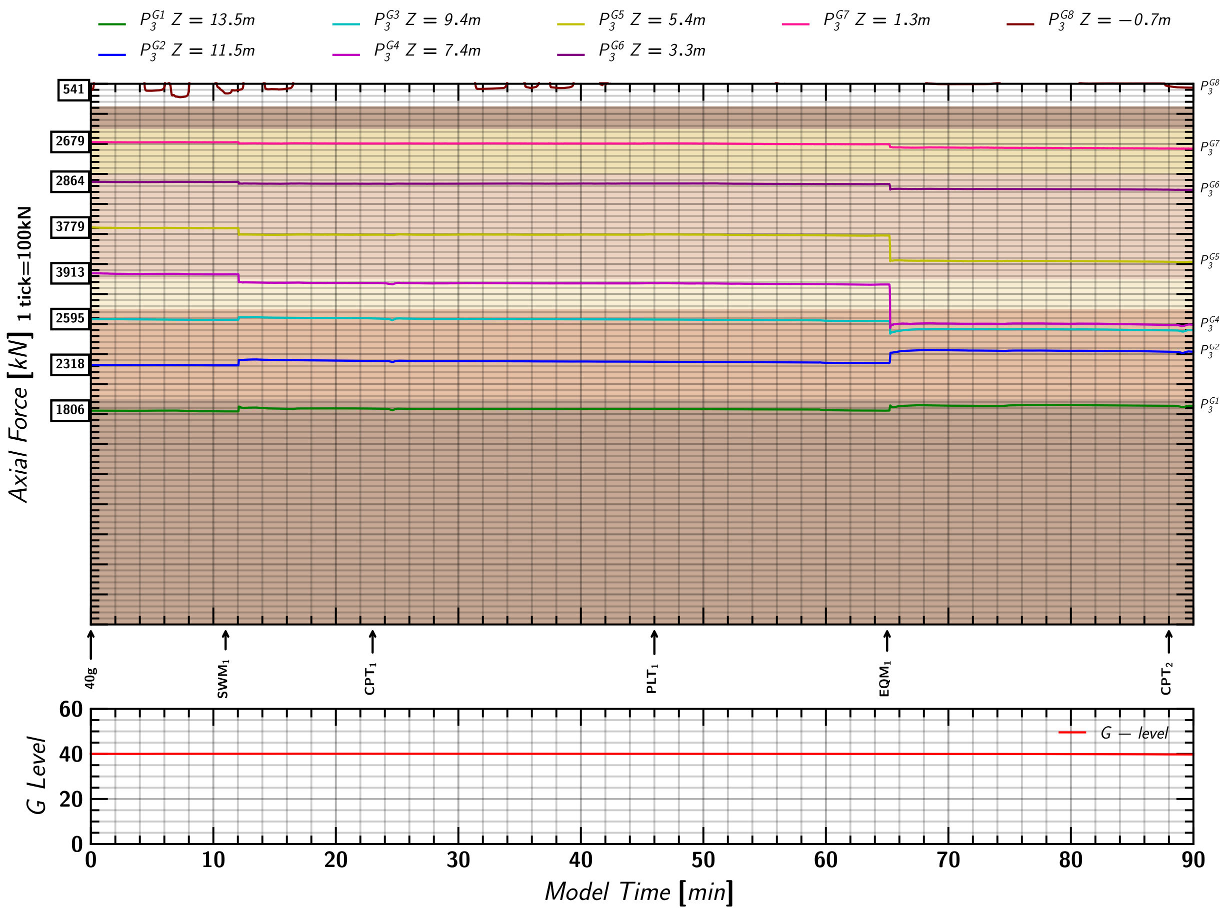

Figure 65. Day 1 Spin 1: Axial load measurements in Pile 3.

A.3 Pore pressure and Axial Load Profile

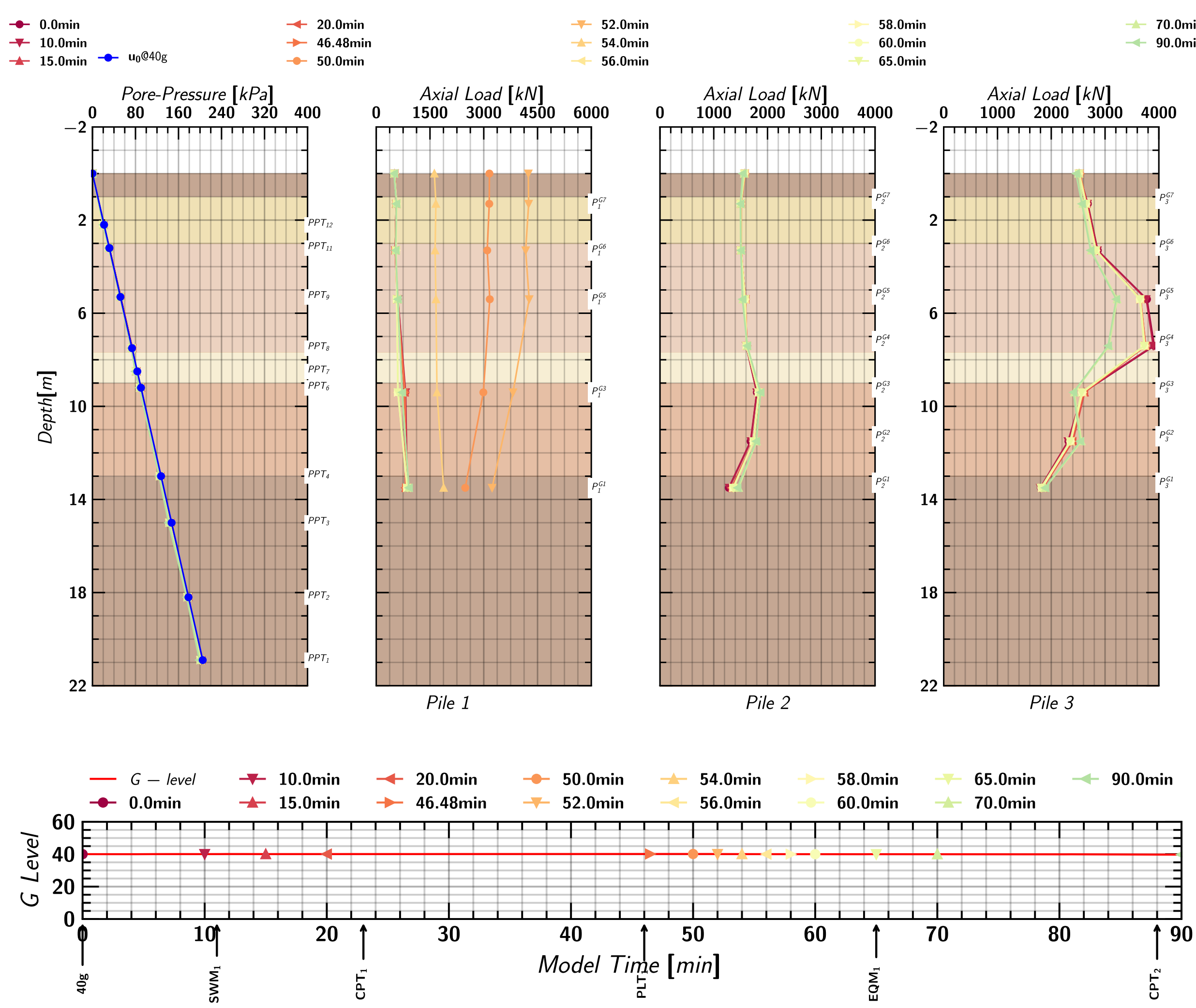

Figure 66. Day 1 Spin 1: Axial load profile of pile 1, pile 2 and pile 3 at different times during the test.

B. DAY 2 Spin 1

B.1 Pore Pressures in Soils

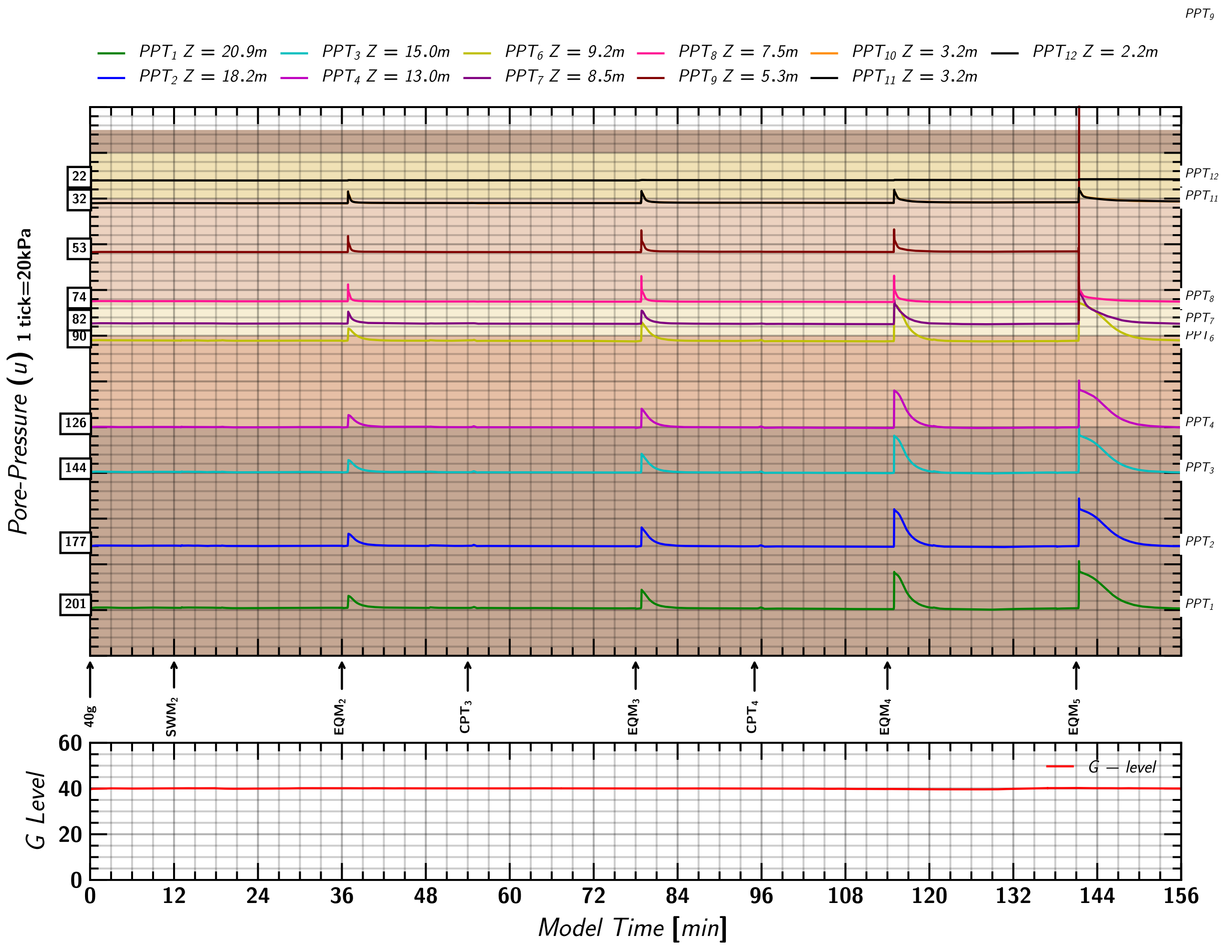

Figure 67. Day 2 Spin 1: Pore pressures measurements in soil from Keller transducers.

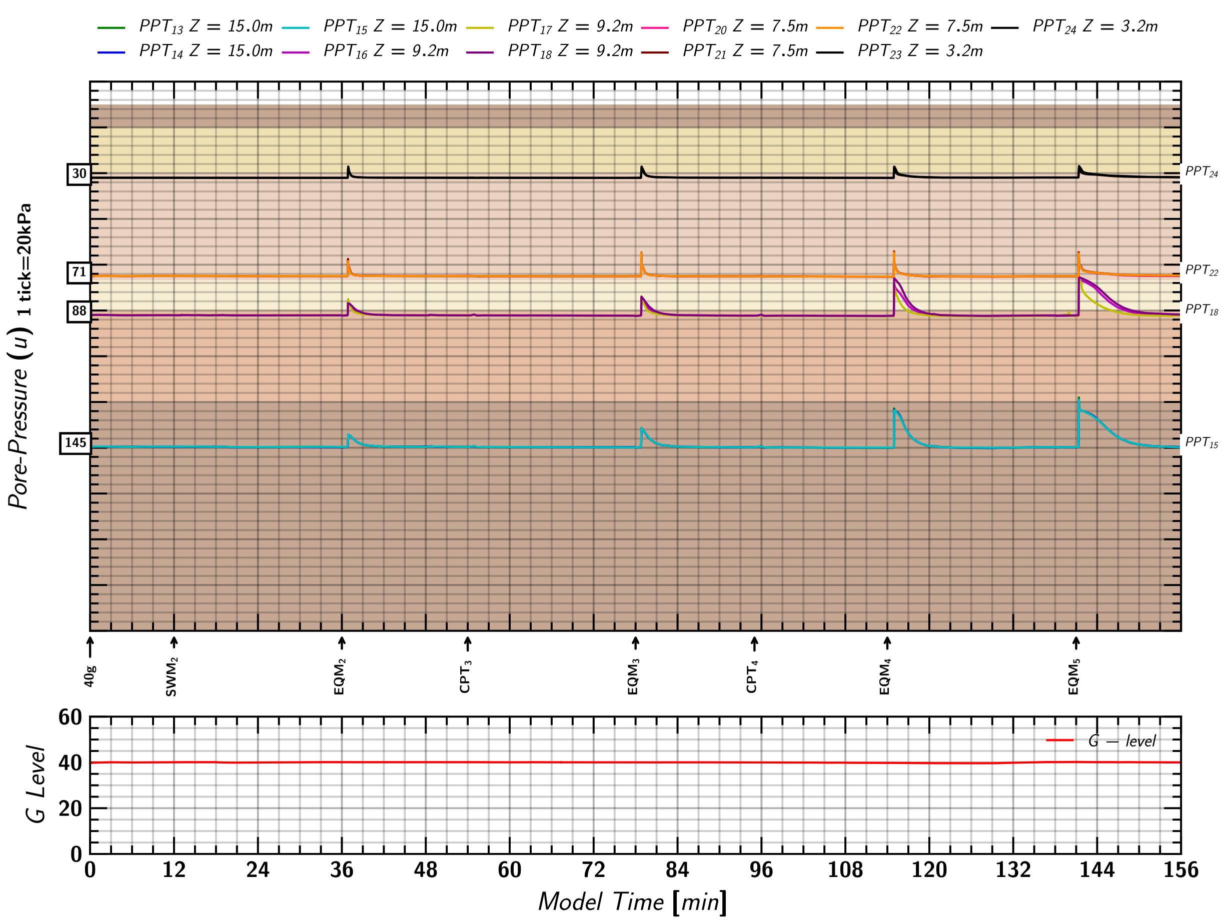

Figure 68. Day 2 Spin 1: Pore pressures measurements in soil from MS54XXX transducers.

Dense Sand | Medium Dense Sand | Clayey Silt | Loose Sand | Clay Crust

B.2 Axial Load in Piles

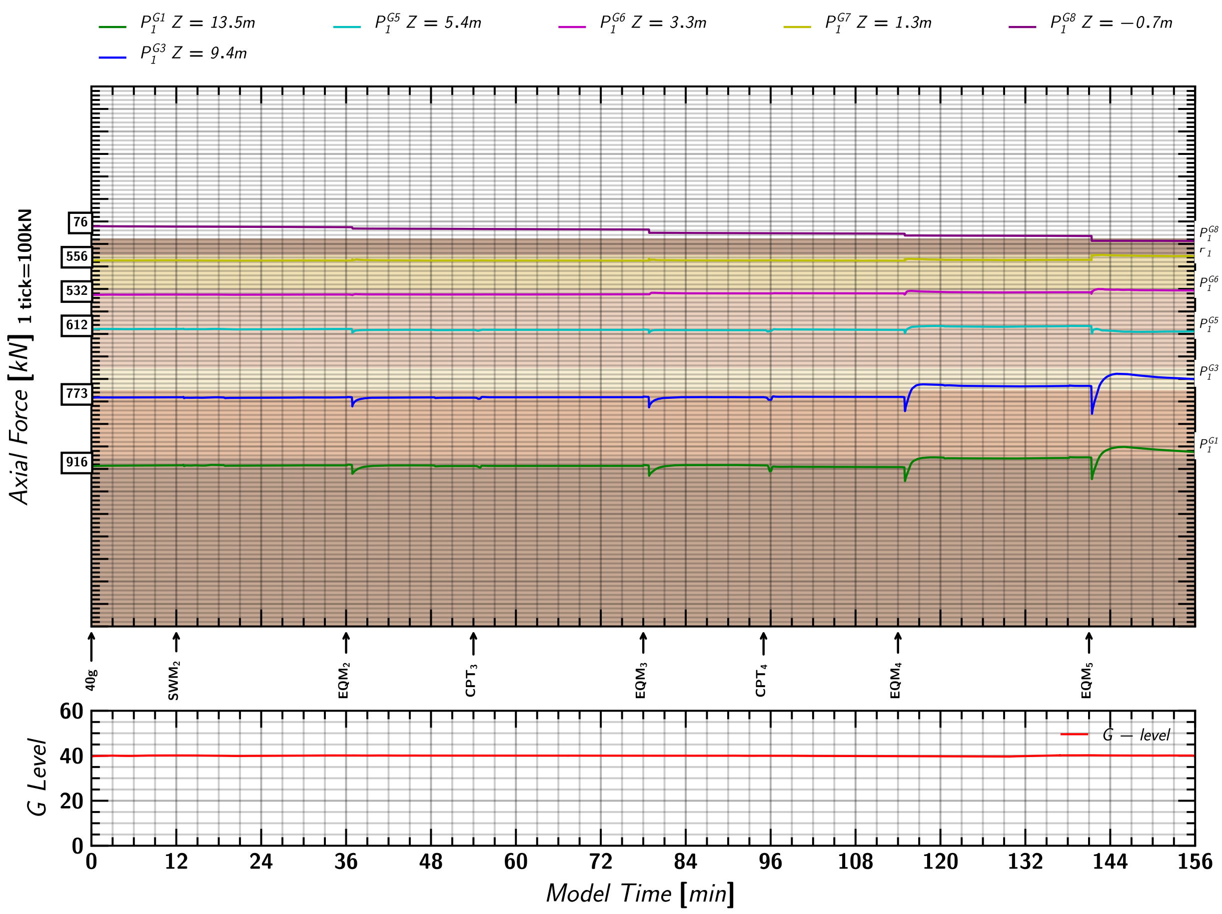

Figure 69. Day 2 Spin 1: Axial load measurements in Pile 1.

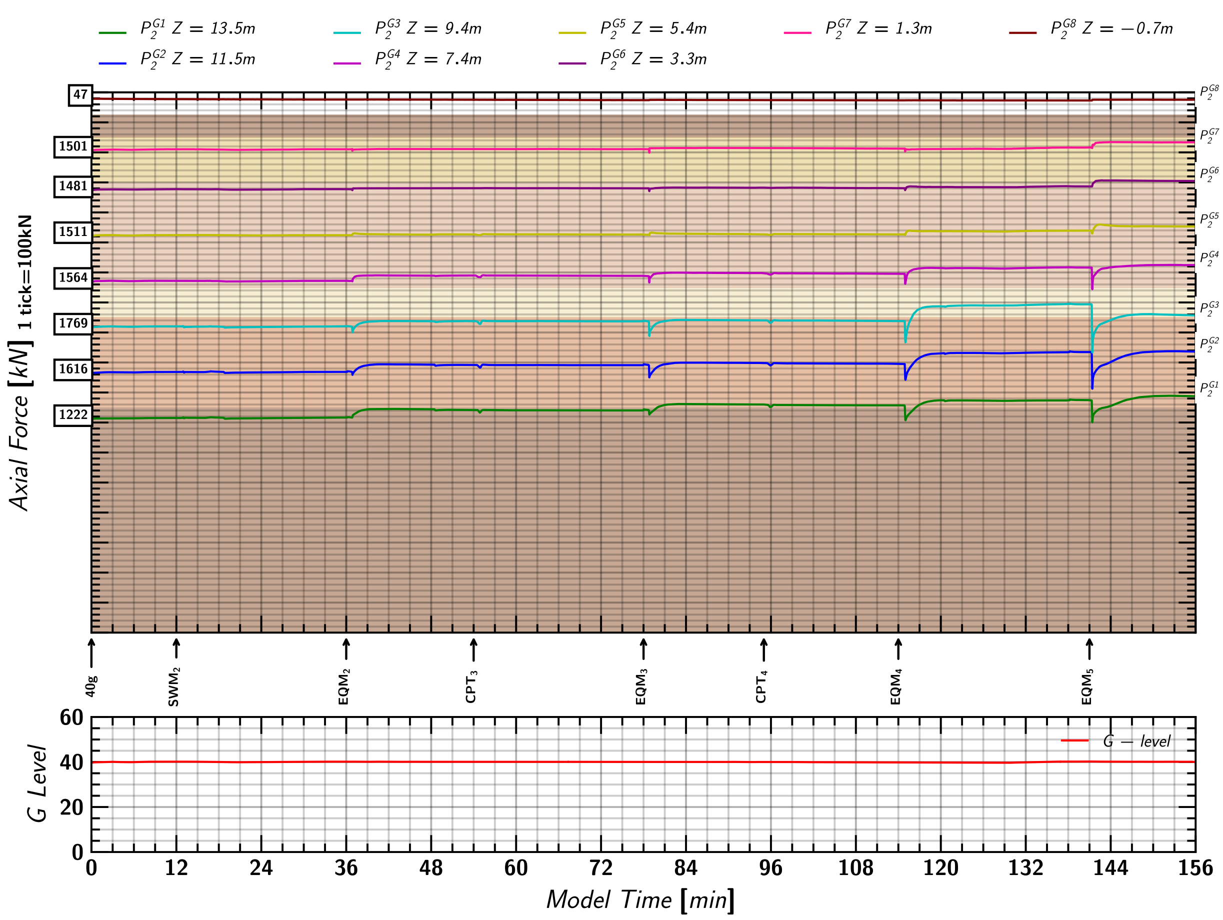

Figure 70. Day 2 Spin 1: Axial load measurements in Pile 2.

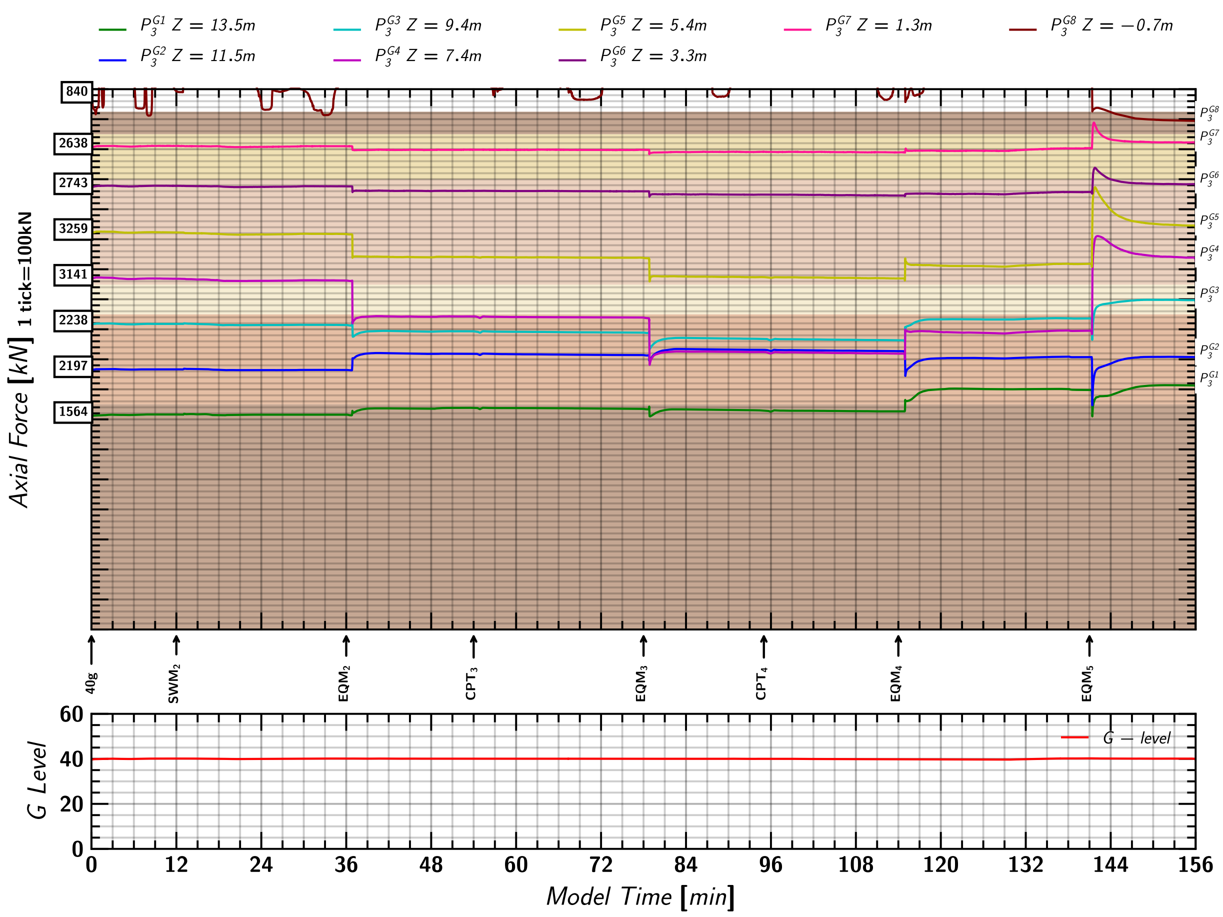

Figure 71. Day 2 Spin 1: Axial load measurements in Pile 3.

B.3 Pore pressure and Axial Load Profile

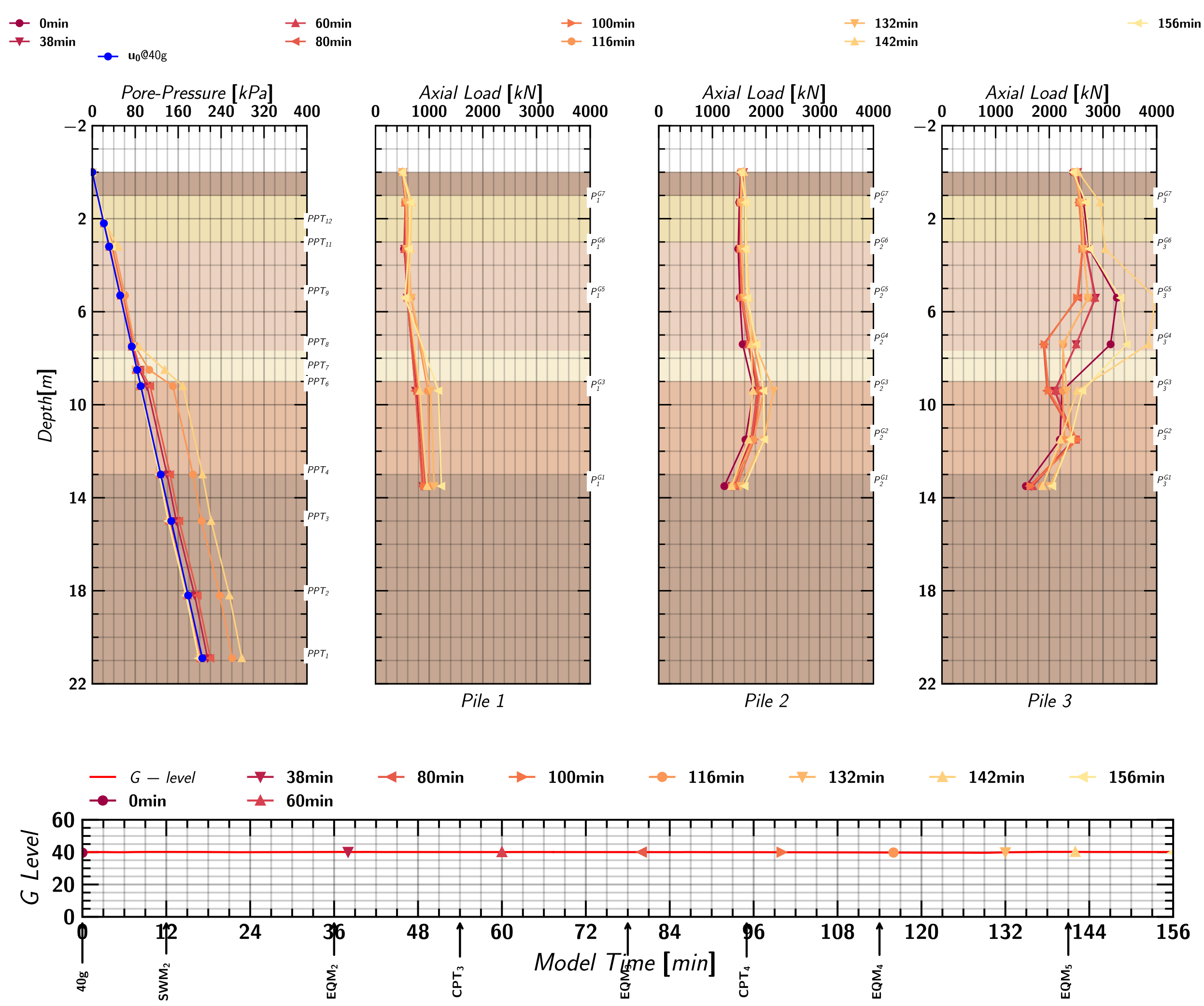

Figure 72. Day 2 Spin 1: Axial load profile of pile 1, pile 2 and pile 3 at different times during the test.

C. DAY 2 Spin 2

C.1 Pore Pressures in Soils

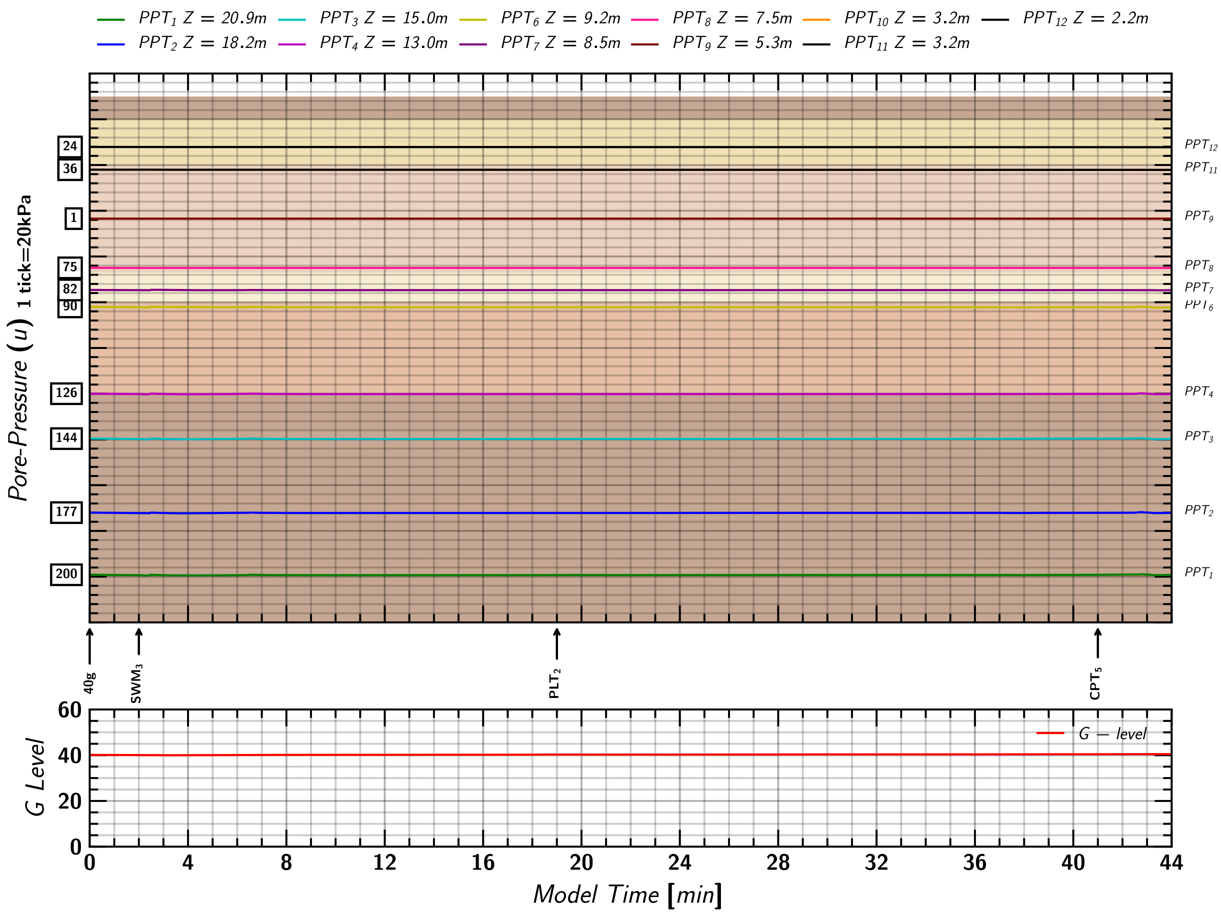

Figure 73. Day 2 Spin 2: Pore pressures measurements in soil from Keller transducers.

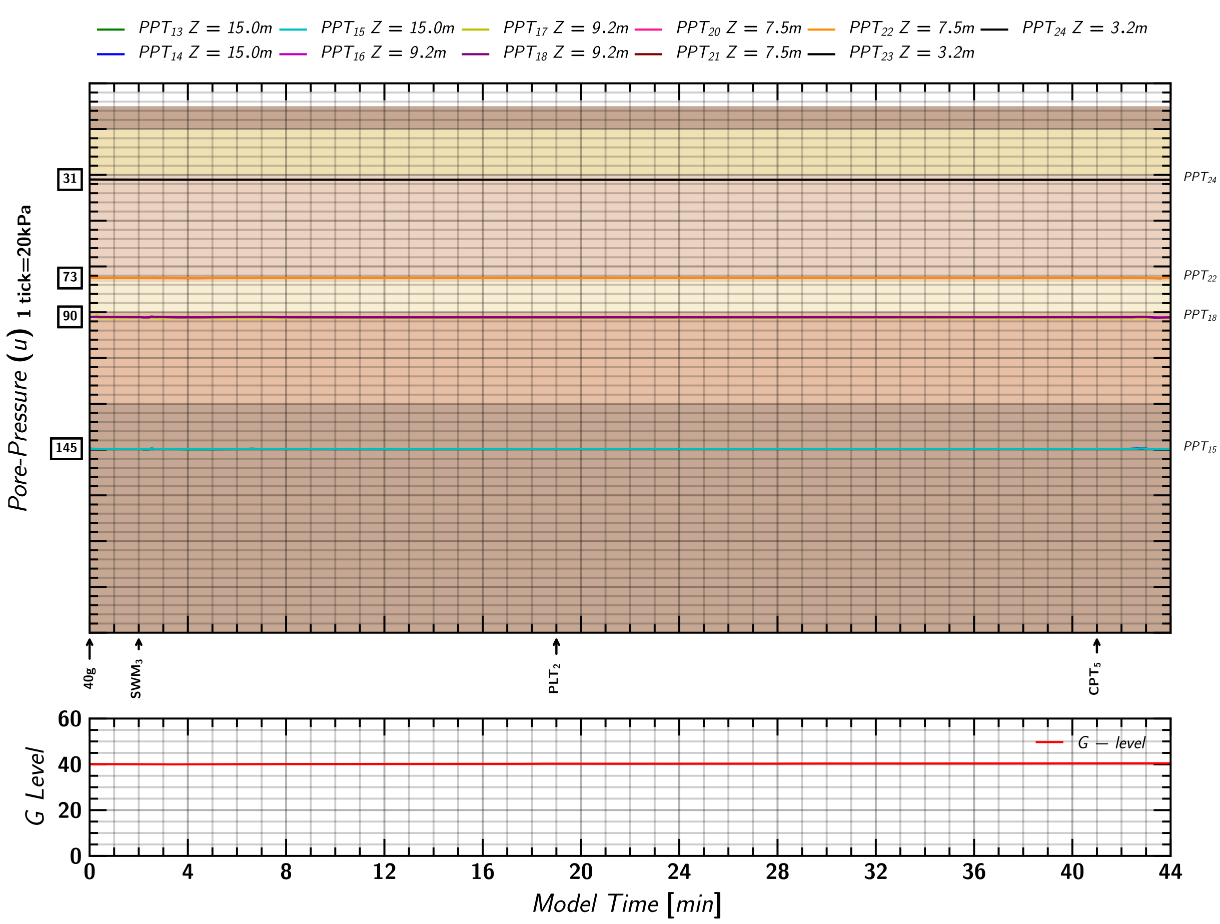

Figure 74. Day 2 Spin 2: Pore pressures measurements in soil from MS54XXX transducers.

C.2 Axial Load in Piles

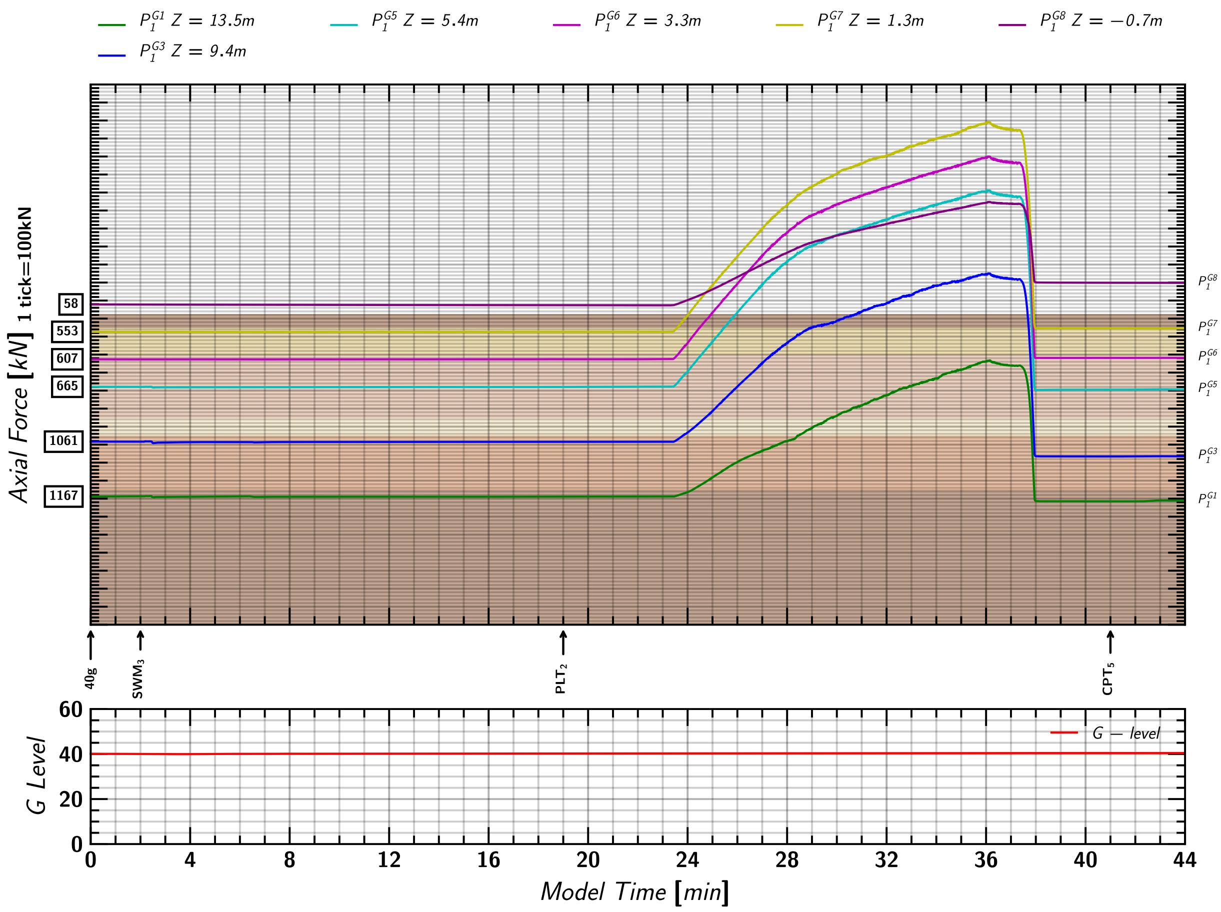

Figure 75. Day 2 Spin 2: Axial load measurements in Pile 1.

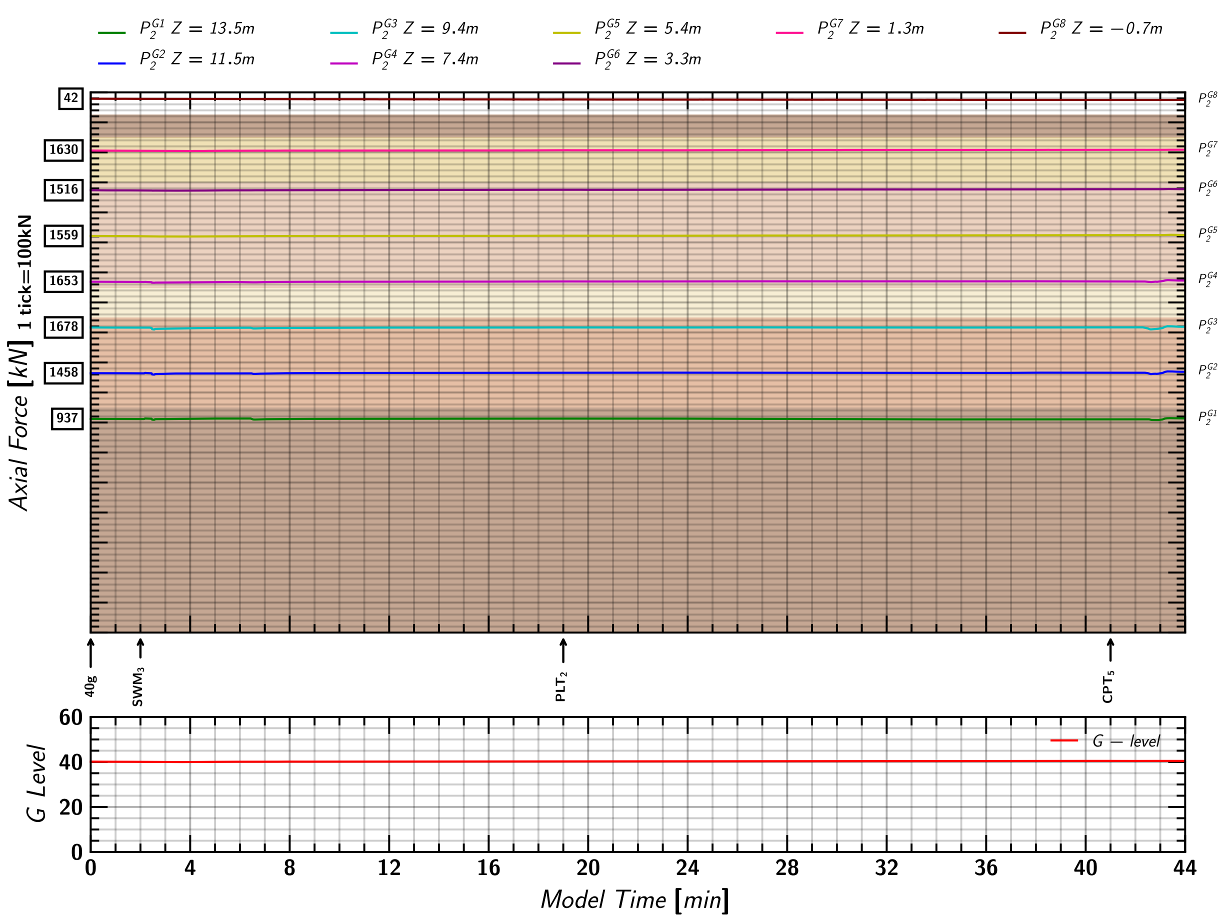

Figure 76. Day 2 Spin 2: Axial load measurements in Pile 2.

Dense Sand | Medium Dense Sand | Clayey Silt | Loose Sand | Clay Crust

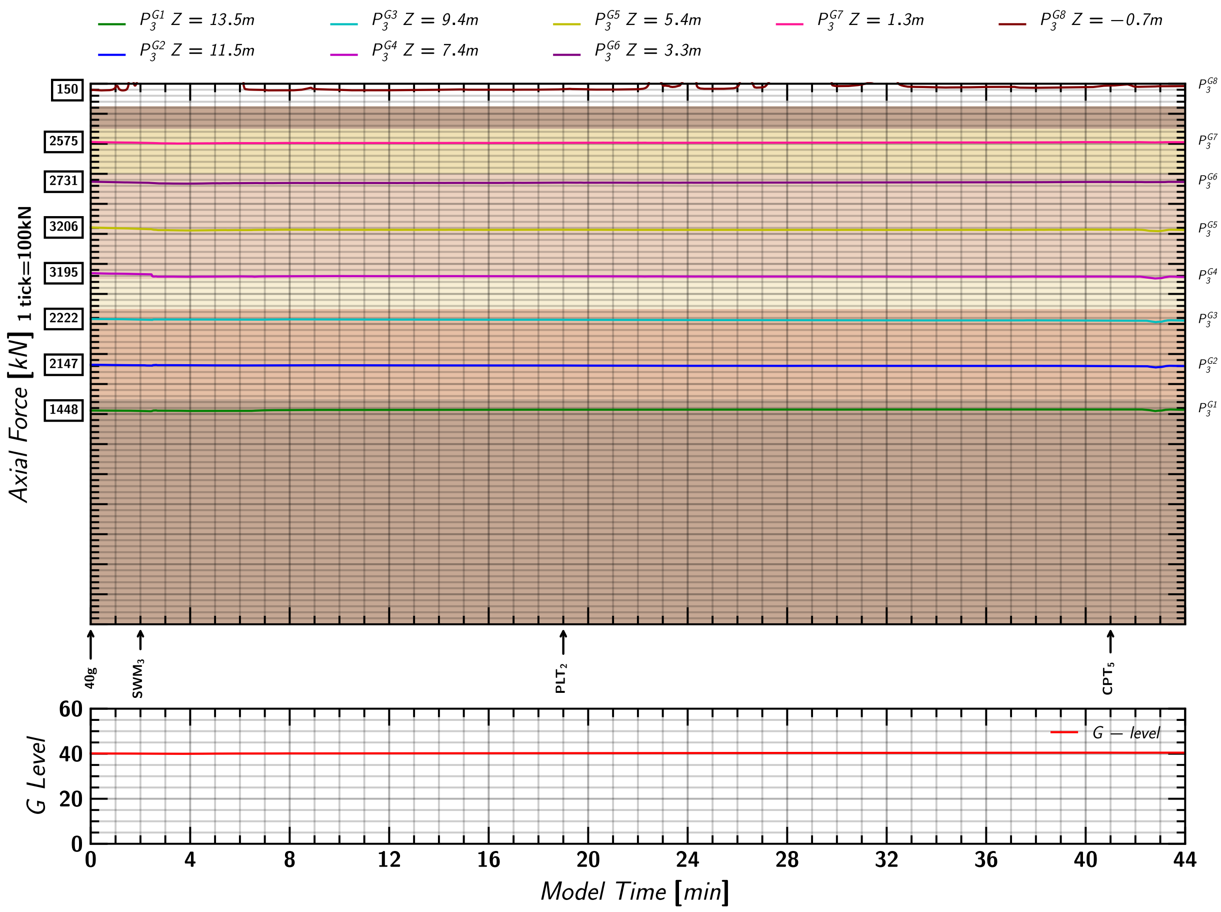

Figure 77. Day 2 Spin 2: Axial load measurements in Pile 3.

C.3 Pore pressure and Axial Load Profile

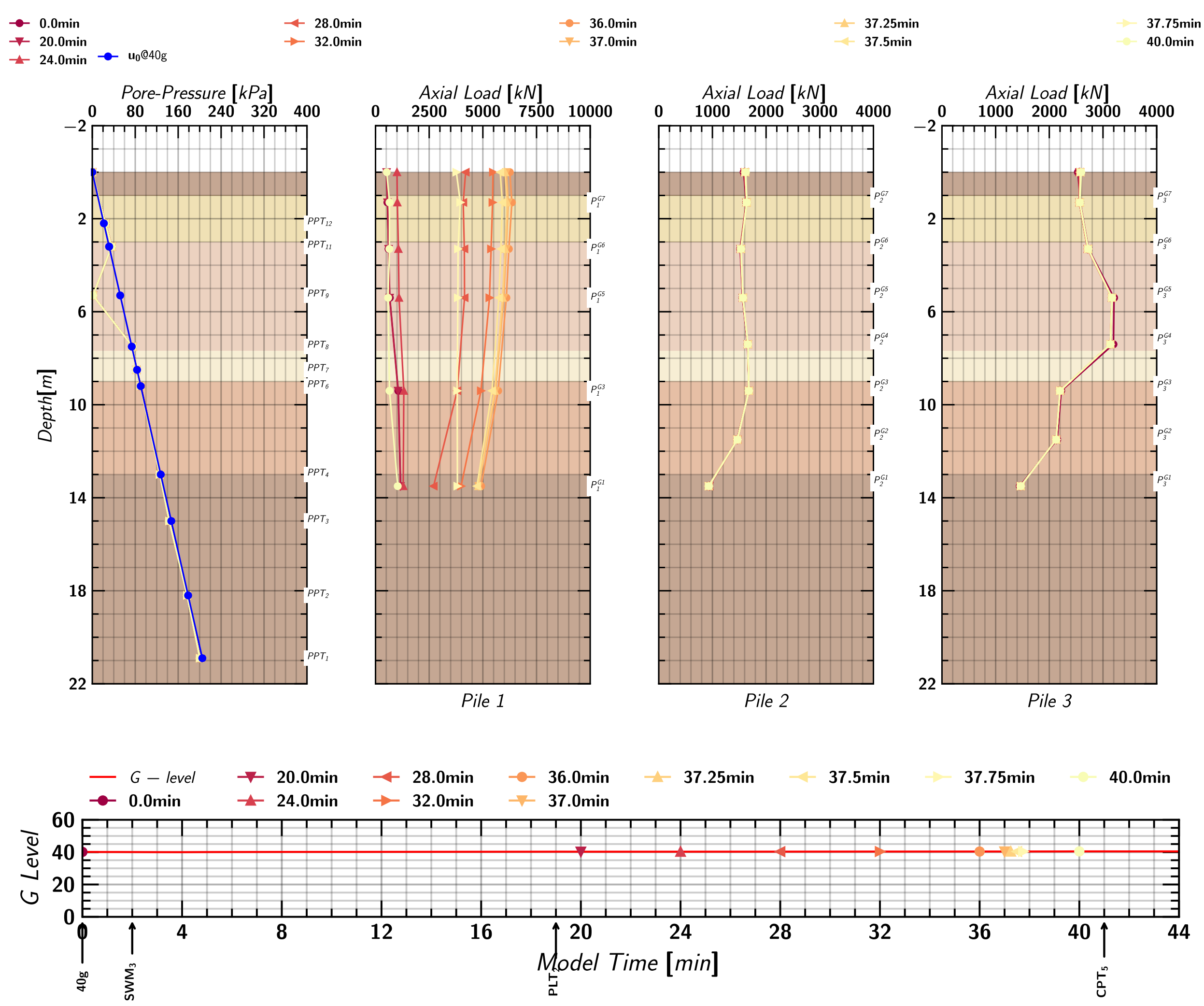

Figure 78. Day 2 Spin 2: Axial load profile of pile 1, pile 2 and pile 3 at different times during the test.

Dense Sand	Medium Dense Sand	Clayey Silt	Loose Sand	Clay Crust

D. EQM$_1$: SMALL SANTA CRUZ EARTHQUAKE (PGA = 0.09g)

D.1 Input Motion

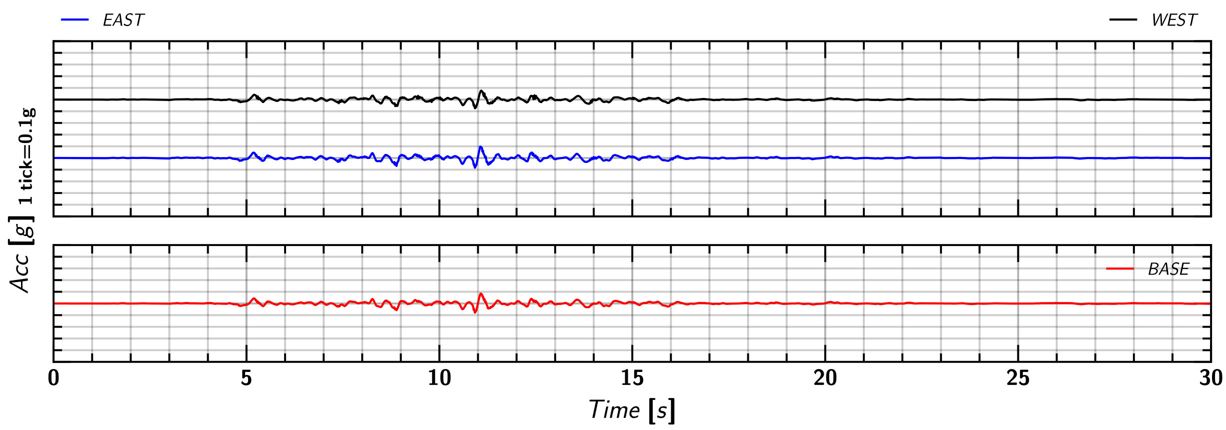

Figure 79. EQM$_1$: Input motion.

D.2 Spectral Acceleration

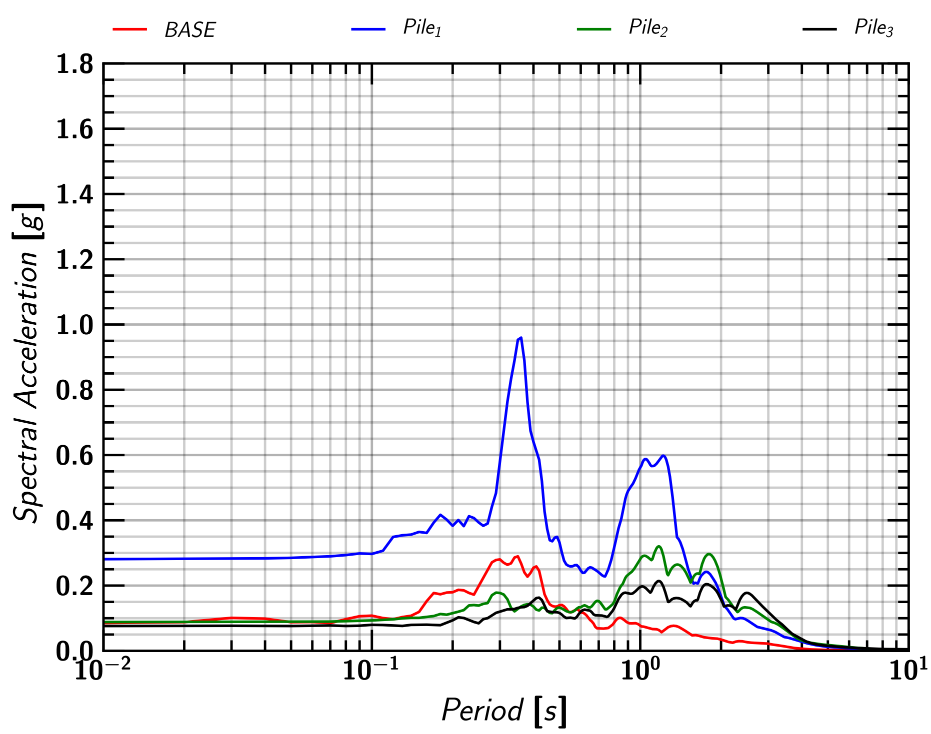

Figure 80. EQM$_1$: Spectral Acceleration.

D.3 Container Acceleration

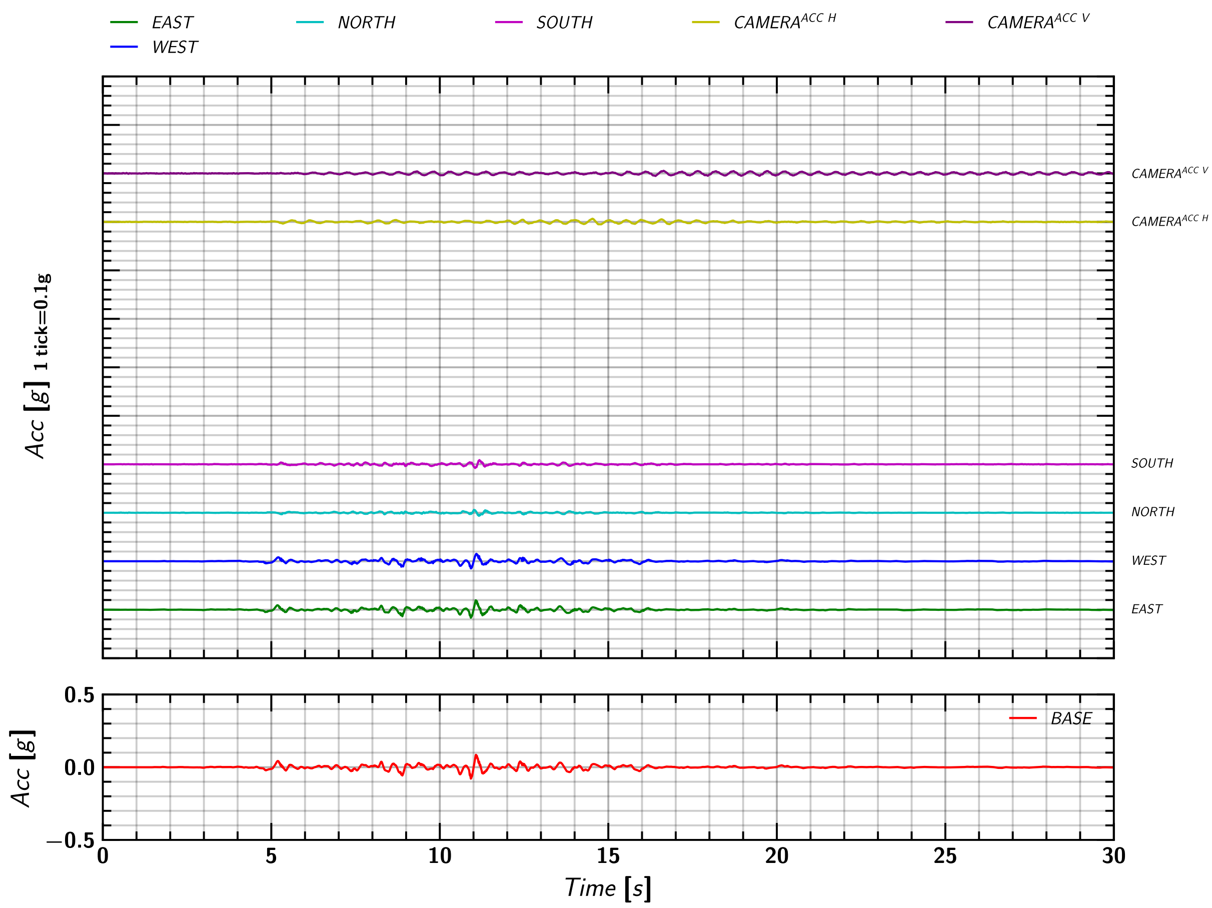

Figure 81. EQM$_1$: Acceleration measurement on container and camera beam.

D.4 Soil Acceleration

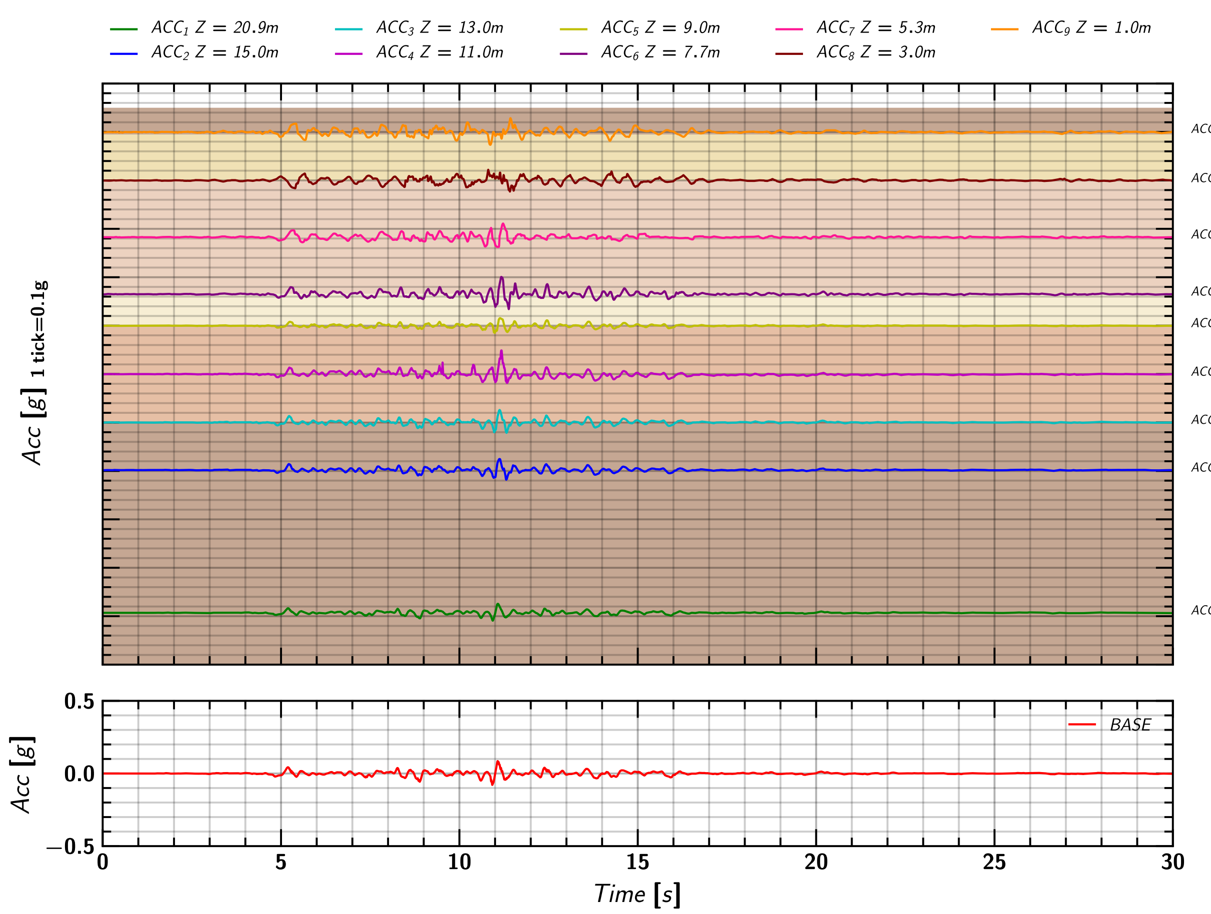

Figure 82. EQM$_1$: Acceleration measurement in soil.

D.5 Pile Mass Acceleration

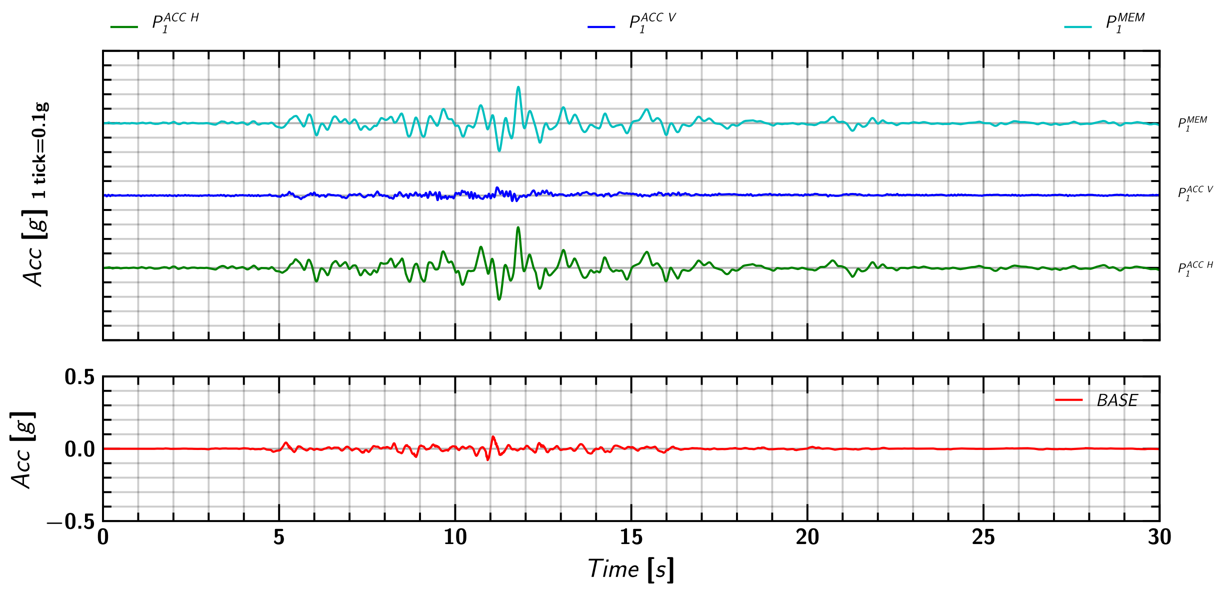

Figure 83. EQM$_1$: Acceleration measurement on pile 1.

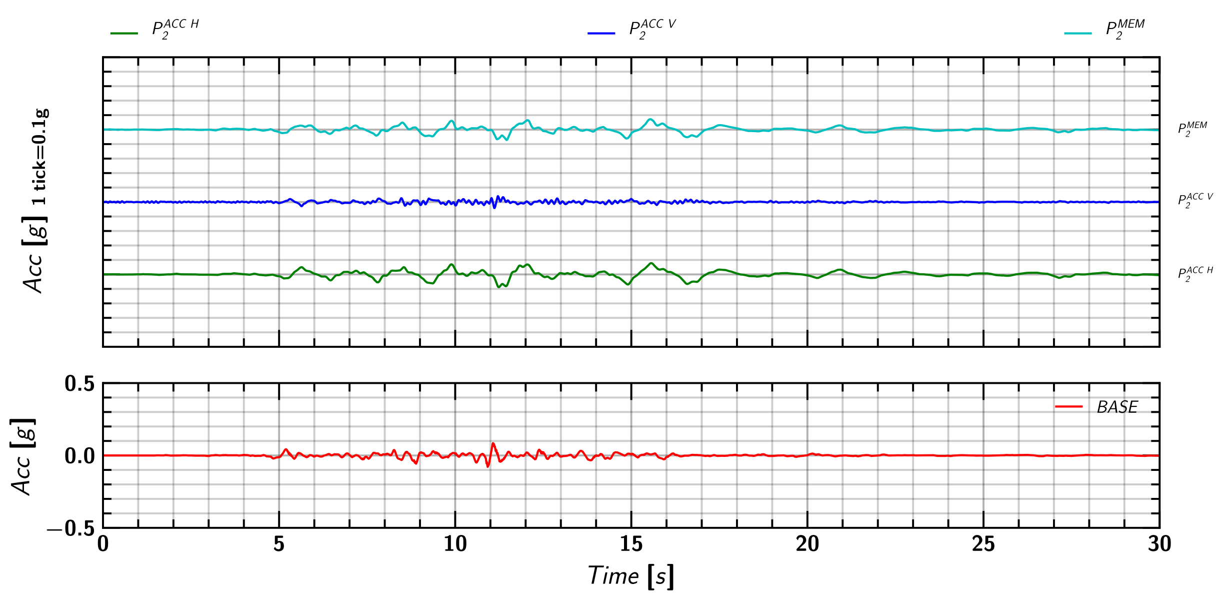

Figure 84. EQM$_1$: Acceleration measurement on pile 2.

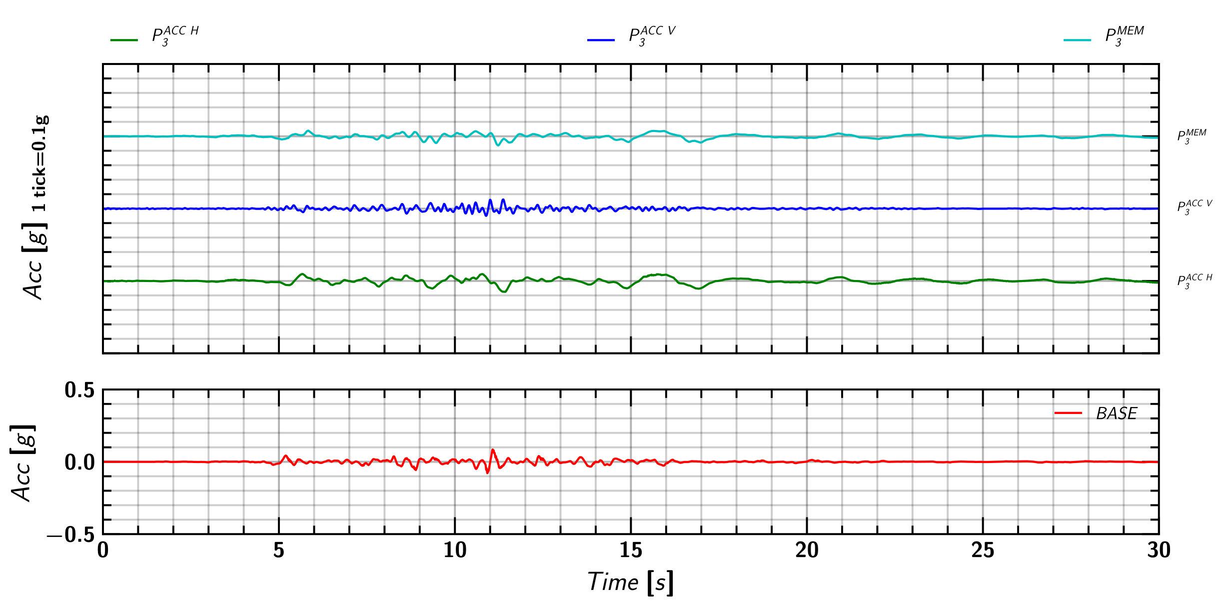

Figure 85. EQM$_1$: Acceleration measurement on pile 3.

D.6 Soil and Pile Mass Lateral Movement in X direction

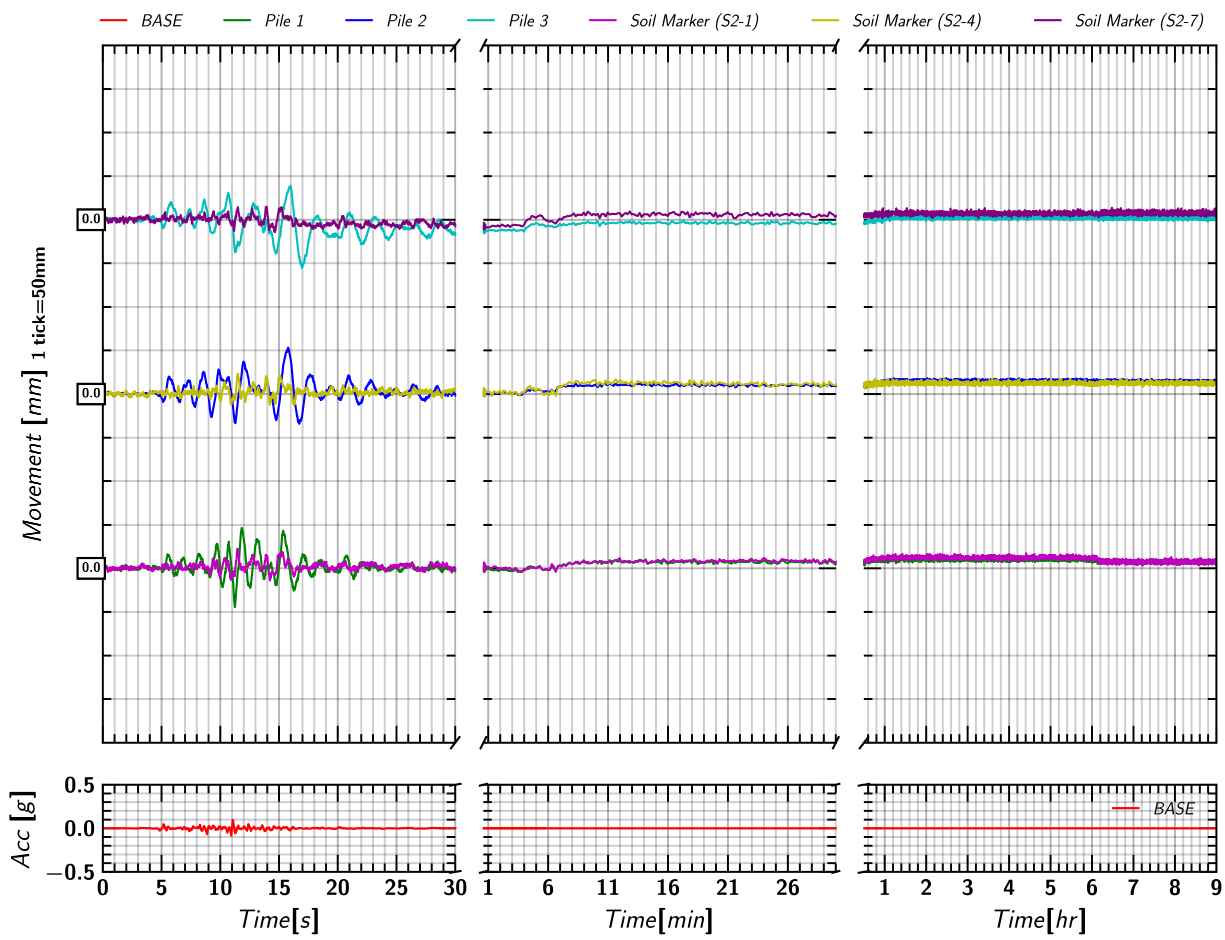

Figure 86. EQM$_1$: Lateral movement of soil and pile relative to container in x-direction during and post shaking.

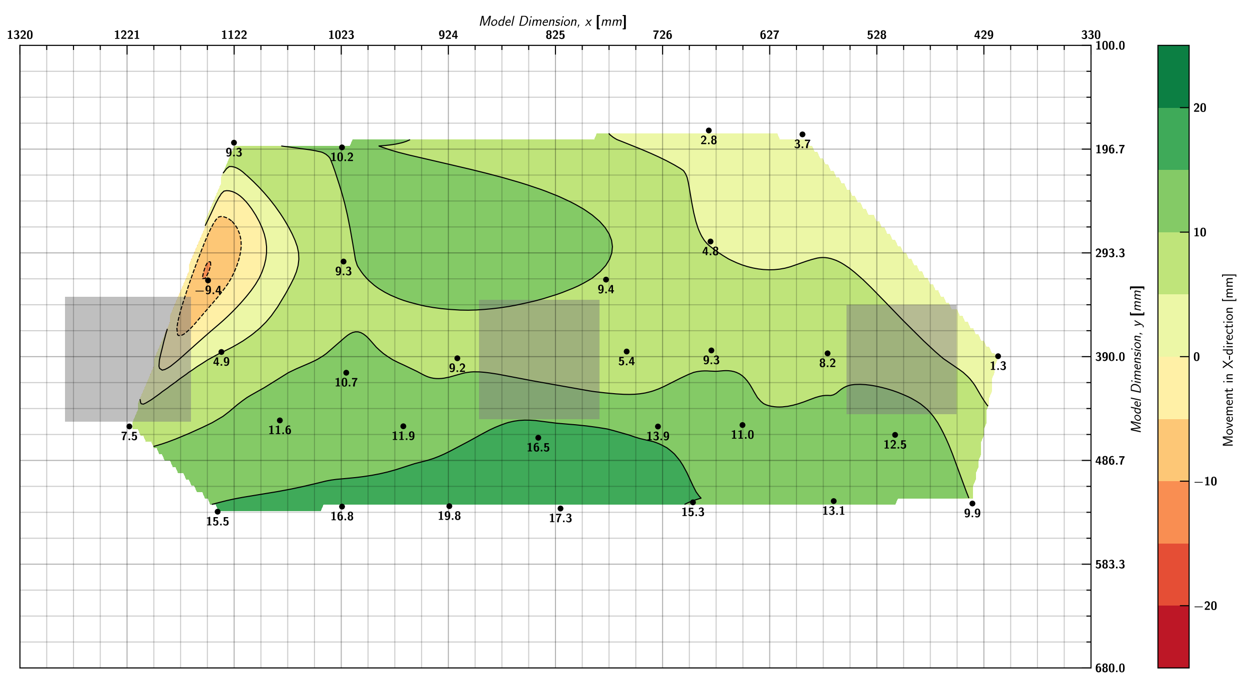

Figure 87. EQM$_1$:Contour of lateral movement of soil with respect to container in x-direction at the end of reconsolidation (t=120 minutes).

D.7 Soil and Pile Settlement (i.e., movement in Z direction)

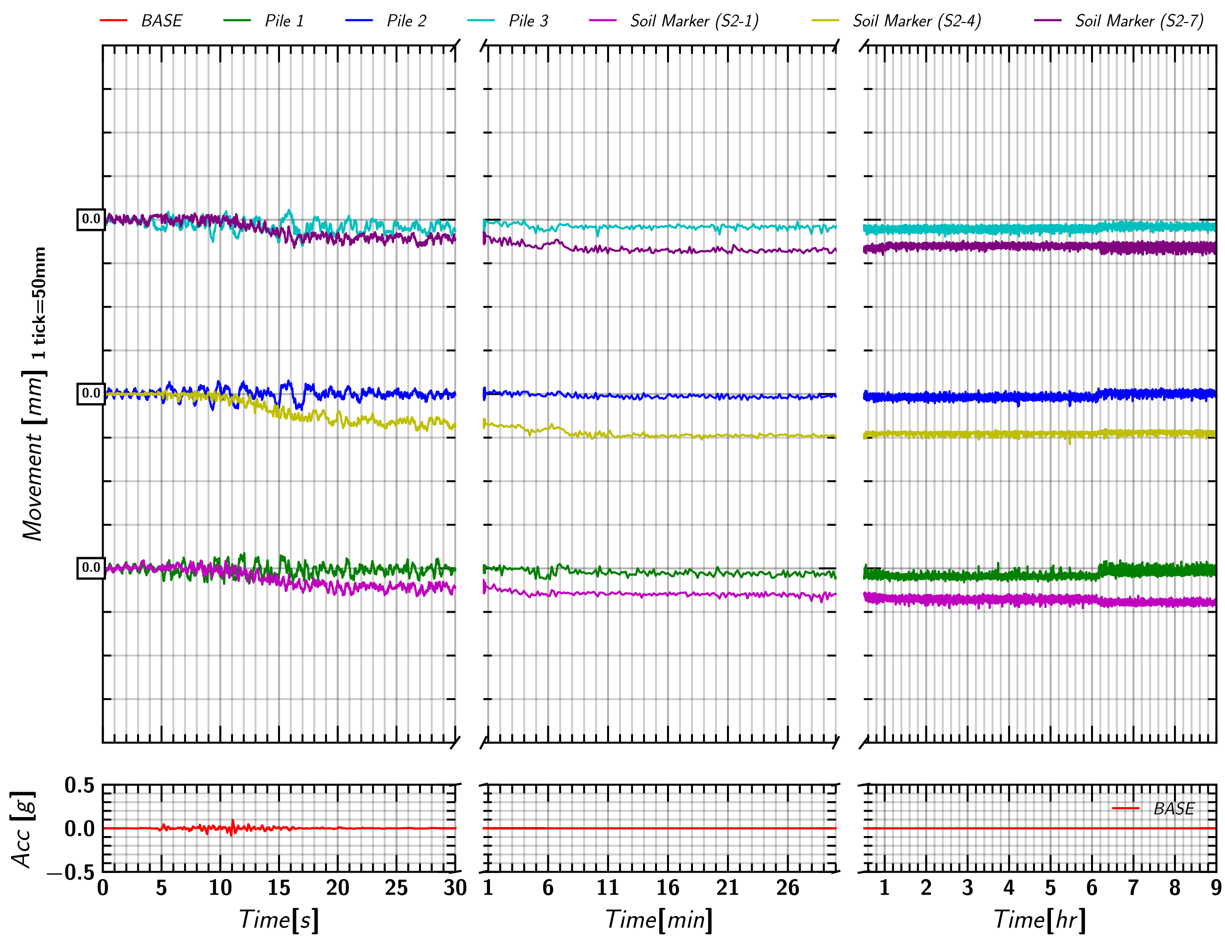

Figure 88. EQM$_1$: Settlement measurement in soil and pile during and post shaking.

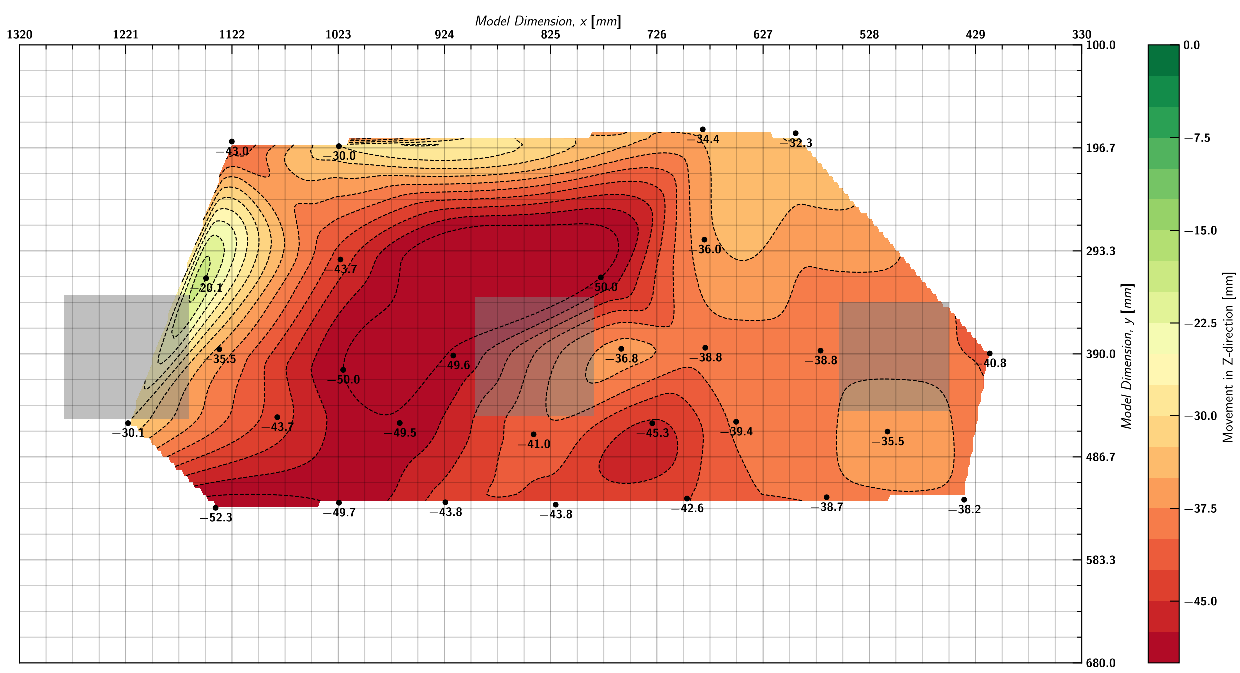

Figure 89. EQM$_1$:Contour of soil settlement with respect to container at the end of reconsolidation (t=120 minutes).

D.8 Pore pressure in Soil Measured by Keller Transducers

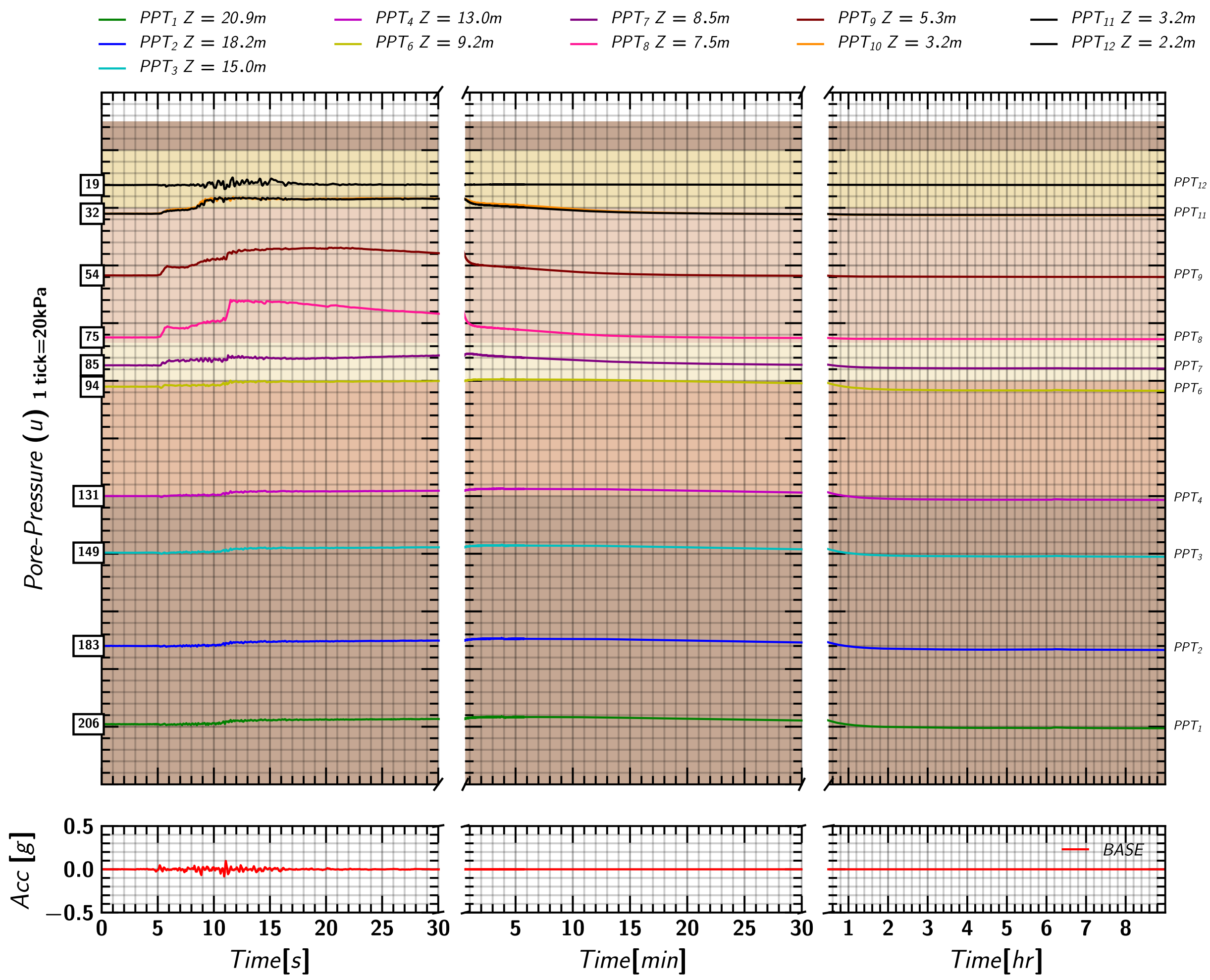

Figure 90. EQM$_1$: Pore pressure measurements in soil from Keller transducers during and post shaking.

D.9 Pore pressure in Soil Measured by MS54XXX Transducers

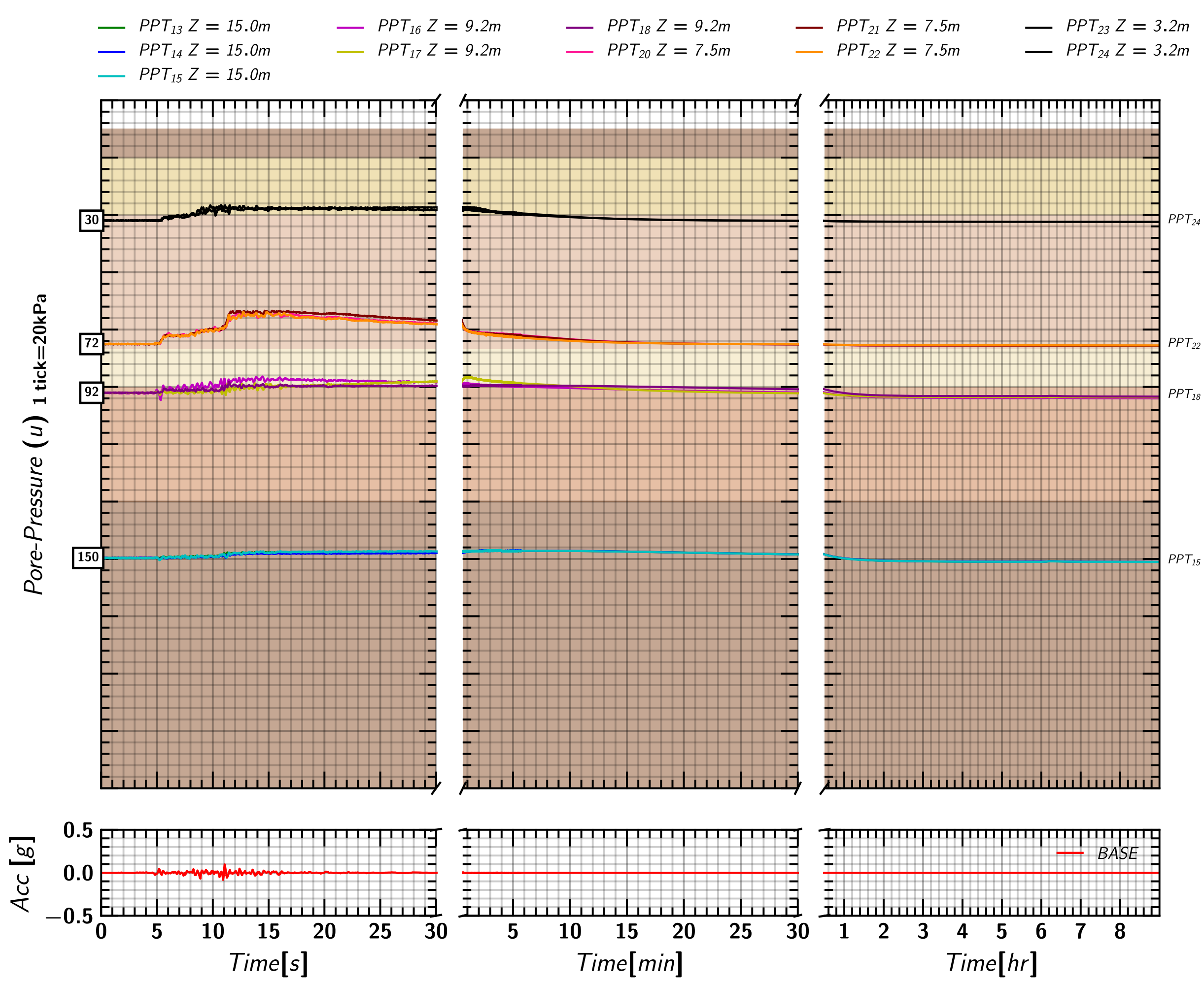

Figure 91. EQM$_1$: Pore pressure measurements in soil from MS54XXX transducers during and post shaking.

Dense Sand | Medium Dense Sand | Clayey Silt | Loose Sand | Clay Crust

D.10 Excess Pore pressures Ratio (r_u) Estimated from Keller Transducers

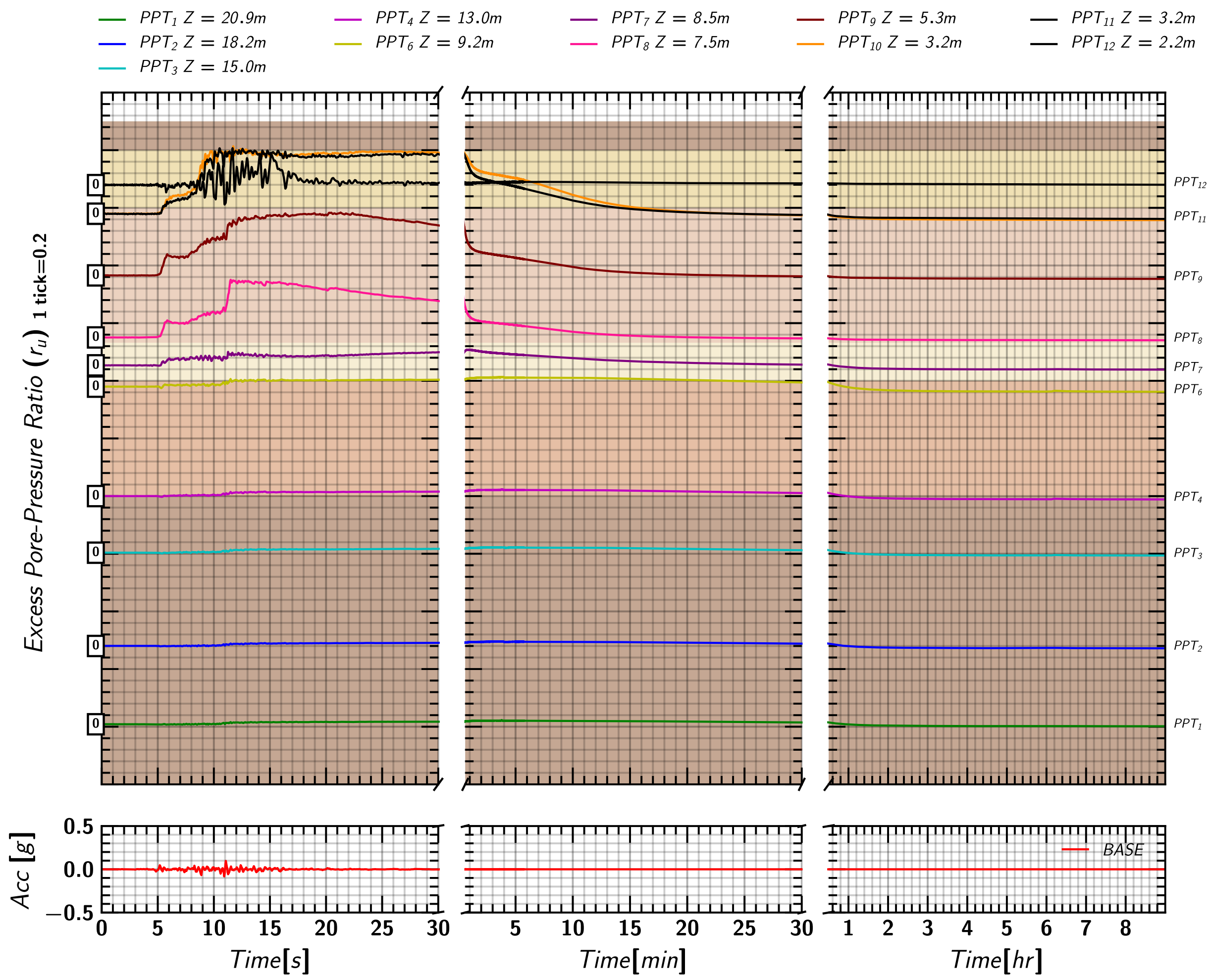

Figure 92. EQM$_1$: Excess pore pressure ratio (r_u) estimated from Keller transducers during and post shaking.

D.11 Excess Pore pressure Ratio (r_u) Estimated from MS54XXX Transducers

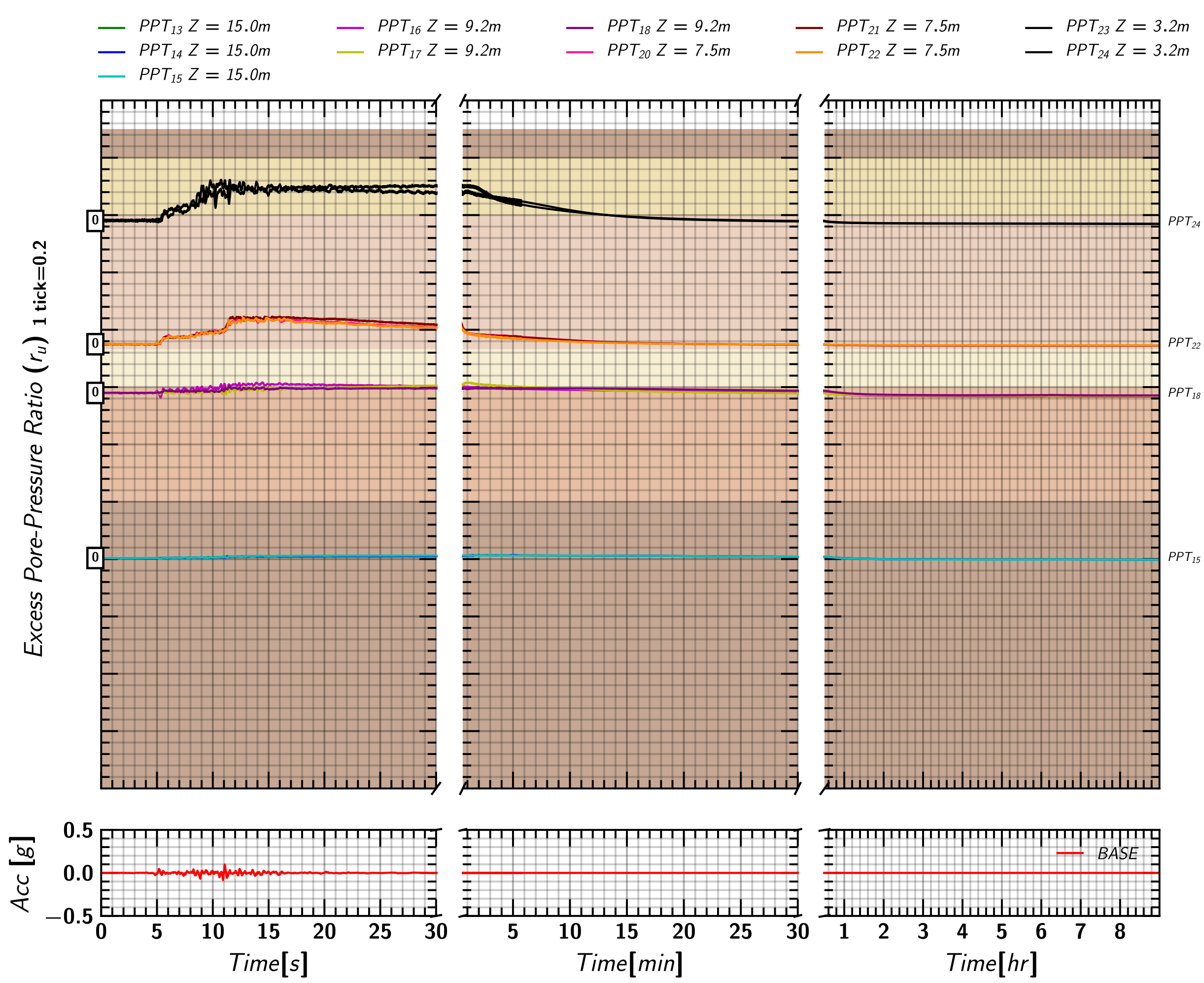

Figure 93. EQM$_1$: Excess pore pressure ratio (r_u) estimated from MS54XXX transducers during and post shaking.

Dense Sand	Medium Dense Sand	Clayey Silt	Loose Sand	Clay Crust

D.12 Axial Load in Pile 1

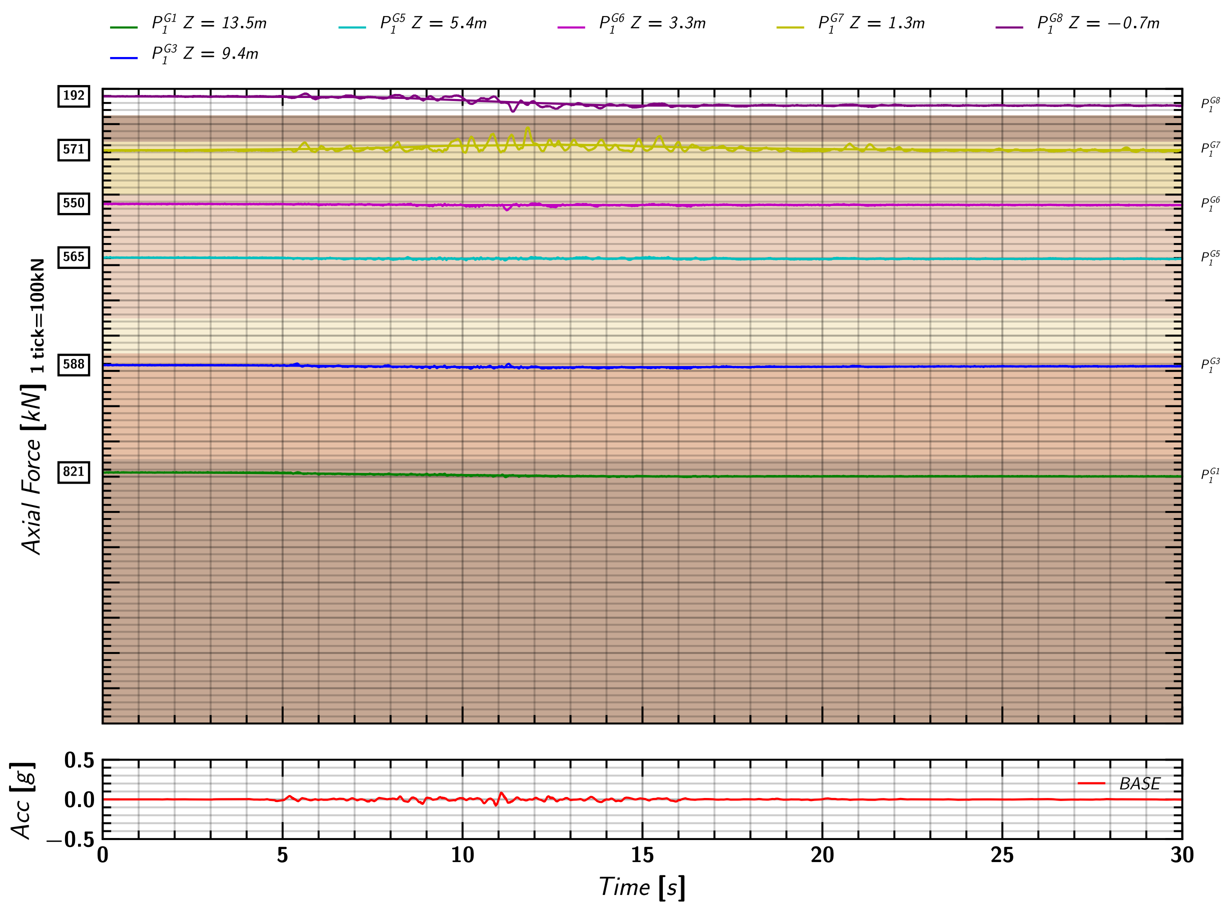

Figure 94. EQM$_1$: Axial load measurements from pile 1 strain gages during shaking.

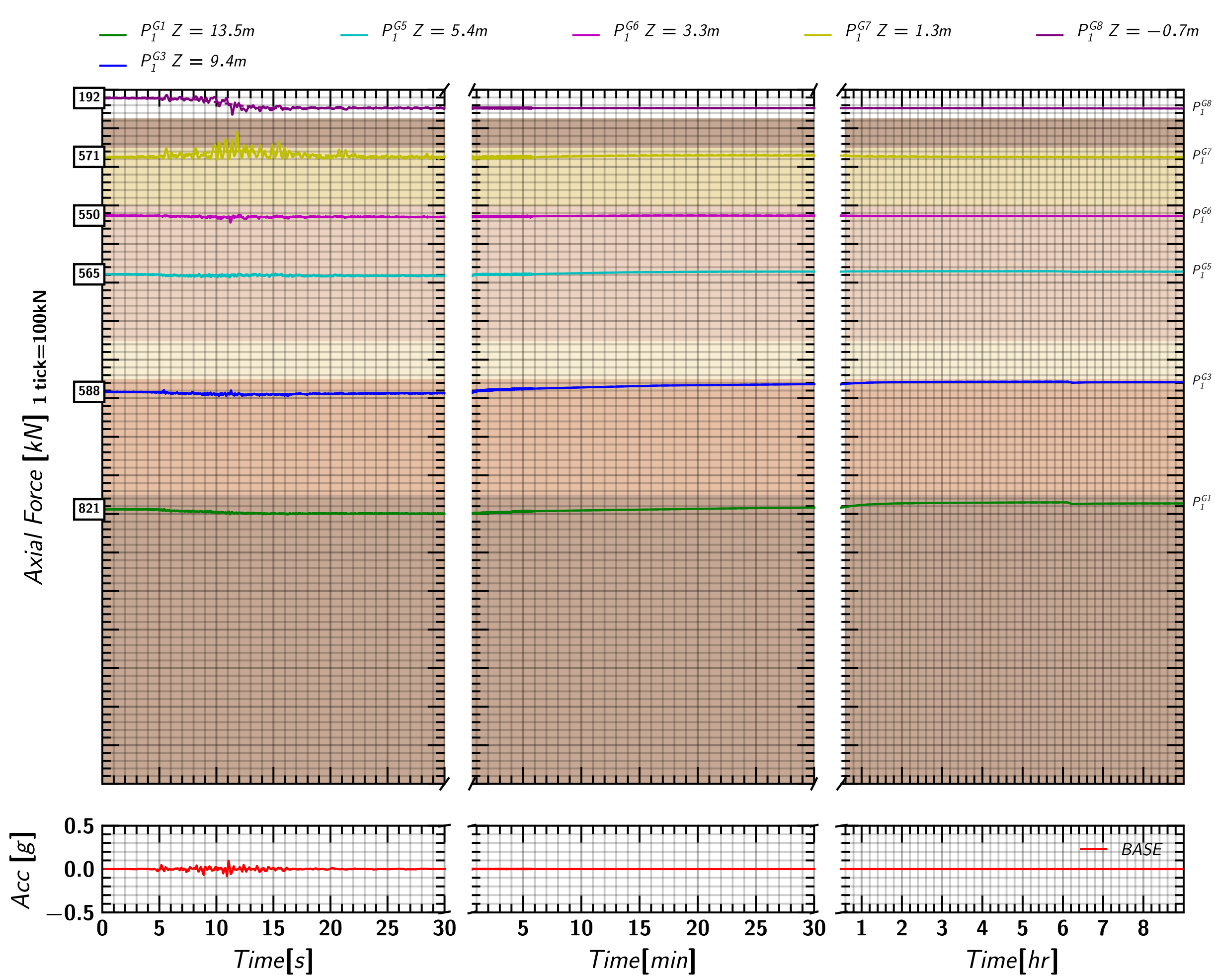

Figure 95. EQM$_1$: Axial load measurements from pile 1 strain gages during and post shaking.

D.13 Axial Load in Pile 2

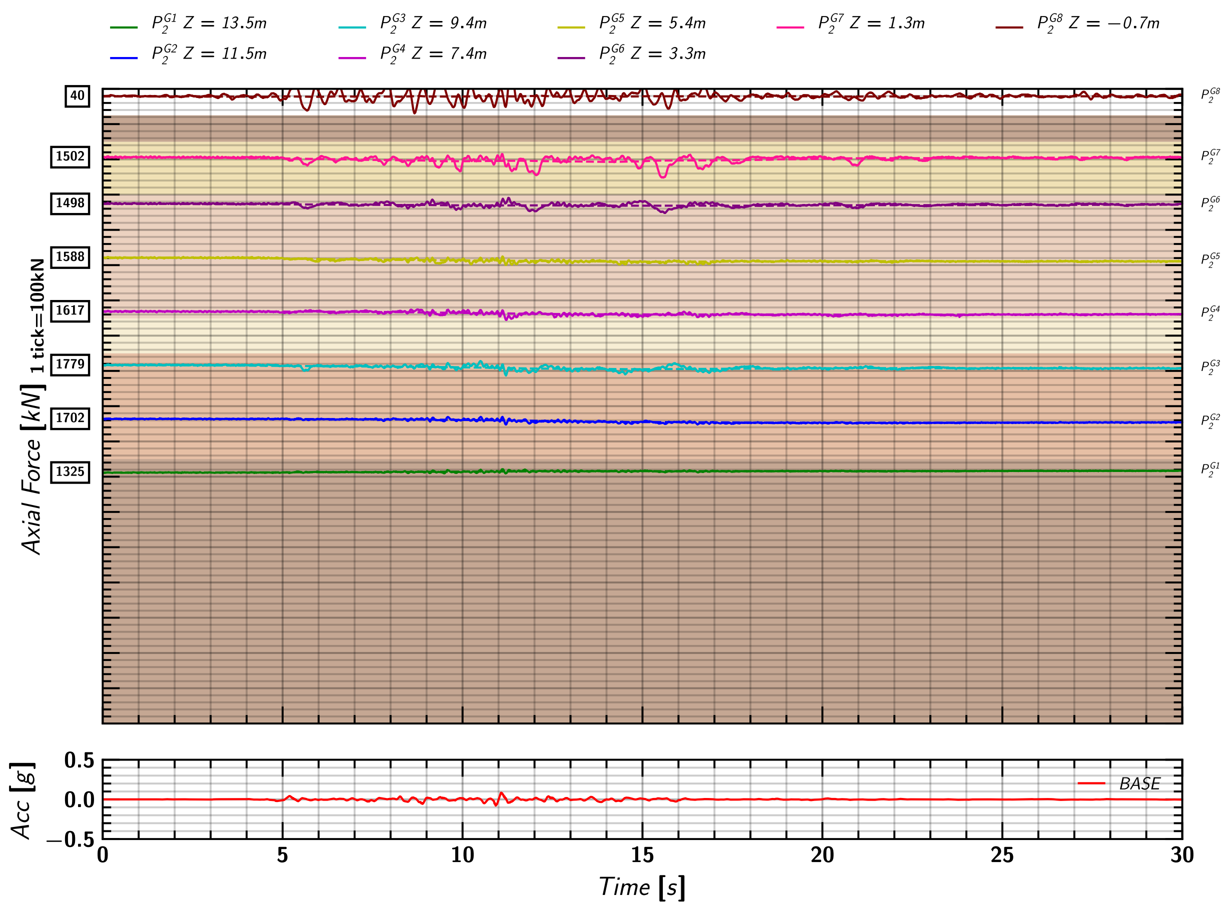

Figure 96. EQM$_1$: Axial load measurements from pile 2 strain gages during shaking.

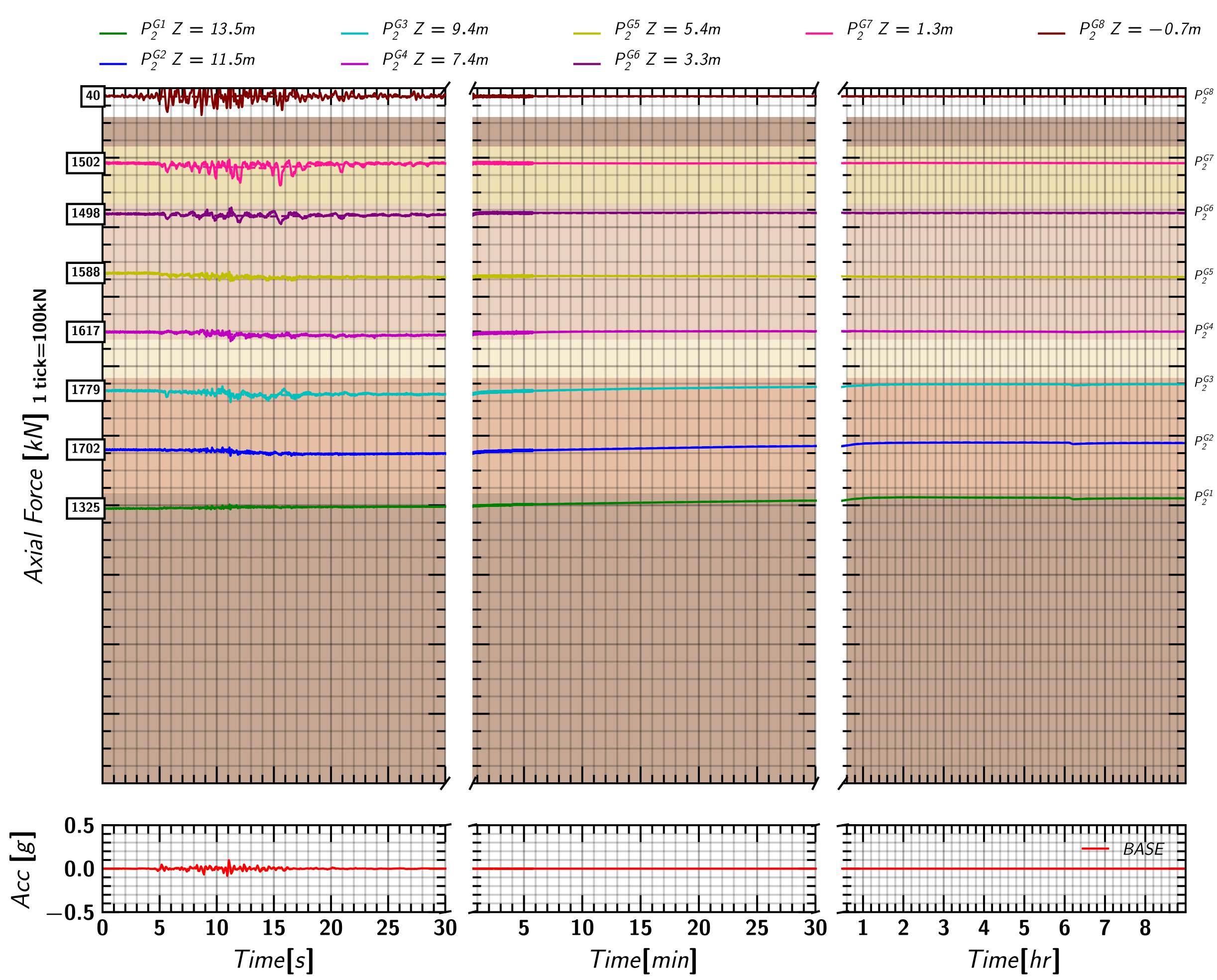

Figure 97. EQM$_1$: Axial load measurements from pile 2 strain gages during and post shaking.

D.14 Axial Load in Pile 3

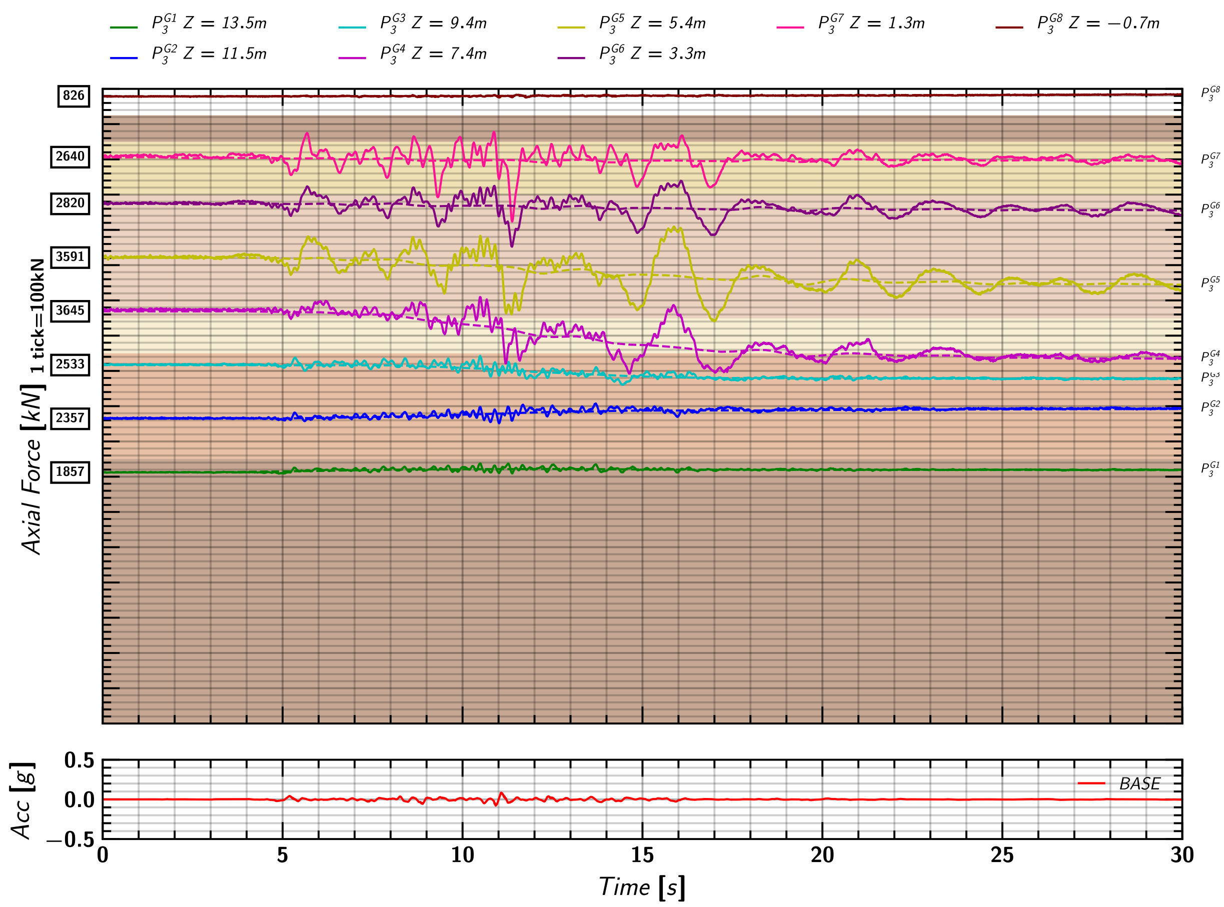

Figure 98. EQM$_1$: Axial load measurements from pile 3 strain gages during shaking.

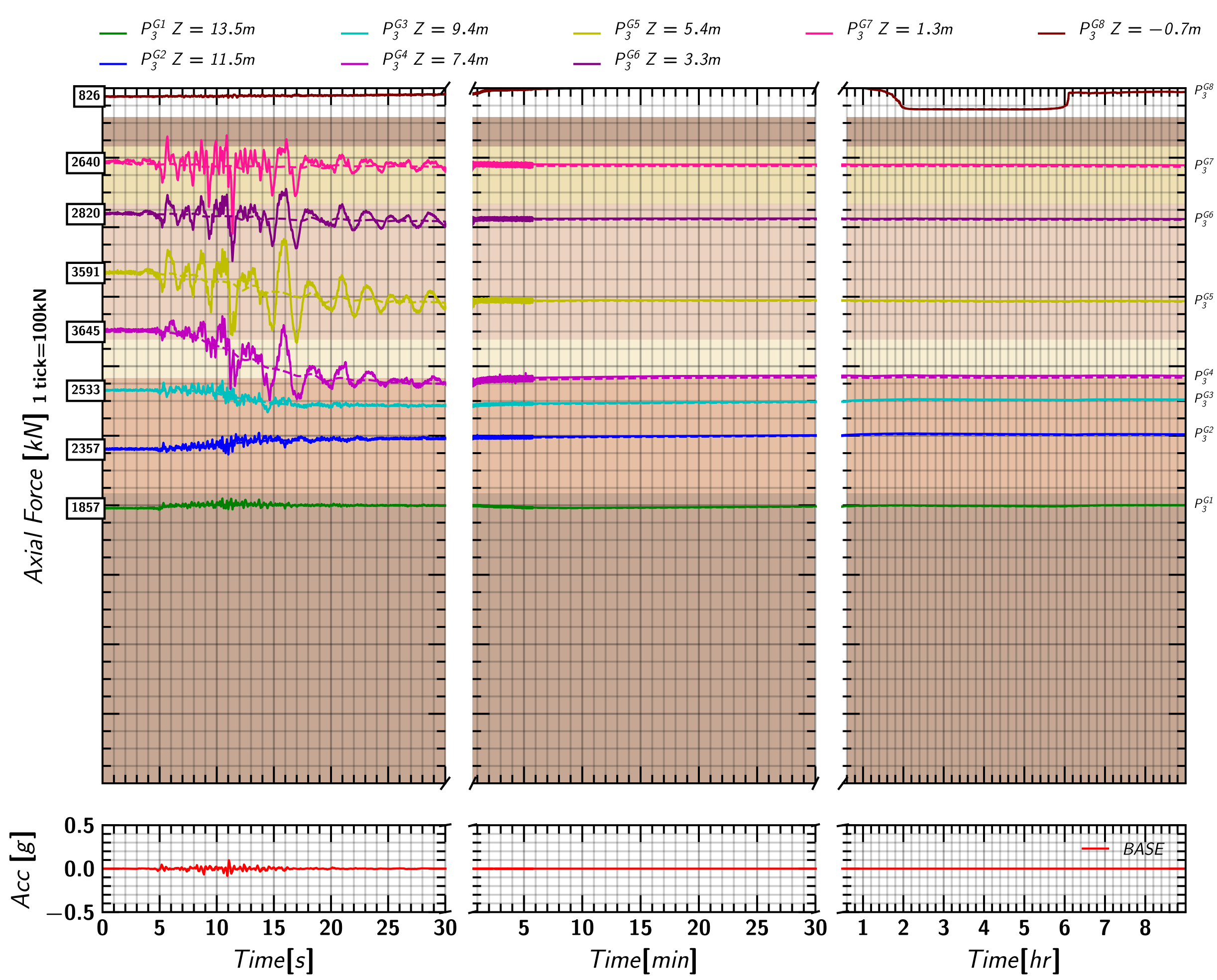

Figure 99. EQM$_1$: Axial load measurements from pile 3 strain gages during and post shaking.

D.15 Pore pressure and Axial Load Profile

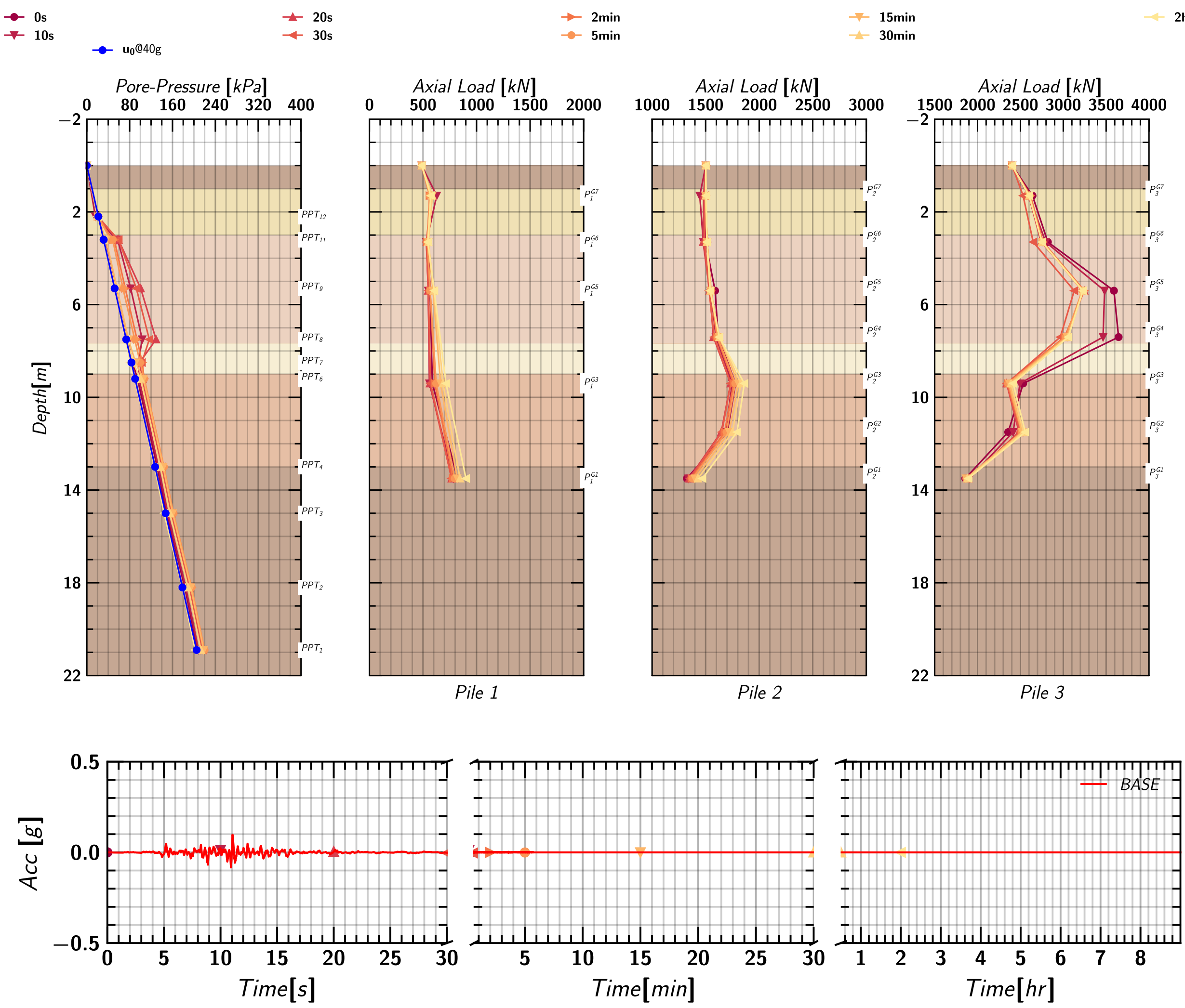

Figure 100. EQM$_1$: Pore pressure and axial load profile in pile 1, pile 2 and pile 3 at different times during and post shaking.

Dense Sand | Medium Dense Sand | Clayey Silt | Loose Sand | Clay Crust

E. EQM1: Soil, Pile, and Container Movements in X and Z

E.1 Container Movement in X

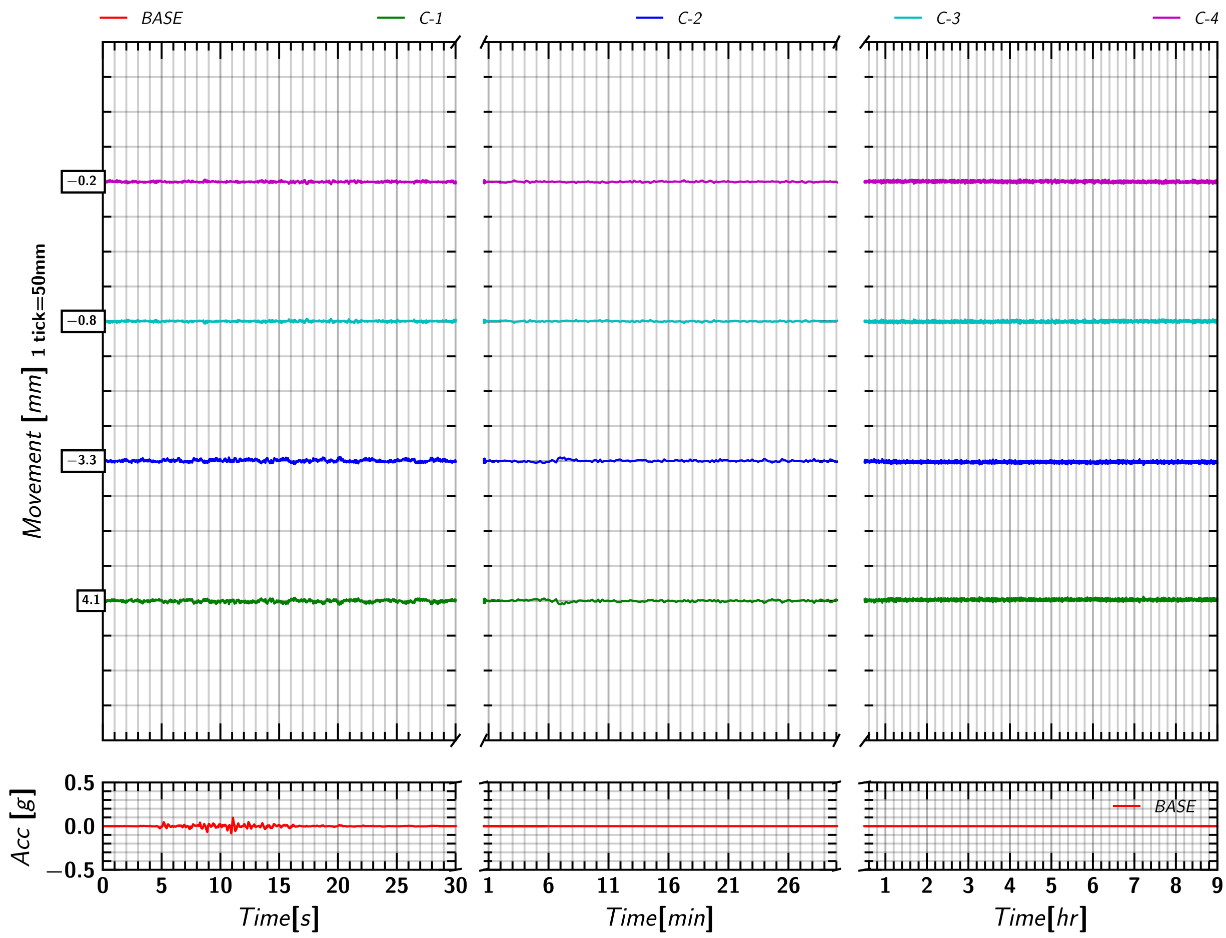

Figure 101. EQM1: Container movement in X-direction relative to the model container during and post shaking.

E.2 Container Movement in Z

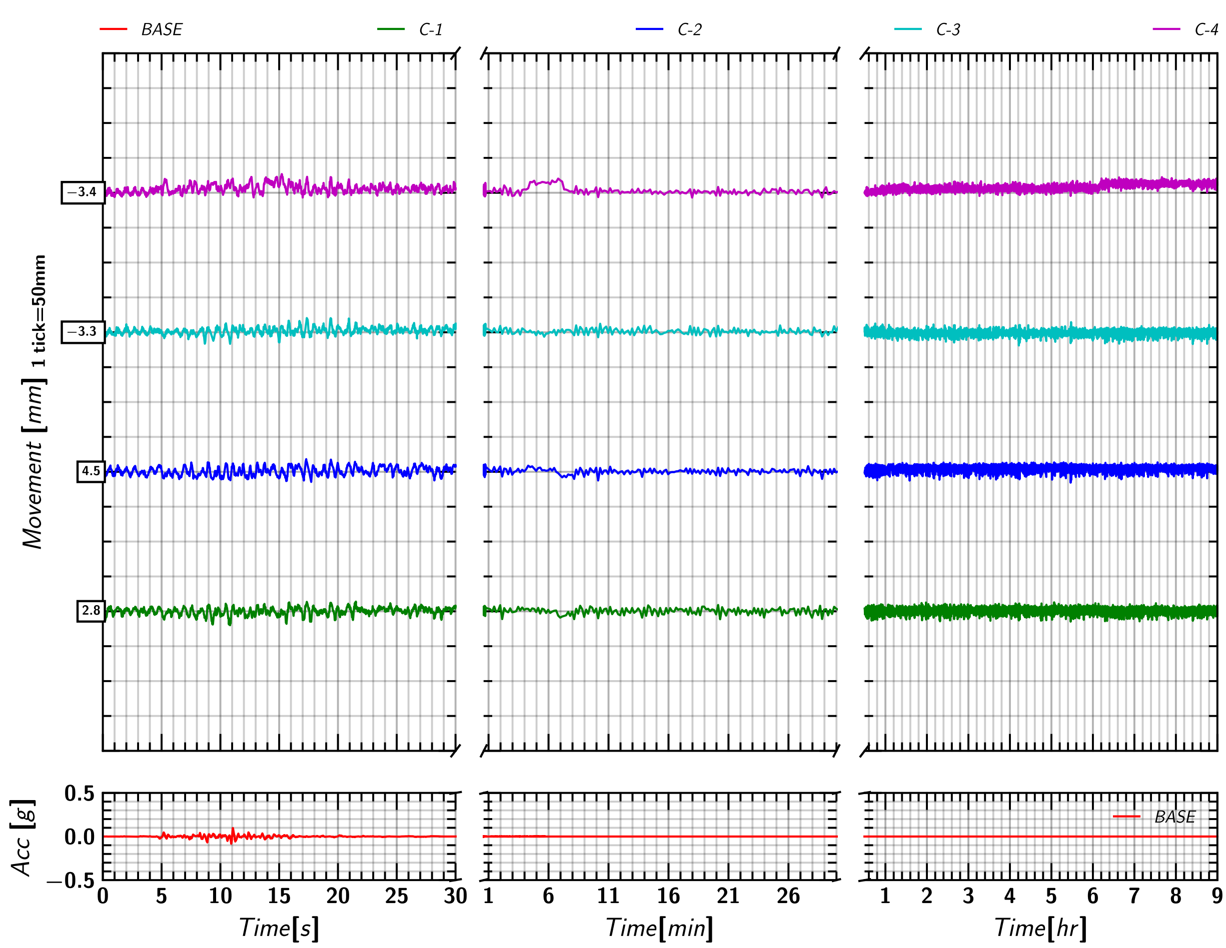

Figure 102. EQM1: Container movement in Z-direction relative to the model container during and post shaking.

E.3 Soil (Row S-1) Movement in X

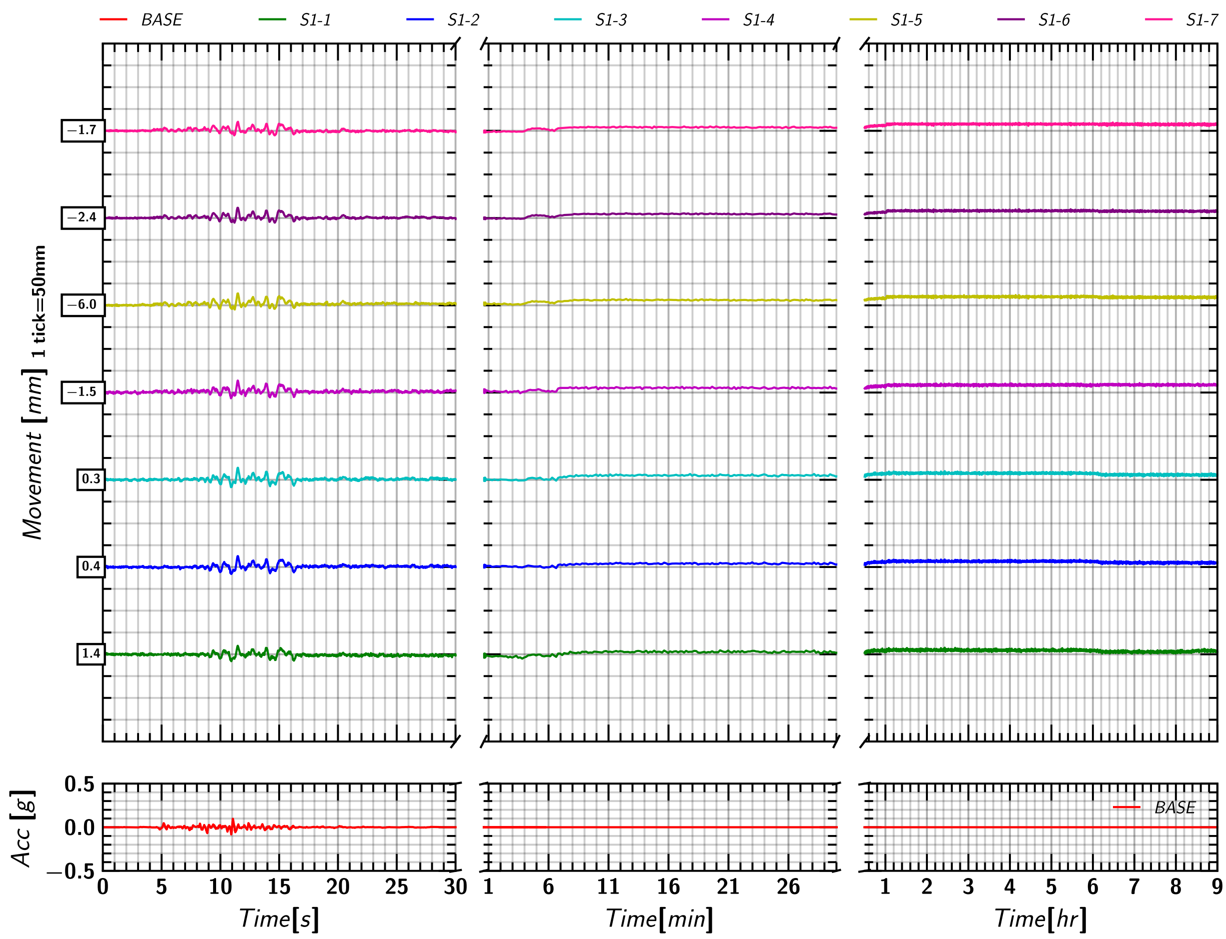

Figure 103. EQM1: Soil (Row S-1) movement in X-direction relative to the model container during and post shaking.

E.4 Soil (Row S-1) Movement in Z

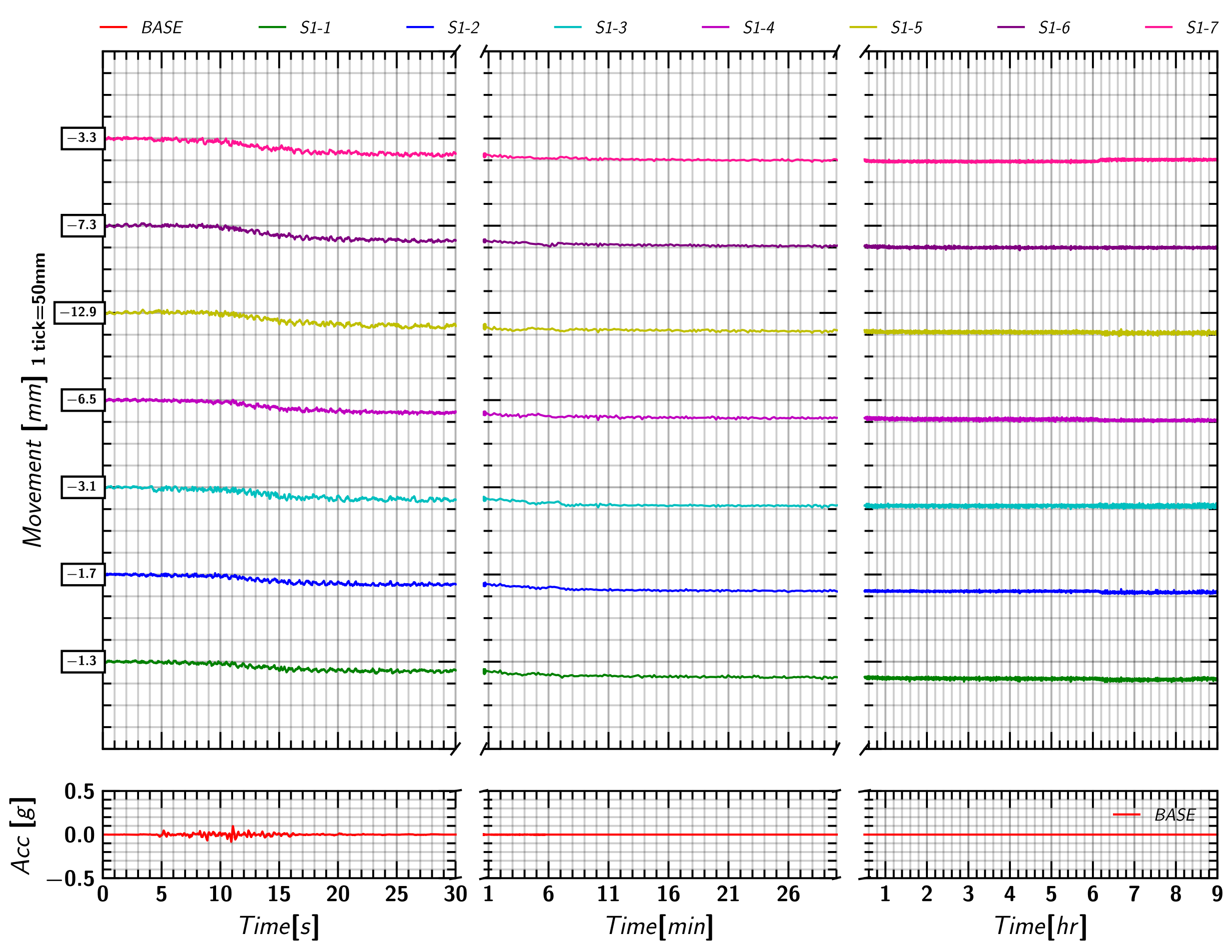

Figure 104. EQM1: Soil (Row S-1) movement in Z-direction relative to the model container during and post shaking.

E.5 Soil (Row S-2) Movement in X

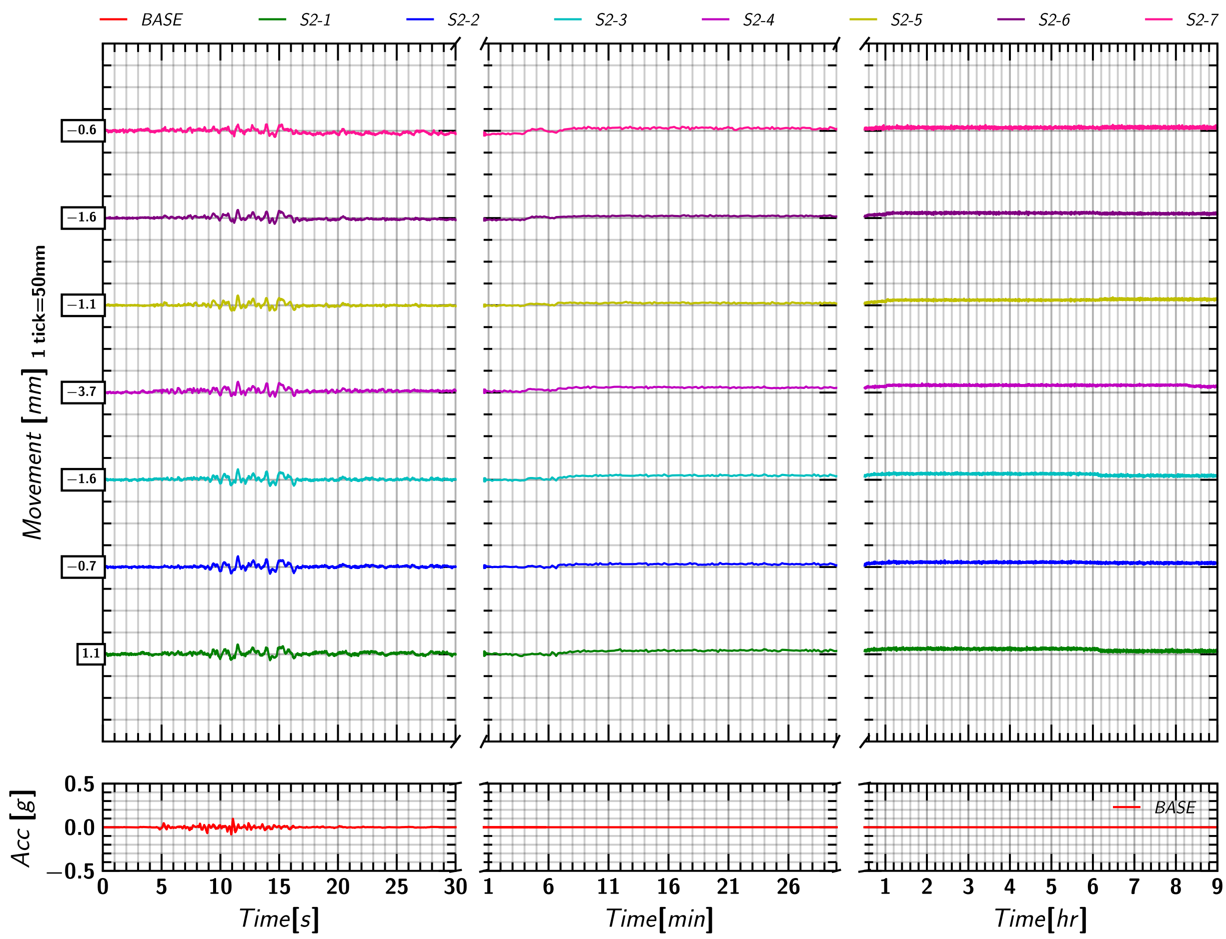

Figure 105. EQM$_1$: Soil (Row S-2) movement in X-direction relative to the model container during and post shaking.

E.6 Soil (Row S-2) Movement in Z

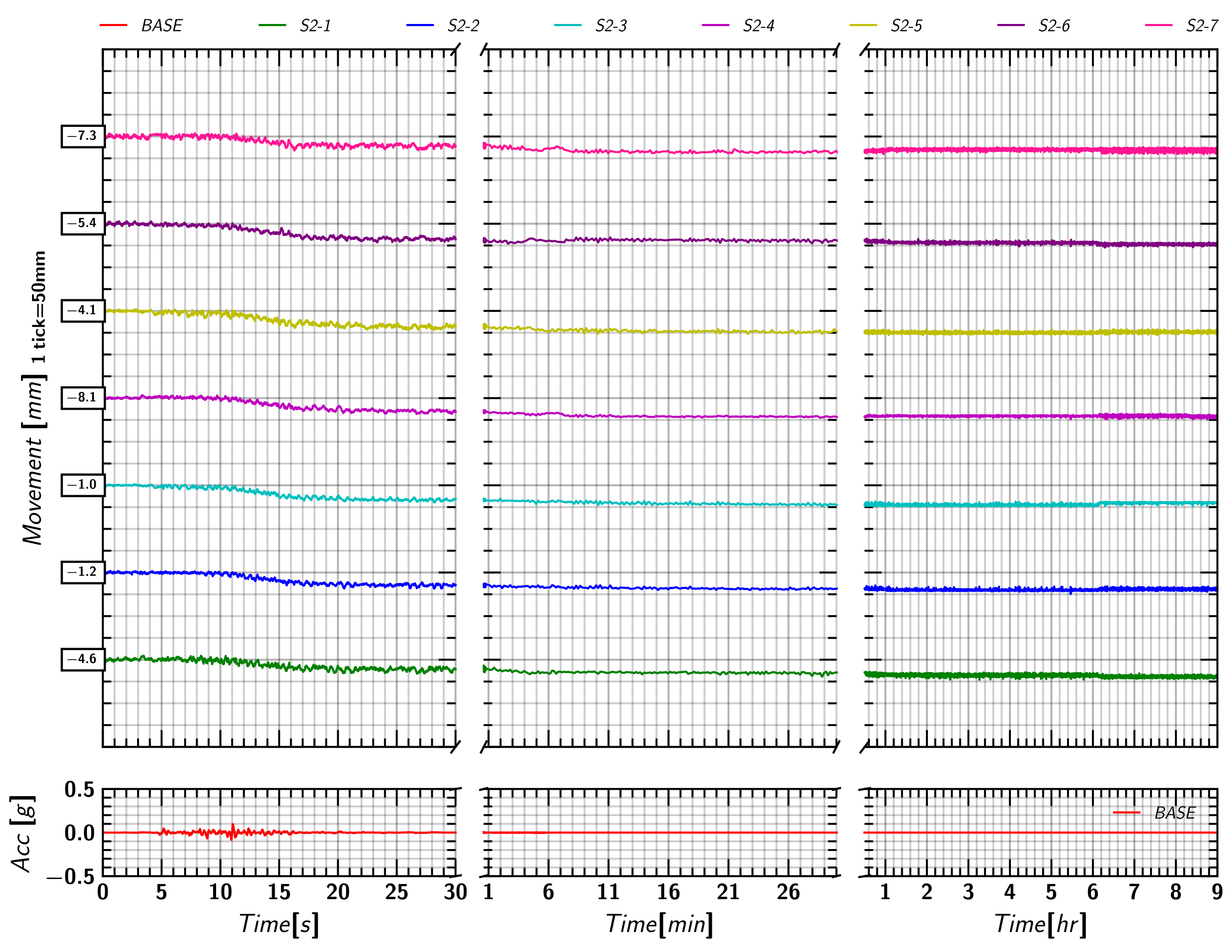

Figure 106. EQM$_1$: Soil (Row S-2) movement in Z-direction relative to the model container during and post shaking.

E.7 Soil (Row S-3) Movement in X

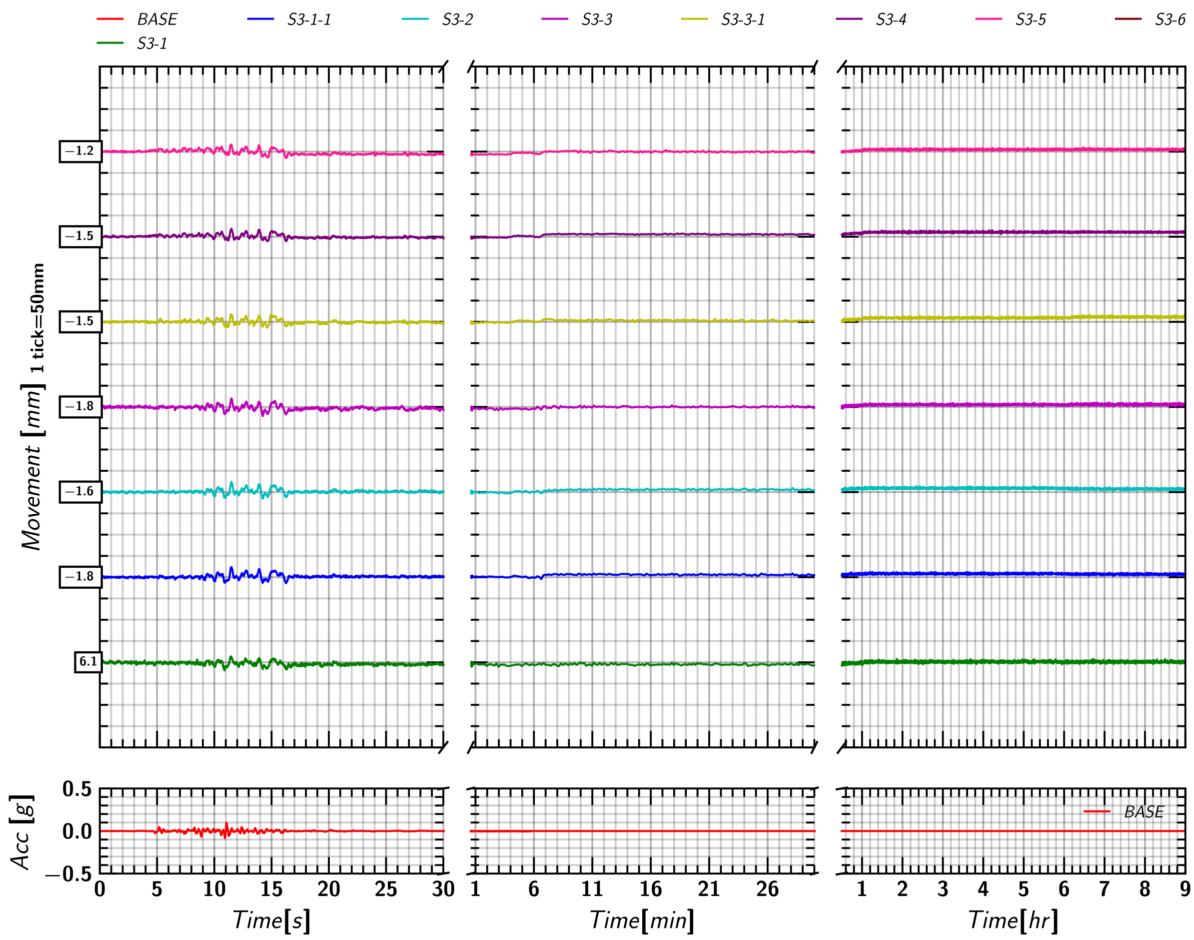

Figure 107. EQM$_1$: Soil (Row S-3) movement in X-direction relative to the model container during and post shaking.

E.8 Soil (Row S-3) Movement in Z

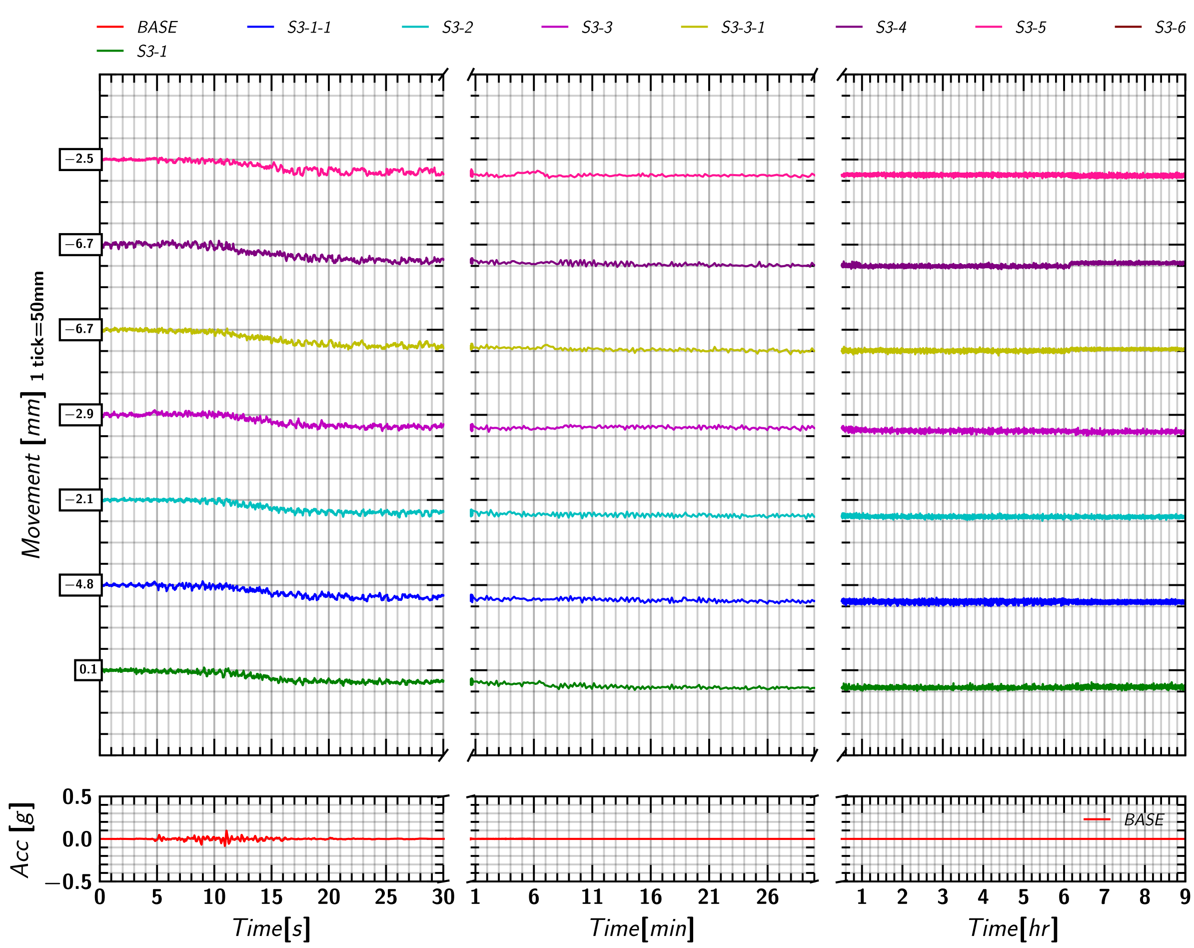

Figure 108. EQM$_1$: Soil (Row S-3) movement in Z-direction relative to the model container during and post shaking.

E.9 Soil (Row S-4) Movement in X

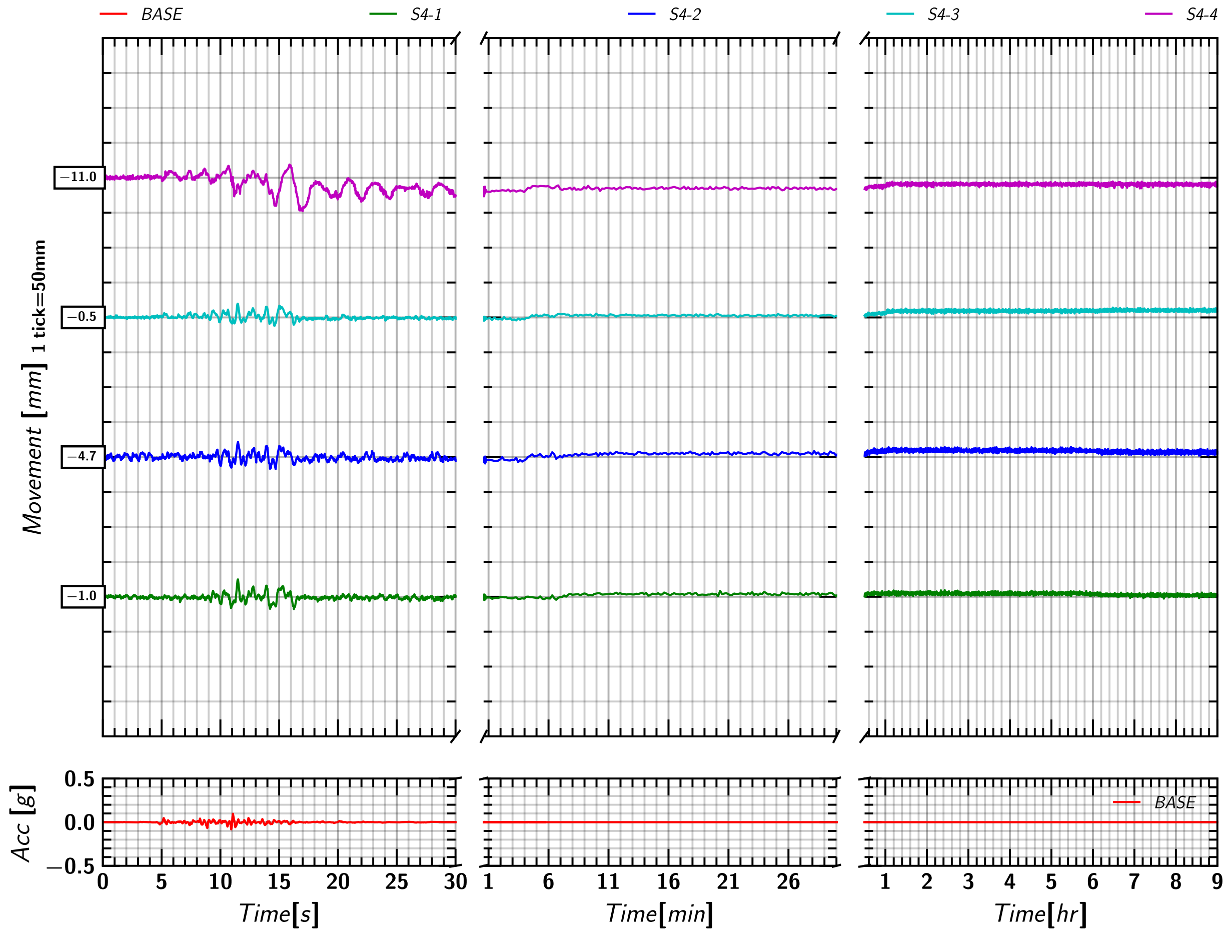

Figure 109. EQM$_1$: Soil (Row S-4) movement in X-direction relative to the model container during and post shaking.

E.10 Soil (Row S-4) Movement in Z

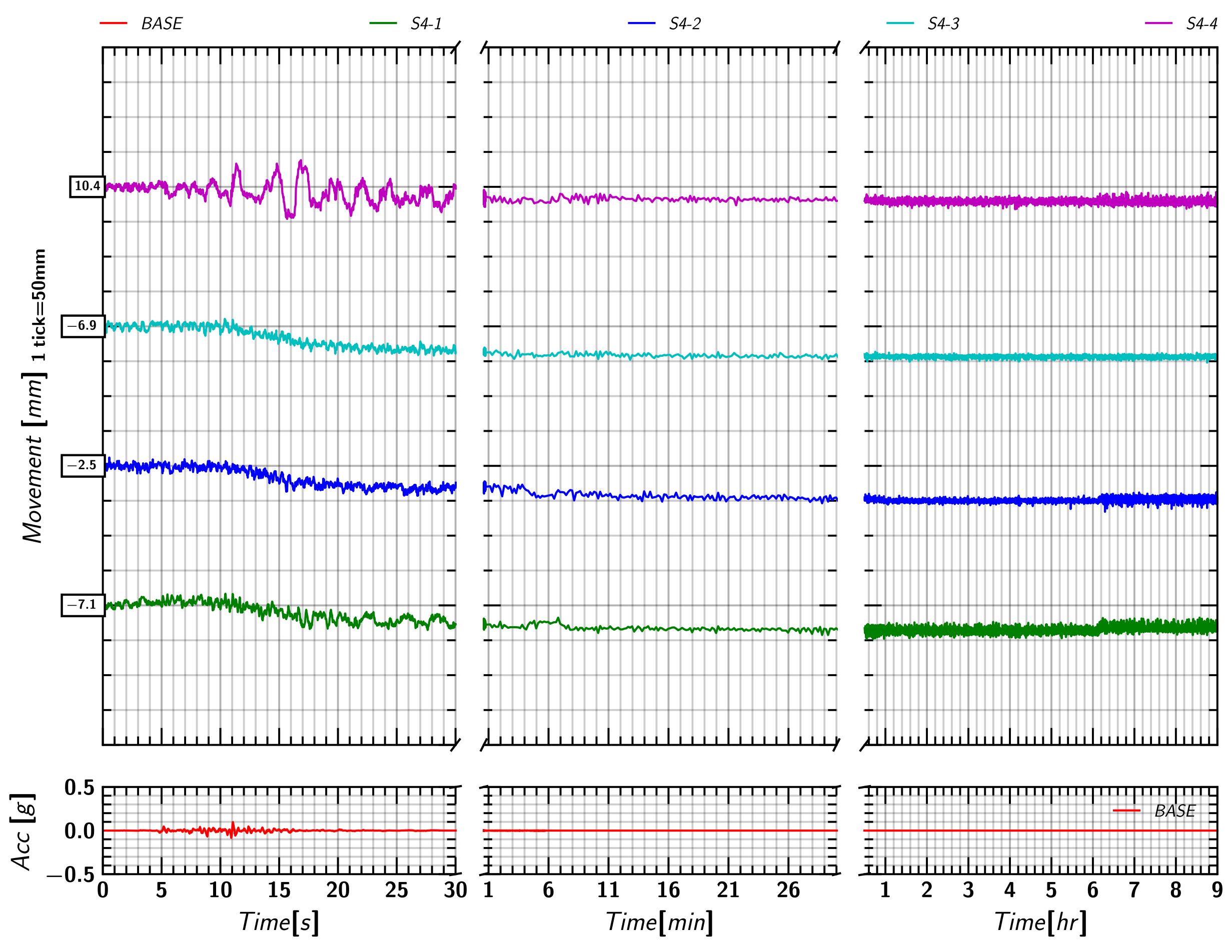

Figure 110. EQM$_1$: Soil (Row S-4) movement in Z-direction relative to the model container during and post shaking.

E.11 Soil (Row S-5) Movement in X

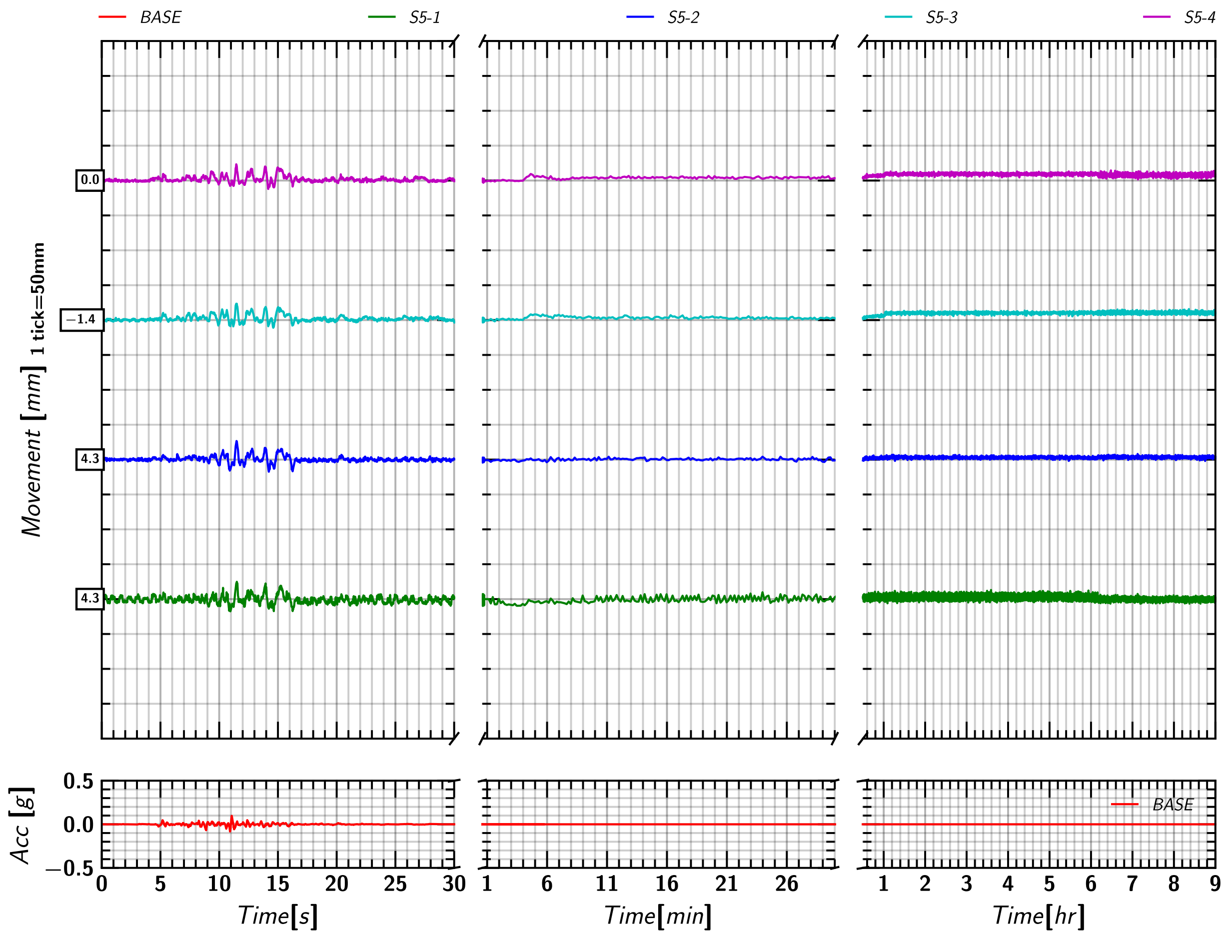

Figure 111. EQM$_1$: Soil (Row S-5) movement in X-direction relative to the model container during and post shaking.

E.12 Soil (Row S-5) Movement in Z

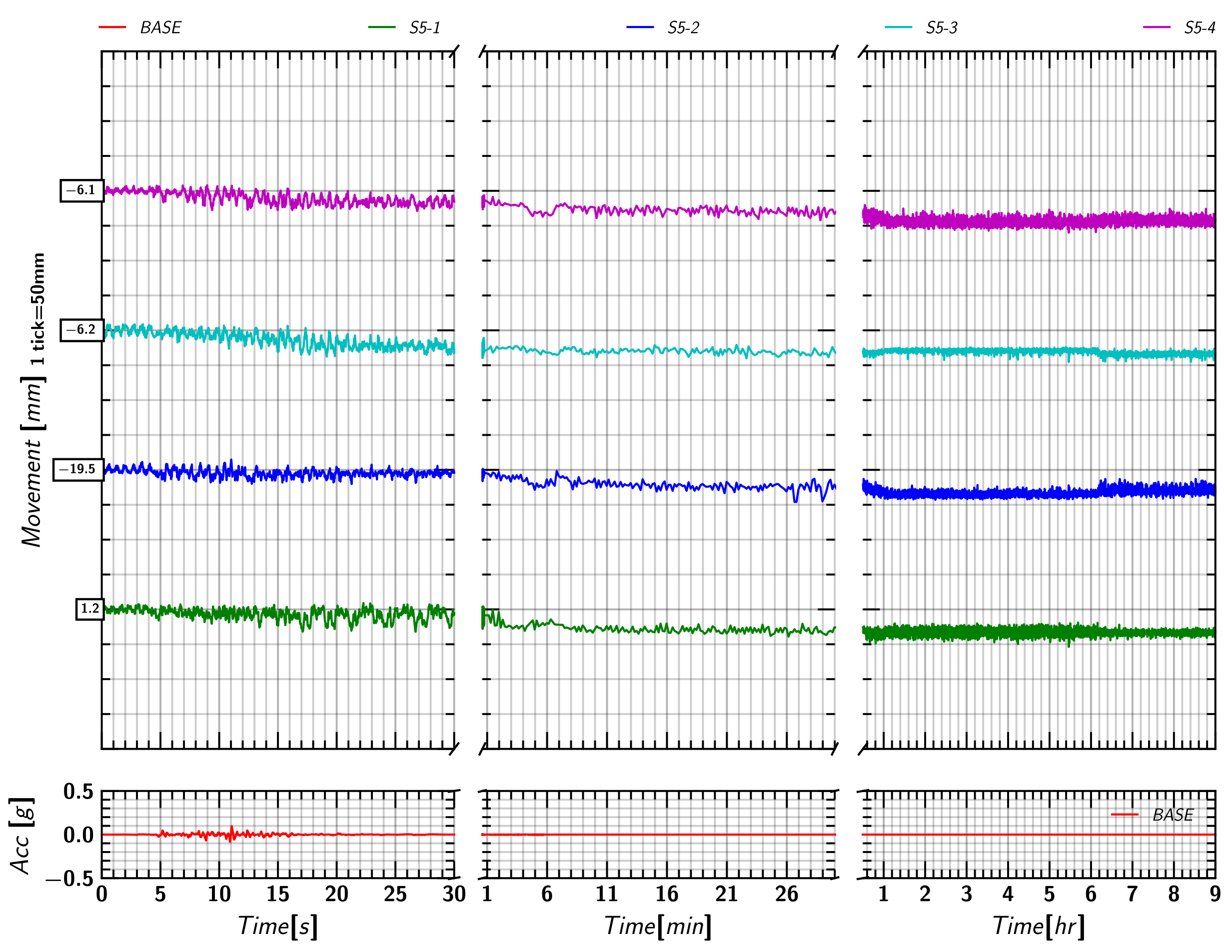

Figure 112. EQM$_1$: Soil (Row S-5) movement in Z-direction relative to the model container during and post shaking.

E.13 Pile 1 Mass Movement in X

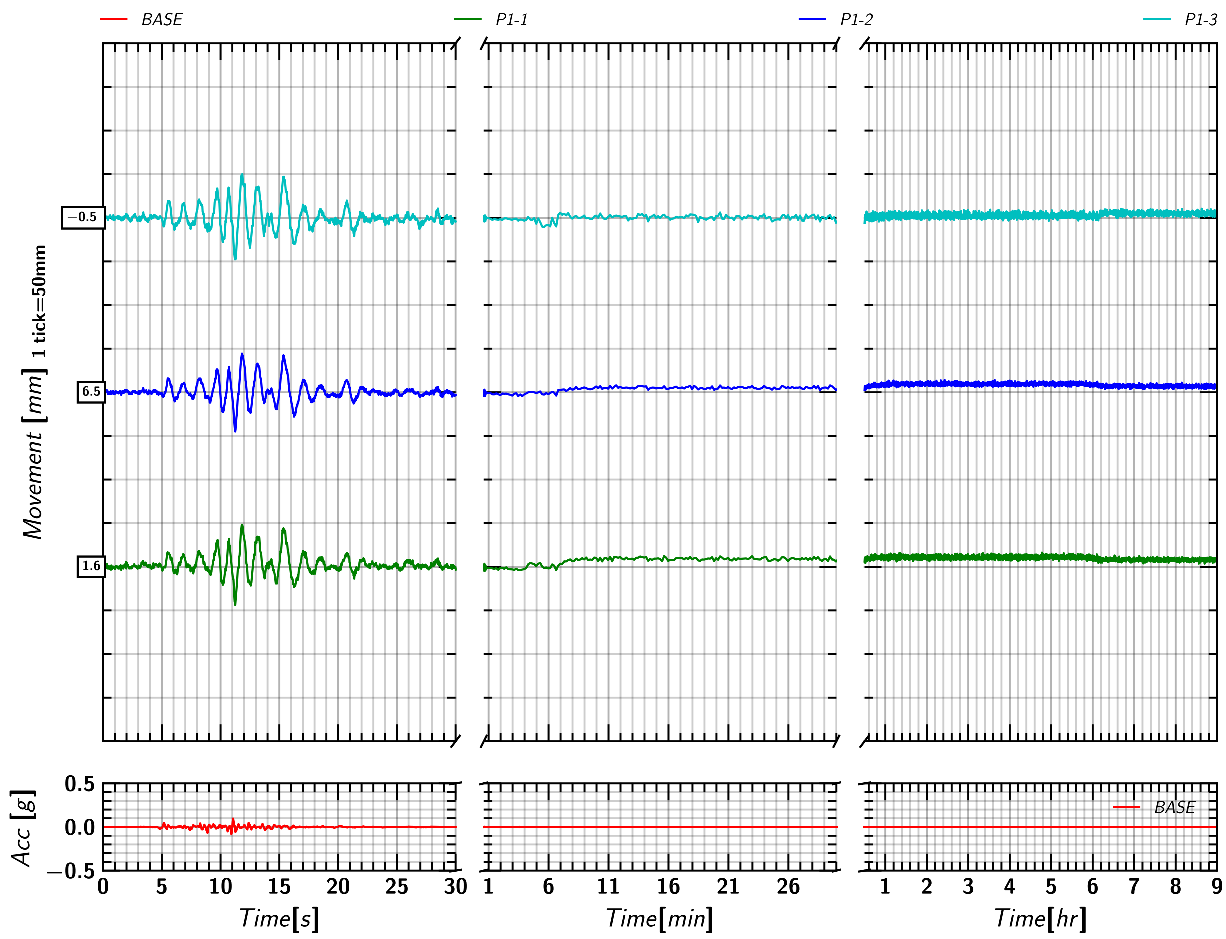

Figure 113. EQM$_1$: Pile 1 movement in X-direction relative to the model container during and post shaking.

E.14 Pile 1 Mass Movement in Z

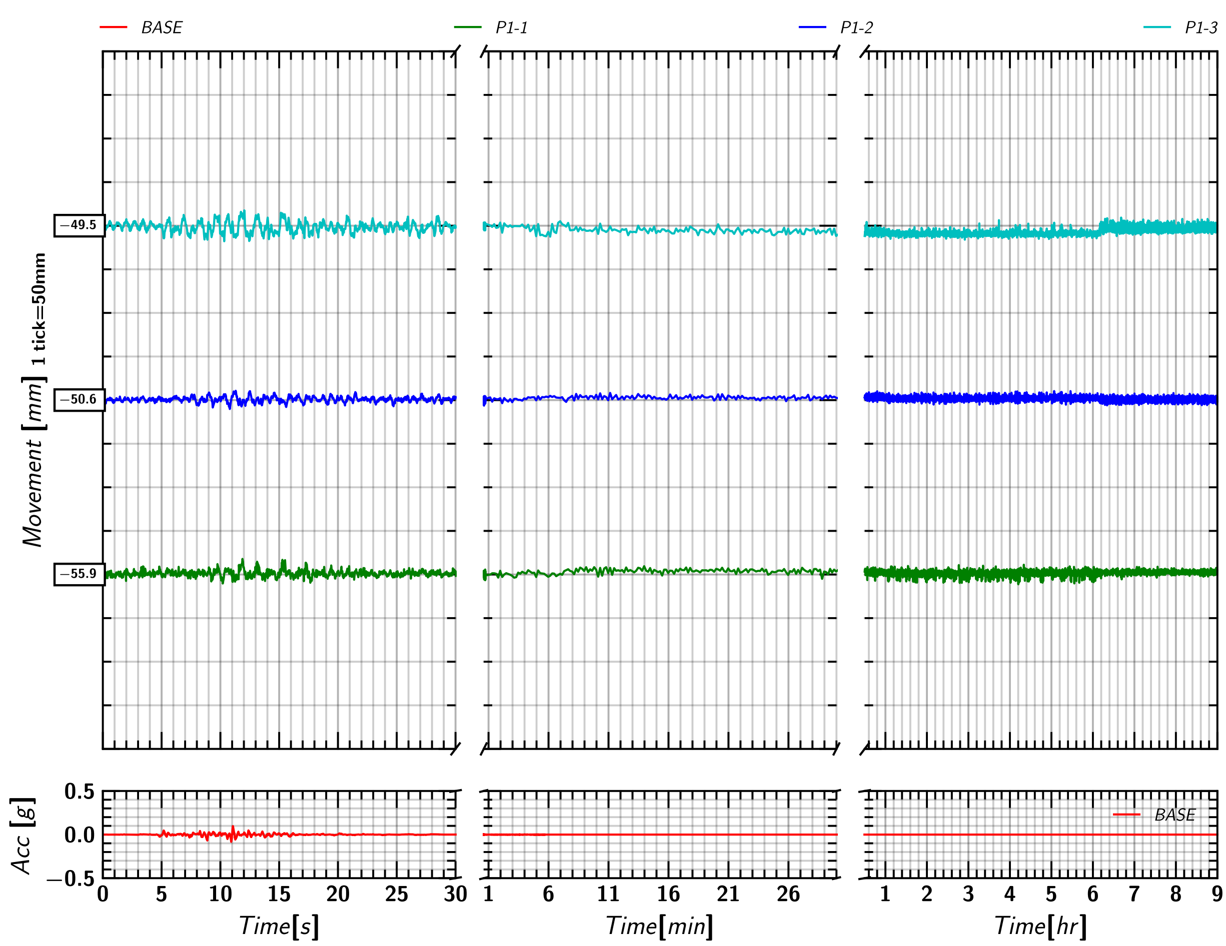

Figure 114. EQM$_1$: Pile 1 movement in Z-direction relative to the model container during and post shaking.

E.15 Pile 2 Mass Movement in X

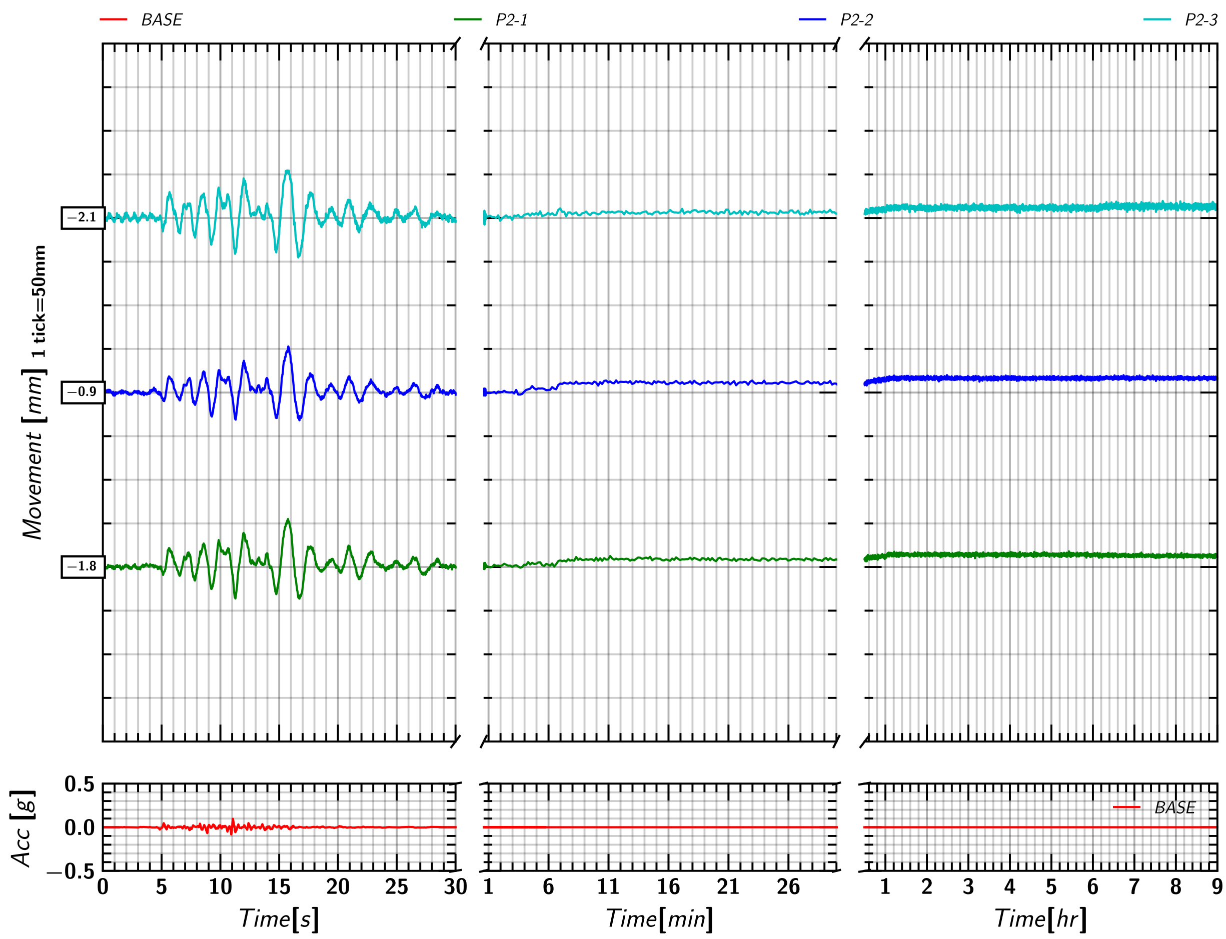

Figure 115. EQM$_1$: Pile 2 movement in X-direction relative to the model container during and post shaking.

E.16 Pile 2 Mass Movement in Z

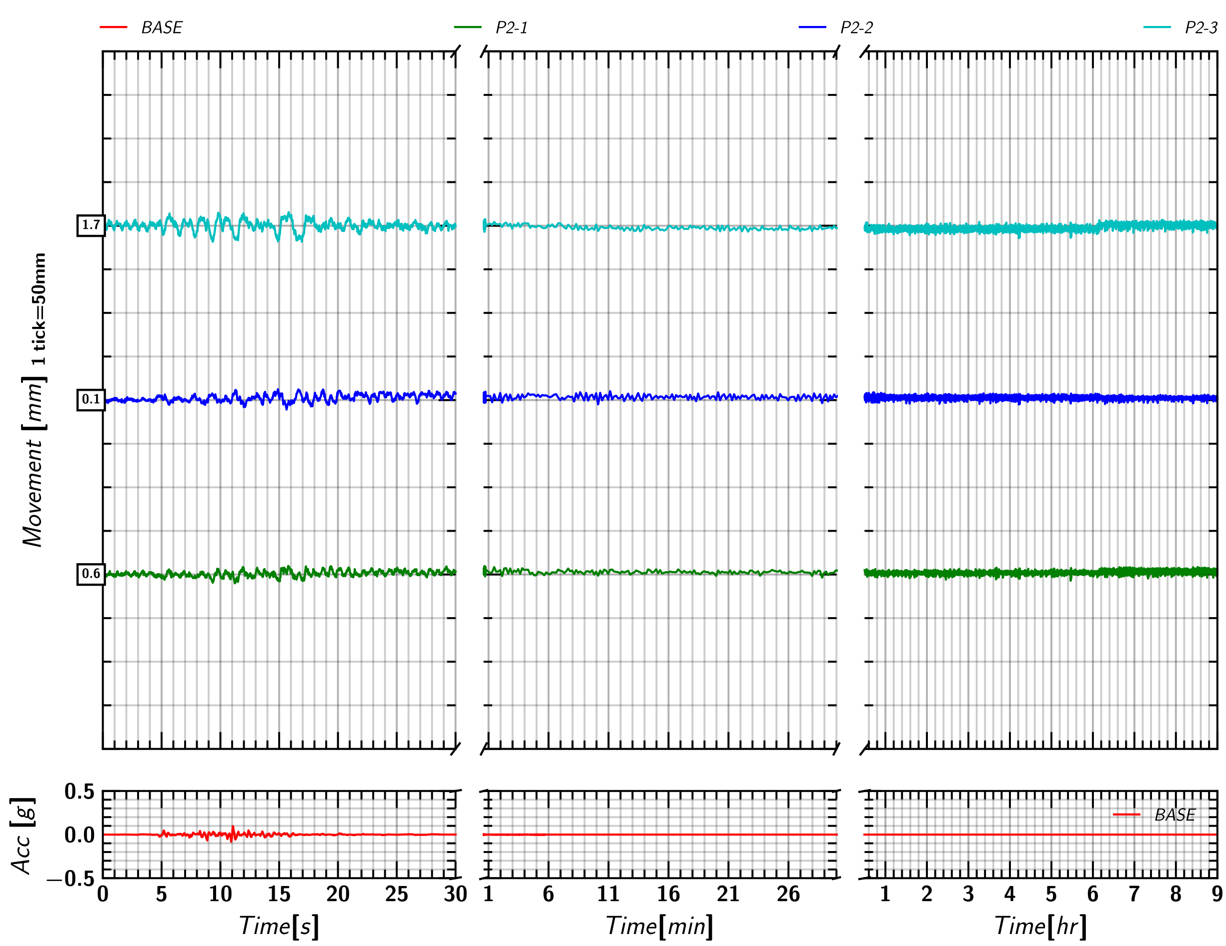

Figure 116. EQM$_1$: Pile 2 movement in Z-direction relative to the model container during and post shaking.

E.17 Pile 3 Mass Movement in X

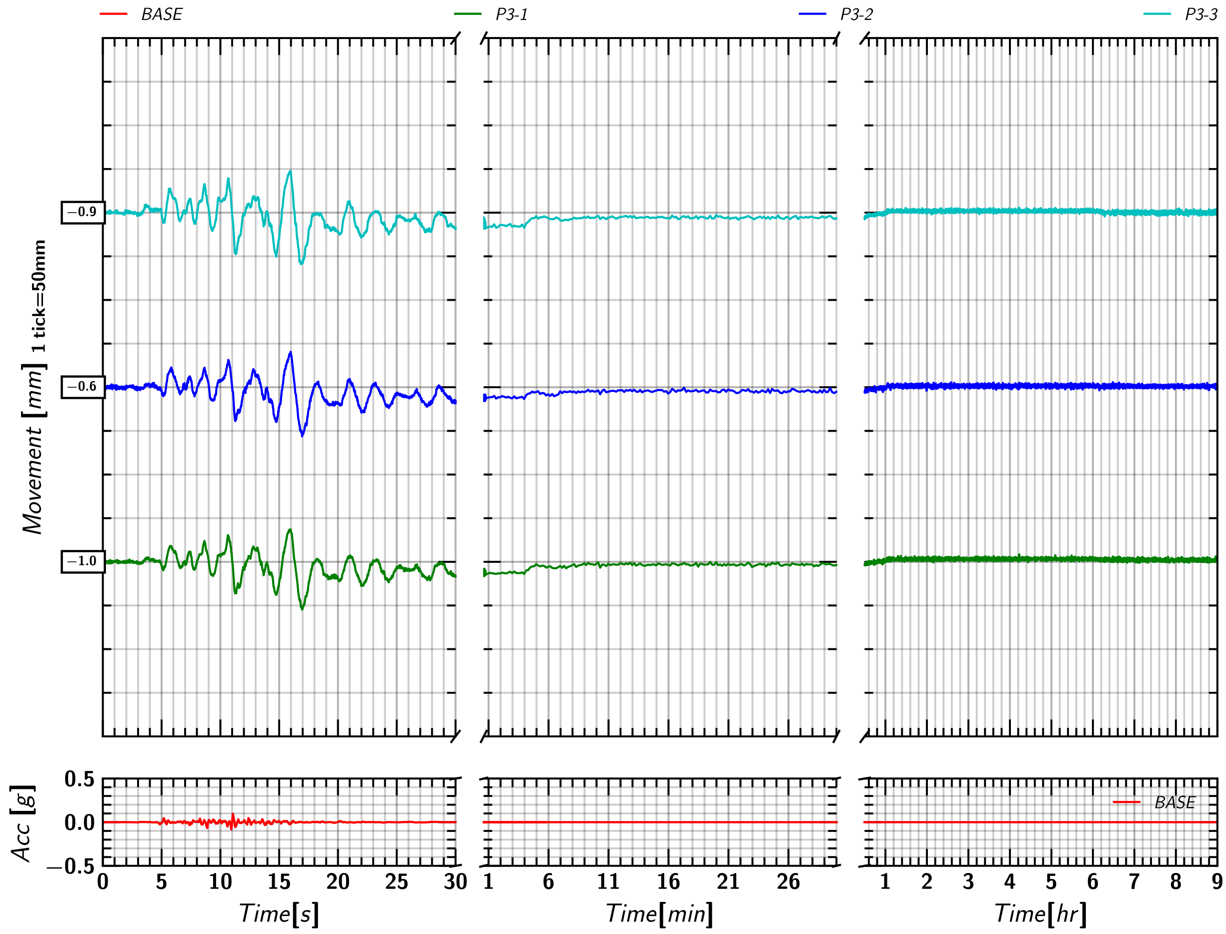

Figure 117. EQM$_1$: Pile 3 movement in X-direction relative to the model container during and post shaking.

E.18 Pile 3 Mass Movement in Z

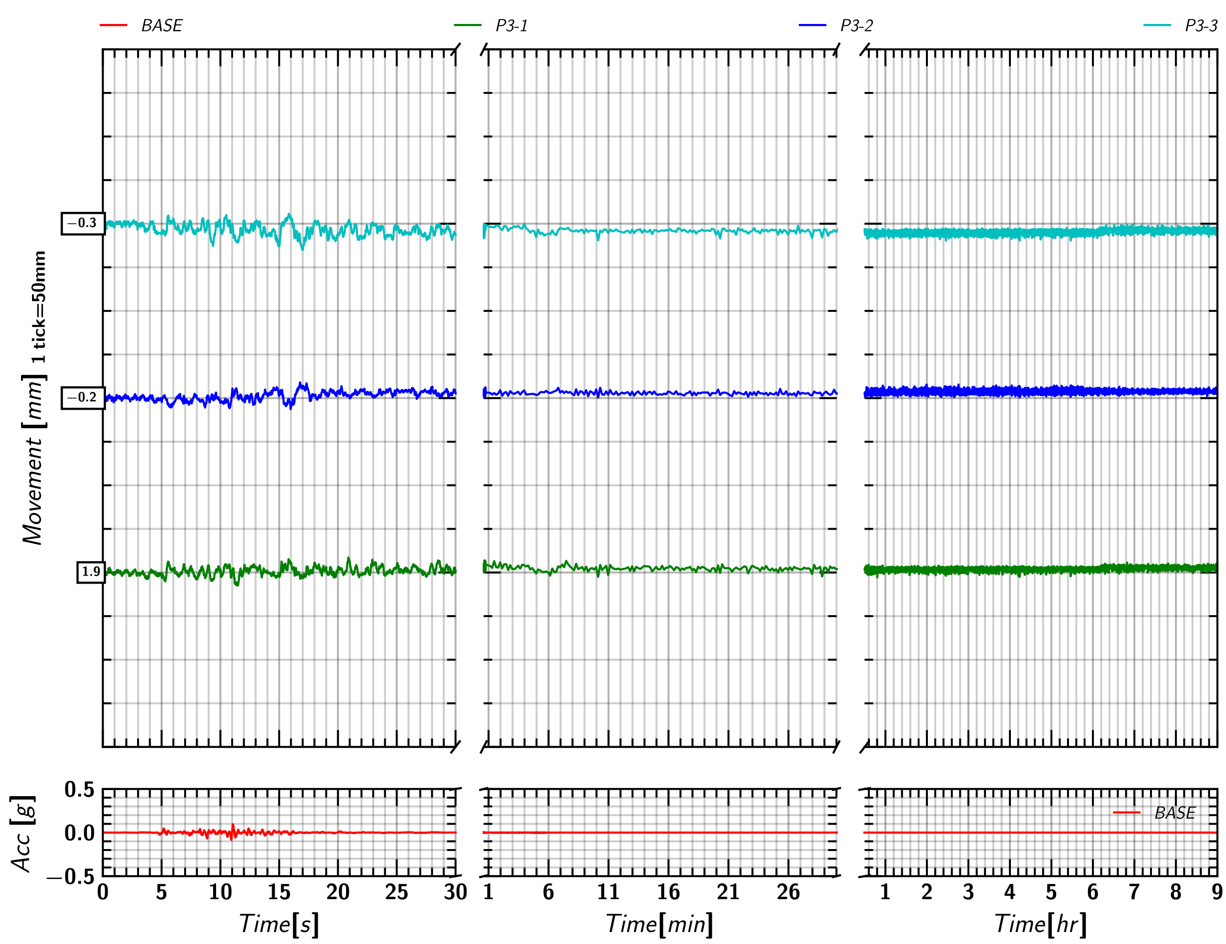

Figure 118. EQM$_1$: Pile 3 movement in Z-direction relative to the model container during and post shaking.

F. EQM$_2$: MEDIUM SANTA CRUZ EARTHQUAKE (PGA= 0.13g)

F.1 Input Motion

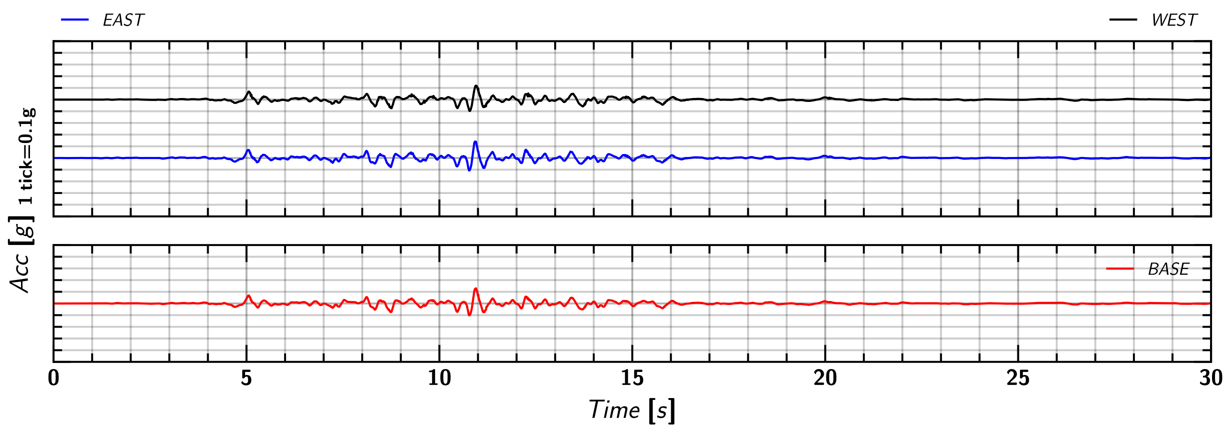

Figure 119. EQM$_2$: Input motion.

F.2 Spectral Acceleration

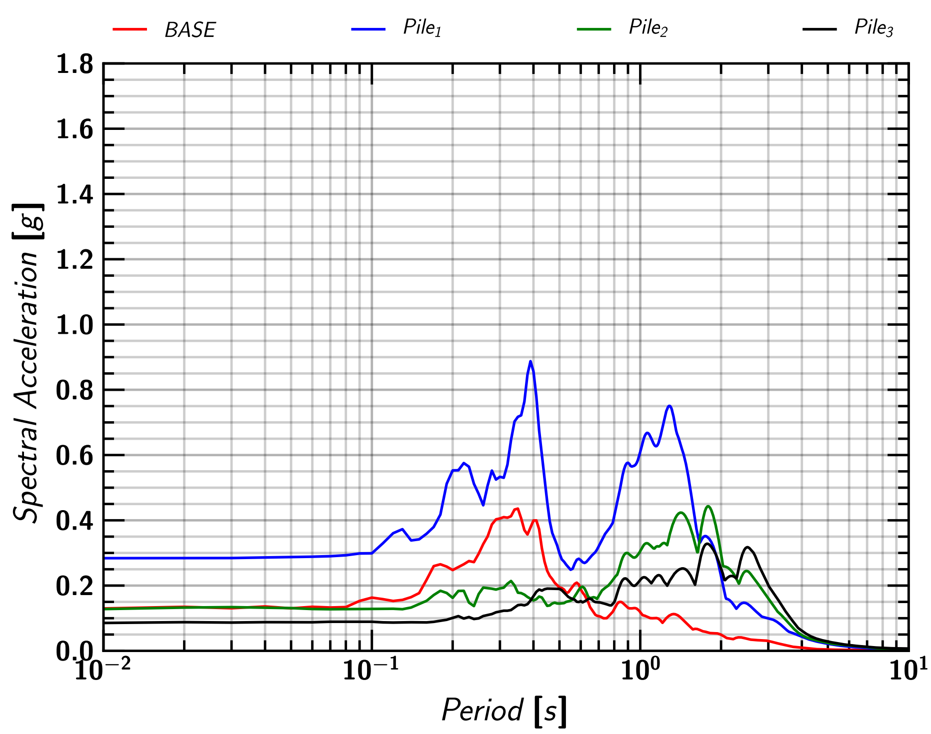

Figure 120. EQM$_2$: Spectral Acceleration.

F.3 Container Acceleration

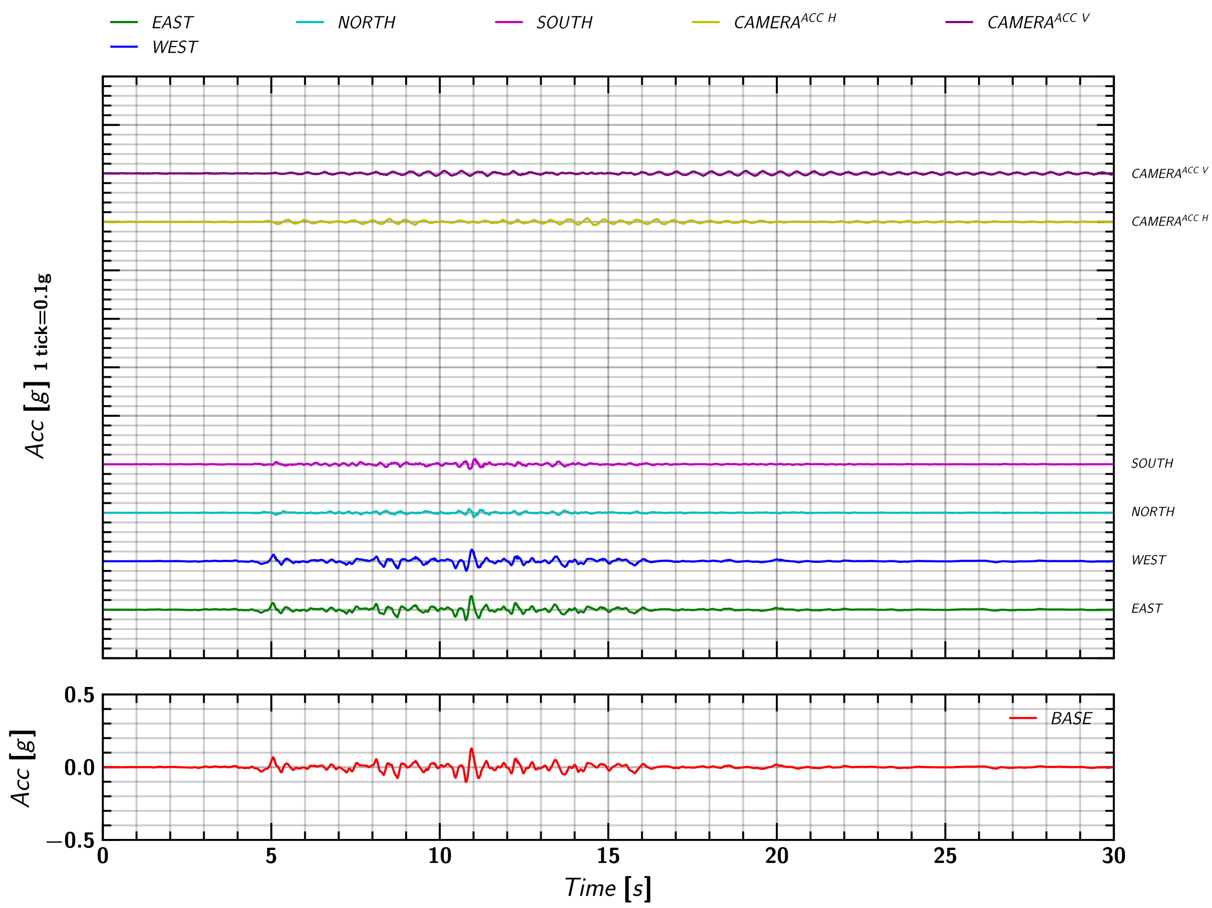

Figure 121. EQM$_2$: Acceleration measurement on container and camera beam.

F.4 Soil Acceleration

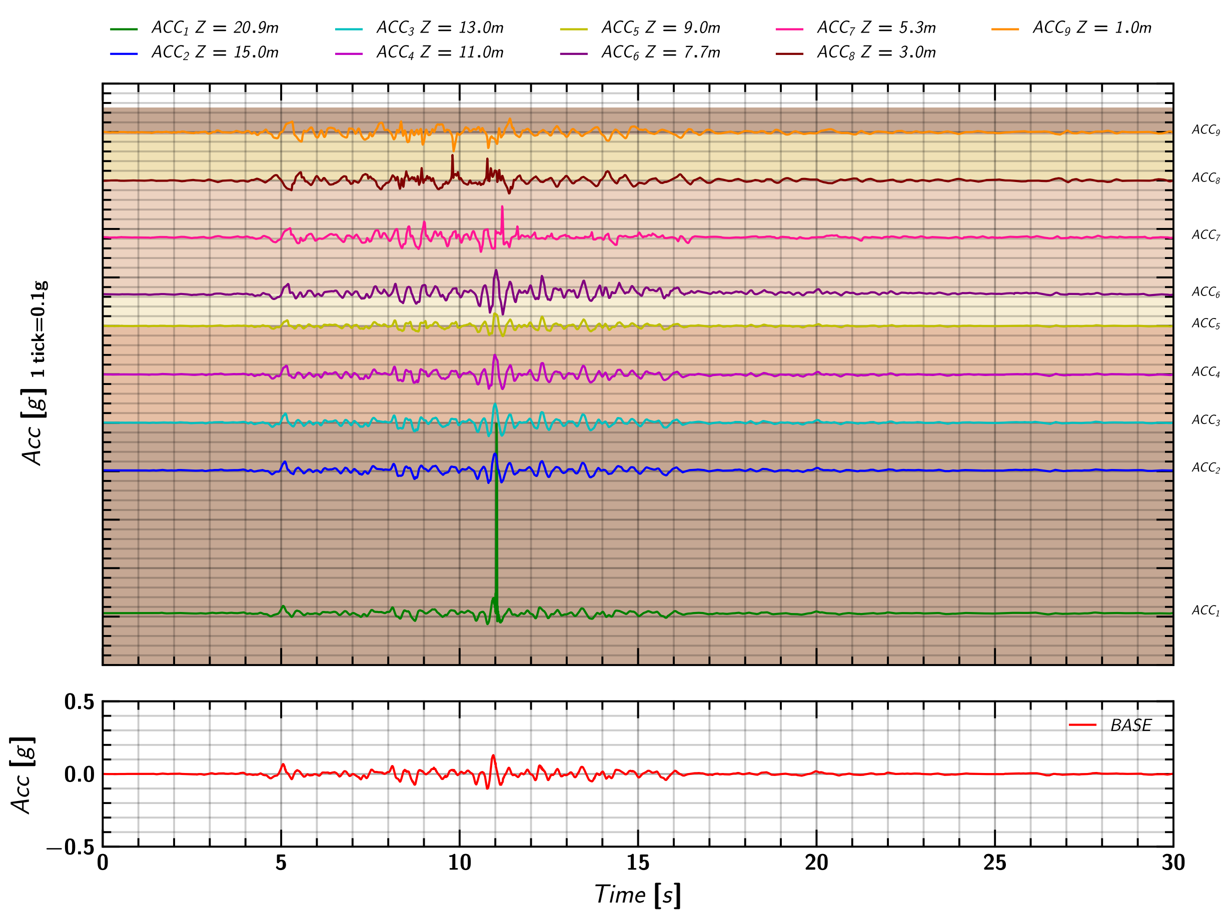

Figure 122. EQM$_2$: Acceleration measurement in soil.

F.5 Pile Mass Acceleration

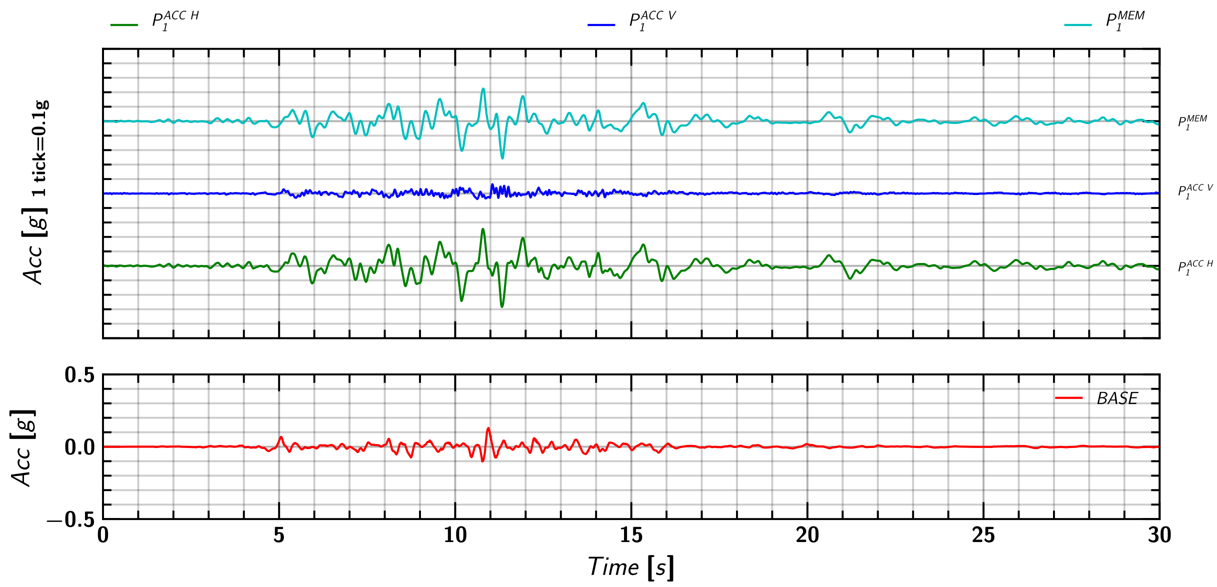

Figure 123. EQM$_2$: Acceleration measurement on pile 1.

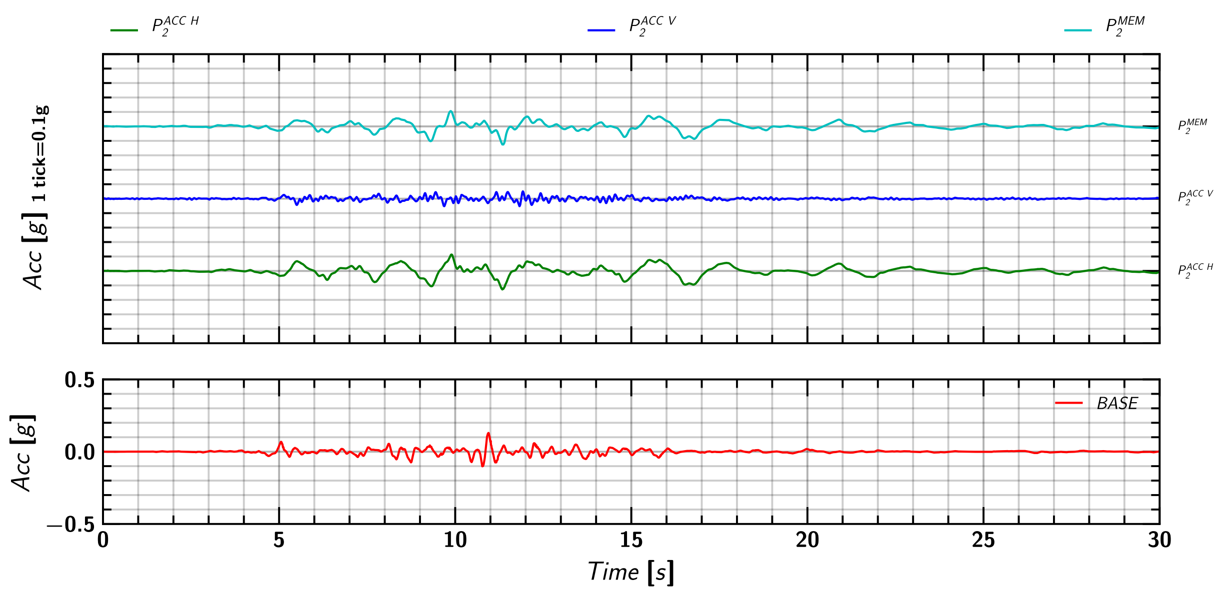

Figure 124. EQM$_2$: Acceleration measurement on pile 2.

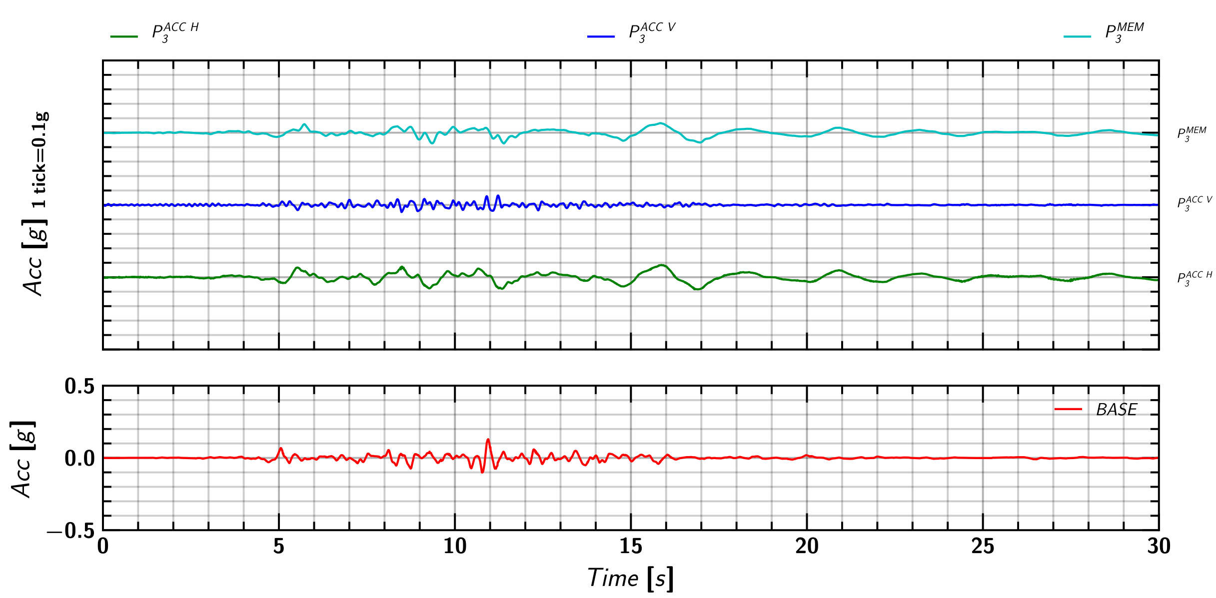

Figure 125. EQM$_2$: Acceleration measurement on pile 3.

F.6 Soil and Pile Lateral Mass Movement in X direction

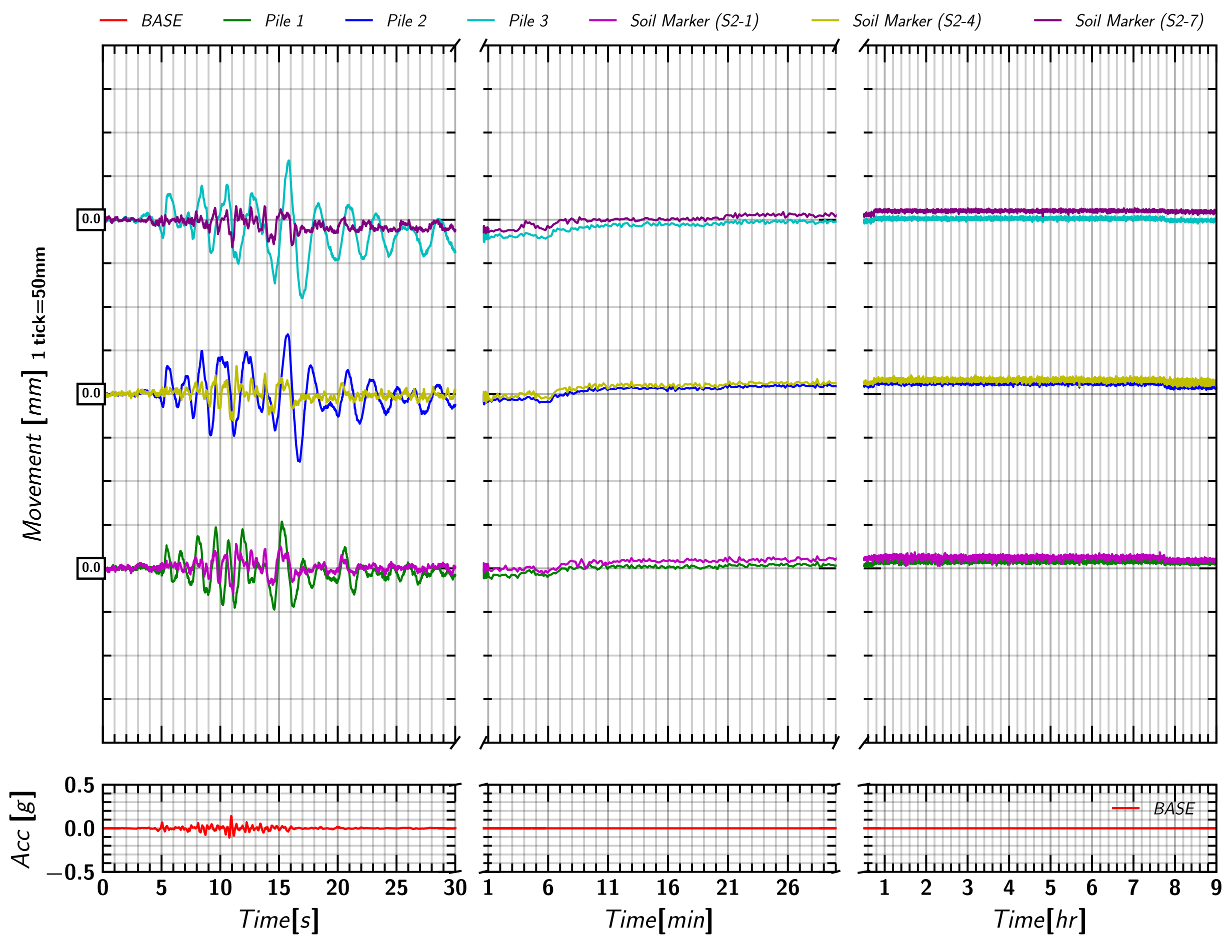

Figure 126. EQM$_2$: Lateral movement of soil and pile in x-direction during and post the applied earthquake motion.

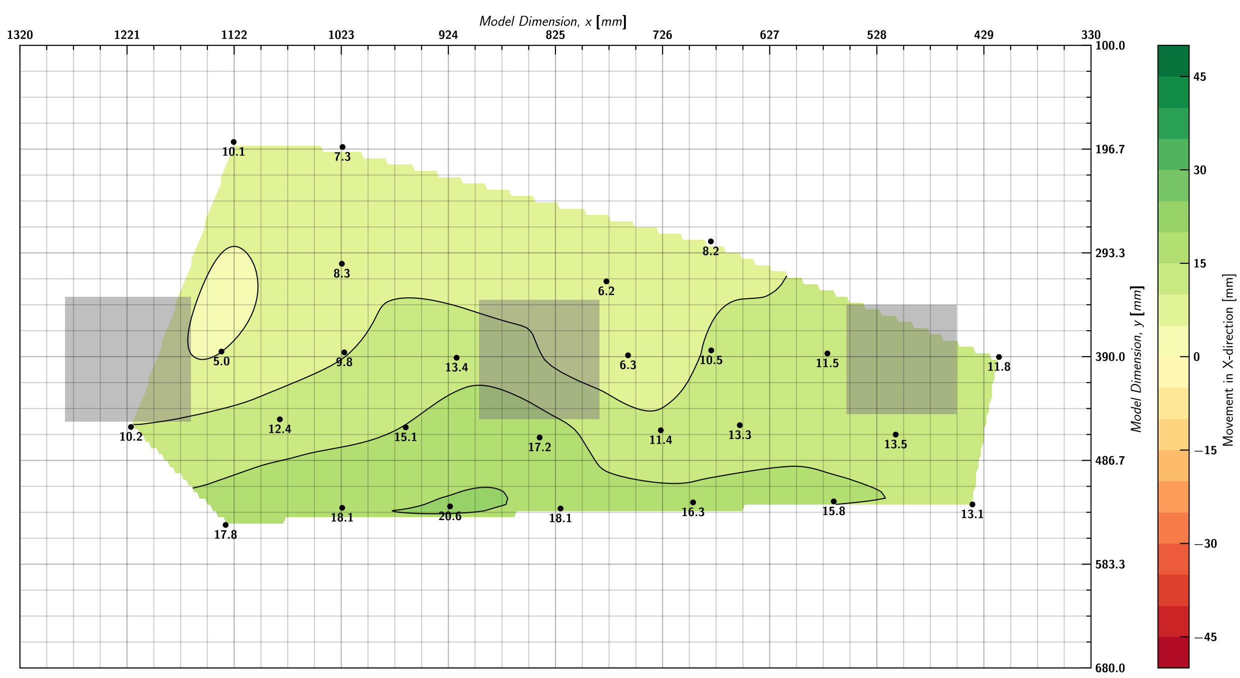

Figure 127. EQM$_2$:Contour of lateral movement of soil with respect to container in x-direction at the end of reconsolidation (t=200 minutes).

F.7 Soil and Pile Settlement (i.e., movement in Z direction)

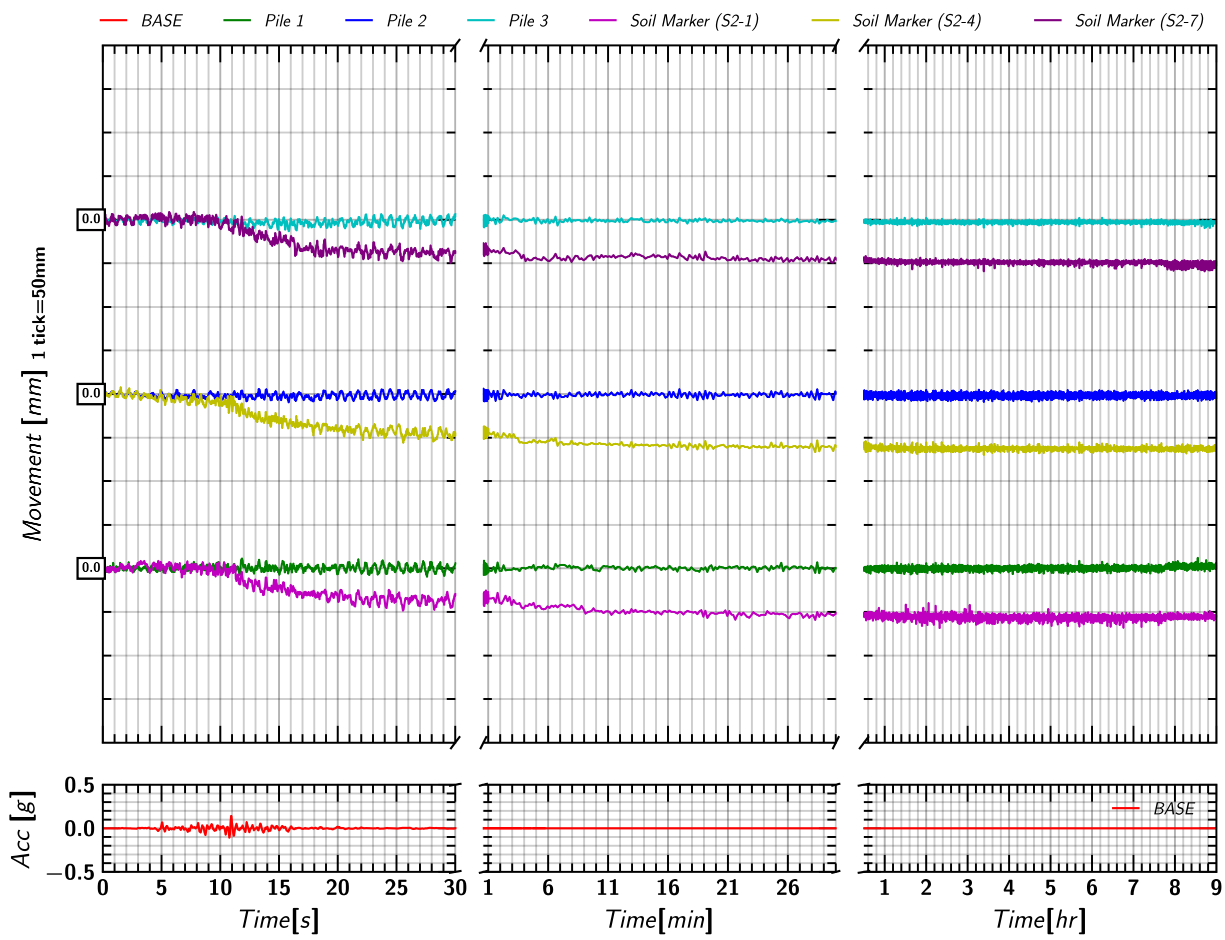

Figure 128. EQM$_2$: Settlement measurement in soil and pile during and post the applied earthquake motion.

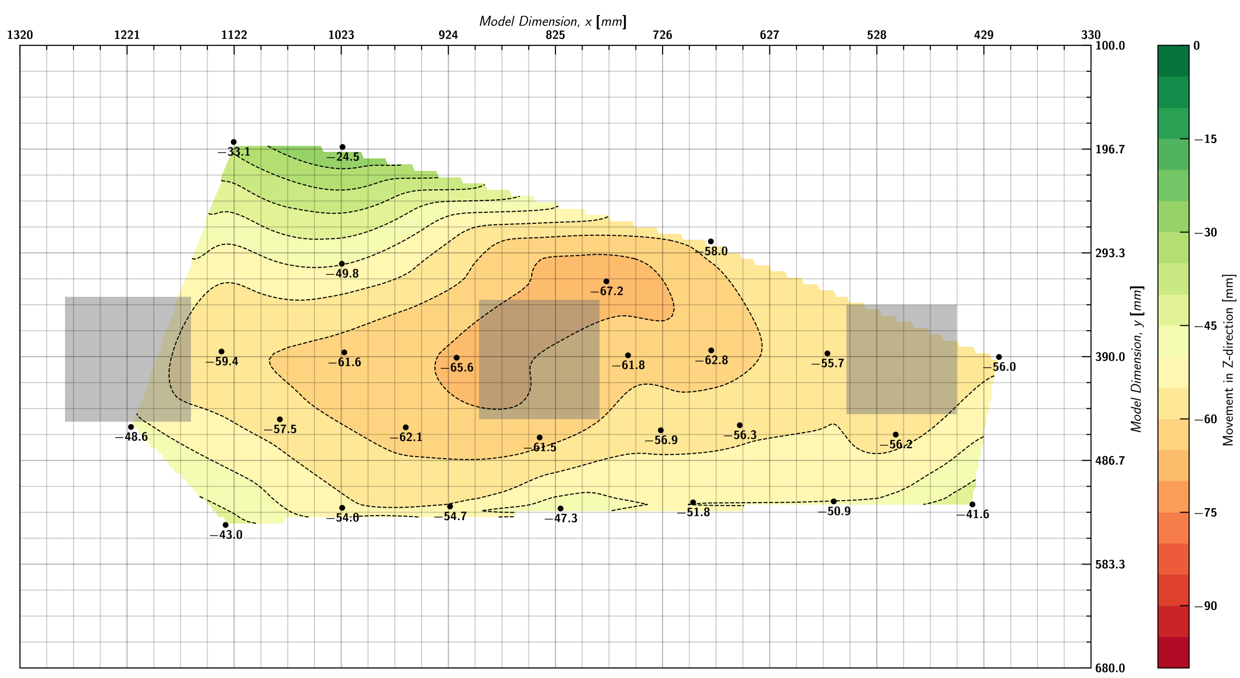

Figure 129. EQM$_2$:Contour of soil settlement with respect to container at the end of reconsolidation (t=200 minutes).

F.8 Pore pressure in Soil Measured by Keller Transducers

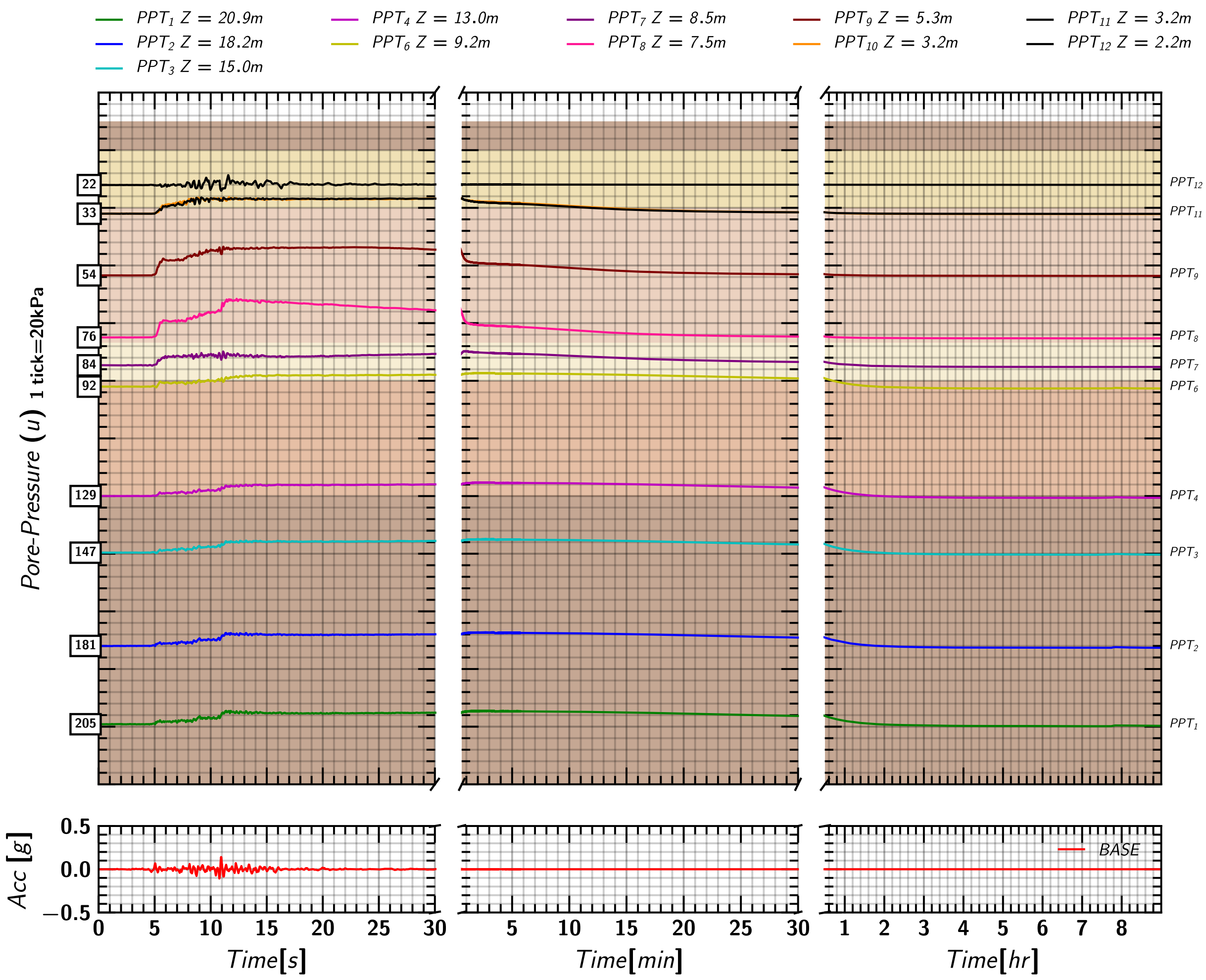

Figure 130. EQM$_2$: Pore pressure measurements in soil from Keller transducers during and post shaking.

F.9 Pore pressure in Soil Measured by MS54XXX Transducers

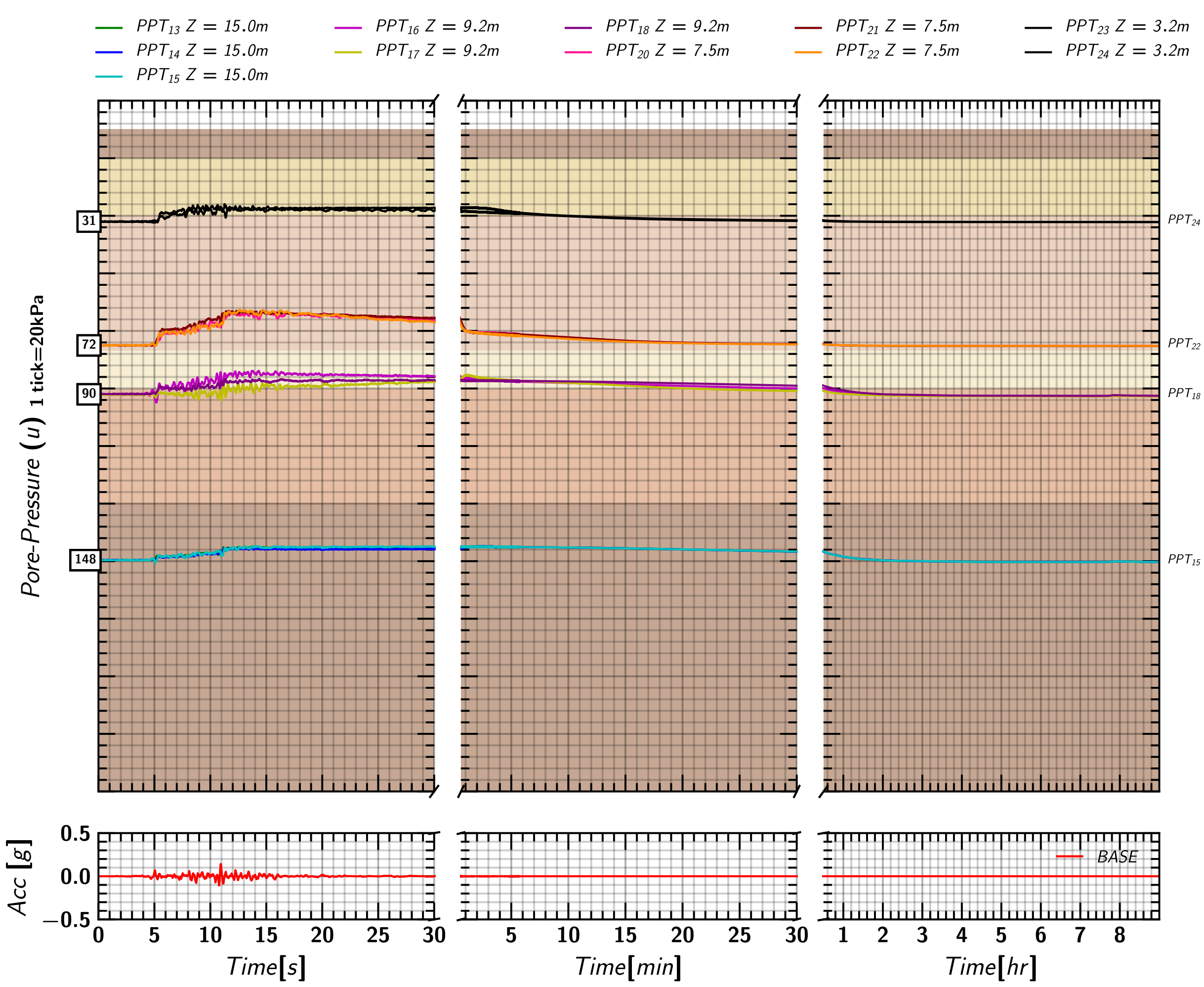

Figure 131. EQM$_2$: Pore pressure measurements in soil from MS54XXX transducers during and post shaking.

Dense Sand	Medium Dense Sand	Clayey Silt	Loose Sand	Clay Crust

F.10 Excess Pore pressures Ratio (r_u) Estimated from Keller Transducers

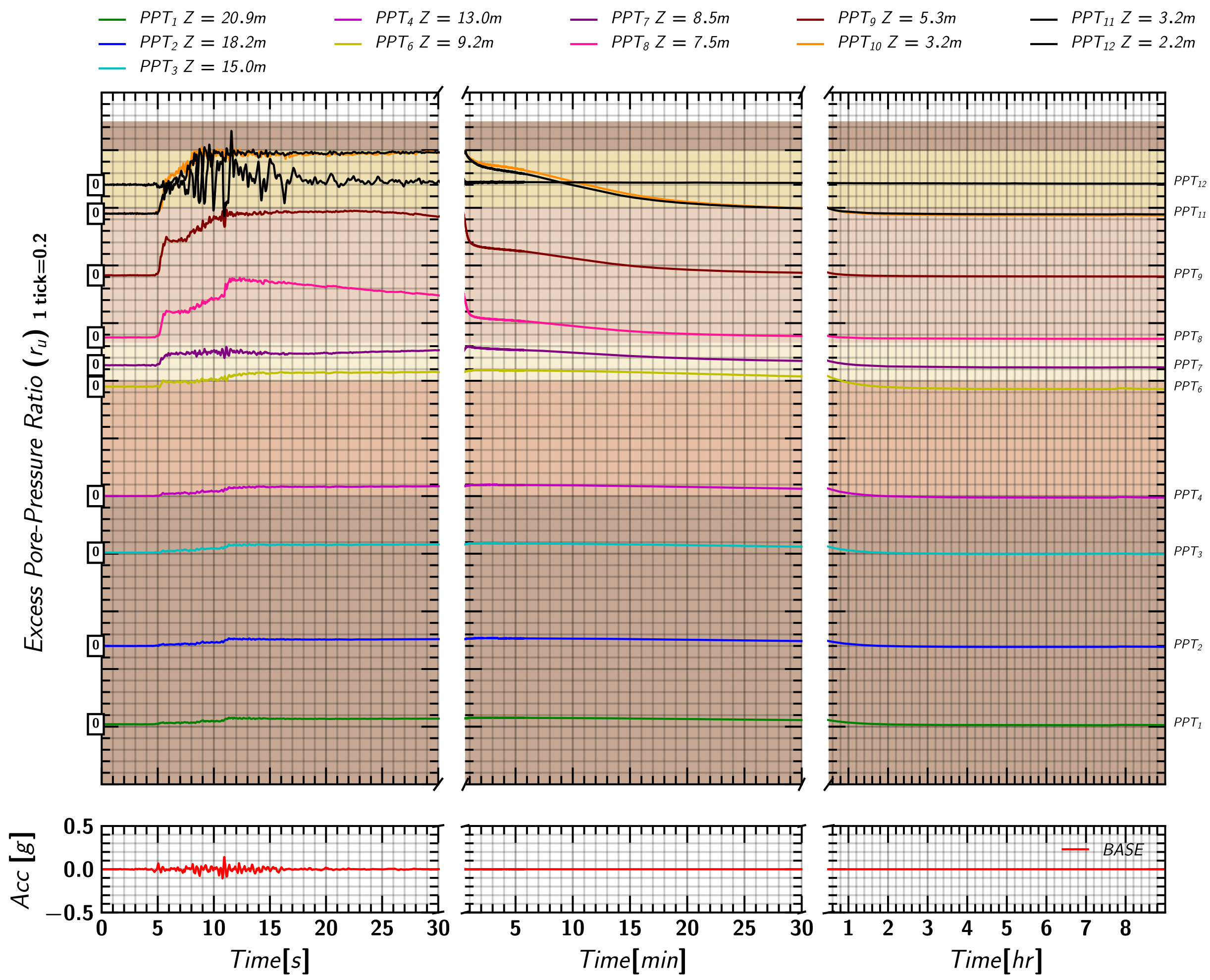

Figure 132. EQM$_2$: Excess pore pressure ratio (r_u) estimated from Keller transducers during and post shaking.

F.11 Excess Pore pressure Ratio (r_u) Estimated from MS54XXX Transducers

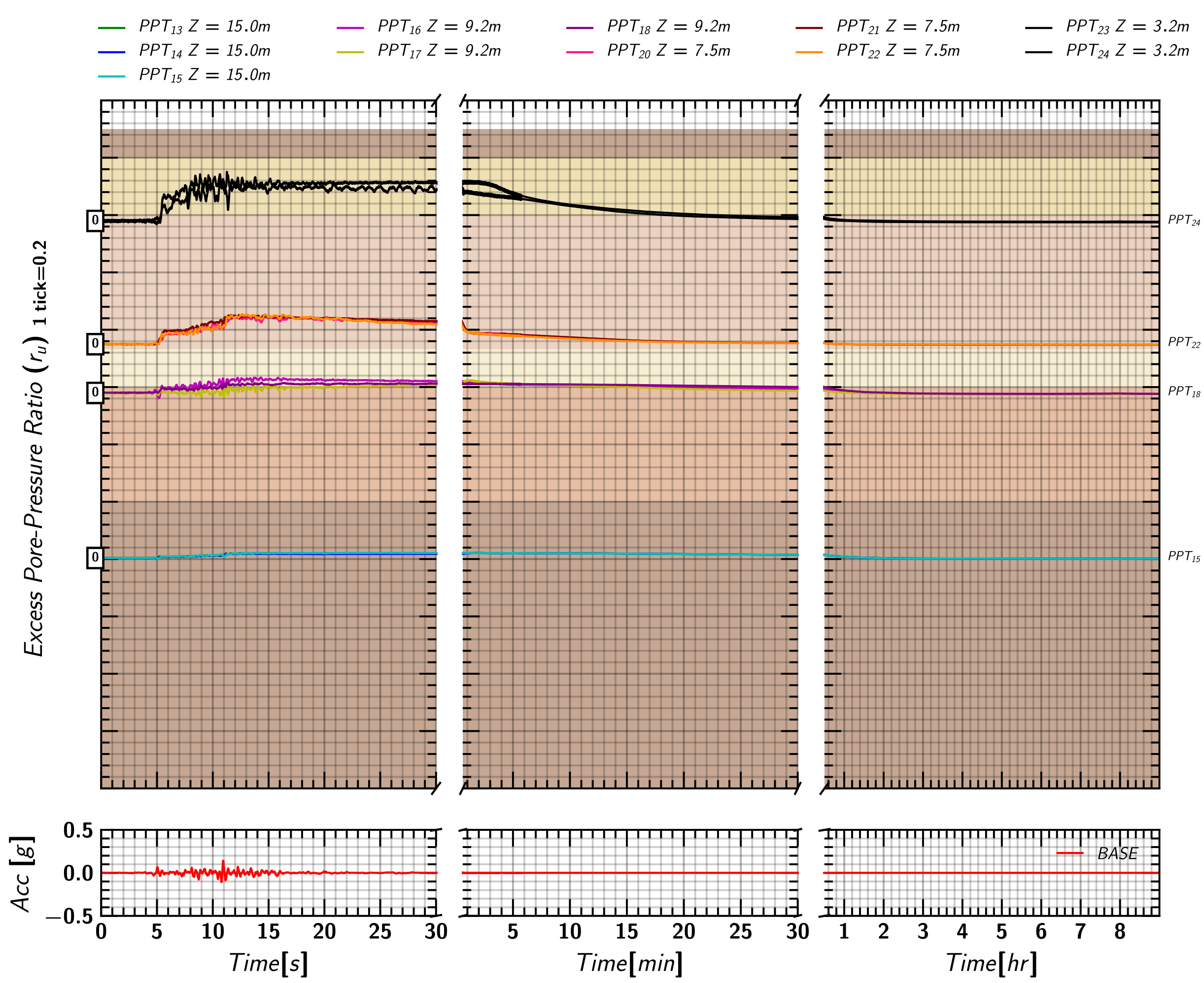

Figure 133. EQM$_2$: Excess pore pressure ratio (r_u) estimated from MS54XXX transducers during and post shaking.

Dense Sand	Medium Dense Sand	Clayey Silt	Loose Sand	Clay Crust

F.12 Axial Load in Pile 1

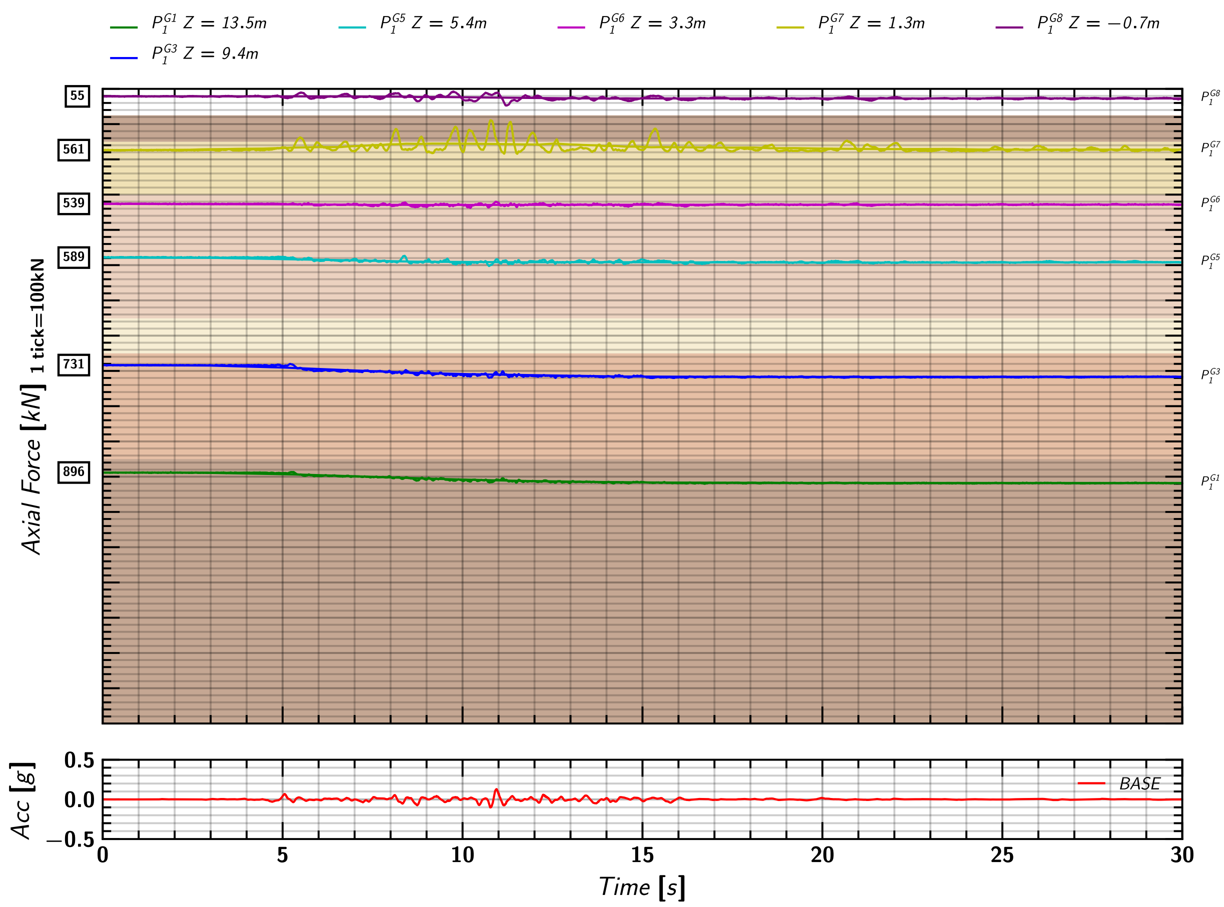

Figure 134. EQM$_2$: Axial load measurements from pile 1 strain gages during shaking.

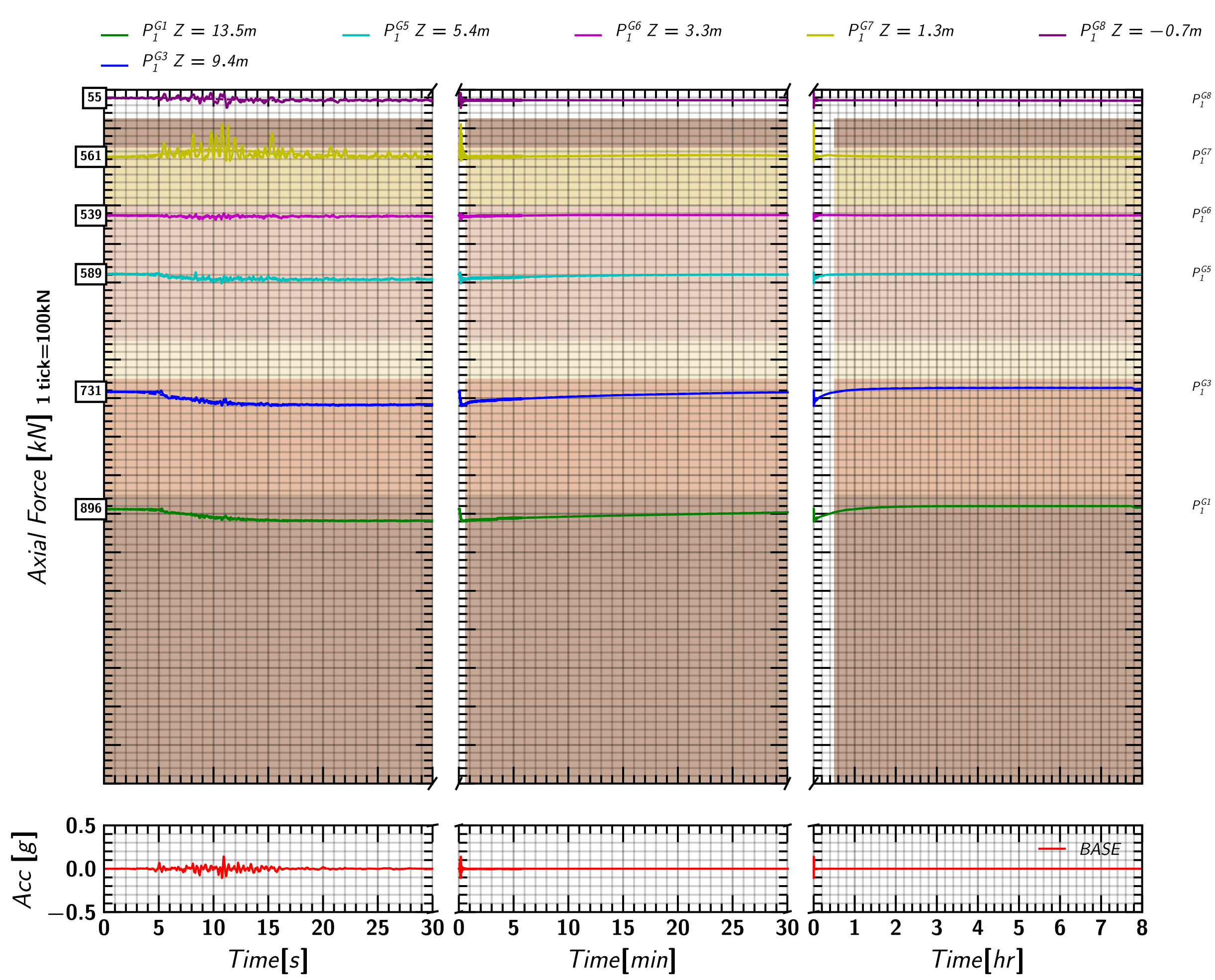

Figure 135. EQM$_2$: Axial load measurements from pile 1 strain gages during and post shaking.

F.13 Axial Load in Pile 2

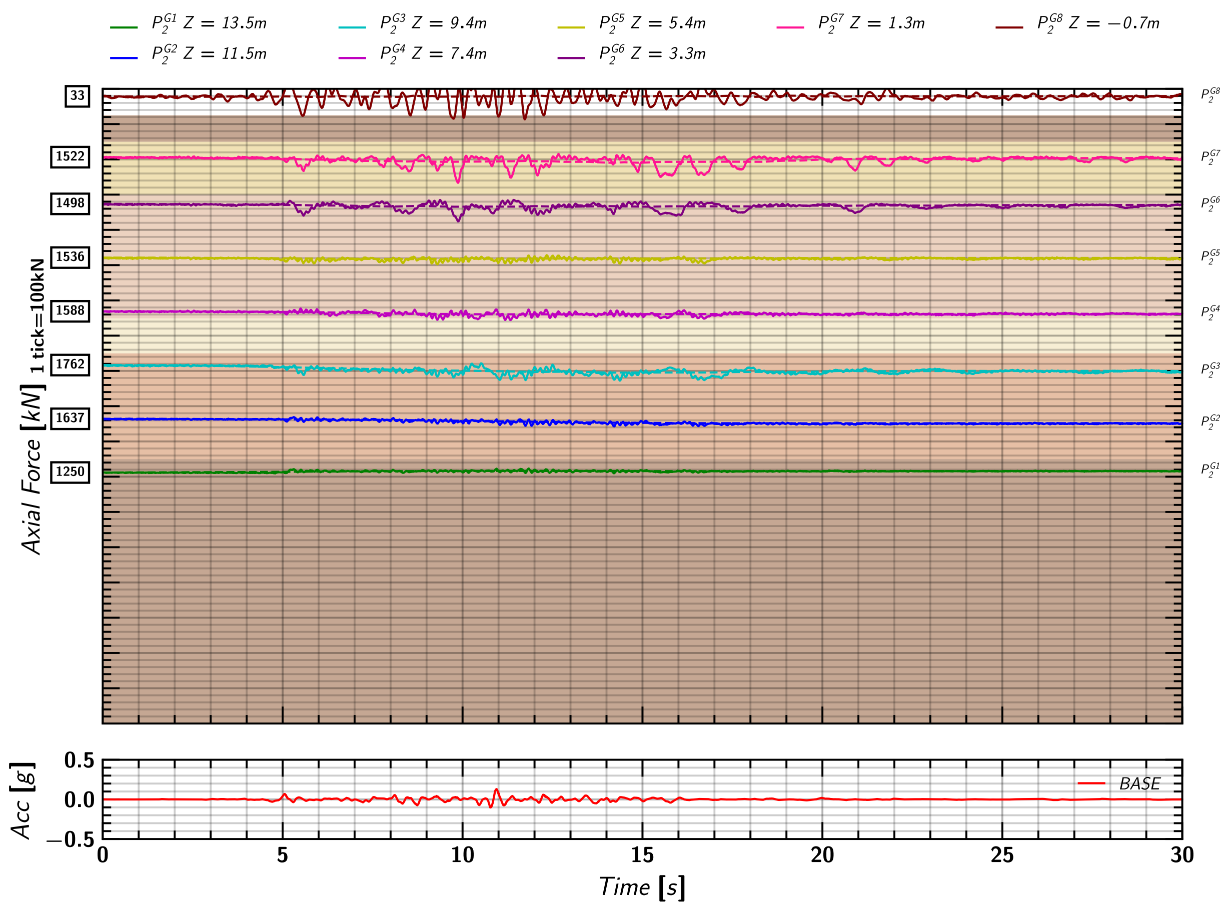

Figure 136. EQM$_2$: Axial load measurements from pile 2 strain gages during shaking.

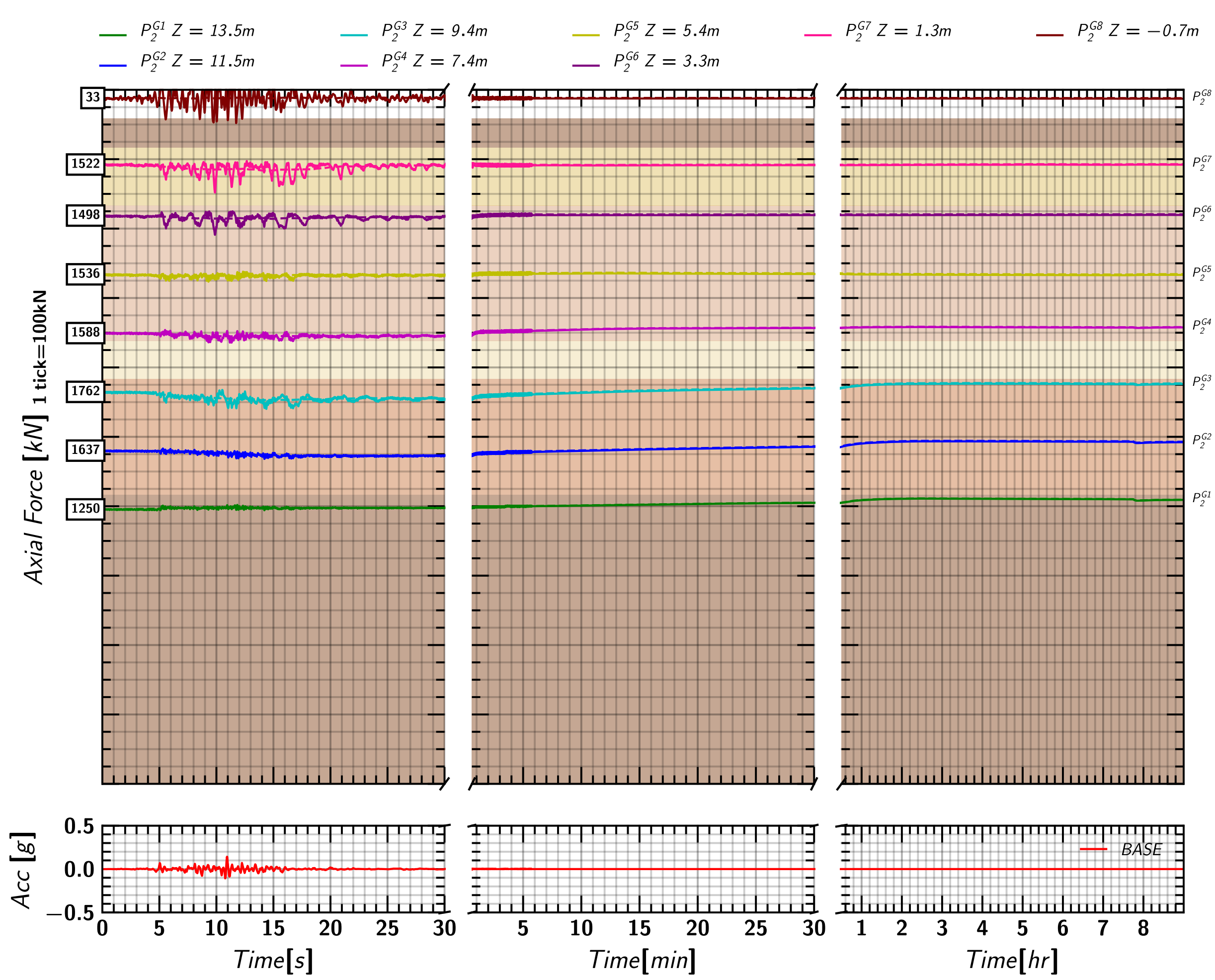

Figure 137. EQM$_2$: Axial load measurements from pile 2 strain gages during and post shaking.

F.14 Axial Load in Pile 3

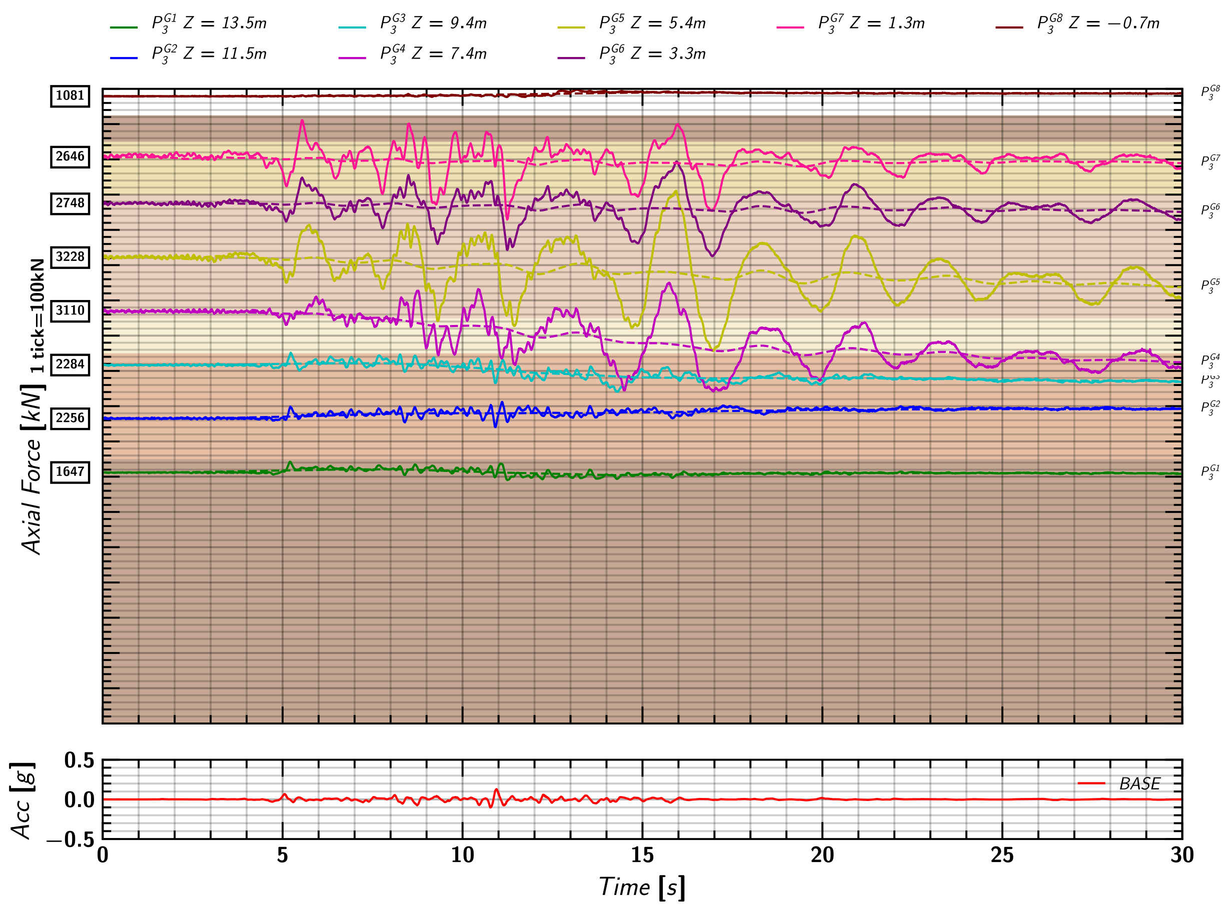

Figure 138. EQM$_2$: Axial load measurements from pile 3 strain gages during shaking.

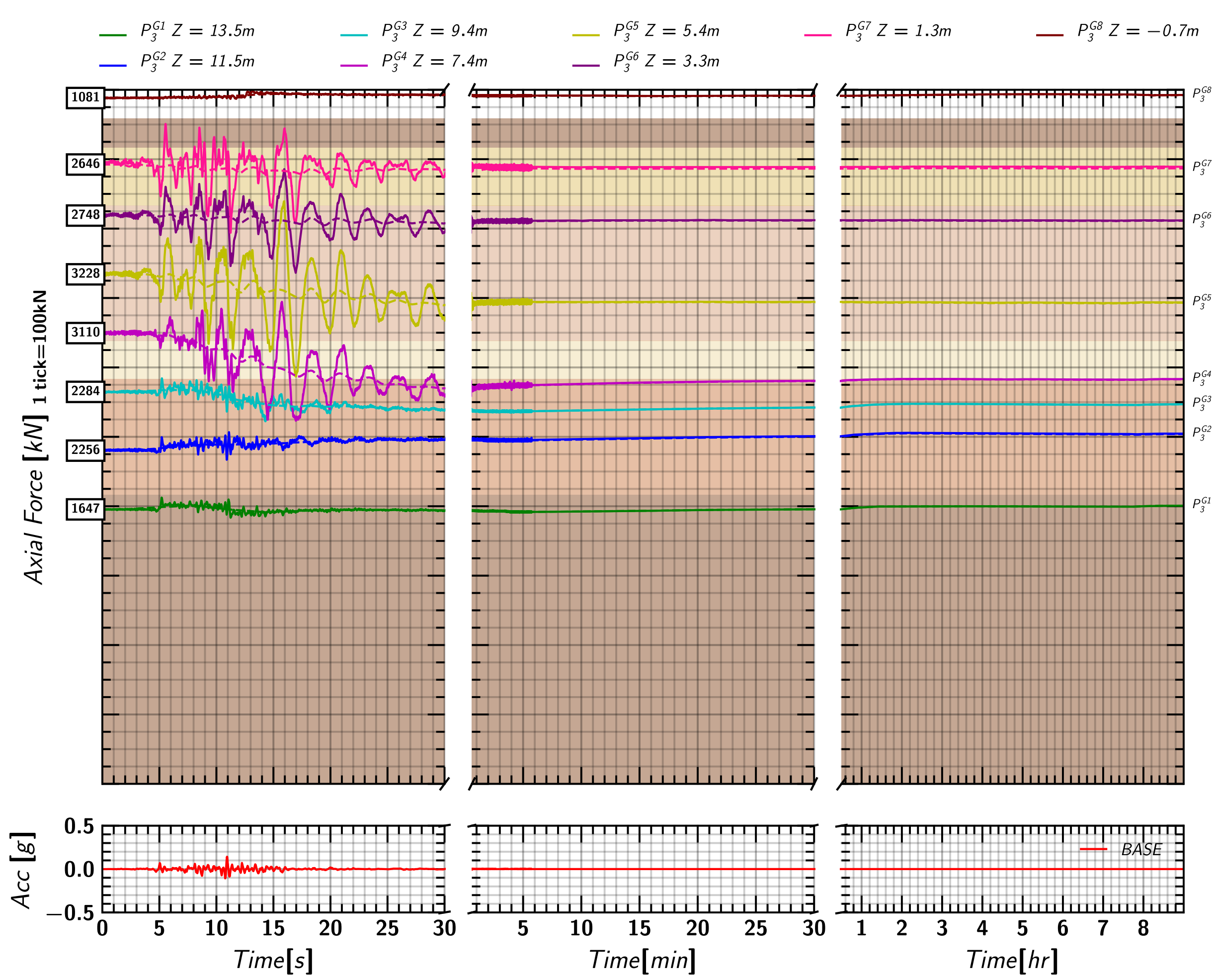

Figure 139. EQM$_2$: Axial load measurements from pile 3 strain gages during and post shaking.

Dense Sand | Medium Dense Sand | Clayey Silt | Loose Sand | Clay Crust

F.15 Pore pressure and Axial Load Profile

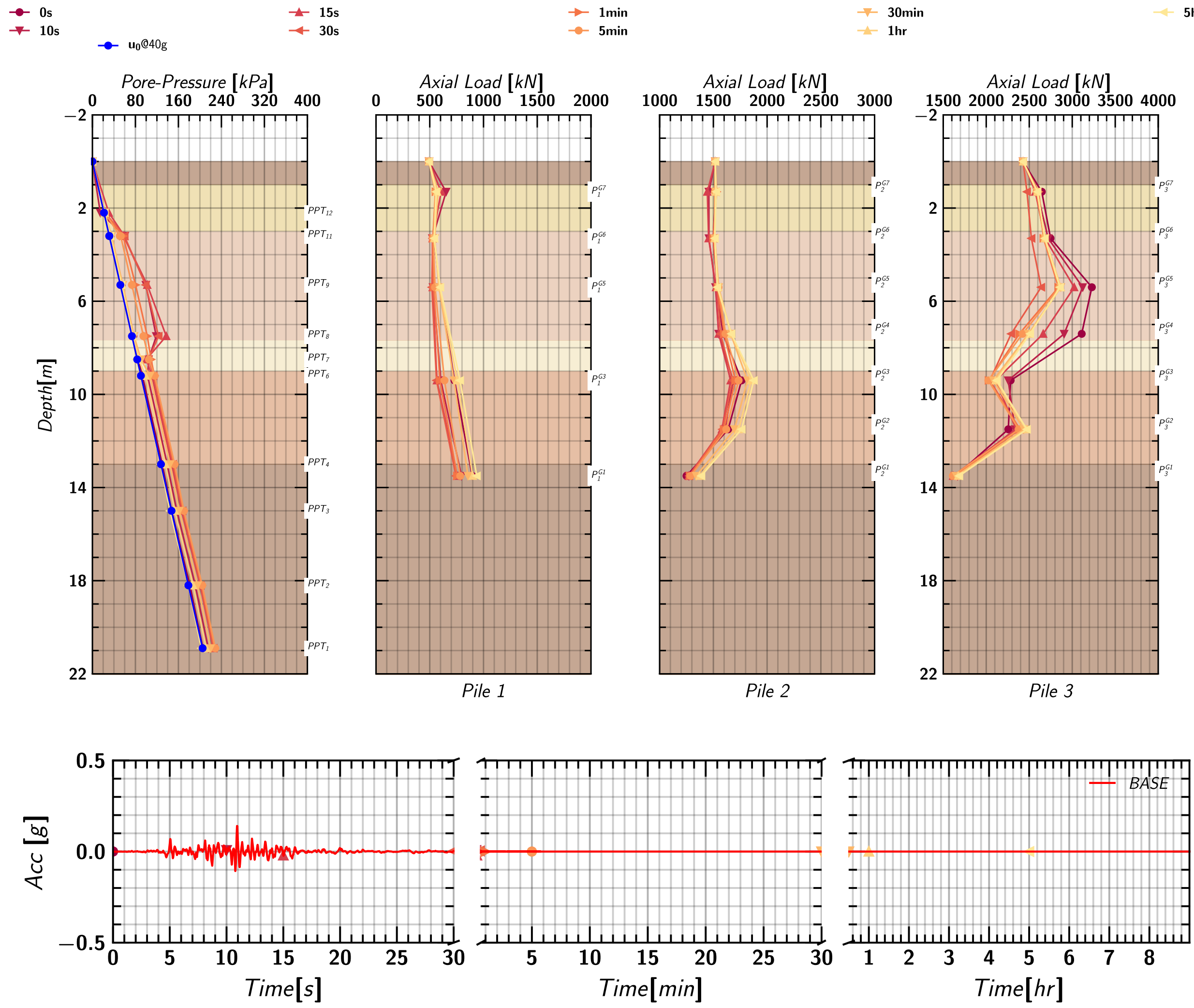

Figure 140. EQM₂: Pore pressure and axial load profile in pile 1, pile 2 and pile 3 at different times during and post shaking.

G. EQM$_2$: Soil, Pile and Container Movements in X and Z

G.1 Container Movement in X

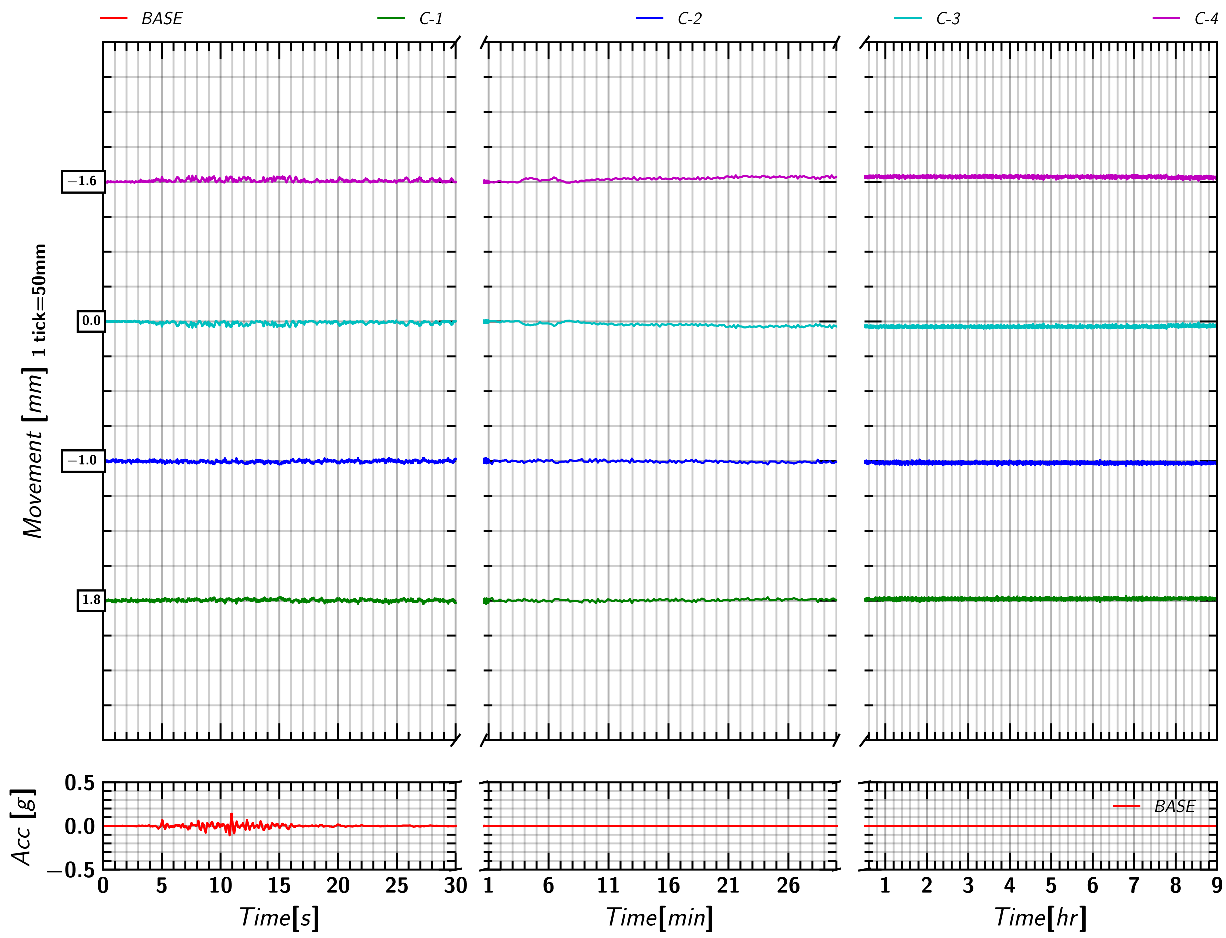

Figure 141. EQM$_2$: Container movement in X-direction relative to the model container during and post shaking.

G.2 Container Movement in Z

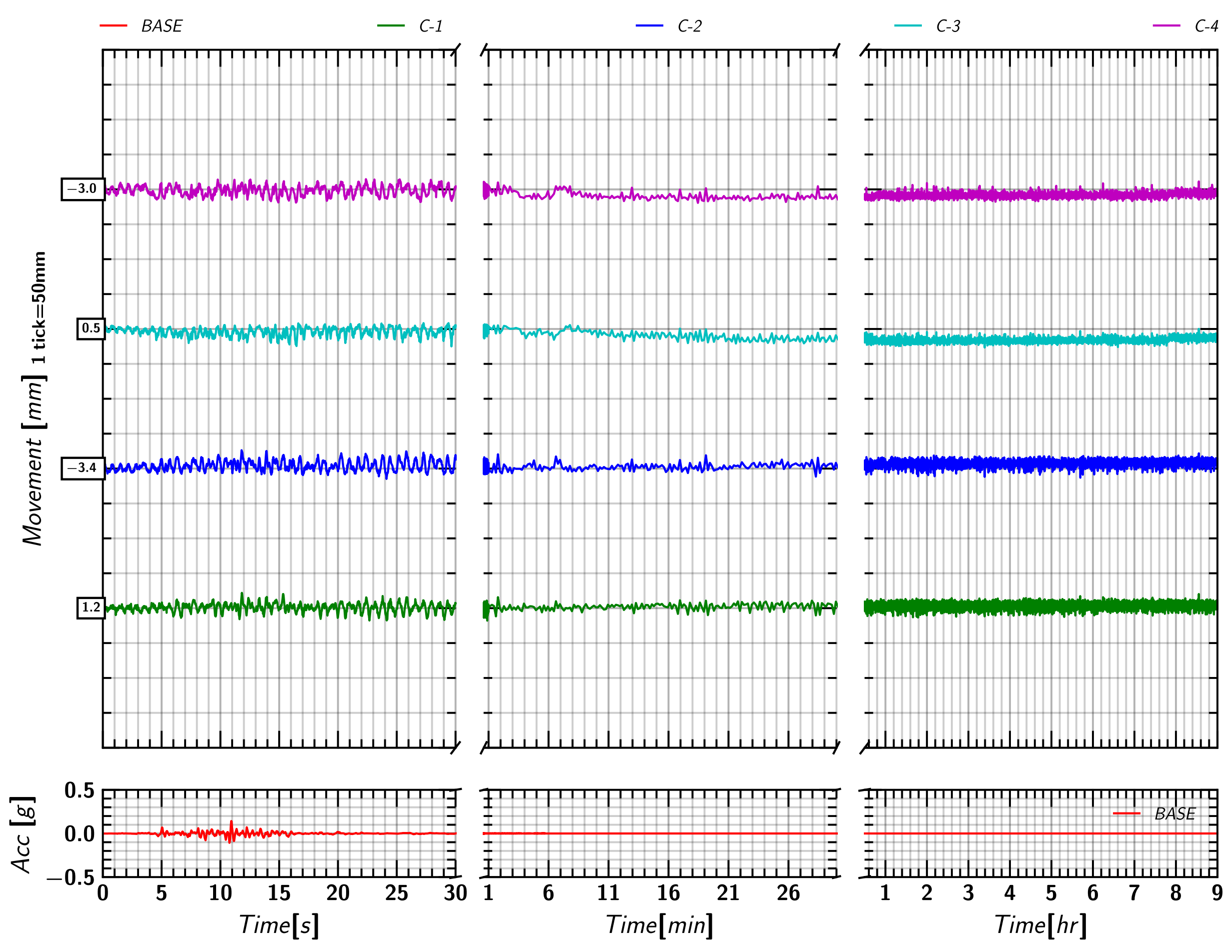

Figure 142. EQM$_2$: Container movement in Z-direction relative to the model container during and post shaking.

G.3 Soil (Row S-1) Movement in X

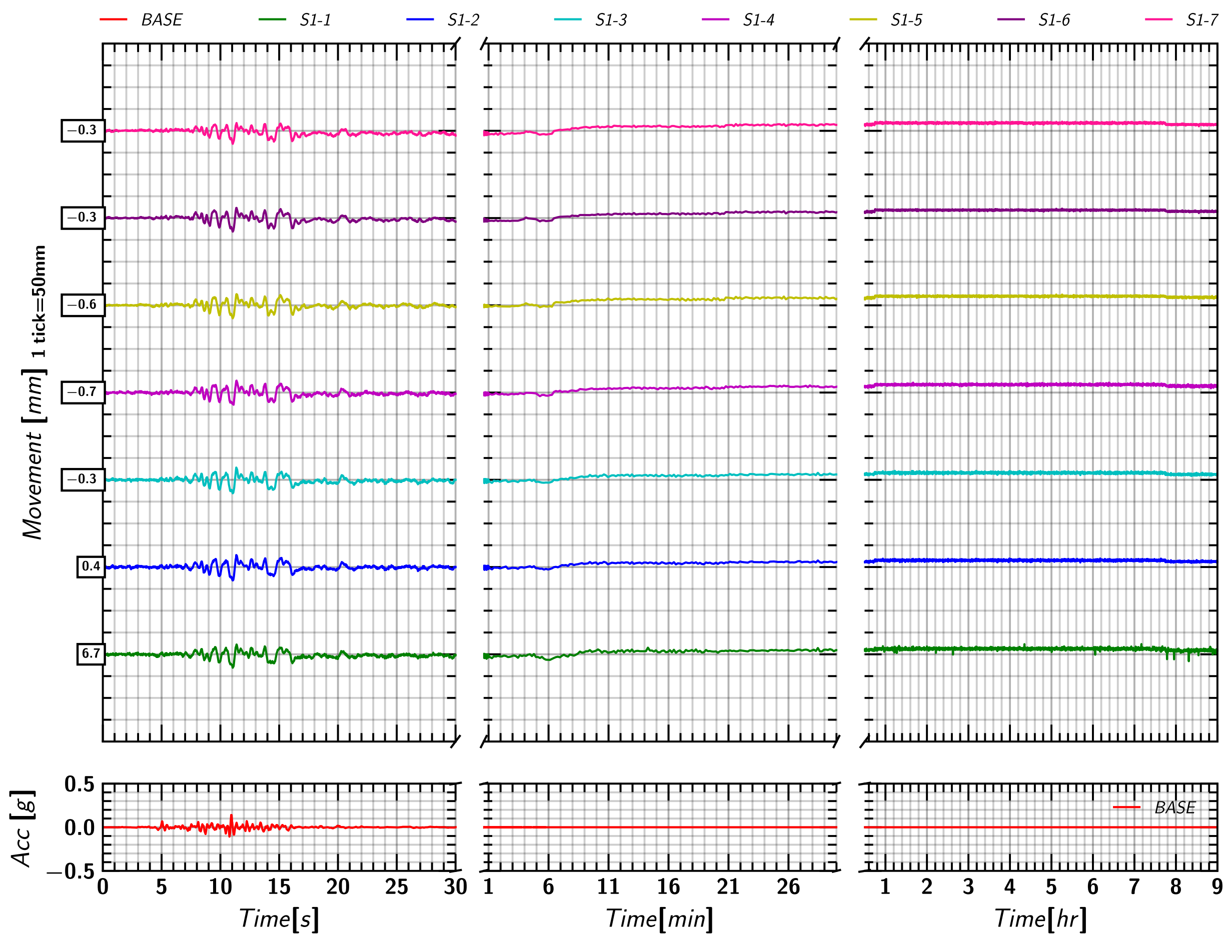

Figure 143. EQM$_2$: Soil (Row S-1) movement in X-direction relative to the model container during and post shaking.

G.4 Soil (Row S-1) Movement in Z

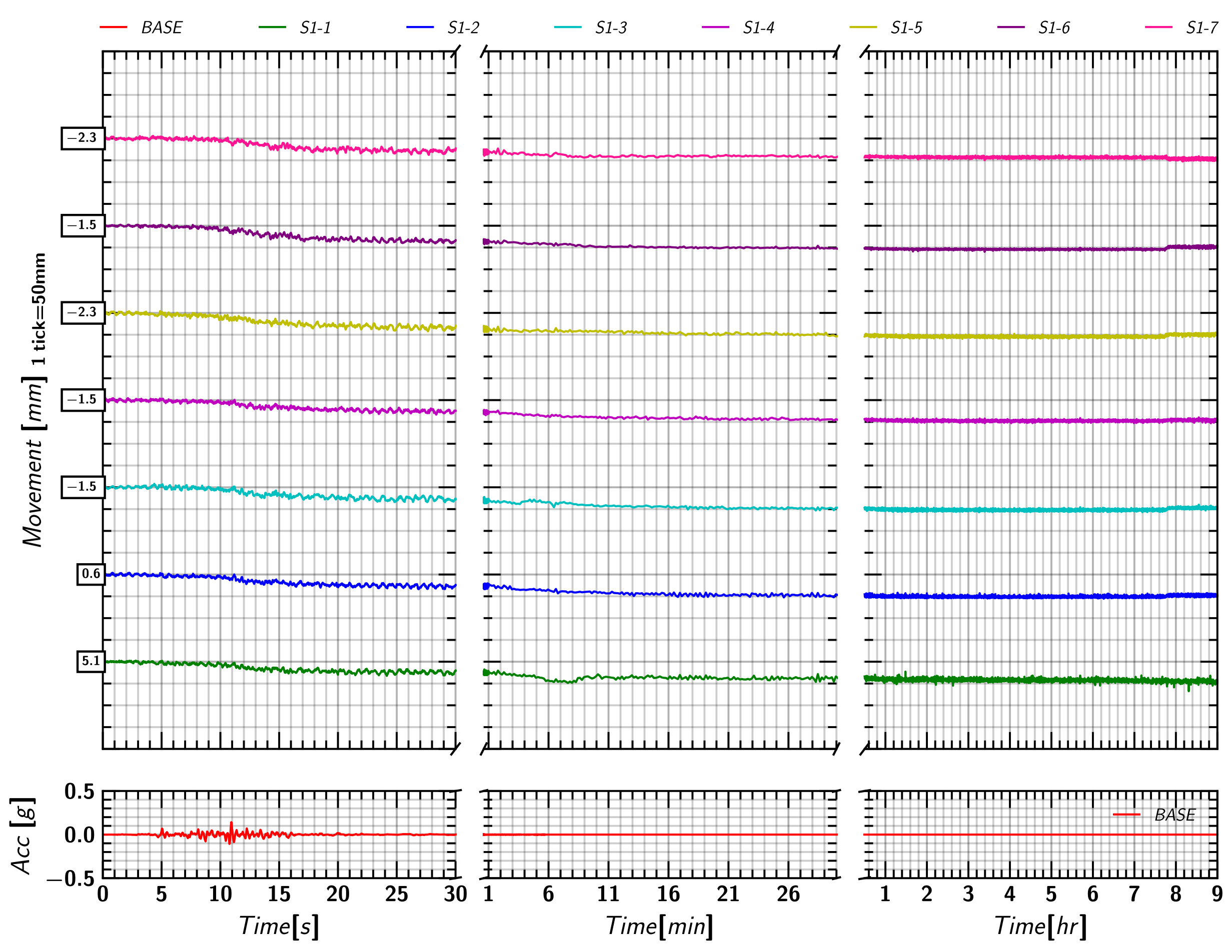

Figure 144. EQM$_2$: Soil (Row S-1) movement in Z-direction relative to the model container during and post shaking.

G.5 Soil (Row S-2) Movement in X

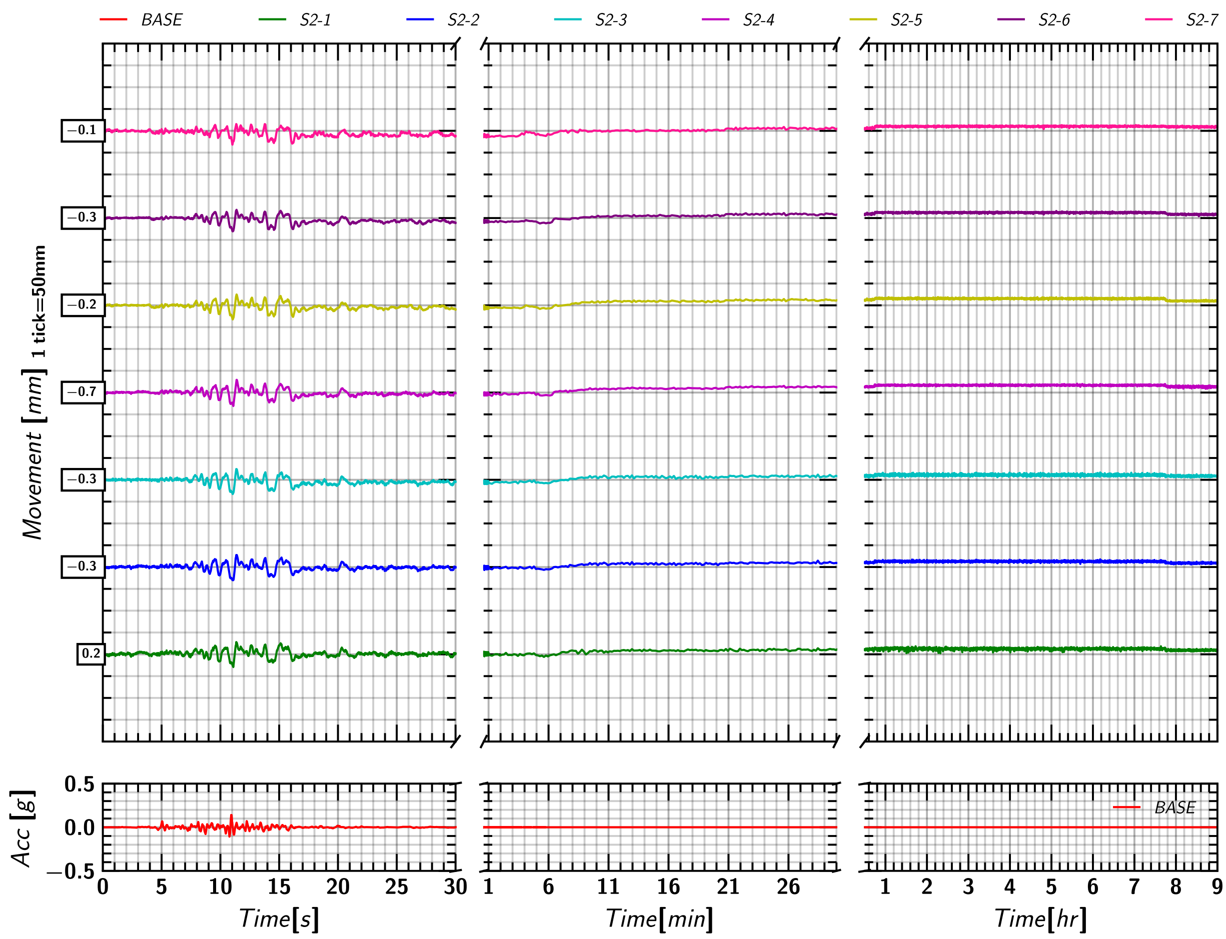

Figure 145. EQM₂: Soil (Row S-2) movement in X-direction relative to the model container during and post shaking.

G.6 Soil (Row S-2) Movement in Z

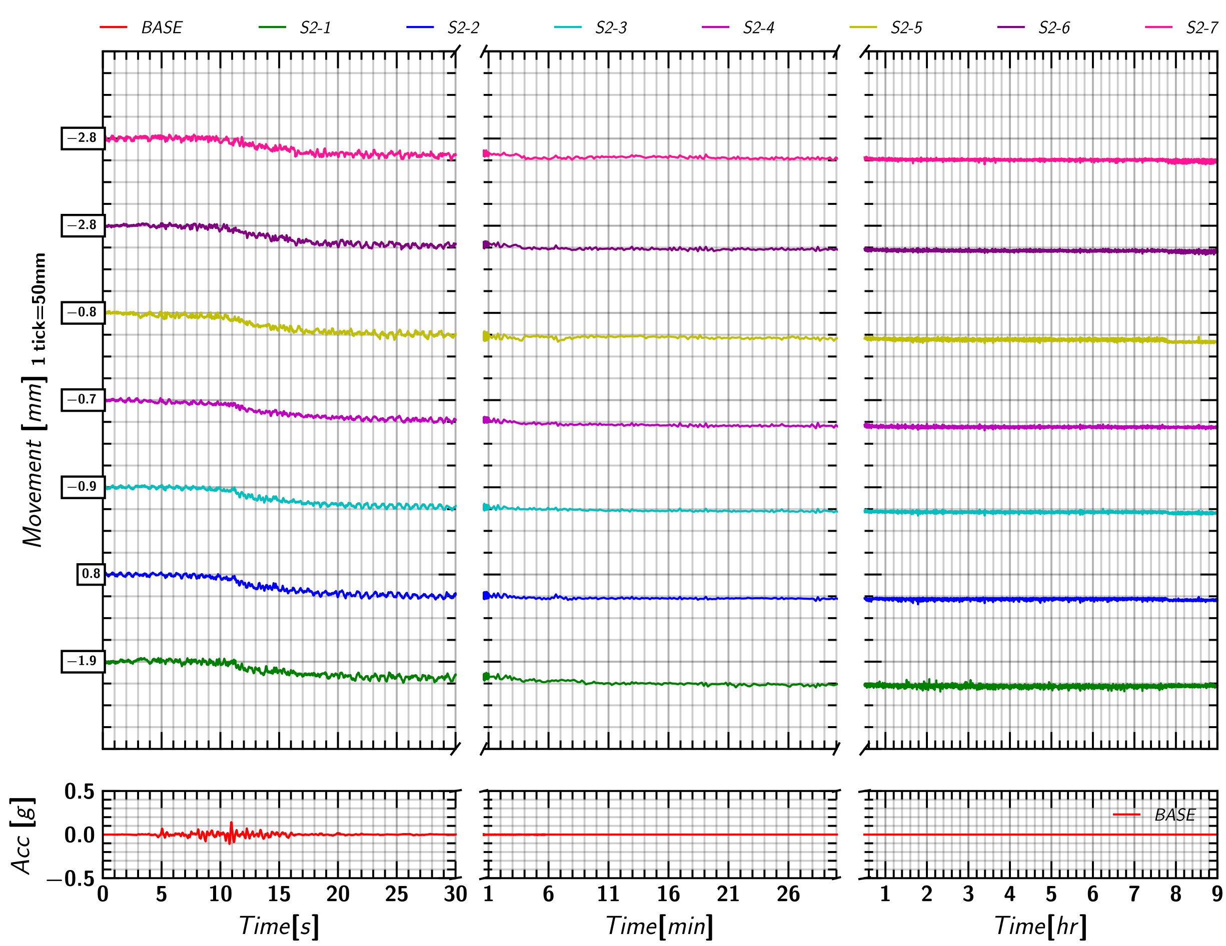

Figure 146. EQM$_2$: Soil (Row S-2) movement in Z-direction relative to the model container during and post shaking.

G.7 Soil (Row S-3) Movement in X

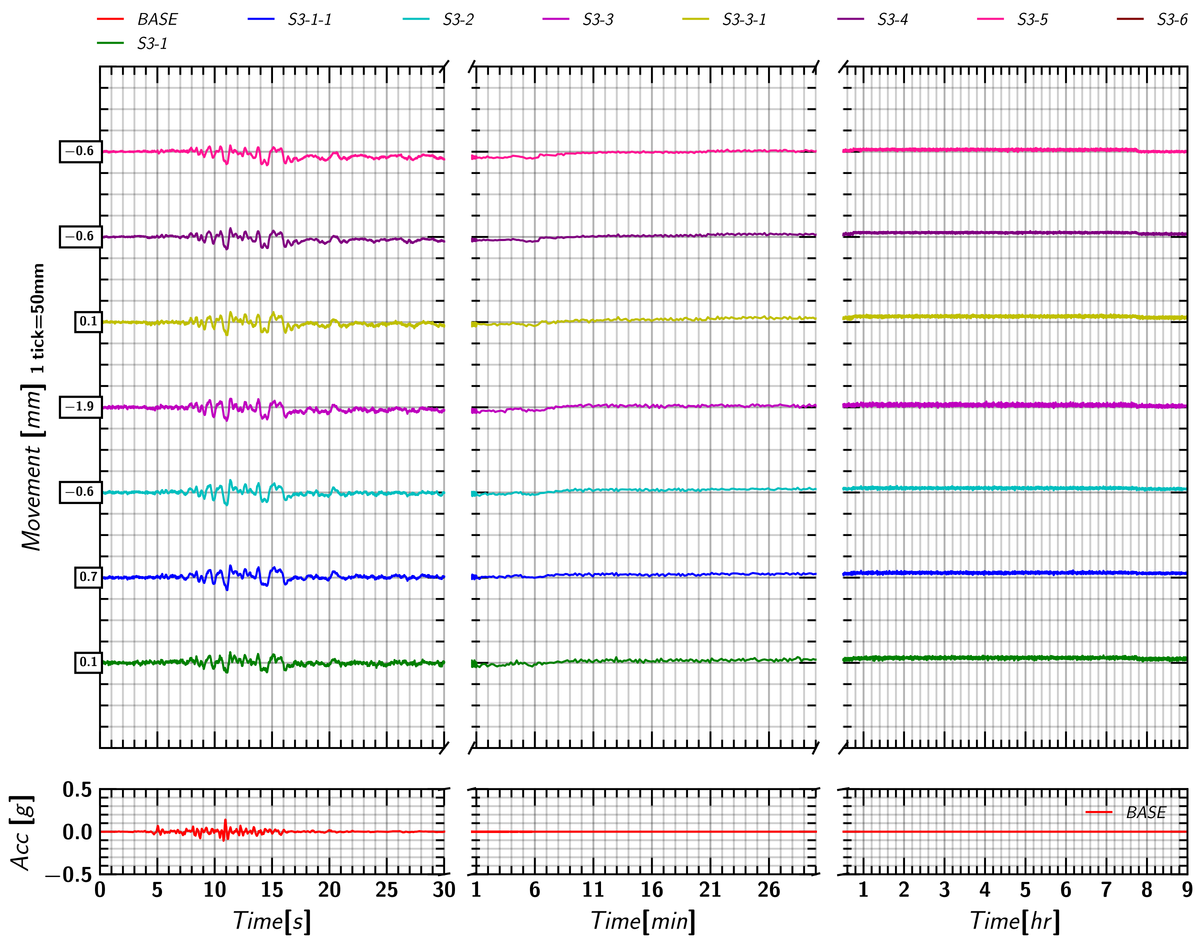

Figure 147. EQM$_2$: Soil (Row S-3) movement in X-direction relative to the model container during and post shaking.

G.8 Soil (Row S-3) Movement in Z

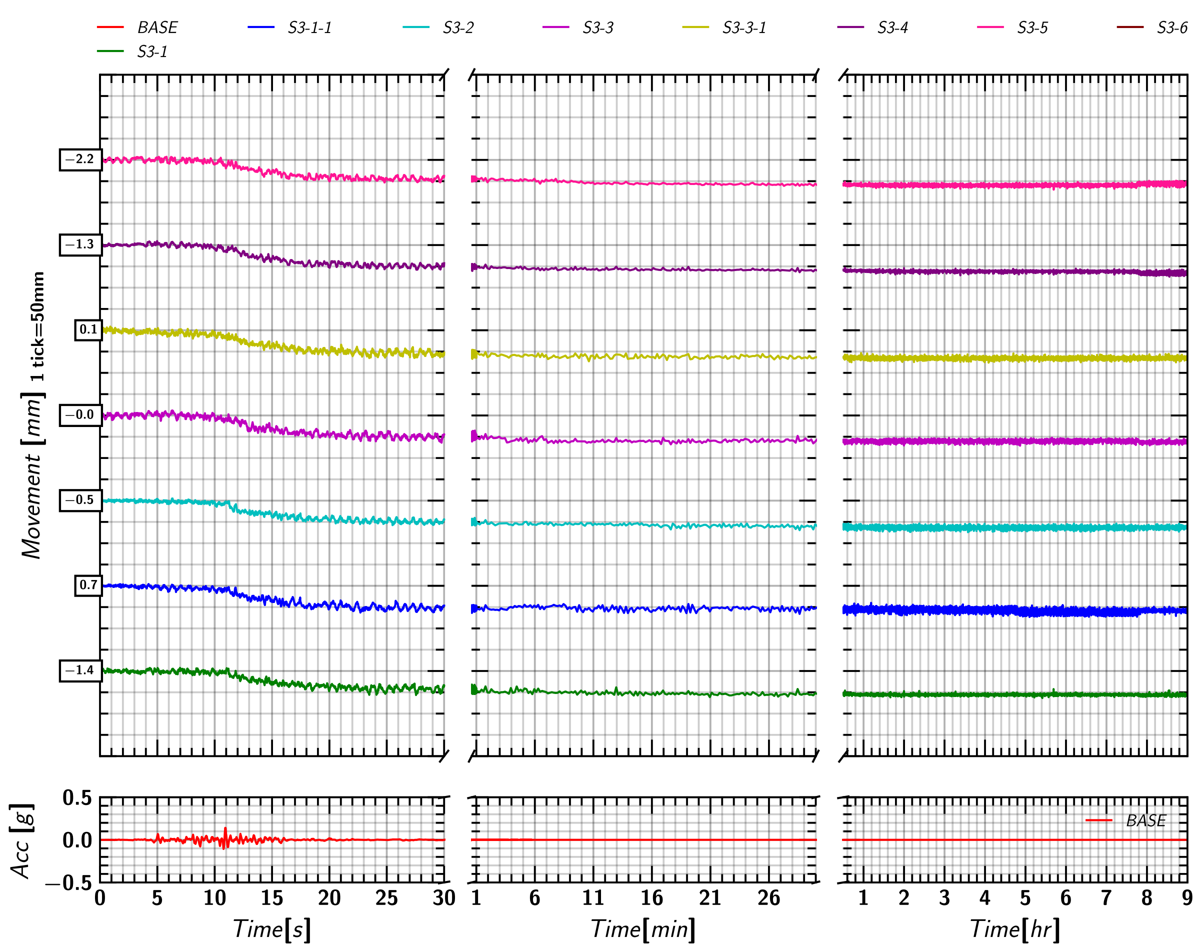

Figure 148. EQM$_2$: Soil (Row S-3) movement in Z-direction relative to the model container during and post shaking.

G.9 Soil (Row S-4) Movement in X

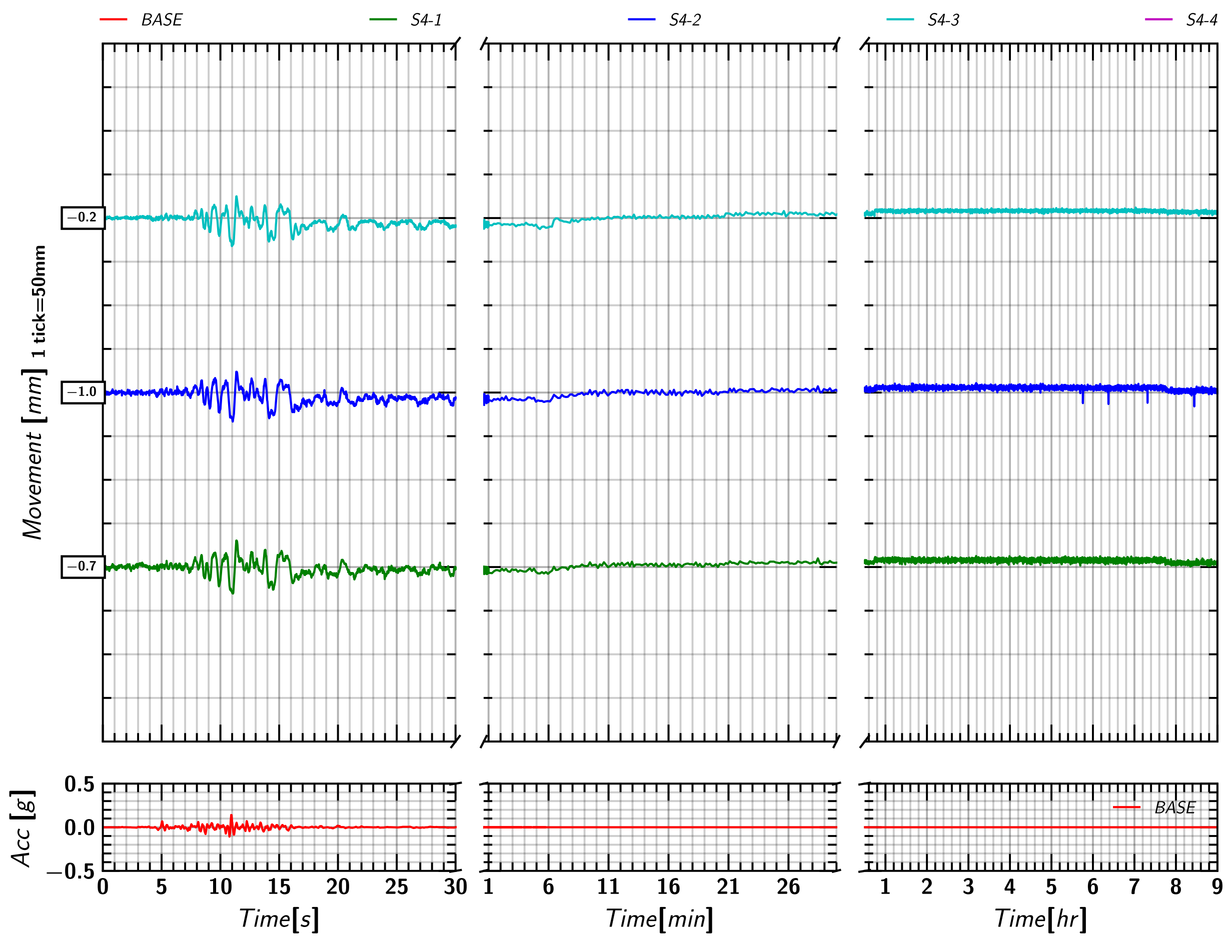

Figure 149. EQM$_2$: Soil (Row S-4) movement in X-direction relative to the model container during and post shaking.

G.10 Soil (Row S-4) Movement in Z

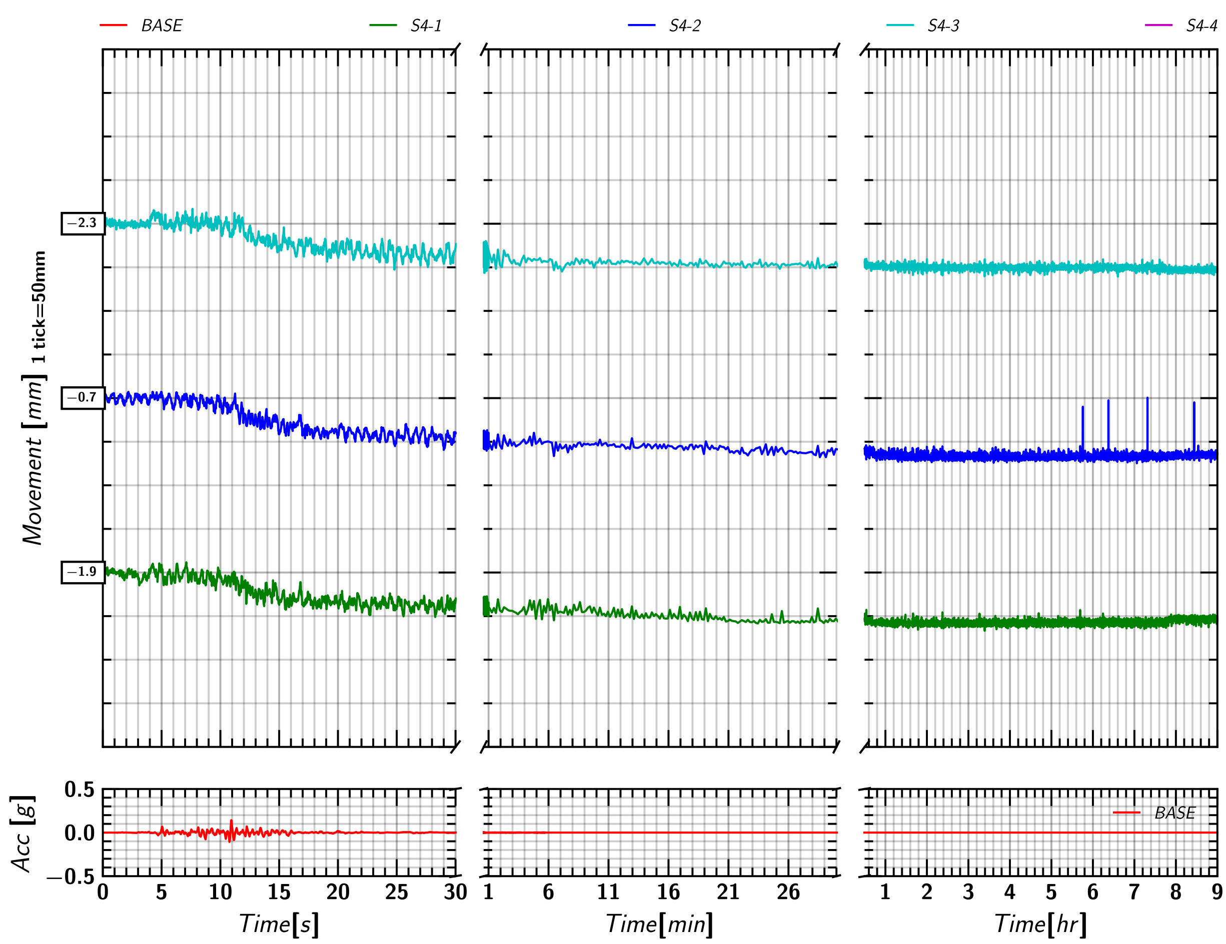

Figure 150. EQM$_2$: Soil (Row S-4) movement in Z-direction relative to the model container during and post shaking.

G.11 Soil (Row S-5) Movement in X

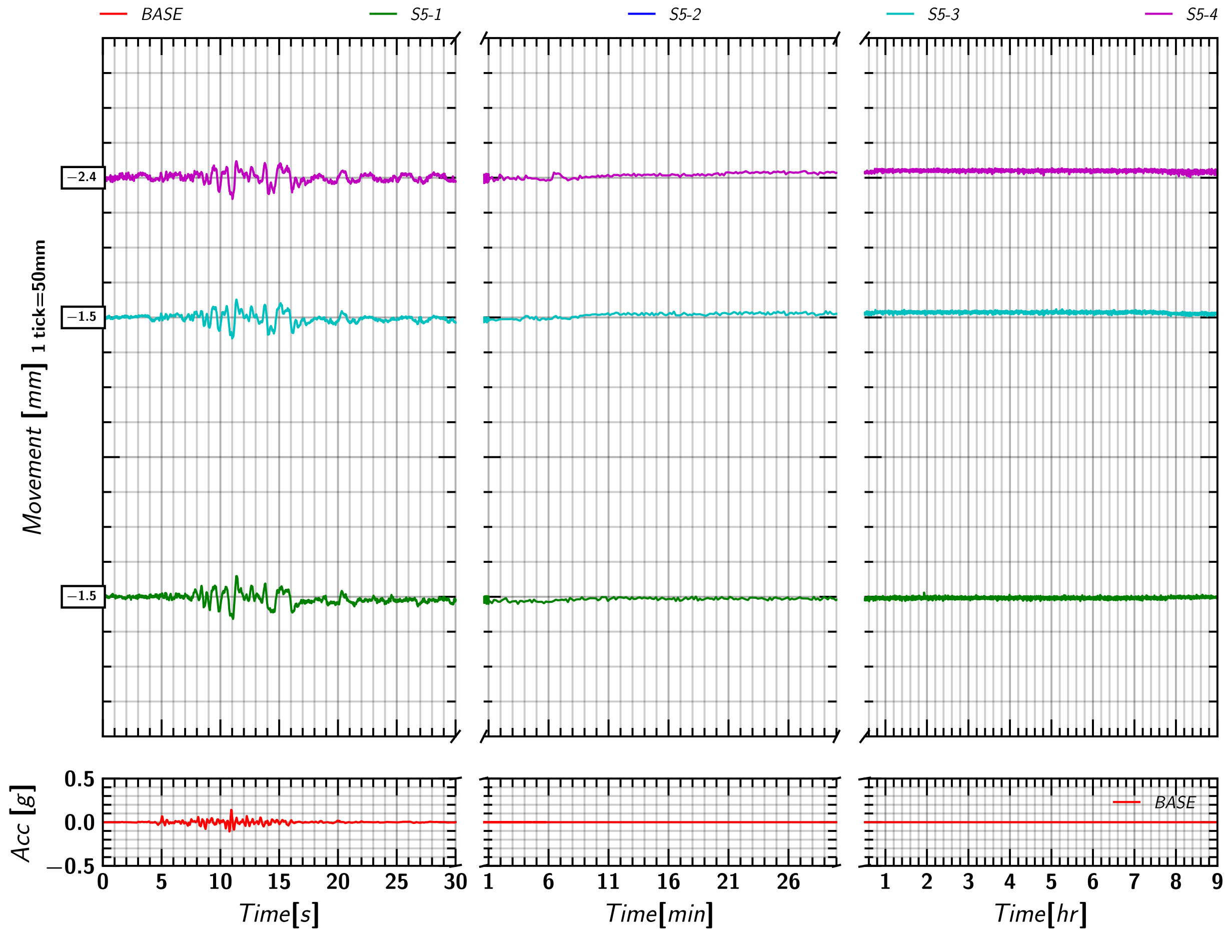

Figure 151. EQM2: Soil (Row S-5) movement in X-direction during the applied earthquake motion.

G.12 Soil (Row S-5) Movement in Z

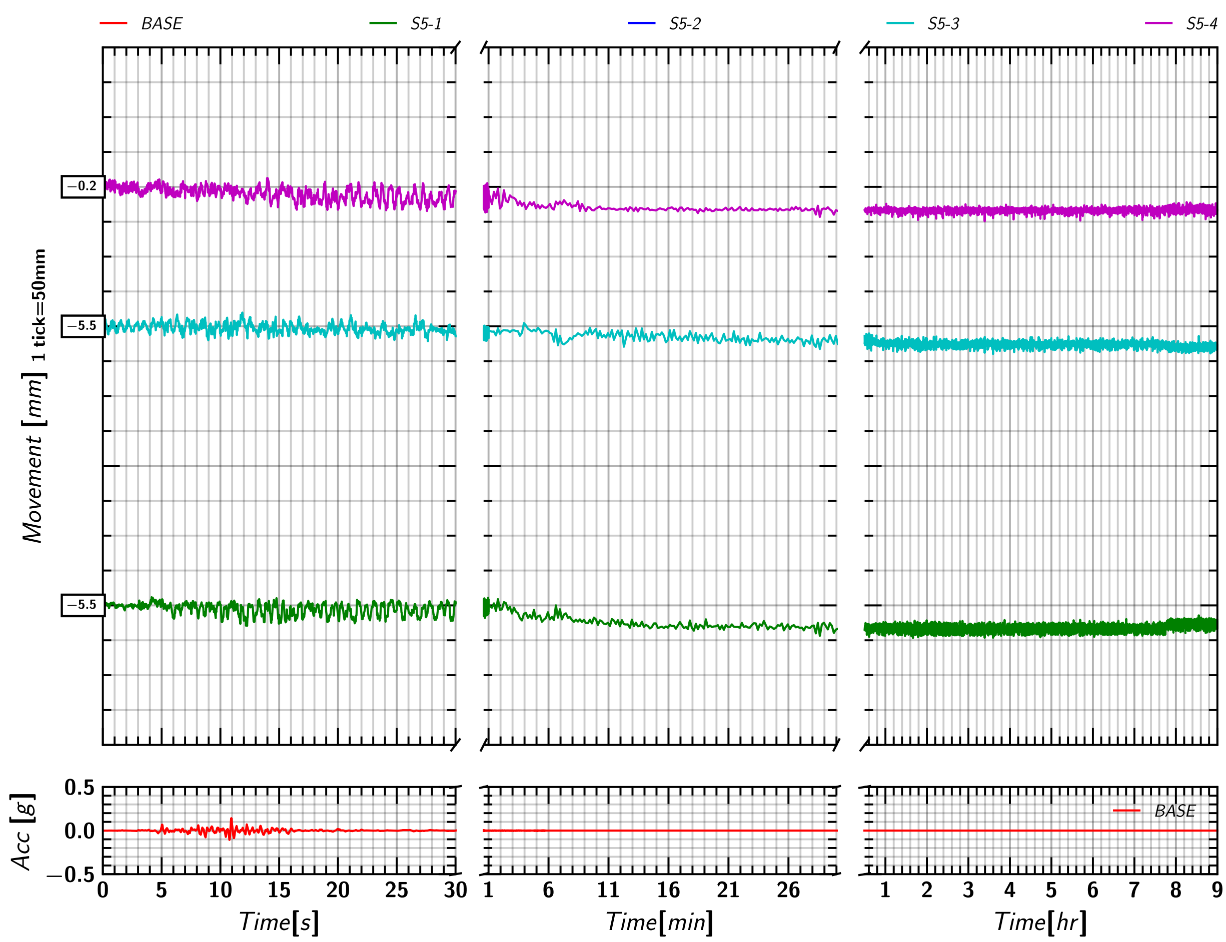

Figure 152. EQM2: Soil (Row S-5) movement in Z-direction relative to the model container during and post shaking.

G.13 Pile 1 Mass Movement in X

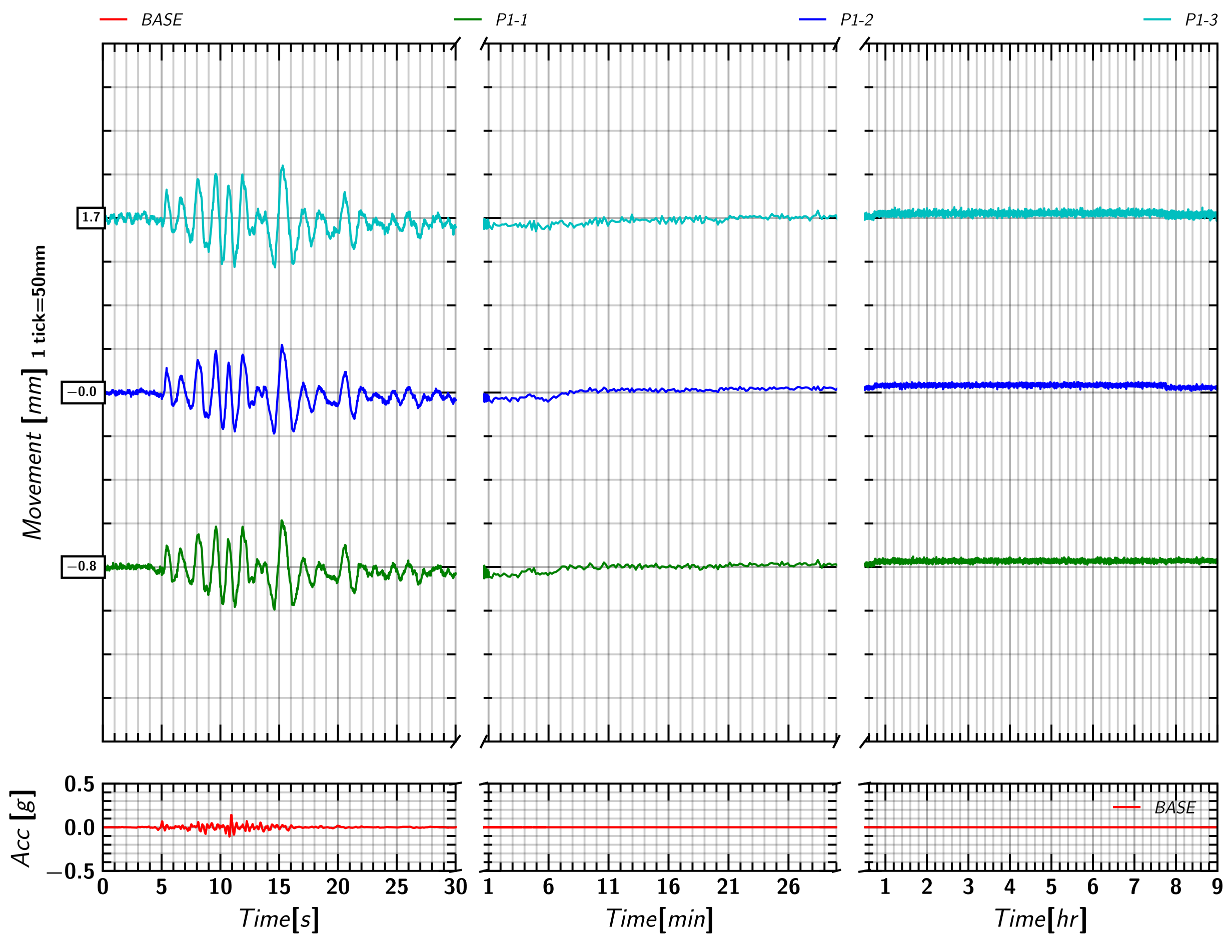

Figure 153. EQM$_2$: Pile 1 movement in X-direction relative to the model container during and post shaking.

G.14 Pile 1 Mass Movement in Z

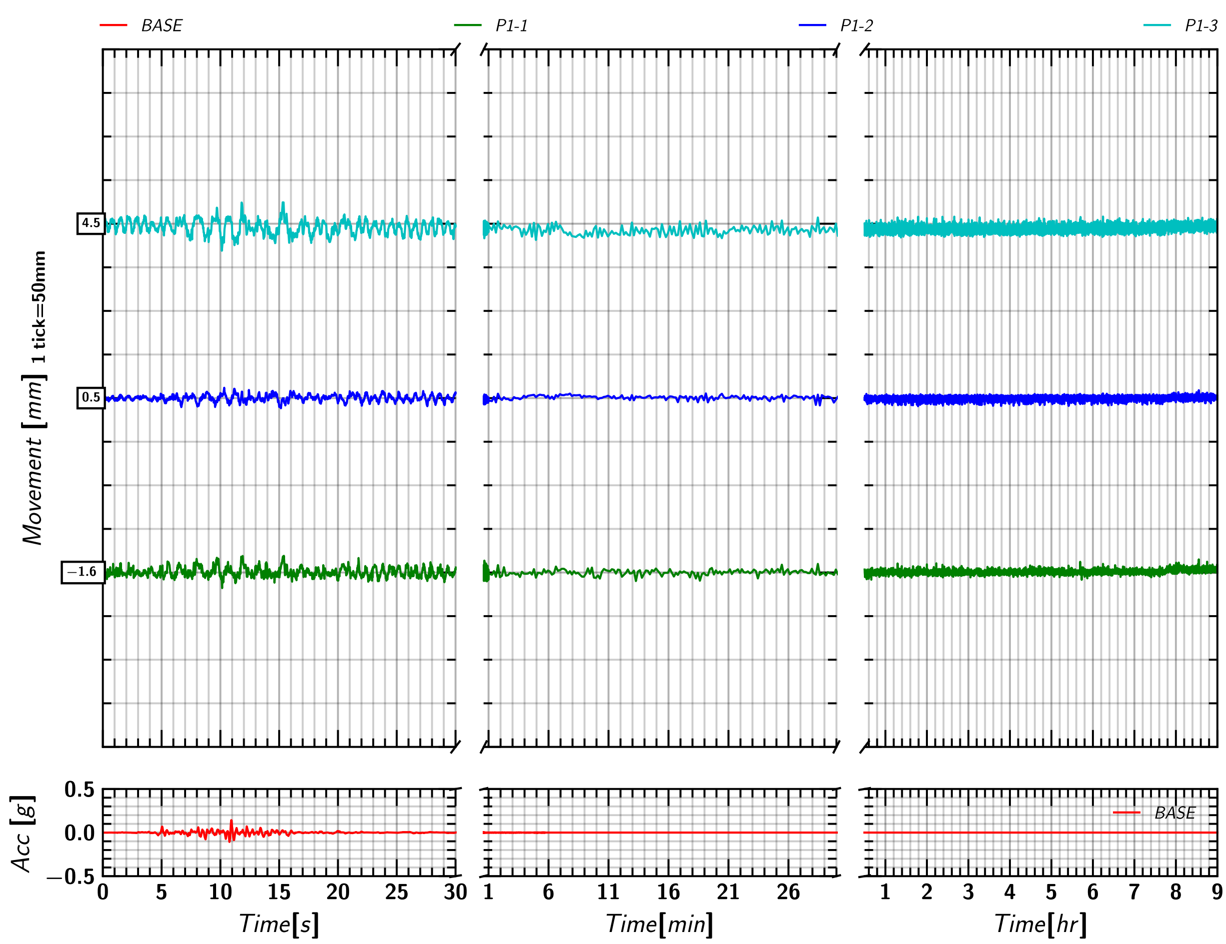

Figure 154. EQM$_2$: Pile 1 movement in Z-direction relative to the model container during and post shaking.

G.15 Pile 2 Mass Movement in X

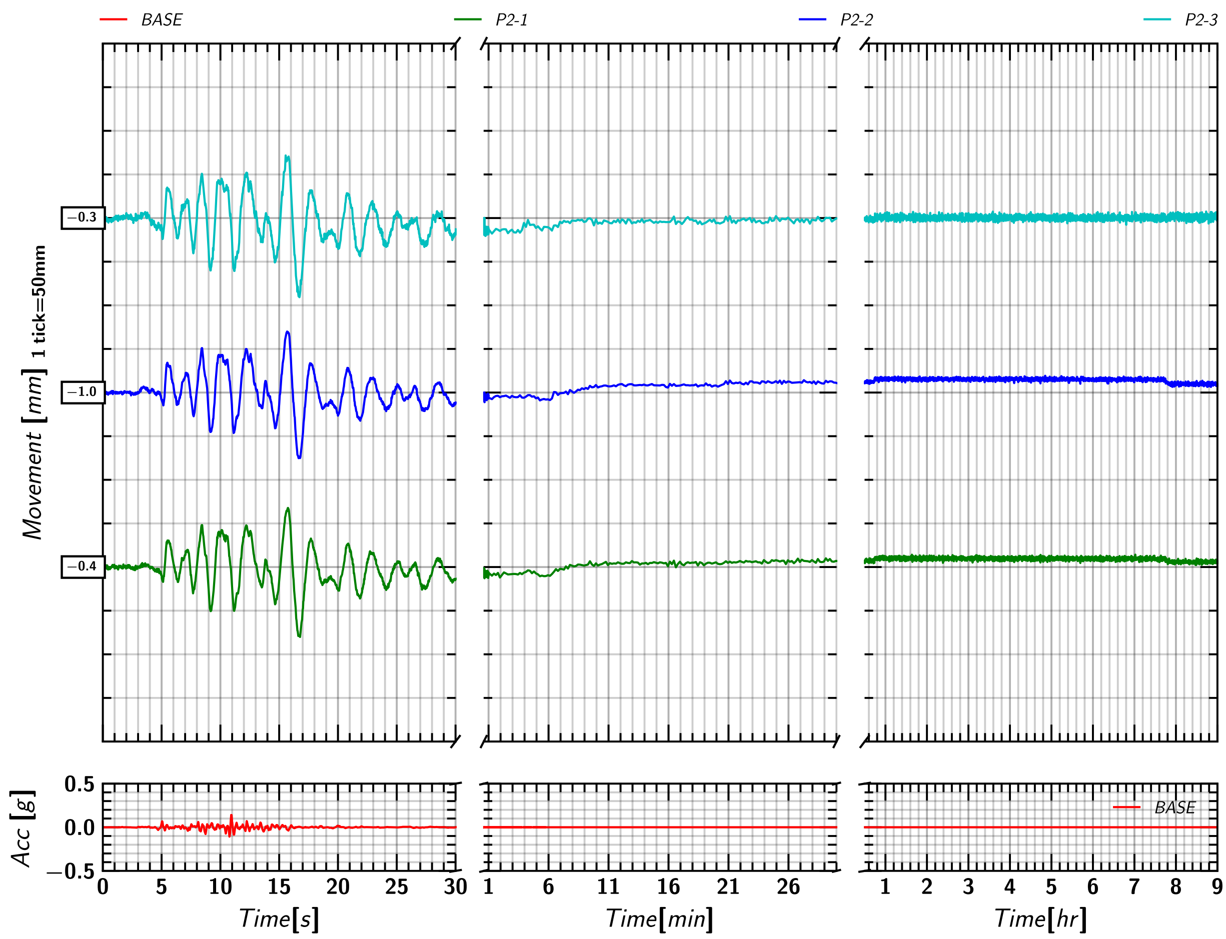

Figure 155. EQM$_2$: Pile 2 movement in X-direction relative to the model container during and post shaking.

G.16 Pile 2 Mass Movement in Z

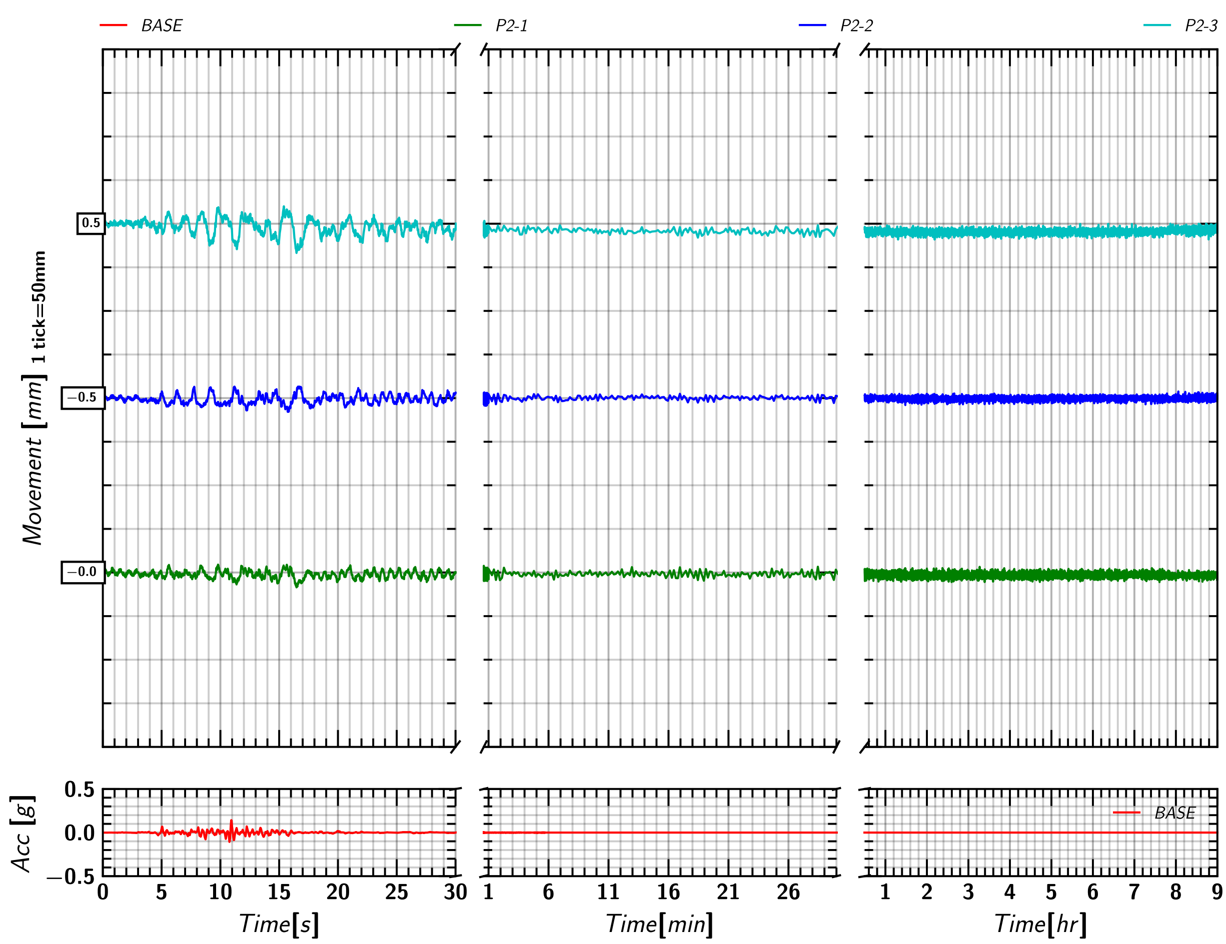

Figure 156. EQM$_2$: Pile 2 movement in Z-direction relative to the model container during and post shaking.

G.17 Pile 3 Mass Movement in X

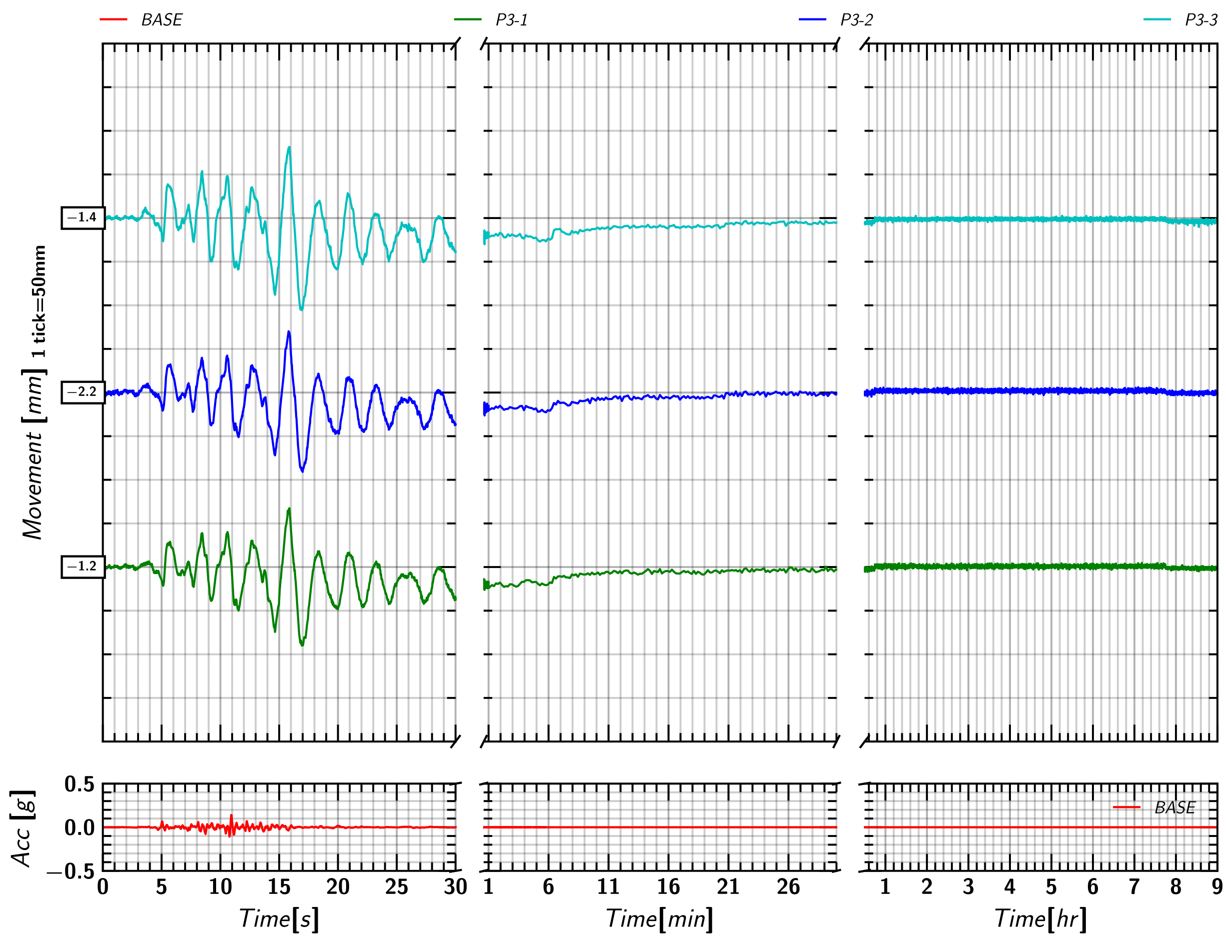

Figure 157. EQM₂: Pile 3 movement in X-direction relative to the model container during and post shaking.

G.18 Pile 3 Mass Movement in Z

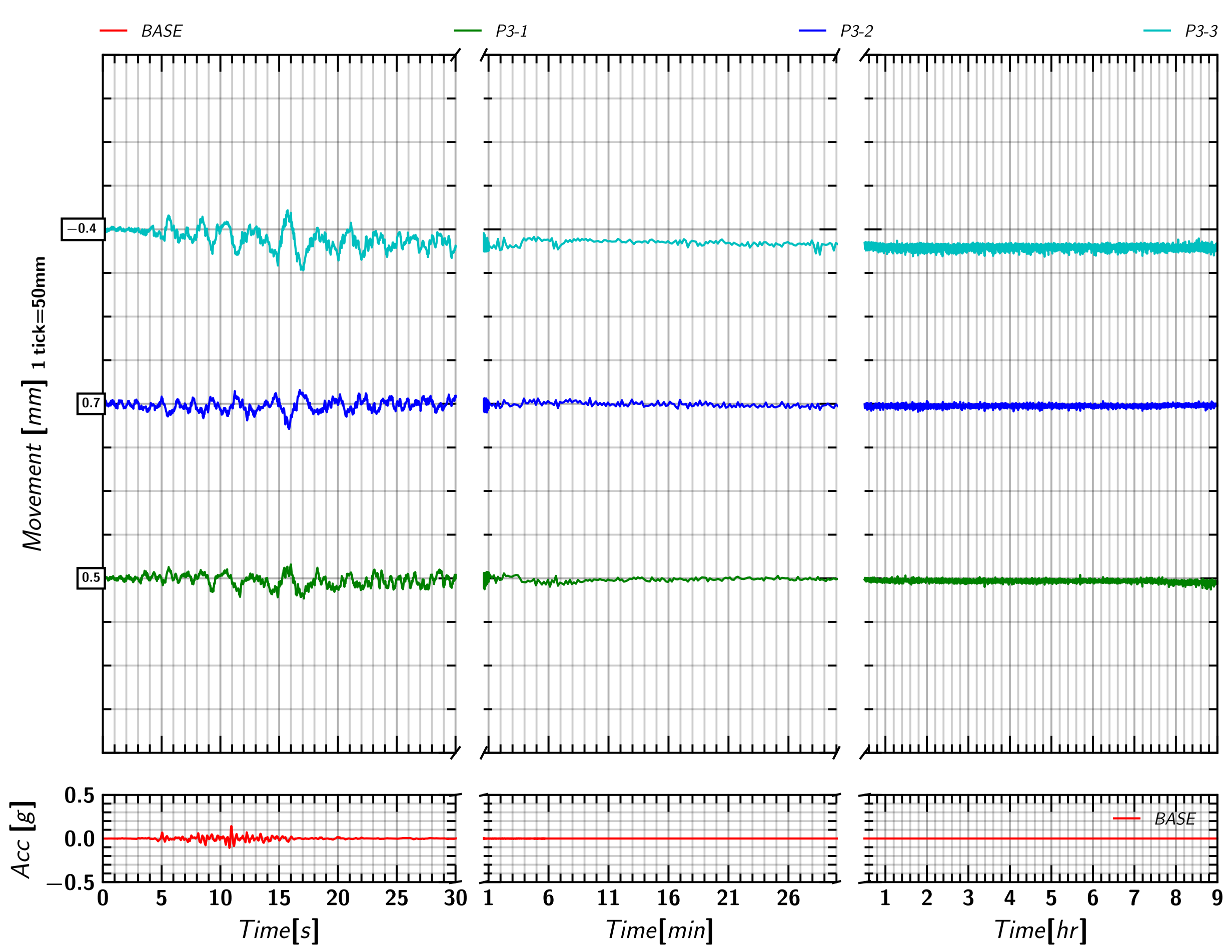

Figure 158. EQM$_2$: Pile 3 movement in Z-direction relative to the model container during and post shaking.

H. EQM$_3$: MEDIUM SANTA CRUZ EARTHQUAKE (PGA=0.18g)

H.1 Input Motion

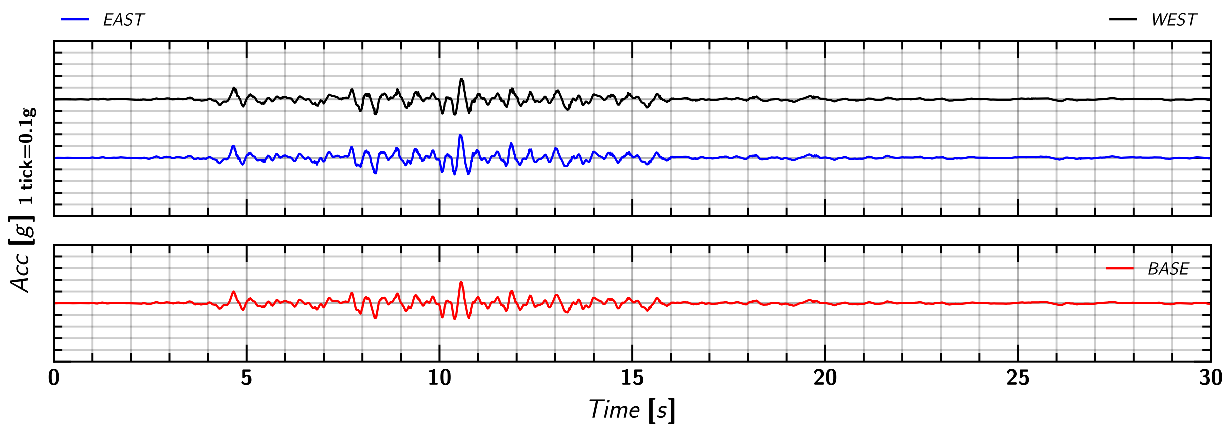

Figure 159. EQM$_3$: Input motion.

H.2 Spectral Acceleration

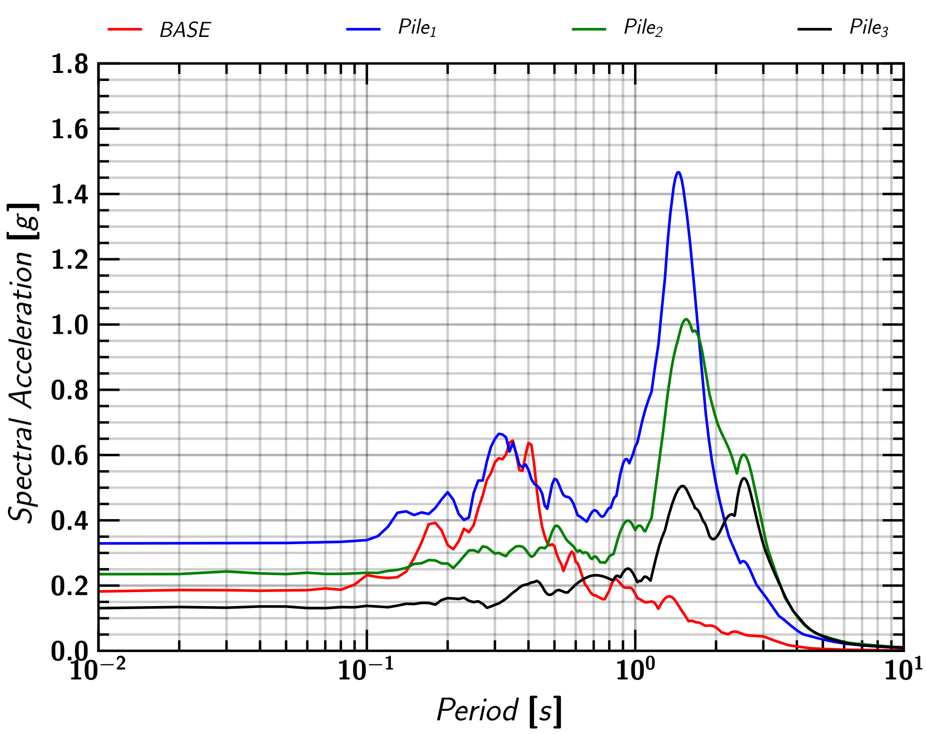

Figure 160. EQM$_3$: Spectral Acceleration.

H.3 Container Acceleration

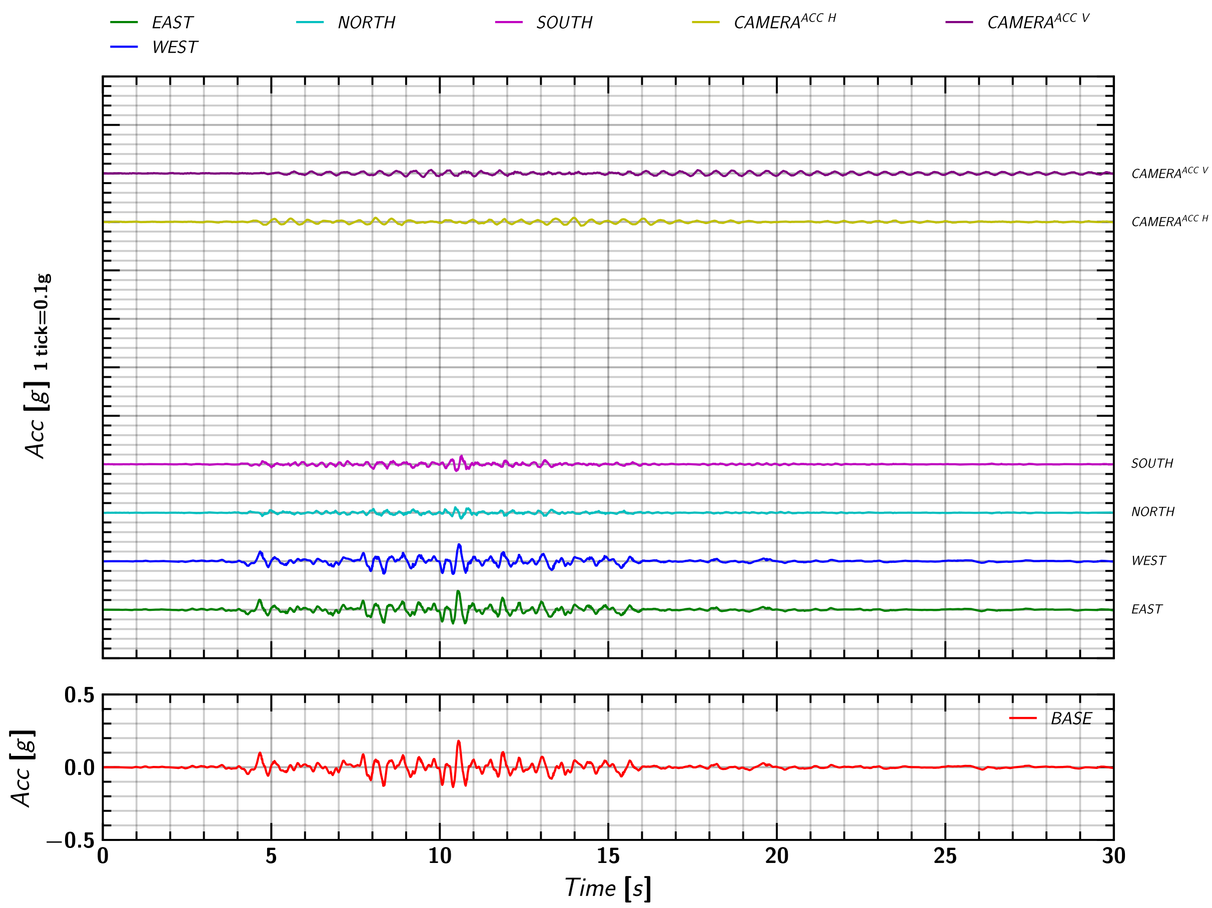

Figure 161. EQM3: Acceleration measurement on container and camera beam.

H.4 Soil Acceleration

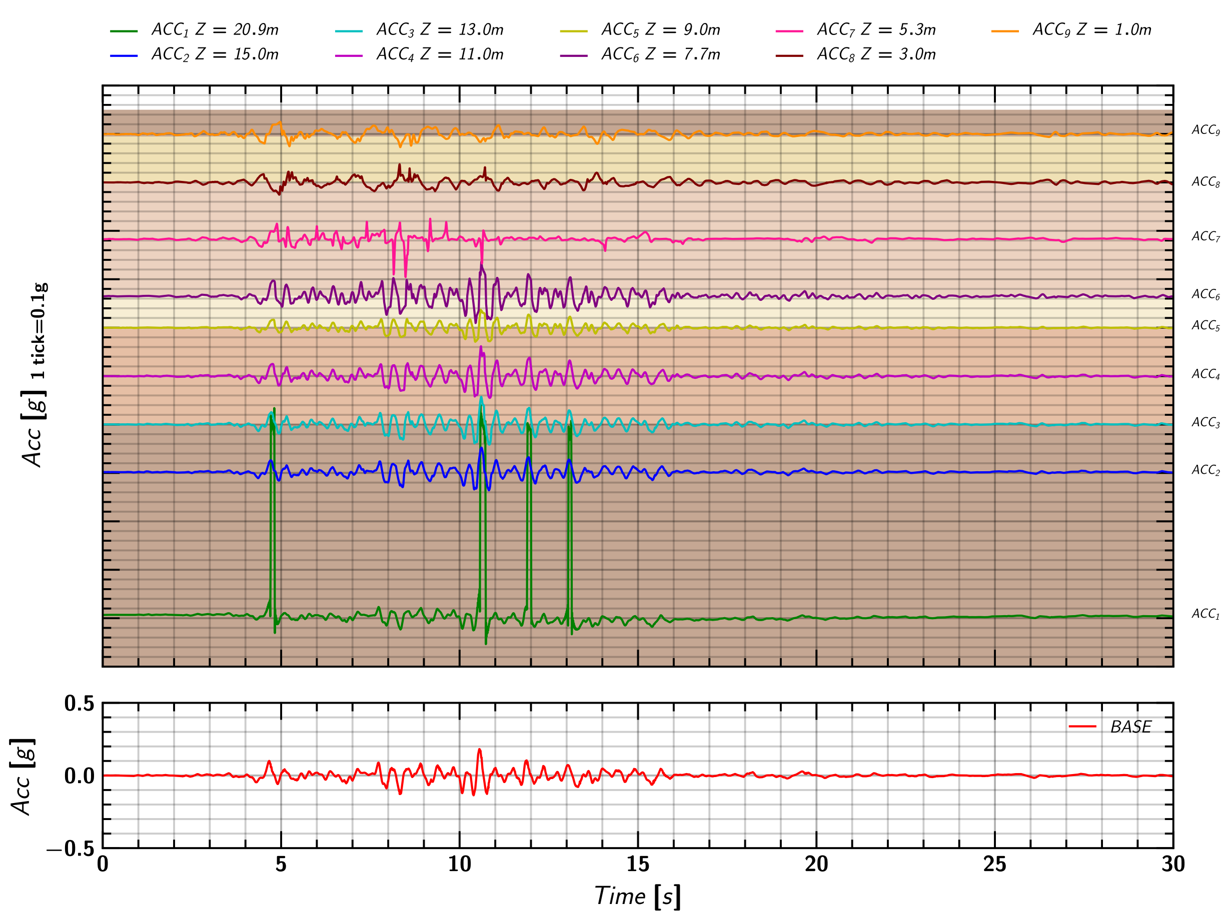

Figure 162. EQM3: Acceleration measurement in soil.

H.5 Pile Mass Acceleration

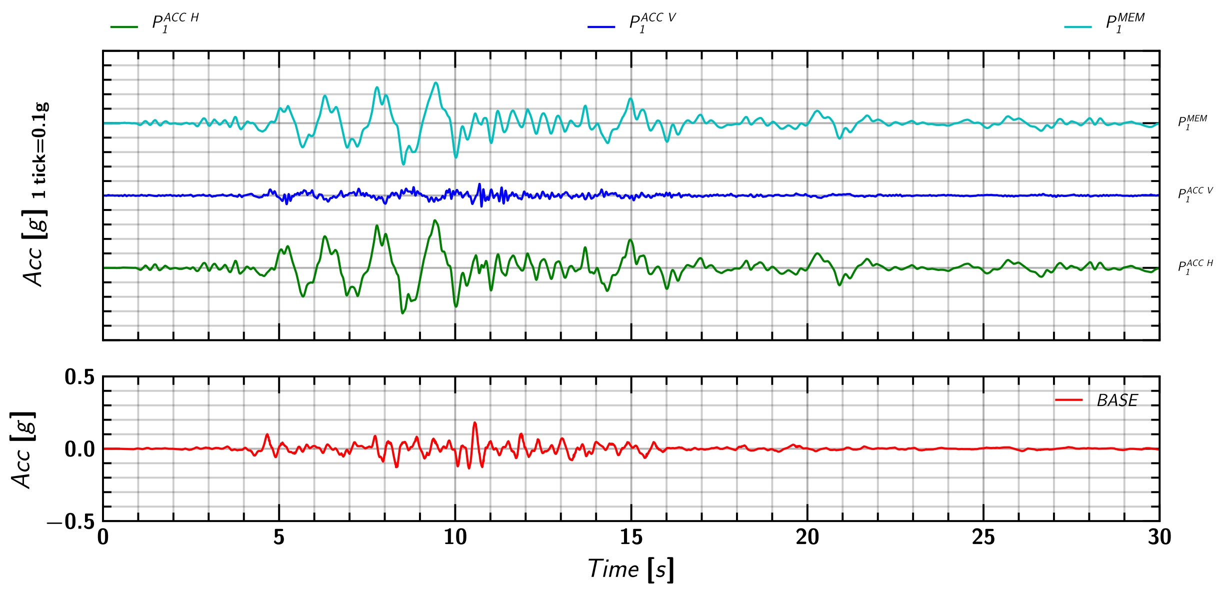

Figure 163. EQM₃: Acceleration measurement on pile 1.

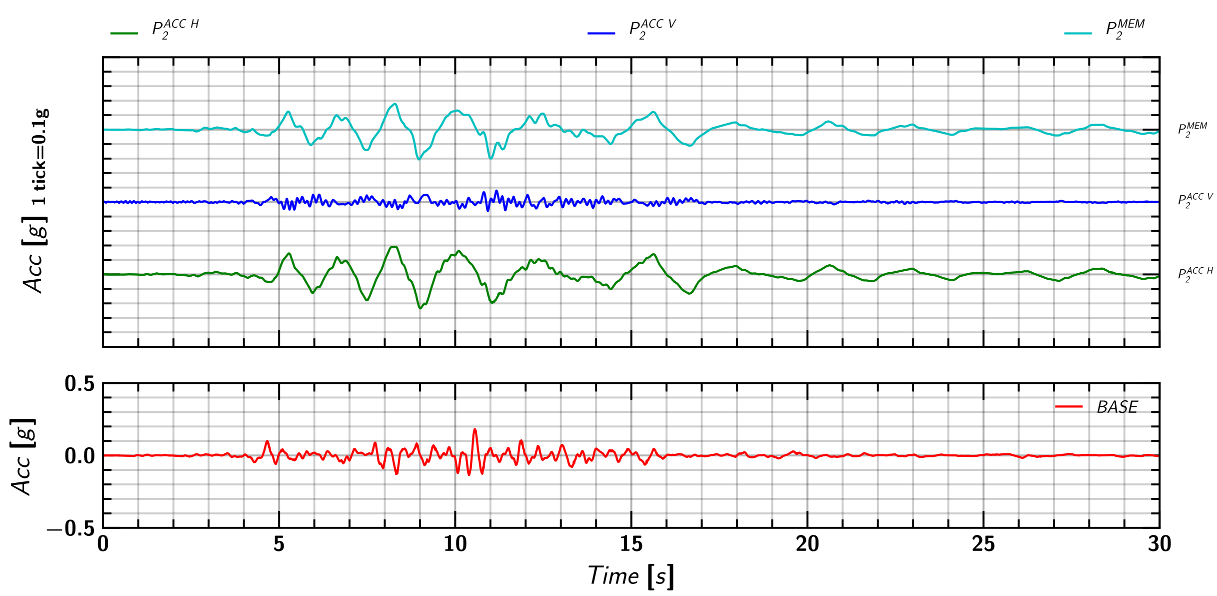

Figure 164. EQM$_3$: Acceleration measurement on pile 2.

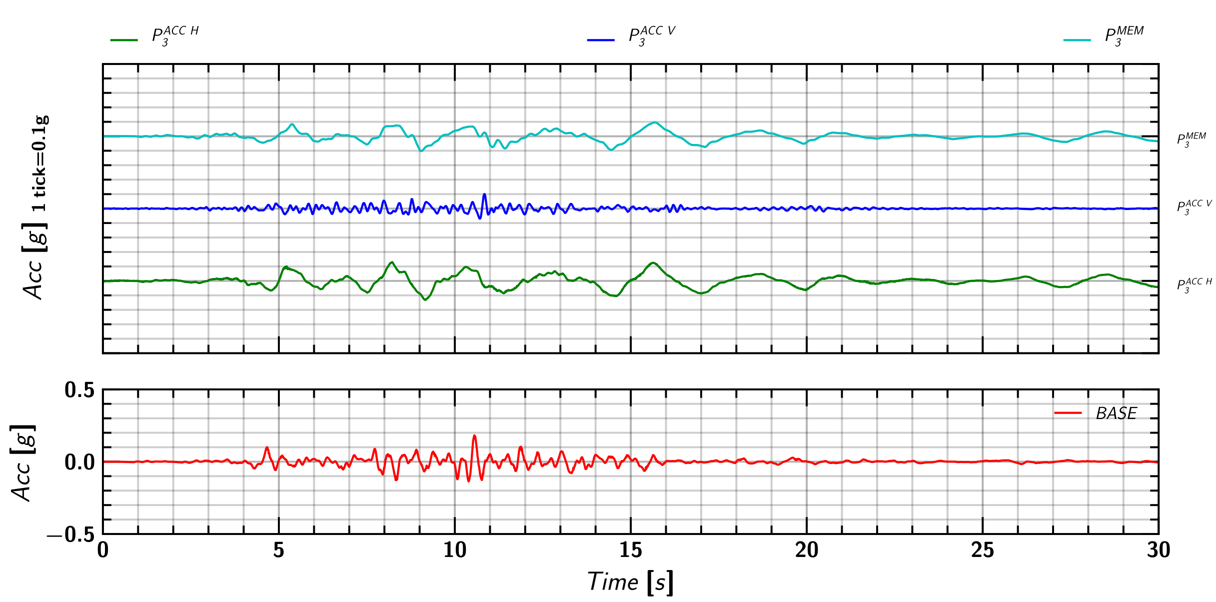

Figure 165. EQM$_3$: Acceleration measurement on pile 3.

H.6 Soil and Pile Mass Lateral Movement in X direction

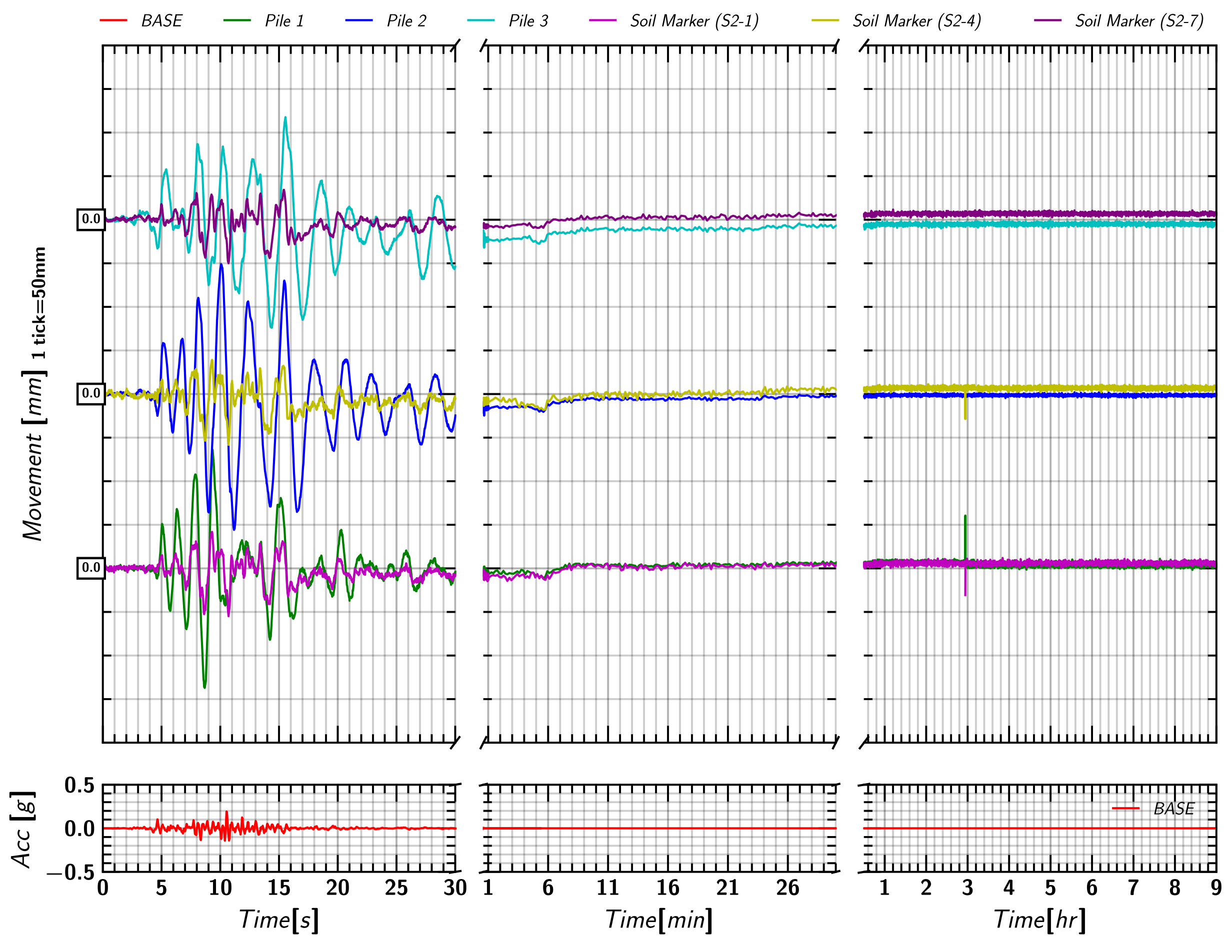

Figure 166. EQM3: Lateral movement of soil and pile in x-direction during and post shaking.

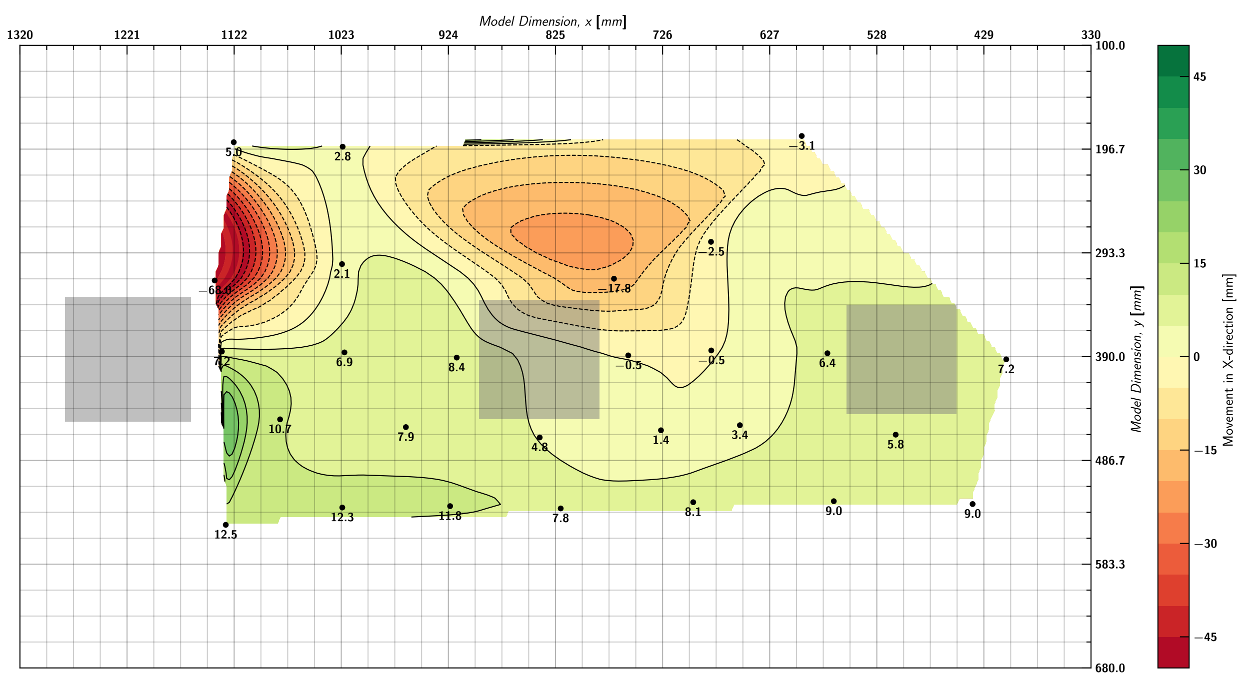

Figure 167. EQM3:Contour of lateral movement of soil with respect to container in x-direction at the end of reconsolidation (t=240 minutes).

H.7 Soil and Pile Settlement (i.e., movement in Z direction)

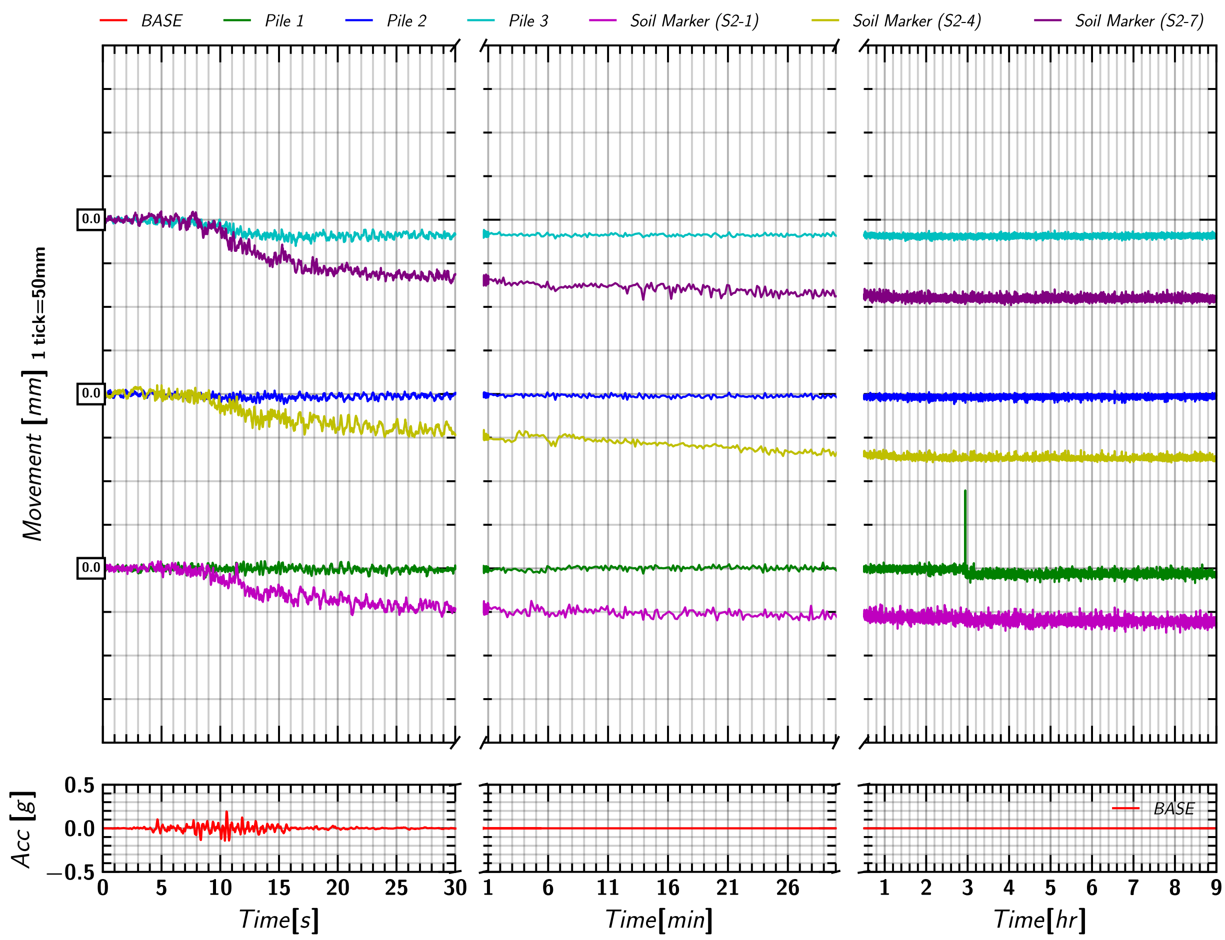

Figure 168. EQM$_3$: Settlement measurement in soil and pile during and post shaking.

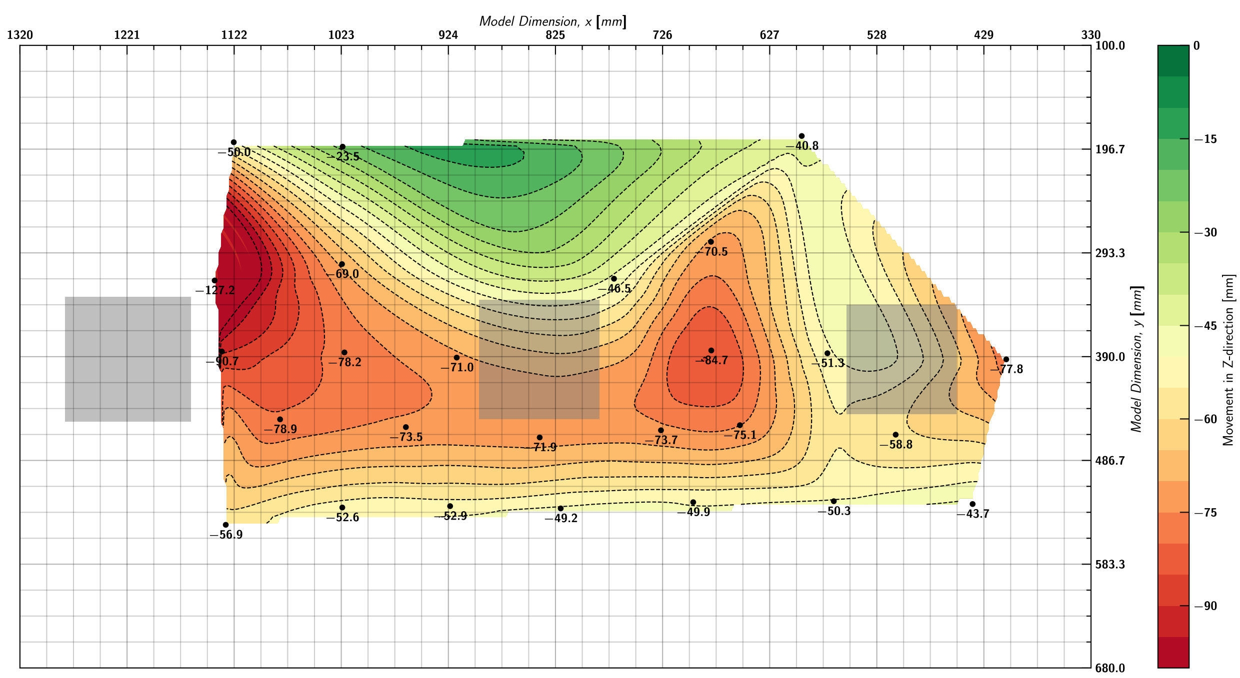

Figure 169. EQM$_3$:Contour of lateral movement of soil with respect to container in x-direction at the end of reconsolidation (t=240 minutes).

H.8 Pore pressure in Soil Measured by Keller Transducers

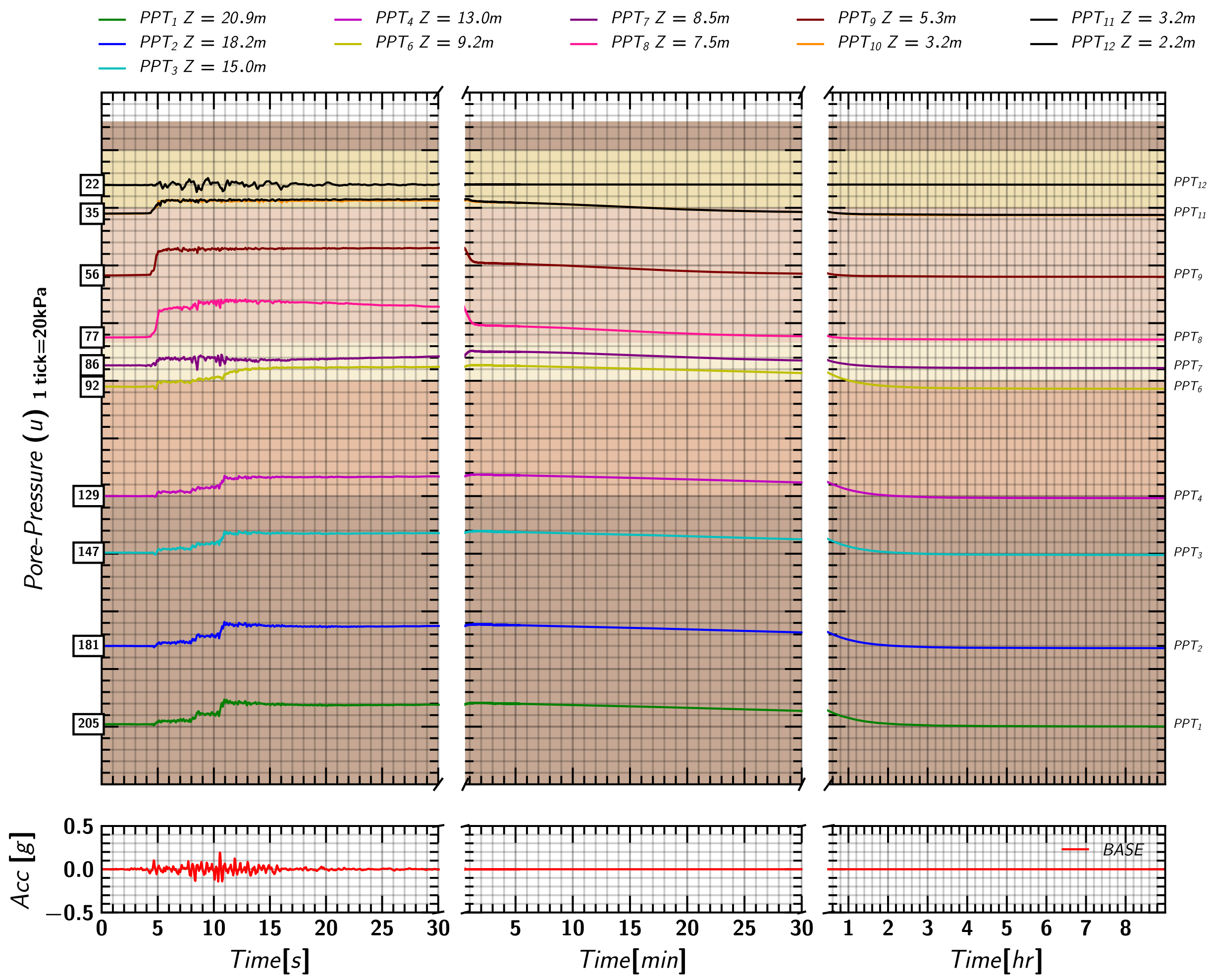

Figure 170. EQM3: Pore pressure measurements in soil from Keller transducers during and post shaking.

H.9 Pore pressure in Soil Measured by MS54XXX Transducers

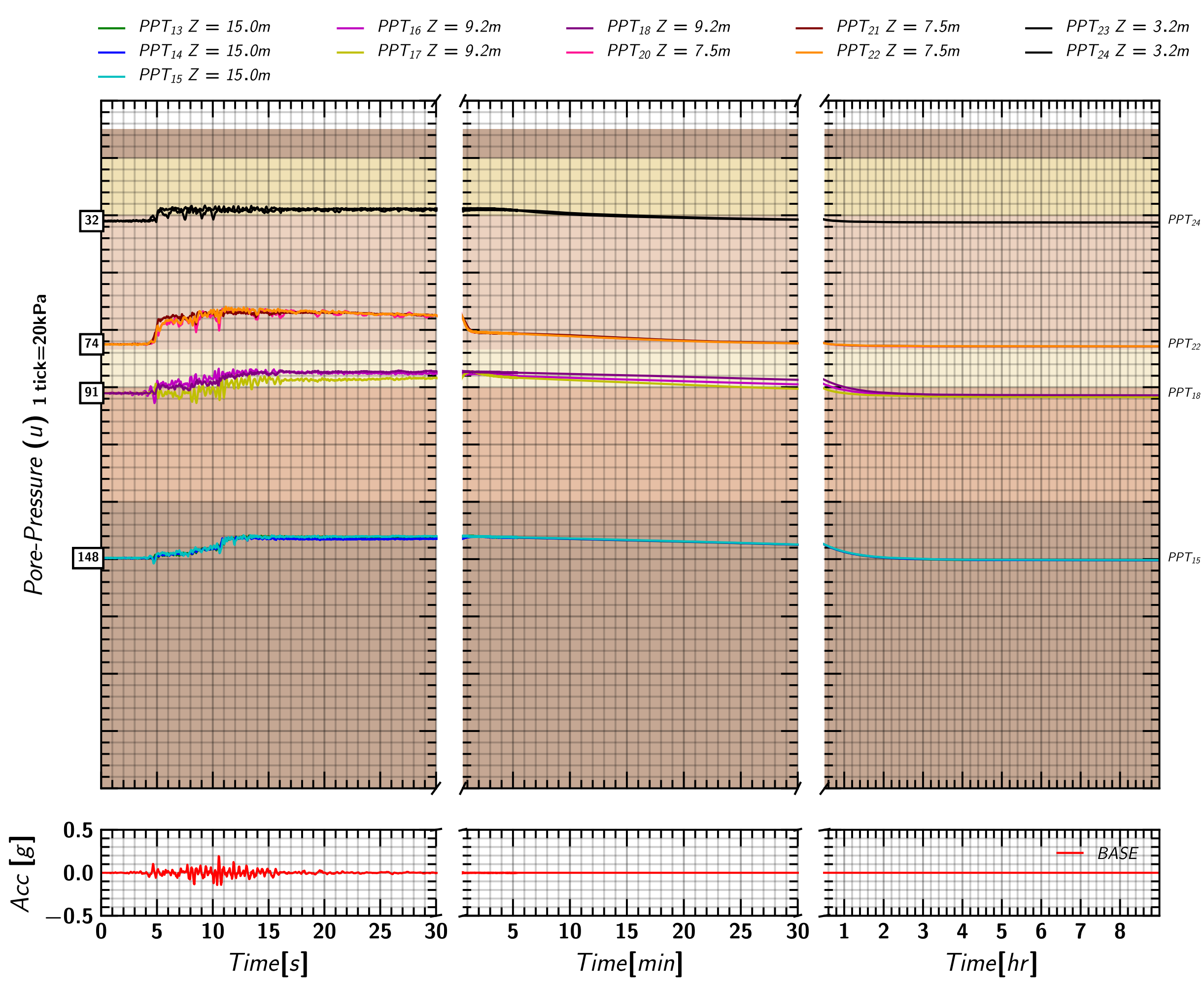

Figure 171. EQM3: Pore pressure measurements in soil from MS54XXX transducers during and post shaking.

Dense Sand	Medium Dense Sand	Clayey Silt	Loose Sand	Clay Crust

H.10 Excess Pore pressures Ratio (r_u) Estimated from Keller Transducers

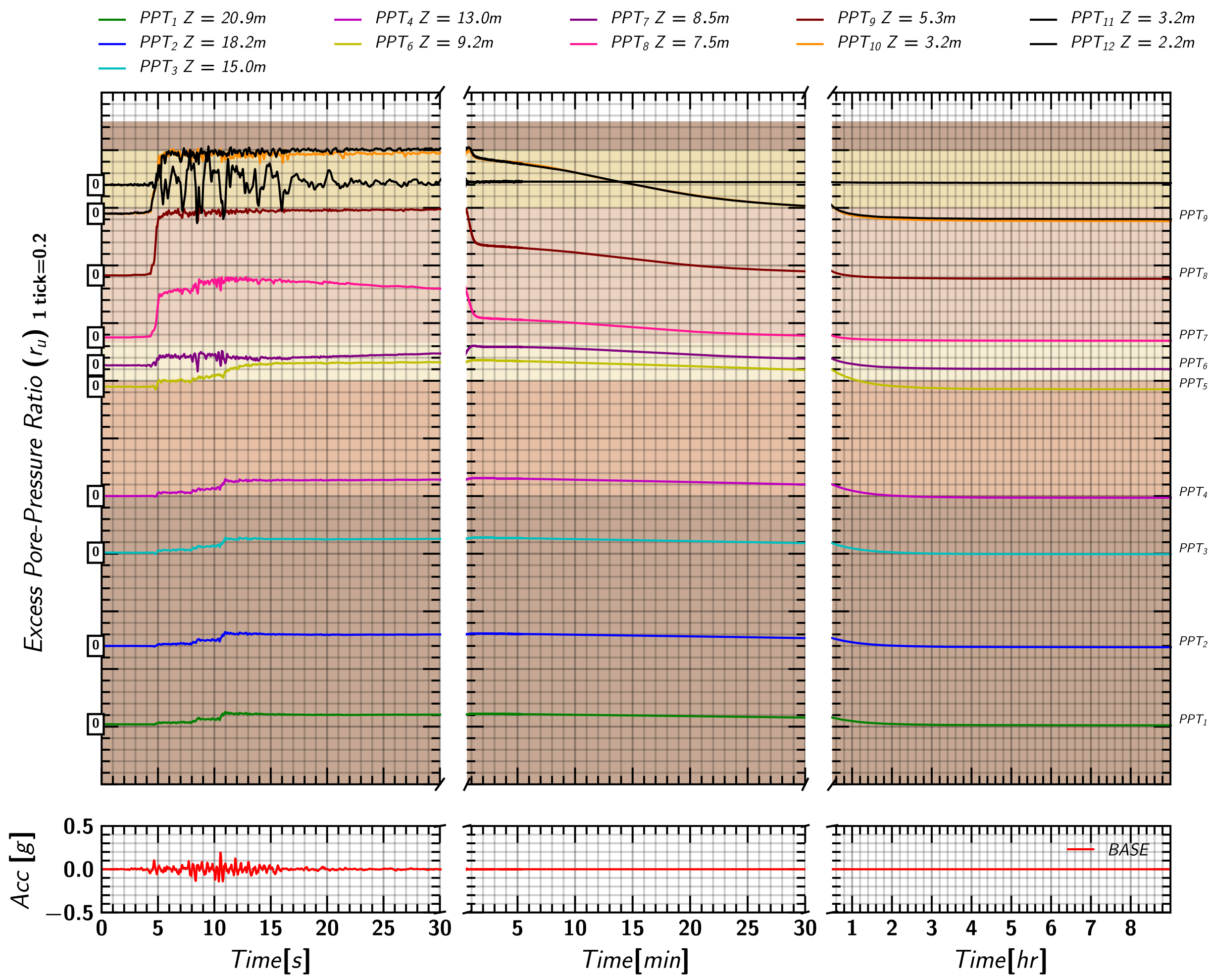

Figure 172. EQM3: Excess pore pressure ratio (r_u) estimated from Keller transducers during and post shaking.

H.11 Excess Pore pressure Ratio (r_u) Estimated from MS54XXX Transducers

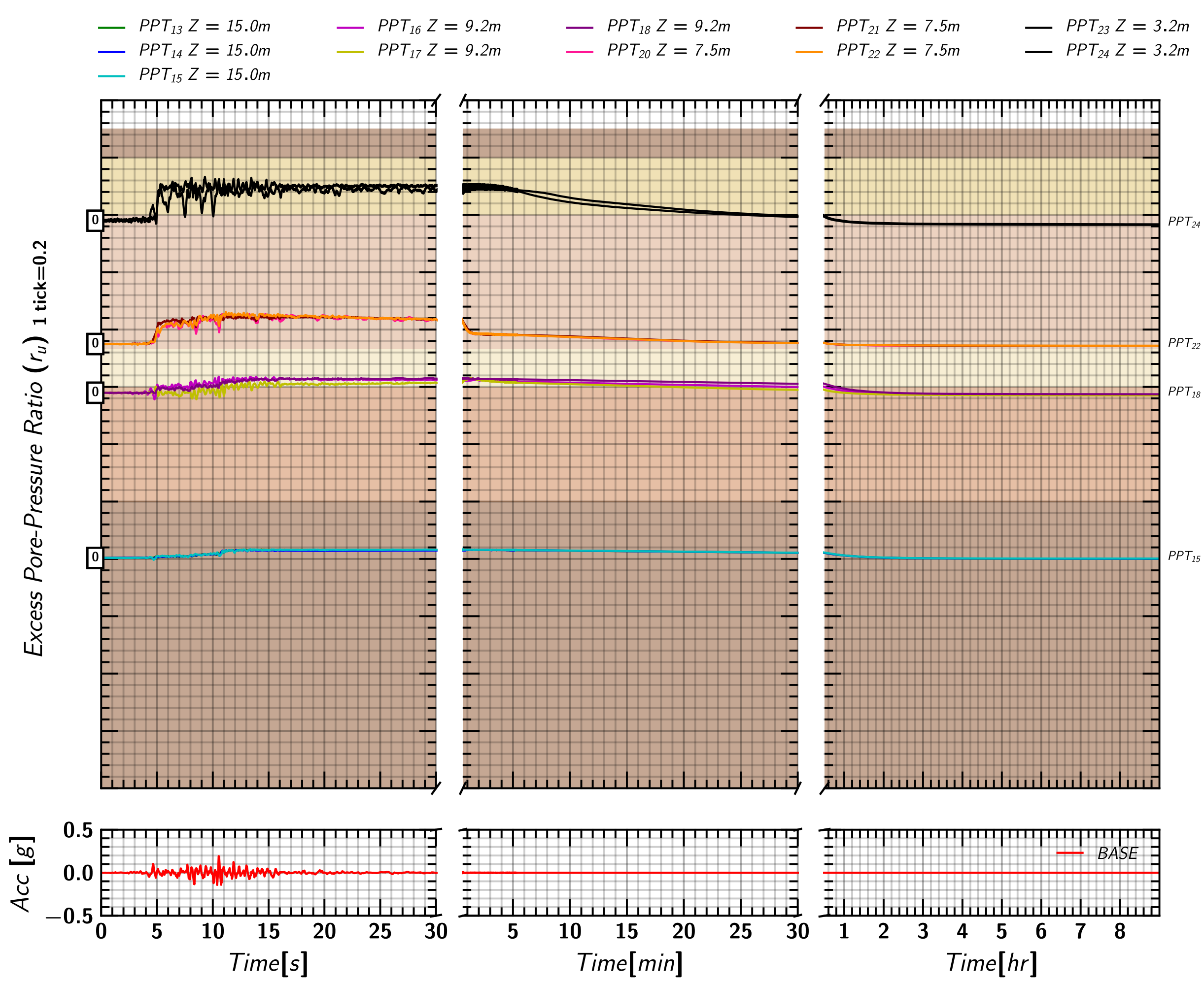

Figure 173. EQM3: Excess pore pressure ratio (r_u) estimated from MS54XXX transducers during and post shaking.

H.12 Axial Load in Pile 1

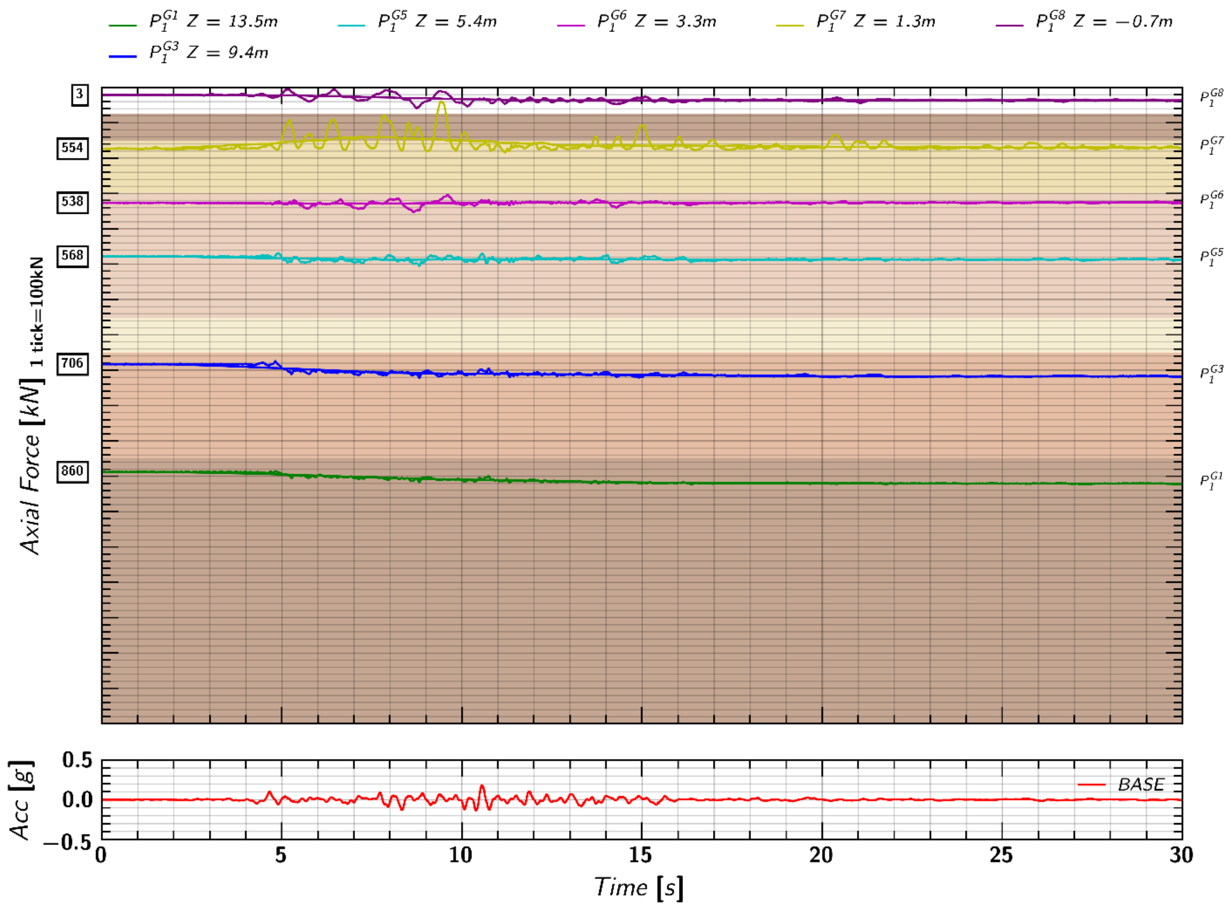

Figure 174. EQM3: Axial load measurements from pile 1 strain gages during shaking.

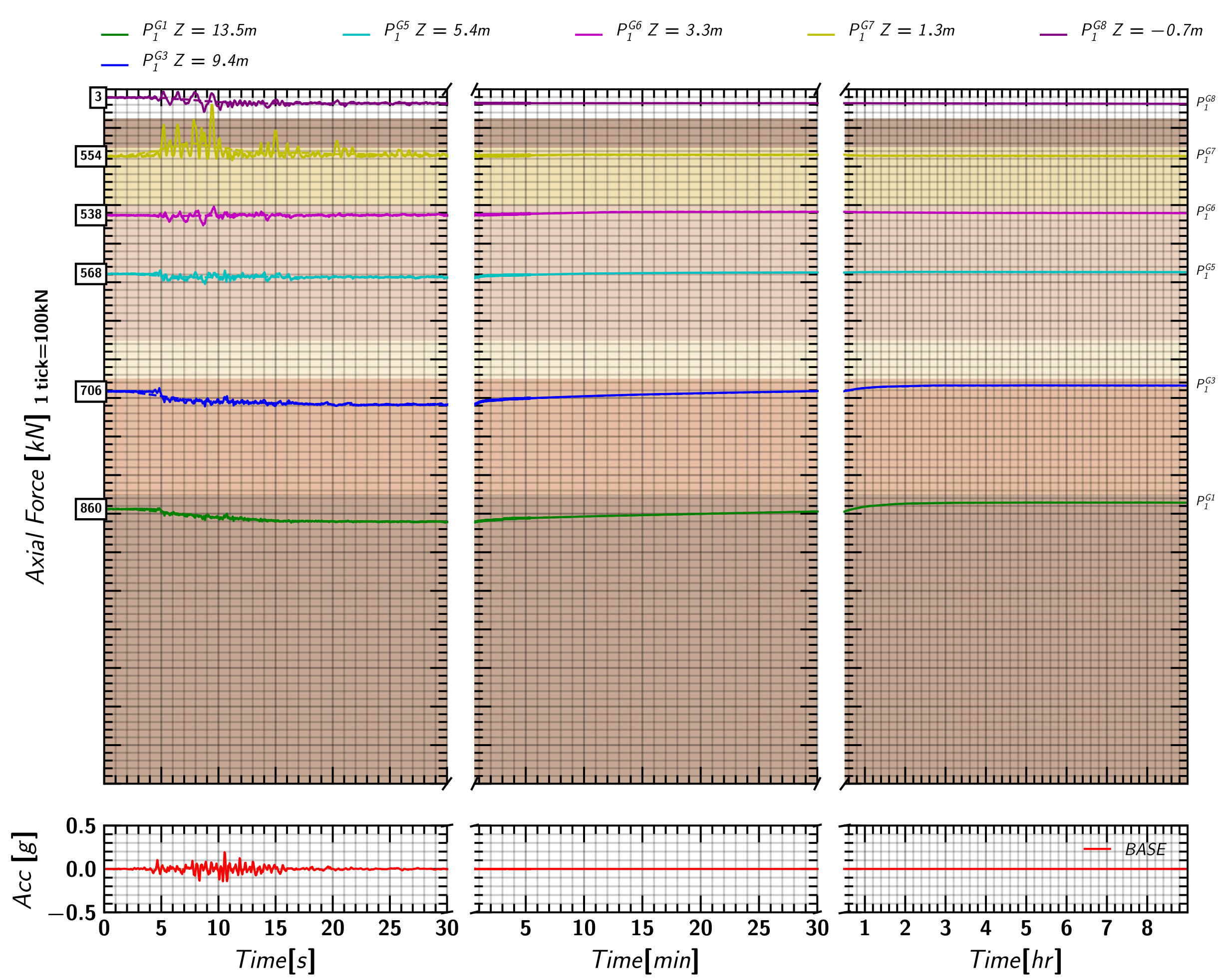

Figure 175. EQM3: Axial load measurements from pile 1 strain gages during and post shaking.

H.13 Axial Load in Pile 2

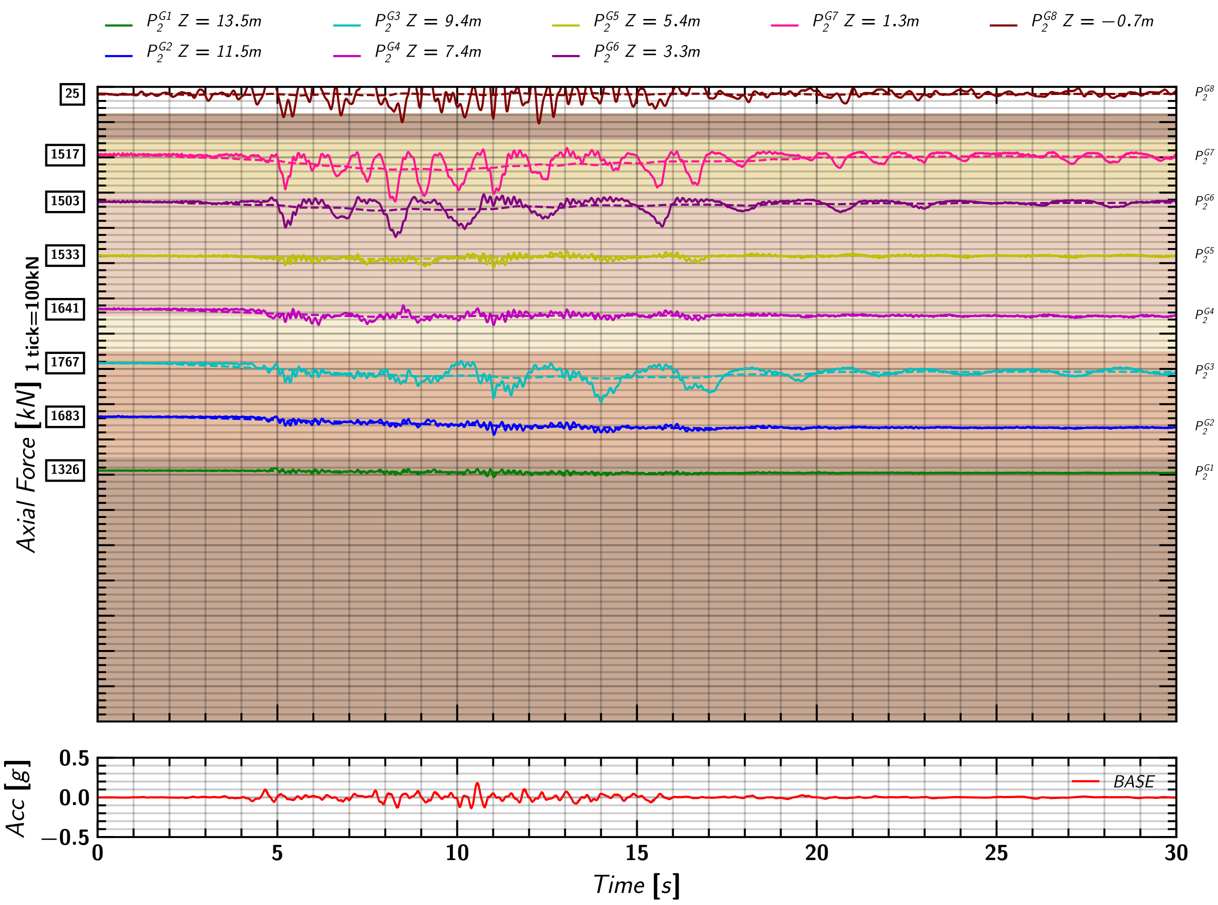

Figure 176. EQM₃: Axial load measurements from pile 2 strain gages during shaking.

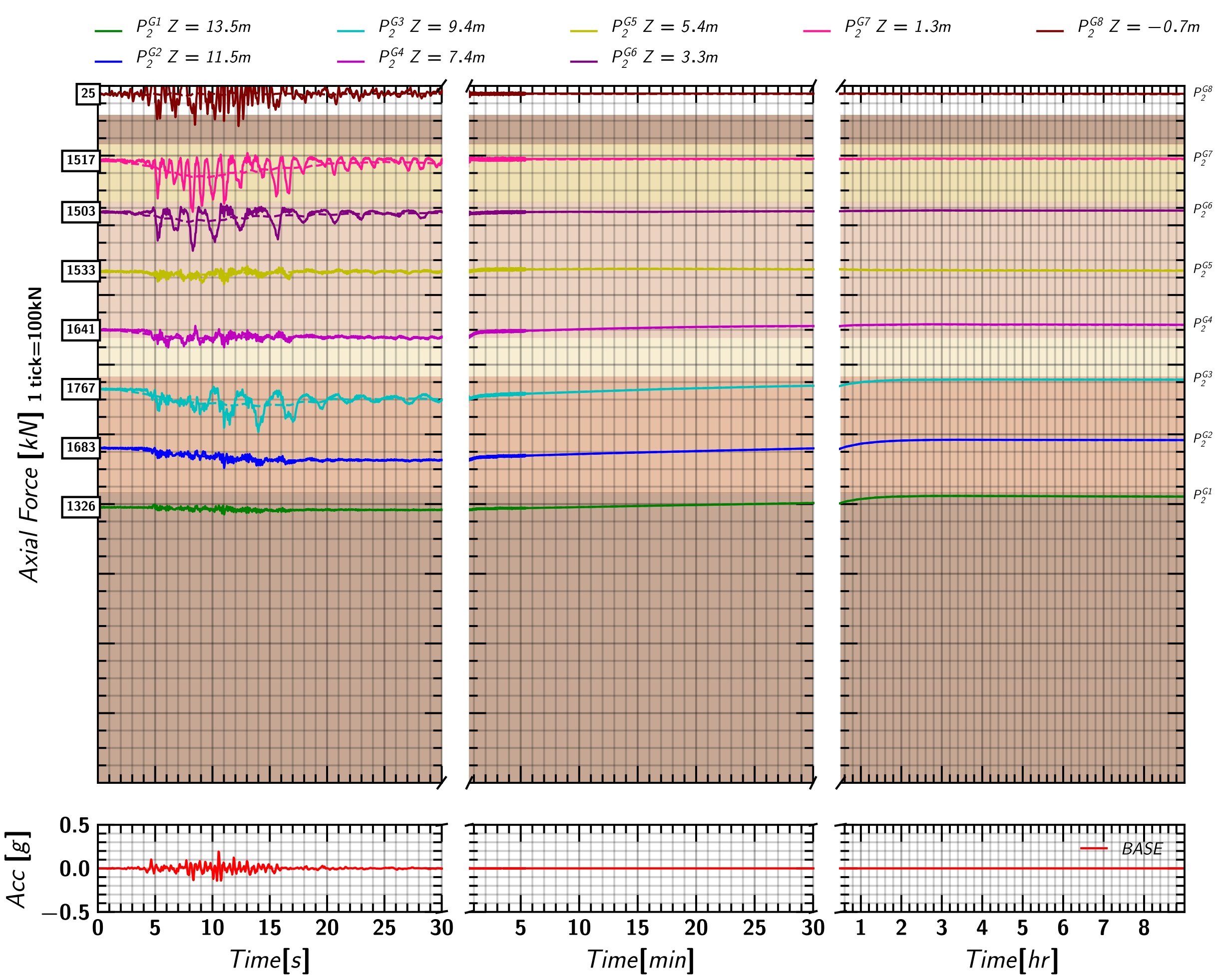

Figure 177. EQM₃: Axial load measurements from pile 2 strain gages during and post shaking.

H.14 Axial Load in Pile 3

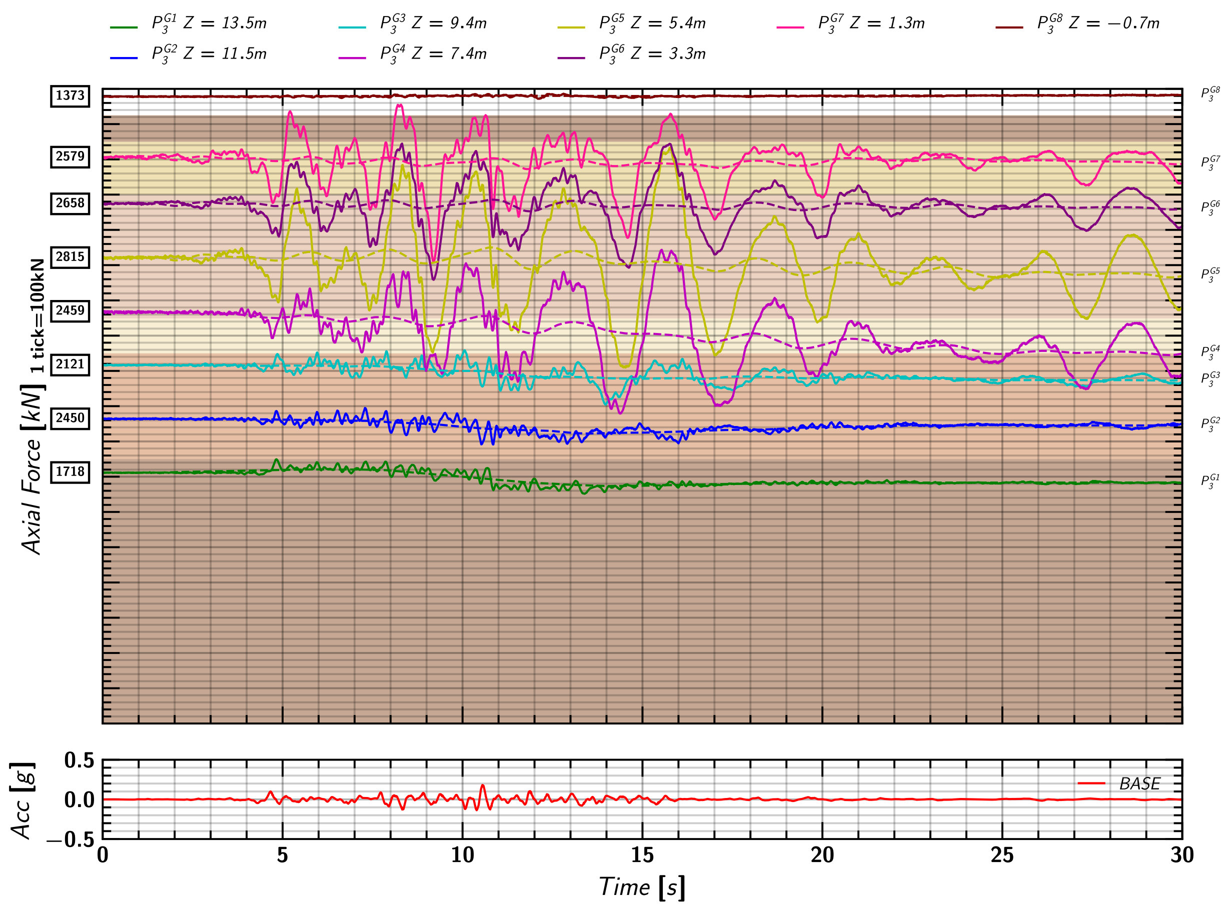

Figure 178. EQM₃: Axial load measurements from pile 3 strain gages during shaking.

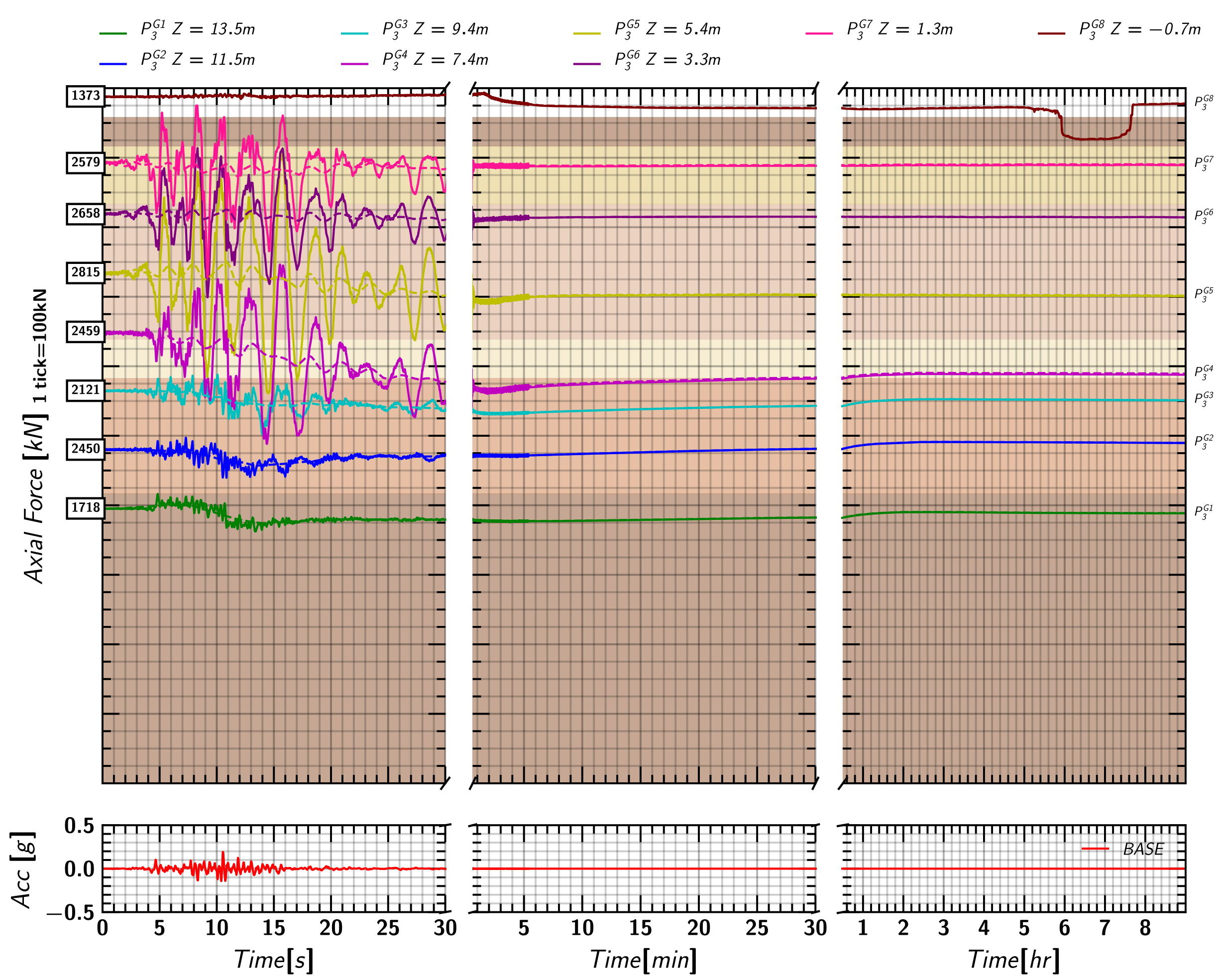

Figure 179. EQM₃: Axial load measurements from pile 3 strain gages during and post shaking.

H.15 Pore pressure and Axial Load Profile

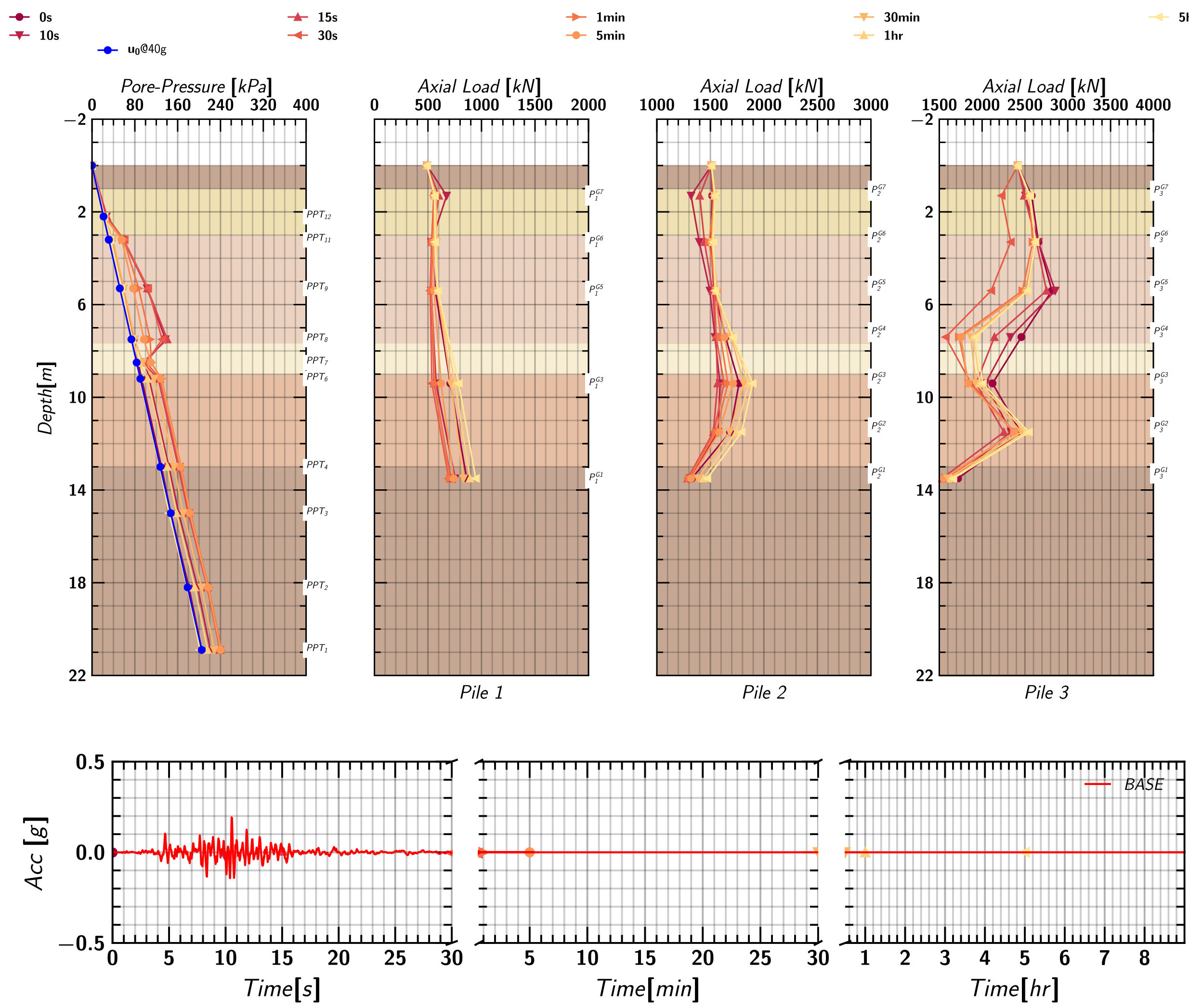

Figure 180. EQM$_3$: Pore pressure and axial load profile in pile 1, pile 2 and pile 3 at different times during and post shaking.

I. EQM3: Soil, Pile, and Container Movements in X and Z

I.1 Container Movement in X

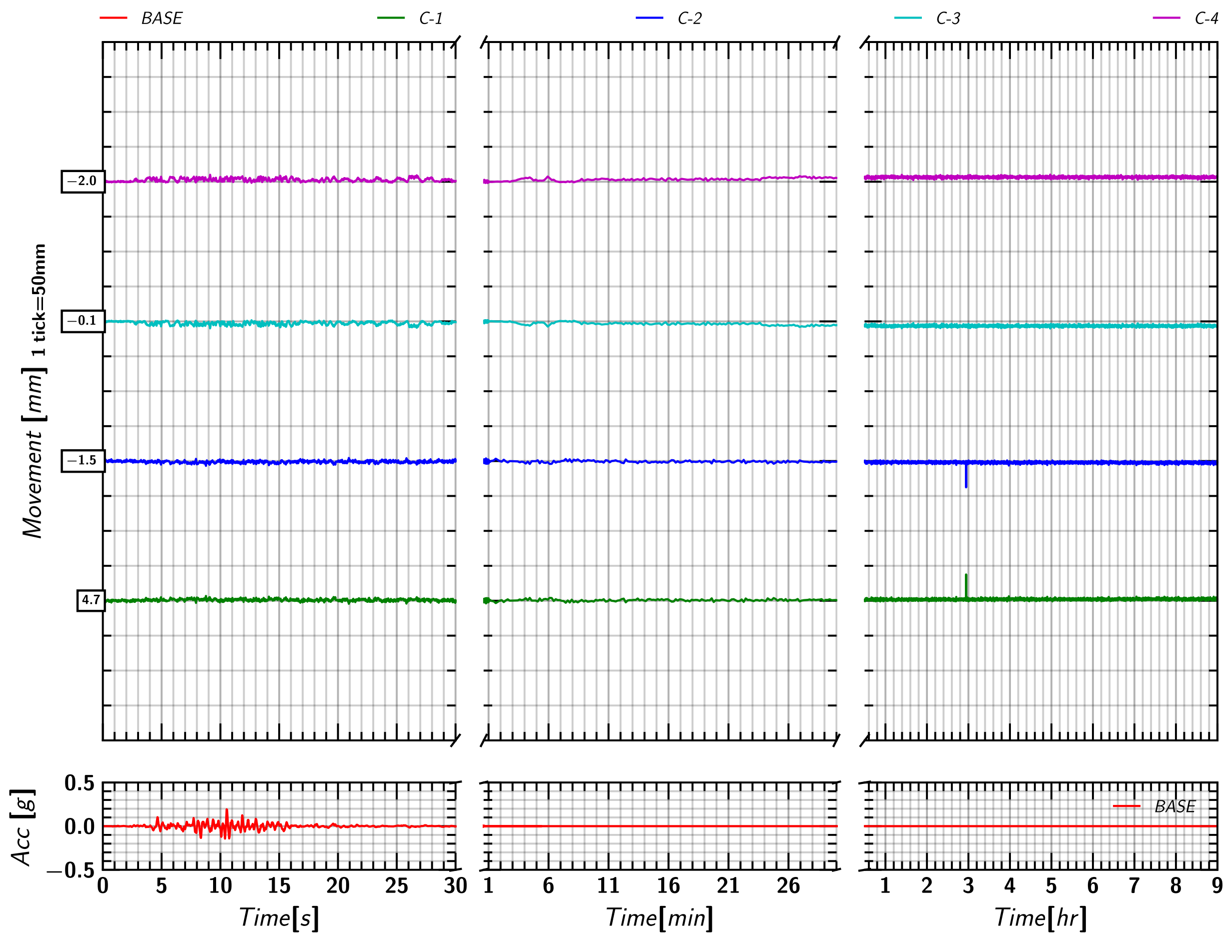

Figure 181. EQM3: Container movement in X-direction relative to the model container during and post shaking.

I.2 Container Movement in Z

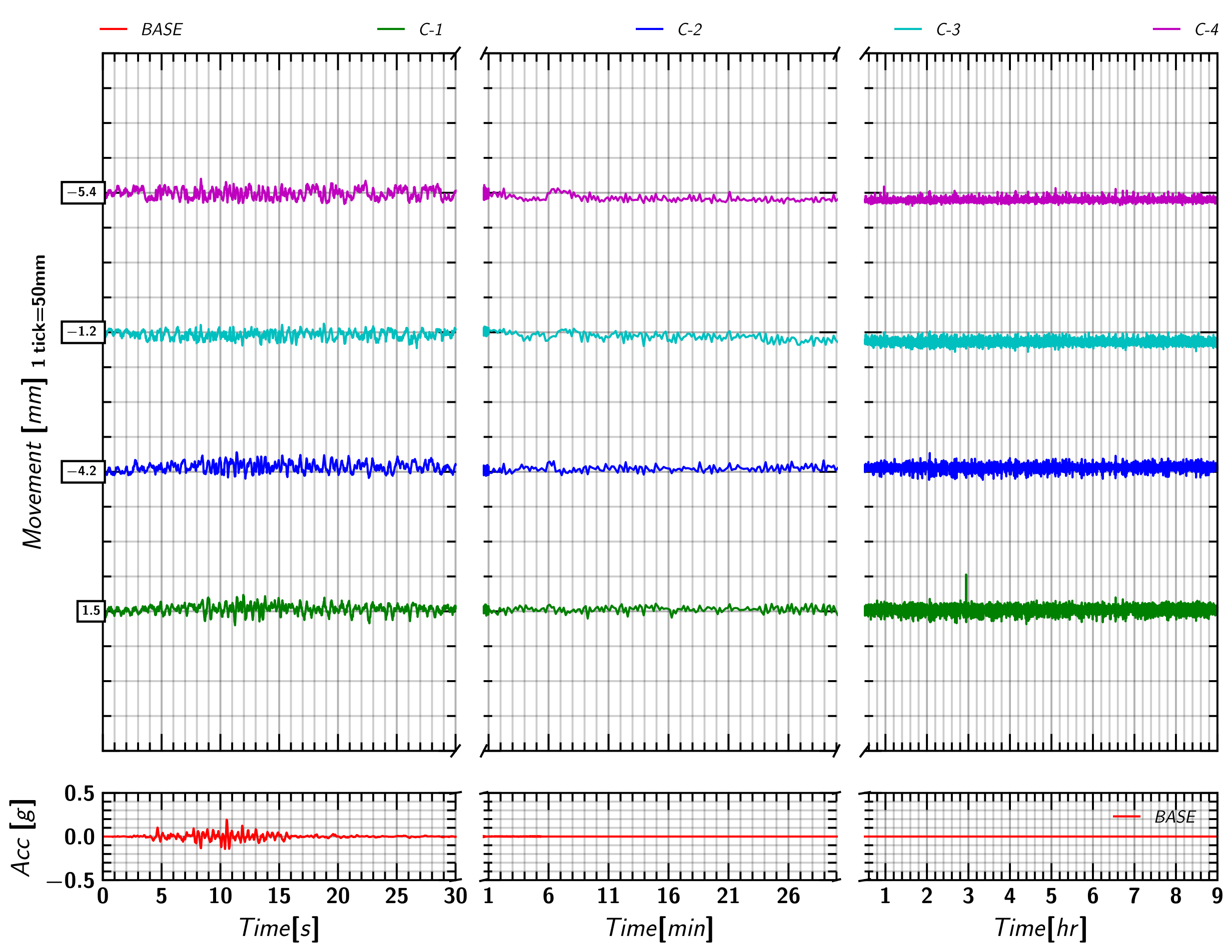

Figure 182. EQM3: Container movement in Z-direction relative to the model container during and post shaking.

I.3 Soil (Row S-1) Movement in X

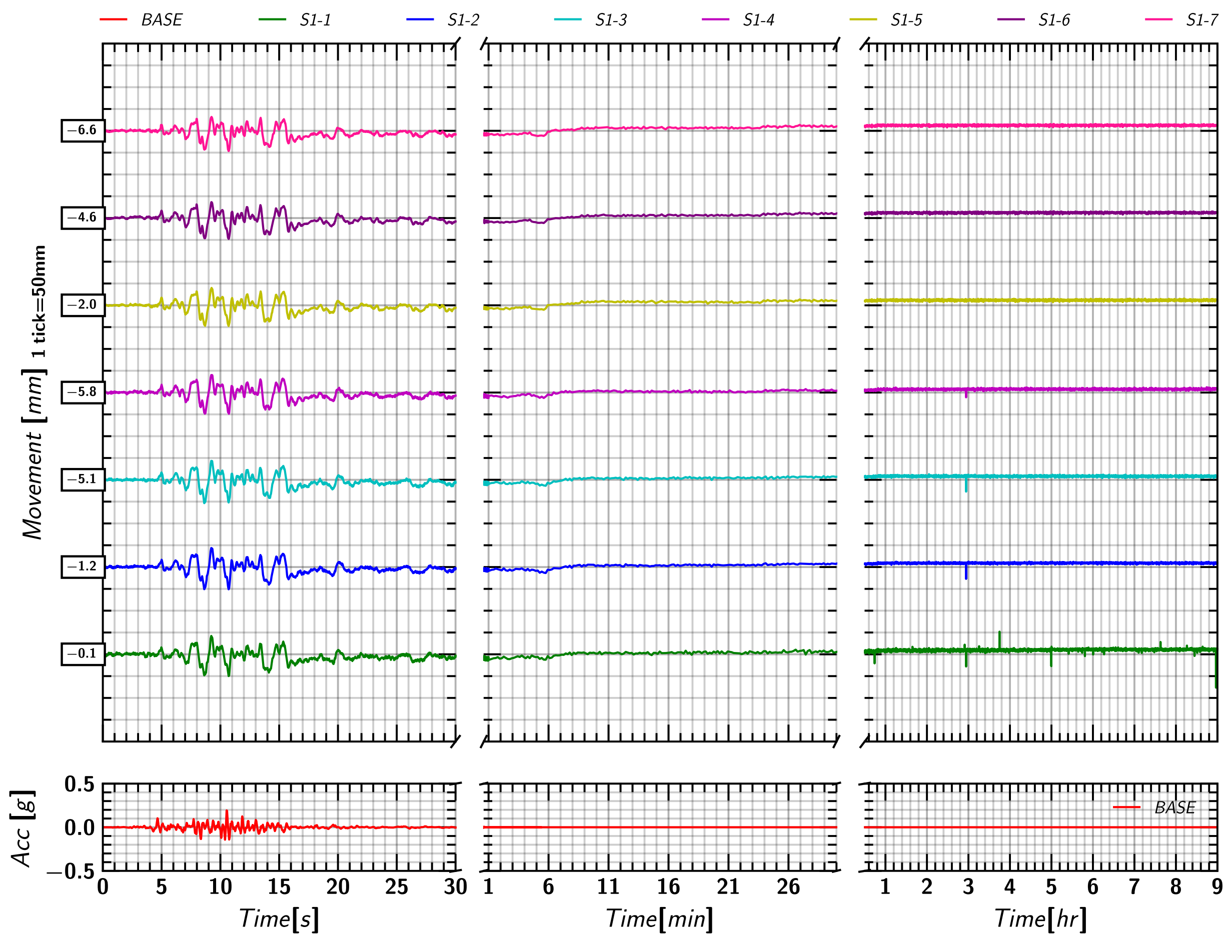

Figure 183. EQM3: Soil (Row S-1) movement in X-direction relative to the model container during and post shaking.

I.4 Soil (Row S-1) Movement in Z

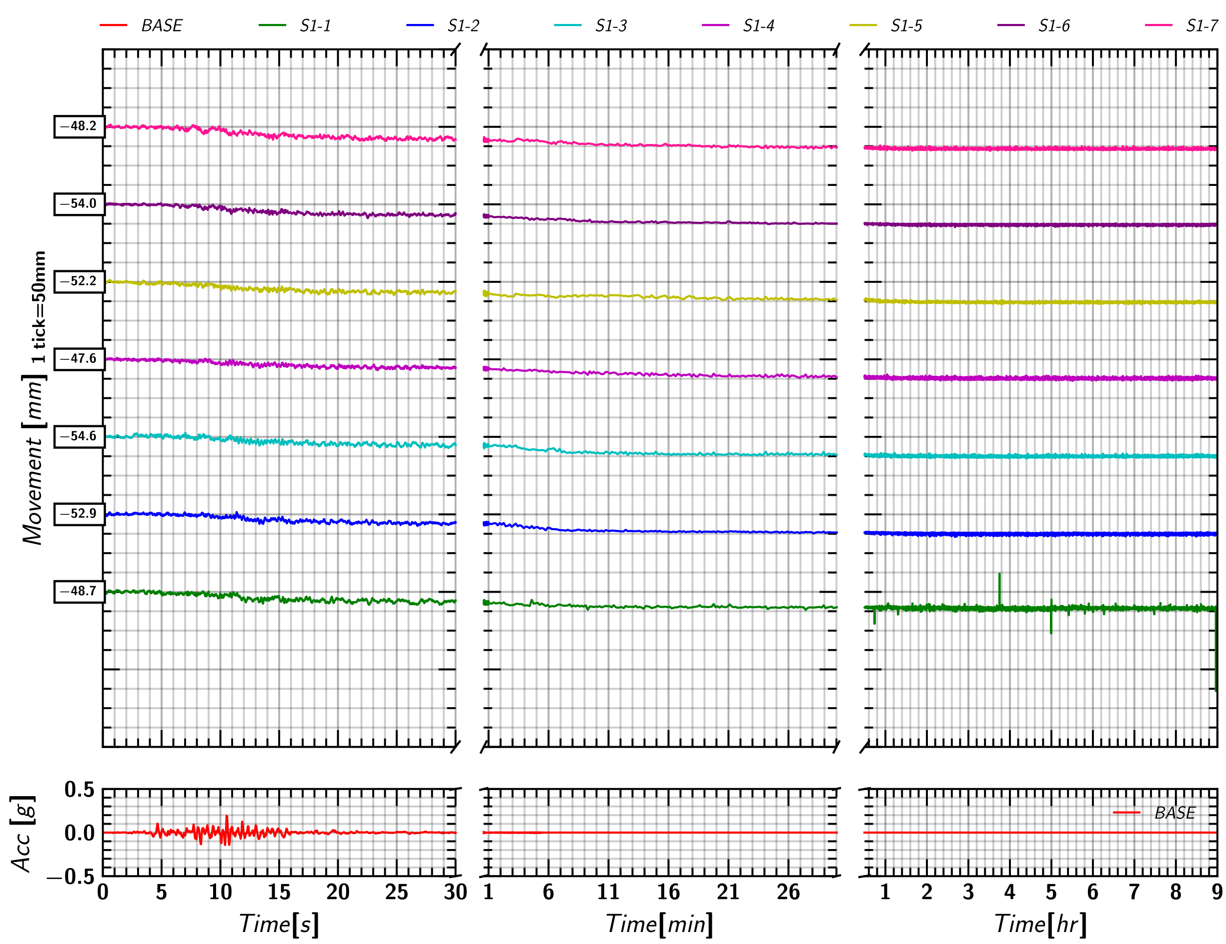

Figure 184. EQM3: Soil (Row S-1) movement in Z-direction relative to the model container during and post shaking.

I.5 Soil (Row S-2) Movement in X

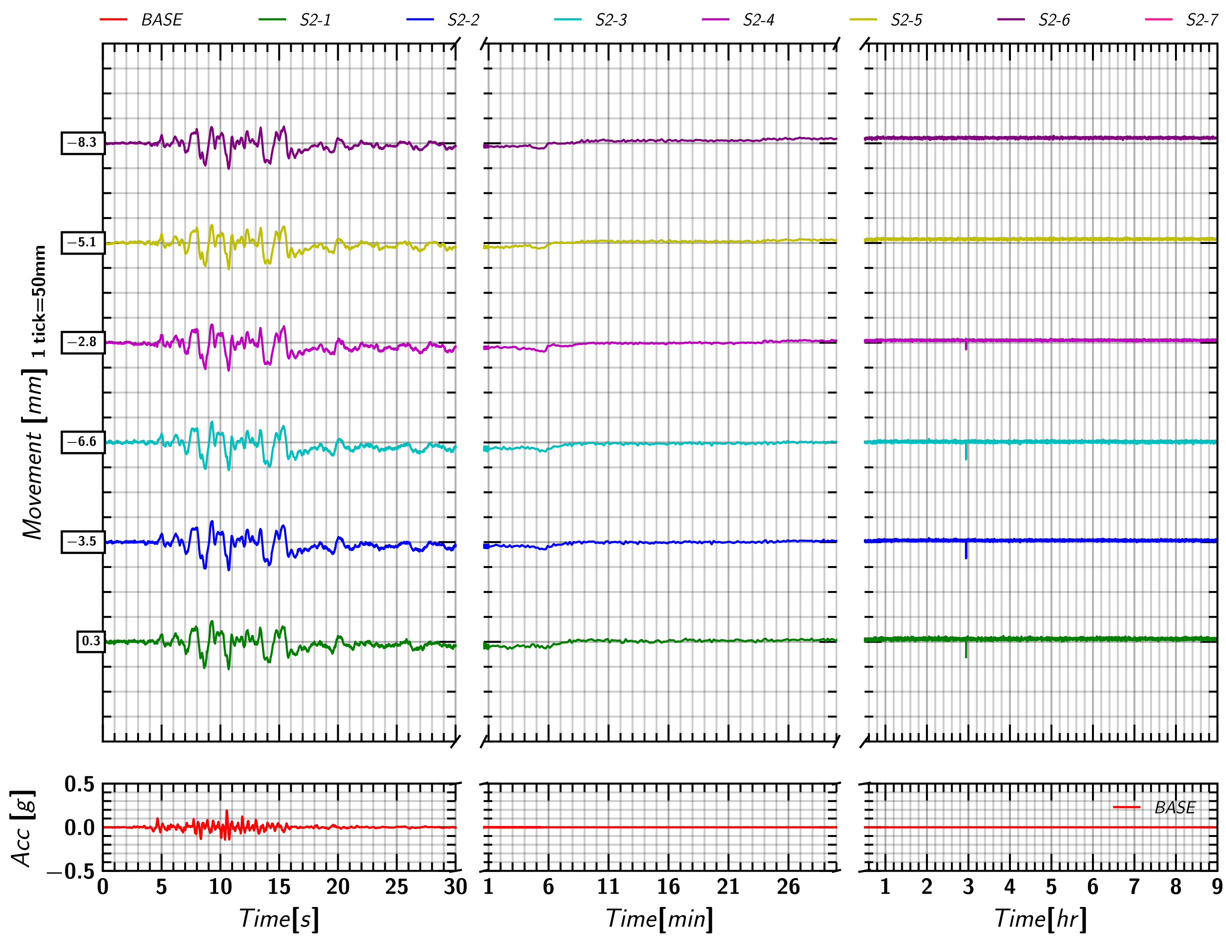

Figure 185. EQM3: Soil (Row S-2) movement in X-direction relative to the model container during and post shaking.

I.6 Soil (Row S-2) Movement in Z

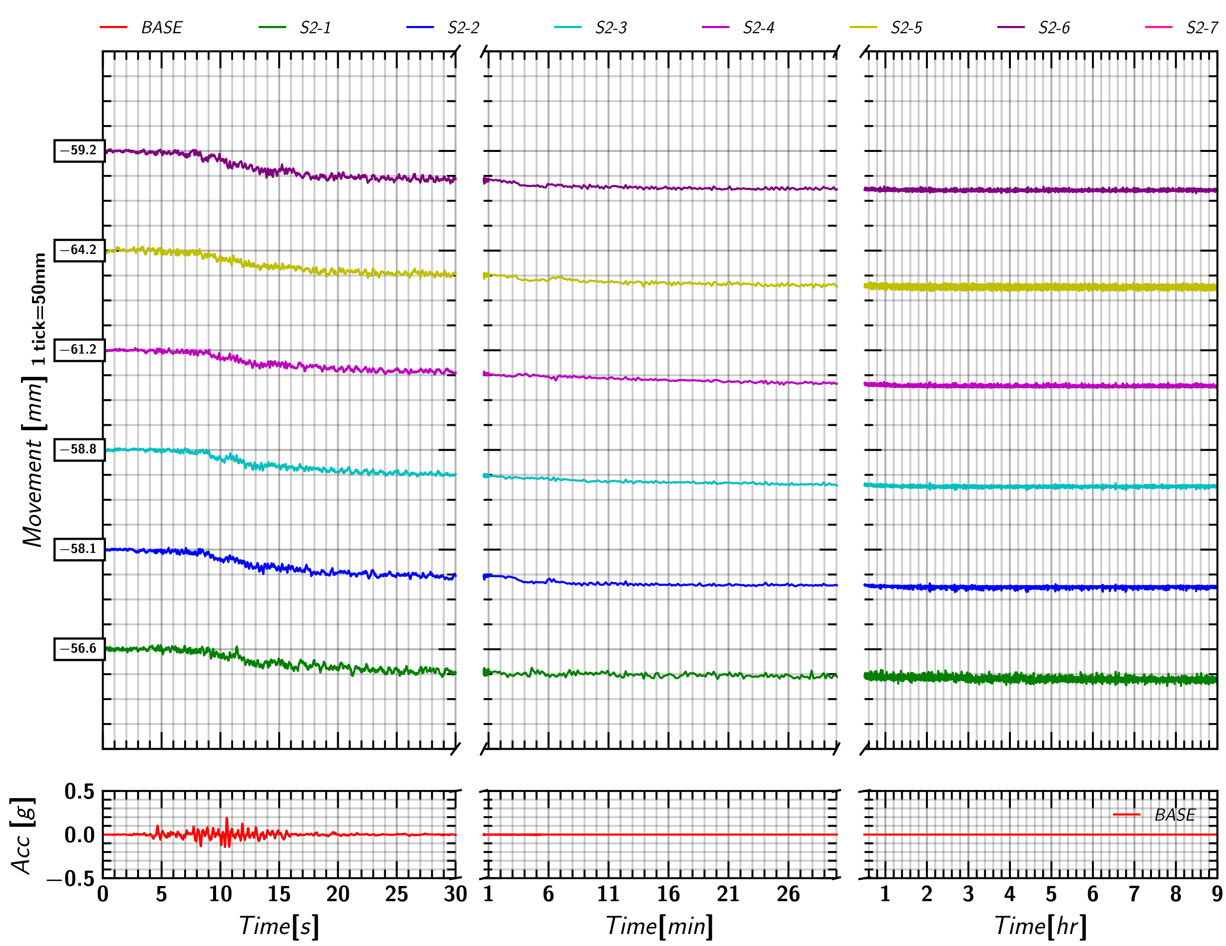

Figure 186. EQM3: Soil (Row S-2) movement in Z-direction relative to the model container during and post shaking.

I.7 Soil (Row S-3) Movement in X

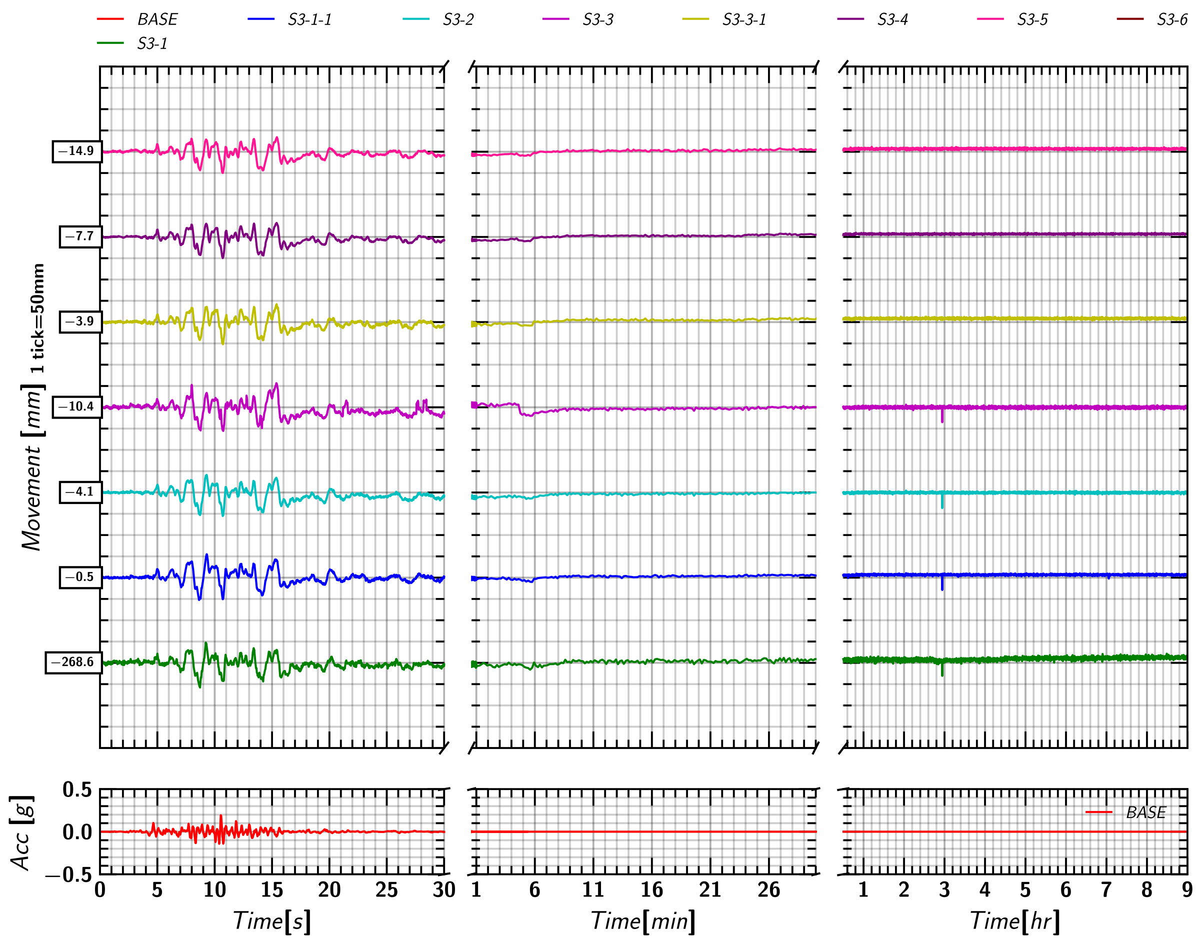

Figure 187. EQM3: Soil (Row S-3) movement in X-direction relative to the model container during and post shaking.

I.8 Soil (Row S-3) Movement in Z

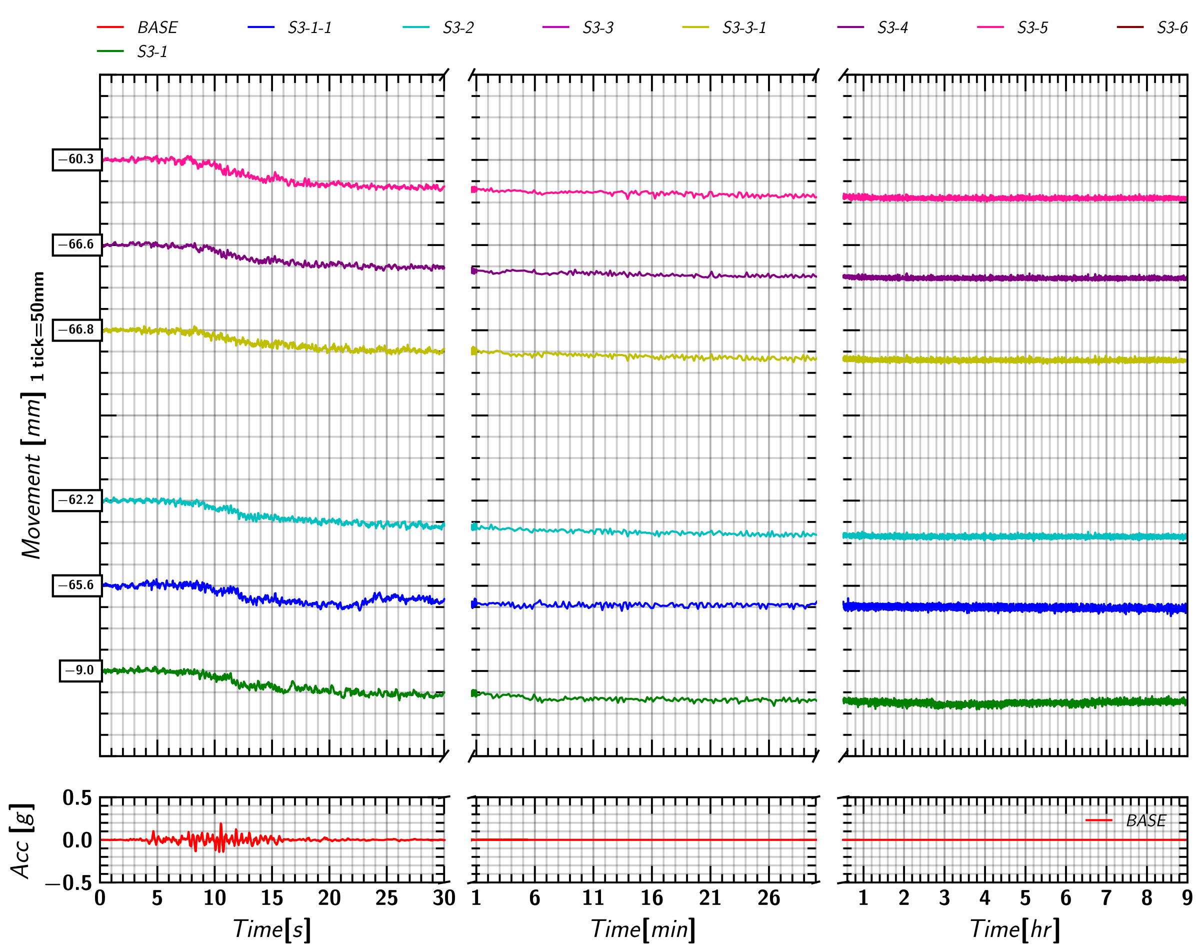

Figure 188. EQM3: Soil (Row S-3) movement in Z-direction relative to the model container during and post shaking.

I.9 Soil (Row S-4) Movement in X

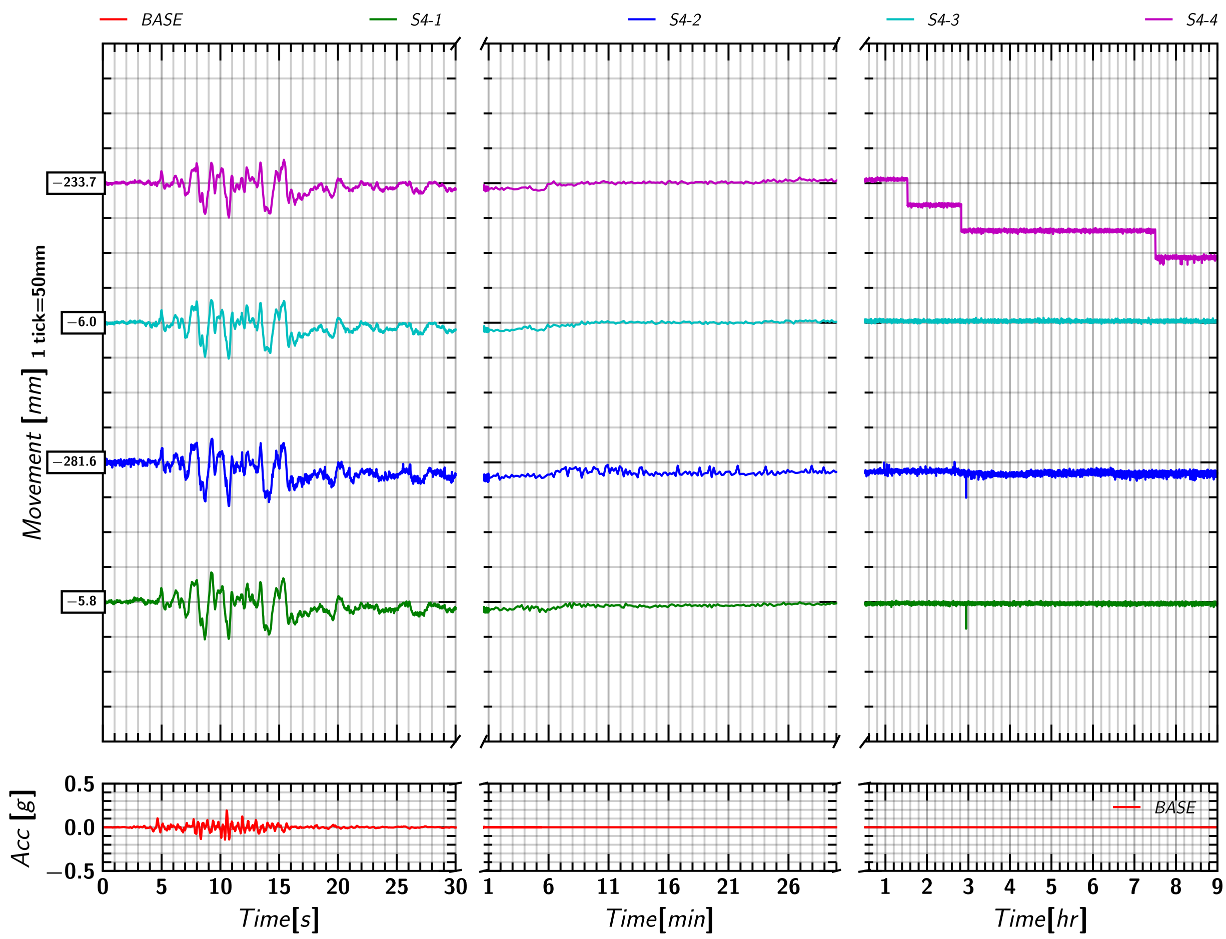

Figure 189. EQM3: Soil (Row S-4) movement in X-direction relative to the model container during and post shaking.

I.10 Soil (Row S-4) Movement in Z

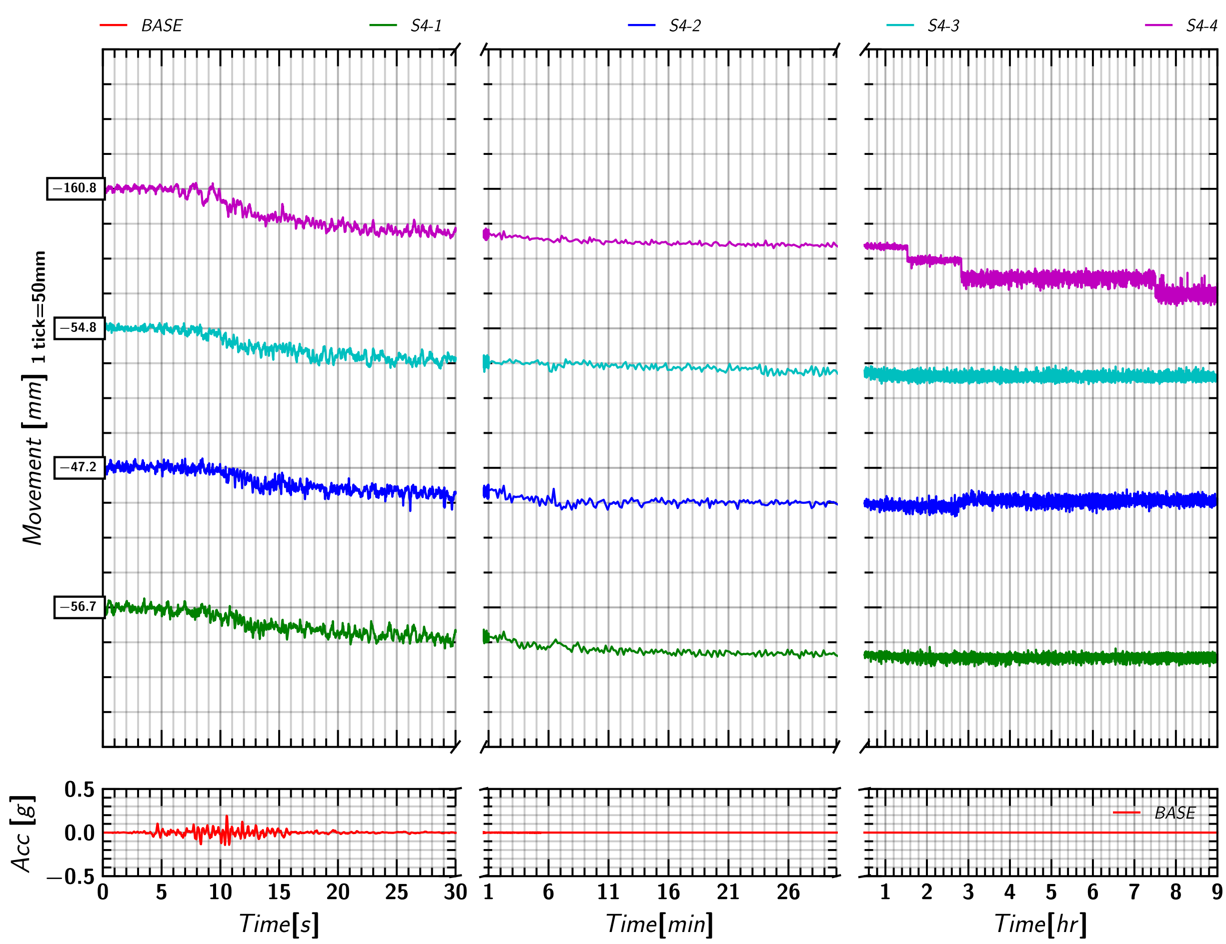

Figure 190. EQM3: Soil (Row S-4) movement in Z-direction relative to the model container during and post shaking.

I.11 Soil (Row S-5) Movement in X

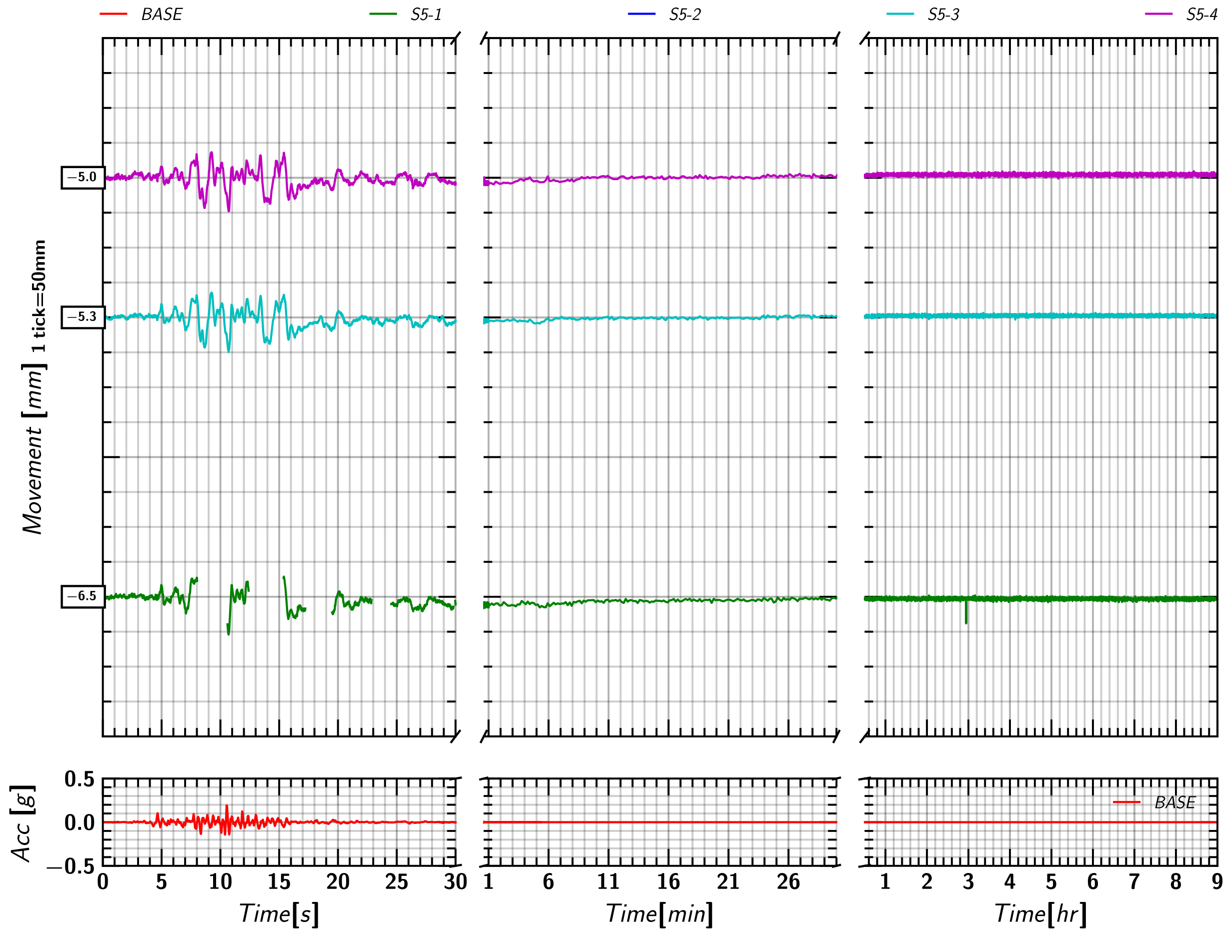

Figure 191. EQM$_3$: Soil (Row S-5) movement in X-direction relative to the model container during and post shaking.

I.12 Soil (Row S-5) Movement in Z

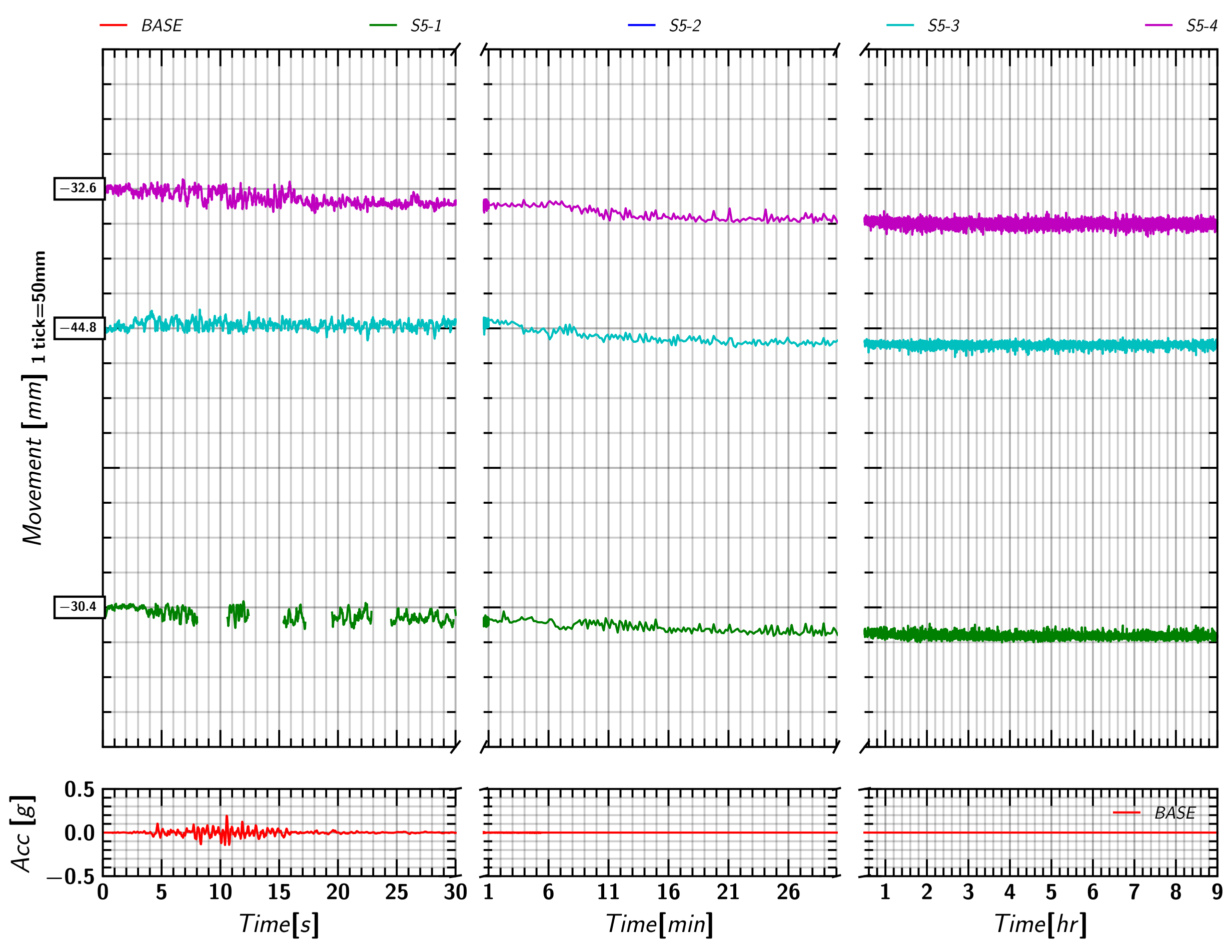

Figure 192. EQM$_3$: Soil (Row S-5) movement in Z-direction relative to the model container during and post shaking.

I.13 Pile 1 Mass Movement in X

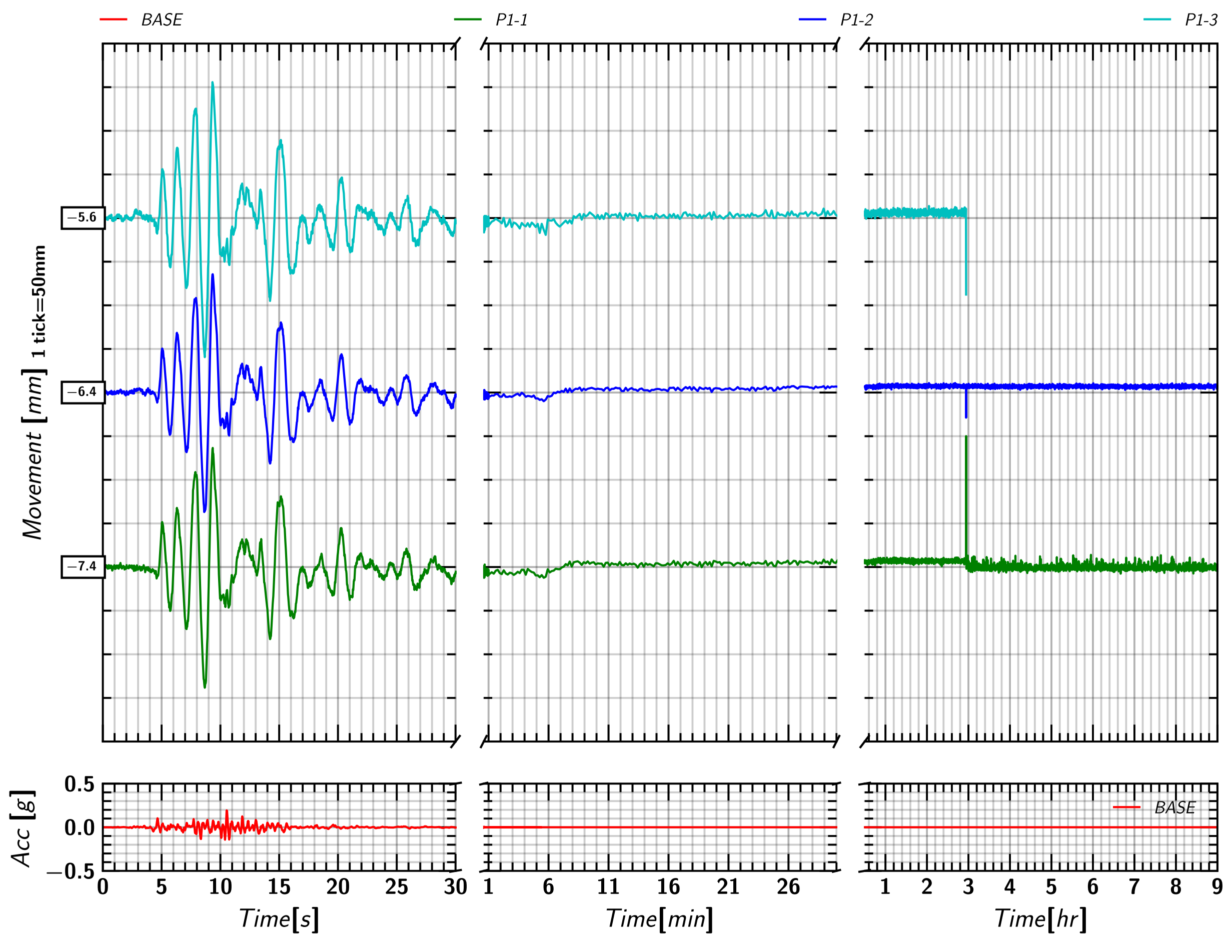

Figure 193. EQM3: Pile 1 movement in X-direction relative to the model container during and post shaking.

I.14 Pile 1 Mass Movement in Z

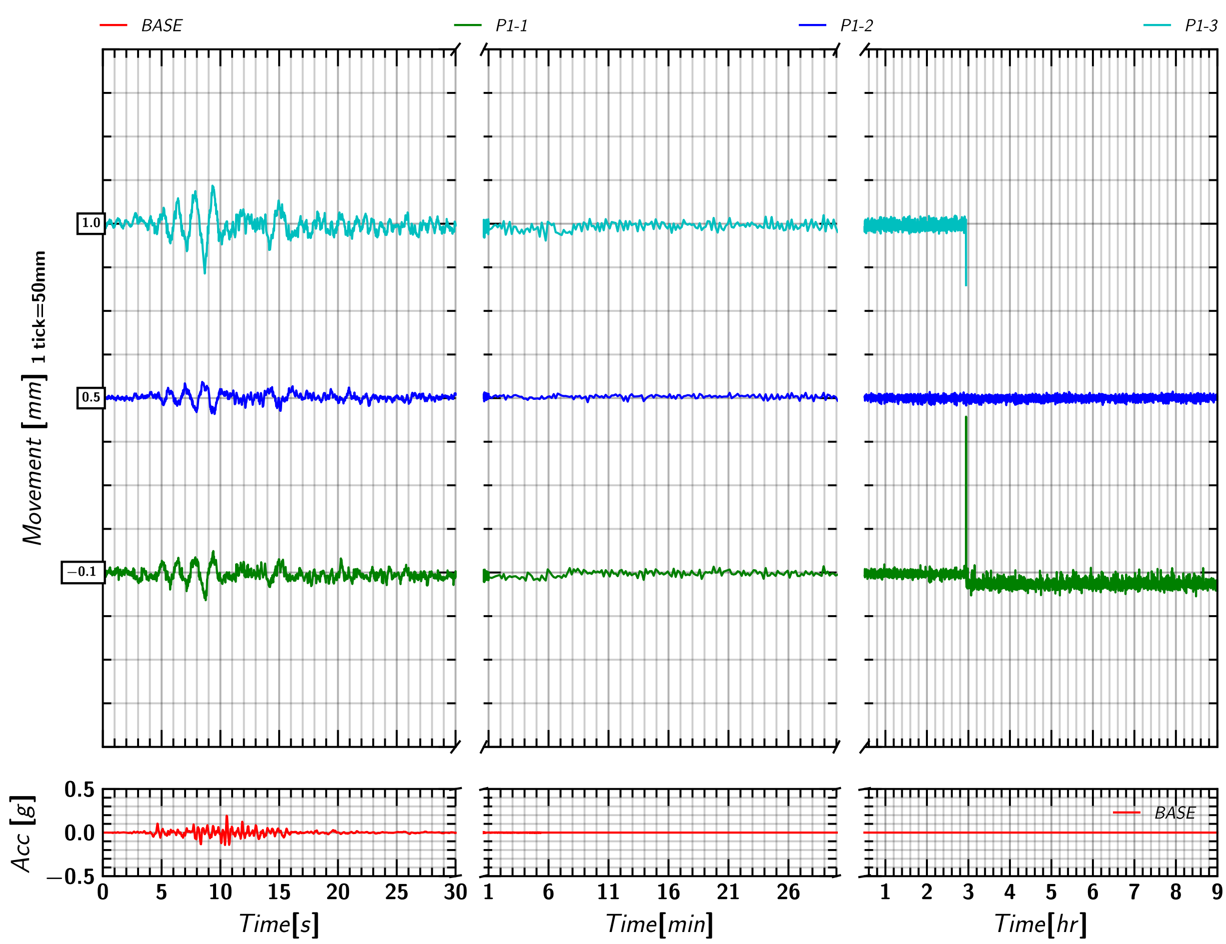

Figure 194. EQM3: Pile 1 movement in Z-direction relative to the model container during and post shaking.

I.15 Pile 2 Mass Movement in X

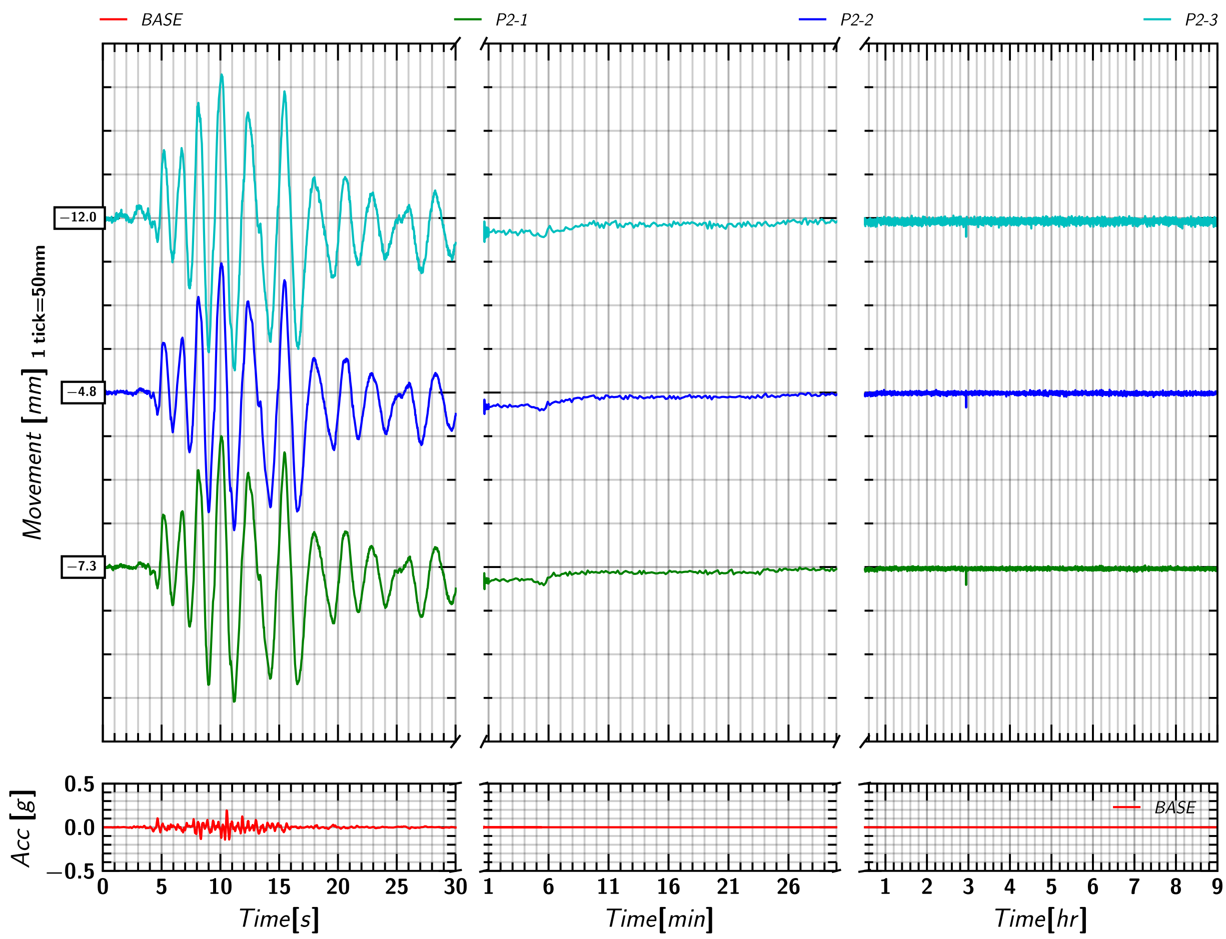

Figure 195. EQM$_3$: Pile 2 movement in X-direction relative to the model container during and post shaking.

I.16 Pile 2 Mass Movement in Z

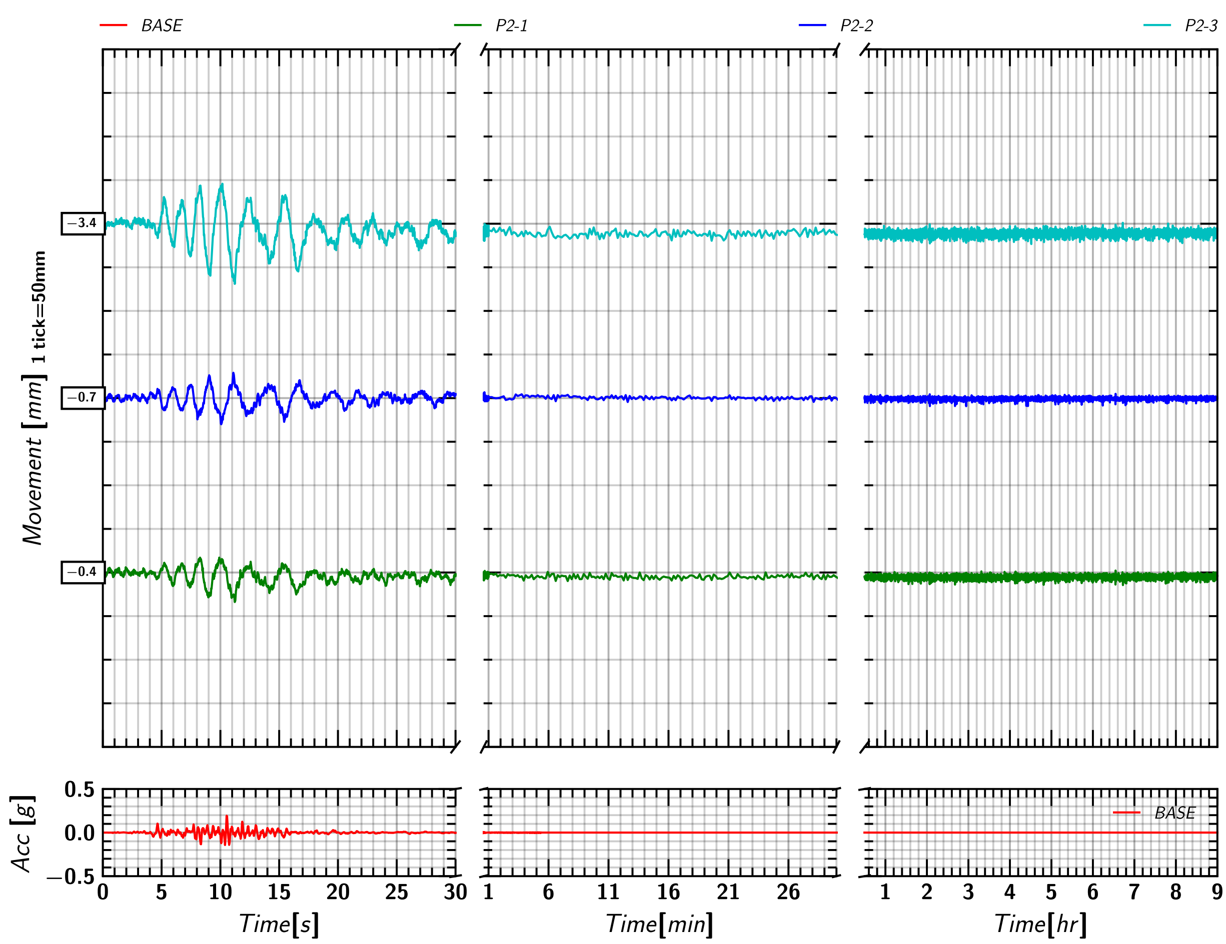

Figure 196. EQM$_3$: Pile 2 movement in Z-direction relative to the model container during and post shaking.

I.17 Pile 3 Mass Movement in X

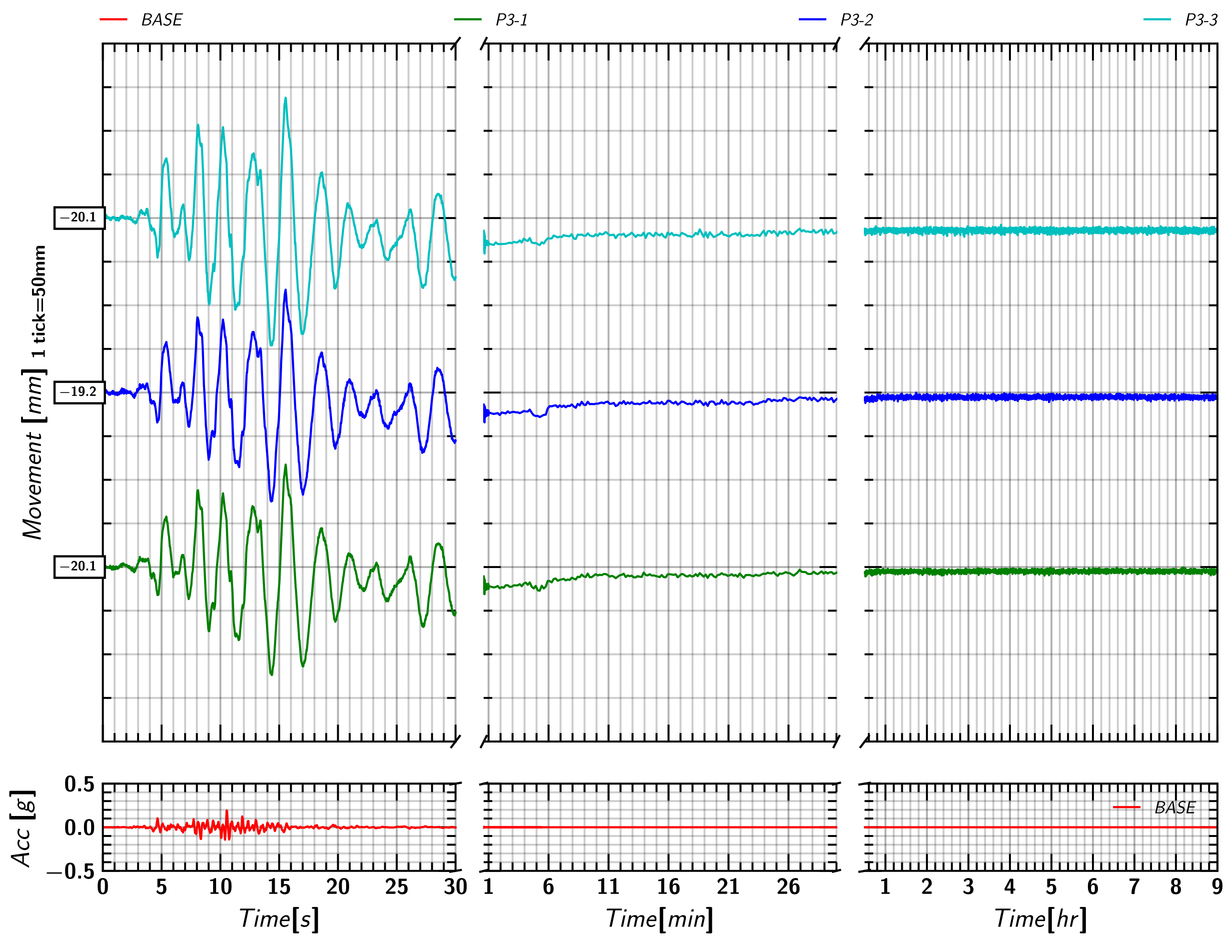

Figure 197. EQM$_3$: Pile 3 movement in X-direction relative to the model container during and post shaking.

I.18 Pile 3 Mass Movement in Z

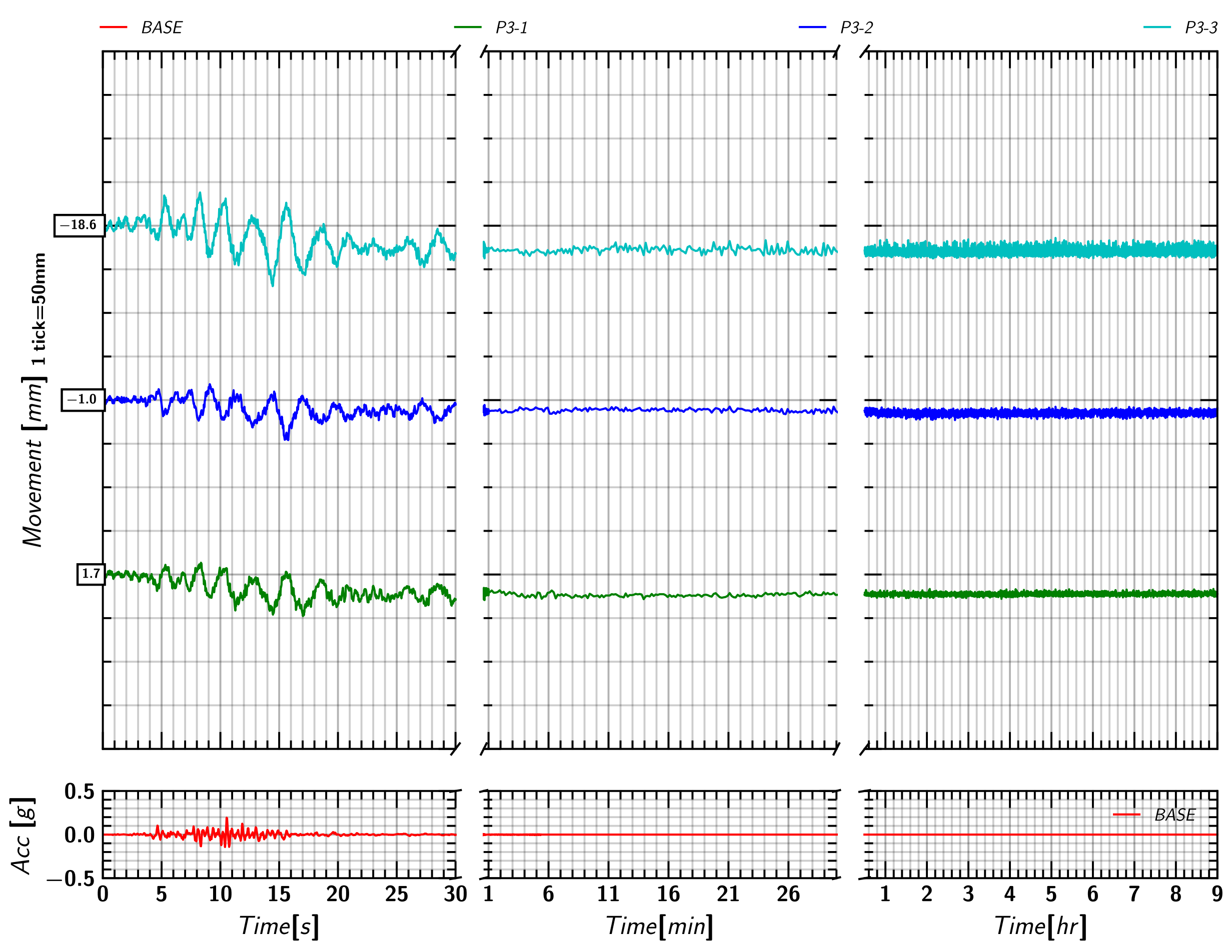

Figure 198. EQM$_3$: Pile 3 movement in Z-direction relative to the model container during and post shaking.

J. EQM₄: Large EJM01 CRUZ EARTHQUAKE (PGA = 0.45g)

J.1 Input Motion

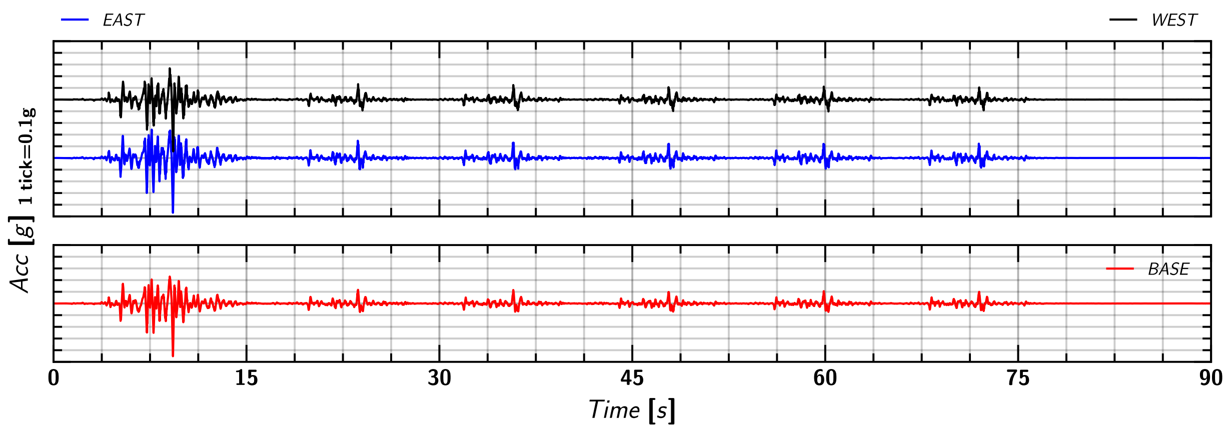

Figure 199. EQM$_4$: Input motion.

J.2 Spectral Acceleration

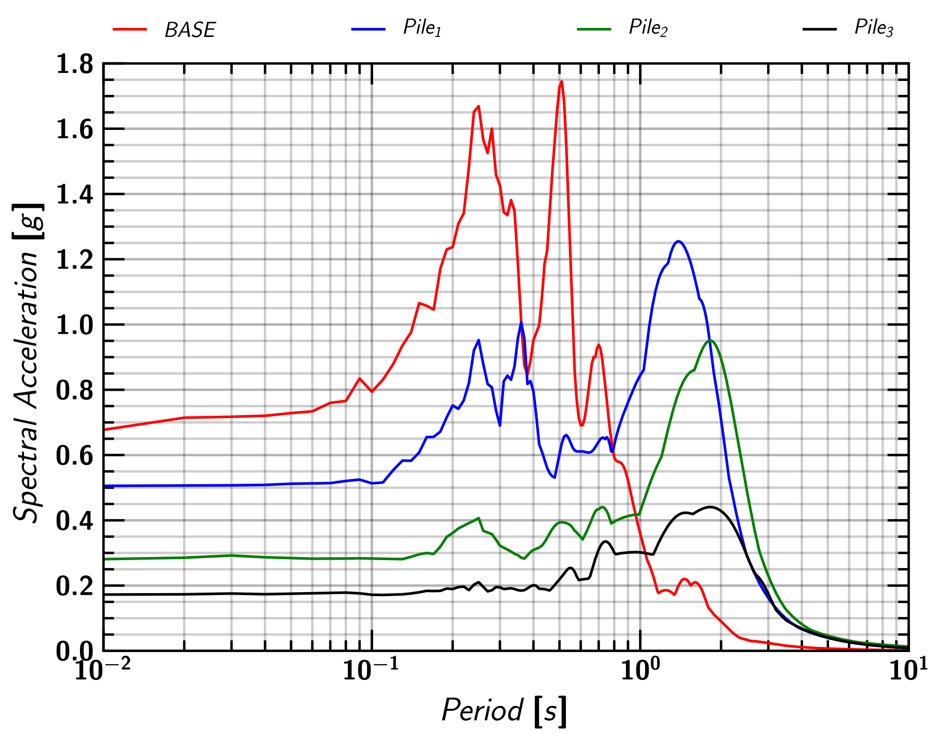

Figure 200. EQM$_4$: Spectral Acceleration.

J.3 Container Acceleration

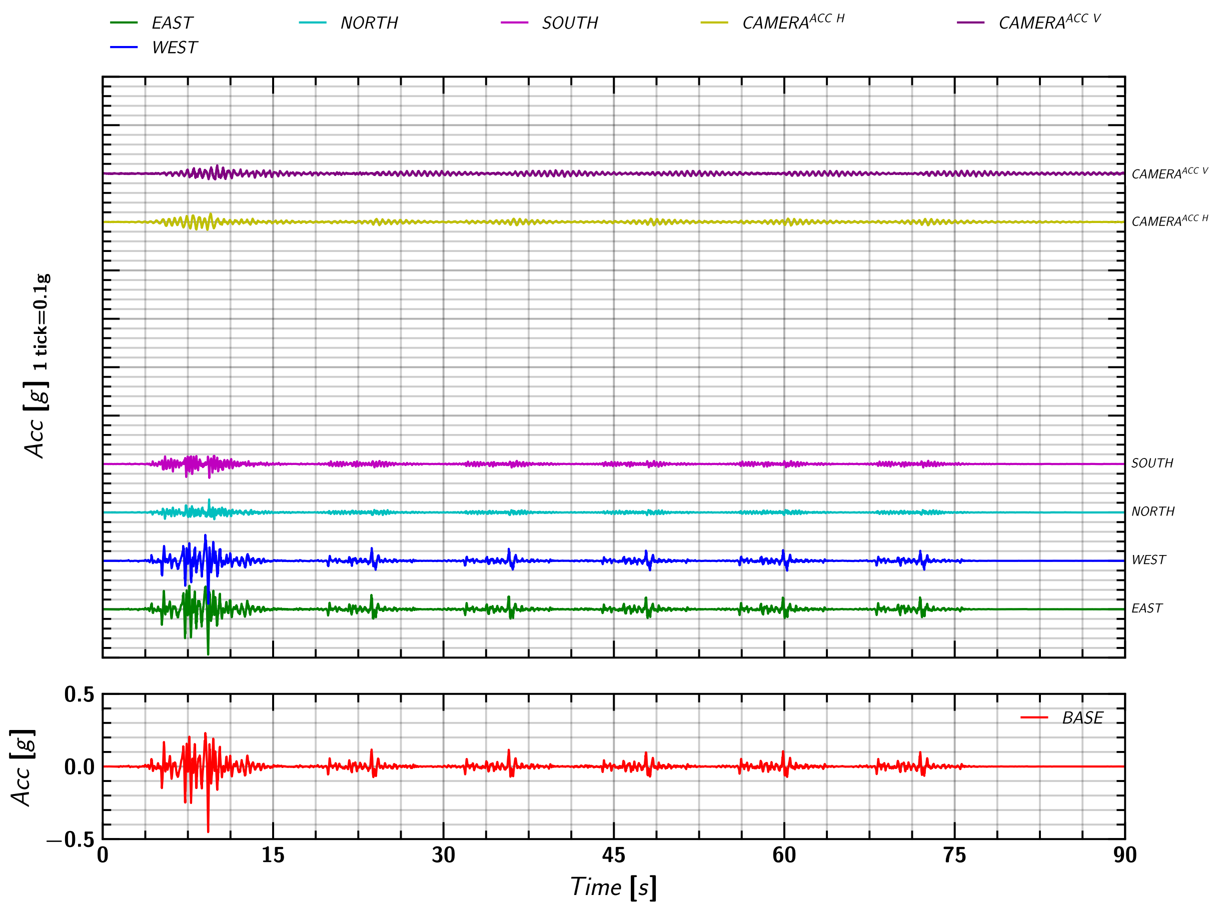

Figure 201. EQM$_4$: Acceleration measurement on container and camera beam.

J.4 Acceleration in Soil

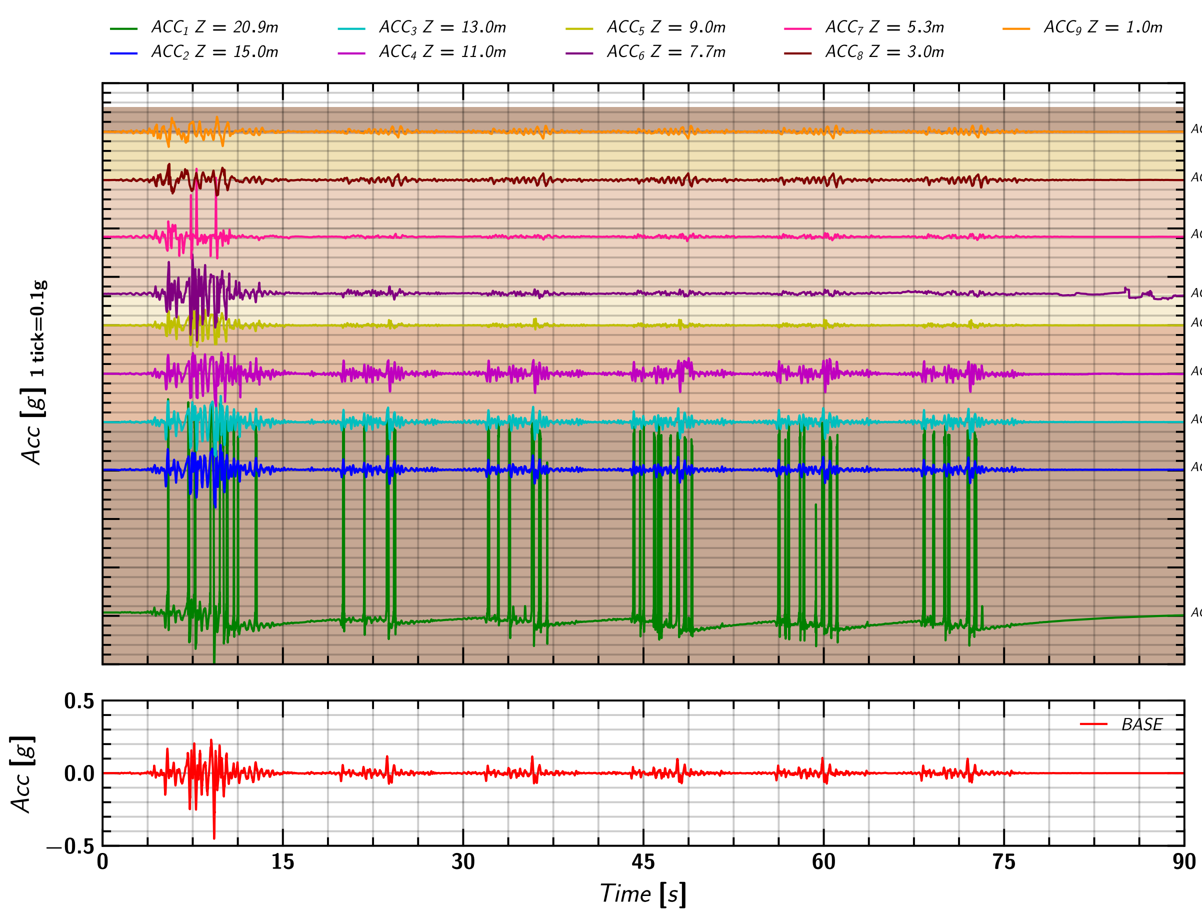

Figure 202. EQM$_4$: Acceleration measurement in soil.

J.5 Pile Mass Acceleration

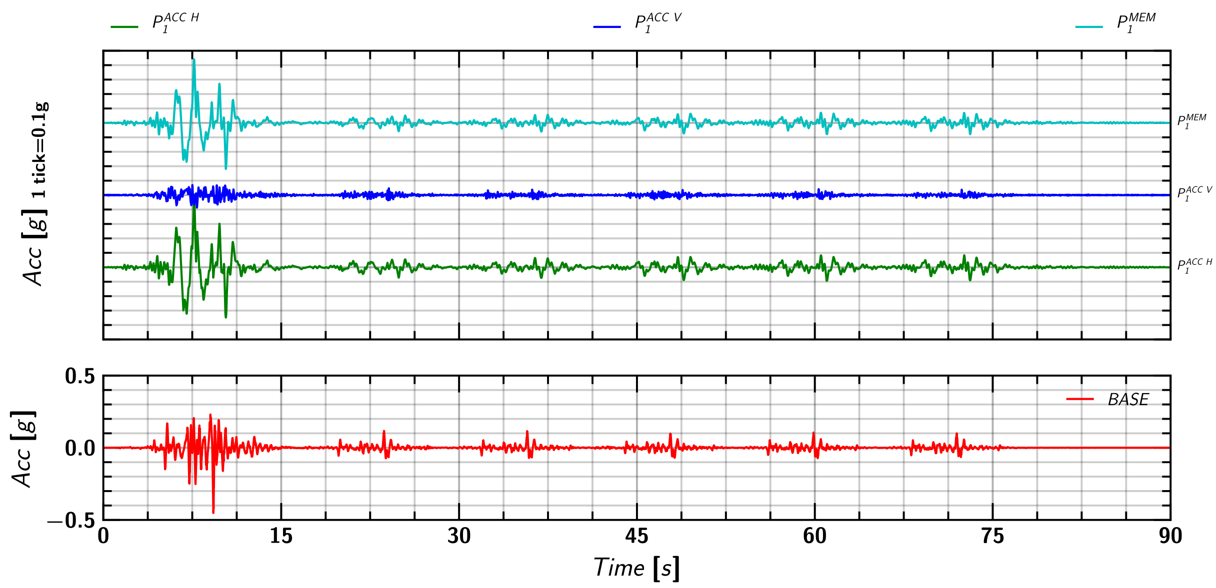

Figure 203. EQM$_4$: Acceleration measurement on pile 1.

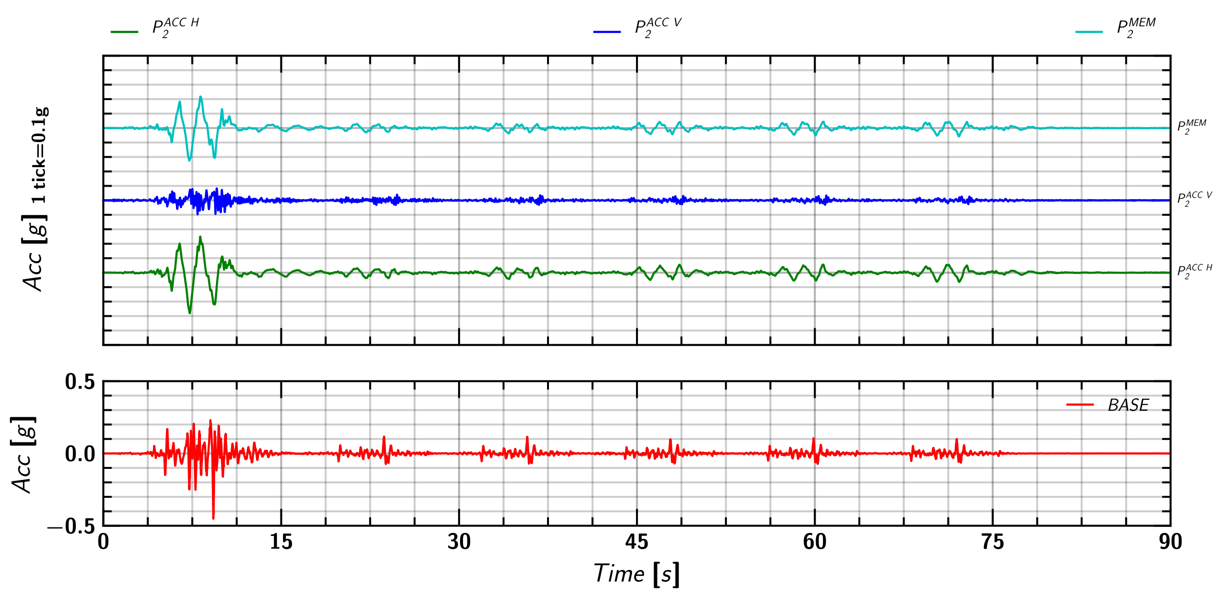

Figure 204. EQM$_4$: Acceleration measurement on pile 2.

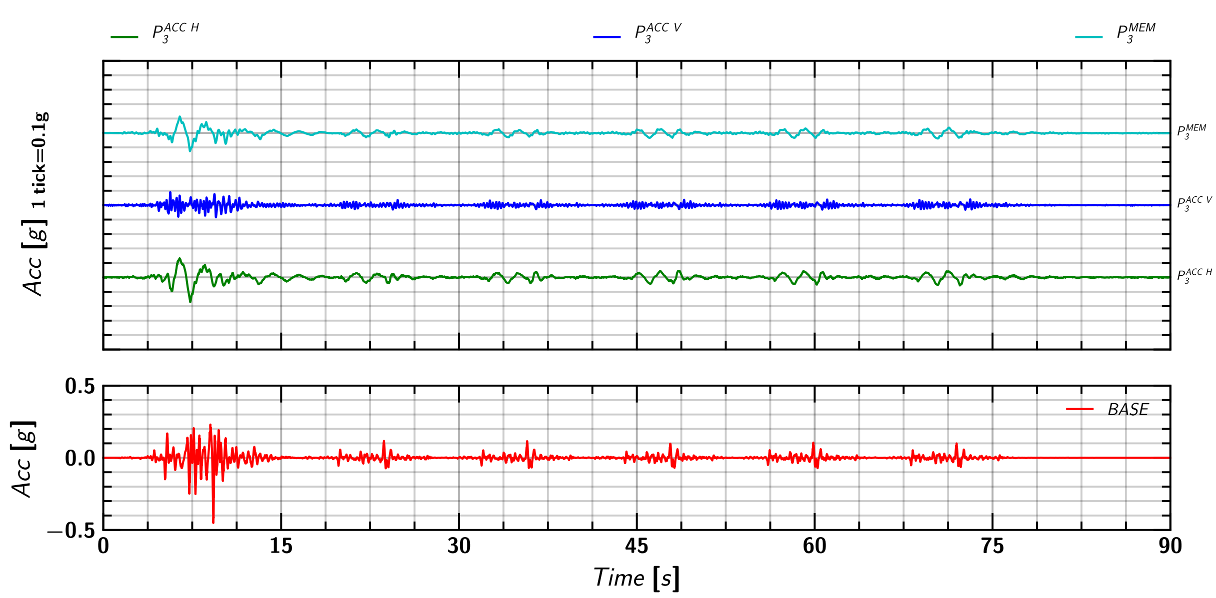

Figure 205. EQM$_4$: Acceleration measurement on pile 3.

J.6 Soil and Pile Mass Lateral Movement in X direction

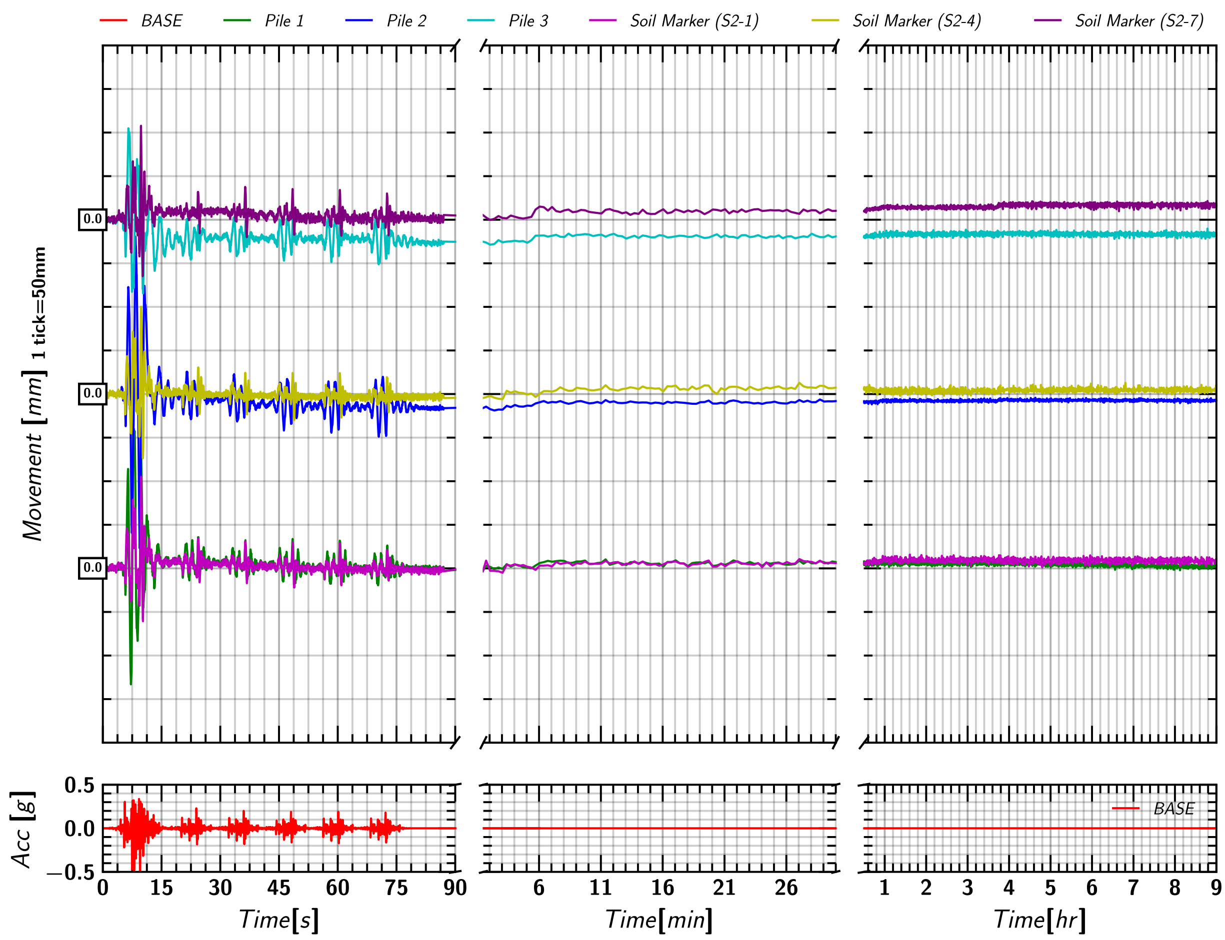

Figure 206. EQM$_4$: Lateral movement of soil and pile in x-direction during and post shaking.

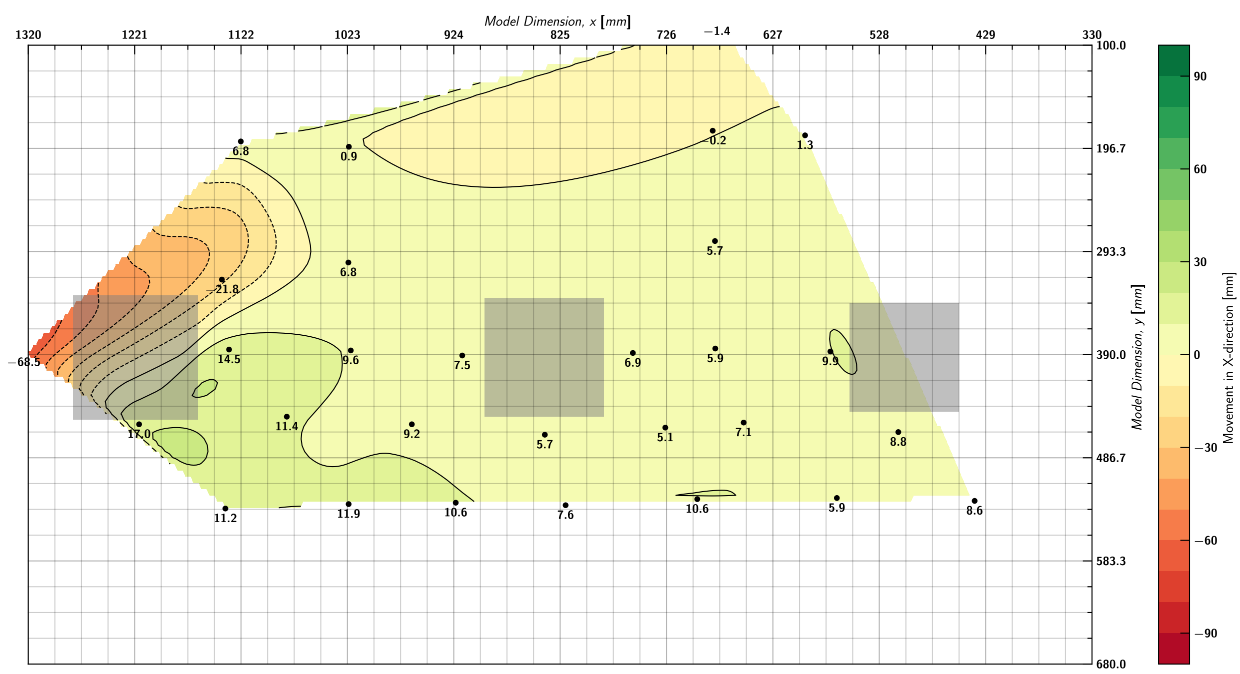

Figure 207. EQM$_4$:Contour of lateral movement of soil with respect to container in x-direction at the end of reconsolidation (t=240 minutes).

J.7 Soil and Pile Settlement (i.e., movement in Z direction)

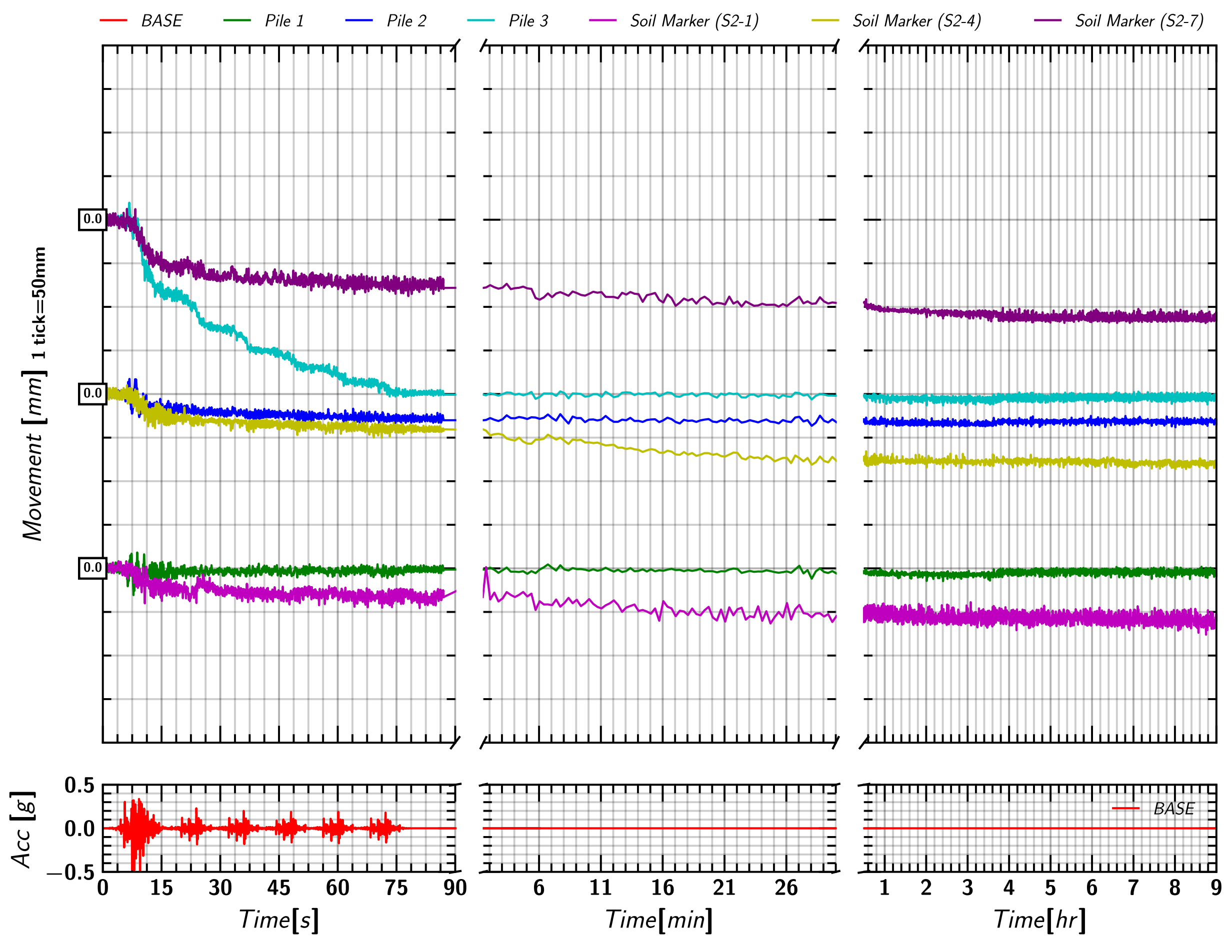

Figure 208. EQM$_4$: Settlement measurement in soil and pile during and post shaking.

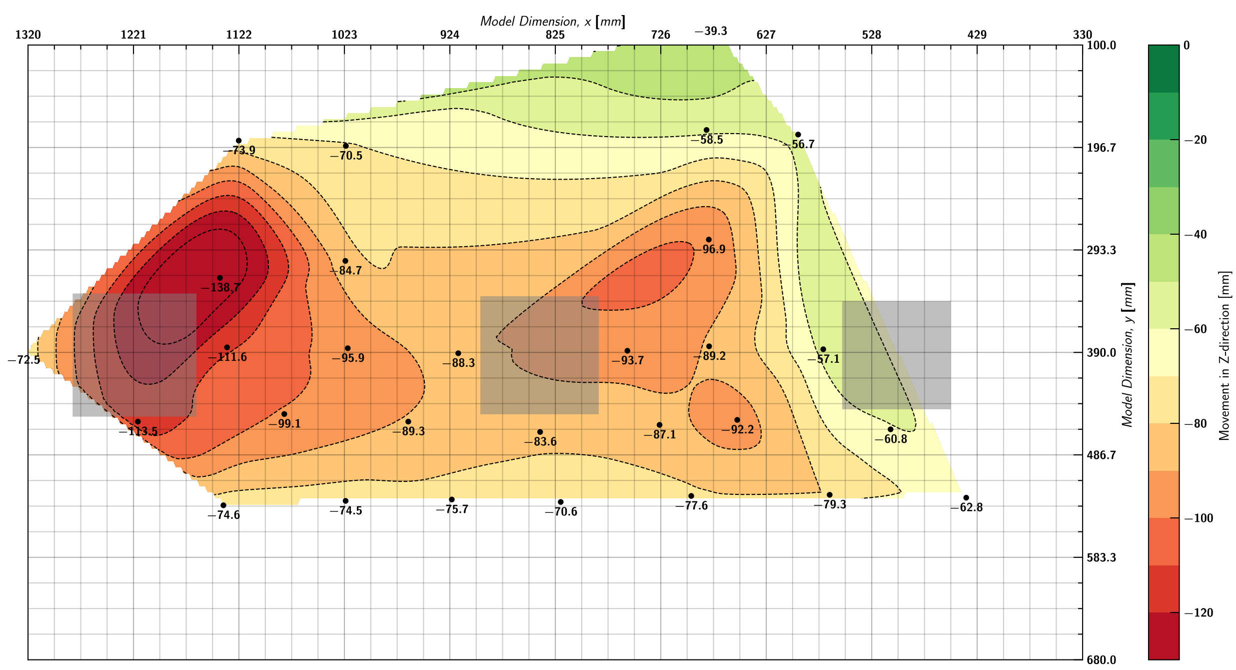

Figure 209. EQM$_4$:Contour of lateral movement of soil settlement at the end of reconsolidation (t=240 minutes).

J.8 Pore pressure in Soil Measured by Keller Transducers

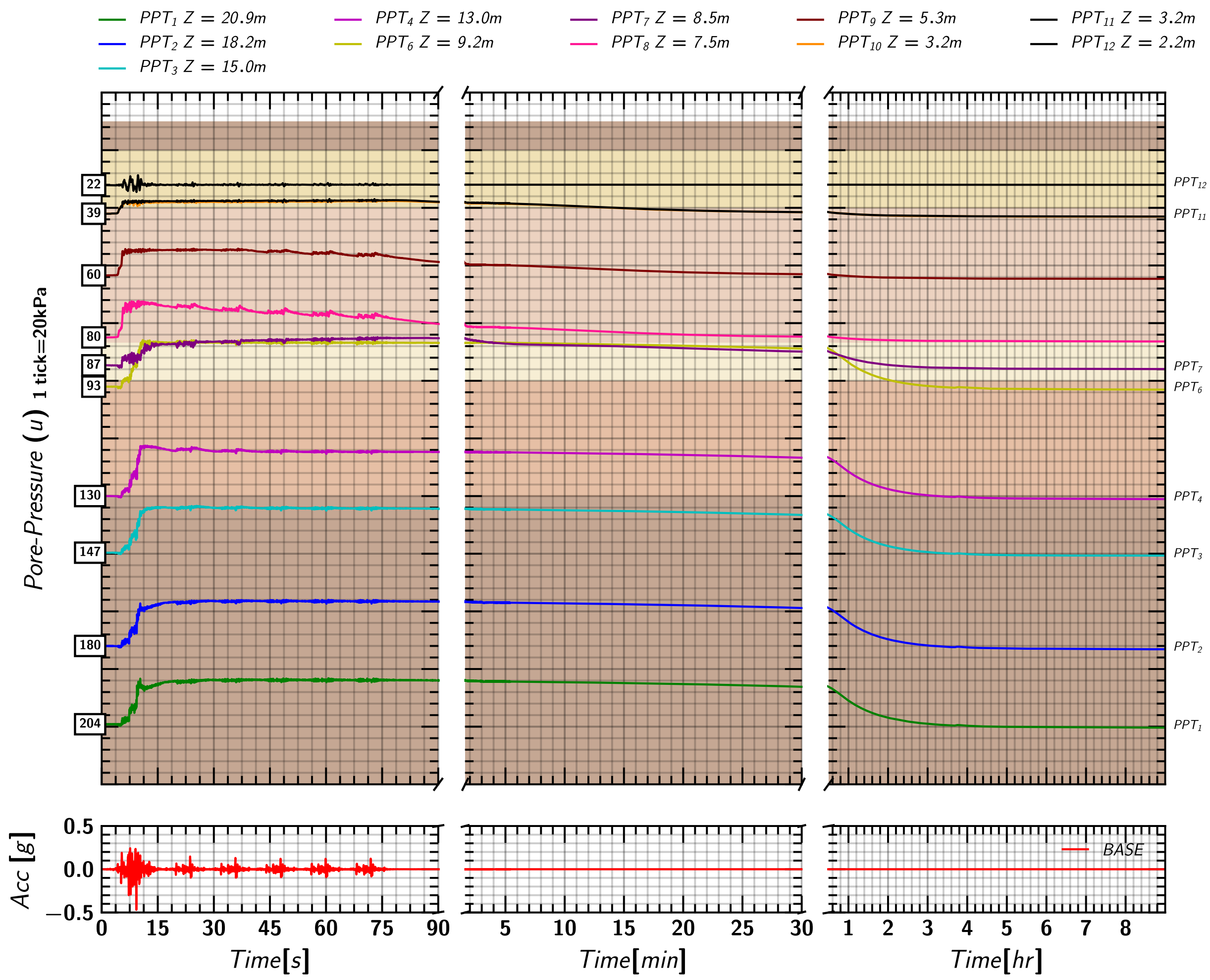

Figure 210. EQM4: Pore pressure measurements in soil from Keller transducers during and post shaking.

J.9 Pore pressure in Soil Measured by MS54XXX Transducers

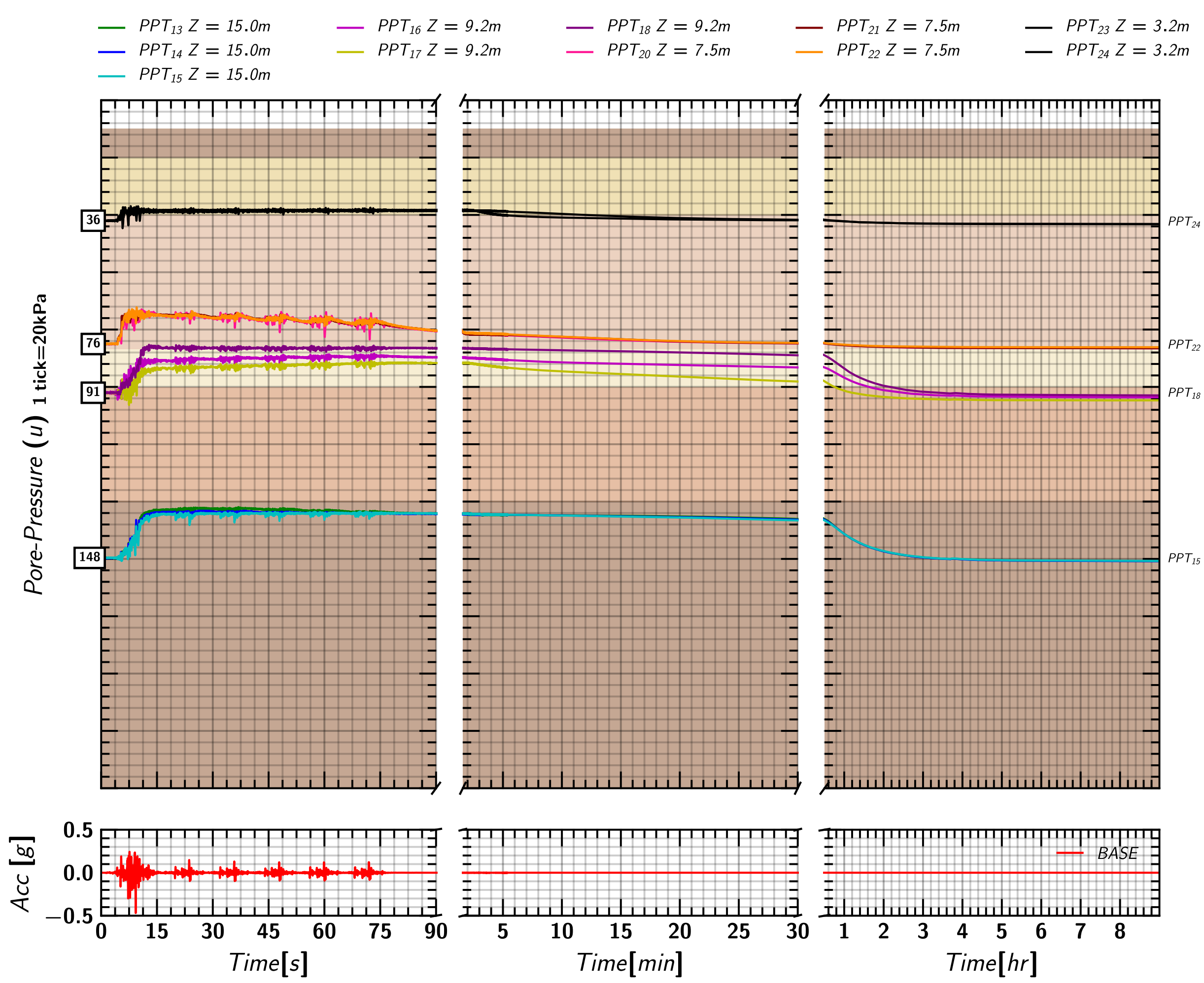

Figure 211. EQM4: Pore pressure measurements in soil from MS54XXX transducers during and post shaking.

J.10 Excess Pore pressures Ratio (r_u) Estimated from Keller Transducers

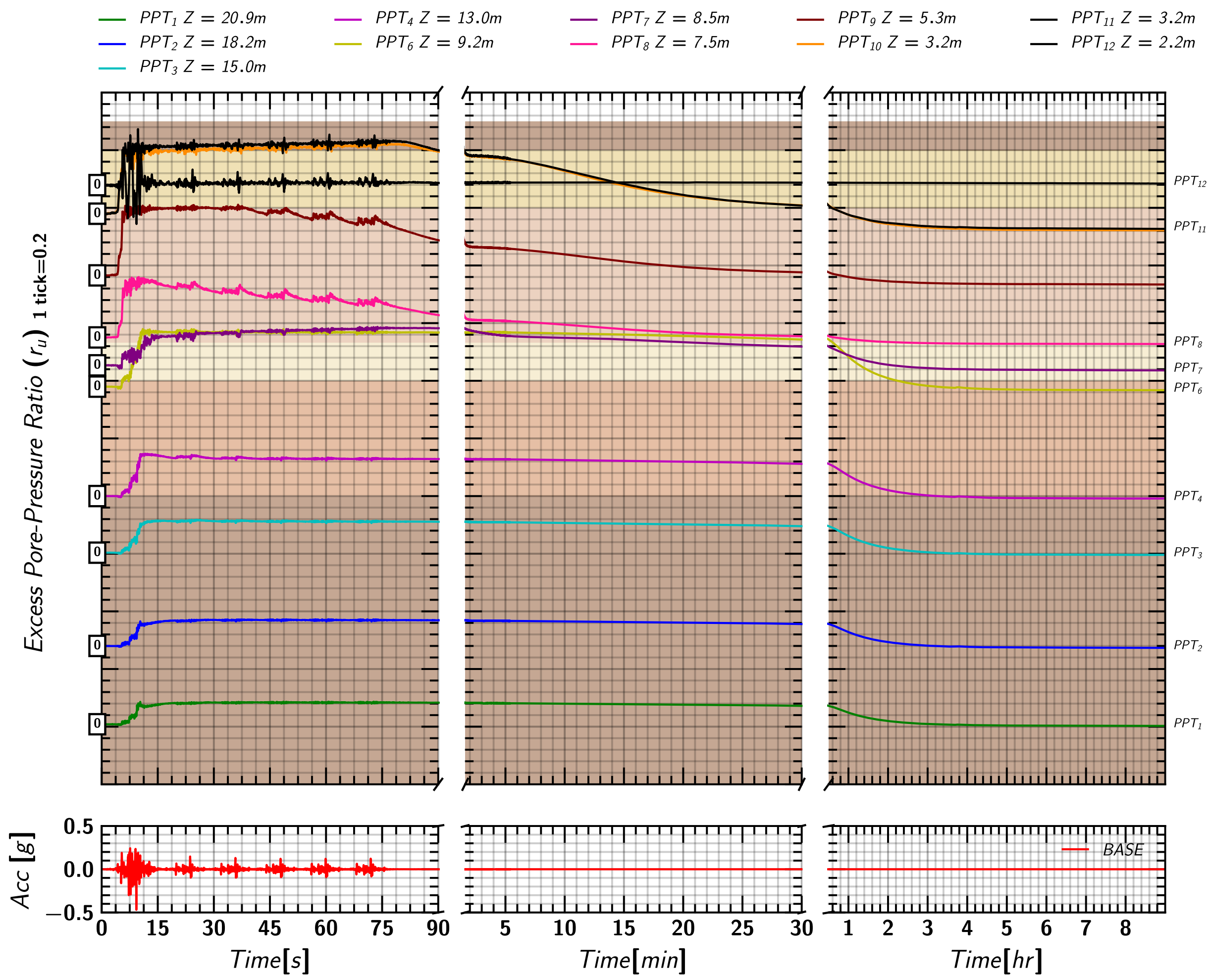

Figure 212. EQM4: Excess pore pressure ratio (r_u) estimated from Keller transducers during and post shaking.

J.11 Excess Pore pressure Ratio (r_u) Estimated from MS54XXX Transducers

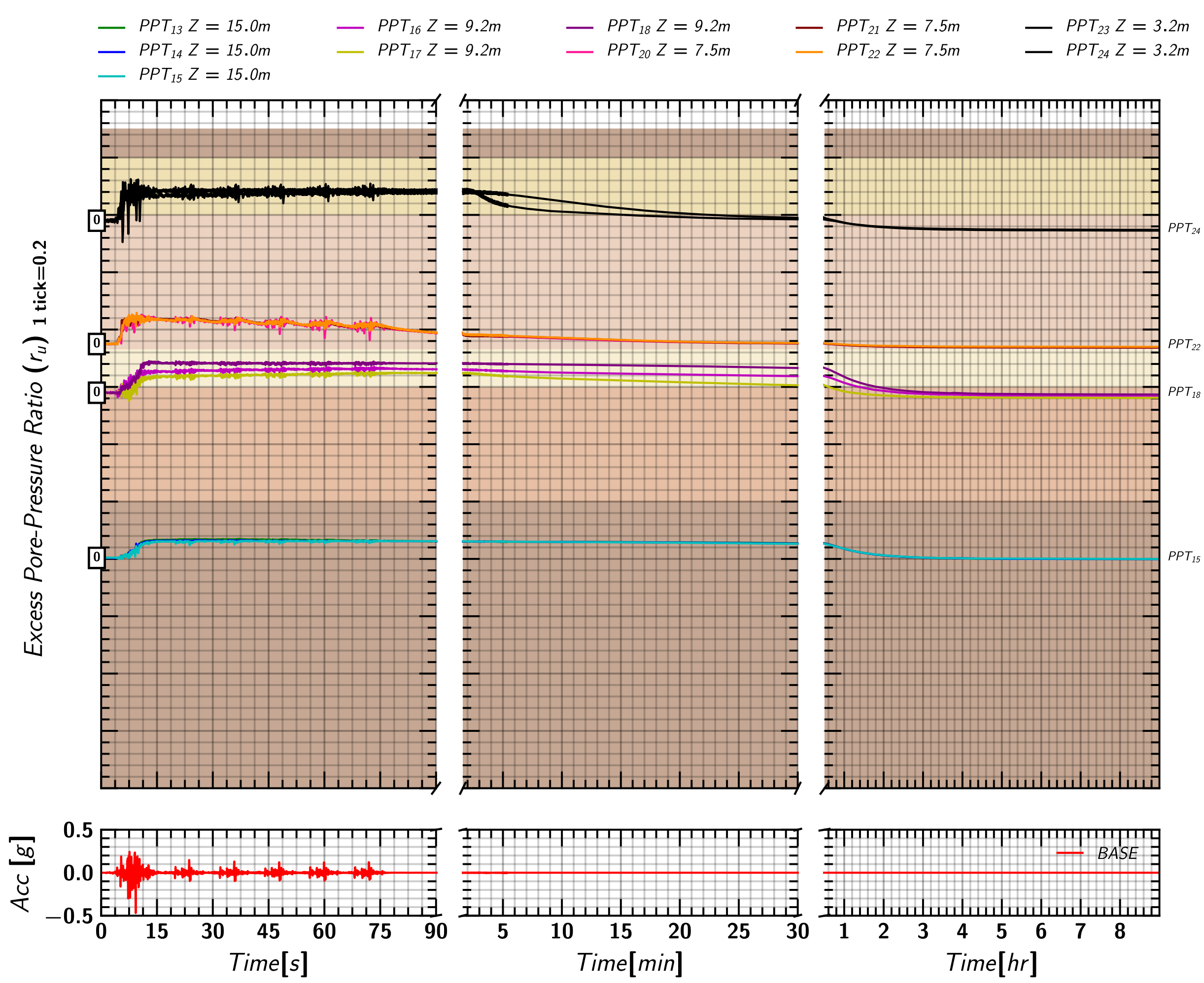

Figure 213. EQM4: Excess pore pressure ratio (r_u) estimated from MS54XXX transducers during and post shaking.

Dense Sand	Medium Dense Sand	Clayey Silt	Loose Sand	Clay Crust

J.12 Axial Load in Pile 1

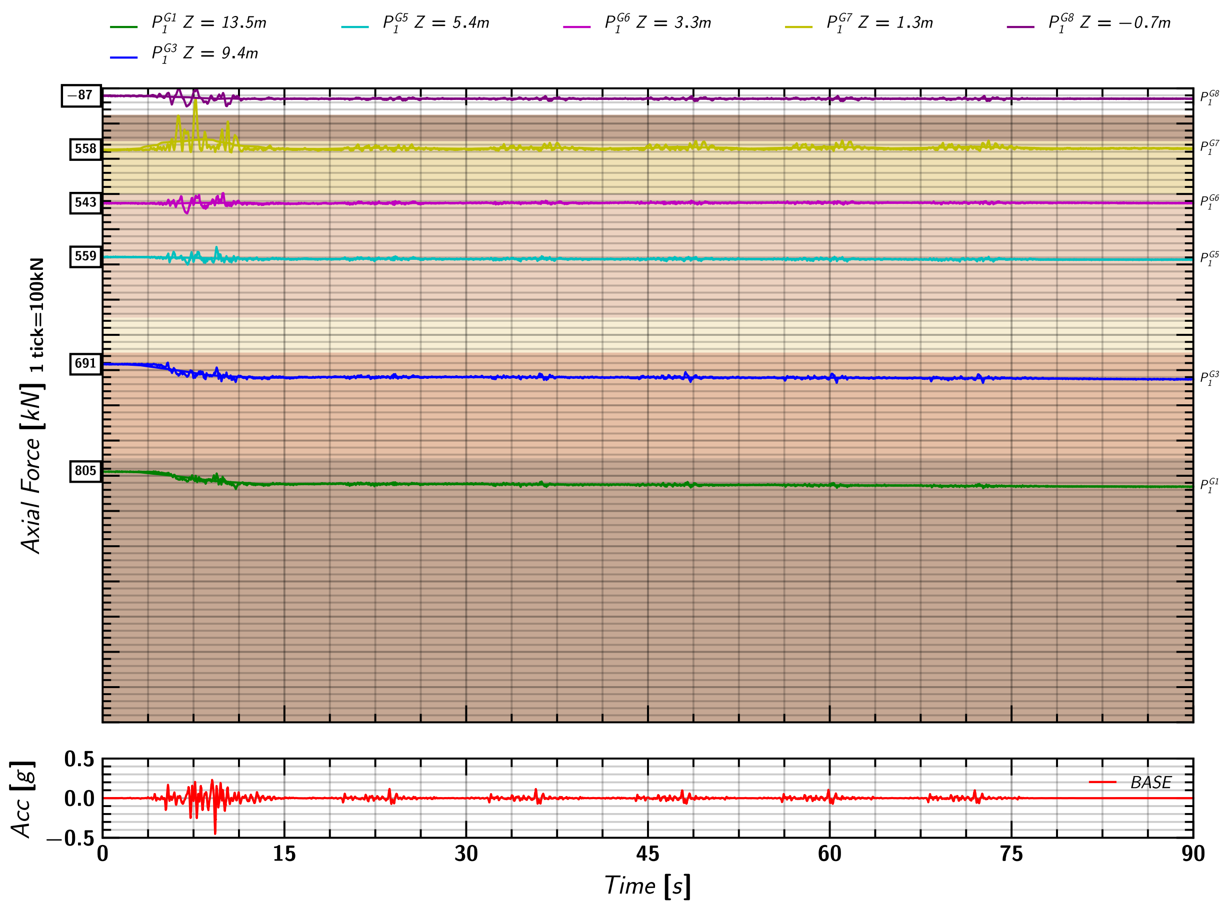

Figure 214. EQM4: Axial load measurements from pile 1 strain gages during shaking.

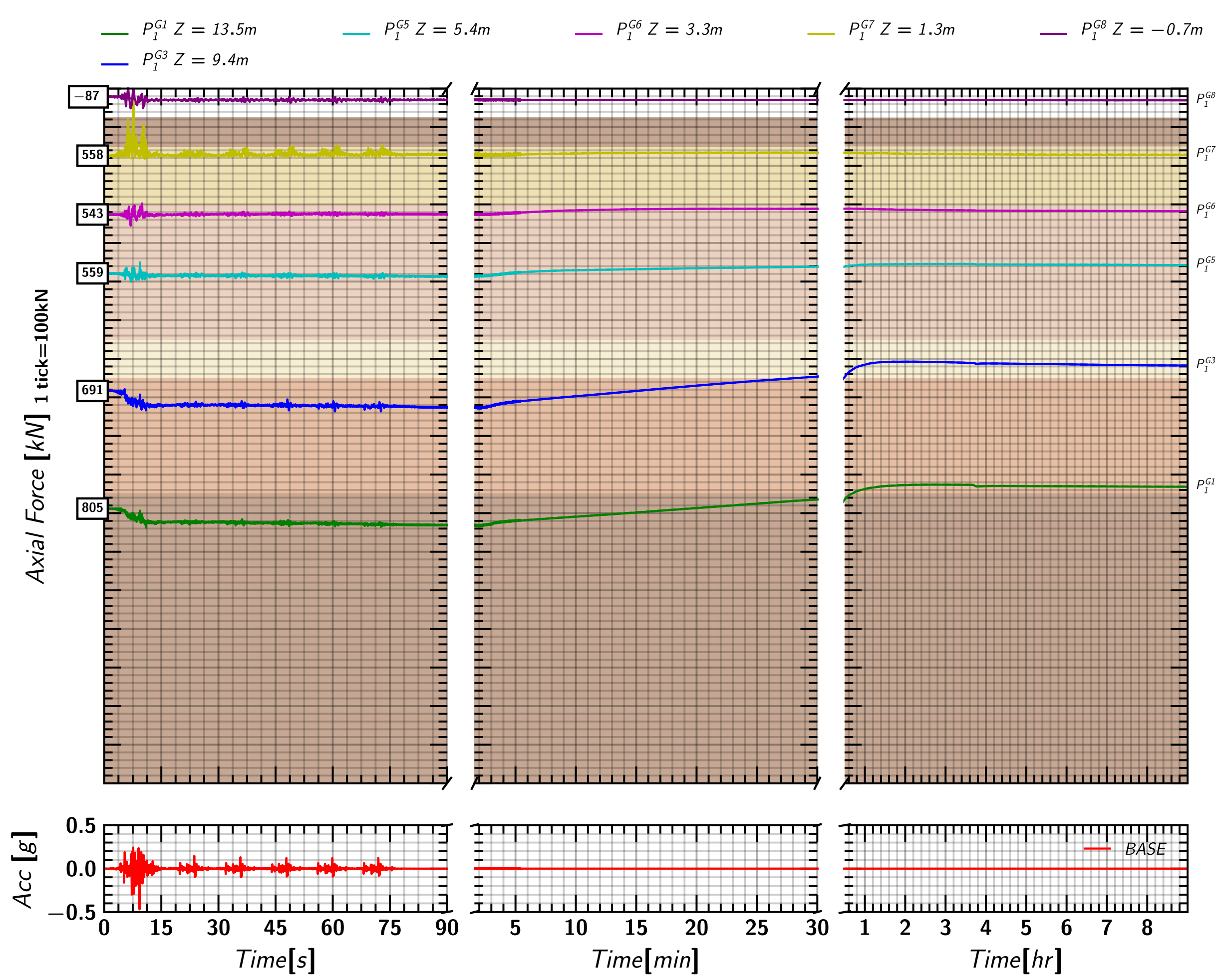

Figure 215. EQM4: Axial load measurements from pile 1 strain gages during and post shaking.

Dense Sand | Medium Dense Sand | Clayey Silt | Loose Sand | Clay Crust

J.13 Axial Load in Pile 2

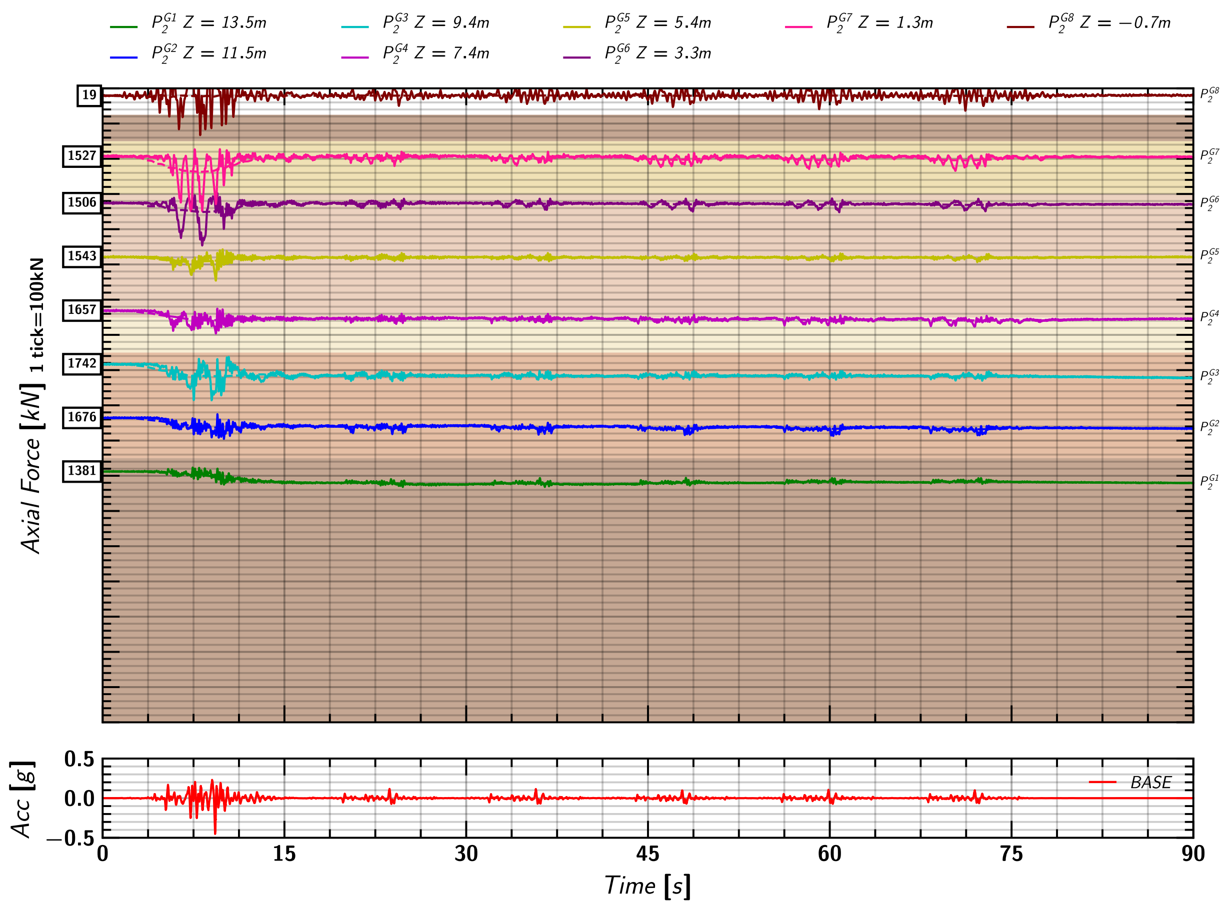

Figure 216. EQM₄: Axial load measurements from pile 2 strain gages during shaking.

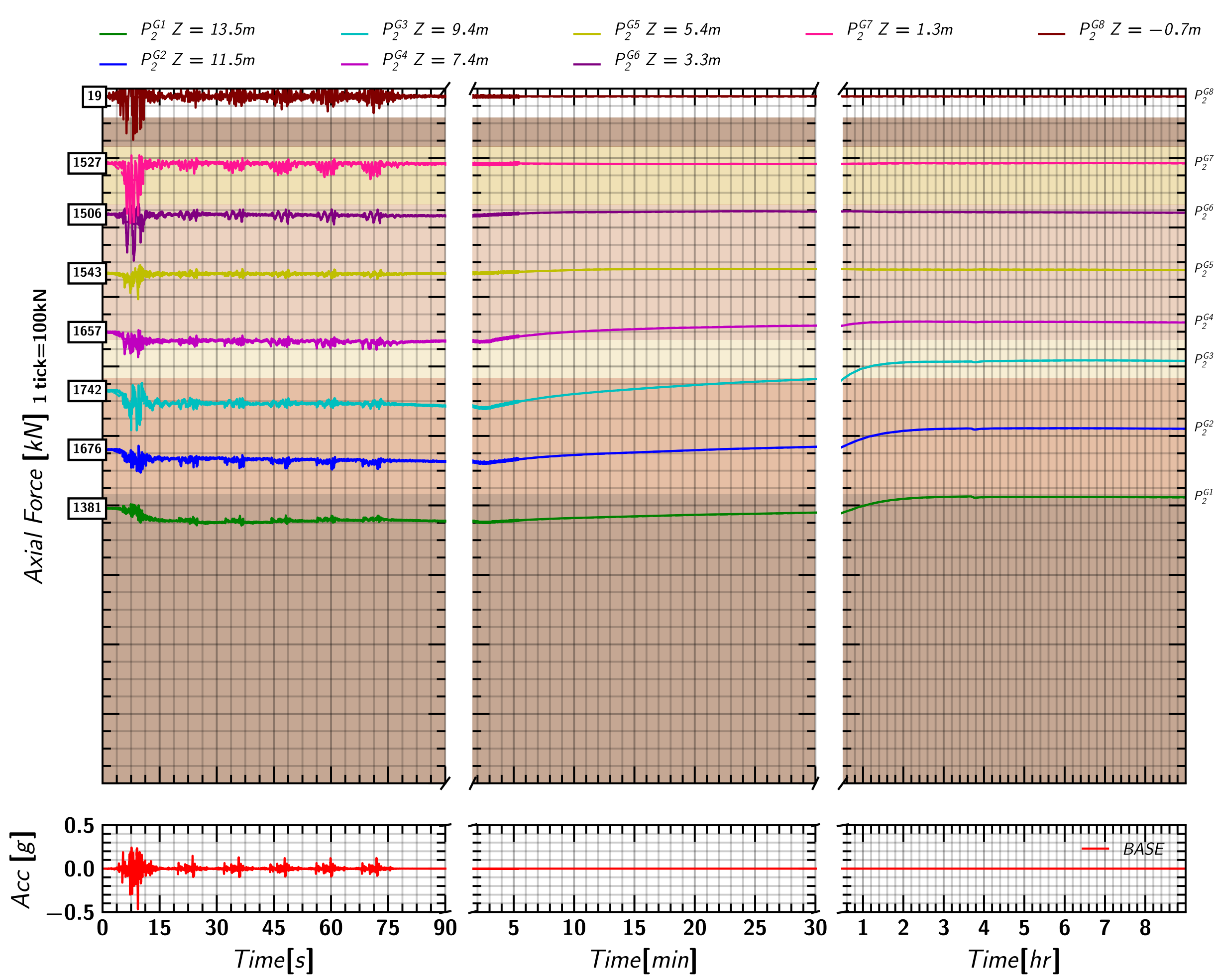

Figure 217. EQM₄: Axial load measurements from pile 2 strain gages during and post shaking.

Dense Sand	Medium Dense Sand	Clayey Silt	Loose Sand	Clay Crust

J.14 Axial Load in Pile 3

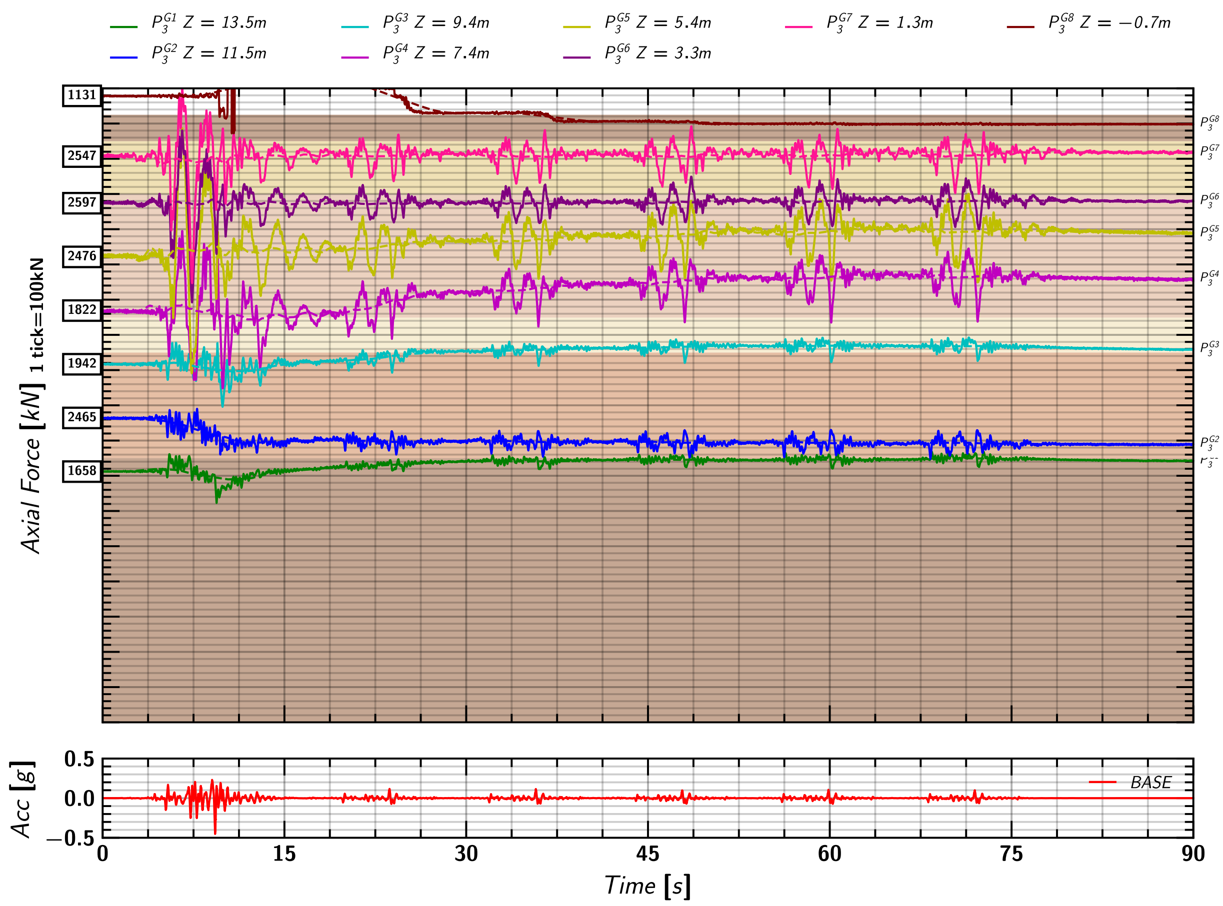

Figure 218. EQM$_4$: Axial load measurements from pile 3 strain gages during shaking.

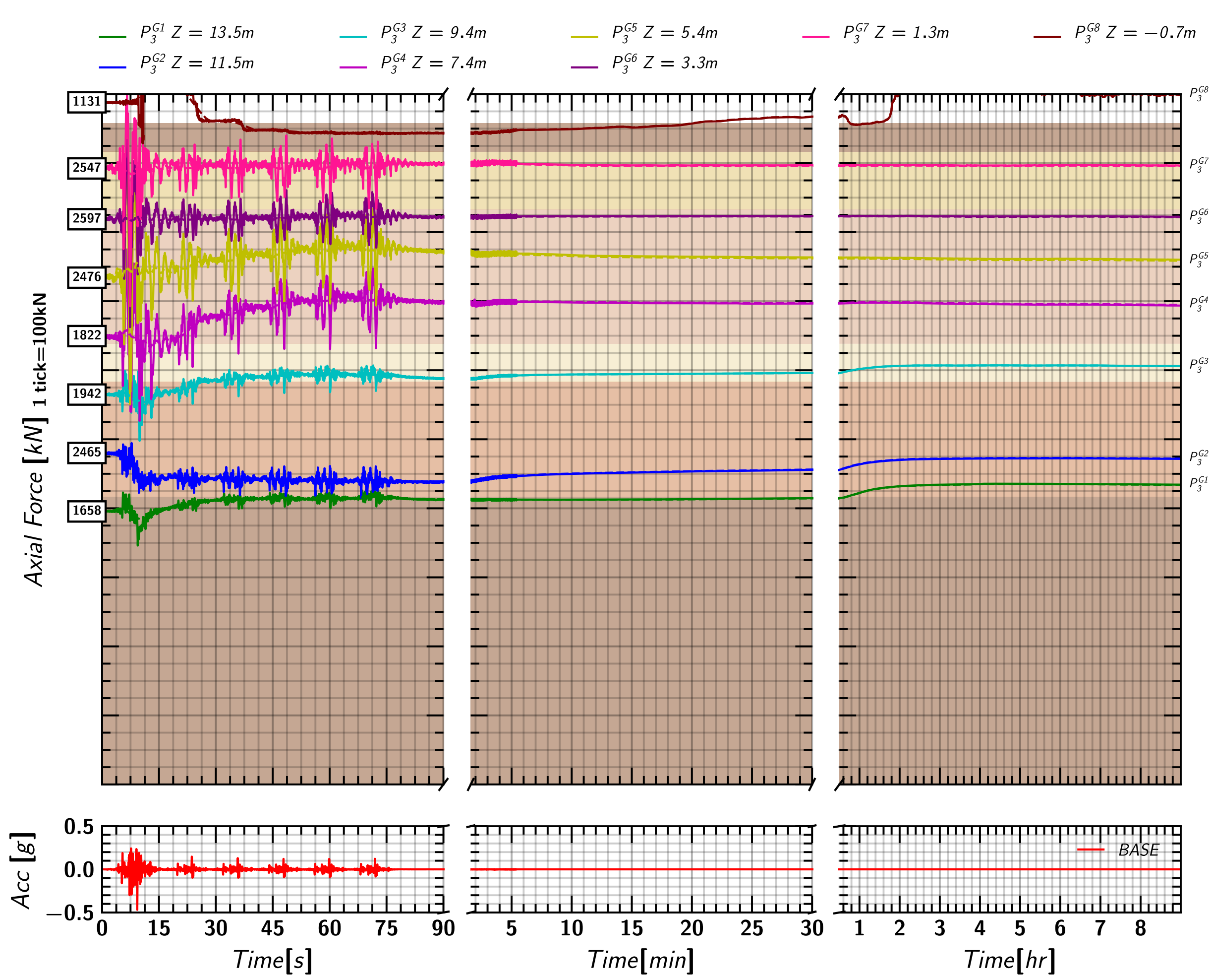

Figure 219. EQM$_4$: Axial load measurements from pile 3 strain gages during and post shaking.

J.15 Pore pressure and Axial Load Profile

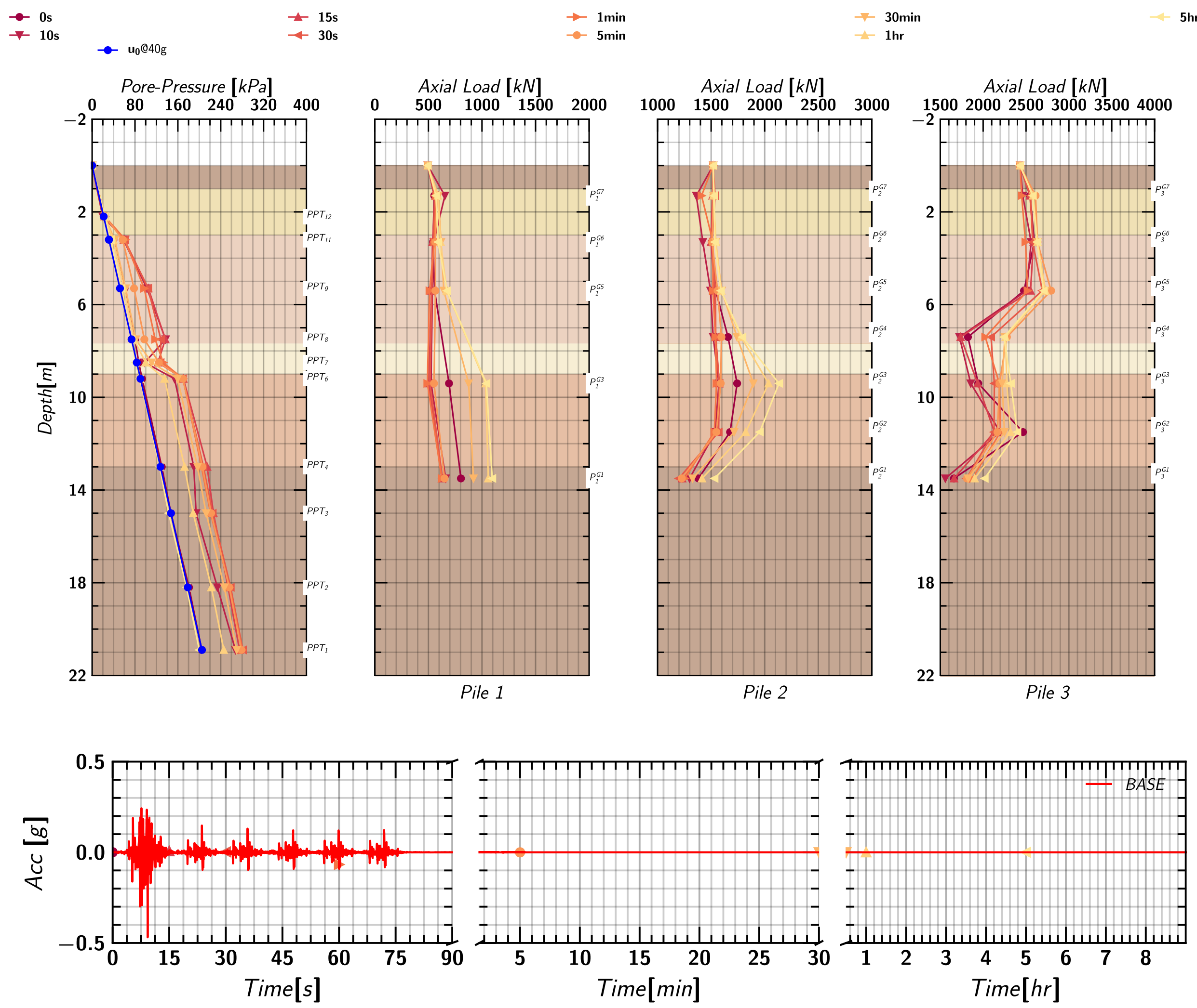

Figure 220. EQM$_4$: Pore pressure and axial load profile in pile 1, pile 2 and pile 3 at different times during and post shaking.

K. EQM₄: Soil, Pile, and Container Movements in X and Z

K.1 Container Movement in X

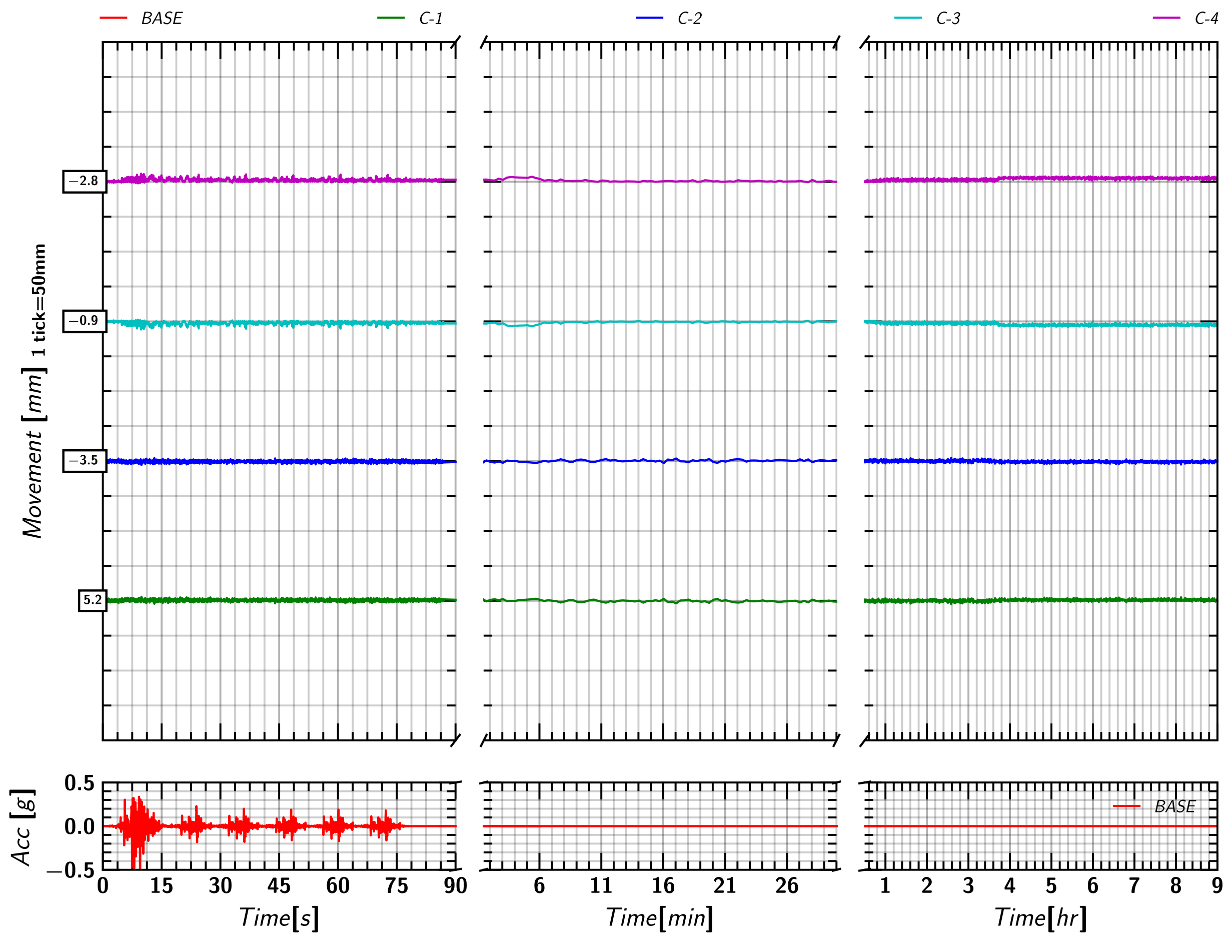

Figure 221. EQM₄: Container movement in X-direction relative to the model container during and post shaking.

K.2 Container Movement in Z

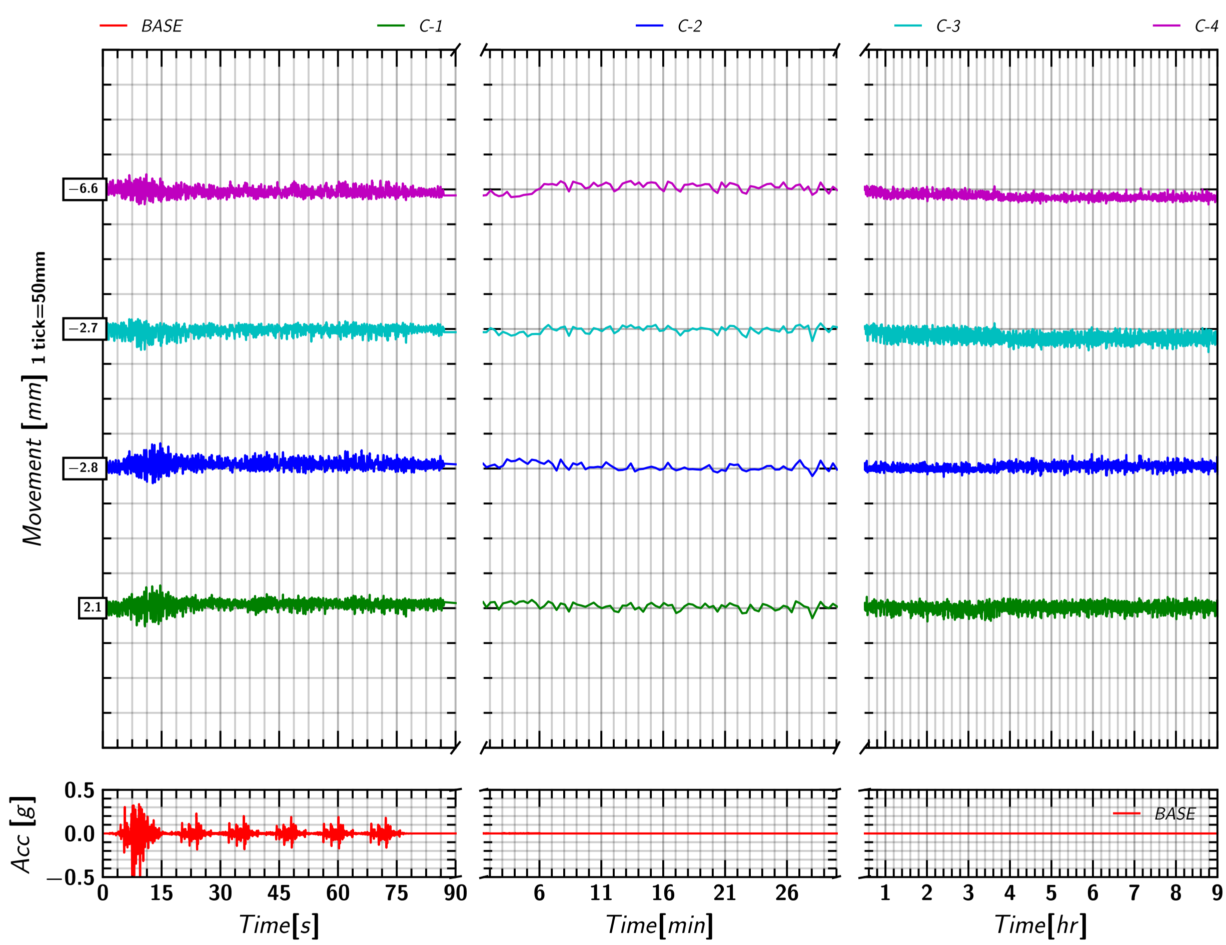

Figure 222. EQM₄: Container movement in Z-direction relative to the model container during and post shaking.

K.3 Soil (Row S-1) Movement in X

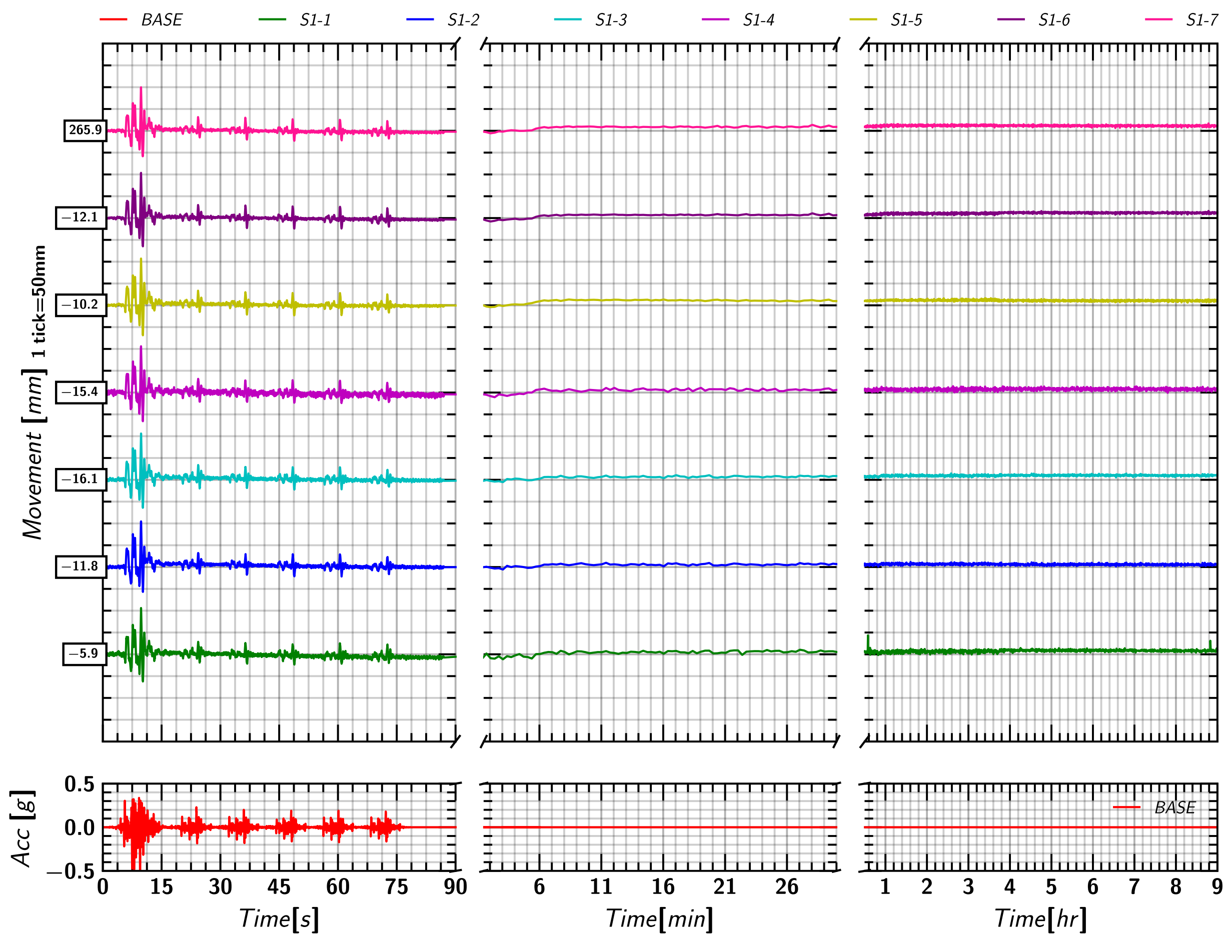

Figure 223. EQM$_4$: Soil (Row S-1) movement in X-direction relative to the model container during and post shaking.

K.4 Soil (Row S-1) Movement in Z

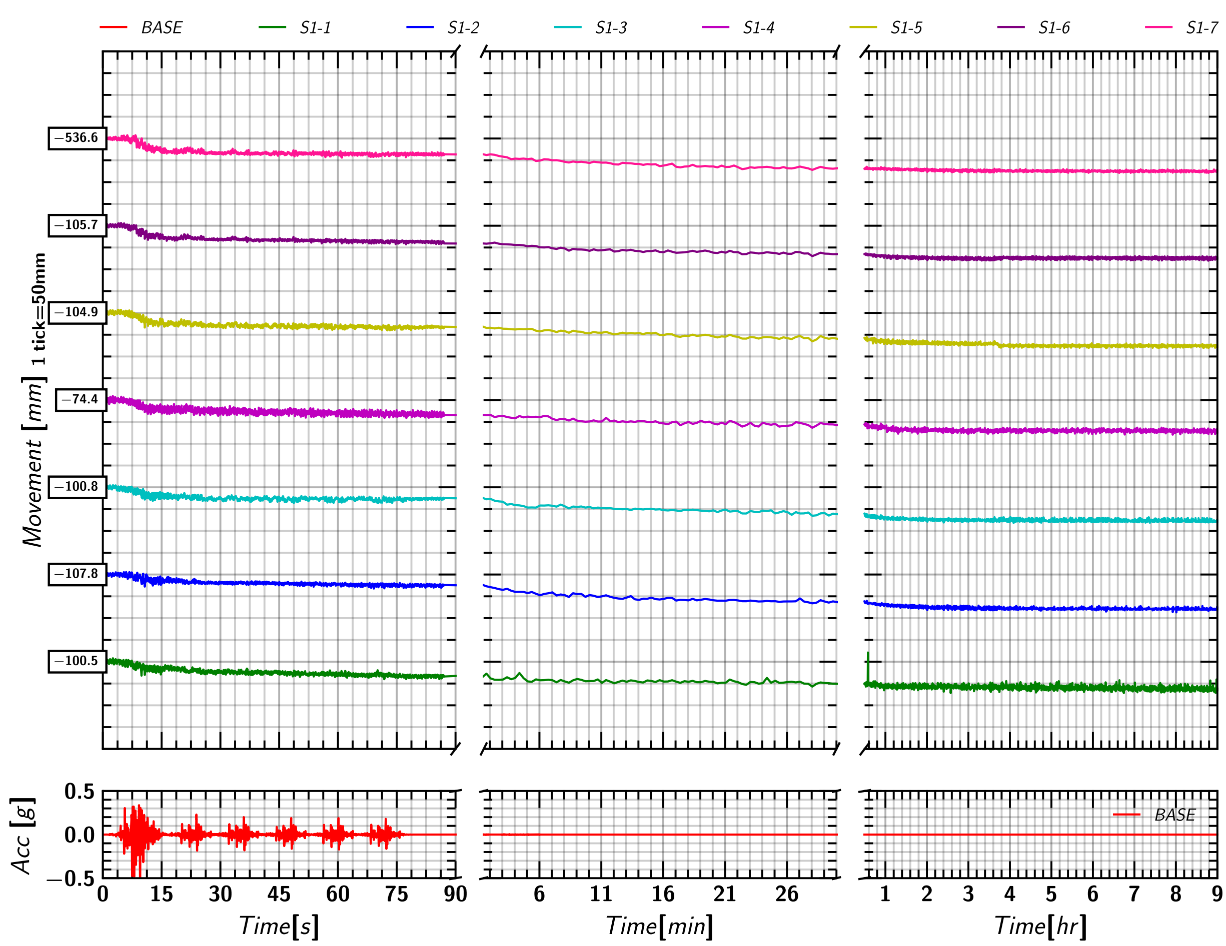

Figure 224. EQM$_4$: Soil (Row S-1) movement in Z-direction relative to the model container during and post shaking.

K.5 Soil (Row S-2) Movement in X

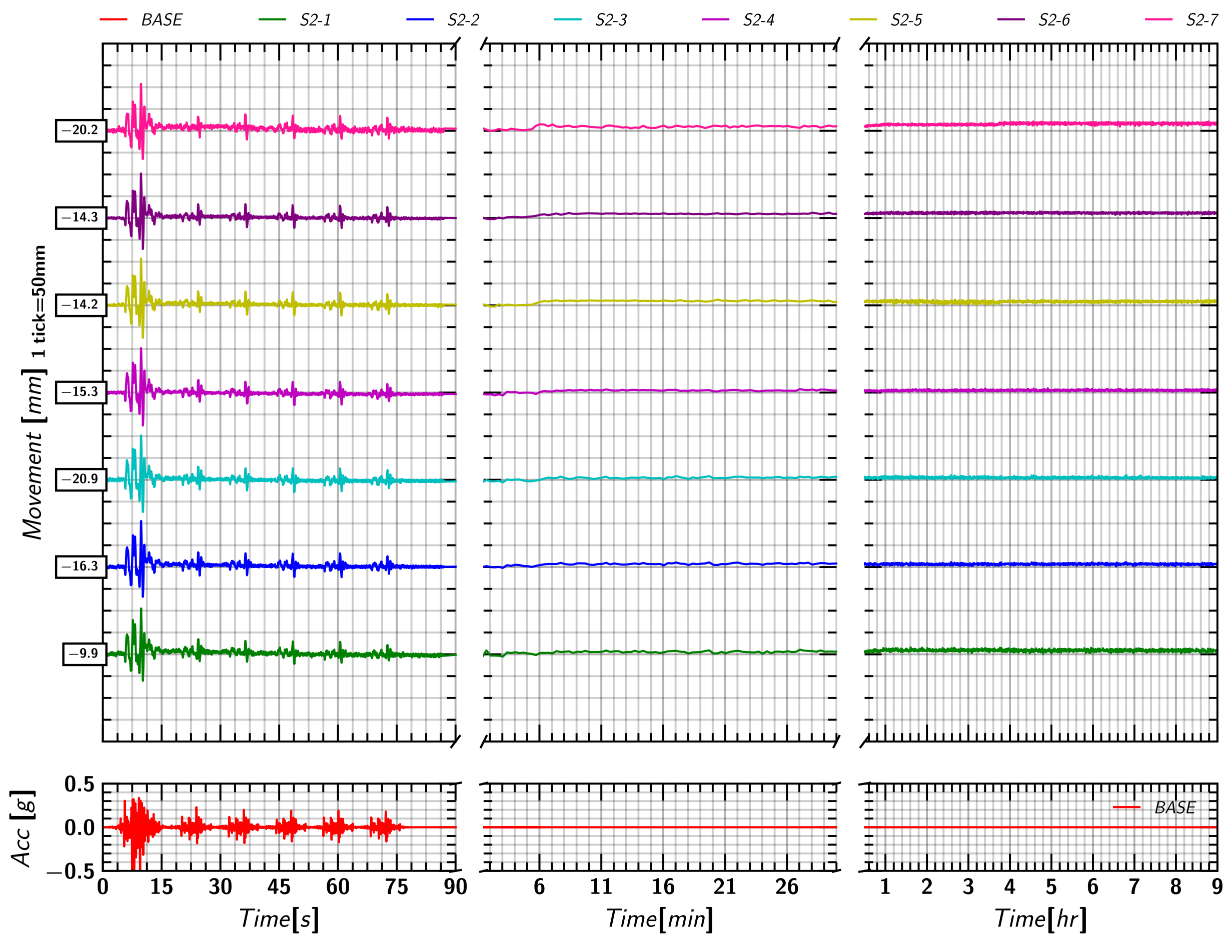

Figure 225. EQM4: Soil (Row S-2) movement in X-direction relative to the model container during and post shaking.

K.6 Soil (Row S-2) Movement in Z

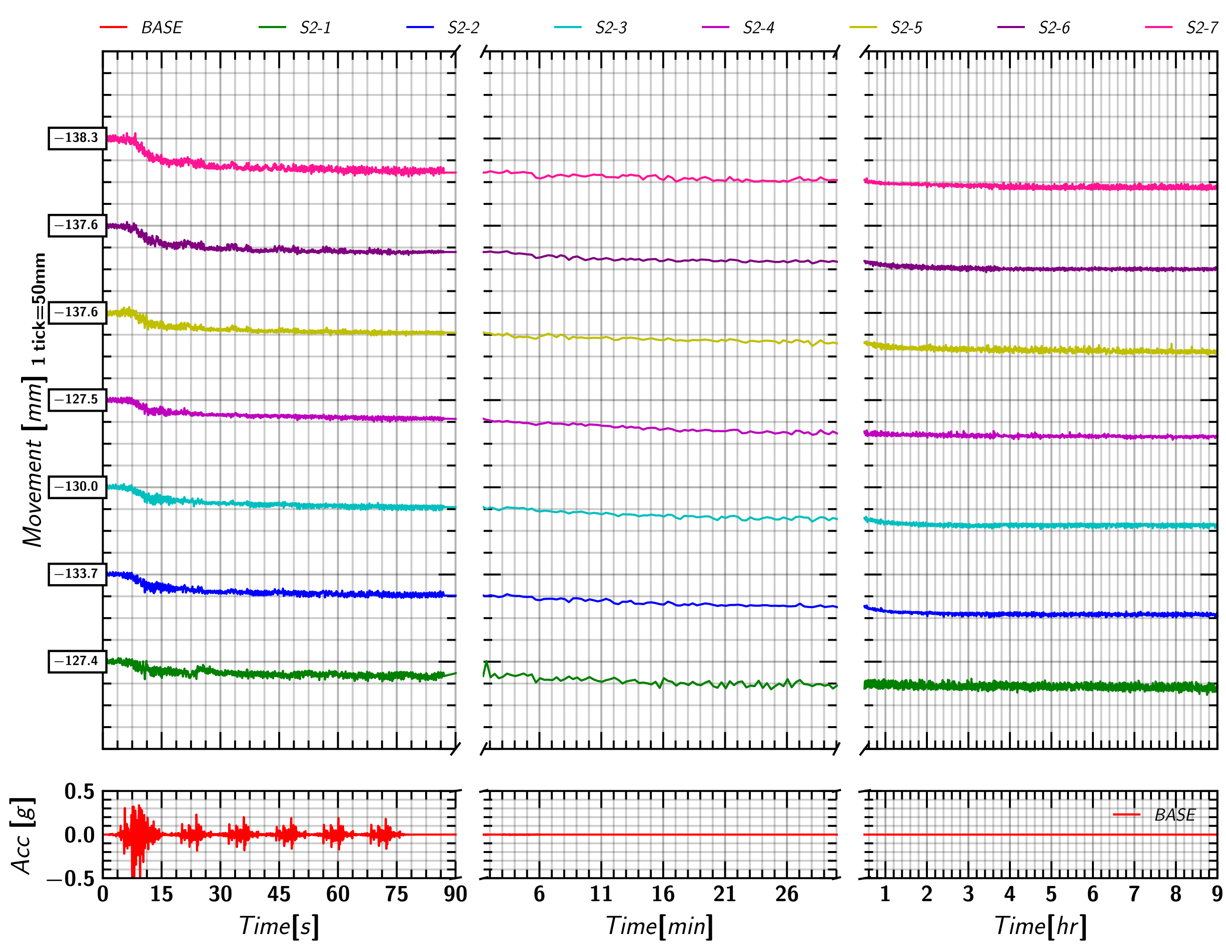

Figure 226. EQM4: Soil (Row S-2) movement in Z-direction relative to the model container during and post shaking.

K.7 Soil (Row S-3) Movement in X

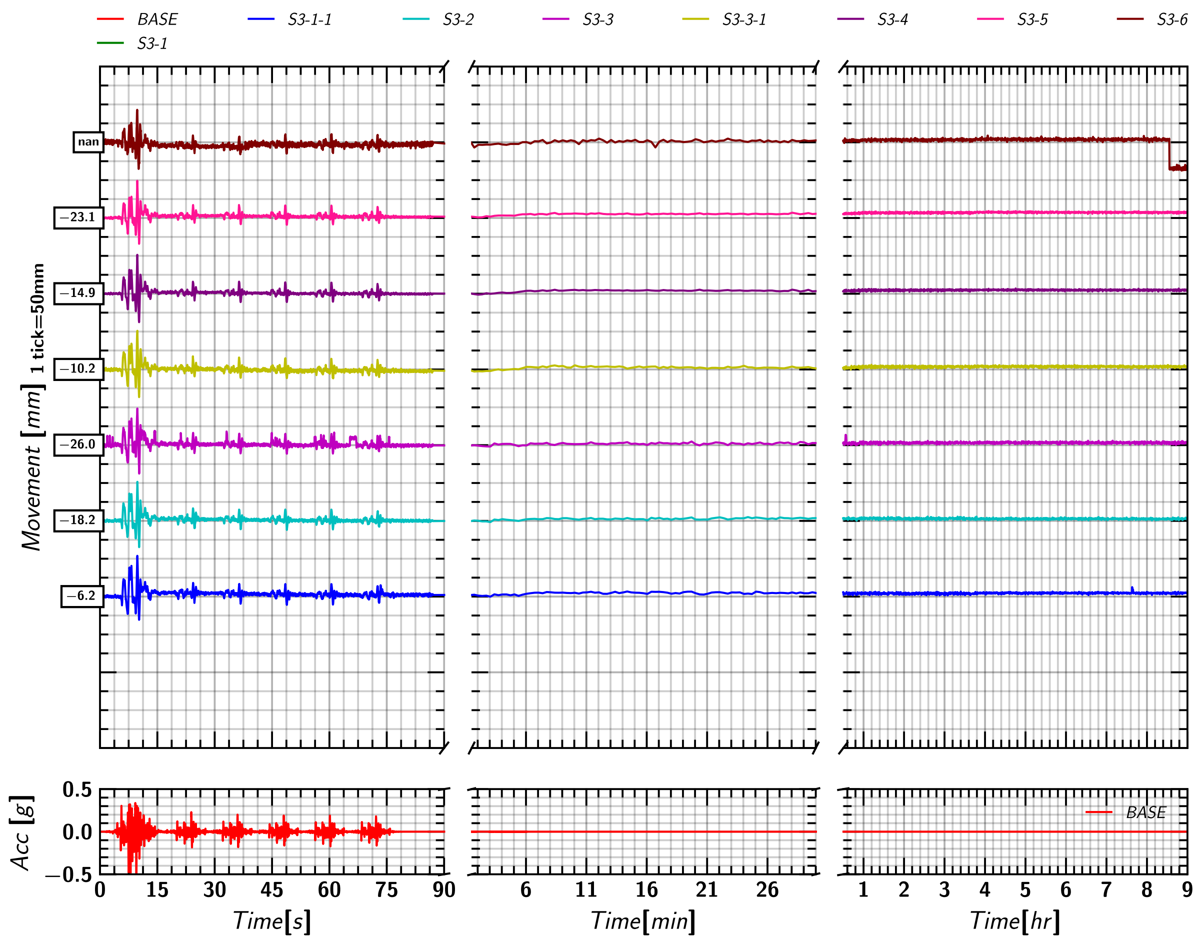

Figure 227. EQM$_4$: Soil (Row S-3) movement in X-direction relative to the model container during and post shaking.

K.8 Soil (Row S-3) Movement in Z

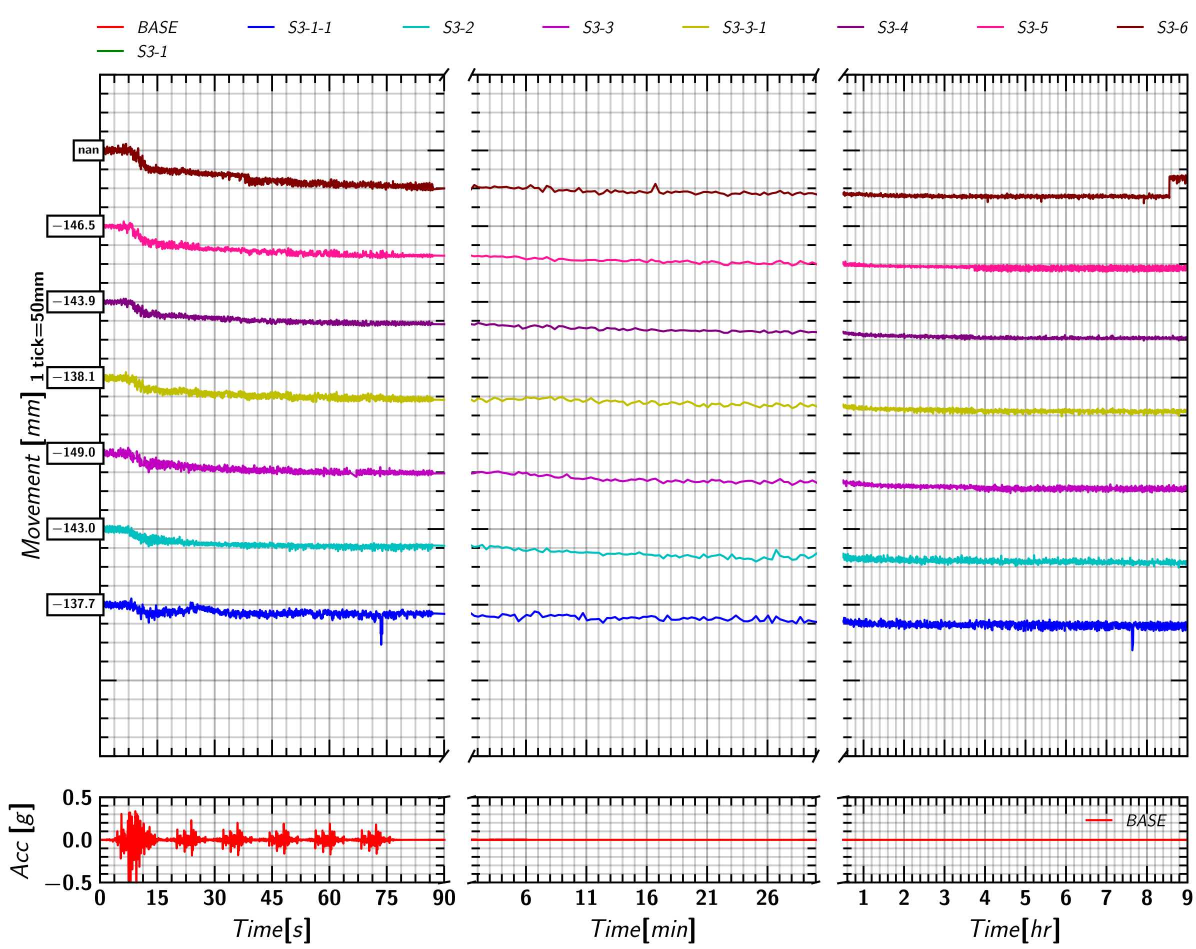

Figure 228. EQM$_4$: Soil (Row S-3) movement in Z-direction relative to the model container during and post shaking.

K.9 Soil (Row S-4) Movement in X

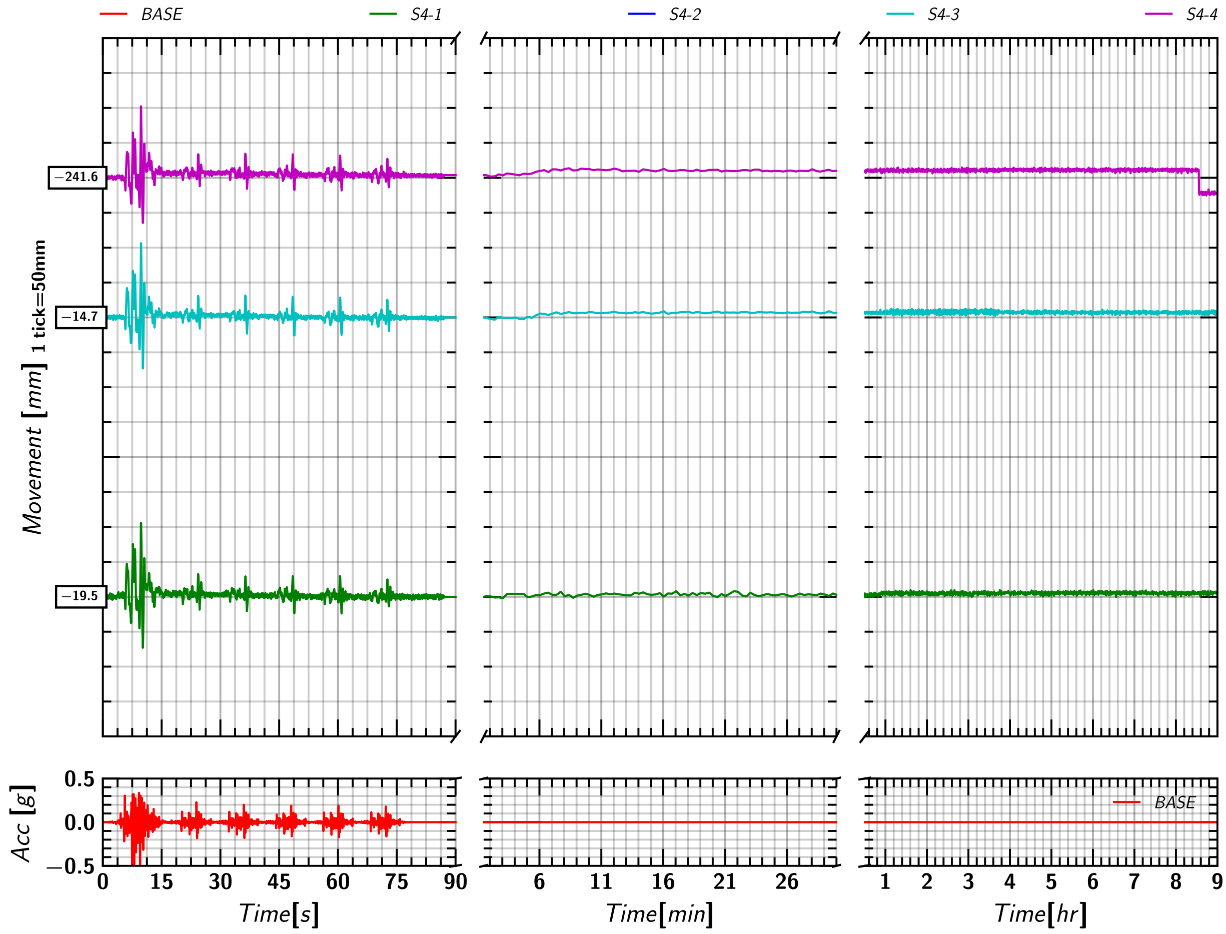

Figure 229. EQM$_4$: Soil (Row S-4) movement in X-direction relative to the model container during and post shaking.

K.10 Soil (Row S-4) Movement in Z

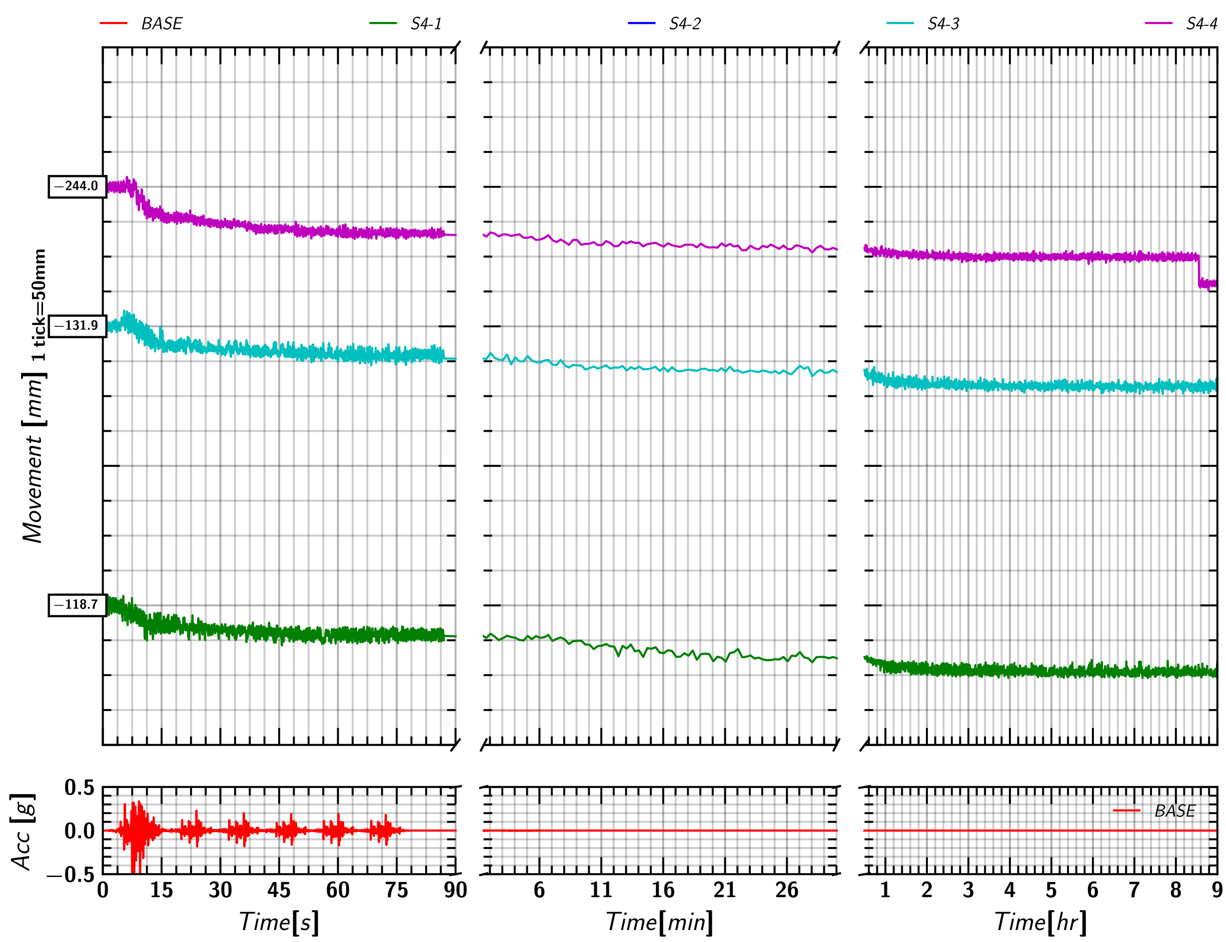

Figure 230. EQM$_4$: Soil (Row S-4) movement in Z-direction relative to the model container during and post shaking.

K.11Soil (Row S-5) Movement in X

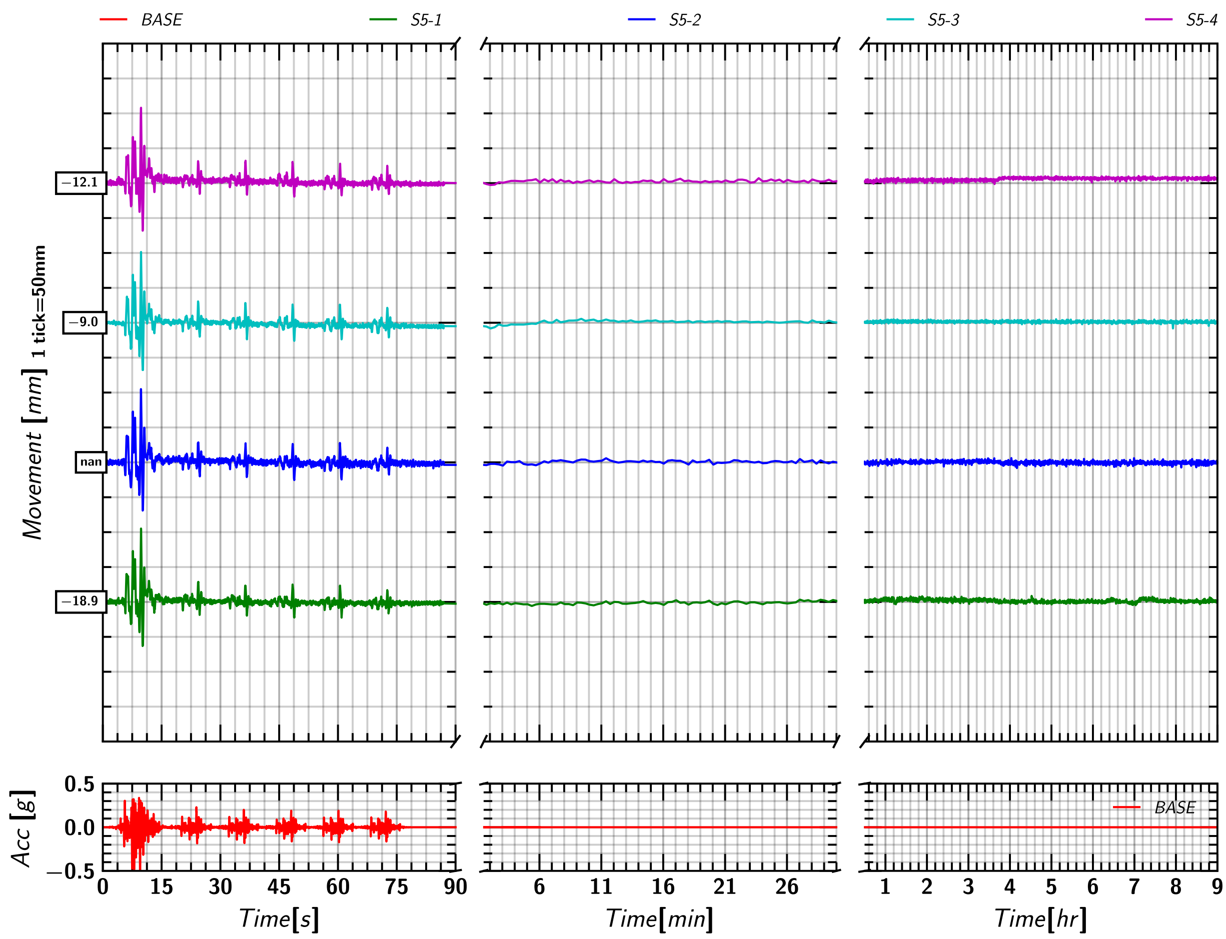

Figure 231. EQM4: Soil (Row S-5) movement in X-direction relative to the model container during and post shaking.

K.12 Soil (Row S-5) Movement in Z

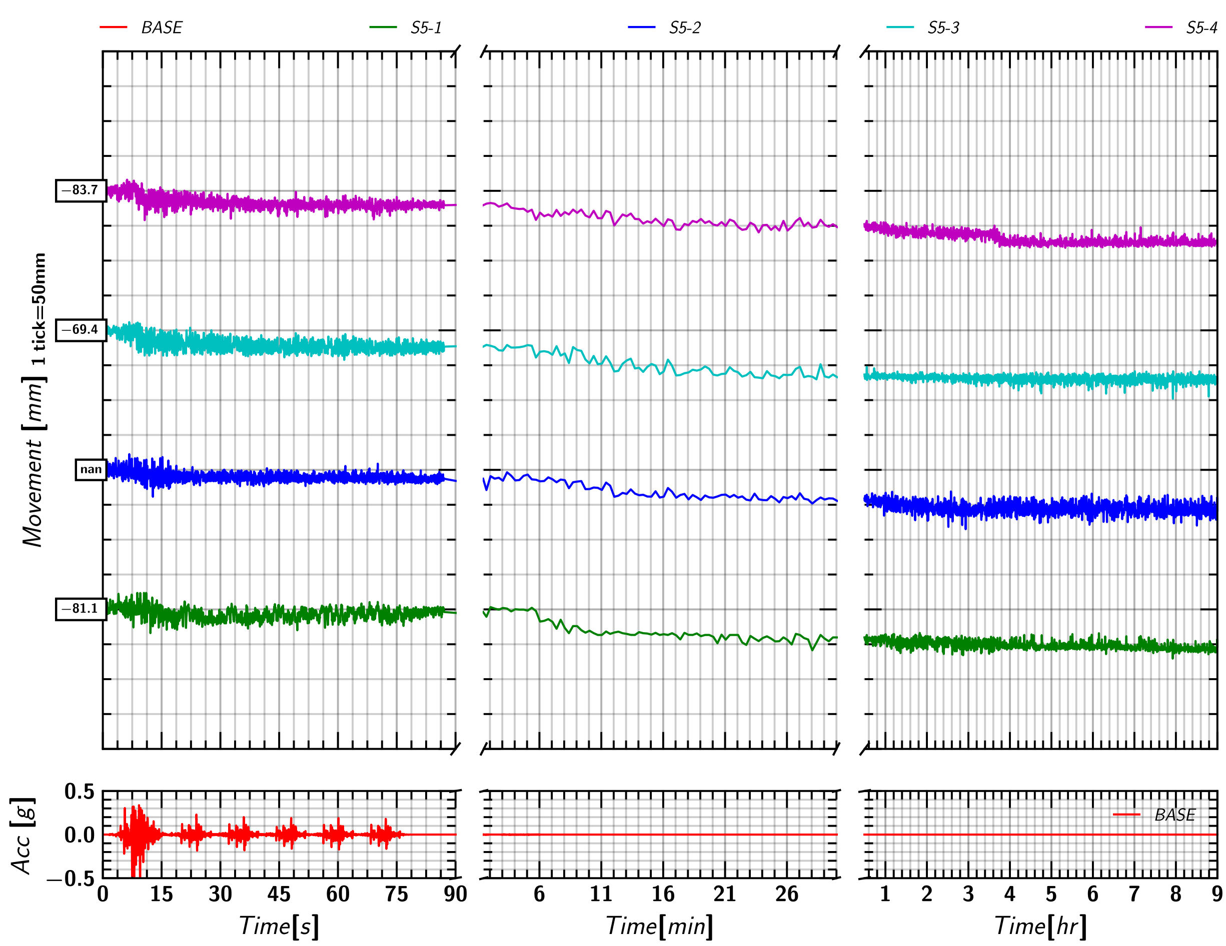

Figure 232. EQM4: Soil (Row S-5) movement in Z-direction relative to the model container during and post shaking.

K.13 Pile 1 Mass Movement in X

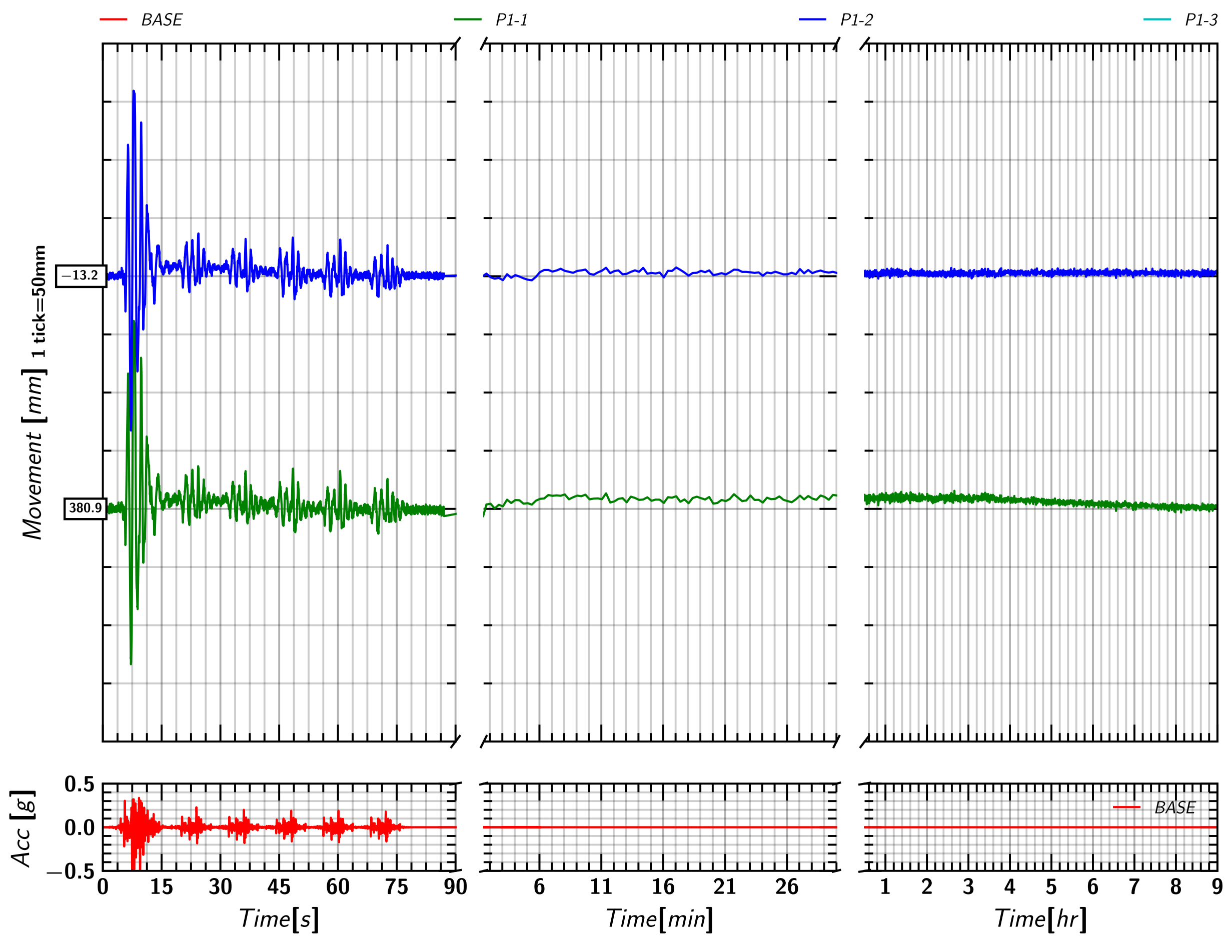

Figure 233. EQM$_4$: Pile 1 movement in X-direction relative to the model container during and post shaking.

K.14 Pile 1 Mass Movement in Z

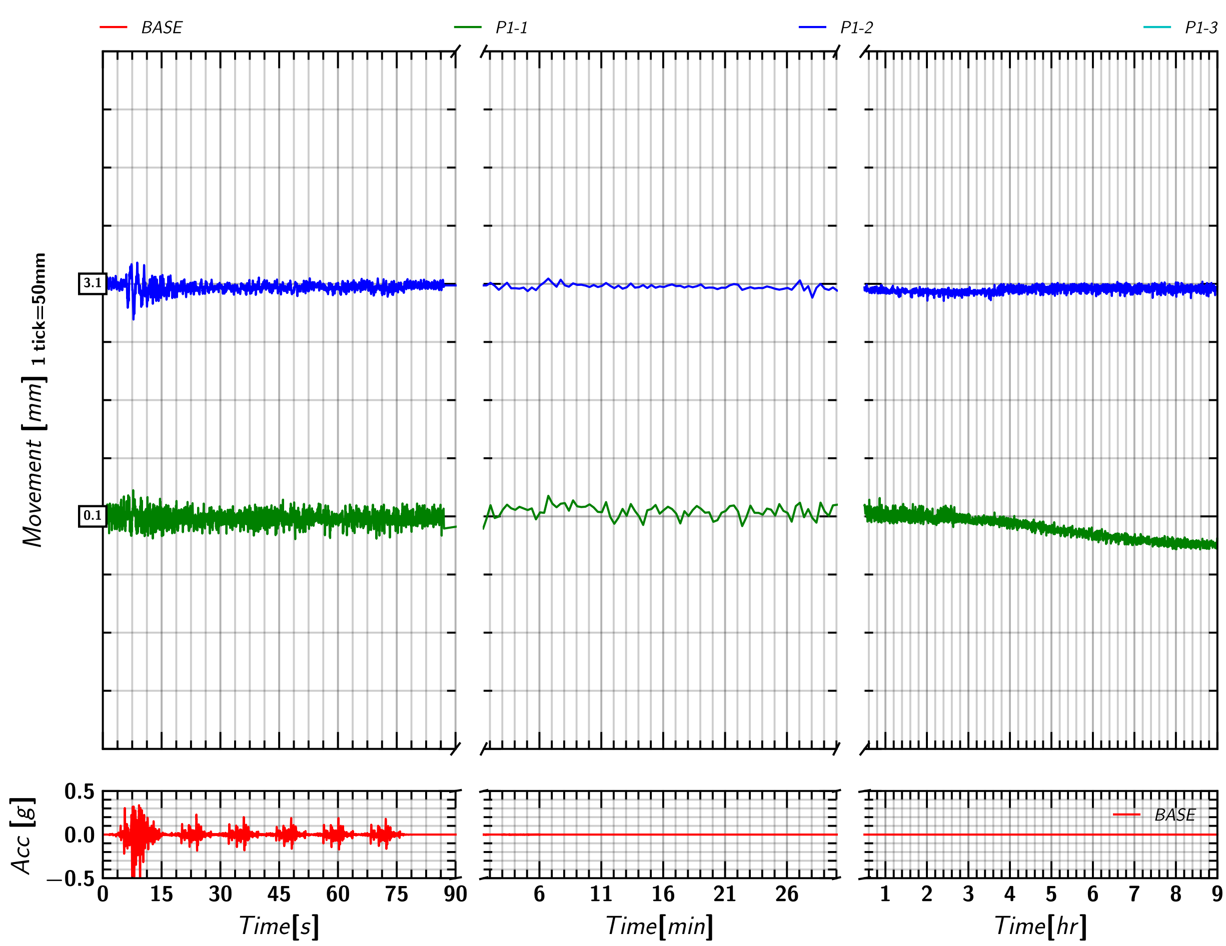

Figure 234. EQM$_4$: Pile 1 movement in Z-direction relative to the model container during and post shaking.

K.15 Pile 2 Mass Movement in X

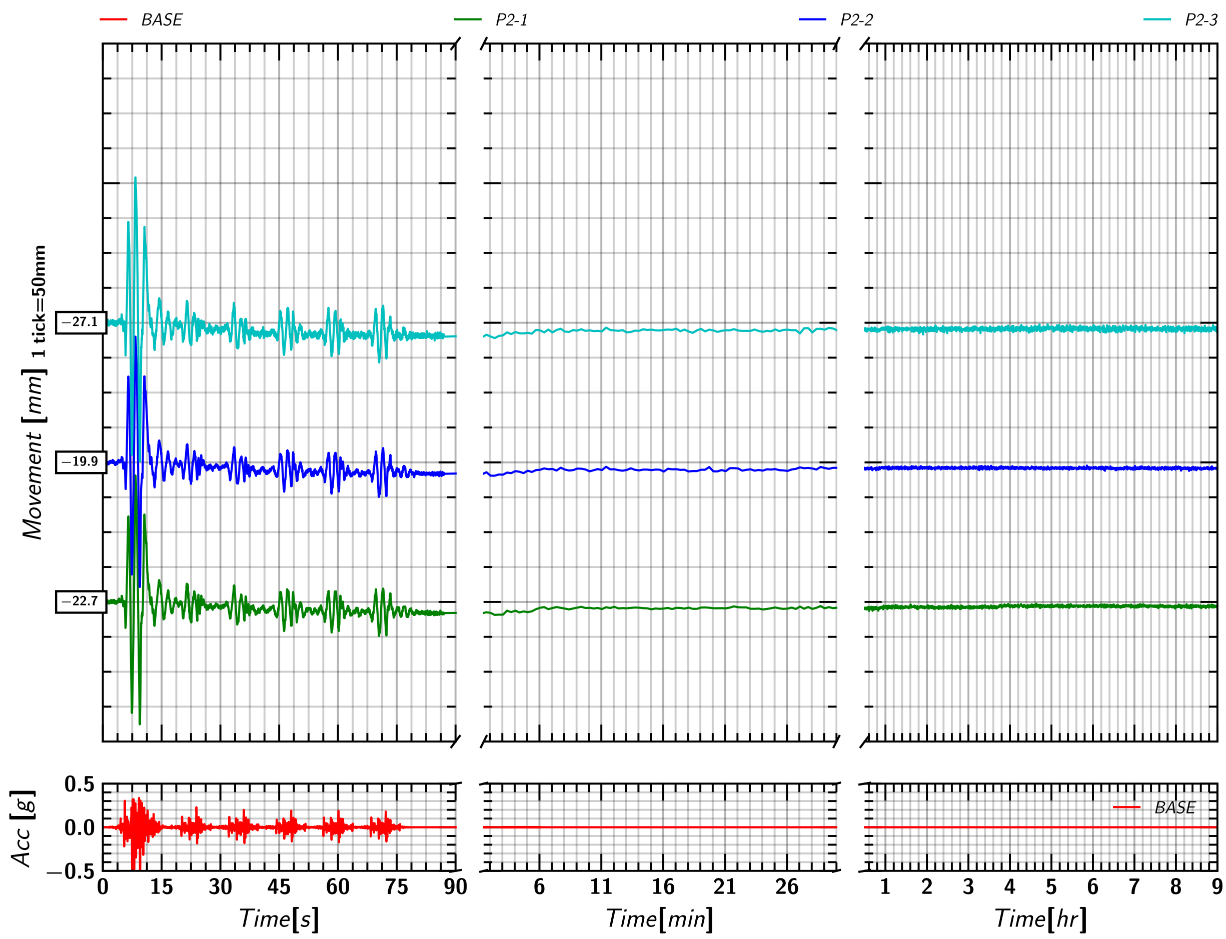

Figure 235. EQM$_4$: Pile 2 movement in X-direction relative to the model container during and post shaking.

K.16 Pile 2 Mass Movement in Z

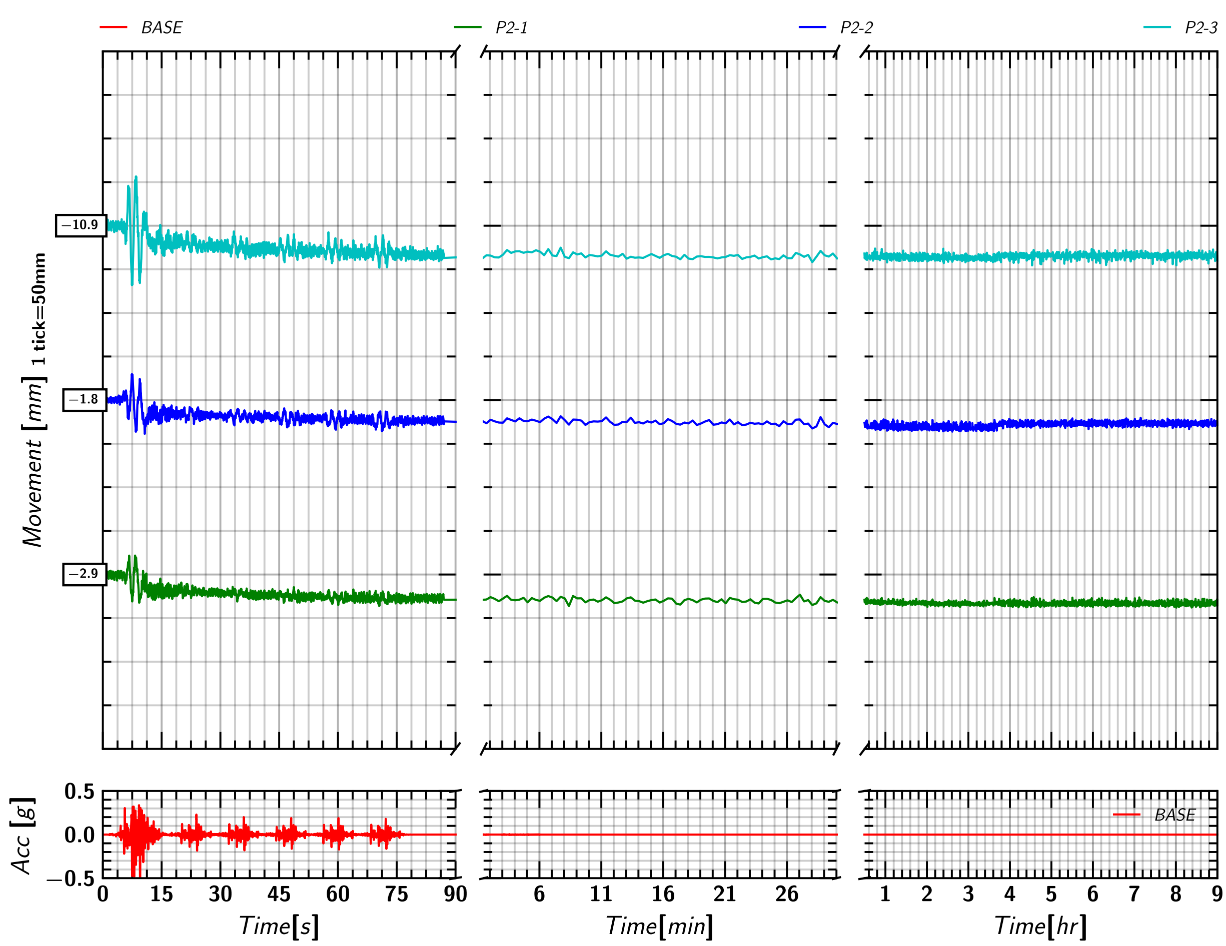

Figure 236. EQM$_4$: Pile 2 movement in Z-direction relative to the model container during and post shaking.

K.17 Pile 3 Mass Movement in X

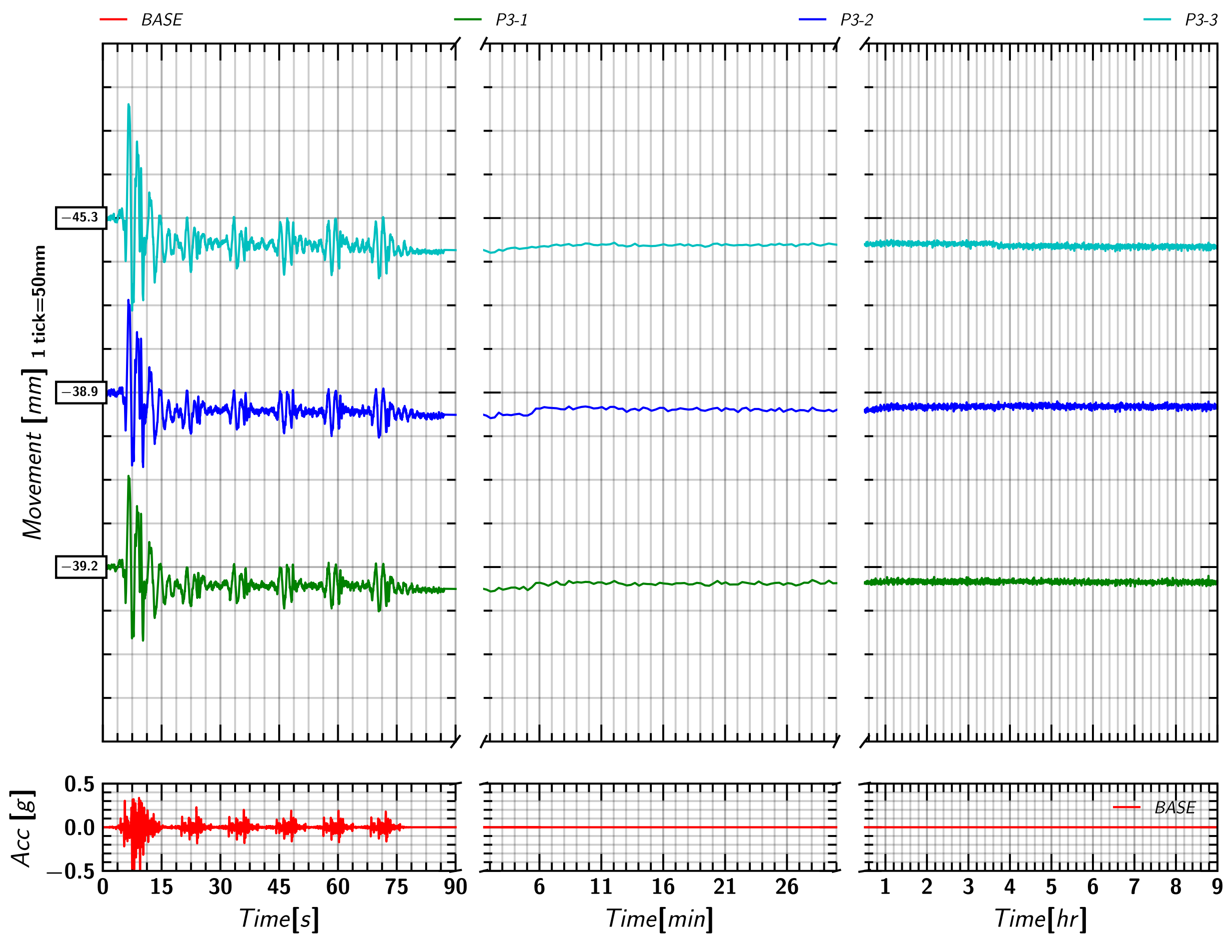

Figure 237. EQM$_4$: Pile 3 movement in X-direction relative to the model container during and post shaking.

K.18 Pile 3 Mass Movement in Z

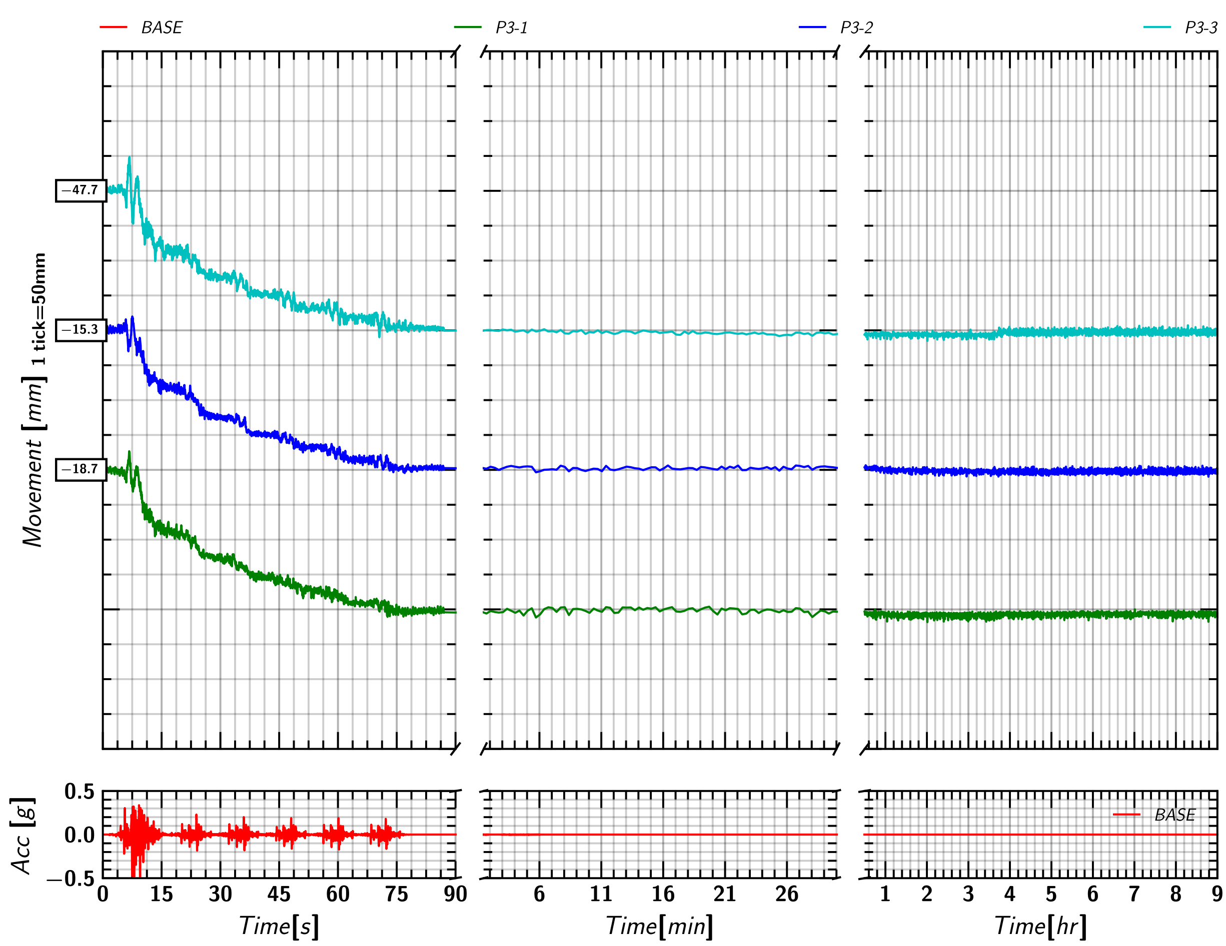

Figure 238. EQM$_4$: Pile 3 movement in Z-direction relative to the model container during and post shaking.

L. EQM$_5$: Large EJM01 CRUZ EARTHQUAKE (PGA = 0.61g)

L.1 Input Motion

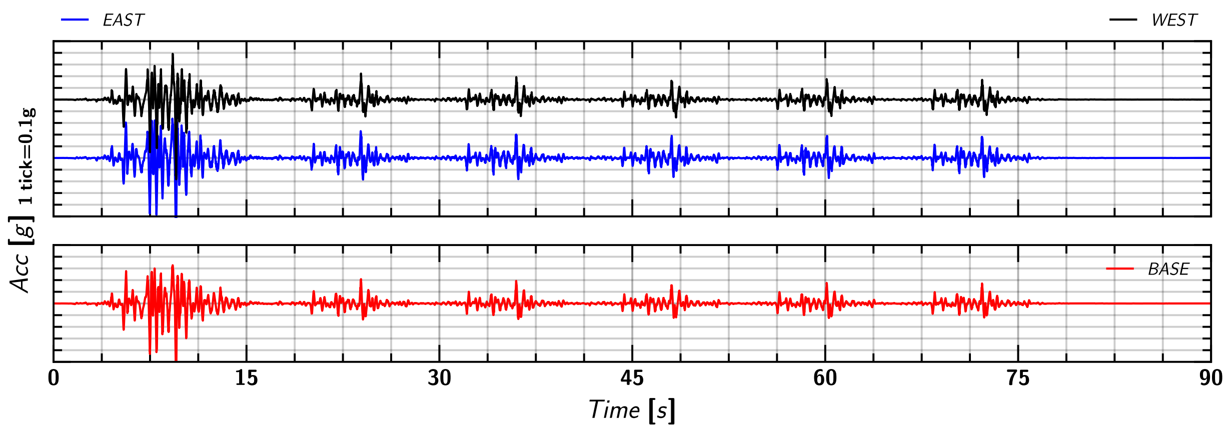

Figure 239. EQM$_5$: Input motion.

L.2 Spectral Acceleration

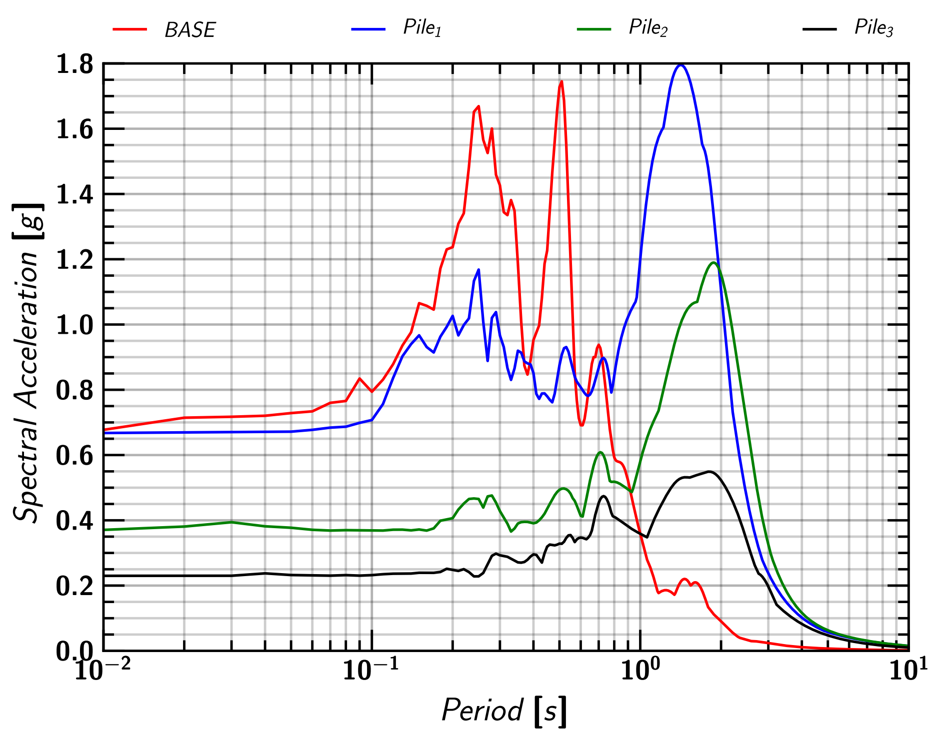

Figure 240. EQM$_5$: Spectral Acceleration.

L.3 Container Acceleration

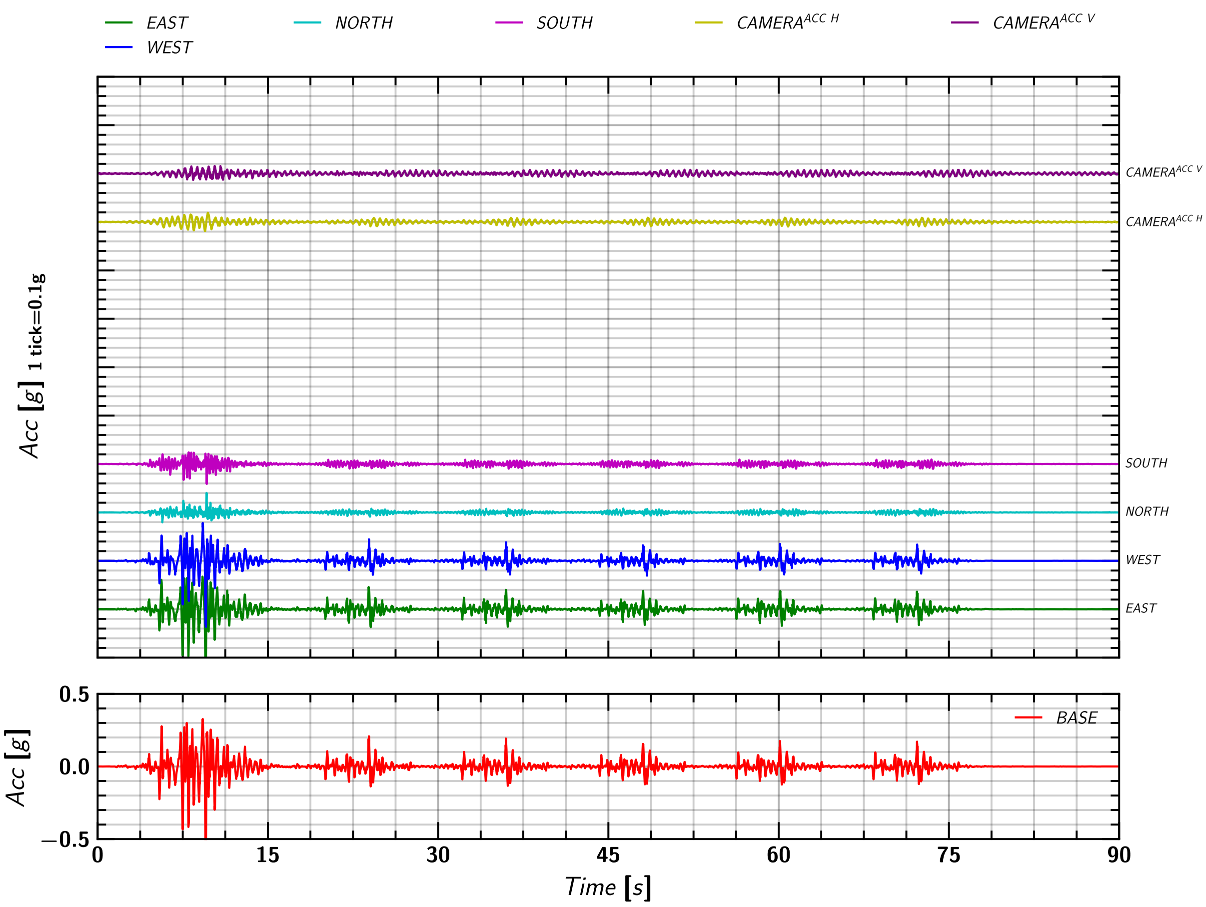

Figure 241. EQM5: Acceleration measurement on container and camera beam.

L.4 Soil Acceleration

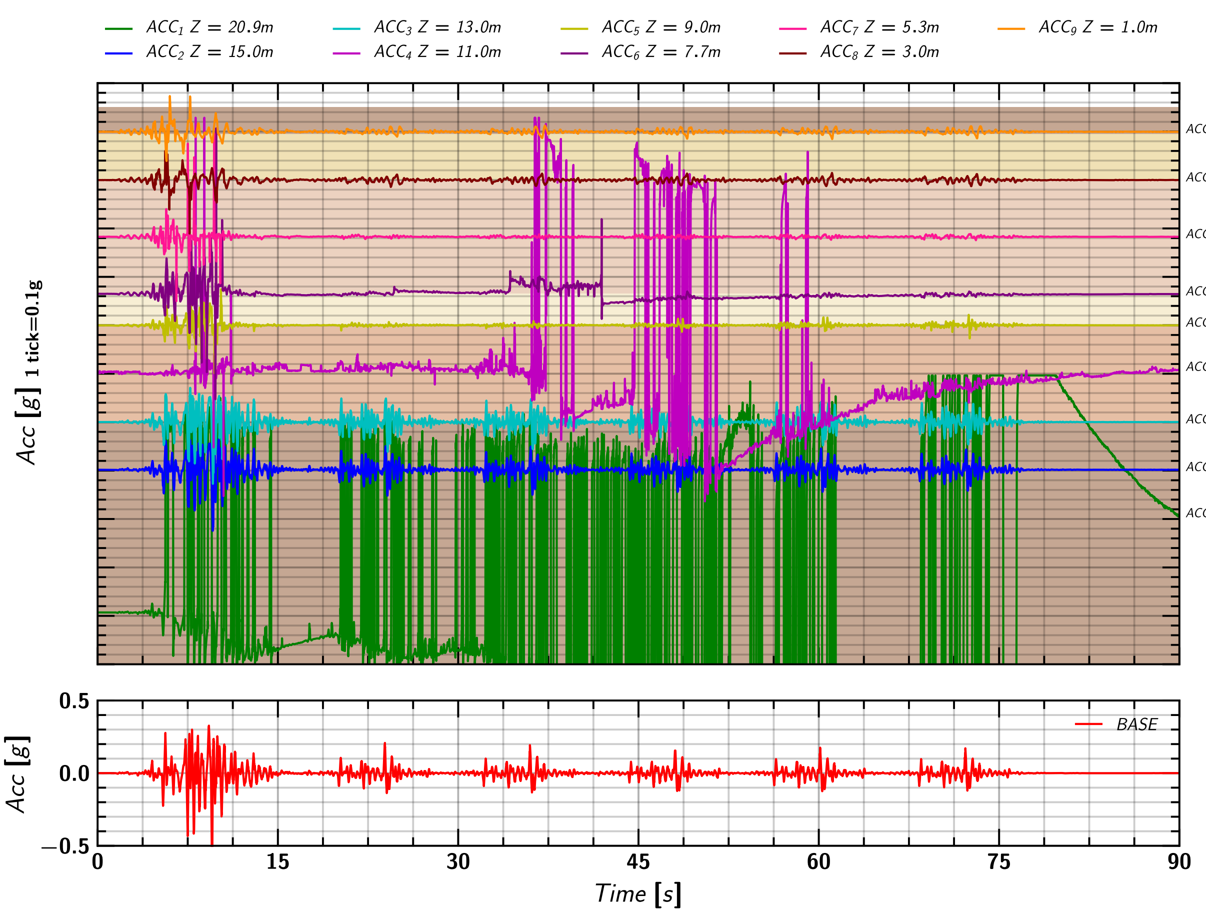

Figure 242. EQM5: Acceleration measurement in soil.

L.5 Pile Mass Acceleration

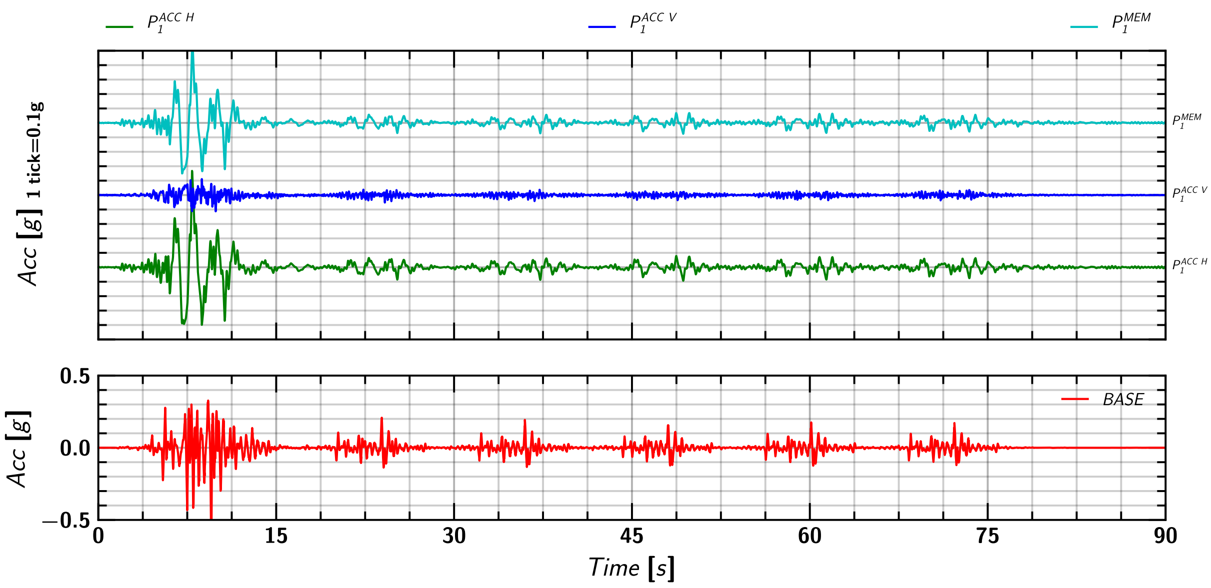

Figure 243. EQM5: Acceleration measurement on pile 1.

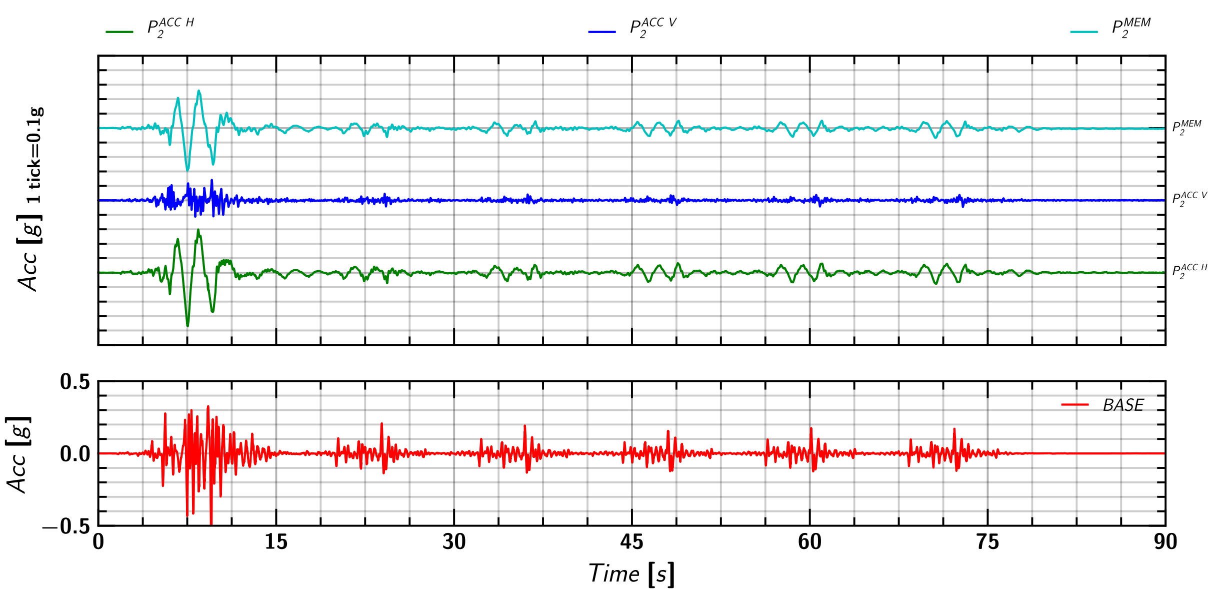

Figure 244. EQM5: Acceleration measurement on pile 2.

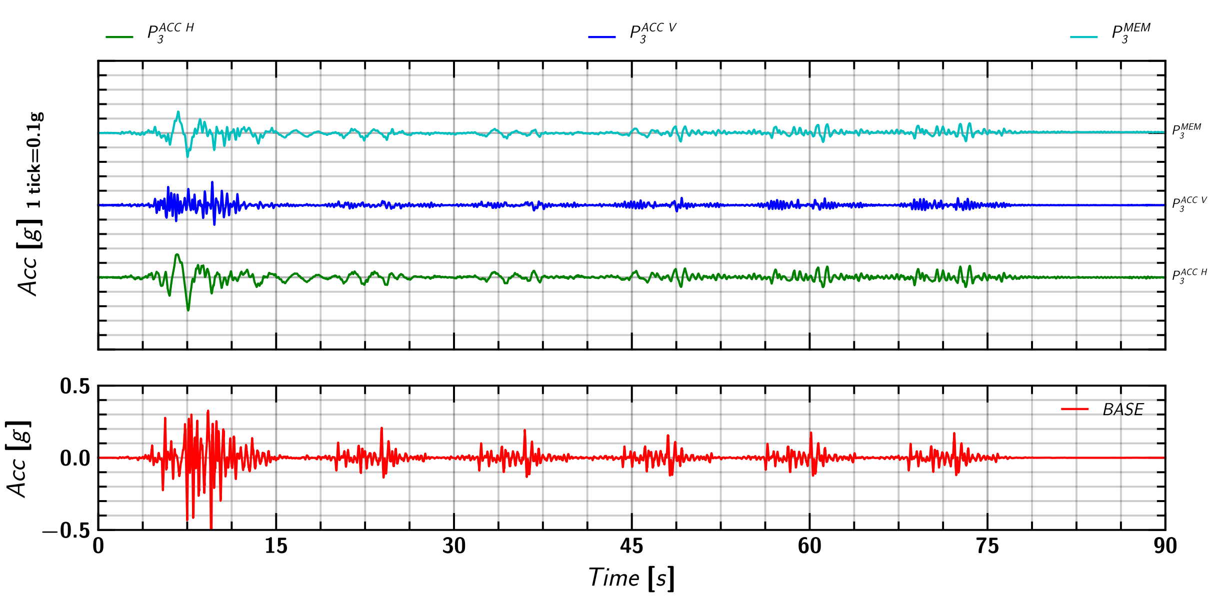

Figure 245. EQM5: Acceleration measurement on pile 3.

L.6 Soil and Pile Lateral Mass Movement in X direction

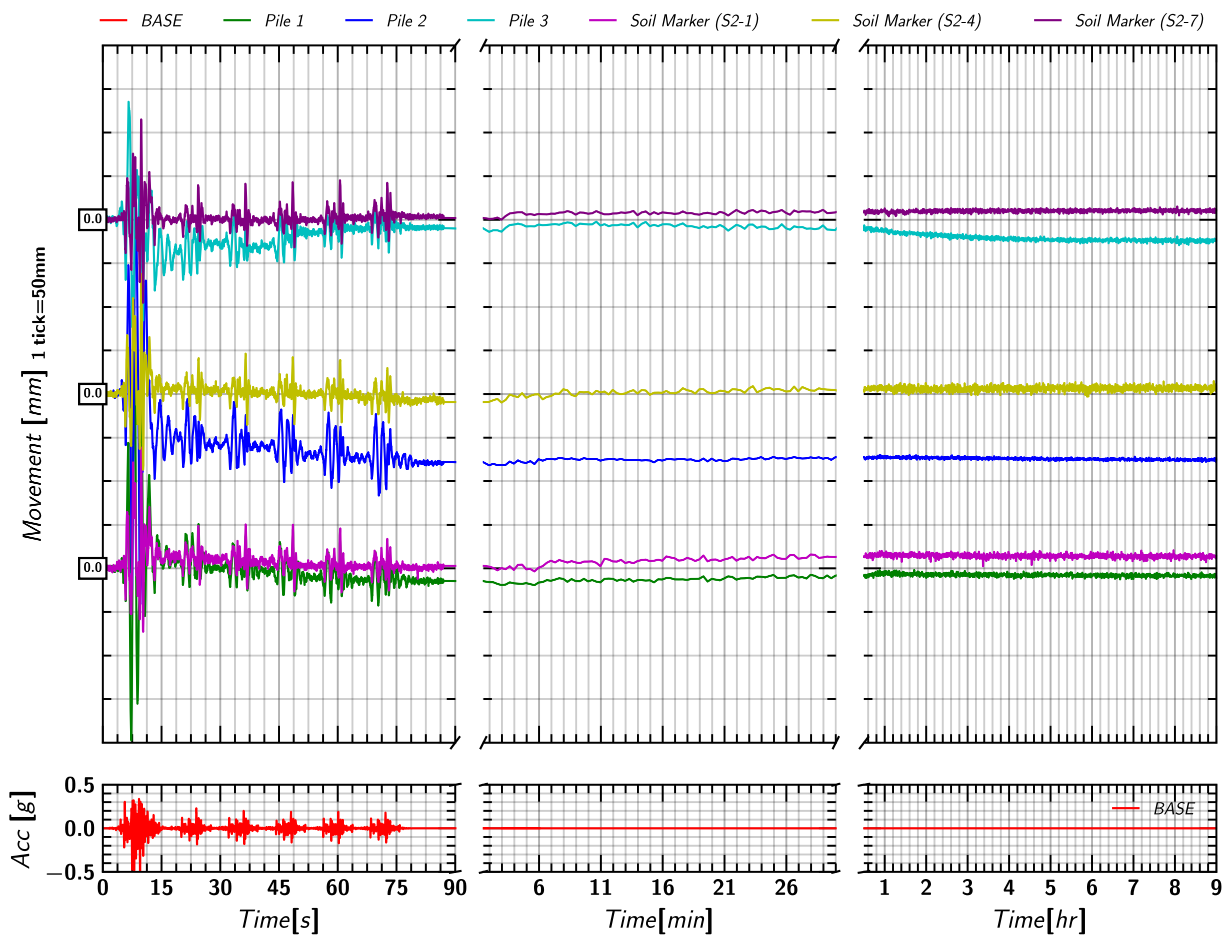

Figure 246. EQM₅: Lateral movement of soil and pile in x-direction during and post shaking.

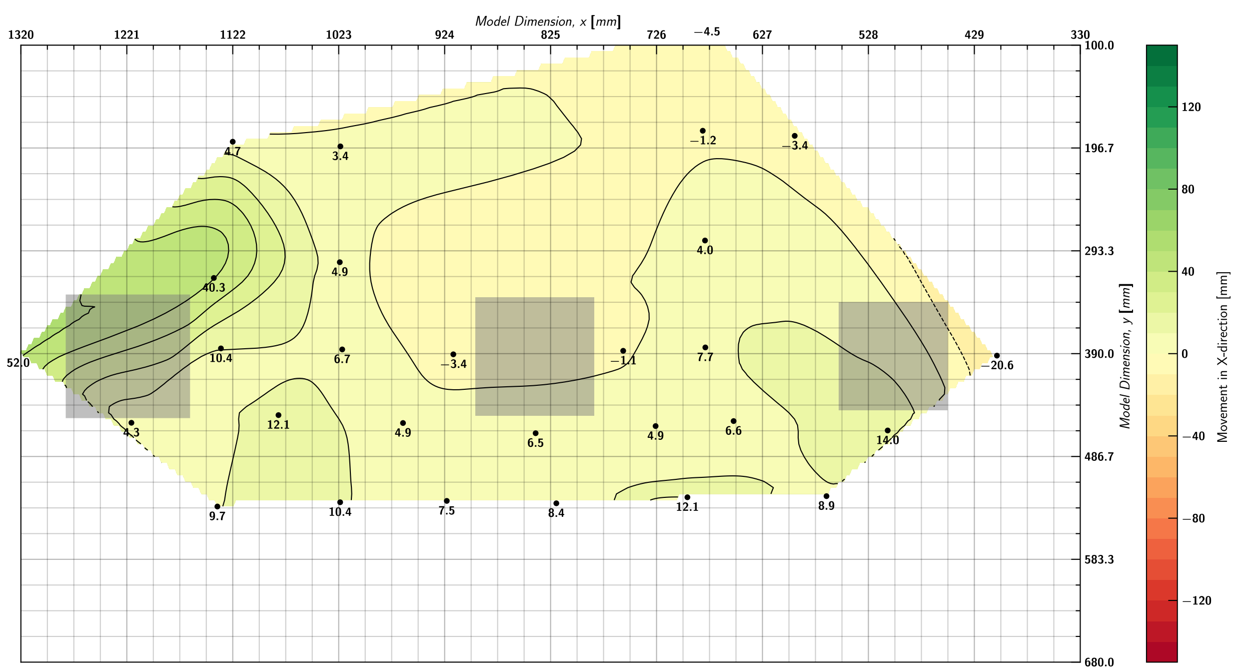

Figure 247. EQM₅:Contour of lateral movement of soil with respect to container in x-direction at the end of reconsolidation (t=300 minutes).

L.7 Soil and Pile Settlement (i.e., movement in Z direction)

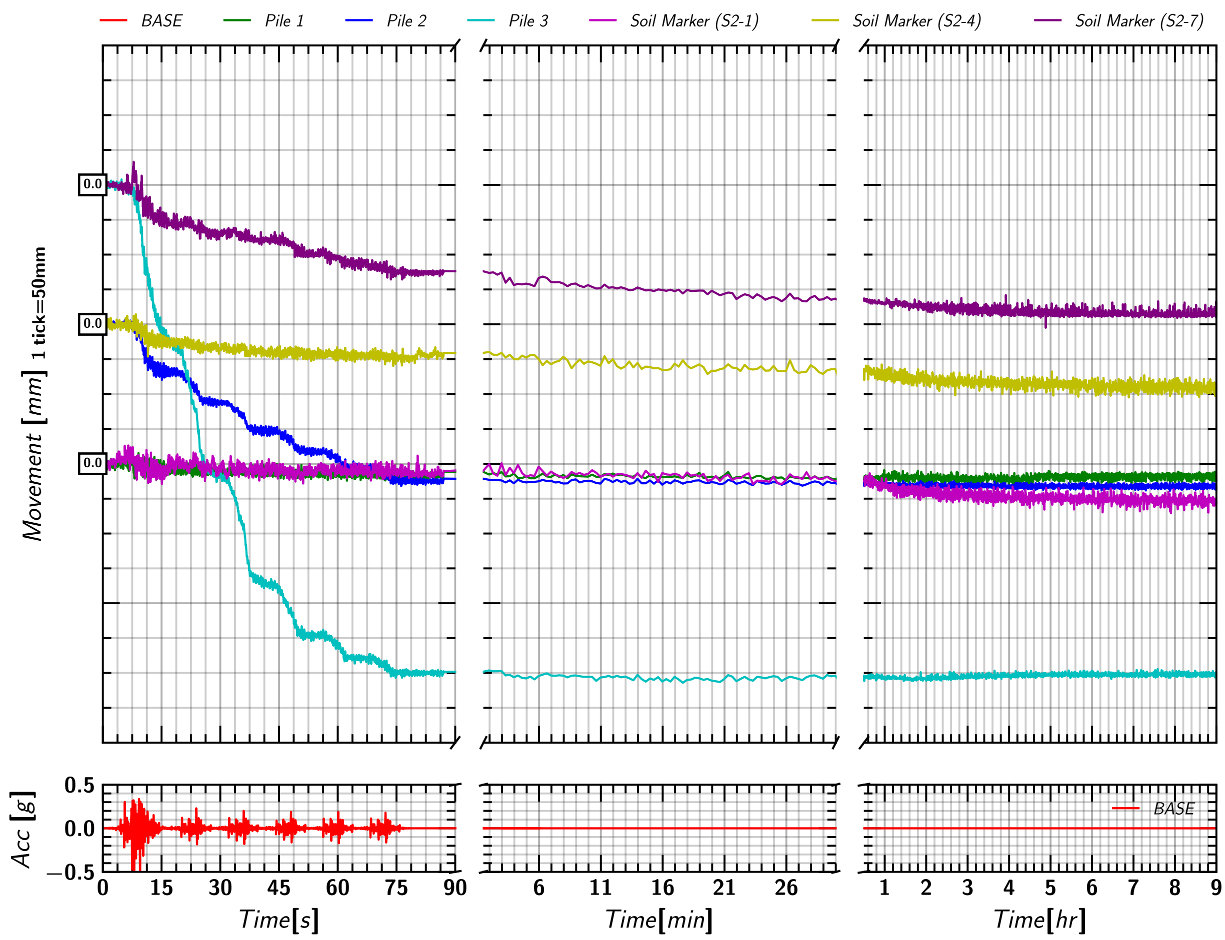

Figure 248. EQM5: Settlement measurement in soil and pile during and post shaking.

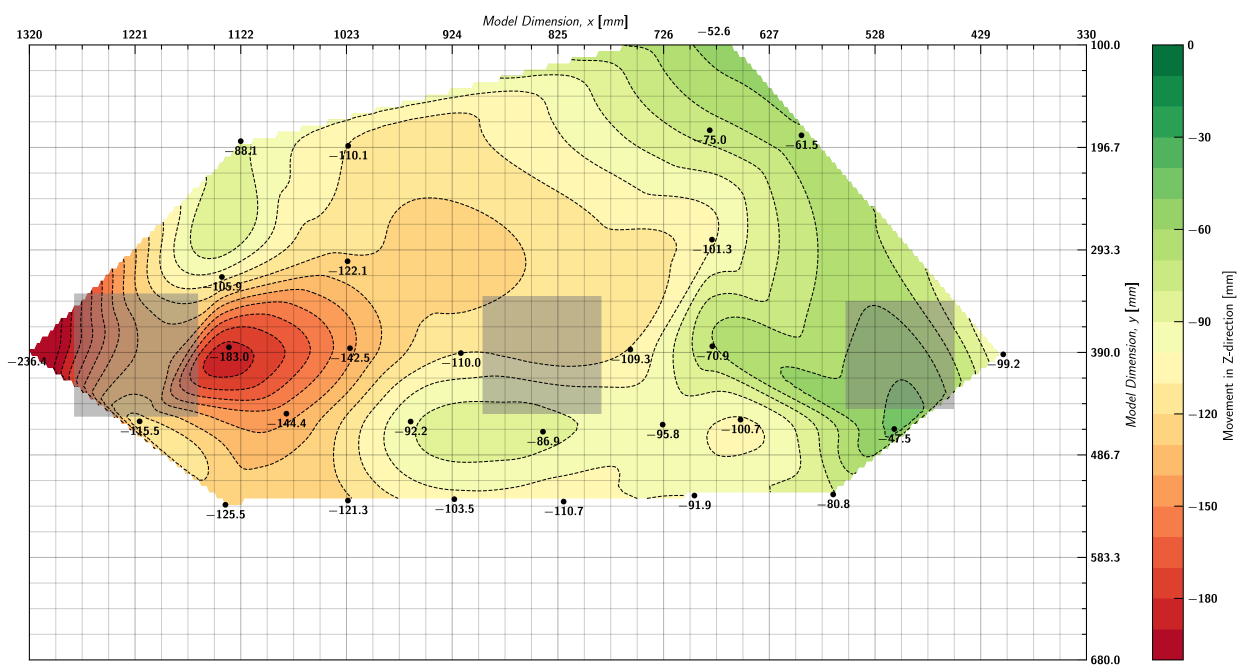

Figure 249. EQM5:Contour of lateral movement of soil with respect to container in x-direction at the end of reconsolidation (t=300 minutes).

L.8 Pore pressure in Soil Measured by Keller Transducers

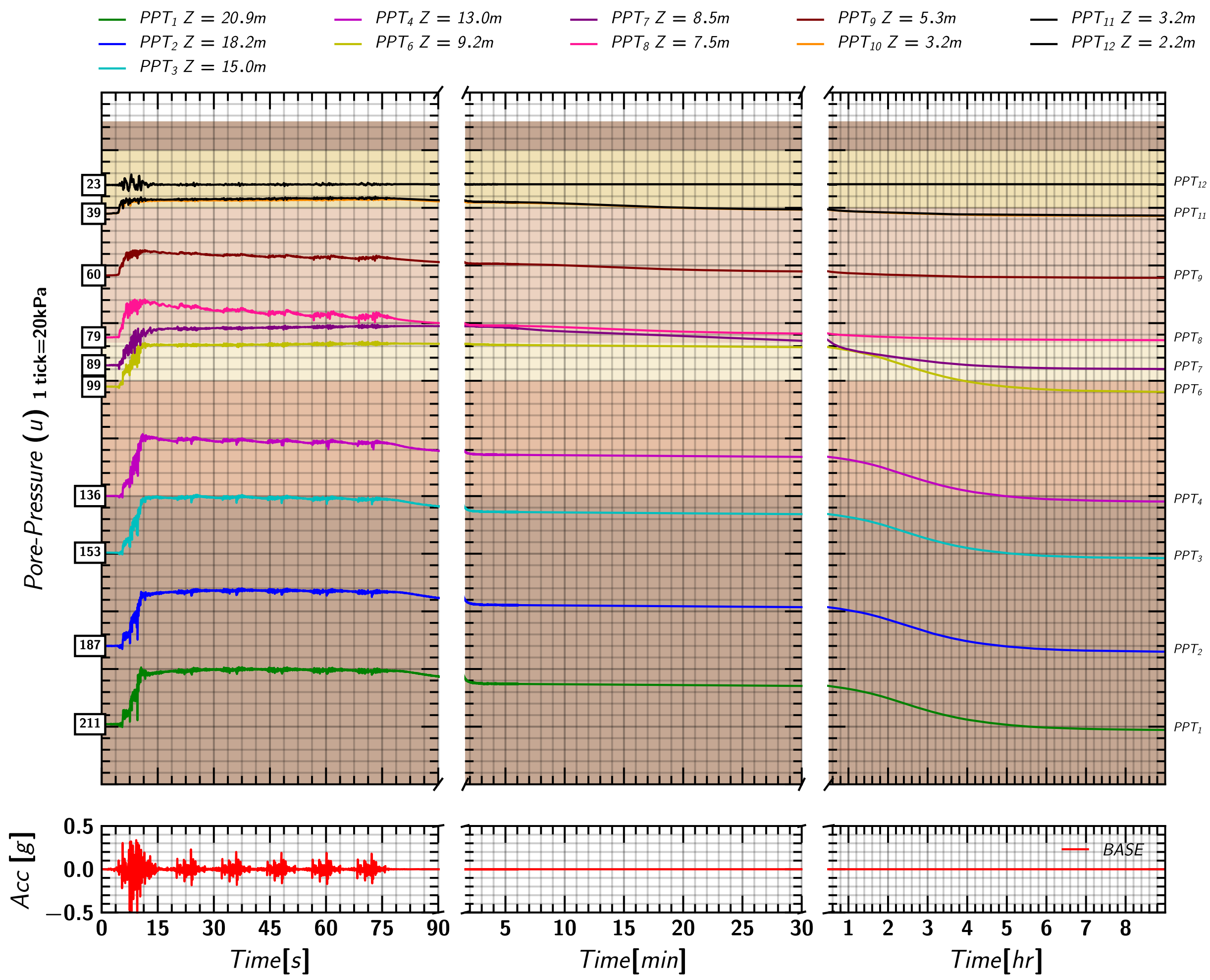

Figure 250. EQM5: Pore pressure measurements in soil from Keller transducers during and post shaking.

L.9 Pore pressure in Soil Measured by MS54XXX Transducers

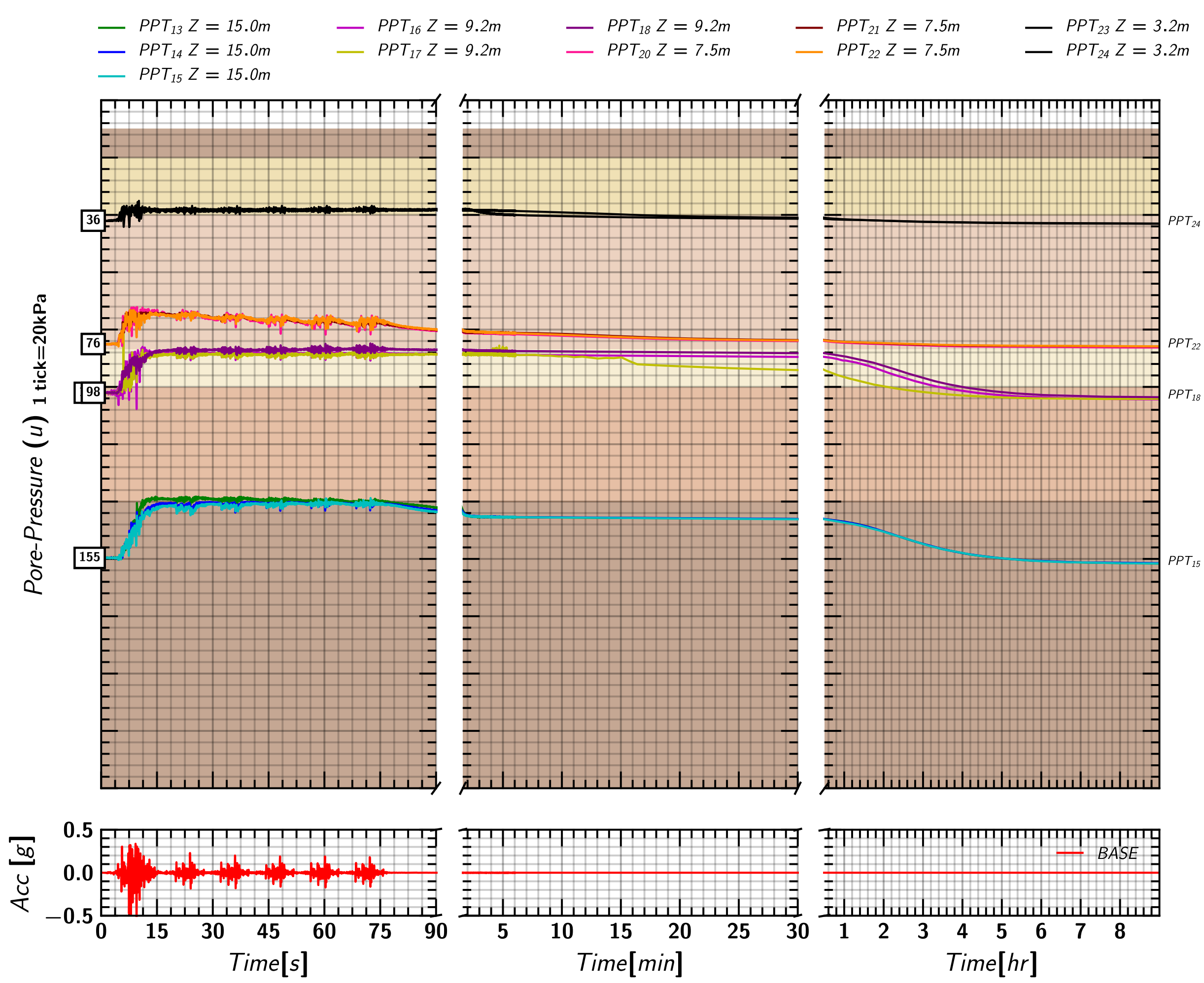

Figure 251. EQM5: Pore pressure measurements in soil from MS54XXX transducers during and post shaking.

Dense Sand	Medium Dense Sand	Clayey Silt	Loose Sand	Clay Crust

L.10 Excess Pore pressures Ratio (r_u) Estimated from Keller Transducers

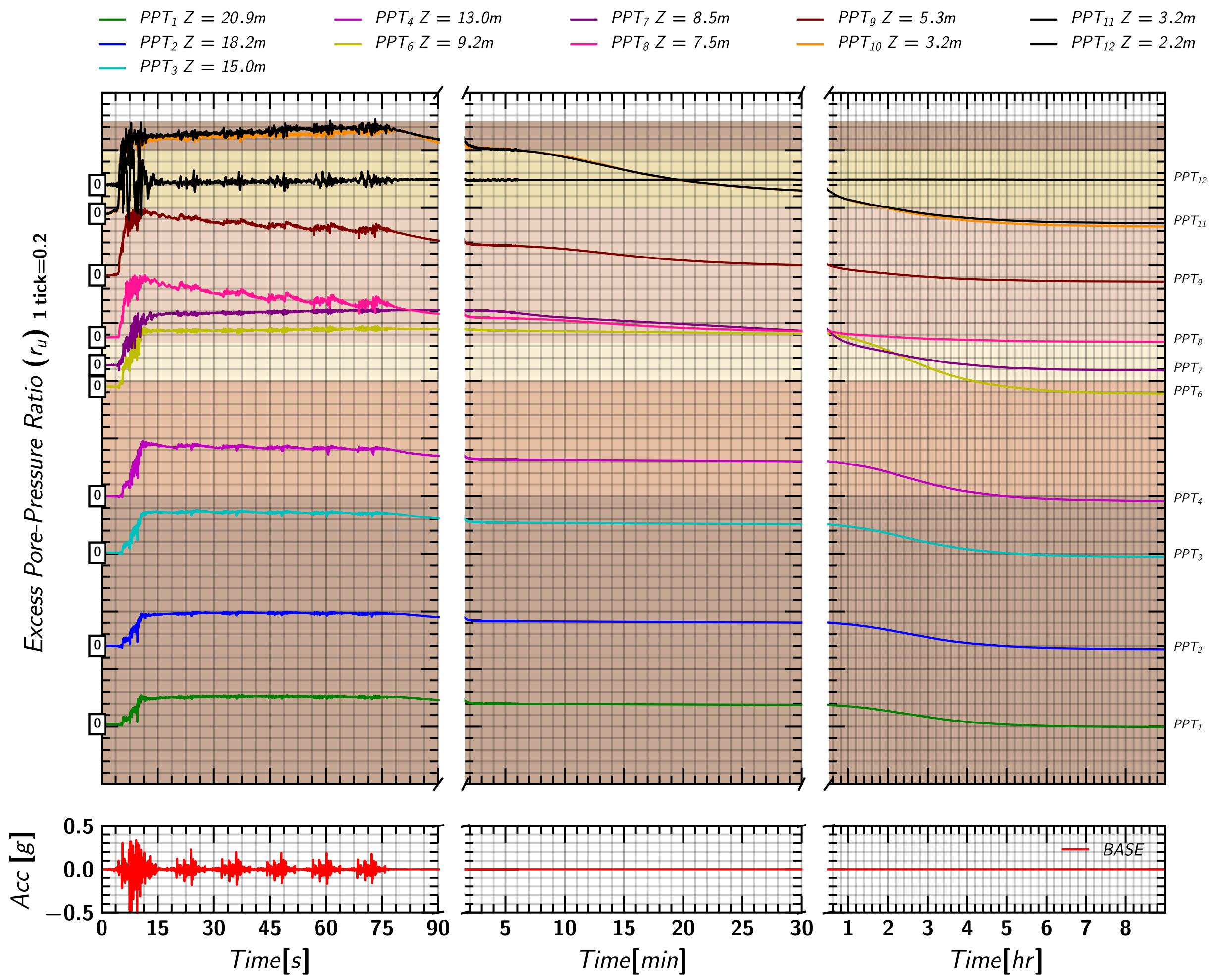

Figure 252. EQM5: Excess pore pressure ratio (r_u) estimated from Keller transducers during and post shaking.

L.11 Excess Pore pressure Ratio (r_u) Estimated from MS54XXX Transducers

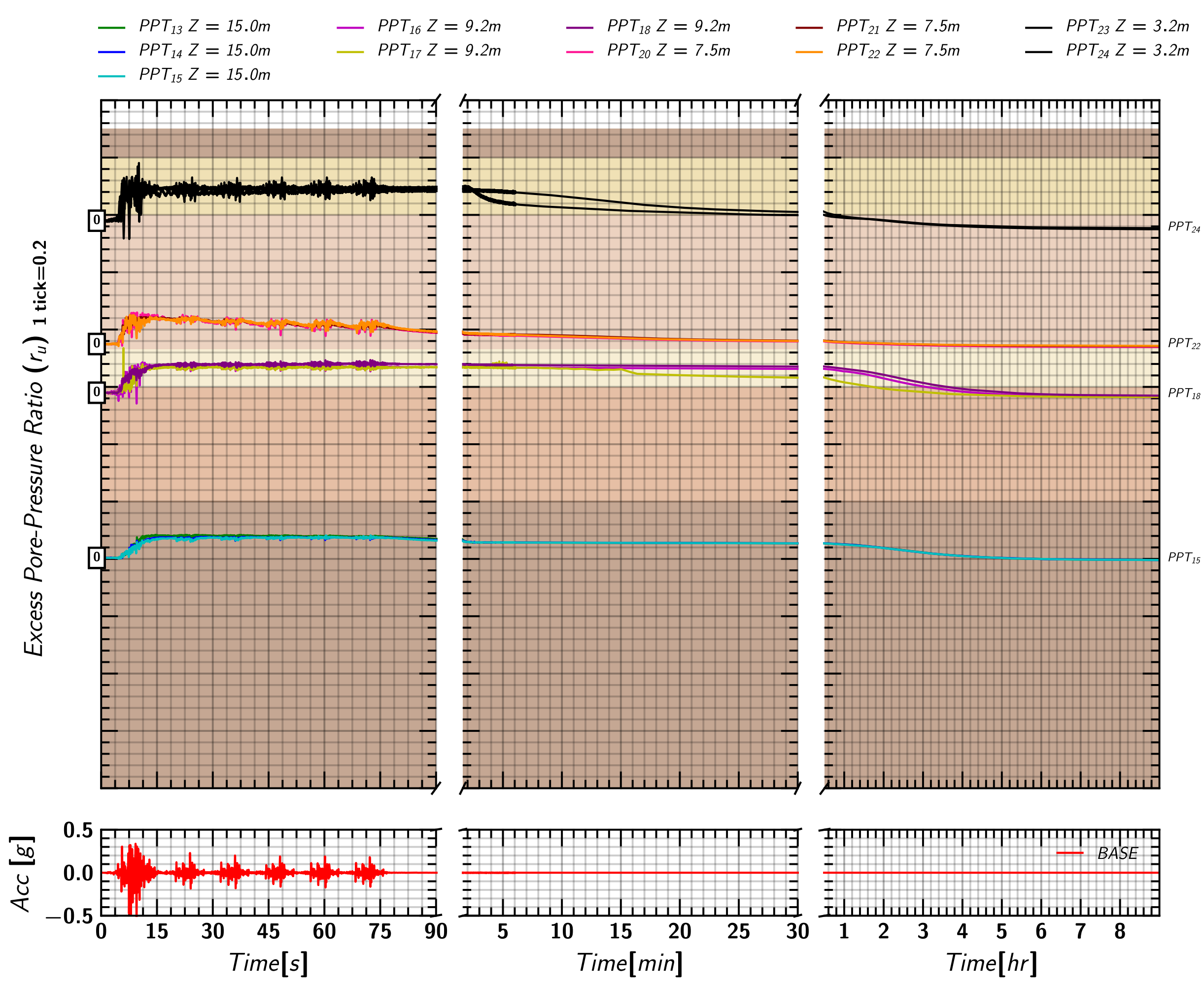

Figure 253. EQM5: Excess pore pressure ratio (r_u) estimated from MS54XXX transducers during and post shaking.

Dense Sand	Medium Dense Sand	Clayey Silt	Loose Sand	Clay Crust

L.12 Axial Load in Pile 1

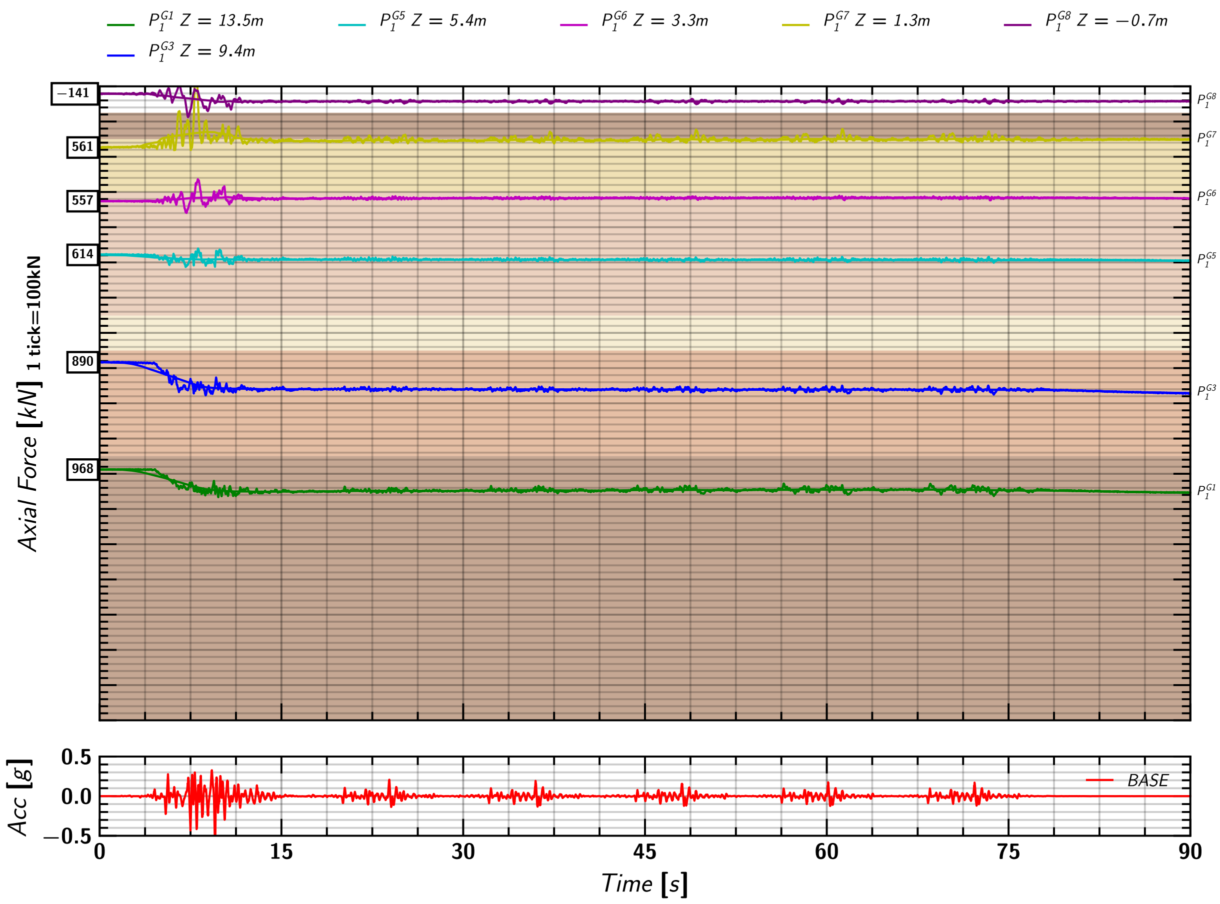

Figure 254. EQM5: Axial load measurements from pile 1 strain gages during shaking.

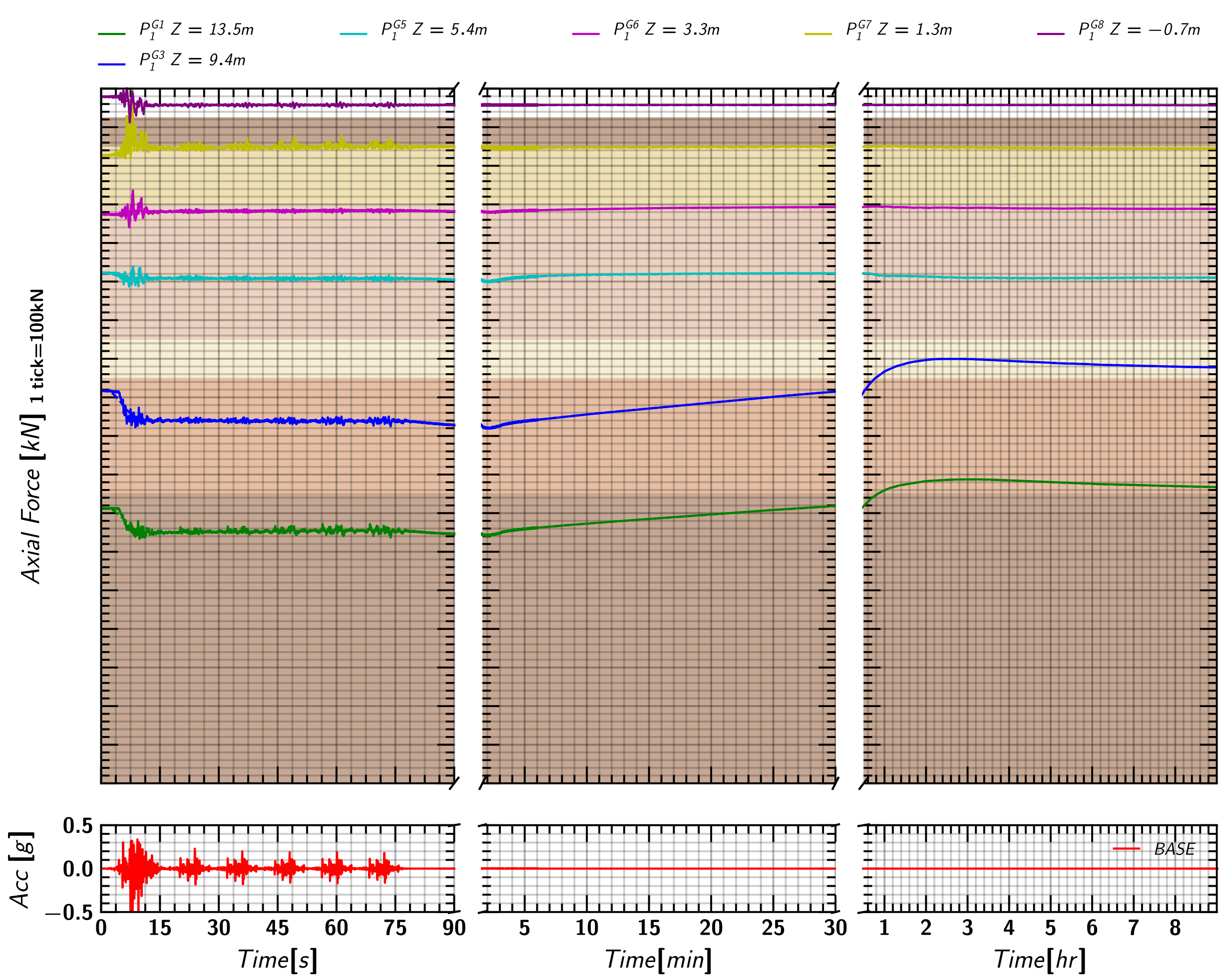

Figure 255. EQM5: Axial load measurements from pile 1 strain gages during and post shaking.

L.13 Axial Load in Pile 2

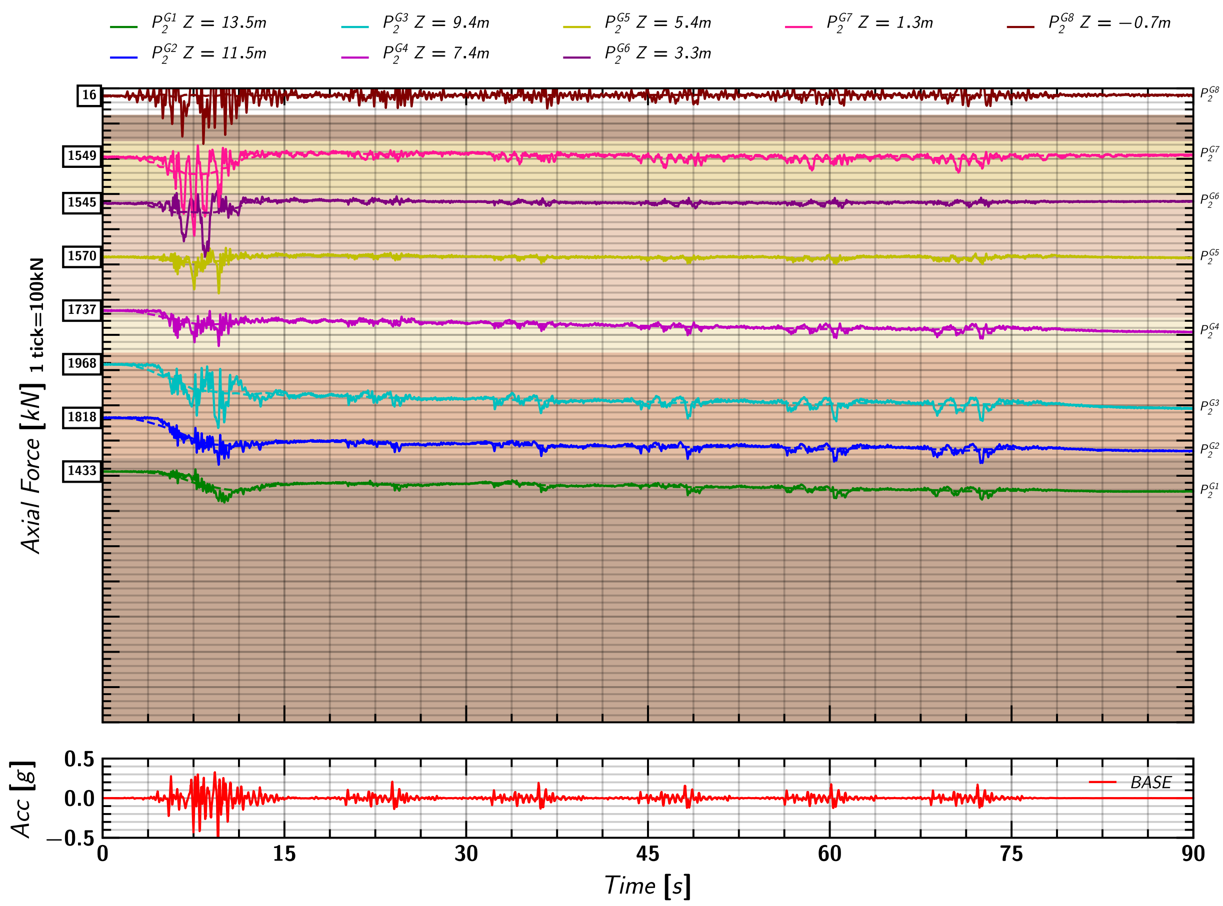

Figure 256. EQM₅: Axial load measurements from pile 2 strain gages during shaking.

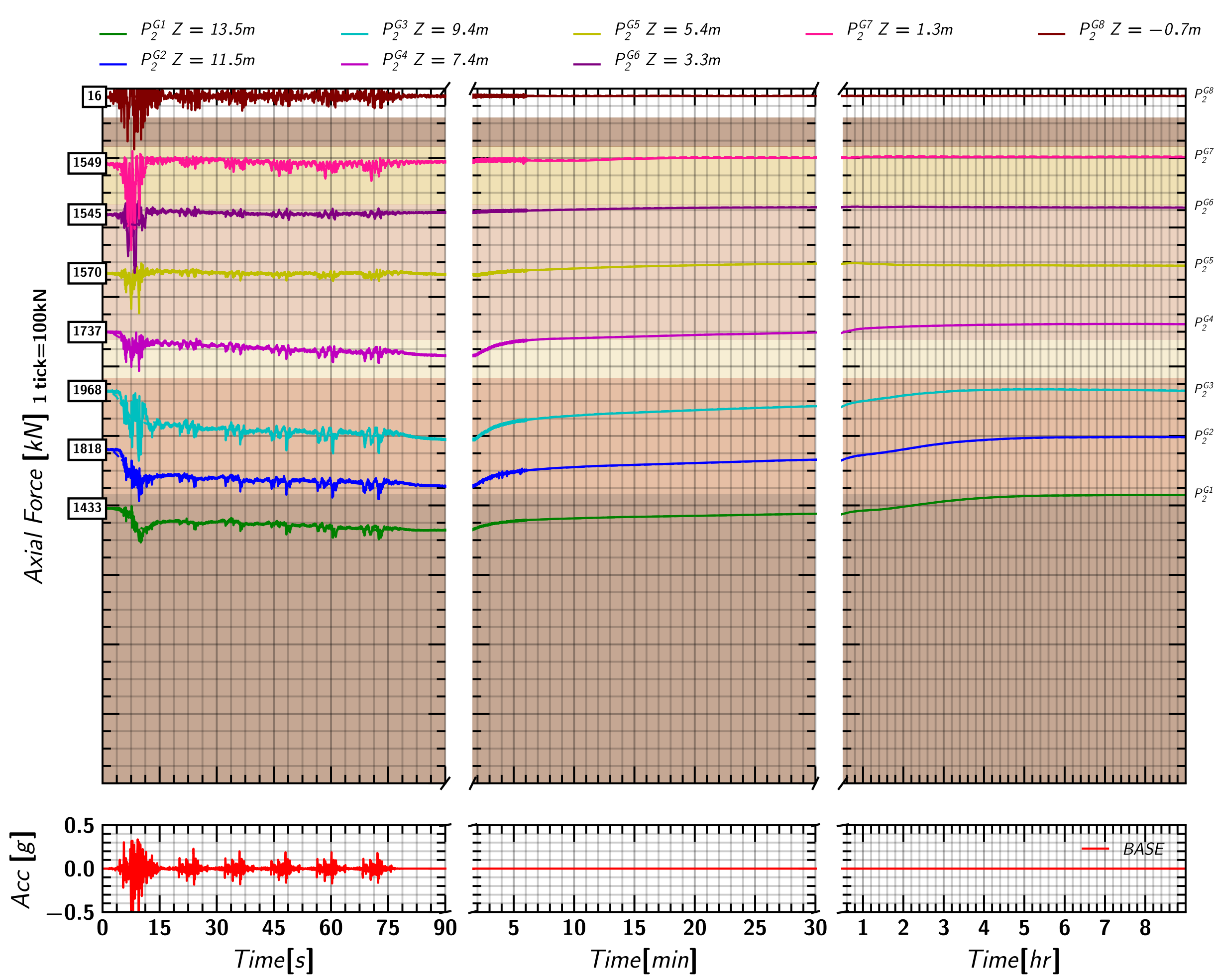

Figure 257. EQM₅: Axial load measurements from pile 2 strain gages during and post shaking.

L.14 Axial Load in Pile 3

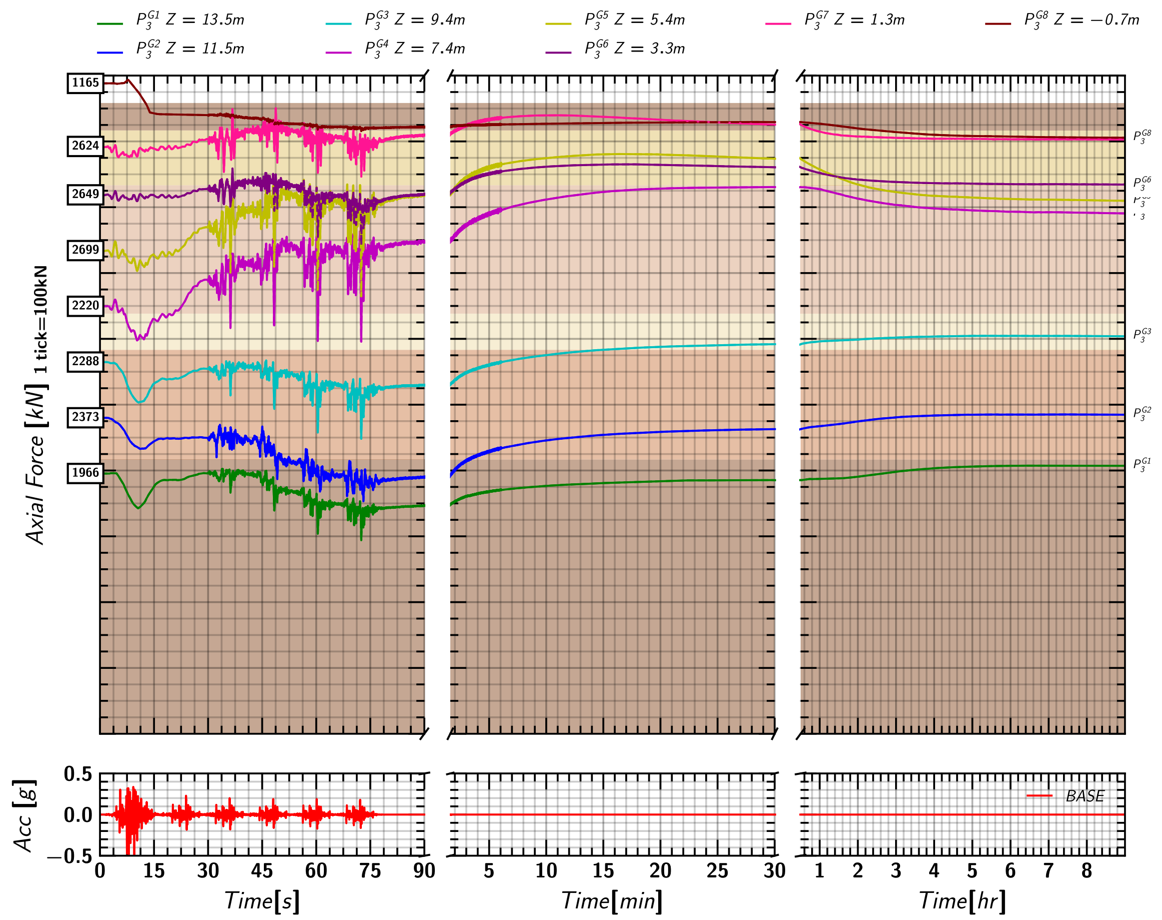

Figure 258. EQM₅: Axial load measurements from pile 3 strain gages during shaking.

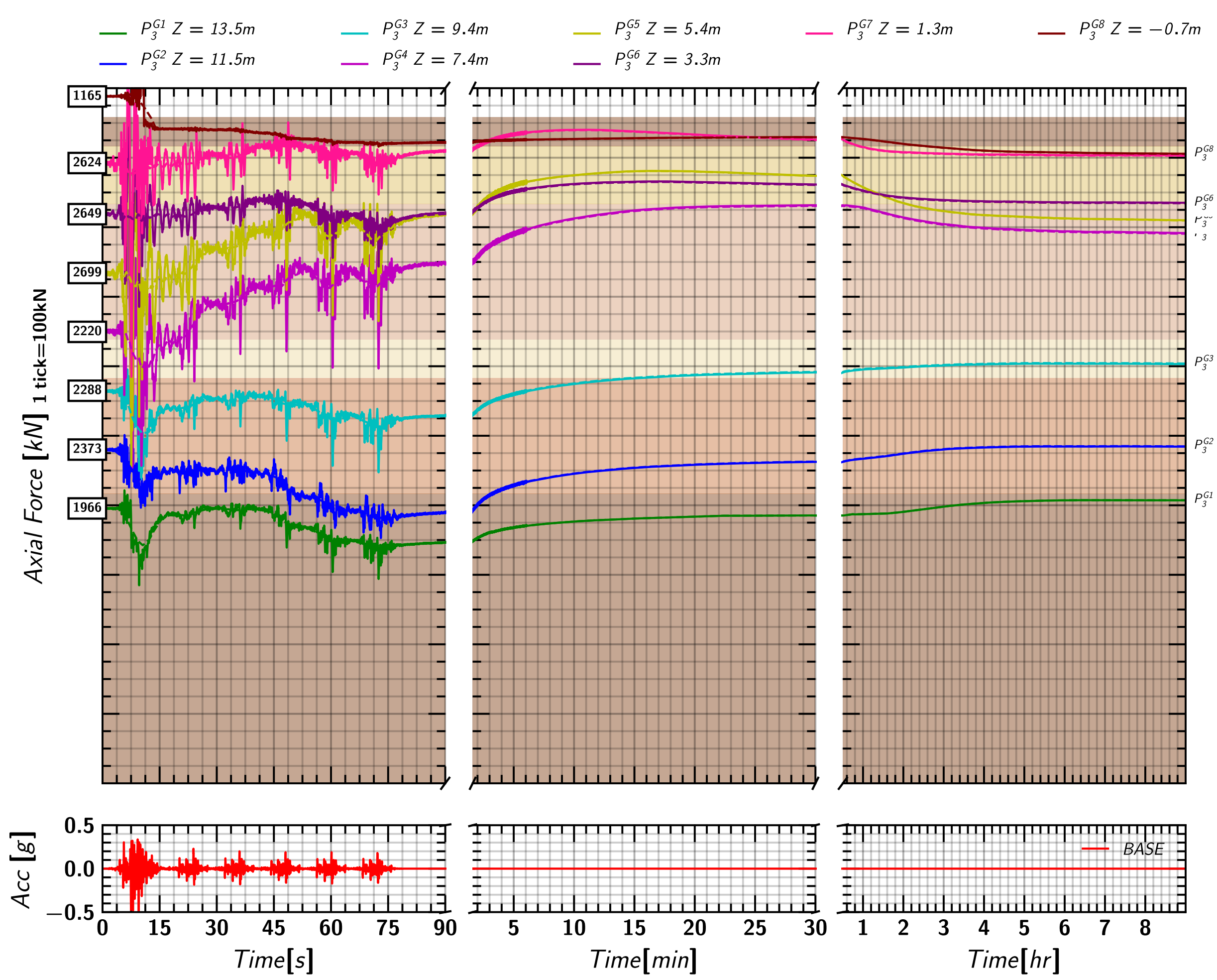

Figure 259. EQM₅: Axial load measurements from pile 3 strain gages during and post shaking.

L.15 Pore pressure and Axial Load Profile

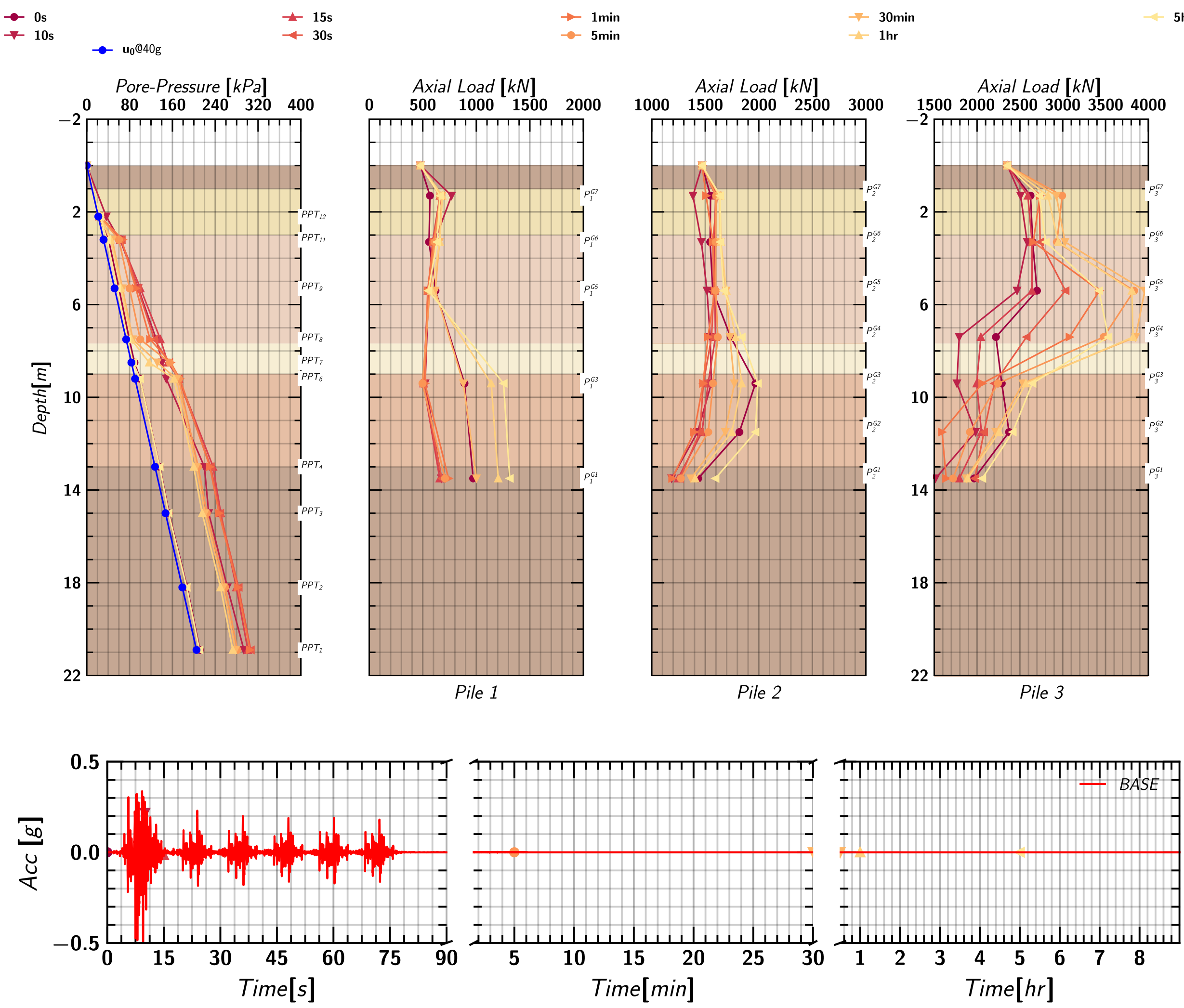

Figure 260. EQM₅: Pore pressure and axial load profile in pile 1, pile 2 and pile 3 at different times during and post shaking.

M. EQM$_5$: Soil, Pile, and Container Movements in X and Z

M.1 Container Movement in X

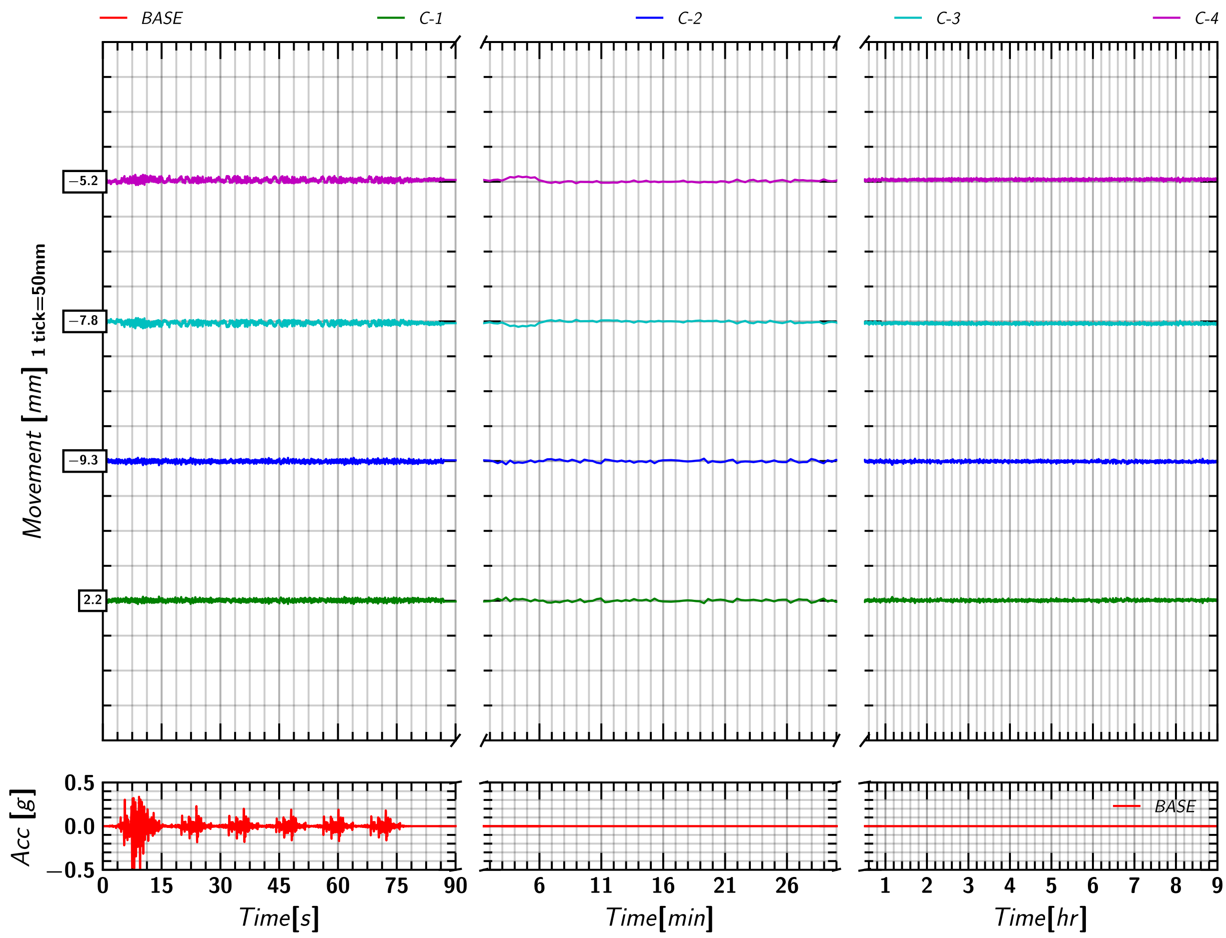

Figure 261. EQM$_5$: Container movement in X-direction relative to the model container during and post shaking.

M.2 Container Movement in Z

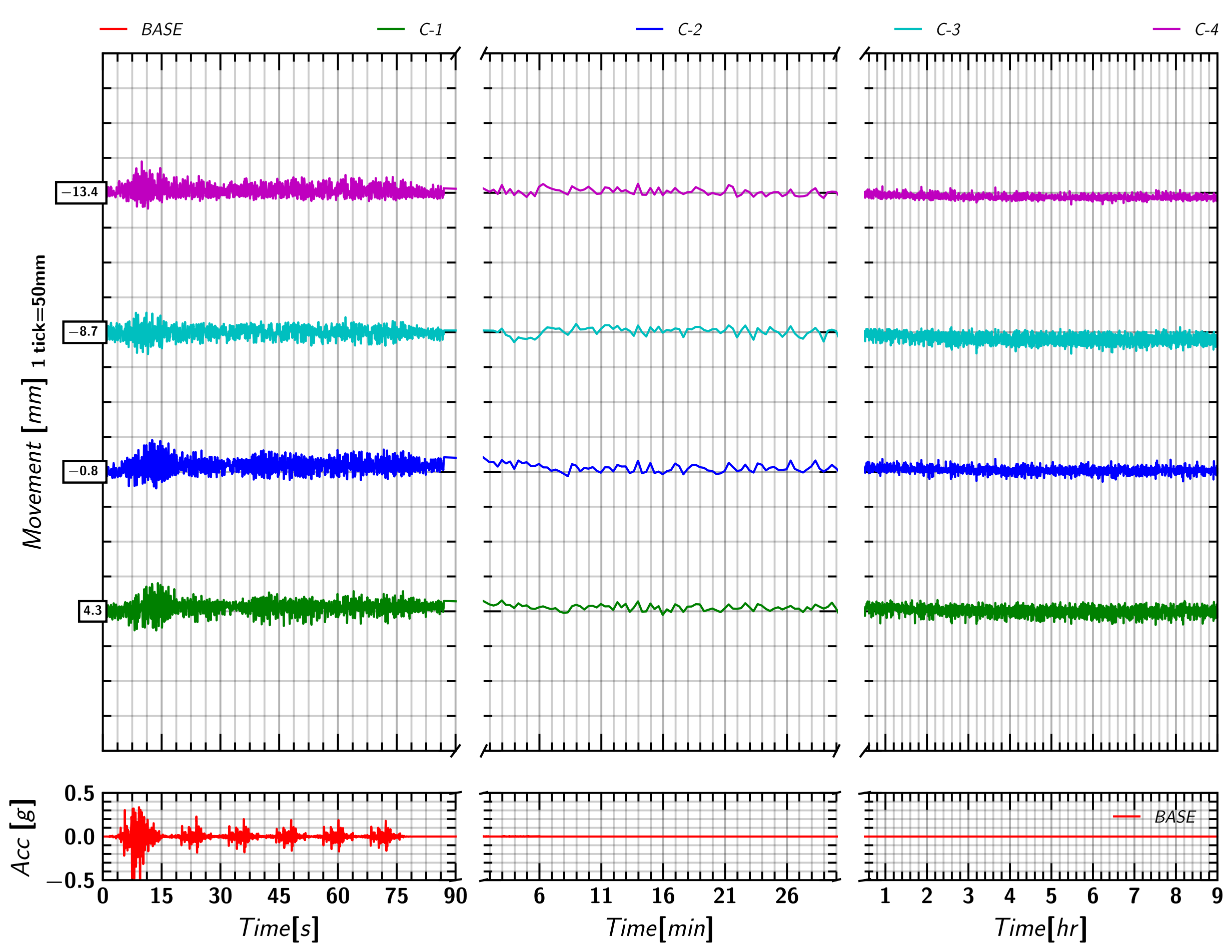

Figure 262. EQM$_5$: Container movement in Z-direction relative to the model container during and post shaking.

M.3 Soil (Row S-1) Movement in X

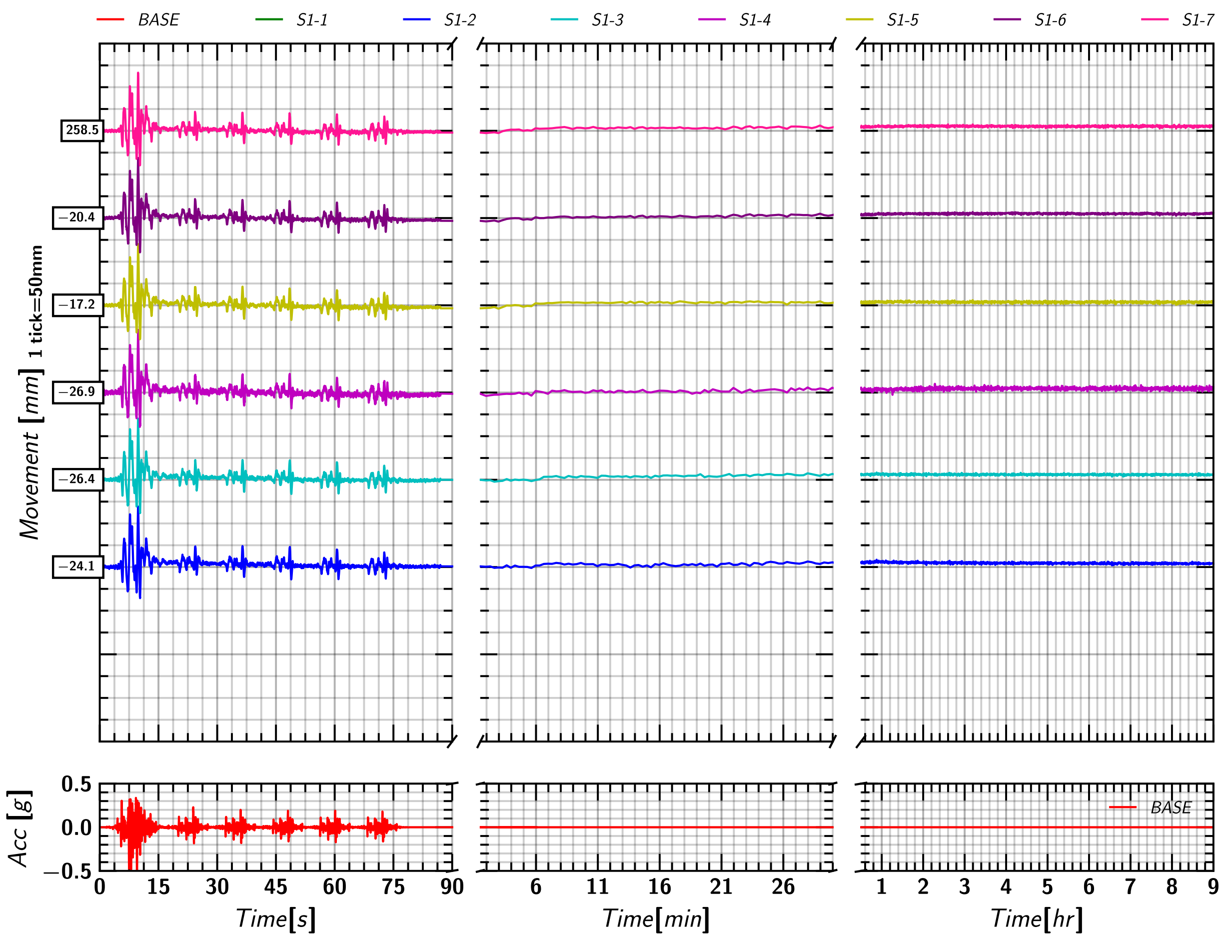

Figure 263. EQM5: Soil (Row S-1) movement in X-direction relative to the model container during and post shaking.

M.4 Soil (Row S-1) Movement in Z

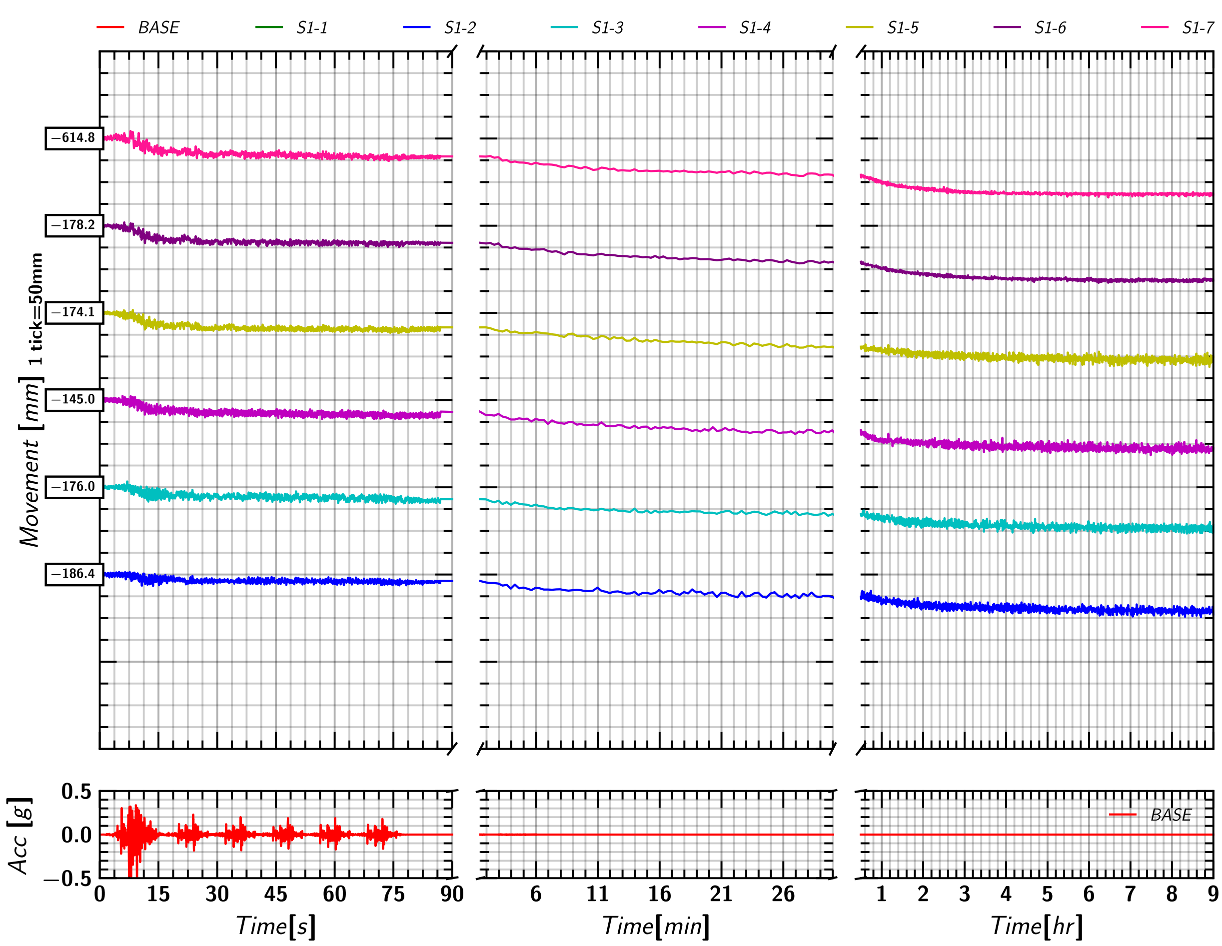

Figure 264. EQM5: Soil (Row S-1) movement in Z-direction relative to the model container during and post shaking.

M.5 Soil (Row S-2) Movement in X

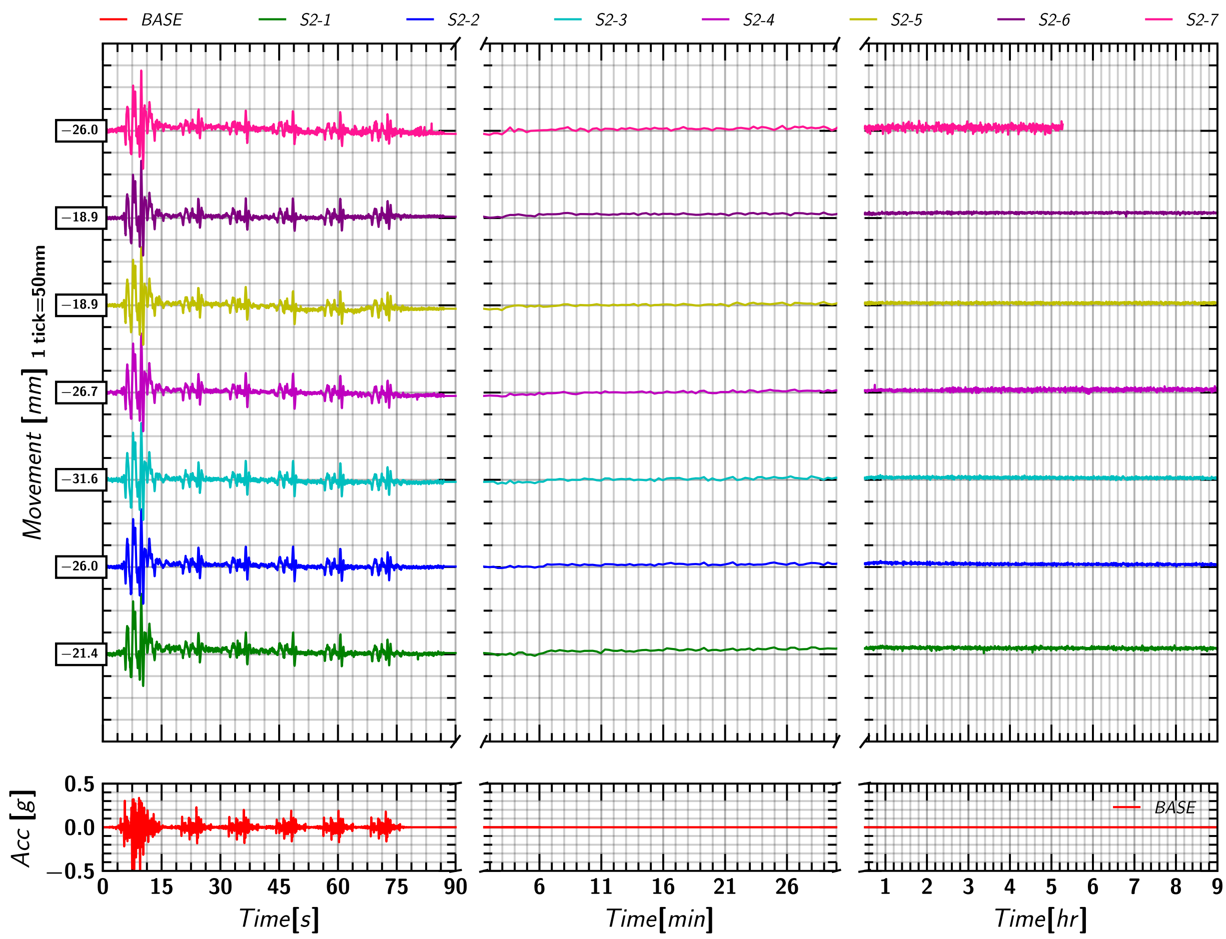

Figure 265. EQM5: Soil (Row S-2) movement in X-direction relative to the model container during and post shaking.

M.6 Soil (Row S-2) Movement in Z

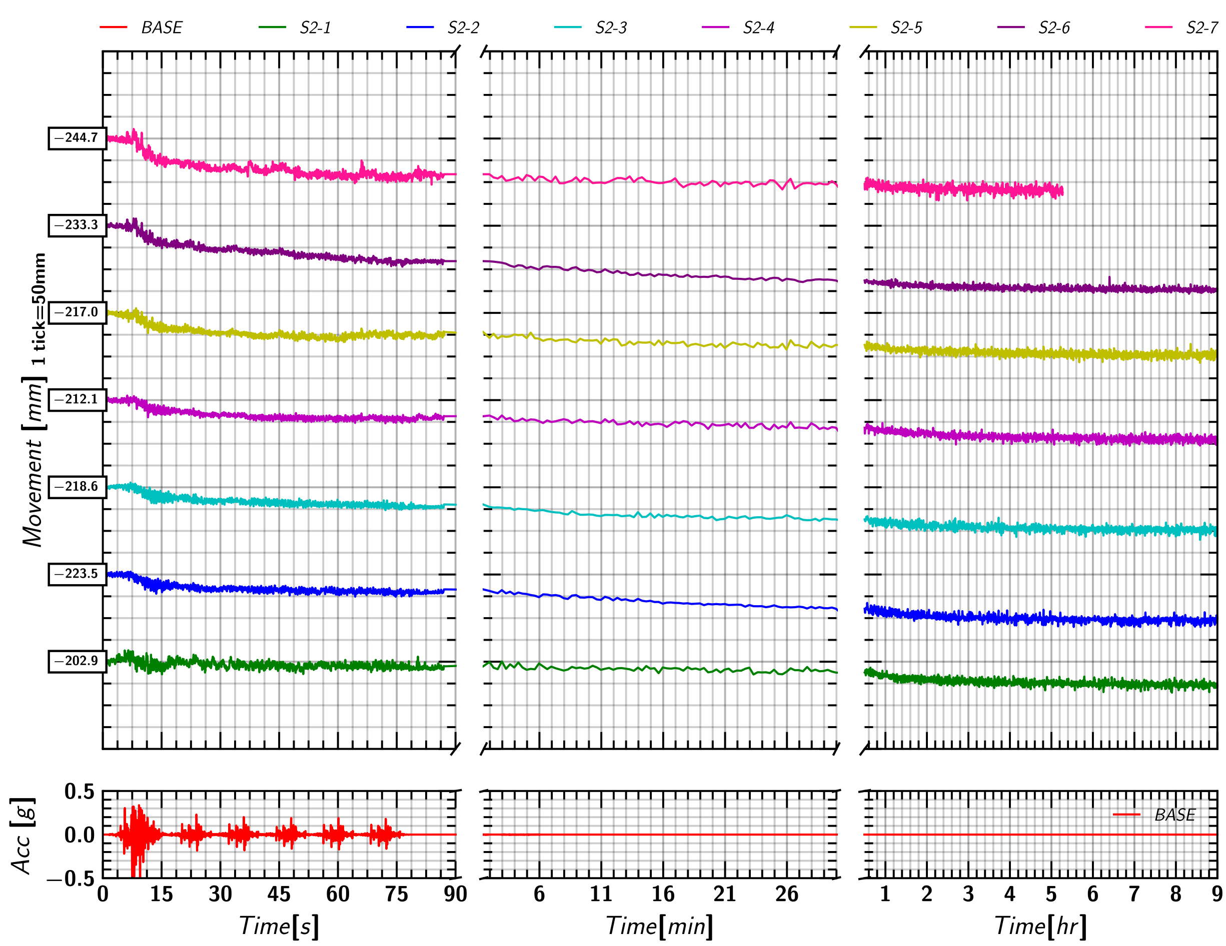

Figure 266. EQM5: Soil (Row S-2) movement in Z-direction relative to the model container during and post shaking.

M.7 Soil (Row S-3) Movement in X

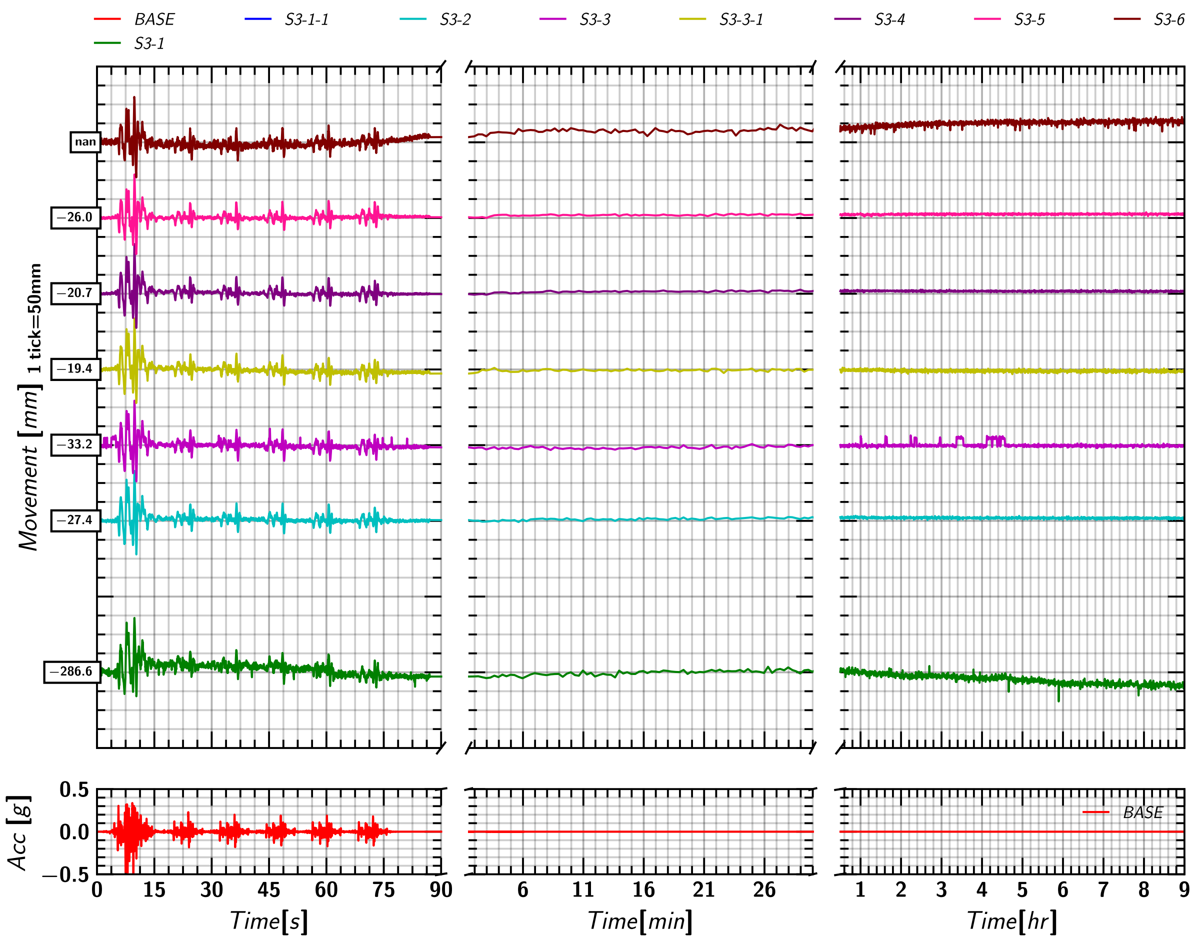

Figure 267. EQM₅: Soil (Row S-3) movement in X-direction relative to the model container during and post shaking.

M.8 Soil (Row S-3) Movement in Z

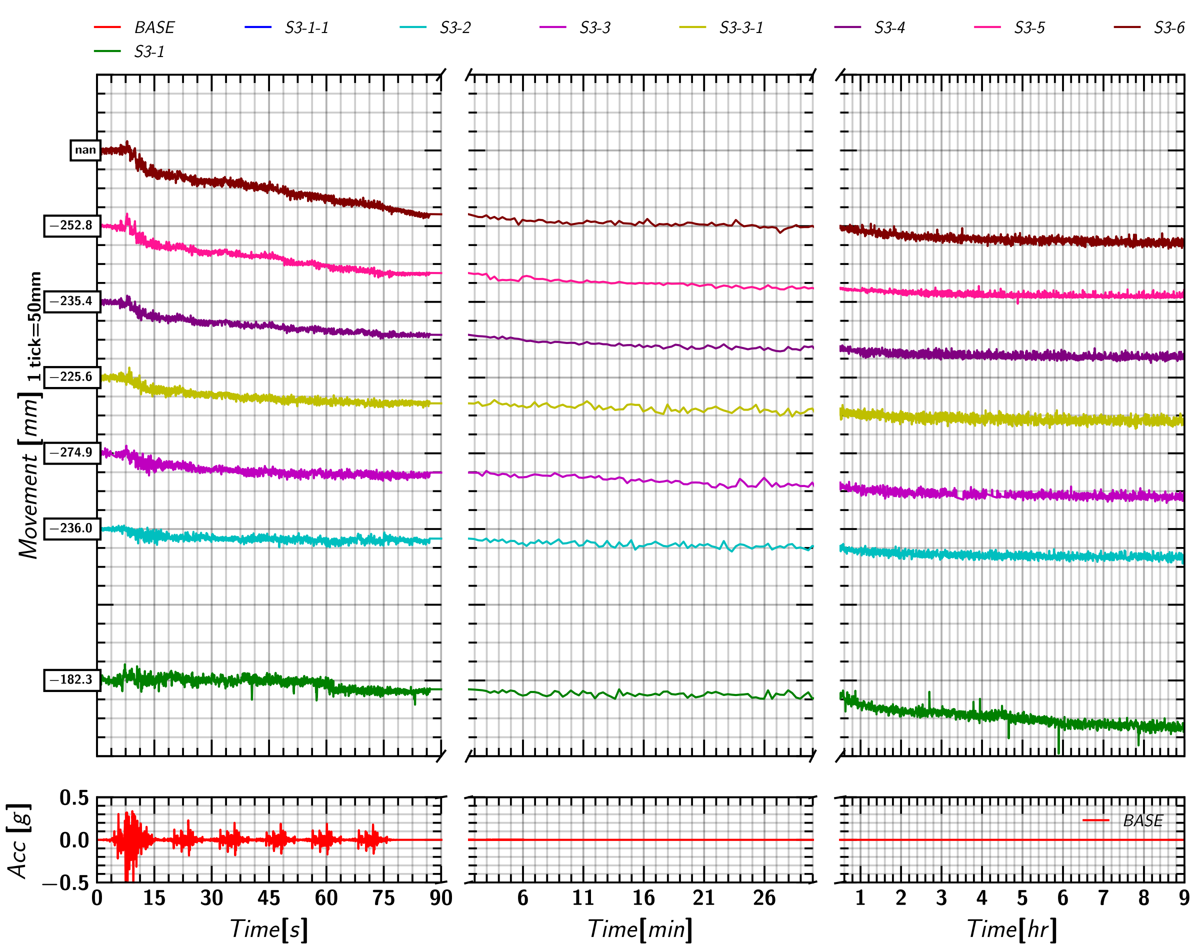

Figure 268. EQM₅: Soil (Row S-3) movement in Z-direction relative to the model container during and post shaking.

M.9 Soil (Row S-4) Movement in X

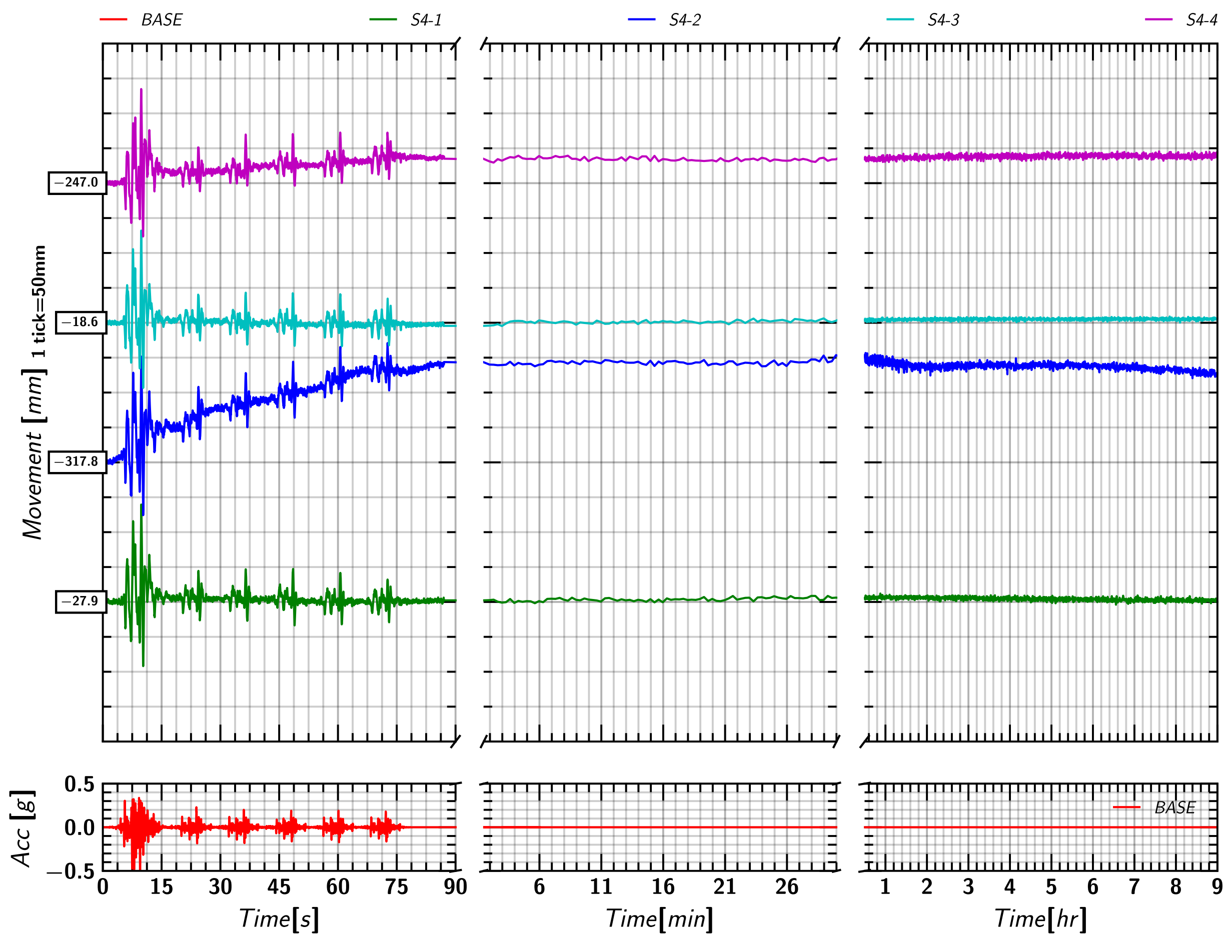

Figure 269. EQM$_5$: Soil (Row S-4) movement in X-direction relative to the model container during and post shaking.

M.10 Soil (Row S-4) Movement in Z

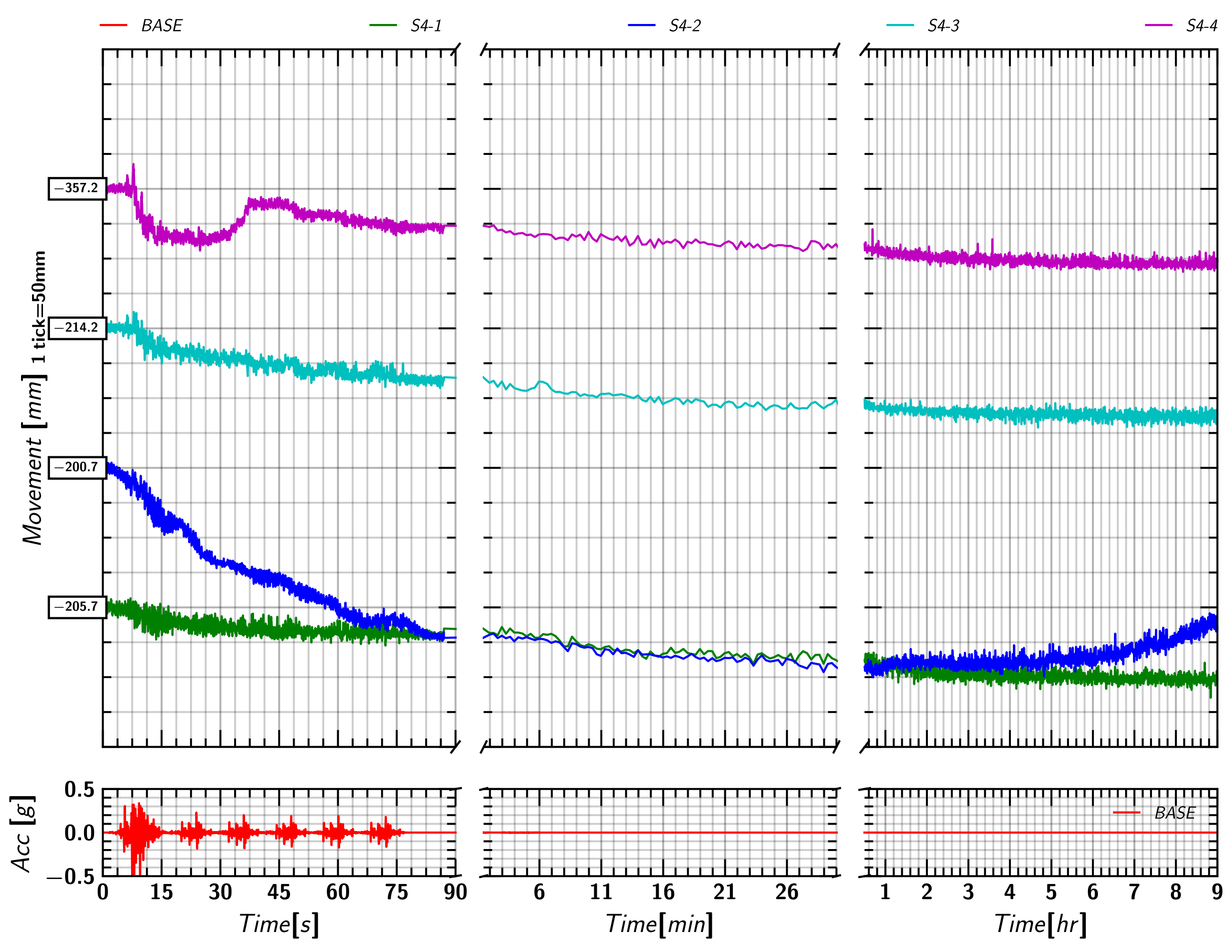

Figure 270. EQM$_5$: Soil (Row S-4) movement in Z-direction relative to the model container during and post shaking.

M.11 Soil (Row S-5) Movement in X

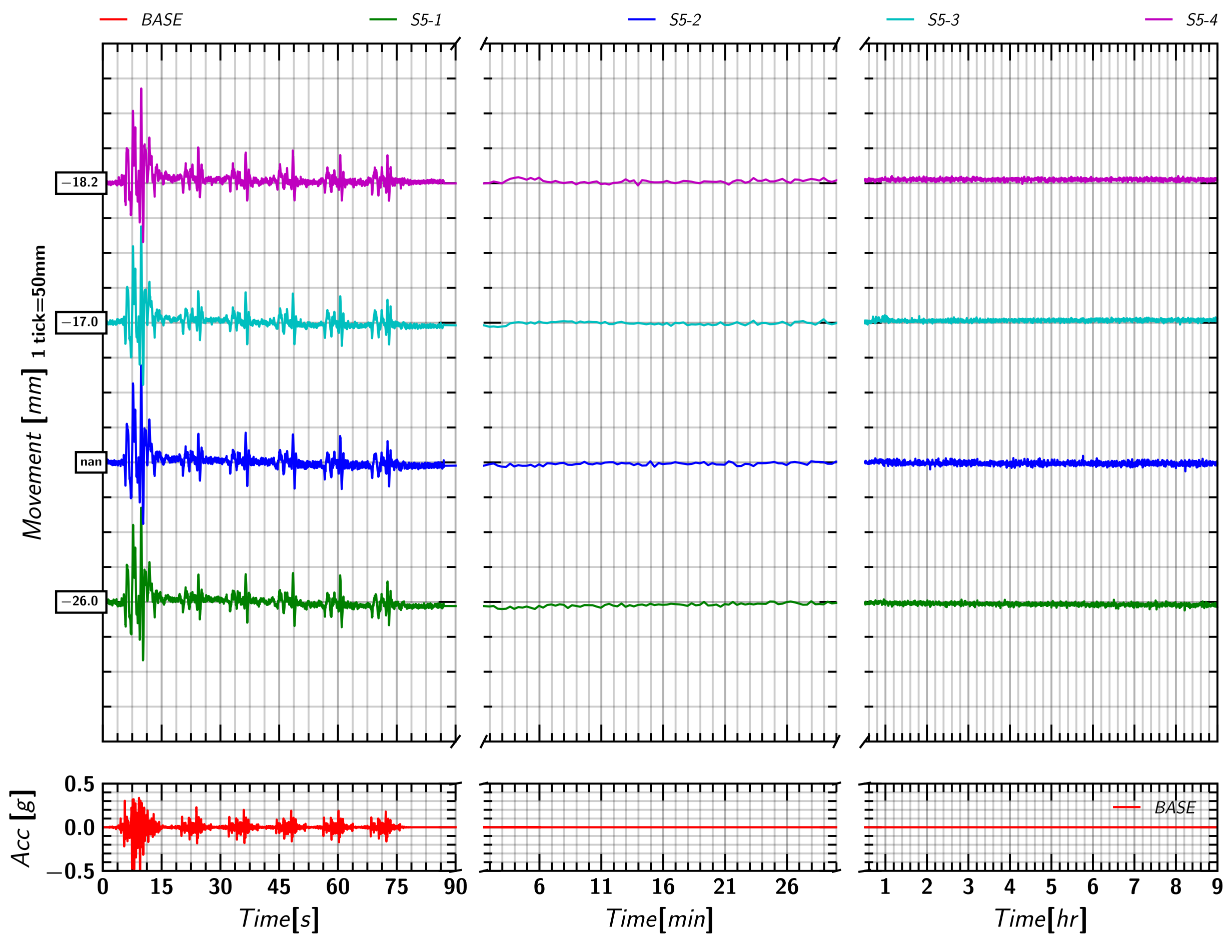

Figure 271. EQM5: Soil (Row S-5) movement in X-direction relative to the model container during and post shaking.

M.12 Soil (Row S-5) Movement in Z

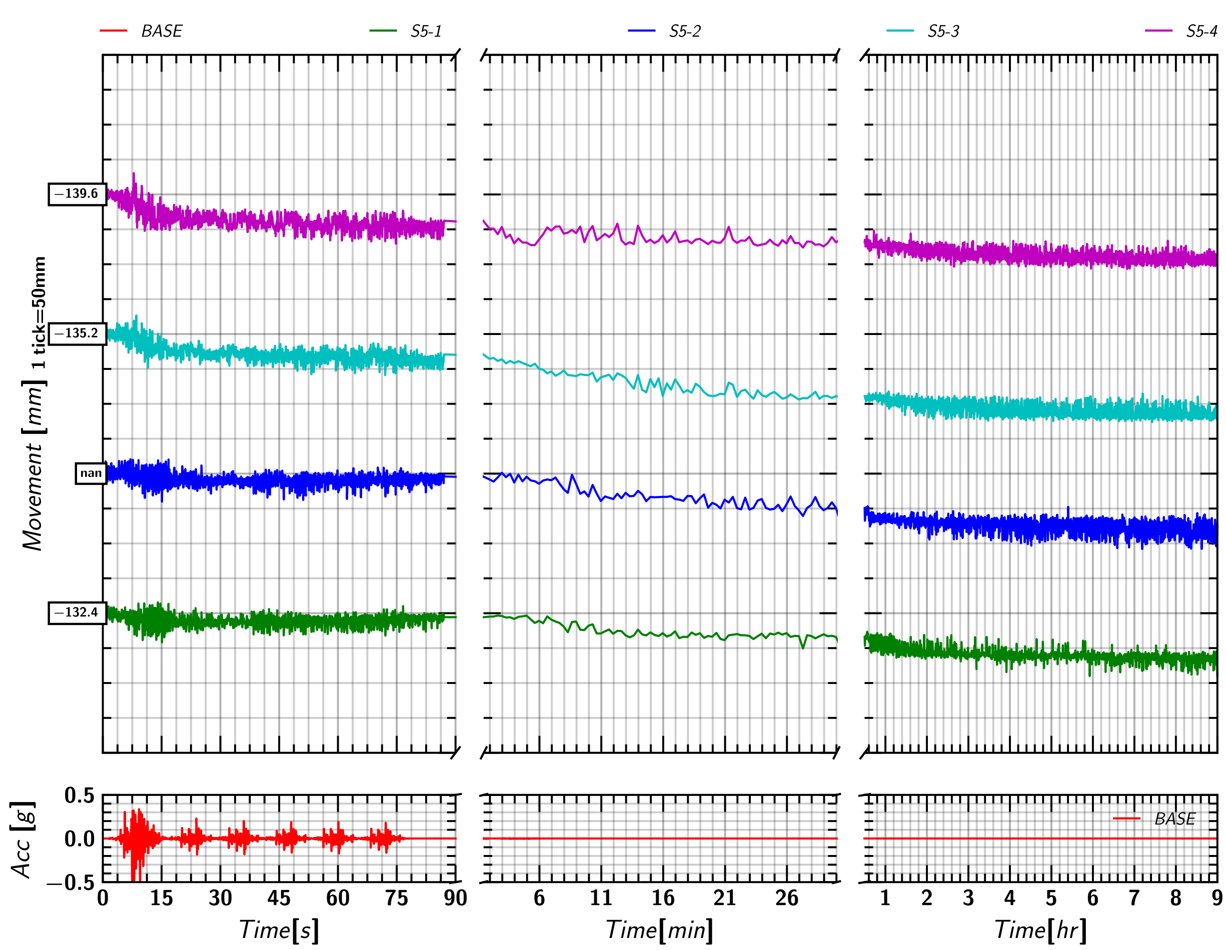

Figure 272. EQM5: Soil (Row S-5) movement in Z-direction relative to the model container during and post shaking.

M.13 Pile 1 Mass Movement in X

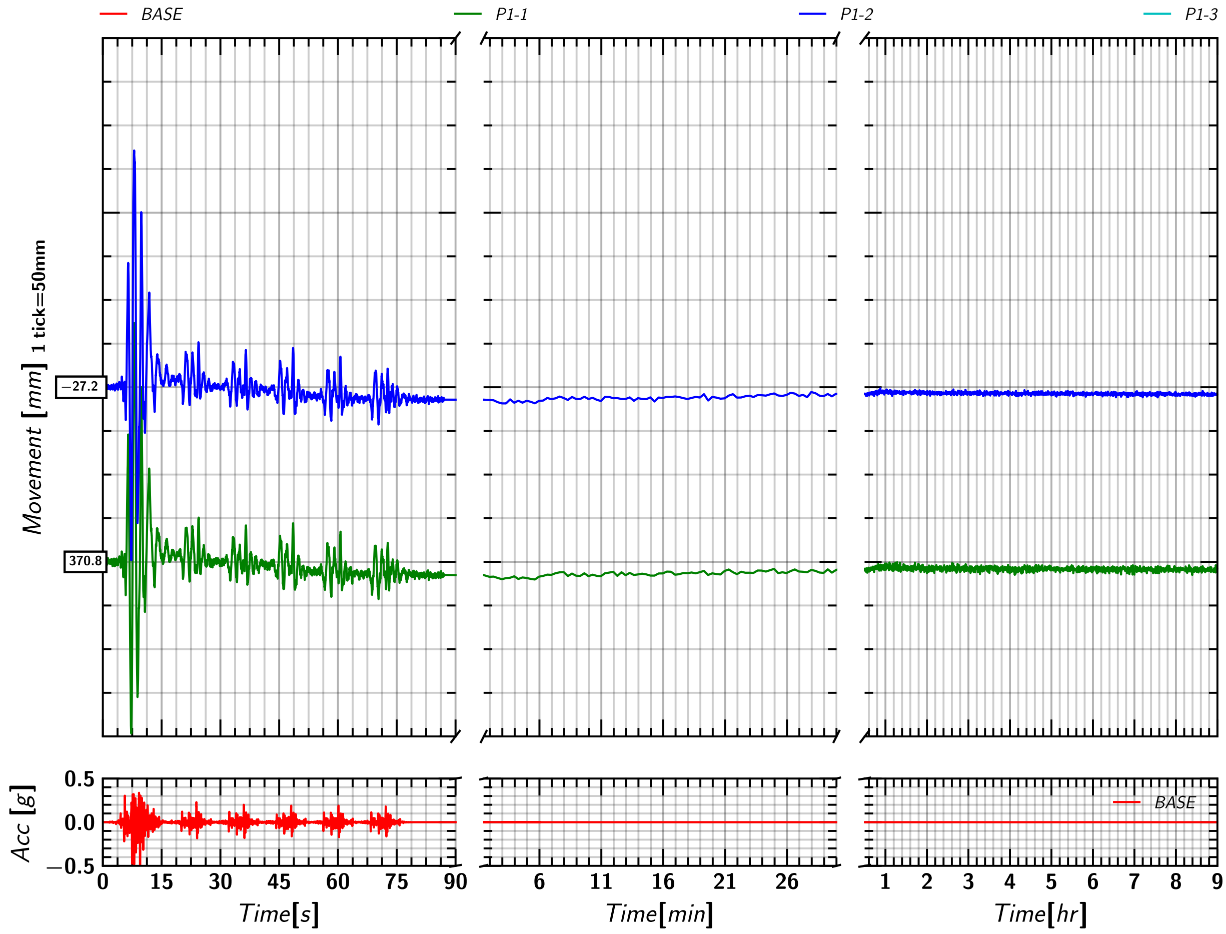

Figure 273. EQM₅: Pile 1 movement in X-direction relative to the model container during and post shaking.

M.14 Pile 1 Mass Movement in Z

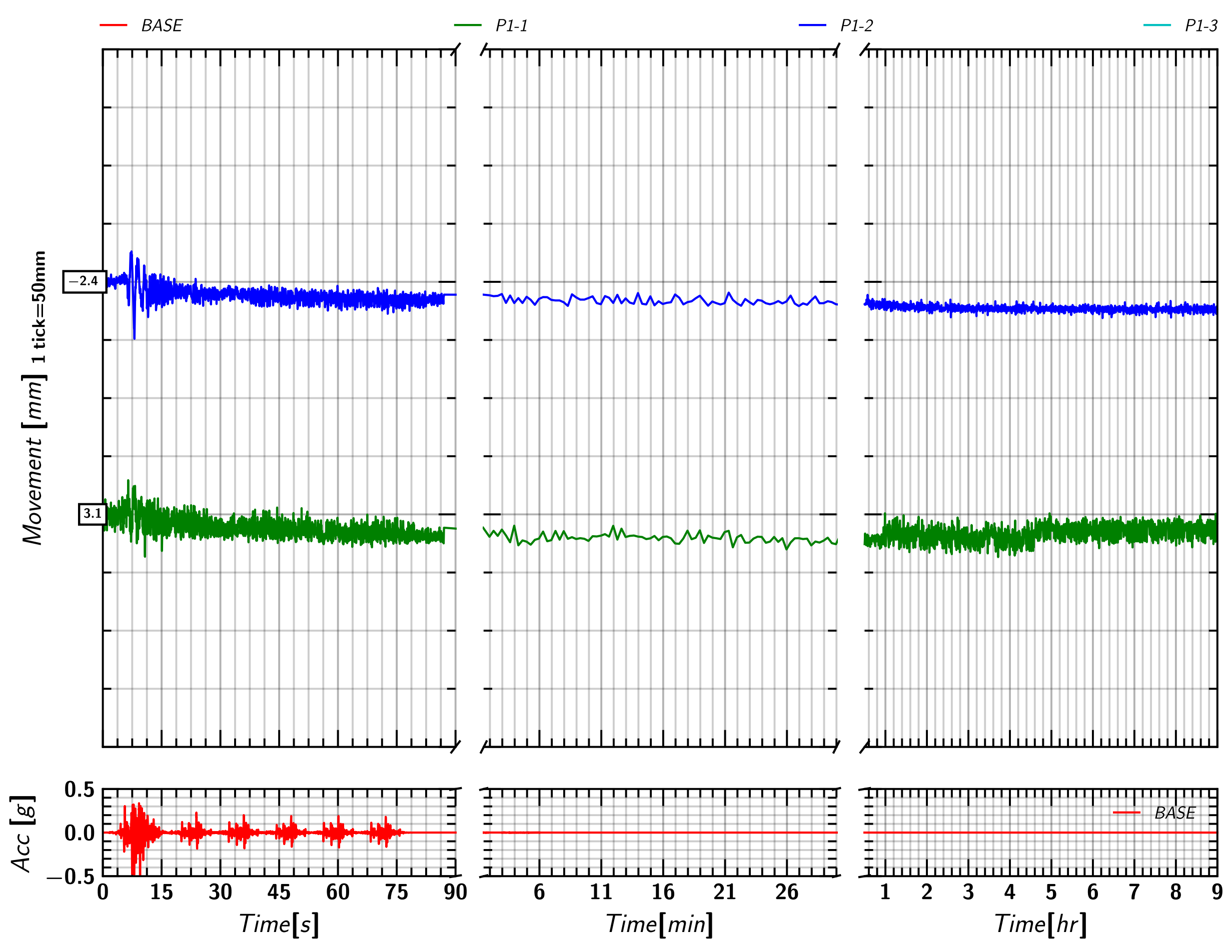

Figure 274. EQM₅: Pile 1 movement in Z-direction relative to the model container during and post shaking.

M.15 Pile 2 Mass Movement in X

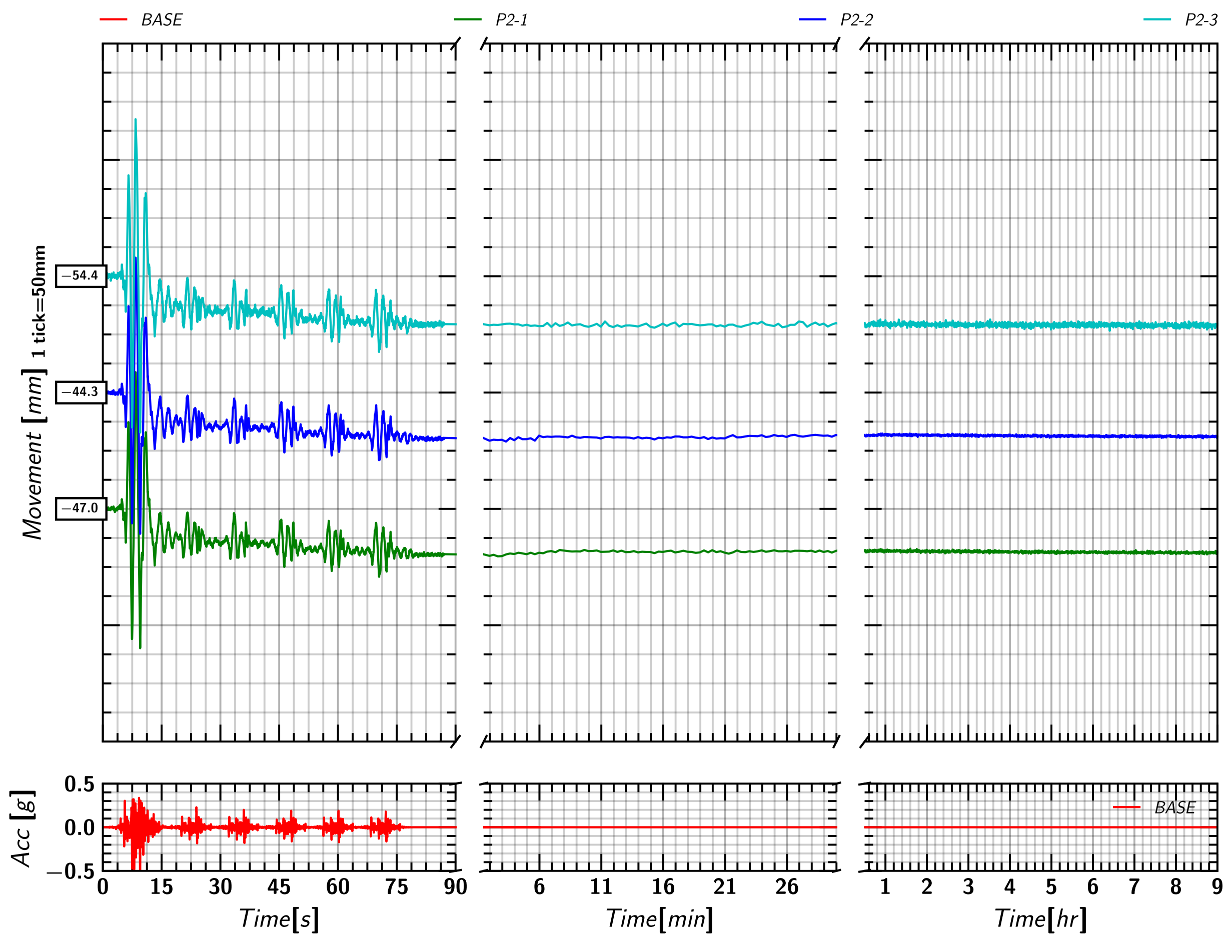

Figure 275. EQM5: Pile 2 movement in X-direction relative to the model container during and post shaking.

M.16 Pile 2 Mass Movement in Z

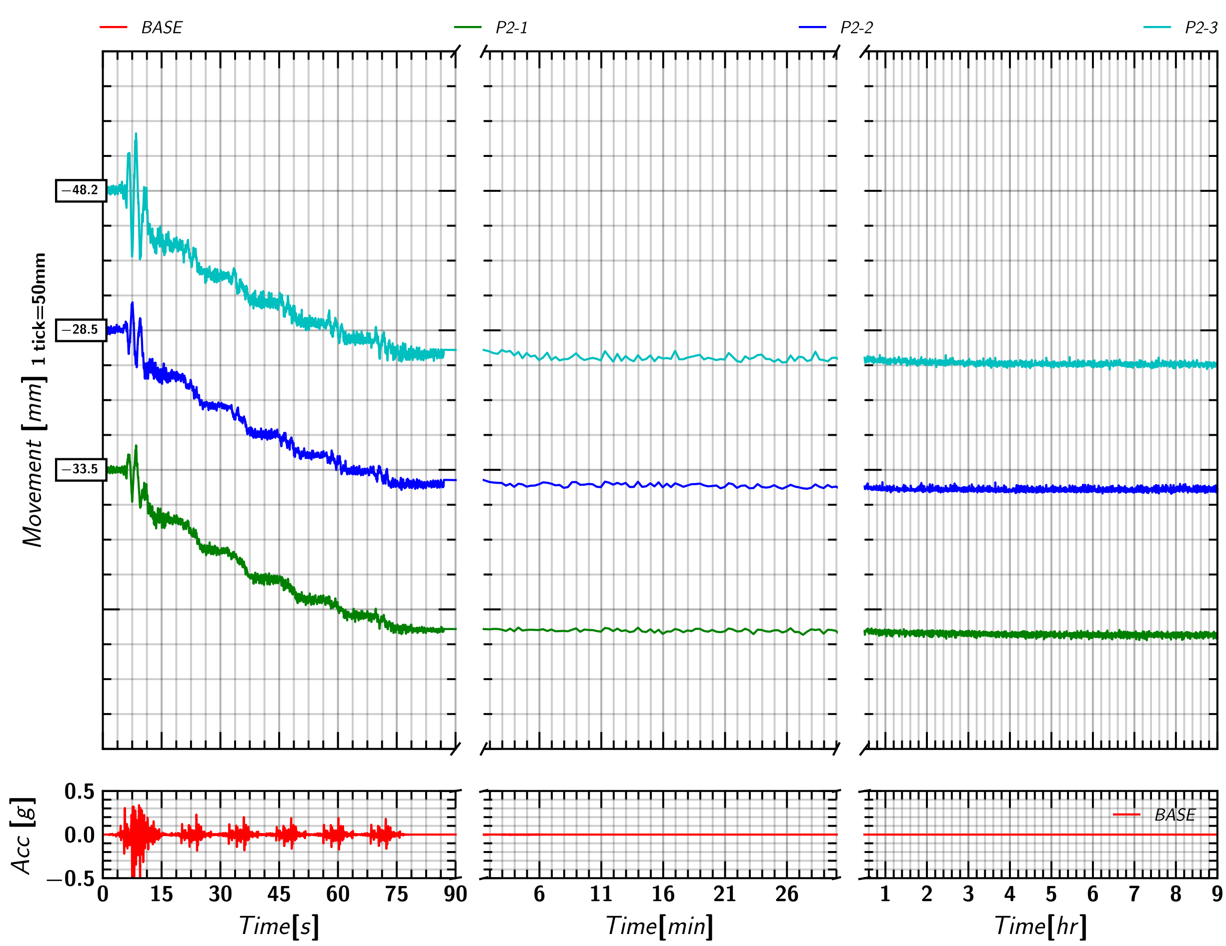

Figure 276. EQM5: Pile 2 movement in Z-direction relative to the model container during and post shaking.

M.17 Pile 3 Mass Movement in X

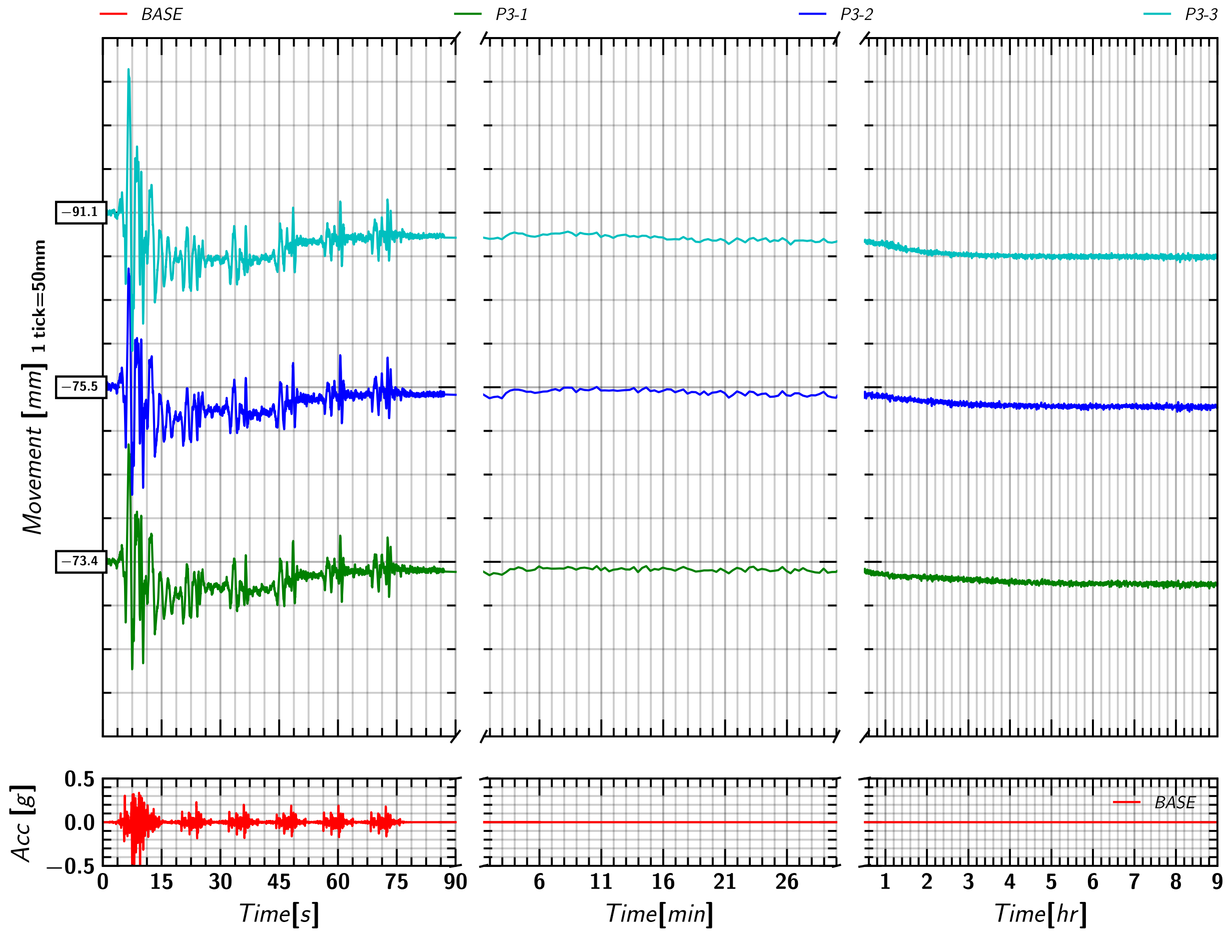

Figure 277. EQM5: Pile 3 movement in X-direction relative to the model container during and post shaking.

M.18 Pile 3 Mass Movement in Z

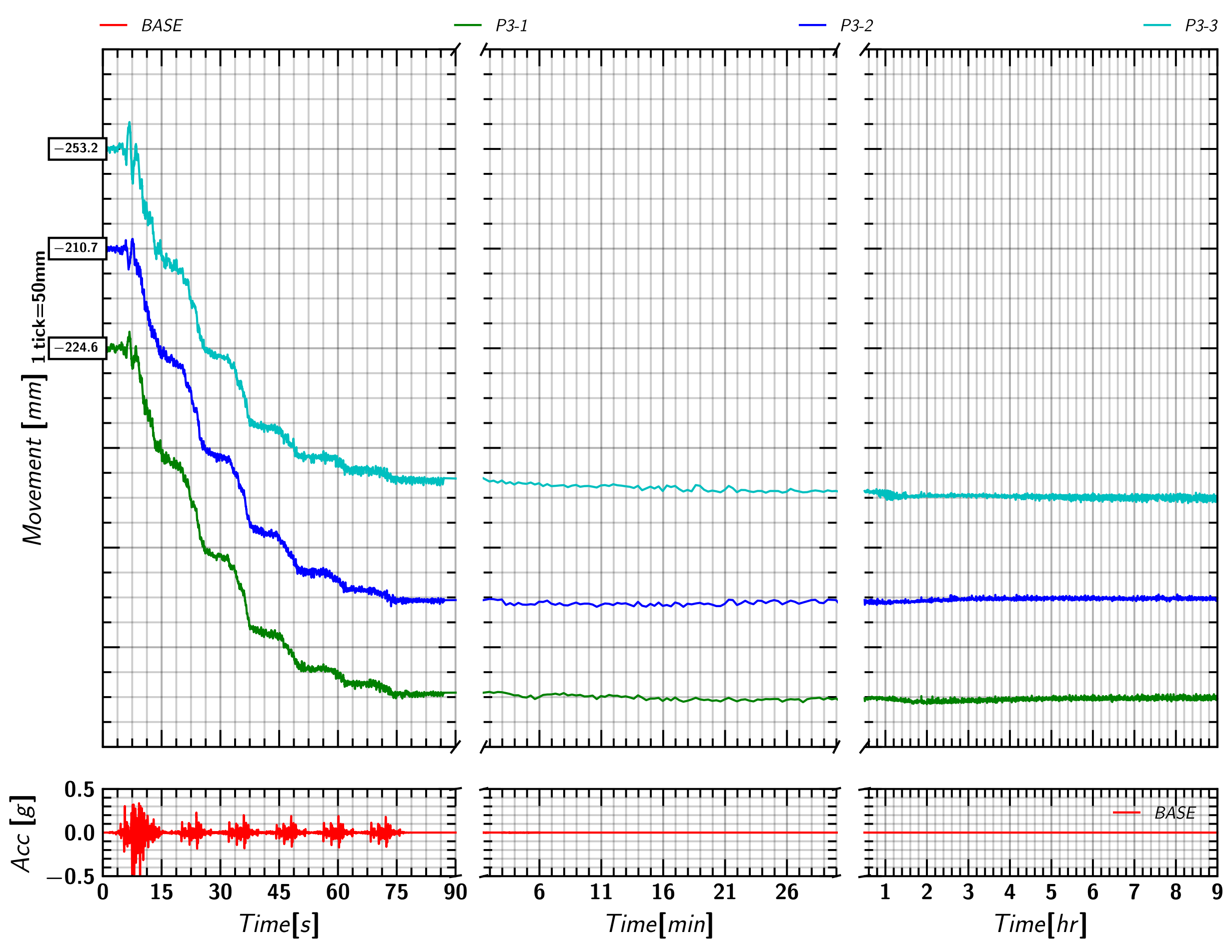

Figure 278. EQM5: Pile 3 movement in Z-direction relative to the model container during and post shaking.